**Patrícia Sofia Menalha Amado**

# Design, Synthesis and *in vitro* Evaluation of a Series of Endoperoxide Hybrids Designed to Tackle Latent Tuberculosis

**UNIVERSIDADE DO ALGARVE**

FACULDADE DE CIÊNCIAS E TECNOLOGIA

Doutoramento em Química

**2023**

**Patrícia Sofia Menalha Amado**

# Design, Synthesis and *in vitro* Evaluation of a Series of Endoperoxide Hybrids Designed to Tackle Latent Tuberculosis

Tese elaborada para a obtenção do grau de Doutor no ramo de Química, especialidade de Química Orgânica

**Trabalho efetuado sob a orientação de:**

Maria de Lurdes dos Santos Cristiano (Universidade do Algarve) – orientadora

Paul Michael O'Neill (University of Liverpool, UK) – co-orientador

**UNIVERSIDADE DO ALGARVE**

FACULDADE DE CIÊNCIAS E TECNOLOGIA

**2023**

# Design, Synthesis and *in vitro* Evaluation of a Series of Endoperoxide Hybrids Designed to Tackle Latent Tuberculosis

Doutoramento em Química, especialidade de Química Orgânica

## Declaração de Autoria do Trabalho

Declaro ser o autor deste trabalho, que é original e inédito. Autores e trabalhos consultados estão devidamente citados no texto e constam da listagem de referências incluídas.

Patrícia Sofia Menalha Amado

…….

## Direitos de cópia ou Copyright

*To my family,*

# *Acknowledgments*

This thesis results from five years of study, investigation, work, inspiration, patience, and perseverance. Throughout my doctoral program, I received assistance, guidance, and support from supervisors, the laboratory team, friends, and family.

I am deeply grateful to my supervisor Professor Maria de Lurdes Cristiano, for all the support, experience, leadership, and encouragement expressed throughout all these years. Thank you for all your guidance and friendship.

To Professor Paul O'Neill, my co-supervisor, I would like to express my gratitude for all the support and enthusiasm and the opportunity to participate in this project at his research group at the University of Liverpool.

Special thanks go to my lab members (and friends), Inês Costa, Joana Leal, Alina Secrieru, and Lília Cabral. None of this would have been possible without your help. I cannot express how important your presence has been during these years. I will never forget our conversations, laughs, lunches, and coffee breaks.

I am also grateful to all the great co-workers I had the pleasure to work with during the project (in Faro, and Liverpool) for sharing valuable professional experiences, constant support, and a pleasant working environment. I express my gratitude for the support in the synthesis by Dr Shirley Leung, in Liverpool.

I also thank the Department of Chemistry (University of Liverpool) and CCMAR (with the operational programs CRESC Algarve 2020 and COMPETE 2020 through projects EMBRC.PT ALG-01-0145-FEDER-022121, UIDB/04326/2020, UIDP/04326/2020, and LA/P/0101/2020) for providing facilities for compounds characterization, namely mass spectrometry, NMR, and elemental analysis.

I want to acknowledge the Liverpool School of Tropical Medicine staff for conducting the biological assays of my compounds. I thank the support given in the computational studies by Professor Neil Berry (University of Liverpool). CQC (Departamento de Química, Universidade de Coimbra), CQC-IMS (Faculdade de Farmácia, Universidade de Coimbra), CFisUC (Departamento de Física, Universidade de Coimbra), CQE (From Instituto Superior Técnico, and Faculdade de Ciências, University of Lisbon), more exactly to Professor Rui Fausto, Professor António José Jesus, Professor José António Paixão, Dr Luís Frija, Dr Jaime Coelho, for all the collaboration and availability in matrix isolation, Hirshfeld surface analysis, X-ray, and DFT computational studies. Together, we contributed to better science.

An enormous acknowledgment to Fundação para a Ciência e Tecnologia (FCT – Portugal) for generous financial support, especially within the Portuguese Science Foundation (Fundação para a Ciência e a Tecnologia (FCT) – Portugal) doctoral grant SFRH/BD/130407/2017 and additional grant COVID/BD/152392/2022. This PhD research in Chemistry was one of my life dreams that became a reality thanks to these grants.

This thesis is truly dedicated to my family, my sister Ana Lúcia, my niece Matilde, and my parents, Ângela and Carlos Amado. Thank you for believing in me and for all the unconditional support and understanding you gave me. Without you, I would never go this far. The word 'thank you' is very small for the unconditional love from you.

I am grateful for all support from Catarina Sardinha within so many years of friendship, filled with moments and calls.

Finally, I want to express my gratitude to Úrsula Maplehurst for always being there for me and her unconditional trust in me. Without her support, understanding, and patience, it would have been much harder to complete this thesis. Thank you so much for everything.

I am also thankful to all those who directly or indirectly helped me during this entire work.

# *Statement*

O presente trabalho foi desenvolvido sob a orientação científica da Professora Doutora Maria de Lurdes dos Santos Cristiano e coorientação do Professor Doutor Paul O'Neill. O trabalho foi elaborado em Portugal, na Universidade do Algarve (Faculdade de Ciências e Tecnologia, Departamento de Química e Farmácia) e no Centro de Ciências do Mar (CCMAR), e no Reino Unido, na Universidade de Liverpool (Departamento de Química). Este trabalho foi financiado pela Fundação para a Ciência e Tecnologia, através de uma bolsa individual de doutoramento com a referência **SFRH/BD/130407/2017** e uma bolsa excecional com a referência **COVID/BD/152392/2022**

This work was developed under the scientific supervision of Professor Maria de Lurdes dos Santos Cristiano and the co-supervision of Professor Paul O'Neill. It was conducted in Portugal, at the University of Algarve (Faculdade de Ciências e Tecnologia, Departamento de Química e Farmácia) and Centre of Marine Sciences (CCMAR), and in the United Kingdom, at the University of Liverpool (Department of Chemistry). The work was financially supported by Fundação para a Ciência e Tecnologia through the doctoral grant **SFRH/BD/130407/2017** and the additional grant **COVID/BD/152392/2022**.

# *Publications*

Part of the original work described in this thesis has been included in the following publications or communications.

**Research articles (Related to this thesis) published in peer reviewed journals:**

**1 - Amado, P. S. M.**; Woodley, C. M.; Cristiano, M. L. S.; O'Neill, P. M. *ACS Omega*, **2022**, *7* (45), 40659-40681. https://doi.org/10.1021/acsomega.2c05307

**2 - Amado, P. S. M.**; Jesus, A. J. L.; Paixão, J. A.; Fausto, R.; Cristiano, M. L. S. *ChemPlusChem*, **2022**, *87* (8), e202200207. https://doi.org/10.1002/cplu.202200207

**3 -** Woodley, C. M.; **Amado, P. S. M.;** Cristiano, M. L. S.; O'Neill, P. M. *Med. Res. Rev*. **2021**, *41* (6), 3062–3095. https://doi.org/10.1002/med.21849

**4 - Amado, P. S. M.;** Frija, L. M. T.; Coelho, J. A. S.; O'Neill, P. M.; Cristiano, M. L. S.; *The Journal of Organic Chemistry*. **2021**, *86* (15), 10608–10620. https://doi.org/10.1021/acs.joc.1c01258

**Book Chapter:**

**1- Amado, P. S. M**.; Frija, L. M. T.; O'Neill, P. M.; Cristiano, M. L. S. Synthesis of Non-Symmetrical 1,2,4,5-Tetraoxanes: Past and Current Routes. *To be published by World Scientific*. *Submitted on 17th February 2022. In editorial Revision.*

**Other Publications during the PhD program:**

**1 -** Leal, J. F.; Bombo, G.; **Amado, P. S. M**.; Pereira, H.; Cristiano, M. L. S. *Foods*, **2023**, *12* (4), 768. https://doi.org/10.3390/foods12040768

**2 -** Mendes, A.; Armada, A.; Cabral, L. I. L.; **Amado, P. S. M.;** Campino L.; Cristiano, M. L. S.; Cortes, S. *Pharmaceuticals*. **2022**, *15* (4), 446. https://doi.org/10.3390/ph15040446

**3- Amado, P. S. M.**; Costa, I. C. C.; Paixão, J. A.; Mendes, R. F.; Cortes, S.; Cristiano, M. L. S. *Molecules*, **2022**, *27* (17), 5401. https://doi.org/10.3390/molecules27175401

**4 -** Leal, J. F.; Guerreiro, B.; **Amado, P. S. M.;** Fernandes, A. L.; Barreira, L.; Paixão, J. A.; Cristiano, M. L. S. *Molecules*. **2021**, *26* (6), 1501-1501. https://doi.org/10.3390/molecules26061501

**5 -** Nunes, C. M.; Pereira, N. A. M.; Reva, I.; **Amado, P. S. M.;** Cristiano, M. L. S.; Fausto, R. *The Journal of Physical Chemistry Letters*. **2020**, *11* (19), 8034-8039. http://dx.doi.org/10.1021/acs.jpclett.0c02272

**6 -** Brás, E. M.; Cabral, L. I. L.; **Amado, P. S. M.;** Abe, M.; Fausto, R.; Cristiano, Maria L. S. *The Journal of Physical Chemistry A*. **2020**, *124* (21), 4202-4210. http://dx.doi.org/10.1021/acs.jpca.0c01974

**7 -** Cabral, L. I. L.; Pomel, S.; Cojean, S.; **Amado, P. S. M.;** Loiseau, P. M.; Cristiano, M. L. S. *Molecules*. **2020**, *25* (3), 465-465. https://doi.org/10.3390/molecules25030465

**Manuscripts in preparation:**

**1 - Amado, P. S. M**.; Woodley, C. M.; Cristiano, M. L. S.; O'Neill, P. M. Synthesis of Endoperoxide-Based Antitubercular Hybrids with Potential for Dual Mechanisms of Action.

**2 - Amado**, **P. S. M**.; Cristiano, M. L. S.; O'Neill, P. M. Classification models on DprE1 inhibitors using machine learning methods.

# *Abstract*

*Mycobacterium tuberculosis* (*Mtb*) is the world's second leading cause of death from infectious diseases (after COVID-19). The ability of *Mtb* to enter the nonreplicating persistence (NRP) and then transition to latent TB contributes to *Mtb*'s drug tolerance and treatment failure in chronically infected individuals.

The DosRST two-component regulatory system regulates the *Mtb* physiology to promote NRP, in which peroxides such as the natural antimalarial drug artemisinin and synthetic 1,2,4-trioxolanes have been demonstrated to inhibit this system and re-sensitize *Mtb*. Hence, we proposed hybridizing two separate anti-TB classes by combining the 1,2,4-trioxane-containing moieties with the indole-2-carboxamide scaffold (MmpL3 inhibitors) and the benzothiazinone scaffold (DprE1 inhibitors), to establish a dual mode of action, by increasing *Mtb*'s sensitivity to the active anti-TB pharmacophore while also targeting the DosRST signalling. These hybrid compounds prepared were evaluated for their *in vitro* antimycobacterial activity, and the drug metabolism and pharmacokinetics parameters were also assessed.

Additionally, we evaluated ~1519 DprE1 inhibitors disclosed in the literature from 2009-2022 by performing an in-depth analysis of physicochemical descriptors and absorption, distribution, metabolism, elimination, and toxicology properties to deepen our understanding of DprE1 inhibitors and build machine learning classification models.

Among organic peroxides, six-membered cyclic 1,2,4-trioxanes and 1,2,4,5-tetraoxanes have gained a great interest in medicinal chemistry, their synthesis being of paramount relevance. The cyclocondensation of a representative library of ketones with *gem*-dihydroperoxides or peroxysilyl alcohols/β-hydroperoxy alcohols to afford the corresponding unsymmetrical 1,2,4,5-tetraoxanes or 1,2,4-trioxanes, mediated by the silica sulfuric acid (SSA) catalyst, was systematically investigated in this thesis, yielding an improved synthetic route to 1,2,4-trioxanes and 1,2,4,5-tetraoxanes.

Despite the endoperoxides' potential pharmaceutical applications, fundamental studies on the structures of trioxolanes and tetraoxanes are scarce. By combining X-ray crystallography and vibrational spectroscopy, along with Hirshfeld surface analysis and calculations (CE-B3LYP/6-31G(d,p)) of pairwise interaction energies of intermolecular contacts existing in the crystal structure, a deeper understanding of the relative reactivity and the properties of these endoperoxide classes was gathered.

***Keywords**:* tuberculosis, endoperoxides, anti-tubercular hybrids, DosRST-inhibitors, silica-supported catalysts, structural analysis, machine learning.

# *Resumo*

A infeção por *Mycobacterium tuberculosis* (*Mtb*) é, atualmente, a segunda principal causa de morte no mundo por doenças infeciosas, estando apenas atrás da COVID-19. Acredita-se que um quarto da população mundial esteja infetado por esta micobactéria e a forma mais prevalente é a tuberculose pulmonar, altamente contagiosa e potencialmente fatal se não tratada.

A capacidade da *Mtb* de entrar no estado não replicativo (NRP) e, em seguida, transitar para a tuberculose latente, contribui para a tolerância/resistência da micobactéria relativamente à terapêutica, levando à falha no tratamento em indivíduos cronicamente infetados. Desta forma, melhorias de tratamento contra a tuberculose (TB) requerem moléculas de ação mais rápida e capaz de contornar o problema da latência.

O sistema regulador de dois componentes DosRST, composto por um gene regulador transcricional, DosR, e duas histidinas quinases, DosS e DosT, regula a fisiologia da *Mtb* para promover o estado não replicativo, o qual é induzido por hipoxia, monóxido de carbono e óxido nítrico no meio celular.

Foi publicado que o antimalárico artemisinina (ART), um 1,2,4-trioxano de origem natural, participa na desregulação das proteínas dependentes do sistema DosRST. Essa inibição foi atribuída à capacidade da ligação peroxídica presente na estrutura 1,2,4-trioxano da ART de interagir com o grupo heme em DosS e DosT, levando à sua inativação. O pré-tratamento com ART aumenta assim a sensibilidade da *Mtb* latente à isoniazida, um medicamento anti-TB de primeira linha, mas sem atividade antimicrobiana contra a *Mtb* latente. Foi também descoberto em 2022 que os peróxidos sintéticos 1,2,4-trioxolano OZ277 e OZ439 podem direcionar a sinalização de hipoxia mediada por DosS em *M. abscessus* e reproduzir o fenótipo "*knock-out*" de DosS, aumentando a sensibilidade da *Mtb* à antibioterapia.

Como os compostos ART, OZ277 e OZ439 demonstraram inibir essas histidina-quinases, postulou-se que outros endoperóxidos sintéticos também poderiam interagir com DosS e DosT. A procura de novas moléculas com dupla ação, capazes de interromper a sinalização de DosRST e, ao mesmo tempo, inibir uma proteína-alvo de *Mtb* conhecida, afigura-se como uma estratégia de tratamento válida para travar a *Mtb* latente. Desta forma, foi proposto hibridizar duas classes de compostos com propriedades anti-TB, através da combinação de um fragmento que contém um endoperóxido com um fragmento indole-2-carboxamida (que inibe a proteína transportadora MmpL3), ou com um fragmento de benzotiazinona (que inibe a flavoenzima DprE1). O tipo de

endoperóxido escolhido para esta tese foi o endoperóxido cíclico 1,2,4-trioxano. Com esta abordagem híbrida, procurou-se estabelecer um modo de ação duplo, aumentando a sensibilidade da *Mtb* ao farmacóforo anti-TB e, ao mesmo tempo, alterar a sinalização do sistema DosRST. Os estudos realizados nesta tese concentram-se no desenho, síntese, estrutura e propriedades de uma biblioteca de novos híbridos de 1,2,4-trioxano, com o fragmento indole-2-carboxamida (IC) e com o fragmento benzotiazinona (BTZ). Esses compostos híbridos foram avaliados quanto à sua atividade antituberculosa *in vitro*, e os seus parâmetros farmacocinéticos e metabolismo (DMPK) foram também avaliados.

A análise dos híbridos de peróxido-IC contra *Mtb* no estado replicativo (forma ativa) demonstrou baixa atividade para a maioria dos compostos ($IC_{50}$ > 10 μM), embora o metabolito controlo 2.84 e o híbrido tetraoxano 2.86 tenham exibido atividade inibitória moderada no crescimento de *Mtb* ($IC_{50}$ = 5,680 e 2,634 μM, respetivamente). Os estudos de modelação molecular explicam a baixa atividade dos híbridos peróxido-IC, uma vez que os resultados obtidos foram pouco satisfatórios para estes compostos, exceto para o análogo IC dimetilado, TIC01. No entanto, verificou-se que este híbrido de peróxido também não era ativo contra o *Mtb*.

Em contrapartida, a síntese dos análogos peróxidos-BTZ resultou em dezasseis novos compostos de híbridos peróxidos-BTZ e levou à identificação de compostos ativos potentes, com valores de $IC_{50}$ na escala nanomolar (1,32-870 nM) e picomolar (< 0,457 nM). Os estudos de modelação molecular demonstraram boa sobreposição entre o sistema de anéis BTZ dos híbridos e o ligando de referência (BTZ043), o que justifica a potente atividade submicromolar observada nessas séries.

Foram efetuados estudos *in silico* para os híbridos endoperoxídicos sintetizados e os dados obtidos foram comparados com os resultados *in vitro* de DMPK. Experimentalmente, os híbridos IC-trioxano **TIC01-03** apresentam lipofilicidades similares e solubilidades baixas a pH 7,4, como previsto para os compostos indole-2-carboxamida. Os perfis metabólicos dos híbridos peróxido-IC e peróxido-BTZ043 apresentaram valores de moderado a bom, enquanto para os híbridos peróxido-PBTZ169 foram de fraco a moderado. Os elevados valores de cLogP obtidos para todos os compostos sintetizados explicam a baixa solubilidade aquosa destas moléculas.

Estudos *in vivo* dos perfis farmacocinéticos dos híbridos peróxido-BTZ **B3**, **P1** e dos compostos controlo indicam que os híbridos endoperóxido-BTZ são metabolicamente menos estáveis do que os correspondentes BTZs. Isto deve-se, possivelmente, à ligação lábil do peróxido na sua estrutura, o que os torna mais suscetíveis ao metabolismo. Comparando com os compostos líder (BTZ043 e PBTZ169), o peróxido-BTZ **B3** exibiu

dados farmacocinéticos semelhantes. Os compostos mais promissores da série endoperóxido-BTZ foram selecionados para avaliação em células *Mtb* modificadas para expressar proteína verde fluorescente ("*green fluorescent protein*", GFP) dependente de DosRST, de forma a avaliar a inibição neste sistema. Estes ensaios celulares encontram-se em avaliação.

A vulnerabilidade não específica da flavoenzima DprE1 pode explicar os resultados promissores obtidos durante o desenvolvimento de híbridos endoperóxido-BTZ. Embora o desenvolvimento de inibidores de DprE1 possa ser complexo, aprofundar a compreensão das suas propriedades físico-químicos (FQ) e características relacionadas com a absorção, distribuição, metabolismo, excreção e toxicidade (ADMET) pode facilitar a descoberta de novos compostos potentes. Com este objetivo em mente foi realizada uma extensa análise dos descritores FQ e dos parâmetros ADMET para aprofundar os conhecimentos acerca dos inibidores de DprE1. Foram avaliadas 1519 moléculas classificadas como inibidores da enzima DprE1, com cobertura da literatura disponível desde 2009 até abril de 2022. Concomitantemente, foram construídos modelos de classificação para os inibidores DprE1, de forma a possibilitar a previsão da atividade de um composto através da análise das suas propriedades químicas.

Para além da utilização no tratamento do *Mtb*, os peróxidos orgânicos, em especial os 1,2,4-trioxanos e os 1,2,4,5-tetraoxanos, em que a funcionalidade peróxido está inserida em anéis de seis membros, têm despertado grande interesse na química medicinal devido ao seu potencial para o tratamento de outras doenças, nomeadamente a malária. Uma parte dos estudos realizados no âmbito desta tese concentrou-se em melhorar os métodos de síntese de peróxidos de seis membros para expandir as bibliotecas destes compostos, facilitando a descoberta de novos candidatos a fármacos. Foi investigada a ciclocondensação de um conjunto de cetonas com *gem*-dihidroperóxidos ou álcoois peroxisilílicos/β-hidroperoxiálcoois para produzir os correspondentes 1,2,4,5-tetraoxanos ou 1,2,4-trioxanos assimétricos, mediada pelo catalisador SSA. Os catalisadores suportados em sílica têm atraído a atenção recentemente devido à sua promissora reatividade, sendo também recicláveis e reutilizáveis, com grandes vantagens económicas e ambientais. As etapas elementares envolvidas na via de ciclocondensação foram investigadas através de cálculos de orbitais moleculares, usando a teoria do funcional de densidade (DFT), no nível de aproximação ωB97XD/def2-TZVPP/PCM(DCM)//B3LYP/6-31G(d). Os resultados sustentam uma proposta mecanística que destaca a função catalítica da SSA, onde a protonação inicial do grupo

carbonilo da cetona pela SSA surge como uma etapa chave no mecanismo. Esta nova abordagem envolvendo o catalisador suportado em sílica oferece várias vantagens sintéticas, nomeadamente a tolerância a uma ampla gama de substratos. Além disso, a fácil preparação, reciclabilidade e propriedades ecológicas do catalisador SSA são características que tornam este método uma ferramenta atraente para desenvolver novos endoperóxidos biologicamente ativos, estabelecendo assim uma abordagem válida para a síntese de novos endoperóxidos biologicamente ativos sem recurso a catalisadores baseados em metais tóxicos.

Apesar das potenciais aplicações terapêuticas dos endoperóxidos, os estudos fundamentais sobre as estruturas dos 1,2,4-trioxolanos e 1,2,4,5-tetraoxanos são escassos. Neste âmbito, combinando a cristalografia de raios-X e a espectroscopia vibracional com a análise de superfície de Hirshfeld e cálculos (CE-B3LYP/6-31G(d,p)) das energias de interação par a par dos contatos intermoleculares existentes na estrutura cristalina, foi possível aprofundar o conhecimento estrutural, o que facilita a compreensão da reatividade relativa e das propriedades dessas classes de endoperóxidos.

***Palavras-chave:*** tuberculose, endoperóxidos, híbridos antituberculares, inibidores de DosRST, catalisadores suportados em sílica, análise estrutural, aprendizagem de máquina.

# *Table of Contents*

# *List of Figures*

# *List of Tables*

# *List of Schemes*

# *Abbreviations*

| | |
|---|---|
| **2-CQ** | 2-carboxyquinoxalines |
| **2-S-BTO** | 2-mercaptobenzothiazoles |
| **4-AQ** | 4-Aminoquinolone piperidine amides |
| **AcOH** | Acetic acid |
| **ACP** | NADH-specific enoyl-acyl carrier protein |
| **Act** | Active |
| **ACT** | Artemisinin Combination Therapy |
| **AD** | Applicability Domain |
| **ADMET** | Absorption, distribution, metabolism, excretion, and toxicity |
| **AG** | Arabinogalactan |
| **AIDS** | Acquired immunodeficiency syndrome |
| **Am** | Amikacin |
| **AMES** | *Salmonella typhimurium* reverse mutation assay |
| **ART** | Artemisinin |
| **Asn** | Asparagine |
| **Asp** | Aspartic acid |
| **ATP** | Adenosine triphosphate |
| **ATR** | Attenuated total reflectance |
| **AUC** | Area under the curve (*Chapter 1*) |
| **$AUC_{inf}$** | Area under the curve to infinity |
| **AUROC** | Receiver operating characteristic curve (also AUC or ROC in *Chapter 3*) |
| **AVMT** | Avermectins |
| **AZA** | 1,4-azaindole |
| **BBB** | Blood-brain barrier penetration |
| **BCG** | *Mycobacterium bovis* Calmette-Guérin |
| **BD** | Benzodioxanes |
| **Bdq** | Bedaquiline |
| **BI** | Benzimidazoles |
| **Boc** | *tert*-Butyloxycarbonyl |
| **br** | Broad |
| **bRo5** | Beyond Ro5 |
| **BSA** | *N,O*-bis-(trimethylsilyl)acetamide |
| **BTO** | Benzothiazoles |
| **BTZ** | Benzothiazinones |
| **CBFP** | Computational bioactivity fingerprints |
| **cBT** | Crowded benzothiazoles |
| **$CC_{50}$** | Half-maximal inhibitory concentration |
| **CD** | 3,4-Dihydrocarostyril derivative |
| **CFU** | Colony forming units |
| **Cfz** | Clofazimine |
| **CI** | Chemical ionisation |

| | |
|---|---|
| **CL** | Clearance |
| **CLint** | Intrinsic clearance |
| **CLND** | Kinetic aqueous solubility |
| **ClogD** | Calculated distribution coefficient at pH=7.4 |
| **ClogP** | Calculated partition coefficient |
| **$C_{max}$** | Maximum plasma concentration |
| **Cmpd** | Compound |
| **CNS** | Central nervous system |
| **CO** | Carbon monoxide |
| **Cov** | Covalent |
| **Cs** | Clycoserine |
| **CV** | Cross validation |
| **CYP** | Cytochrome P450 |
| **Cys** | Cysteine |
| **d** | Doublet (spectral) |
| **DCE** | Dichloroethane |
| **DCM** | Dichloromethane |
| **dd** | Doublet of doublets (spectral) |
| **DFT** | Density functional theory |
| **DHP** | *Gem*-dihydroperoxide |
| **Dlm** | Delamanid |
| **DMF** | *N*,*N*-dimethylformamide |
| **DMPK** | Drug Metabolism and Pharmacokinetics |
| **DMSO** | Dimethyl sulfoxide |
| **DNA** | Deoxyribonucleic acid |
| **DNB** | Dinitrobenzamides |
| **DNPT** | 3,5-Dinitrophenyl 1,2,4-triazoles |
| **DOT** | Directly observed treatment |
| **DPA** | Decaprenyl-phospho-arabinose |
| **DPG** | Diphosphatidylglycerol |
| **DPR** | Decaprenyl-phospho-ribose |
| **DprE1** | Decaprenylphosphoryl-β-$_D$-ribose oxidase |
| **DprE2** | Decaprenylphosphoryl-$_D$-2-keto erythro pentose reductase |
| **DPX** | Decaprenyl-phospho-2'-keto-$_D$-arabinose |
| **DS** | Drug-susceptible (*Chapter 1*) or down-sampling dataset (*Chapter 3*) |
| **DS-TB** | Drug-susceptible tuberculosis |
| **$ED_{99}$** | Effective dose that reduced bacterial burden by 99% |
| **EDC** | *N'*-ethylcarbodiimide hydrochloride |
| **EMB** | Ethambutol |
| **ESAT-6** | Early secreted antigenic target of 6 kDa |
| **ESX-1** | ESAT-6 secretion system-1 |
| **$Et_2O$** | Diethyl ether |
| **EtOAc** | Ethyl acetate |
| **dq** | Doublet of quartets |

| | |
|---|---|
| **dt** | Doublet of triplets |
| **ECFP** | Extended-connectivity fingerprint |
| **EDC·HCl** | 1-ethyl-3-(3-(dimethylamino)-propyl)carbodiimide hydrochloride |
| **eRo5** | Extended Ro5 |
| **eq.** | Equivalent |
| **ESI** | Electrospray ionization |
| **Eto** | Ethionamide |
| **EWG** | Electron-withdrawing group |
| **EWH** | Electrophilic warhead |
| **Exp** | Experimental |
| **FAD** | Flavin adenine dinucleotide |
| **FCFP** | Functional-class fingerprints |
| **FDA** | Food and Drug Administration |
| **FInd** | Flexibility index |
| **Fmoc** | Fluorenylmethyloxycarbonyl |
| **FN** | False negatives |
| **FP** | False positives |
| **FTIR** | Fourier-Transform Infrared |
| **GBM** | Glioblastoma multiforme |
| **GBMs** | Gradient boosting machines |
| **GFP** | Green fluorescent protein |
| **Gly** | Glycine |
| **GOLD** | Genetic Optimization for Ligand Docking |
| **GSK** | GlaxoSmithKline |
| **GT** | Golden triangle |
| **H** | High |
| **HBA** | Hydrogen bond acceptor |
| **HBC** | High burden countries |
| **HBD** | Hydrogen bond donor |
| **HepG2** | Human hepatocellular carcinoma |
| **hERG** | Human ether-a-gogo-related gene |
| **His** | Histine |
| **HIV** | Human immunodeficiency virus |
| **HLM** | Human liver microsomes |
| **HOBt** | Hydroxybenzotriazole |
| **HPA** | β-hydroxy hydroperoxide alcohols |
| **HPLC** | High performance liquid chromatography |
| **HSP** | Hydroxy silyl peroxide |
| **HSs** | Hirshfeld surfaces |
| **HTS** | High throughput screening |
| **Hu PPB** | Human PPB |
| **HYD** | Hydantoin |
| **IC** | Indole-2-carboxamide |
| **$IC_{50}$** | Half maximal (50%) inhibitory concentration of a substance |

| | |
|---|---|
| **IGRAs** | Interferon-γ release assay |
| **Ile** | Isoleucine |
| **INH** | Isoniazid |
| **Ipm-Cln** | Imipenem–cilastatin |
| **IR** | Inhibition rate (*Chapter 3*) or Infrared (*Chapter 5*) |
| **iv or IV** | Intravenous |
| **KasA** | β-ketoacyl ACP synthase |
| **KNN** | K-nearest neighbours |
| **LA** | Lewis acid |
| **LAM** | Lipoarabinomannan |
| **LE** | Ligand efficiency |
| **Leu** | Leucine |
| **Lfx** | Levofloxacin |
| **LLE** | Ligand lipophilicity efficiency |
| **LM** | Lipomannan |
| **LogS** | Intrinsic aqueous solubility |
| **LTBI** | Latent tuberculosis infection |
| **Lys** | Lysine |
| **Lzd** | Linezolid |
| **M** | Medium |
| **MABA** | Microplate alamar blue assay |
| **MACCS** | Molecular access System keys |
| **MAs** | Mycolic acids |
| **MBC** | Minimum bactericidal concentration |
| **MCC** | Matthews correlation coefficient |
| **MCZ** | Macozinone |
| **Md** | Median |
| **MDR** | Multidrug-resistant |
| **Mfx** | Moxifloxacin |
| **MIC** | Minimum inhibitory concentration |
| **$MIC_{50}$** | Lowest drug concentration that inhibits growth of more than 50% of a bacterial population |
| **$MIC_{99}$** | Lowest drug concentration that inhibits growth of more than 99% of a bacterial population |
| **ML** | Machine learning |
| **MLM** | Mouse liver microsomes |
| **MoA** | Mechanism of action |
| **MIM** | Mycobacterial inner membrane |
| **MmpL3** | Transporter mycobacterial membrane protein large 3 |
| **Mn** | Mean |
| **MOM** | Specialized mycobacterial outer membrane |
| **MP** | Morpholine-pyrimidine |
| **Mpm** | Meropenem |
| **MsCl** | Mesyl chloride |

| | |
|---|---|
| ***Mtb*** | *Mycobacterium tuberculosis* |
| **MW** | Molecular weight |
| **MXF** | Moxifloxacin |
| **NAct** | Not active |
| **NAHPC** | *N*-alkyl-5-hydroxypyrimidinone carboxamides |
| **NBTO** | Nitrobenzothiazole |
| **NC BTZ** | Non-covalent benzothiazinone |
| **NCov** | Non-covalent |
| **NHMS** | *N*-(4-hydroxy-3-mercaptonaphthalenyl) sulfonamide |
| **NIAID** | National Institute of Allergy and Infectious Diseases |
| **NMR** | Nuclear magnetic resonance |
| **NO** | Nitric oxide |
| **NQs** | Nitroquinoxalines |
| **NRP** | Nonreplicating persistence |
| **NTZs** | 3-nitro-1,2,4-triazoles |
| **ORTEP** | Oak ridge thermal-ellipsoid plot |
| **OS** | Original sample dataset |
| **P** | Precision |
| **PAINS** | Pan Assay Interference compounds |
| **PAMPA** | Parallel artificial membrane permeability assay |
| **$P_{app}$** | Apparent permeability |
| **PAS** | *P*-aminosalicylic acid |
| **PBTZ** | 2-Piperazino-benzothiazinone |
| **PC** | Physicochemical |
| **PCC** | Pyridinium chlorochromate |
| **PCR** | Polymerase chain reaction |
| **PDB** | Protein data bank |
| **PDE6** | Phosphodiesterase 6 |
| **PE** | Phosphatidylethanolamine |
| **PFI** | Property Forecast Index score |
| **PG** | Peptidoglycan |
| **P-gp** | P-glycoprotein |
| **Ph** | Phenyl |
| **Phe** | Phenylalanine |
| **PIMs** | Phosphatidyl-myo-inositol mannosides |
| **PK** | Pharmacokinetics |
| **PMF** | Proton motive force |
| **po** | Oral administration |
| **PP** | Pyrazolopyridones |
| **PPB** | Plasma protein binding |
| **Pred** | Predicted |
| **PTD** | Pyrrolothiadiazole |
| **Pto** | Prothionamide |
| **PYR** | Pyrazinamide |

| | |
|---|---|
| **q** | Quartet (spectral) |
| **Q** | Accuracy |
| **QSAR** | Quantitative structure–activity relationship |
| **$R^2$** | Squared Correlation Coefficient |
| **RBF** | Radial basis functions |
| **RIF** | Rifampicin |
| **RF** | Random forest |
| **RMSD** | Root Mean Square Deviation |
| **RNA** | Ribonucleic acid |
| **RND** | Resistance-nodulation-cell |
| **Ro5** | Rule of 5 |
| **ROTBS** | Number of rotatable bonds |
| **rt** | Room temperature |
| **s** | Singlet (spectral) |
| **S** | Streptomycin |
| **SA** | Structural alerts |
| **SAR** | Structure-activity relationship |
| **SD** | Standard deviation |
| **SE** | Sensitivity |
| **SI** | Selectivity index |
| **SP** | Specificity |
| **SSA** | Silica sulfuric acid |
| **SVM** | Support vector machine |
| **t** | Triplet (spectral) |
| **$t_{1/2}$** | Half-life |
| **TAG** | Triacylglycerol |
| **TAMRA** | Carboxytetramethylrhodamine |
| **TEA** | Triethylamine |
| **TB** | Tuberculosis |
| **TC** | Tanimoto coefficient |
| **TCS** | Two-component regulatory system |
| **td** | Triplet of doublets (spectral) |
| **TDM** | Trehalose dimycolate |
| **TFA** | Trifluoroacetic acid |
| **thd** | 2,2,6,6-tetramethyl-3,5-heptanedionate |
| **THF** | Tetrahydrofuran |
| **TLC** | Thin layer chromatography |
| **TM** | Transmembrane helices |
| **$T_{max}$** | Time of maximal plasma concentration |
| **TMM** | Trehalose monomycolate |
| **TMS** | Tetramethylsilane |
| **TN** | True negatives |
| **TNF** | Tumour necrosis factor |
| **TP** | True positives |

| | |
|---|---|
| **TPA** | Thiophene-arylamide compounds |
| **TPSA** | Topological polar surface area |
| **Trd** | Terizidone |
| **Trp** | Tryptophan |
| **TS** | Transition state |
| **TSTs** | Tuberculin skin tests |
| **Tyr** | Tyrosine |
| **US** | Up-sampling dataset |
| **Val** | Valine |
| **WHA** | World Health Assembly |
| **WHO** | World Health Organization |
| **XDR** | Extensively drug-resistant |
| **XGB** | Extreme gradient boosting |

# *General organization of the thesis*

*Mycobacterium tuberculosis* (*Mtb*) is the world's second leading cause of death from infectious diseases (after COVID-19). The ability of *Mtb* to enter the nonreplicating persistence (NRP) and then transition to latent TB contributes to *Mtb*'s drug tolerance and treatment failure in chronically infected individuals. Considering this, developing novel, effective, and safe chemotherapeutic drugs for tuberculosis treatment remains a key priority.

This PhD thesis includes six chapters:

**Chapter 1** introduces tuberculosis's epidemiology, symptoms, diagnosis, and pathology. The licensed vaccine, potential candidates, and approved drugs for TB treatment were also addressed concisely, along with a discussion of the limitations of TB therapy and the concerns of TB resistance associated with these regimens approved by WHO. TB discovery initiatives have uncovered several novel protein targets, such as the transporter mycobacterial membrane protein large 3 (MmpL3) and the flavoenzyme decaprenylphosphoryl-β-$_D$-ribose 2′-epimerase (DprE1). These are two prominent targets for which several inhibitors have been identified through hit discovery, preclinical investigations, and clinical trials. Finally, the function and structure of DosS, DosT, and DosR were examined concerning the role of DosRST signalling in *Mtb* latency.

**Chapter 2** presents the synthetic approaches and reaction conditions followed during the preparation of our series of trioxane hybrids. Two separate anti-TB classes were selected by combining peroxide-containing moieties with the indole-2-carboxamide scaffold (MmpL3 inhibitors) and the benzothiazinone scaffold (DprE1 inhibitors), choosing the 1,2,4-trioxane core for this research. This chapter also provides the results of a detailed structural investigation of representative compounds to understand better their chemical reactivity and properties, including biological activity. It presents the results of *in vitro* activity tests of the synthesized compounds against replicant *M. tuberculosis*. In parallel, this section describes and explores studies for lipophilicity/solubility evaluation and docking simulations.

**Chapter 3** depicts a computational analysis of the physicochemical and ADMET properties of DprE1 inhibitors and the development of machine learning classification models for identifying potential DprE1 inhibitors.

**Chapter 4** describes a novel protocol for preparing non-symmetrical 1,2,4,5-tetraoxanes and 1,2,4-trioxanes promoted by the heterogeneous Silica Sulfuric Acid (SSA) catalyst. Different ketones react under mild conditions with *gem*-dihydroperoxides or

peroxysilyl alcohols/β-hydroperoxy alcohols to generate the corresponding endoperoxides in good yields. Our mechanistic proposal, assisted by molecular orbital calculations, at the ωB97XD/def2-TZVPP/PCM(DCM)//B3LYP/6-31G(d) level of theory, enhances the role of SSA in the cyclocondensation step. This novel procedure differs from previously reported methods by using readily available and inexpensive reagents with recyclable properties, establishing a valid alternative approach for synthesising new biologically active endoperoxides.

**Chapter 5** presents a general overview of the results obtained from our investigations on the structure of endoperoxides with moieties 1,2,4,5-tetraoxane and 1,2,4-trioxolane. By combining X-ray crystallography and vibrational spectroscopy, along with Hirshfeld surface analysis and calculations (CE-B3LYP/6-31G(d,p)) of pairwise interaction energies of intermolecular contacts existing in the crystal structure, it allowed us to deepen the understanding of the relative reactivity and the properties of these endoperoxide classes.

**Chapter 6** provides an overview of the work completed throughout this PhD project, alongside the conclusions and some perspectives for future work.

# Chapter 1

## Overview of Tuberculosis and emergent MmpL3, DprE1, and DosRST Inhibitors

## 1.1. Tuberculosis – background

Tuberculosis (TB) is an airborne illness caused by a single infectious agent, *Mycobacterium tuberculosis* (*Mtb*), one of the world's top ten infectious killers.[1] TB is a well-known infectious bacterial illness that has tormented humanity for millennia. Although reports date the earliest evidence of infection to 9000-year-old human remains,[2] and archaeological discoveries on mummies in ancient Egypt as early as 1500 BC,[3,4] the etiological agent was not discovered until the late 19$^{th}$ century.[5,6] The 19$^{th}$ century saw substantial advances in our understanding of illness pathogenesis. Eventually, in 1882, Robert Koch discovered the tubercle bacillus, which allowed the disease to be accurately called tuberculosis.[7,8]

*Mtb* is predicted to infect around 2 billion people, mainly in the latent form, with a risk of individuals contracting the disease's most aggressive form (generally 5-10% of the cases, predominantly among those with comorbidities such as diabetes or AIDS).[1] Even though tuberculosis is normally treatable, the rise of drug-resistant strains, combined with the continual increase in infection rates in Africa and Asia's poorest regions, prompted the World Health Organization (WHO) to proclaim tuberculosis as a global health emergency in 1993.[9] Worldwide, 10.6 million new cases of TB were reported in 2021, with men accounting for 54% of this total, 32% in adult women, and 14% in children, among HIV-negative people. For the HIV-positive people, 51% were in men, 38% were in women, and 11% were in children.[1] Moreover, the spread of multidrug-resistant (MDR) and extensively drug-resistant (XDR) tuberculosis, and the simultaneous pandemic of HIV-TB co-infection, together with a deficient healthcare infrastructure and the lack of an effective vaccine, all contribute to the disease's endurance.[10,11]

## 1.2. Epidemiology

About a quarter of the world's population is infected with *M. tuberculosis*, although the prevalence of the disease is not homogenous. Only 30 countries account for 86–90% of cases (**Figure 1.1**).[1] The list of "high burden countries" (HBC) comprises essentially countries from sub-Saharan Africa, south-east Asia, and Western Pacific.[1] The most affected regions are primarily connected with a poor economy, a low quality of life, and frequently lack access to medical care, all of which significantly restrict the attempts to control efficiently the disease. Simultaneously, the TB burden in the poorest regions – particularly in Africa – correlates significantly with HIV infection prevalence.[12,13] In

2021, over 1.4 million HIV-negative, together with 187,000 HIV-positive individuals, died of TB.[1] HIV-TB co-infection has been shown to be a substantial risk factor leading to the progression of the disease.[14] The proportion of tuberculosis cases co-infected with HIV was highest in WHO African Region countries, reaching 50% in areas of southern Africa.[1]

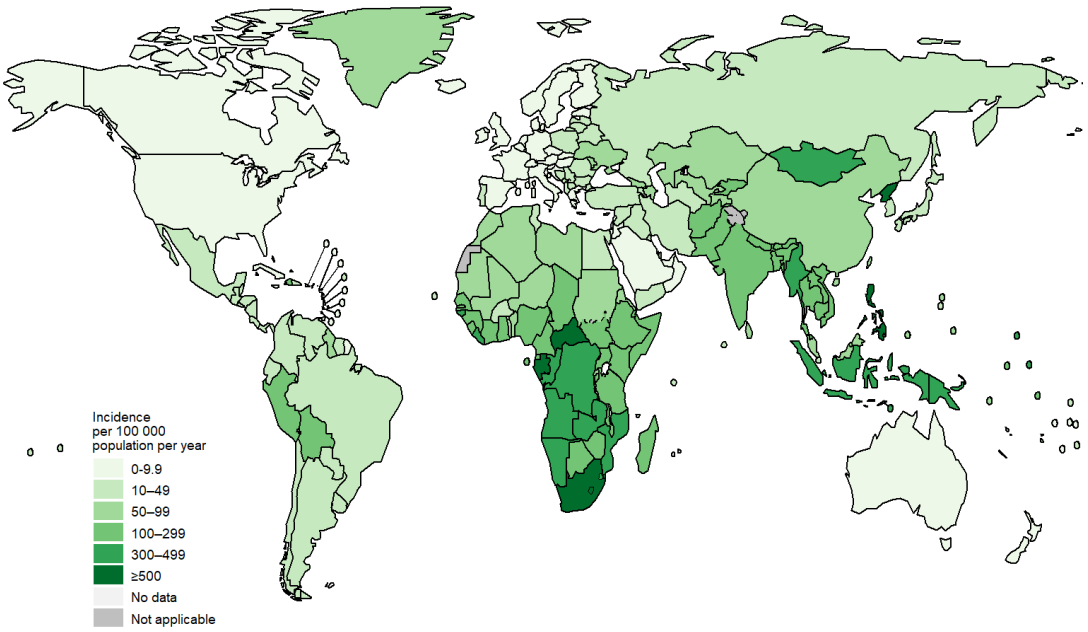


**Figure 1.1.** Estimated TB incidence rates in 2021. Source from WHO.[15]

Over the last century, public health initiatives combined with the introduction of several chemotherapeutic drugs have resulted in a sharp decline in the incidence and mortality rates of disease in the western world, also demonstrating comparable results in countries with a more considerable tuberculosis burden. Unfortunately, the rapid proliferation of drug-resistant *Mycobacterium* strains has significantly hindered efforts to eradicate the illness. The first examples of drug resistance date back to streptomycin's initial clinical trials, prompting the development of combination drugs required for effective therapy.[16]

Nonetheless, decades of ineffective antibiotic delivery resulted in the onset of mycobacteria resistance to not one but numerous antitubercular drugs. With the rise of multidrug-resistant tuberculosis (MDR-TB), extensively drug-resistant tuberculosis (XDR-TB) and, more recently, the identified strains classified as totally drug-resistant

tuberculosis (TDR-TB),[17,18] the inevitability need for increased drug-discovery efforts and global initiatives to control and stop the spread of TB became imperative.

As such, the World Health Assembly (WHA) issued a resolution in 2014 establishing a global program called 'Ending the TB epidemic'.[19] The program's ultimate goal is to reduce worldwide infection rates by 90% and mortality rates by 95%, till 2035.[20] The policy will require additional funding and commitment from governments to facilitate access to health care and to improve people's quality of life, particularly in regions with a high prevalence of disease and a poor economic status. Simultaneously, the initiative anticipates greater financing to develop innovative antitubercular vaccines and drugs.[1,21]

## 1.3. The spectrum of tuberculosis infection and disease

Although mainly a respiratory pathogen, *M. tuberculosis* can cause systemic infection and TB ranges from asymptomatic infection to life-threatening illness.[22,23] In terms of clinical and public health, TB patients can be defined as having latent TB infection (LTBI), non-transmissible and asymptomatic, or active TB disease, which is transmissible and can be diagnosed by culture-based or molecular methods.

The spectrum of TB infection is illustrated in **Figure 1.2**, showing that exposure *to Mtb* can result in two outcomes: the pathogen is either eliminated or persists. In the first scenario, the pathogen is eradicated either by innate immune responses (in which tuberculin skin tests (TSTs) or interferon-γ release assays (IGRAs) may be negative) or by adaptive immune responses (in which TSTs and IGRAs can be positive or negative).[22,23] Nevertheless, in case *Mtb* infection is not totally eradicated, the mycobacteria might remain dormant (LTBI), and the infected person will frequently get positive TST and IGRA results, and be asymptomatic. However, a positive TST or IGRA test does not always imply LTBI, as individuals who have successfully eradicated the infection may still have a positive TST or IGRA due to memory T cell responses.[22,23] These outcomes help to explain why TSTs and IGRAs have a low predictive (prognostic) value.[24]

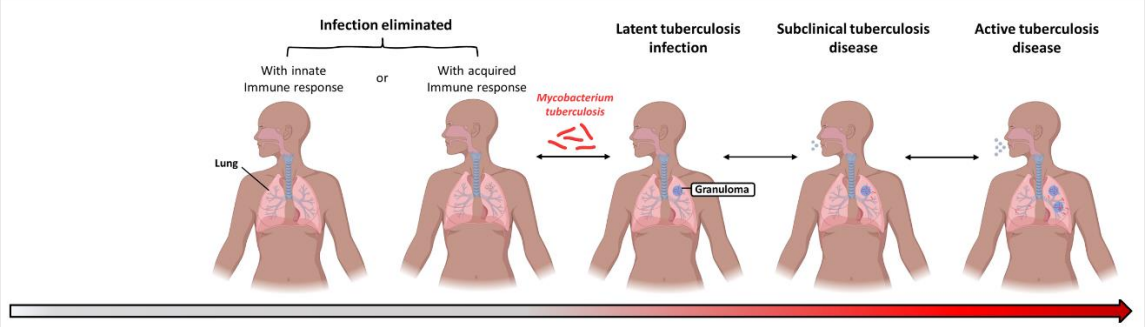


| | | | | | |
|---|---|---|---|---|---|
| TST | - | + | + | + | Usually positive |
| IGRA | - | + | + | + | Usually positive |
| Culture | - | - | - | Intermittently positive | + |
| Sputum smear | - | - | - | Usually positive | Positive or negative |
| Infectious | No | No | No | Sporadically | Yes |
| Symptoms | None | None | None | Mild or none | Mild to severe |

**Figure 1.2.** The spectrum of tuberculosis infection and disease— from infection to active (pulmonary) disease. Adapted from Furin *et al.*[25] and Pai *et al.*[26]

### 1.3.1. Symptoms

Active TB is characterized by persistent cough, unexplained weight loss, fever, and, if severe, night sweats and bloody coughing. Active pulmonary tuberculosis is contagious, and in the early stages of the disease, active TB may be asymptomatic in around 25% of cases.[27] Extrapulmonary TB may present more complicated symptoms, depending on the organ systems affected.[28]

### 1.3.2. Diagnosis

The diversity of TB symptoms makes diagnosis difficult. Therefore, *Mtb* must be found in a biological sample before a definitive diagnosis of tuberculosis is issued. TB TST or TB blood tests are employed to identify *Mtb* in the body. Their positive result merely indicates that a person has been infected with the mycobacteria; it does not indicate if the individual has LTBI or has developed TB illness. Therefore, further tests (such as a chest X-ray and sputum sample) are required to diagnose TB.[29,30]

In many countries with a high incidence of tuberculosis, sputum-smear microscopy is the principal diagnostic tool for examining individuals with tuberculosis symptoms. However, this approach has several drawbacks, including poor sensitivity and the inability to differentiate between drug-susceptible and drug-resistant TB strains. The current gold standard for bacteriological confirmation of tuberculosis is culture using a commercially available liquid medium. Yet, due to high cost, biosafety constraints, and lengthy result-generating time, it is rarely employed as a primary diagnostic test in most

countries with a high TB prevalence.[31–34]

## 1.4. Tuberculosis Infection Cycle

TB is an airborne disease spread through respiratory fluid droplets of individuals with active TB. *Mtb* has a limited ability to survive outside a human host and has no other known animal reservoir; hence *Mtb* relies on humans with latent infections as a critical biological reservoir.[35]

*Mtb* enters the body *via* the respiratory system; after inhalation, it is translocated to the lower respiratory tract, infecting alveolar macrophages, the mycobacteria's primary target cell type.[26,36] These cells absorb the mycobacteria by receptor-mediated phagocytosis, a process that is facilitated by a broad range of receptors.[26,37] After internalization, *Mtb* actively blocks phagosome fusion with the lysosome (phagosome-lysosome fusion), to ensure its survival.[38] *M. tuberculosis* can then breach the phagosomal membrane *via* the early secreted antigenic target of 6 kDa (ESAT-6) secretion system-1 (ESX-1), releasing bacterial products into the macrophage cytosol, including mycobacterial DNA.[39,40]

Subsequently, mycobacteria can obtain access to the lung interstitium through two possible mechanisms: *Mtb* infection of epithelial cells and transmigration of *Mtb*-infected macrophages across the epithelium, where the infection process evolves. Monocytes and dendritic cells travel synchronously to lymph nodes, where T-cell priming can take place. Consequently, lymphocytes T-cells and B-cells initiate a multicellular host reaction, also known as a granuloma, at the site of the infection. The granuloma formation is vital to control a chronic infection. It comprises mainly of the recruitment at the infectious stage of macrophages, highly differentiated cells such as epithelioid, Foam, and multinucleated giant cells, containing the infection from the surrounding tissues with layers by T-cells and B-cells. While granuloma initially restricts the infection, certain mycobacteria can persist within these structures for lengthy periods in a dormant state.[41–44] These granulomas consist of neutrophils, lymphocytes, and other immune cells and become covered in calcified fibrotic components;[26] in 95% of cases, transmission leads to a latent infection that presents no symptoms. While latent TB is most frequently associated with lung granulomas, *in situ* polymerase chain reaction (PCR) studies have identified latent *Mtb* in adipose tissues surrounding several organs other than the lungs.[45] Although the disease remains asymptomatic in most infected people, the granulomas may occasionally

be unable to stop the spread of bacteria. The bacteria reproduce within the granuloma as it grows. If the mycobacterial load is too high, the granuloma will not be able to control the infection, and the mycobacteria will eventually spread to other organs (brain included). At this stage, the mycobacteria can reach the bloodstream or re-enter the respiratory system to be discharged; the infected host now has an active, highly contagious TB infection and is symptomatic. The mechanisms of progression are not fully understood. A significant risk factor has been found as compromised immune system function in the host, such as HIV co-infection. Necrosis of the granuloma and development of the so-called caseum are caused by an insufficient supply of nutrients and oxygen to the centre of a granuloma.[46] Ultimately, liquefaction of the granuloma occurs, releasing the content and enabling disease progression into the clinical stage. The release of infected necrotic tissue into the lung alveoli is characterized by a chronic cough, a hallmark sign of pulmonary TB. The infected human is highly contagious, and the aerosolized germs may infect a second host. In addition, the discharged germs may enter the bloodstream and spread to other organs, where they might cause the extrapulmonary form of the disease to develop.[47]

In healthy individuals, contact with *Mtb*-containing aerosol is only likely to cause infection in 5% of cases where an active infection is acquired directly, or the latent infection becomes reactivated. The reactivation rate is much higher for immunocompromised individuals, such as those positive for HIV. Active TB occurs mainly in the pulmonary form, mainly affecting the lungs, while extrapulmonary TB contributes to 15% of all cases. The most common forms of extrapulmonary TB are lymphatic, pleural, and disseminated TB.[45]

## 1.5. Mycobacterial cell envelope

All mycobacterial species are distinguished by their cell envelope. The structure representation of the cell envelope of *Mycobacterium tuberculosis* is illustrated in **Figure 1.3.** *Mtb* has a distinctive cell envelope, contributing to its success as the most successful pathogen of our time. *Mtb*'s unique cell membrane is particularly rich in lipids, making it waxy and robust,[48] which confers in the mycobacteria, resistance, a hydrophobic barrier to antibiotics,[49] and its key virulence properties.[50–52] Given these features and the fact that many drugs for tuberculosis inhibit the transport or synthesis of complex lipids, a better

knowledge of *Mtb*'s lipid structures and synthesis is a major focus of current research, with the potential for the development of novel drug targets. Mycobacteria's envelope is suggested to have a dual membrane structure: a specialized mycobacterial outer membrane (MOM) composed of an inner layer of mycolic acids (MAs) and an outer layer of free lipids.[53–56] Mycolic acids are long-chained (70-90 carbons) $\alpha$-alkyl, $\beta$-hydroxy fatty acids, representing 40-60% of the cell's dry weight.[57–59] Even though the free lipids are not linked to the envelope and can be removed, the MA layer is covalently bonded to the polysaccharide cell wall,[53,60] which is not observed in Gram-negative bacteria. This linkage is a component of the mycoloylarabinogalactan–peptidoglycan complex (mAGP), containing branched arabinose domains esterified on the outer surface with MAs and linked to the peptidoglycan (PG) through the arabinogalactan (AG) galactan helices.[61–63] Due to the large size of the periplasmic space of *Mtb*, enzymatic reactions can occur, and the material can be processed and transported to the MOM.[55,64,65] Initially, it was believed that the inner membrane of *Mtb* was a conventional bacterial membrane; however, lipid studies have demonstrated that the phospholipid composition is primarily phosphatidyl-myo-inositol mannosides (PIMs). $PIM_2$ (two mannose sugars on the inositol moiety) appears to be present primarily in the inner layer of the inner membrane, whereas $PIM_6$ (with six mannose residues) is believed to fill the outer leaflet.[66] The strong packing of these chains results in a membrane that is more stable, less fluid, and less permeable to drugs, denominated as the mycobacterial inner membrane (MIM).[56,67] The lipoglycans lipoarabinomannan (LAM) and lipomannan (LM), which are most likely extend from the MIM into the periplasm, both contain lipid anchors based on PIMs. The phospholipids as diphosphatidylglycerol (DPG) and phosphatidylethanolamine (PE) are also found in the outer leaflet.[57,68–70]

For *Mtb* to maintain its virulence and intracellular survival, the integrity of the mycobacterial cell envelope is crucial. Understanding its biosynthesis and structure is essential in the search for novel drugs to halt the ever-increasing rise of resistance.[57,68–70] Due to its limited drug permeability, this efficient barrier is the one of the reasons for the intense antibiotic treatment of tuberculosis. Nevertheless, this distinctive cell wall has several unique biosynthetic pathways, including several mycobacterial-specific enzymes that serve as targets for antimycobacterial treatment. As a result, it is unsurprising that a wide range of antitubercular drugs acts as cell wall biosynthesis inhibitors.

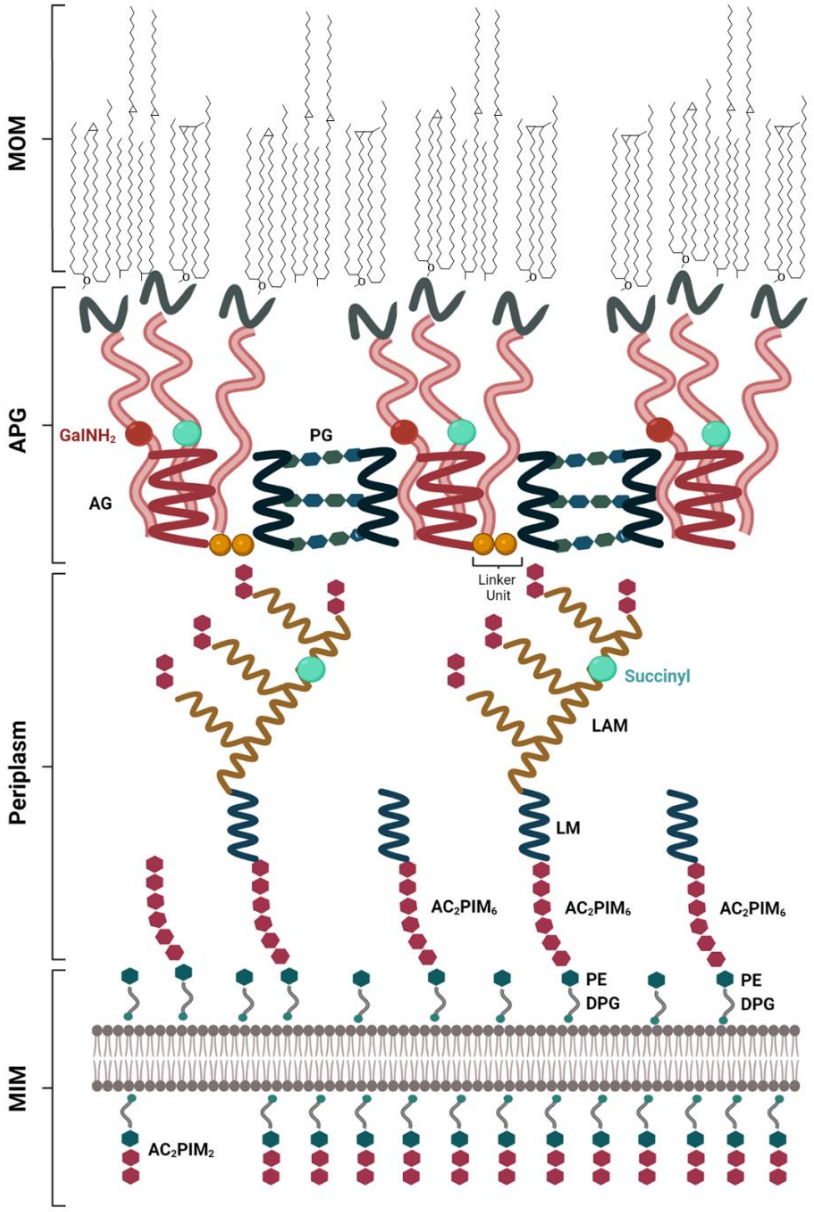


**Figure 1.3.** Schematic illustration of the cell envelope of *Mycobacterium tuberculosis*. Adapted by Batt *et at*.[71] *Please note that, due to the molecular complexity, structure representations of mycolic acids in MOM have been simplified.*

## 1.6. Prevention: TB vaccines

Human TB protection from bovine bacilli was suggested when *M. tuberculosis* was identified and distinguished from *M. bovis*.[72] However, early studies demonstrated that *M. bovis* is particularly pathogenic in humans, and infection can cause sickness. Albert Calmette and Camille Guérin discovered a less virulent bovine pathogen in 1908.[73] After 13 years of subculturing, researchers found a less virulent strain that could not cause the development of the disease in animal studies.[74] The first human Bacillus Calmette-

Guérin (BCG) vaccine was administered in 1921, and it is still the only clinically authorized tuberculosis vaccine.[75]

Despite a century of global use and intense research, the disease-protective efficacy is still unpredictable.[75] Overall analysis indicates that protection should extend for 10-15 years following immunization,[76] in which antigen reactivity has been observed to diminish significantly within the first years in some individuals while being persistent for more than 40 years in others.[77] Nevertheless, additional factors were indicated to be significant, including disease dissemination within the population, pre-exposure to non-tuberculous mycobacteria in the environment,[78] and even the BCG vaccine strain employed.[79] While BCG's efficacy in adults is mainly unpredictable, it has been found to provide a strong protective immunity in new-borns, notably against disseminated TB and tuberculosis meningitis.[80] According to previous research, earlier exposure to mycobacteria may prime the immune system, resulting in a faster reaction to bovine bacilli administration and reducing the expected stimulatory impact.[78,81] These findings encourage ongoing neonatal administration, especially in disease-prone areas.[82] Conversely, live bacilli in BCG might cause infection, especially in immunocompromised patients. The vaccine is no longer recommended for HIV-infected new-borns.[83] Thus, widely administered in most of the 20$^{th}$ century, many first-world countries have stopped routine administration of the BCG vaccine due to the low risk of contracting TB within these countries. The exception to this is in infants who are at high risk for TB.[84]

The need for new vaccines is evident considering the lack of predictable efficacy of the BCG vaccine; the poor expected benefit in adults, especially those pre-exposed to mycobacteria, and the higher risk of side effects in HIV-positive individuals. Yet, no new antitubercular vaccines have entered the market in the last century.[85]

There are currently several novel TB vaccines that achieve a less variable immune response in adult populations. MVA85A, based on a virus modified to produce the mycobacterial antigen Ag85A, was the first novel agent to reach human effectiveness trials since 1921.[86] Several months after the initial inoculation, the vaccine was administered to improve the efficacy of BCG. However, although effective in animal models, MVA85A failed to demonstrate clinical success.[87] Following the development of MVA85A, new candidates based on different vaccine technologies and formulation strategies started filling the antitubercular vaccine pipeline. As of 2022, there are 16 vaccine candidates in the pipeline at multiple phases I, II, and III of clinical development.[82,88] The most effective to date is M72/AS01$_E$, an adjuvant vaccine

developed by GlaxoSmithKline (GSK) in association with Aeras containing of a fusion protein of two mycobacterial antigens, Rv1196 and Rv0125.[1,89] M72/AS01$_E$ is the first vaccine that could provide efficacy against clinical disease, showing 54% protection against progression to pulmonary tuberculosis in *Mtb*-infected patients in Kenya.[90,91] The immunogenicity analysis at the completion of the three-year follow-up period revealed that M72/AS01$_E$ induced an immune response and protected against progression to pulmonary tuberculosis for at least three years.[90,91] The vaccine has been licensed by Bill & Melinda Gates Medical Research Institute for further development after completing Phase IIb clinical trials.[92,93]

## 1.7. Tuberculosis treatment

Since 1943, when streptomycin was discovered from *Streptomyces griseus*, several more anti-TB drugs have been found. The tuberculosis persistence and its ability to resistance have led to stricter treatment requirements.[94–97] Currently, treating TB needs drugs to be administered under the observation of a healthcare professional to guarantee that the entire course of treatment is completed. This practice is referred to as community- or home-based directly observed treatment (DOT) and is the recommended form of administration by the WHO.[98]

These medications have downsides, including long treatments, unwanted side effects, drug interactions, poor patient compliance, and drug resistance conferred by *Mycobacterium* mutations.[99,100] Searching for better medications and therapy regimens is crucial in maintaining disease control.[101,102]

### 1.7.1. First-line treatment for drug-susceptible tuberculosis

There have been no notable changes in drug-susceptible tuberculosis (DS-TB) treatment since the 1970s.[103–105] Typically, new TB patients have unknown drug susceptibility at therapy initiation. Unless there is a risk of drug-resistant disease is identified, a DS antituberculosis regimen is initiated.[106] The structure representations of the first-line drugs recommended by the current WHO guidelines for DS tuberculosis treatment are shown in **Figure 1.4.** This regimen comprises four first-line drugs: isoniazid (INH, H), pyrazinamide (PZA, Z), ethambutol (EMB, E), and rifampicin (RIF, R), for the primary treatment course.[98,104] For TB patients who did not finish, or relapsed from their first treatment course, the retreatment regimen includes the four first-line drugs HRZE

and streptomycin (S), a second-line TB medicine.[11,107–109] Since the earliest research, it has been noted that introducing any single antibiotic results in fast emergence of resistance. Data from clinical trials demonstrated that monotherapy with INH resulted in resistance, whereas combination therapy with streptomycin or *para*-aminosalicylic acid (PAS) inhibited resistance development.[16,110] These discoveries resulted in the development of multi-drug therapy using a combination of antibiotics. Until the early 1970s, the average period of antituberculosis treatment was eighteen months or longer. With the addition of rifampicin in the antibiotic therapy, the length of therapy was reduced to nine months. In the 1980s, the substitution of PZA for streptomycin resulted in the six-month short-course oral therapy regimen.[110,111]

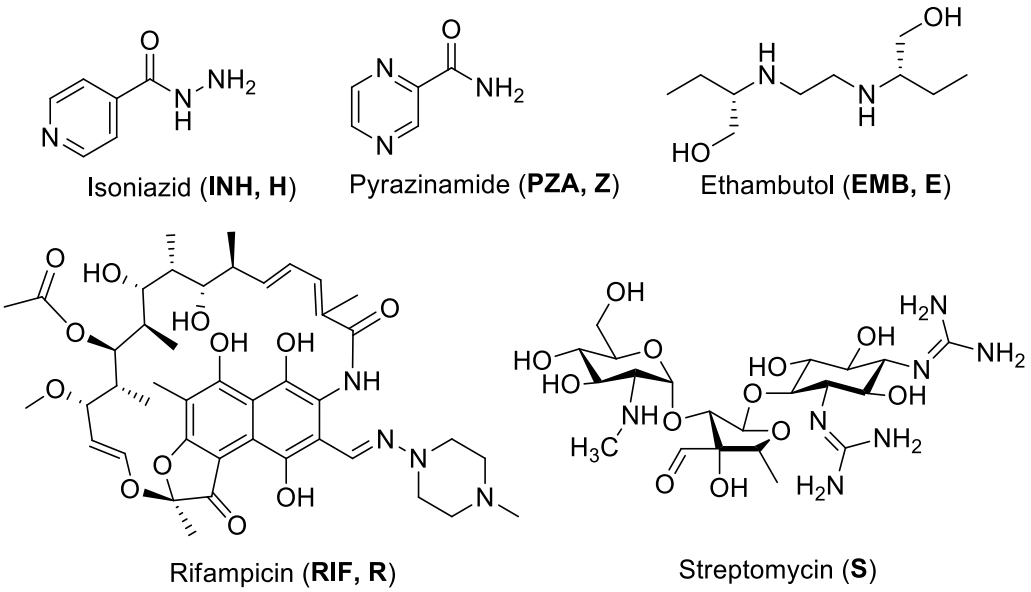


**Figure 1.4.** Structure representations of the molecules approved for the treatment of DS-TB.

As depicted in **Table 1.1**, treatment of drug-sensitive TB involves a DOT short course comprising a two-month intensive phase of treatment with INH, RIF, PZA, EMB (2HRZE), and a four-month continuation phase with RIF and INH (4RH). The first intensive phase consists of a once-daily four-drug therapy for two months, enabling rapid bacillary load reduction as the treatment eliminates effectively growing bacteria.[112] Four further months of two-drug therapy constitute the continuation phase.[113,114] This four-drug regimen achieves up to 95% cure rates for DS-TB in six months when administered under DOT.[11,45,115] It is currently implemented for pulmonary and most forms of extrapulmonary tuberculosis.[11,16,98,116]

For TB patients returning after relapsing or defaulting from their first treatment course, they can receive the retreatment regimen consisting of an eight-month therapy

2HRZES/1HRZE/5HRE.[107]

**Table 1.1:** Treatment schemes for drug-susceptible TB, recommended by WHO.

| | Type | Duration | Combination |
|---|---|---|---|
| **Drug-susceptible TB** | First-line | 6 months | **2HRZE/4HR:**<br>2 months INH + RIF + PYR + EMB<br>4 months INH+RIF |
| **Relapse Situations Drug-susceptible TB** | First-line | 8 months | **2HRZES/1HRZE/5HRE:**<br>2 months INH + RIF + PYR + EMB + S<br>1 month INH + RIF + PYR + EMB<br>5 months INH + RIF + EMB |

Since its discovery in 1952, INH, an isonicotinic acid hydrazide, has been regarded as one of the most specific and efficient antituberculosis drugs for DS-TB.[117] First synthesized in 1912,[118] INH was substantially more potent than other modern antituberculosis drugs, with selectivity for mycobacteria and activity against streptomycin-resistant strains.[109] The mechanism of action of INH is quite complex, affecting several pathways associated with macromolecular synthesis, including mycolic acid synthesis. INH is a prodrug activated by the catalase-peroxidase hemoprotein (KatG), and the corresponding active drug inhibits beta-ketoacyl ACP synthase (KasA) and InhA, an NADH-specific enoyl-acyl carrier protein (ACP) reductase, both of which participate in fatty acid synthesis.[119–124] Consequently, this drug inhibits cell wall synthesis. Reports indicate that it has a high early bactericidal impact on actively growing *Mtb*, causing a fast drop in sputum bacilli during the first two weeks of treatment.[125] It is ineffective against the nonreplicating subpopulation of mycobacteria and in anaerobic conditions.[126] INH can be administered as a monotherapy to prevent the reactivation of latent TB infection.[121,125] Hepatotoxicity (including hepatitis development) and neurotoxicity (in particular peripheral neuropathy) are the most significant adverse reactions associated when taking INH.[125,126]

Pyrazinamide (PZA, Z) is an analogue of nicotinamide that was initially synthesized in 1936 and first used as an antimycobacterial in 1952. PZA, unlike other first-line anti-TB drugs, has efficacy against semi-dormant, nonreplicating *M. tuberculosis* persisters;[127] hence, PZA is the basis of a 6-month first-line therapy regimen

for DS-TB.[105,128] This makes pyrazinamide one of the key drugs of combination chemotherapies against drug-resistant tuberculosis, such as MDR-TB.[129] This sterilizing action is unique among TB medications. Recent preclinical studies to establish effective medication combinations with novel pharmacological candidates for shortening TB therapy, for example, revealed that PZA is the only medicine that cannot be substituted without reducing treatment effectiveness.[130–132] PZA is a prodrug that must be converted into the active pyrazinoic acid form by *Mtb* PZase/nicotinamidase (PZase).[133,134] It is generally acknowledged that pyrazinoic acid may not have a particular target but produces acidification in the cytoplasm. There are several hypotheses on the mechanism by which pyrazinoic acid induces cell death in *Mtb*, ranging from acidification of the cytoplasm to direct inhibition of cellular targets. One biological target is the translation-involved ribosomal protein S1 (RpsA), the suppression of which would limit protein synthesis.[135] Most examples of PZA resistance are due to mutations in the genes producing PZase/nicotinamidase and RpsA, which result in decreased activation or inhibition of the target.[134] Nevertheless, more recent investigations on resistance have indicated that mutations in the panD gene provide modest PZA resistance. PanD encodes an aspartate decarboxylase involved in pantothenate and coenzyme A production, an essential mechanism for *Mtb* survival; this may provide an alternate target for PZA.[136] Other processes observed following PZA administration include disruption of important cellular functions through inhibition of essential enzymes, of membrane transport, or protein and RNA production.[128,137,138] PZA can induce hypersensitivity reactions (pruritis, urticaria, and skin rashes), liver damage, and gastrointestinal issues.[139]

Ethambutol, discovered in 1961, is a bacteriostatic drug active against actively growing bacteria of the genus *Mycobacterium* but devoid of activity on nonreplicating tubercle bacilli. It increases the efficacy of rifamycins, aminoglycosides, and quinolones.[140] The bacteriostatic effects of EMB are attributed to the suppression of the arabinosyltransferase enzymes EmbA, EmbB, and EmbC, with EmbB being the primary target, in which EmbA, B, and C are essential in cell-wall arabinogalactan biosynthesis.[141–144] Resistance to EMB is mainly caused by mutations in EmbB and the arabinose biosynthesis pathway.[145] The most often seen adverse effect of EMB is ocular neuropathy, which may be permanent. The occurrence of this adverse drug event is unexpected, thus therapeutic monitoring is necessary.[140,145]

Streptomycin was identified as the first aminoglycoside antibiotic. Although it is used less frequently, due to the high likelihood of resistance, it can replace amikacin,

when the latter is unavailable or there is documented resistance.[129] The most recent WHO guidelines recommend against unnecessarily exposure of DS-TB patients to streptomycin, due to its substantial toxicity.[98,146]All aminoglycosides may affect the eighth cranial nerve resulting in loss of balance, hearing loss, or both.[147] Moreover, neurotoxicity (apnea and muscle paralysis) and nephrotoxicity have been detected, together with milder side effects such as headaches, rashes, and nausea.[148,149]

Rifampicin (RIF), also known as rifampin, is a semisynthetic derivative of structurally similar natural rifamycins.[150] RIF, an antituberculosis medication with a strong sterilizing effect, was first synthesized in 1959 and brought into clinical use in 1972. By establishing a stable drug-enzyme complex, RIF inhibits bacterial DNA-dependent RNA synthesis by attaching itself to the RNA polymerase in its β-subunit, thus intervening in the RNA transcription and expression. Inhibition of bacterial transcription activity results in death of the mycobacteria.[151–154] The selectivity for bacterial over human RNA polymerase means that, compared to other RNA polymerase inhibitors, RIF is relatively safe and does not inhibit the mammalian enzyme.[154,155] Resistance to this chemotype was initially detected during the early stages of RIF development, when it was recognized that a single mutation conferred substantial levels of resistance in bacteria. The most clinically significant mutations are in the rpoB gene encoding for RNA polymerase.[156] The administration of RIF results in reduced adverse effects. It may produce some gastrointestinal distress but hepatotoxicity is minimal with RIF alone, and less frequent than with isoniazid treatment.[126,152] RIF-induced cytochrome P450 enzymes result in drug-drug interactions with several antiretroviral drugs.[116,157]

## 1.7.2. Second-line treatment for multi-drug resistance tuberculosis

Second-line antituberculosis drugs are employed when resistance to first-line therapy is manifested.

MDR-TB is defined as TB resistant to at least INH or RIF among the first-line TB drugs, prompting the employment of second and third-line anti-TB treatments with low toxicological profiles. Due to the more difficult-to-treat nature of MDR-TB, the mortality rate is roughly 40% and causes about 20% of all TB deaths. Extensively drug-resistant (XDR) displays the same antibiotic resistance observed in MDR-TB, in addition to resistance to any fluroquinolones and at least one of three injectable second-line drugs, namely kanamycin and amikacin, and bears a mortality rate of roughly 60%.[158] Totally

drug-resistant tuberculosis (TDR-TB) refers to *Mtb* clinical strains that show *in vitro* resistance to all first- and second-line drugs tested, and the fatality rate is high. The treatment of TDR-TB comprises antibiotics with limited effectiveness against *Mtb*. Therefore, the main objective of therapy is to treat the acute infection rather than to achieve a complete cure.[159,160]

Patients with MDR-TB are treated with different combinations of second-line drugs, usually for extended periods (18 months or more).[107] Well-known antibiotics, such as fluoroquinolones, linezolid, aminoglycosides, and carbapenems, have also been demonstrated to have anti-TB action, and are widely used in MDR-TB and XDR-TB treatment regimens due to their established safety and availability. Indeed, most second-line medications recommended by WHO for MDR-TB treatment were not developed for TB. Bedaquiline (Bdq) and delamanid (Dlm) are the two exceptions that gained conditional authorization from the European Medicines Agency in 2014 to treat MDR-TB. The US Food and Drug Administration (FDA) gave Bdq accelerated approval to treat tuberculosis resistance, making it the first TB drug approved by the FDA in 40 years.[107]

Following a comprehensive evaluation of the relative benefits and risks, WHO developed recommendations for each medication and categorized them into three groups:[107]

- Group A: fluoroquinolones (moxifloxacin and levofloxacin), bedaquiline, and linezolid were deemed highly efficacious and strongly suggested for inclusion in all regimens, unless otherwise noted.
- Group B: clofazimine, cycloserine or terizidone were conditionally indicated as second-choice medicines.
- Group C: includes all additional medicines employed when a regimen cannot be formulated with drugs of Group A or Group B. In Group C drugs are ranked according to the relative balance of projected benefits and risks.

The WHO guidelines of the second-line drugs for treatment of MDR-TB and XDR-TB and their structure representations are shown in **Table 1.2** and **Figure 1.5.** Bedaquiline (Bdq) and delamanid (Dlm) are the most recently approved drugs for the treatment of MDR-TB, bedaquiline in 2012 and delamanid in 2014.[161]

**Table 1.2:** Combination of medicines recommended to treat MDR-TB and XDR-TB infection, advised by WHO[107]

| Groups | Medicine | |
|---|---|---|
| **Group A:** Include all three medicines | Levofloxacin or moxifloxacin | Lfx Mfx |
| | Bedaquiline | Bdq |
| | Linezolid | Lzd |
| **Group B:** Add one or both medicines | Clofazimine | Cfz |
| | Cycloserine or terizidone | Cs Trd |
| **Group C:** Add to complete the regimen and when medicines from Groups A or B cannot be used | Ethambutol | EMB |
| | Delamanid | Dlm |
| | Pyrazinamide | PZA |
| | Imipenem–cilastatin or meropenem | Ipm-Cln Mpm |
| | Amikacin (or streptomycin) | Am (S) |
| | Ethionamide or prothionamide | Eto Pto |
| | *p*-aminosalicylic acid | PAS |

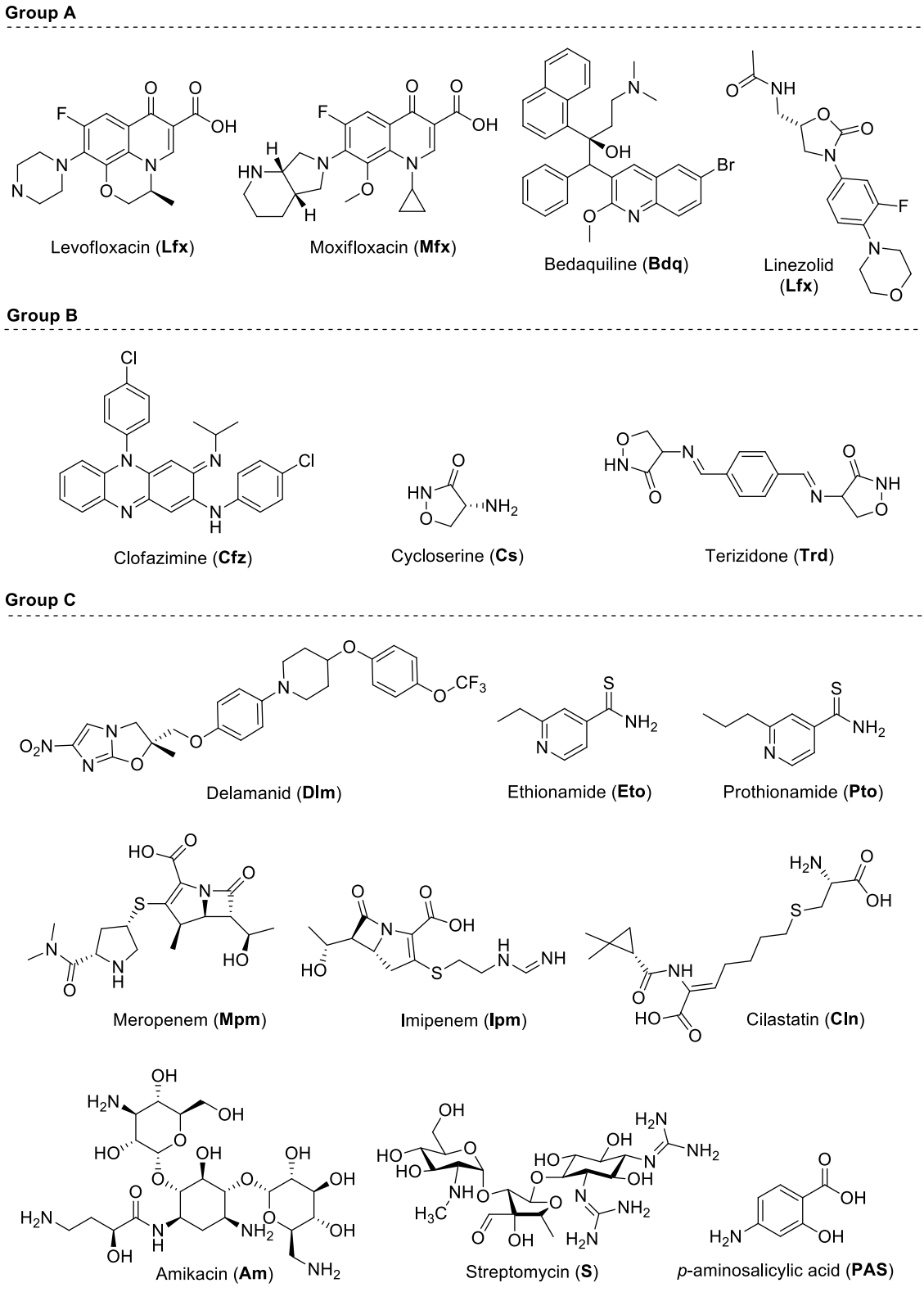


**Figure 1.5.** Structure representations of the second-line anti-TB drugs for drug-resistant tuberculosis treatment.

## 1.8. Drugs in clinical development and emerging anti-TB drug targets

There is a resurgence in demand for new TB drugs due to increased drug resistance and a 40-year shortage of approved TB drugs. Several compounds from new classes (i.e., those with new targets and/or novel modes of action) or with beneficial features have advanced in the drug development pipeline for tuberculosis treatment over the past several years.[162] The *Working Group on New TB Drugs* currently lists 32 active antituberculosis drug discovery initiatives in the discovery phase and many more in clinical development, as shown in **Figure 1.6**.[162]

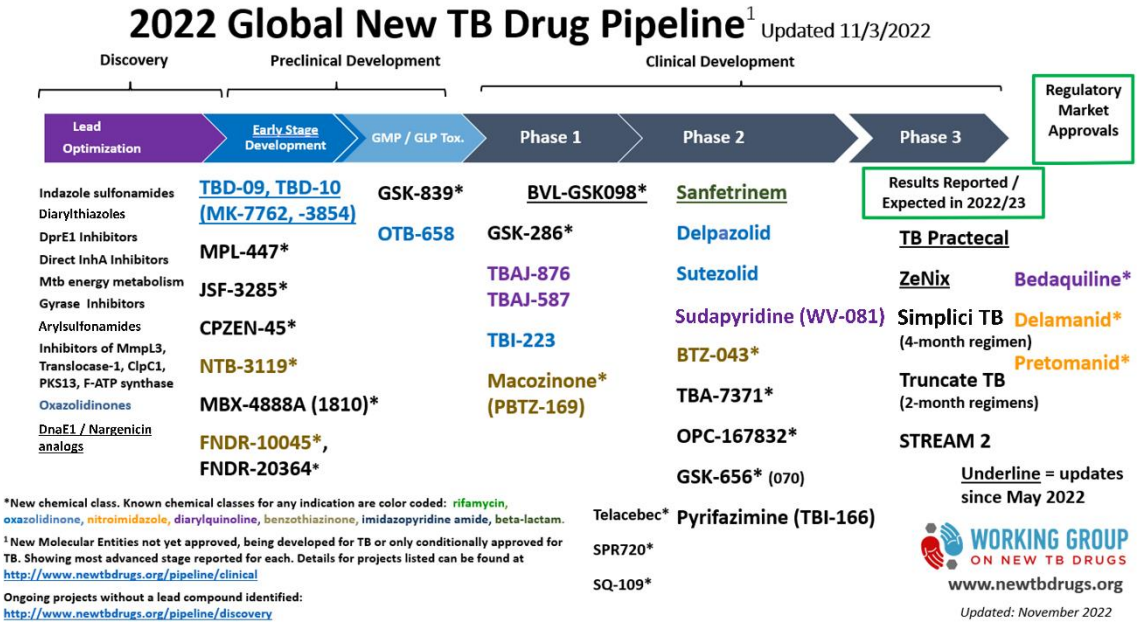


**Figure 1.6.** Novel anti-TB drugs in the pipeline. Source on *Working Group on New TB Drugs*.[163]

These discovery initiatives have uncovered several novel protein targets, such as the transporter mycobacterial membrane protein large 3 (MmpL3) and the flavoenzyme decaprenylphosphoryl-β-D-ribose 2′-epimerase (DprE1). These are two prominent targets for which several inhibitors have been identified through hit discovery, preclinical investigations, and clinical trials.[164,165]

### 1.8.1. MmpL3

MmpL3 is a membrane protein that belongs to the resistance-nodulation-cell division (RND) protein superfamily. MmpL (*M*ycobacterial *m*embrane *p*rotein *L*arge) transporters export lipids and glycolipids across the plasma membrane to the cell surface in mycobacteria, including trehalose monomycolate (TMM), mycobactins, di- and poly-acyltrehaloses, phthiocerol dimycocerosates, monomycolyldiacylglycerol, sulfolipids, and glycopeptidolipids.[57,166–170] MmpL3 is essential for the survival of *Mtb*, making this protein an appealing target, demonstrating that MmpL3 inhibitors can potentially shorten TB therapy.[57,171,172]

MmpL3 consists of 12 transmembrane helices (TMs 1–12), two periplasmic loops (loops 1 and 2), and one *C*-terminal cytoplasmic domain. The periplasmic loops are necessary for the function of MmpL3 and play a role in substrate binding.[173] It has been hypothesized that the *C*-terminal domain serves as a signal for polar localization of the protein.[174] MmpL3 employs the proton motive force (PMF) as an energy source to transport TMM over the cell membrane into the periplasmic space, in which it functions as a mycolic acid donor to another TMM molecule, to generate trehalose dimycolate (TDM) or arabinogalactan. Conformational changes in the transmembrane domain of MmpL3 take place during the flux of protons, which is required for TMM translocation. This is supported by mutagenesis experiments, demonstrating that charged residues in the transmembrane region are necessary for MmpL3 function and probably participate in this proton relay channel.[174,175] The mechanism and scope of TMM transport mediated by MmpL3 remain under study. Assays on spheroplasts indicate that MmpL3 acts as a flippase.[175] Recent refinement of the crystal structure of MmpL3 provided information on the potential mechanism of TMM translocation, revealing that TMM binds to purified MmpL3 with a $K_d$ of 3.7 ± 1.3 μM, while there was no binding was observed when TDM was analyzed.[176,177] The transmembrane domain is believed to be the channel for proton translocation mediated by the aspartate-tyrosine pairs (Asp256 and Tyr257 with Tyr646 and Asp645) on TM4 and TM10, which forms hydrogen bonds between these two helices.[176,178,179] Three out of four of these residues have been demonstrated to be necessary for MmpL3 function.[173] It has been demonstrated that these MmpL3 inhibitors bind to the same pocket in the transmembrane region of the protein, causing conformational changes that impair the connection between the two Asp-Tyr pairs required in proton translocation (**Figure 1.7-A/B**).[176] Additionally, most MmpL

transporters, except MmpL7, share this catalytic tetrad, indicating that all MmpL transporters operate with the same mechanism to induce substrate translocation.[173] It has been shown that the transmembrane domain is the binding site for numerous drug classes. The binding site can be separated into five subsites (**Figure 1.7-C**), four of which are hydrophobic (S1, S2, S3, and S5), and S4 is hydrophilic. The steric bulk of the hydrophobic amino-acid side chains determines the cavity size of hydrophobic subsites. The hydrophilic two pair of aspartate and tyrosine residues have been observed to mediate hydrogen bonding interactions with ligands at the S4 subsite.[176]

#### 1.8.1.1. Inhibitors of MmpL3

In recent years, a diversity of scaffolds, depicted in **Table 1.3**, have been reported[180] to inhibit MmpL3. These inhibitors span from several chemical classes, including diarylpyrroles,[181,182] 1,2-diamine derivatives,[183] adamantyl ureas,[184,185] benzimidazoles,[186–188] indolecarboxamides,[189–192] tetrahydropyrazolo pyrimidine carboxamides,[193,194] dihydro-spiro [piperidine-4,4'-thieno[3,2-*c*]pyrans],[193,195] piperidinols,[196] acetamides,[197] carboxamides.[198] *This dissertation will focus on indolecarboxamides, as the investigation of this scaffold in the context of MmpL3 inhibition* and *TB chemotherapy was one of our research aims. The reader is then directed to* ***Chapter 2*** *for an overview of this class in deeper detail.*

Numerous chemically distinct scaffolds, including the anti-tubercular clinical candidate SQ109[183] (**Table 1.3**), have been found to act as a MmpL3 inhibitor, giving this protein a reputation as a promiscuous drug target.[165,180]

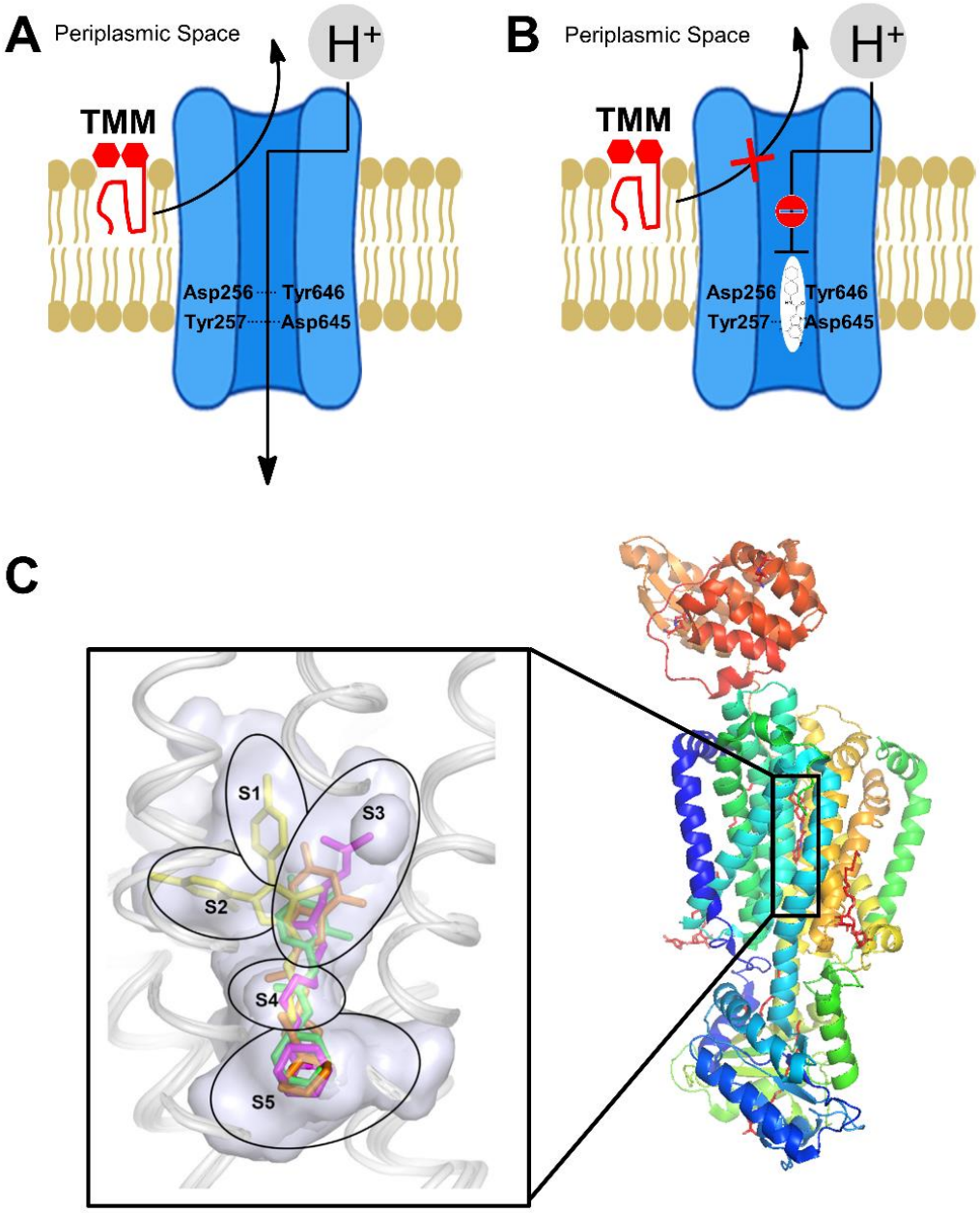


**Figure 1.7.** Structure representation of MmpL3 and its mechanism of action. **(A)** Mechanism of transport of MmpL3: the PMF in the transmembrane region of MmpL3 induces conformational changes that result in the transport of TMM into the periplasmic space**. (B)** Inhibition of MmpL3: inhibitors bind to a pocket in the transmembrane region of MmpL3, hampering the connection between the two Asp-Tyr pairs, disrupting TMM transport. **(C)** Crystal structure of *Mtb* MmpL3 and the inhibitors at the binding site (with sub-sites of the MmpL3 transmembrane pore displayed with docked structures of inhibitors; PDB: 6AJJ, inhibitor ICA38).[176] Adapted from Degiacomi *et al*.[164] and Zhang *et al*.[176]

**Table 1.3:** Compounds reported to inhibit the MmpL3 protein.

| Chemical Class | Compound | Structure | MIC (μM) | REF |
|---|---|---|---|---|
| **Diarylpyrroles** | BM212 | 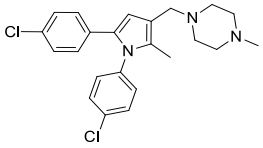 | 3.6 | 181 |
| **1,2-diamine derivatives** | SQ109 | 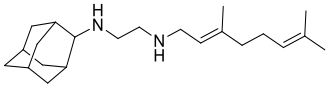 | 0.78 | 183 |
| **Adamantyl urea** | AU1235 | 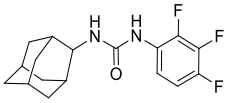 | 0.3 | 184,185 |
| **Benzimidazoles** | C215 | 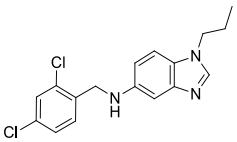 | 16.0 | 186 |
| **Indolecarboxamides** | NIDT349 | 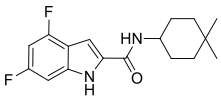 | 0.023 | 189,199 |
| **Tetrahydropyrazolo pyrimidine carboxamide** | THP P | 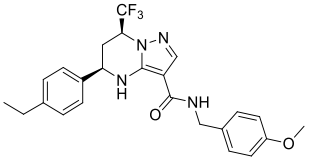 | 0.3 | 193 |
| **Dihydrospiro[piperidine-4,4'-thieno[3,2-*c*]pyrans]** | SPIRO | 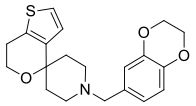 | 0.3 | 193,199 |
| **Piperidinols** | PIPD1 | 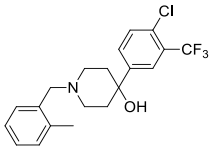 | 1.28 | 196 |
| **Acetamides** | E11 | 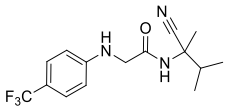 | 8.0 | 197 |
| **Carboxamides** | HC2091 | 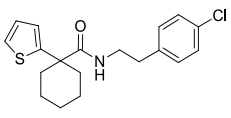 | 19.3 | 198 |

## 1.8.2. DprE1

DprE1, also known as decaprenylphosphoryl-β-$_D$-ribose 2′-epimerase, is an indispensable flavoenzyme involved in forming the *Mtb* cell wall.[200] It catalyzes the two-step epimerization of decaprenyl-phospho-ribose (DPR) to decaprenyl-phospho-arabinose (DPA), the precursor for arabinogalactan and lipoarabinomannan synthesis, in conjunction with decaprenylphosphoryl-$_D$-2-keto erythro pentose reductase (DprE2, **Figure 1.8-A**).[200–202] DprE1 initiates the first step of the epimerization process, where DPR is oxidized to the intermediate decaprenyl-phospho-2'-keto-$_D$-arabinose (DPX), co-factored by flavin adenine dinucleotide (FAD), yielding $FADH_2$. The DprE2, which is NADH-dependent, subsequently converts DPX to DPA.[203–205] The epimerization happens in the periplasmic region, which explains DprE1's vulnerability as a target[205], making this flavoenzyme a promising target for developing novel therapeutic candidates to tackle TB.

DprE1 is formed of a substrate-binding domain and a FAD-binding domain within which FAD is firmly entrenched, with an isoalloxazine ring residing at the interface between the substrate- and FAD-binding domains. By comparing the crystal structures of bound and unbound DprE1, it is possible to observe that the residues around the substrate-binding pocket are flexible. **Figure 1.8-B** shows a comparison between unbound DprE1 (*top*, PDB: 4FEH) and DprE1 bound to a covalent inhibitor (CT319, *bottom*, PDB: 4FDO). The substrate binding pocket is noticeably blocked in the bound structure, and FAD is barely perceptible.[206]

The druggable yet promiscuous nature of DprE1 has led to a significant number of DprE1 inhibitors with diverse molecular scaffolds and pharmacological profiles[164,207–211], as evidenced by an increasing number of publications on the subject. There have been twenty-three new classes of DprE1 inhibitors identified with antimycobacterial activity. These inhibitors are divided into two types, according to their mechanism of action (MoA): (1) Covalent binders, where five classes have been shown to irreversibly inhibit DprE1 by generating a covalent adduct with the C387 residue, and (2) non-covalent inhibitors, in which seventeen reported classes were experimentally confirmed to act as competitive inhibitors. Several DprE1 inhibitor reviews have been written over the last decade, covering scaffold and docking studies.[164,165,207–210,212]

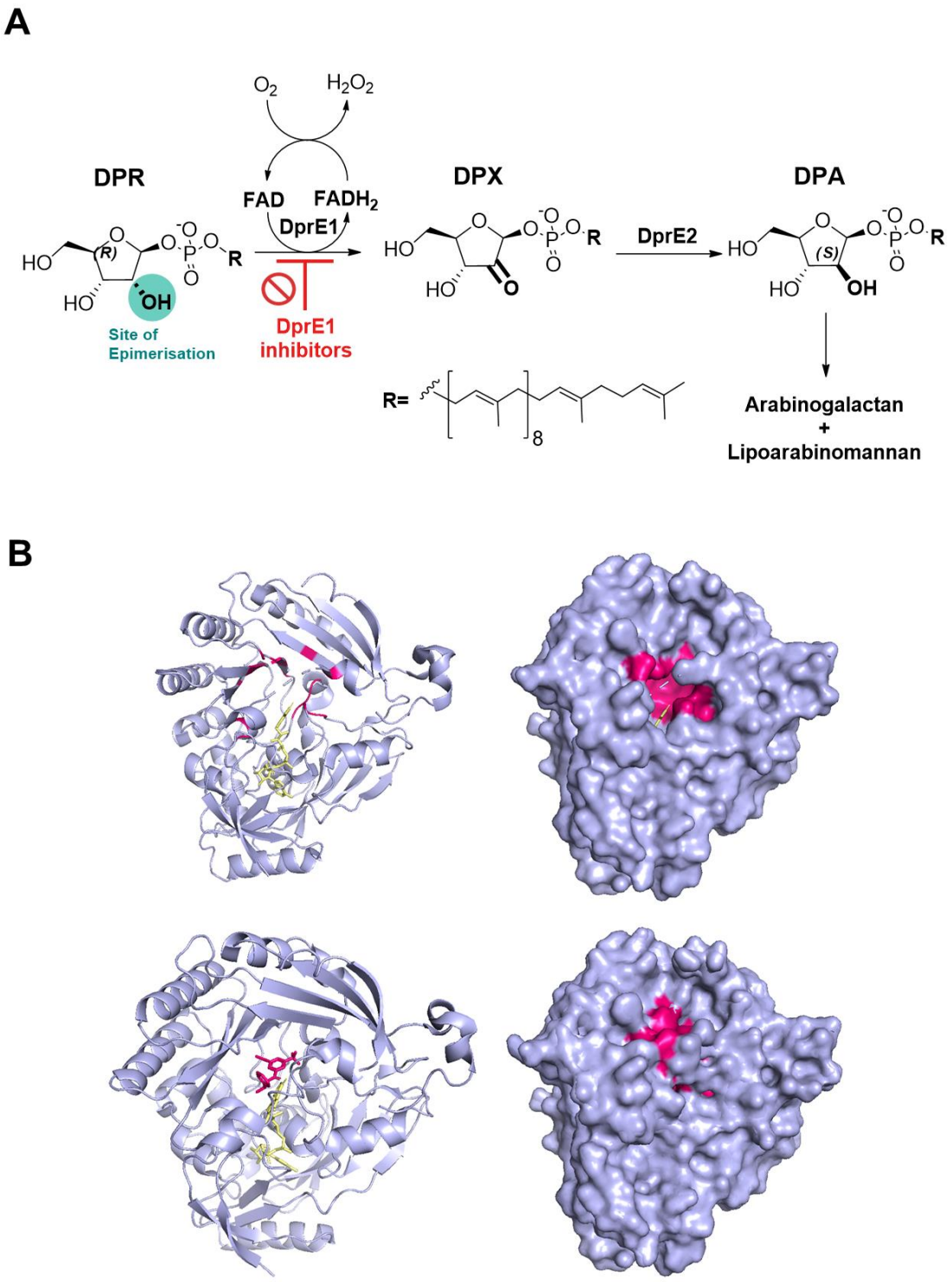


**Figure 1.8.** Structure representation of DprE1 and its mechanism of action. **(A)** The DPA biosynthetic pathway: in the presence of the co-factor FAD, the DprE1 and DprE2 enzymes catalyze the epimerization of the 2'-OH group in DPR to form DPA. **(B)** Cartoon and surface representation of unbound DprE1 (*top*, PDB: 4FEH) and bound to a covalent inhibitor CT319 (*bottom*, PDB: 4FDO) with the substrate binding pocket being significantly narrowed in the bound representation (*in pink*).

### 1.8.2.1. Covalent inhibition

DprE1 was first discovered as a target of benzothiazinones, which inhibit the flavoenzyme DprE1 irreversibly through the formation of a covalent adduct with the amino acid Cys387. Makarov and colleagues demonstrated that benzothiazinones (BTZ) are capable of strongly suppressing DprE1 activity *in vitro* and *in vivo*. Compound BTZ043 (**Figure 1.9**) is one of the most promising benzothiazinones synthesized, with a minimum inhibitory concentration (MIC) of 1 ng/mL (2.3 nM), which is significantly superior to the MICs for frontline medications such as EMB (15 mg/mL) and INH (0.02-0.2 mg/mL).[213–215] BTZ043 acts as a prodrug in the presence of $FADH_2$, where the nitro group on the benzothiazinone core is reduced to its nitroso derivative **1.1** The reactive nitroso form **1.1** reacts with the thiol group on the Cys387 residue in DprE1, producing a semi-mercaptal bond and a covalent adduct, irreversibly inhibiting the enzyme as a suicide substrate (**Figure 1.9**). Despite its exceptional potency (MIC = 2.3 nM), BTZ043's efficacy in a mouse model of TB was lower than expected due to poor solubility, though it has moderate hydrophobicity (logP = 2.84).[206,213,216–220]

Makarov and co-workers addressed these issues to improve the pharmacological properties of the benzothiazinones, producing substituted 2-piperazino-benzothiazinones (PBTZ) with increased lipophilicity.[220] This new series included a diverse range of compounds substituted in the piperazine ring's *N*-4 position; when hydrophilic groups such as alcohols, carboxylic acids, secondary or tertiary amines were introduced, activity was reduced or eliminated, comparatively to BTZ043. The most potent compounds were the piperidines alkyl substituted at *N*-4 position, with MIC values ranging from 0.41 to 1.69 nM. The most active compound in this series was PBTZ169, also known as Macozinone (MCZ, **Table 1.4**), bearing a cyclohexylmethyl group as the piperazine *N*-4 substituent. PBTZ169 had a much more significant bactericidal effect in the lungs than BTZ043 at the same dose, reducing colony-forming units (CFU) by >0.5 log units.[220,221] Compound PBTZ169 has successfully completed Phase I clinical trials and demonstrated synergy with Bdq and PZA, establishing this combination as a viable novel tuberculosis treatment regimen.[222] Compounds BTZ043 and PBTZ169 are currently in Phase 1/2[222] and 2a[223] of clinical trials for the treatment of both drug-susceptible TB and MDR-TB. *This dissertation will focus on the class of benzothiazinones, as the investigation of this class of DprE1 inhibitors with the aim of developing peroxide-based hybrids for TB chemotherapy was one of our research objectives. The reader is then directed to* ***Chapter 2*** *for an overview*

*of this class in deeper detail.*

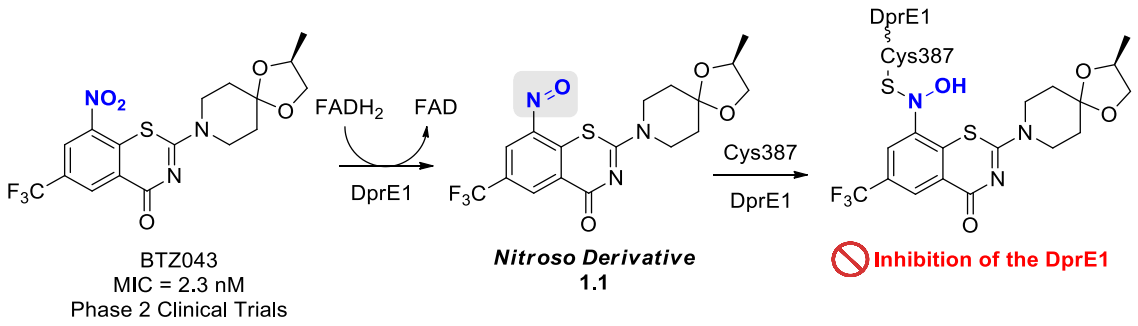


**Figure 1.9.** Mechanism of bioactivation and action of nitrobenzothiazinones: formation of the active nitroso compound from BTZ043 and its reaction with the DprE1, leading to irreversible inhibition of the enzyme.

The presence of a nitro group and its correlation with activity against DprE1 mutants C387A and C387S were taken as typical characteristics of covalent DprE1 inhibitors.[224]

DprE1 has also been identified as the target of nitrobenzothiazoles (NBTO)[225,226], dinitrobenzamides (DNBs),[227] nitroquinoxalines (NQs),[228] and 3-nitro-1,2,4-triazoles (NTZs),[186] all of which inhibit DprE1 covalently (**Table 1.4**). *For a more comprehensive review of covalent DprE1 inhibitors the reader is referred to* ***Chapter 3****, where a perspective on research directions for this topic will be offered.*

### 1.8.2.2. Non-covalent inhibition

Numerous scaffolds acting as non-covalent inhibitors of DprE1 have also been investigated for their activity against *Mtb***.** These inhibitors, depicted in **Table 1.5**, include non-nitro-substituted BTZ analogues (NC BTZ),[229–231] benzothiazoles (BTO),[232,233] 1,2,3-triazole-2-mercaptobenzothiazoles (2-S-BTO),[234] 1,4-azaindoles (AZA),[235–240] benzimidazoles (BI),[241] pyrazolopyridones (PP),[242] 4-aminoquinolone piperidine amides (4-AQ),[243] 2-carboxyquinoxalines (2-CQ),[244] pyrrolothiadiazoles (PTD)**,**[245,246] morpholine-pyrimidines (MP),[247] *N*-alkyl-5-hydroxypyrimidinone carboxamides (NAHPC),[248,249] hydantoins (HYD),[250,251] benzodioxanes (BD),[252] 3,4-dihydrocarbostyril derivatives (CD),[253–257] thiophene-arylamides (TPA),[258] *N*-(4-hydroxy-3-mercaptonaphthalenyl) sulfonamides (NHMS),[259] and avermectins (AVMT).[260] *For a more comprehensive review of non-covalent DprE1 inhibitors the reader is referred to* ***Chapter 3****, where a perspective on research directions for this topic will be provided.*

**Table 1.4:** Compounds reported to target DprE1 covalently, with irreversible inhibition.

| Structure | MIC (μM) | REF | Structure | MIC (μM) | REF |
|---|---|---|---|---|---|
| **Benzothiazinones (BTZ)**<br>BTZ043 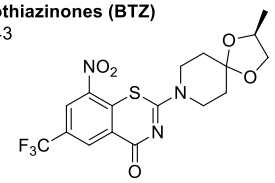 | 2.3 nM | 213 | **Dinitrobenzamides (DNB)**<br>DNB1 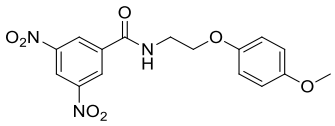 | 0.08 | 227 |
| PBTZ169 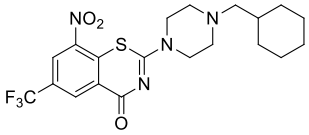 | <0.42 nM | 220 | **Nitroquinoxalines (NQ)**<br>VI-22484 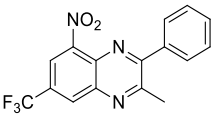 | 0.75 | 228 |
| **Nitrobenzothiazoles (NBTO)**<br>*N*-BTO 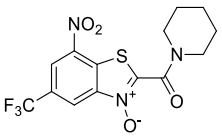 | 0.08 | 225,226 | **3-Nitro-1,2,4-Triazoles (NTZ)**<br>377790 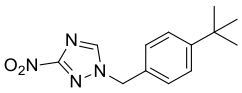 | 0.50[a] | 186 |
| BT 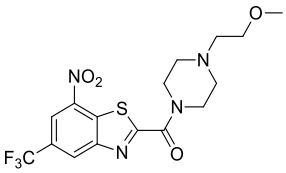 | 0.50 | 225,226 | **Possibly covalent** | | |
| cBT 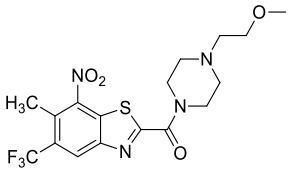 | 4.62 | 225,226 | **3,5-Dinitrophenyl-Containing 1,2,4-Triazoles (DNPT)** 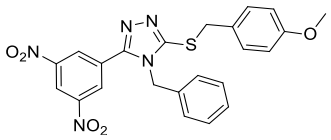 | 0.03 | 261 |

[a] $MIC_{90}$

**Table 1.5:** Compounds reported to target DprE1 non-covalently.

| Structure | MIC (μM) | REF | Structure | MIC (μM) | REF |
|---|---|---|---|---|---|
| **Non-covalent Benzothiazinones (NC-BTZ)** 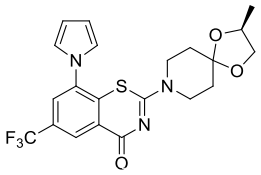 | 0.35 | 229 | **Pyrrolothiadiazoles (PTD)** GSK710 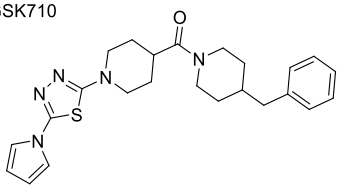 | 0.4 | 245 |
| **Benzothiazole derivatives (BTO)** TCA1 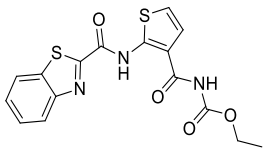 | 0.027 | 232 | **Morpholino-pyrimidines (MP)** 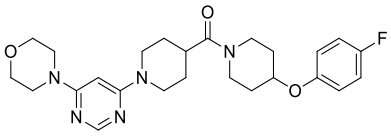 | 1.7 | 247 |
| **1,2,3-Triazole-2-mercaptobenzothiazoles (2-S-BTO)** 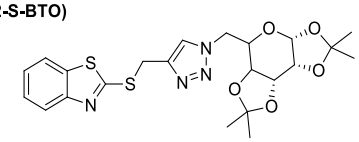 | 16.3 | 234 | ***N*-Alkyl-5-hydroxypyrimidinone Carboxamides (NAHPC)** 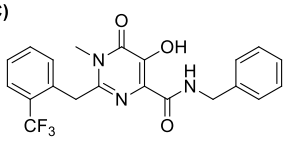 | 4.7 | 248 |
| **2-carboxyquinoxaline derivatives (2-CQ)** Ty38c 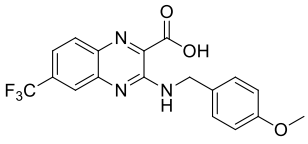 | 3.1[a] | 244 | **Hydantoins (HYD)** 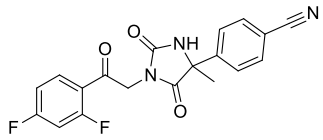 | 8.3 | 251 |
| **1,4-Azaindoles (AZA)** TBA-7371 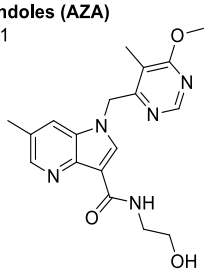 | 1.56-3.12 | 239,240 | **Benzodioxanes (BD)** 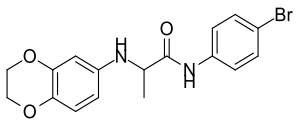 | 6.5 | 252 |
| **Benzimidazole (BI)** 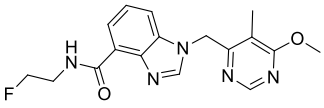 | 1.56 | 241 | **3,4-Dihydrocarbostyril Derivatives (CD)** OPC-167832 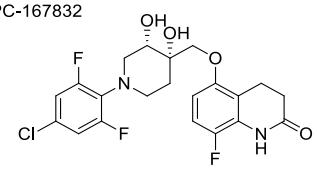 | 0.00044 -0.52 | 253,256, 257 |

| | | | | | |
|---|---|---|---|---|---|
| **4-Aminoquinolones (4-AQ)** 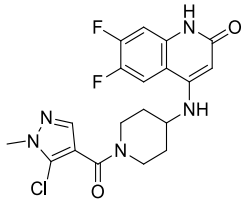 | 0.08 | 243 | **Thiophene-arylamides (TPA)** 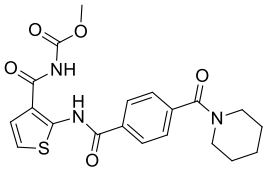 | 0.027 | 258 |
| **Pyrazolopyridones (PP)** 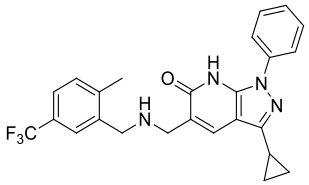 | 0.1 | 242 | **Avermectins (AVMT)** Selamectin 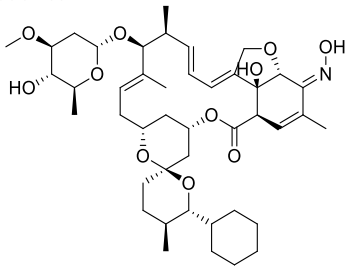 | 5.20 | 260 |
| **N-(4-hydroxy-3-mercaptonaphthalenyl) sulfonamide (NHMS)** 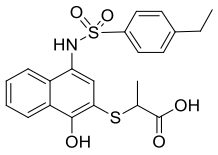 | > 10; 0.38[b] | 259 | | | |

[a] $MIC_{99;}$ [b] $MIC_{50}$ *Ms*

## 1.9. Latent tuberculosis infection (LTBI)

LTBI is described as the presence of antibodies to tuberculosis antigens in the absence of clinical or radiologic manifestations of TB disease.[89,262] Consequently, LTBI screening and treatment are crucial components of overall tuberculosis control and eradication initiatives.[262,263]

Nowadays, four major antimycobacterial regimens are available for treating LTBI: INH monotherapy, RIF monotherapy, and combinations of INH and RIF.[263] In around 90% of patients, INH monotherapy is effective in delaying progression to TB illness, but its lengthy duration and hepatotoxicity result in low compliance and completion rates.[264] Notably, there is no evidence of an increased incidence of INH-resistant or RIF-resistant tuberculosis after having preventive LTBI therapies comprising these drugs.[265,266]

### 1.9.1. DosRST two-component regulatory system

The ability of *Mtb* to enter nonreplicating persistence (NRP) and then transition to latent TB contributes to *Mtb*'s drug tolerance and treatment failure in chronically infected individuals, which is a limitation and causes a significant burden on patients and healthcare infrastructure. The NRP is a specific condition in the mycobacterial infection cycle in which the mycobacteria have a low metabolism, allowing for non-inherited resistance to most antimycobacterial treatments.[267–269]

As part of its pathogenesis, *Mtb* must overcome various obstacles the immune system provides, including survival in hostile environments such as the macrophage and granuloma.[267] The inhibition of aerobic respiration induced by oxygen deficiency or exposure to carbon monoxide (CO) and nitric oxide (NO) is a typical stressor of intra- and extracellular pathogenic mycobacteria.[267–269] *Mtb* can thrive in hypoxia despite the fact that it is an obligate aerobe.[270] However, this can only be accomplished by gradually decreasing oxygen levels, which appears to be the situation during granuloma development. *Mtb* survives this stress by triggering a regulon of 48 genes that promotes its entrance into a NRP while adjusting its metabolism to maintain energy levels and a redox balance suitable for survival in the absence of respiration.[267,269,271–273] This response is controlled by the two-component regulatory system (TCS), DosRST. DosRST was discovered to be involved with *Mycobacterium spp*. virulence and survival under hypoxia;[274–277] DosR is a response regulator, and DosS is a sensor histidine kinase (**Figure 1.10**). Along with DosRS, another sensor kinase, DosT, enhances the sensibility to hypoxia and NO.[278] In response to hypoxia, NO and CO, DosS and DosT autophosphorylate. Both kinases directly interact with and phosphorylate DosR.[272,279] This latter domain depends on divalent metals (e.g., $Mg^{2+}$, $Mn^{2+}$) to catalyze autophosphorylation and phosphoryl-transfer reactions employing adenosine triphosphate (ATP).[280,281] DosT, the sensor with the lowest oxygen affinity ($K_d = 26$ μM), is the first to be enzymatically activated when the oxygen concentration decreases, followed by DosS ($K_d = 3$ μM) at an even lower oxygen level, where they are able to phosphorylate the essential transcription factor DosR. [281] Phospho-DosR then binds directly to a conserved DNA motif and controls an estimated 50-gene core regulon.[267,269,271–273] DosS also contains phosphatase activity, which is aerobically active and dephosphorylates DosR to restrict expression.[282] Alternately, spontaneous dephosphorylation of phospho-DosR may contribute to the signal diminishing.[274]

Supported with biochemical investigations of kinase activation, DosS is assumed to operate as a redox and oxygen sensor, while DosT is thought to sense hypoxia.[283] Nevertheless, reports show that DosS has a slow auto-oxidation rate and operates in a reduced ferrous state, suggesting this histidine kinase may serve predominantly as an oxygen sensor.[284] DosS and DosT have similar structures in that they both include prosthetic heme groups; however, the native oxidation state of their iron centres differs, which has consequences for their respective roles.[285] Oxidized heme in DosS is shifted to the ferrous form under hypoxic conditions, while oxygen-bound heme in DosT converts to the deoxy form, activating the kinases *via* the heme.[286,287] It was reported that ferrous DosS showed more potent autophosphorylation activity than Fe(III)-containing DosS, indicating that reduction promotes DosR activation, hence facilitating NRP. After treatment with NO or CO, the autophosphorylation activity of ferrous DosS was equivalent to that of reduced DosS. This observation suggests that DosS serves as a redox sensor in the DosRST regulon.[272] In addition, DosS may play a pivotal DosR-independent role in macrophage replication, tumour necrosis factor (TNF) suppression, and autophagy pathways, as recently uncovered.[288]

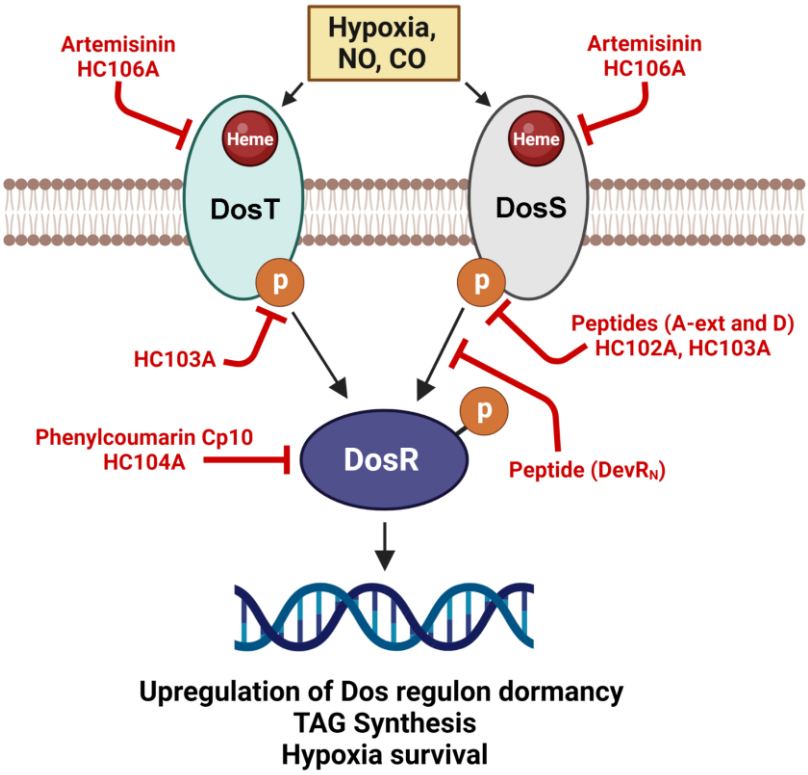


**Figure 1.10**. Diagram of the DosRST signaling pathway showing examples of how peptides and small compounds inhibit DosRST signaling. Adapted from Zheng *et al.*[273] Legend: TAG – triacylglycerol.

## 1.9.2. Inhibitors targeting the DosRST pathway

Since DosRST is initiated during infection and is essential for survival in hypoxic granulomas, there is an interest in developing new drugs that target this pathway. Inhibitors targeting the response of the regulator DosR or the two sensor histidine kinases, DosS and DosT, are being investigated due to their potential to curtail TB therapy and reduce relapse rates when paired with first-line drugs.[276,277] Inhibiting TCS DosRST may shorten the period of therapy by eliminating dormant *Mtb*, whereas earlier research focused on the response regulator DosR.[277,289] To identify TCS inhibitors, whole-cell reporter-based high-throughput screenings (HTS) have been performed.[269,290,291] *In silico* pharmacophore-based screening with a library of 2.5 million compounds, a phenylcoumarin (**1.2**, **Figure 1.11**) was found to inhibit DosR binding to target DNA, down-regulate dormancy gene transcription and significantly impair hypoxic survival, but not nutrient-deprived dormant bacteria or actively developing organisms.[292]

Through phage-display techniques *in vitro* biochemical assays, DosR mimetic peptides that bind to DosS and block autokinase activity or phosphotransfer to DosR were identified.[293,294] This research revealed TLHLHHL as a potential inhibitor for this system.[294] This peptide reduced *Mtb* viability by 95% under hypoxia, but only 50% under aerobic conditions, suggesting a preference for dormancy. However, the high peptide concentration (5 mM) needed for this biological inhibitor likely hampered further progress.[294] Using DosS as bait in phage-display revealed four peptide sequences. These peptides shared similarities with the DosR protein's conserved sequences, leading to the development of further synthetic peptides.[293] Two peptide sequences, VRLPD and SGYVVK-DIKGME, also proved to inhibit DosR-regulated transcription, decreasing *Mtb* survival in hypoxia (40–70%) but not in aerobic (15%) conditions. Although these compounds did not halt phosphoryl-transfer activity, these peptides reduced DosS kinase domain autophosphorylation.[293]

In another report, disclosed in 2017, a whole-cell phenotypic screening assay was employed to screen a library of 540,288 compounds for DosRST inhibition.[295] This screening procedure yielded six distinct groups of compounds as DosRST regulon inhibitors, with the six most effective compounds from each class being selected and designated as HC101 through HC106 (**Figure 1.11**). Initial experiments using HC101A [artemisinin (ART)], HC102A, and HC103A (**Figure 1.11**) demonstrated a lack of selectivity in general. In this situation, the DosR-strongly controlled hspX promoter was

cloned upstream of green fluorescent protein (GFP) on a replicating plasmid, and *Mtb* was transformed. Significant hypoxia and NO-induced GFP fluorescence were seen in the reporter strain.[295] Initial research to unravel the mechanism of action was conducted on ART, HC102A, and HC103A. Comparatively to a DosR mutant control strain, RNAseq transcriptional profiling experiments revealed that these compounds disrupt the DosR regulon.[276,295] Treatment with ART, HC102, and HC103 significantly reduced triacylglycerol (TAG) accumulation. Combining these drugs with INH (to which latent *Mtb* is often resistant) reduced *Mtb* viability very effectively.[295,296] This result is consistent with prior research demonstrating that mutants of the TAG synthase gene tgs1 have a lower tolerance to INH.[297] Further research suggests that ART may change the heme of DosS and DosT by an alkylation mechanism, resulting in different sensor phenomena. ART inhibits the sensing module of DosS and DosT by oxidizing and alkylating the heme group contained in these proteins.[295] In contrast, HC102A and HC103A did not modify the heme (no oxidation or detectable alkylation) but hampered the autophosphorylation activity of the sensors, with HC103A being the most effective.[295]

In 2020, inhibitors HC104A and HC106A were investigated (**Figure 1.11**).[276] HC104A had no effect on *Mtb* survival in a hypoxia model, in which HC106A reduced *Mtb* survival by 50%, suggesting that HC104A inhibits DosR-regulated genes that are not required for survival. It was revealed that these compounds did not affect the autophosphorylation activities of DosS and DosT. Though, HC104A prevented DosR from binding to DNA, whereas HC106A altered the electronic spectrum of deoxy-DosS. This spectroscopic profile for DosS was divergent from ART, indicating that HC106A may bind directly to the heme iron without affecting impairment.[276] HC104A was evaluated for interactions with DosS, through UV-visible spectroscopy and kinase autophosphorylation assays, but no effect was observed. HC104A might operate by inhibiting the dimerization of the response regulator transcription factor DosR and its DNA binding due to its structural similarities with virstatin.[272,298] Virstatin is known to inhibit the dimerization of the ToxT transcription factor in *Vibrio cholera*.[298,299]

Additional structure-activity relationship investigations for HC106A revealed that the isoxazole moiety is required for inhibition. Contrary to ART, which did not reduce NO-driven signalling, HC106 inhibited the DosR regulon when it was triggered by NO and in infected macrophages.[276,295] HC106 suppressed NRP-associated physiologies, such as TAG accumulation and survival during hypoxia, opposite to HC104. Resistance to HC106 was increased by DosS overexpression, demonstrating that DosRST was

the targeted pathway.[276] These results support the existence of diverse groups of small molecules with multiple mechanisms for TCS DosRST inhibition.[300]

As described previously, ART was identified as an inhibitor of DosRST signaling, persistence, and antibiotic tolerance. This endoperoxide operates by oxidizing and alkylating the heme group within DosS and DosT, hence inactivating the sensing module of the proteins.[276,295] In 2022, it was discovered that synthetic 1,2,4-trioxolanes OZ277 and OZ439 (**Figure 1.11**) could target DosS-mediated hypoxia signaling in *M. abscessus* and reproduce the DosS knock-out phenotype. In chronically infected mice, OZ439 demonstrated bactericidal activity comparable to standard-of-care antibiotics, enhancing the efficacy of antibiotics administered in combination.[301]

Multiple mechanisms have been found for inhibitors of DosRST signaling, including inhibition of autophosphorylation, disruption of phosphotransfer to DosR, suppression of DosR DNA binding, heme-binding, oxidation/alkylation of heme of the kinases DosS/T.[273] It is anticipated that merging these approaches may enhance the drugs' synergistic effects.[273] These experiments showed that the DosS/heme-based T's sensor is vulnerable to chemical inhibition. The knowledge of these small molecules as DosS/T inhibitors opens a pathway for *in silico* screening of novel inhibitors that may target the heme or bind in this susceptible sensory domain.

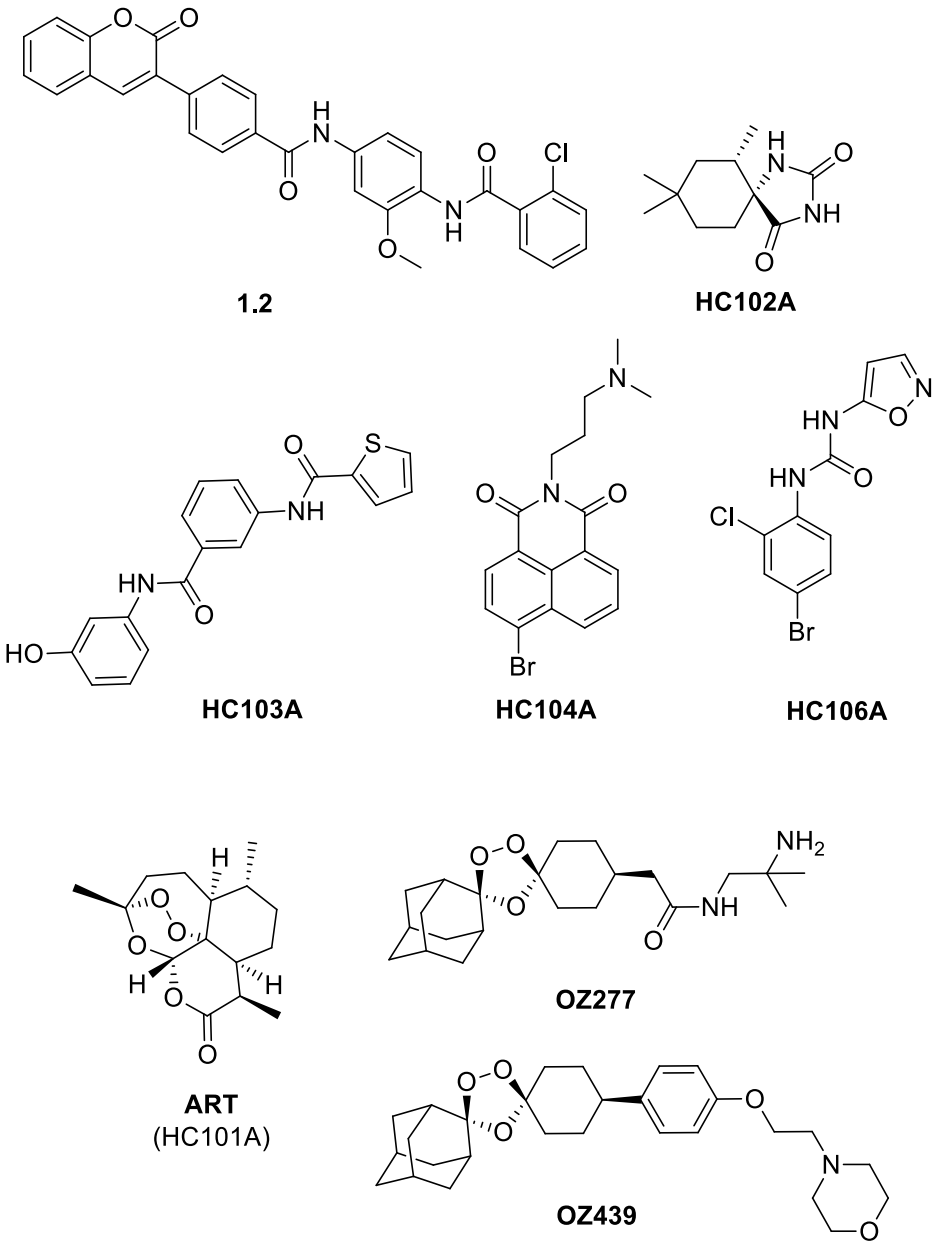


**Figure 1.11.** Structure representations of DosRST signalling inhibitors.

## 1.10. Summary

This chapter introduced the epidemiology, symptoms, diagnosis, and pathology of tuberculosis. The licensed vaccine, potential candidates, and approved drugs for TB treatment were also addressed concisely, along with a discussion of the limitations of TB therapy and the concerns of TB resistance associated with these regimens approved by WHO.

TB discovery initiatives have uncovered several novel protein targets, such as the transporter mycobacterial membrane protein large 3 (MmpL3) and the flavoenzyme

decaprenylphosphoryl-β-$_D$-ribose 2′-epimerase (DprE1). These are two prominent targets for which several inhibitors have been identified through hit discovery, preclinical investigations, and clinical trials. A brief review of potential inhibitors for MmpL3 and DprE1 was given, demonstrating their high potential for developing novel drugs to achieve the aim of TB eradication.

Finally, the function and structure of DosS, DosT, and DosR were examined concerning the role of DosRST signalling in *Mtb* latency. Antimalarial artemisinin and synthetic peroxides can disrupt DosRST signalling and potentiate antibiotics' activity in latent TB when used in combination. These findings could be instrumental in developing solutions that could overcome growing resistance and enhance treatment effects, particularly in cases of latent infection. We followed this path to contribute to the continuous demand for better anti-TB drugs with novel mechanisms of action.

## 1.11. Presentation of the research project and its aims

The subsequent chapters of this dissertation will focus on the research conducted during the Ph.D. program and can be divided into four sections:

- Chapter 2: Synthesis of 1,2,4-Trioxane-Containing Antitubercular Hybrids with Potential for Dual Mechanisms of Action.
- Chapter 3: Computational Analysis of Physicochemical and ADMET Properties of DprE1 Inhibitors and Development of Predictive Classification Models for Identifying Potential DprE1 Inhibitors.
- Chapter 4: Synthesis of Non-Symmetrical Dispiro 1,2,4,5-Tetraoxanes and 1,2,4-Trioxanes Catalysed by Silica Sulfuric Acid.
- Chapter 5: Unravelling the Structure of Peroxides with Antiparasitic Activity: Relative Impact of a Trioxolane or a Tetraoxane Pharmacophore on the Overall Molecular Structure and Photoinduced Reactivity Studies in a Dispiro-1,2,4,5-tetraoxane.

Along the thesis, a similar distribution of topics will be adopted.

This PhD project benefited from established collaborations between CCMar, Universidade do Algarve (Portugal), and other national and international institutions: CQC, Departamento de Química, Universidade de Coimbra; CQC-IMS, Faculdade de Farmácia, Universidade de Coimbra (Portugal); CFisUC, Departamento de Física,

Universidade de Coimbra (Portugal); CQE, from Instituto Superior Técnico, and Faculdade de Ciências, University of Lisbon; Department of Chemistry, University of Liverpool (United Kingdom); Liverpool School of Tropical Medicine, University of Liverpool (United Kingdom).

## 1.12. References


(1) WHO. *WHO. Global Tuberculosis Report 2022*.

(2) Hershkovitz, I.; Donoghue, H. D.; Minnikin, D. E.; Besra, G. S.; Lee, O. Y.-C.; Gernaey, A. M.; Galili, E.; Eshed, V.; Greenblatt, C. L.; Lemma, E.; Bar-Gal, G. K.; Spigelman, M. Detection and Molecular Characterization of 9000-Year-Old *Mycobacterium tuberculosis* from a Neolithic Settlement in the Eastern Mediterranean. *PLoS One* **2008**, *3* (10), e3426. https://doi.org/10.1371/journal.pone.0003426.

(3) Bedeir, S. A. Tuberculosis in Ancient Egypt. In *Tuberculosis*; Tuberculosis. Springer, Berlin, H., Ed.; 2004; pp 3–13. https://doi.org/10.1007/978-3-642-18937-1_1.

(4) Nerlich, A. G.; Haas, C. J.; Zink, A.; Szeimies, U.; Hagedorn, H. G. Molecular Evidence for Tuberculosis in an Ancient Egyptian Mummy. *Lancet* **1997**, *350* (9088), 1404. https://doi.org/10.1016/S0140-6736(05)65185-9.

(5) Murray, J. F. A Century of Tuberculosis. *Am. J. Respir. Crit. Care Med.* **2004**, *169* (11), 1181–1186. https://doi.org/10.1164/rccm.200402-140OE.

(6) Wallstedt, H.; Maeurer, M. History of Tuberculosis Management in Sweden. *Int. J. Infect. Dis.* **2015**, *32*, 179–182. https://doi.org/10.1016/j.ijid.2015.01.018.

(7) Barberis, I.; Bragazzi, N. L.; Galluzzo, L.; Martini, M. The History of Tuberculosis: From the First Historical Records to the Isolation of Koch's Bacillus. *J. Prev. Med. Hyg.* **2017**, *58*, 9–12.

(8) Madkour, M. M.; Al-Otaibi, K. E.; Swailem, R. Al. Historical Aspects of Tuberculosis. In *Tuberculosis*; 2004; pp 15–30. https://doi.org/10.1007/978-3-642-18937-1_2.

(9) Maher, D.; Raviglione, M. Global Epidemiology of Tuberculosis. *Clin. Chest Med.* **2005**, *26* (2), 167–182. https://doi.org/10.1016/j.ccm.2005.02.009.

(10) Lechartier, B.; Rybniker, J.; Zumla, A.; Cole, S. T. Tuberculosis Drug Discovery in the Post-Post-Genomic Era. *EMBO Mol. Med.* **2014**, *6* (2), 158–168. https://doi.org/10.1002/emmm.201201772.

(11) Zumla, A.; Nahid, P.; Cole, S. T. Advances in the Development of New Tuberculosis Drugs and Treatment Regimens. *Nat. Rev. Drug Discov.* **2013**, *12* (5), 388–404. https://doi.org/10.1038/nrd4001.

(12) Spence, D. P. S.; Hotchkiss, J.; Williams, C. S. D.; Davies, P. D. O. Tuberculosis and Poverty. *Br. Med. J.* **1993**, *307* (6907), 759–761. https://doi.org/10.1136/bmj.307.6907.759.

(13) Barter, D. M.; Agboola, S. O.; Murray, M. B.; Bärnighausen, T. Tuberculosis and Poverty: The Contribution of Patient Costs in Sub-Saharan Africa – a Systematic Review. *BMC Public Health* **2012**, *12*, 980. https://doi.org/10.1186/1471-2458-12-980.

(14) Pawlowski, A.; Jansson, M.; Sköld, M.; Rottenberg, M. E.; Källenius, G. Tuberculosis and HIV Co-Infection. *PLoS Pathog.* **2012**, *8* (2), e1002464. https://doi.org/10.1371/journal.ppat.1002464.

(15) https://www.who.int/teams/global-tuberculosis-programme/tb-reports/global-tuberculosis-report-2022/tb-disease-burden/2-1-tb-incidence (accessed on 27th March, 2023).

(16) Gillespie, S. H. Evolution of Drug Resistance in *Mycobacterium tuberculosis*: Clinical and Molecular Perspective. *Antimicrob. Agents Chemother.* **2002**, *46* (2), 267–274. https://doi.org/10.1128/AAC.46.2.267–274.2002.

(17) Udwadia, Z. F.; Amale, R. A.; Ajbani, K. K.; Rodrigues, C. Totally Drug-Resistant Tuberculosis in India. *Clin Infect Dis* **2012**, *54* (4), 579–581.

https://doi.org/10.1093/cid/cir889.
(18) Udwadia, Z. F. MDR, XDR, TDR Tuberculosis: Ominous Progression. *Thorax* **2012**, *67* (4), 286–288. https://doi.org/10.1136/thoraxjnl-2012-201663.
(19) Uplekar, M.; Weil, D.; Lonnroth, K.; Jaramillo, E.; Lienhardt, C.; Dias, H. M.; Falzon, D.; Floyd, K.; Gargioni, G.; Getahun, H.; Gilpin, C.; Glaziou, P.; Grzemska, M.; Mirzayev, F.; Nakatani, H.; Raviglione, M. WHO's New End TB Strategy. *Lancet* **2015**, *385* (9979), 1799–1801. https://doi.org/10.1016/S0140-6736(15)60570-0.
(20) WHO. *Implementing The End TB Strategy: The Essentials*; 2015.
(21) Khawbung, J. L.; Nath, D.; Chakraborty, S. Drug Resistant Tuberculosis: A Review. *Comp. Immunol. Microbiol. Infect. Dis.* **2021**, *74*, 101574. https://doi.org/10.1016/j.cimid.2020.101574.
(22) Barry III, C. E.; Boshoff, H. I.; Dartois, V.; Dick, T.; Ehrt, S.; Flynn, J.; Schnappinger, D.; Wilkinson, R. J.; Young, D. The Spectrum of Latent Tuberculosis: Rethinking the Biology and Intervention Strategies. *Nat. Rev. Microbiol.* **2009**, *7* (12), 845–855. https://doi.org/10.1038/nrmicro2236.
(23) Esmail, H.; Barry, C. E.; Young, D. B.; Wilkinson, R. J. The Ongoing Challenge of Latent Tuberculosis. *Philos. Trans. R. Soc. B* **2014**, *369* (1645), 20130437. https://doi.org/10.1098/rstb.2013.0437.
(24) Rangaka, M. X.; Wilkinson, K. A.; Glynn, J. R.; Ling, D.; Menzies, D.; Mwansa-kambafwile, J.; Fielding, K.; Pai, M. Predictive Value of Interferon-γ Release Assays for Incident Active Tuberculosis: A Systematic Review and Meta-Analysis. *Lancet Infect. Dis.* **2012**, *12* (1), 45–55. https://doi.org/10.1016/S1473-3099(11)70210-9.
(25) Furin, J.; Cox, H.; Pai, *M. tuberculosis. Lancet* **2019**, *393* (10181), 1642–1656. https://doi.org/10.1016/S0140-6736(19)30308-3.
(26) Pai, M.; Behr, M. A.; Dowdy, D.; Dheda, K.; Divangahi, M.; Boehme, C. C.; Ginsberg, A.; Swaminathan, S.; Spigelman, M.; Getahun, H.; Menzies, D.; Raviglione, *M. tuberculosis*. *Nat. Rev. Dis. Prim.* **2016**, *2*, 16076. https://doi.org/10.1038/nrdp.2016.76.
(27) Lawn, S. D.; Zumla, A. I. Tuberculosis. *Lancet* **2011**, *378* (9785), 57–72. https://doi.org/10.1016/S0140-6736(10)62173-3.
(28) Alshoabi, S. A. Tuberculous Meningitis, Vasculitis, and Pericarditis Presented by Deep Coma. *Pak J Med Sci* **2018**, *34* (6), 1576–1578. https://doi.org/10.12669/pjms.346.16350.
(29) Campbell, I. A.; Bah-Sow, O. Pulmonary Tuberculosis: Diagnosis and Treatment. *Br. Med. J.* **2006**, *332* (7551), 1194–1197. https://doi.org/10.1136/bmj.332.7551.1194.
(30) Golub, J. E.; Bur, S.; Cronin, W. A.; Gange, S.; Baruch, N.; Comstock, G. W.; Chaisson, R. E. Delayed Tuberculosis Diagnosis and Tuberculosis Transmission. *Int. J. Tuberc. Lung Dis.* **2006**, *10* (1), 24–30.
(31) WHO. *Xpert MTB/RIF Assay for the Diagnosis of Pulmonary and Extrapulmonary TB in Adults and Children*; 2013.
(32) Tortoli, E.; Russo, C.; Piersimoni, C.; Mazzola, E.; Monte, P. D.; Pascarella, M.; Borroni, E.; Mondo, A.; Piana, F.; Scarparo, C.; Coltella, L.; Lombardi, G.; Cirillo, D. M. Clinical Validation of Xpert MTB/RIF for the Diagnosis of Extrapulmonary Tuberculosis. *Eur. Respir. J.* **2012**, *40* (2), 442–447. https://doi.org/10.1183/09031936.00176311.
(33) Donovan, J.; Thu, D. D. A.; Phu, N. H.; Dung, V. T. M.; Quang, T. P.; Nghia, H. D. T.; Oanh, P. K. N.; Nhu, T. B.; Chau, N. V. V.; Ha, V. T. N.; Hang, V. T. T.; Trinh, D. H. K.; Geskus, R. B.; Tan, L. Van; Thuong, N. T. T.; Thwaites, G. E. Xpert MTB/RIF Ultra versus Xpert MTB/RIF for the Diagnosis of Tuberculous Meningitis: A Prospective, Randomised, Diagnostic Accuracy Study. *Lancet Infect. Dis.* **2020**, *20* (3), 299–307. https://doi.org/10.1016/S1473-3099(19)30649-8.
(34) *WHO Operational Handbook on Tuberculosis*; 2021.
(35) Gagneux, S. Host – Pathogen Coevolution in Human Tuberculosis. *Philos. Trans. R. Soc. B* **2012**, *367* (1590), 850–859. https://doi.org/10.1098/rstb.2011.0316.
(36) Orme, I. M.; Robinson, R. T.; Cooper, A. M. The Balance between Protective and Pathogenic Immune Responses in the TB-Infected Lung. *Nat. Immunol.* **2015**, *16* (1), 57–63. https://doi.org/10.1038/ni.3048.
(37) Walzl, G.; Ronacher, K.; Hanekom, W.; Scriba, T. J.; Zumla, A. Immunological

Biomarkers of Tuberculosis. *Nat. Rev. Imunol.* **2011**, *11* (5), 343–354. https://doi.org/10.1038/nri2960.

(38) Russell, D. G. *Mycobacterium tuberculosis* and the Intimate Discourse of a Chronic Infection. *Immunol. Rev.* **2011**, *240* (1), 252–268. https://doi.org/10.1111/j.1600-065X.2010.00984.x.

(39) Wel, N. van der; Hava, D.; Houben, D.; Fluitsma, D.; Zon, M. van; Pierson, J.; Brenner, M.; Peters, P. J. *M. tuberculosis* and *M . leprae* Translocate from the Phagolysosome to the Cytosol in Myeloid Cells. *Cell* **2007**, *129* (7), 1287–1298. https://doi.org/10.1016/j.cell.2007.05.059.

(40) Houben, D.; Demangel, C.; Ingen, J. van; Perez, J.; Baldeón, L.; Abdallah, A. M.; Caleechurn, L.; Bottai, D.; Zon, M. van; Punder, K. de; Laan, T. van der; Kant, A.; Vries, R. B.; Willemsen, P.; Bitter, W.; Soolingen, D. van; Brosch, R.; Wel, N. van der; Peters, P. J. ESX-1-Mediated Translocation to the Cytosol Controls Virulence of Mycobacteria. *Cell. Microbiol.* **2012**, *14* (8), 1287–1298. https://doi.org/10.1111/j.1462-5822.2012.01799.x.

(41) Rubin, E. J. The Granuloma in Tuberculosis — Friend or Foe? *N. Engl. J. Med.* **2009**, *360* (23), 2471–2473. https://doi.org/10.1056/nejmcibr0902539.

(42) Silva Miranda, M.; Breiman, A.; Allain, S.; Deknuydt, F.; Altare, F. The Tuberculous Granuloma: An Unsuccessful Host Defence Mechanism Providing a Safety Shelter for the Bacteria? *Clin. Dev. Immunol.* **2012**, *2012*, 139127. https://doi.org/10.1155/2012/139127.

(43) Marakalala, M. J.; Raju, R. M.; Sharma, K.; Zhang, Y. J.; Eugenin, E. A.; Prideaux, B.; Daudelin, I. B.; Chen, P.-Y.; Booty, M. G.; Kim, J. H.; Eum, S. Y.; Via, L. E.; Behar, S. M.; Barry III, C. E.; Mann, M.; Dartois, V.; Rubin, E. J. Inflammatory Signaling in Human Tuberculosis Granulomas Is Spatially Organized. *Nat. Med.* **2016**, *22* (5), 531–538. https://doi.org/10.1038/nm.4073.

(44) Liu, C. H.; Liu, H.; Ge, B. Innate Immunity in Tuberculosis: Host Defense vs Pathogen Evasion. *Cell. Mol. Immunol.* **2017**, *14* (12), 963–975. https://doi.org/10.1038/cmi.2017.88.

(45) Koul, A.; Arnoult, E.; Lounis, N.; Guillemont, J.; Andries, K. The Challenge of New Drug Discovery for Tuberculosis. *Nature* **2011**, *469* (7331), 483–490. https://doi.org/10.1038/nature09657.

(46) Grosset, J. *Mycobacterium tuberculosis* in the Extracellular Compartment: An Underestimated Adversary. *Antimicrob. Agents Chemother.* **2003**, *47* (3), 833–836. https://doi.org/10.1128/AAC.47.3.833–836.2003.

(47) Yang, D.; Kong, Y. The Bacterial and Host Factors Associated with Extrapulmonary Dissemination of *Mycobacterium tuberculosis*. *Front. Biol.* **2015**, *10* (3), 252–261. https://doi.org/10.1007/s11515-015-1358-y.

(48) Asselineau, J.; Lederer, E. Structure of the Mycolic Acids of Mycobacteria. *Nature* **1950**, *166* (4227), 782–783. https://doi.org/10.1038/166782a0.

(49) Brennan, P. J.; Nikaido, H. The Envelope of Mycobacteria. *Annu. Rev. Biochem.* **1995**, *64*, 29–63. https://doi.org/10.1146/annurev.bi.64.070195.000333.

(50) Maeda, N.; Nigou, J.; Herrmann, J.-L.; Jackson, M.; Amara, A.; Lagrange, P. H.; Puzo, G.; Gicquel, B.; Neyrolles, O. The Cell Surface Receptor DC-SIGN Discriminates between *Mycobacterium* Species through Selective Recognition of the Mannose Caps on Lipoarabinomannan. *J. Biol. Chem.* **2003**, *278* (8), 5513–5516. https://doi.org/10.1074/jbc.C200586200.

(51) Reed, M. B.; Domenech, P.; Manca, C.; Su, H.; Barczak, A. K.; Kreiswirth, B. N.; Kaplan, G.; Barry III, C. E. A Glycolipid of Hypervirulent Tuberculosis Strains That Inhibits the Innate Immune Response. *Nature* **2004**, *431* (7004), 84–87. https://doi.org/10.1038/nature02837.

(52) Mohandas, P.; Budell, W. C.; Mueller, E.; Au, A.; Bythrow, G. V; Quadri, L. E. N. Pleiotropic Consequences of Gene Knockouts in the Phthiocerol Dimycocerosate and Phenolic Glycolipid Biosynthetic Gene Cluster of the Opportunistic Human Pathogen *Mycobacterium marinum*. *FEMS Microbiol. Lett.* **2016**, *363* (5), fbw016. https://doi.org/10.1093/femsle/fnw016.

(53) Christensen, H.; Garton, N. J.; Horobin, W.; Minnikin, D. E.; Barer, M. R. Lipid Domains of Mycobacteria Studied with Fluorescent Molecular Probes. *Mol. Microbiol.* **1999**, *31* (5), 1561–1572. https://doi.org/10.1046/j.1365-2958.1999.01304.x.

(54) Barksdale, L.; Kim, K. *Mycobacterium*. *Bacteriol. Rev.* **1977**, *41* (1), 217–372. https://doi.org/10.1128/br.41.1.217-372.1977.

(55) Zuber, B.; Chami, M.; Houssin, C.; Dubochet, J.; Griffiths, G.; Daffé, M. Direct Visualization of the Outer Membrane of Mycobacteria and Corynebacteria in Their Native State. *J. Bacteriol.* **2008**, *190* (16), 5672–5680. https://doi.org/10.1128/JB.01919-07.

(56) Brennan, P. J. Structure, Function, and Biogenesis of the Cell Wall of *Mycobacterium tuberculosis*. *Tuberculosis* **2003**, *83* (1–3), 91–97. https://doi.org/10.1016/S1472-9792(02)00089-6.

(57) Grzegorzewicz, A. E.; Pham, H.; Gundi, V. A. K. B.; Scherman, M. S.; North, E. J.; Hess, T.; Jones, V.; Gruppo, V.; Born, S. E. M.; Korduláková, J.; Chavadi, S. S.; Morisseau, C.; Lenaerts, A. J.; Lee, R. E.; McNeil, M. R.; Jackson, M. Inhibition of Mycolic Acid Transport across the *Mycobacterium tuberculosis* Plasma Membrane. *Nat. Chem. Biol.* **2012**, *8* (4), 334–341. https://doi.org/10.1038/nchembio.794.

(58) Dmitriev, B. A.; Ehlers, S.; Rietschel, E. T.; Brennan, P. J. Molecular Mechanics of the Mycobacterial Cell Wall: From Horizontal Layers to Vertical Scaffolds. *Int. J. Med. Microbiol.* **2000**, *290* (3), 251–258. https://doi.org/10.1016/S1438-4221(00)80122-8.

(59) Dmitriev, B.; Toukach, F.; Ehlers, S. Towards a Comprehensive View of the Bacterial Cell Wall. *Trends Microbiol.* **2005**, *13* (12), 569–574. The Bacterial and Host Factors Associated https://doi.org/10.1016/j.tim.2005.10.001.

(60) Liu, J.; Rosenberg, E. Y.; Nikaido, H. Fluidity of the Lipid Domain of Cell Wall from *Mycobacterium chelonae*. *Proc. Natl. Acad. Sci.* **1995**, *92* (24), 11254–11258. https://doi.org/10.1073/pnas.92.24.11254.

(61) Barry, C. E.; Crick, D. C.; McNeil, M. R. Targeting the Formation of the Cell Wall Core of *M. tuberculosis*. *Infect. Disord. - Drug Targets* **2007**, *7* (2), 182–202. https://doi.org/10.2174/187152607781001808.

(62) Crick, D. C.; Mahapatra, S.; Brennan, P. J. Biosynthesis of the Arabinogalactan-Peptidoglycan Complex of *Mycobacterium tuberculosis*. *Glycobiology* **2001**, *11* (9), 107–118. https://doi.org/10.1093/glycob/11.9.107r.

(63) Crick, D. C.; Chatterjee, D.; Scherman, M. S.; McNeil, M. R. Structure and Biosynthesis of the Mycobacterial Cell Wall. *Compr. Nat. Prod. II* **2010**, *6*, 381–406. https://doi.org/10.1016/B978-008045382-8.00173-8.

(64) Mishra, A. K.; Driessen, N. N.; Appelmelk, B. J.; Besra, G. S. Lipoarabinomannanand Relatedglycoconjugates: Structure, Biogenesis and Role in *Mycobacterium tuberculosis* Physiology and Host-Pathogen Interaction. *FEMS Microbiol. Rev.* **2011**, *35* (6), 1126–1157. https://doi.org/10.1111/j.1574-6976.2011.00276.x.

(65) Kaur, D.; Guerin, M.; Škovierová, H.; Brennan, P. J.; Jackson, M. Biogenesis of the Cell Wall and Other Glycoconjugates of *Mycobacterium tuberculosis*. *Adv. Appl. Microbiol.* **2009**, *69*, 23–78. https://doi.org/10.1016/S0065-2164(09)69002-X.

(66) Bansal-Mutalik, R.; Nikaido, H. Mycobacterial Outer Membrane Is a Lipid Bilayer and the Inner Membrane Is Unusually Rich in Diacyl Phosphatidylinositol Dimannosides. *Proc. Natl. Acad. Sci.* **2014**, *111* (13), 4958–4963. https://doi.org/10.1073/pnas.1403078111.

(67) Maitra, A.; Munshi, T.; Healy, J.; Martin, L. T.; Vollmer, W.; Keep, N. H.; Bhakta, S. Cell Wall Peptidoglycan in *Mycobacterium tuberculosis*: An Achilles' Heel for the TB-Causing Pathogen. *FEMS Microbiol. Rev.* **2019**, *43* (5), 548–575. https://doi.org/10.1093/femsre/fuz016.

(68) Brennan, P. J.; Crick, D. C. The Cell-Wall Core of *Mycobacterium tuberculosis* in the Context of Drug Discovery. *Curr. Top. Med. Chem.* **2007**, *7* (5), 475–488. https://doi.org/10.2174/156802607780059763.

(69) Ghazaei, C. *Mycobacterium tuberculosis* and Lipids: Insights into Molecular Mechanisms from Persistence to Virulence. *J. Res. Med. Sci.* **2018**, *23*, 63. https://doi.org/10.4103/jrms.JRMS.

(70) Hoffmann, C.; Leis, A.; Niederweis, M.; Plitzko, J. M.; Engelhardt, H. Disclosure of the Mycobacterial Outer Membrane: Cryo-Electron Tomography and Vitreous Sections Reveal the Lipid Bilayer Structure. *Proc. Natl. Acad. Sci.* **2008**, *105* (10), 3963–3967. https://doi.org/10.1073/pnas.0709530105.

(71) Batt, S. M.; Minnikin, D. E.; Besra, G. S. The Thick Waxy Coat of Mycobacteria, a Protective Layer against Antibiotics and the Host's Immune System. *Biochem. J.* **2020**, *477* (10), 1983–2006. https://doi.org/10.1042/BCJ20200194.

(72) Burke, D. S. Of Postulates and Peccadilloes: Robert Koch and Vaccine (Tuberculin) Therapy for Tuberculosis. *Vaccine* **1993**, *11* (8), 795–804. https://doi.org/10.1016/0264-410X(93)90354-Z.

(73) Vacchelli, E.; Galluzzi, L.; Eggermont, A.; Fridman, W. H.; Galon, J.; Sautès-Fridman, C.; Tartour, E.; Zitvogel, L.; Kroemer, G. Trial Watch: FDA-Approved Toll-like Receptor Agonists for Cancer Therapy. *Oncoimmunology* **2012**, *1* (6), 894–907. https://doi.org/10.4161/onci.20931.

(74) Luca, S.; Mihaescu, T. History of BCG Vaccine. *Mædica - a J. Clin. Med.* **2013**, *8* (1), 53–58.

(75) Andersen, P.; Doherty, T. M. The Success and Failure of BCG — Implications for a Novel Tuberculosis Vaccine. *Nat. Rev. Microbiol.* **2005**, *3* (8), 656–662. https://doi.org/10.1038/nrmicro1211.

(76) Abubakar, I.; Pimpin, L.; Ariti, C.; Beynon, R.; Mangtani, P.; Sterne, J. A. C.; Fine, P. E. M.; Smith, P. G.; Lipman, M.; Elliman, D.; Watson, J. M.; Drumright, L. N.; Whiting, P. F.; Vynnycky, E.; Rodrigues, L. C. Systematic Review and Meta-Analysis of the Current Evidence on the Duration of Protection by Bacillus Calmette–Guérin Vaccination against Tuberculosis. *Health Technol. Assess. (Rockv).* **2013**, *17* (37), 1–372. https://doi.org/10.3310/hta17370.

(77) Nguipdop-Djomo, P.; Heldal, E.; Rodrigues, L. C.; Abubakar, I.; Mangtani, P. Duration of BCG Protection against Tuberculosis and Change in Effectiveness with Time since Vaccination in Norway: A Retrospective Population-Based Cohort Study. *Lancet Infect. Dis.* **2016**, *16* (2), 219–226. https://doi.org/10.1016/S1473-3099(15)00400-4.

(78) Brandt, L.; Cunha, J. F.; Olsen, A. W.; Chilima, B.; Hirsch, P.; Appelberg, R.; Andersen, P. Failure of the *Mycobacterium bovis* BCG Vaccine: Some Species of Environmental Mycobacteria Block Multiplication of BCG and Induction of Protective Immunity to Tuberculosis. *Infect. Immun.* **2002**, *70* (2), 672–678. https://doi.org/10.1128/IAI.70.2.672–678.2002.

(79) Ritz, N.; Hanekom, W. A.; Robins-Browne, R.; Britton, W. J.; Curtis, N. Influence of BCG Vaccine Strain on the Immune Response and Protection against Tuberculosis. *FEMS Microbiol. Rev.* **2008**, *32* (5), 821–841. https://doi.org/10.1111/j.1574-6976.2008.00118.x.

(80) Trunz, B. B.; Fine, P.; Dye, C. Effect of BCG Vaccination on Childhood Tuberculous Meningitis and Miliary Tuberculosis Worldwide: A Meta- Analysis and Assessment of Cost-Effectiveness. *Lancet* **2002**, *367* (9517), 1173–1180. https://doi.org/10.1016/S0140-6736(06)68507-3.

(81) Roordink, D.; Williams, A.; Fritzell, B.; Laddy, D. J.; Gerdil, E.; Graffin, A. M.; Tait, D.; Pol, L. van der; Brink, I. van den; Holleman, M.; Thole, J.; Voss, G.; Lempicki, M.; Thiry, G. The TB Vaccine Development Pathway – An Innovative Approach to Accelerating Global TB Vaccine Development. *Tuberculosis* **2021**, *126*, 102040. https://doi.org/10.1016/j.tube.2020.102040.

(82) Martin, C.; Aguilo, N.; Marinova, D.; Gonzalo-Asensio, J. Update on TB Vaccine Pipeline. *Appl. Sci.* **2020**, *10* (7), 2632. https://doi.org/10.3390/app10072632.

(83) WHO. *Revised BCG Vaccination Guidelines for Children with HIV Infection*; 2007.

(84) Zwerling, A.; Behr, M. A.; Verma, A.; Brewer, T. F.; Menzies, D.; Pai, M. The BCG World Atlas: A Database of Global BCG Vaccination Policies and Practices. *PLoS Med.* **2011**, *8* (3), e1001012. https://doi.org/10.1371/journal.pmed.1001012.

(85) Ahmed, A.; Rakshit, S.; Adiga, V.; Dias, M.; Dwarkanath, P.; D'Souza, G.; Vyakarnam, A. A Century of BCG: Impact on Tuberculosis Control and Beyond. *Immunol. Rev.* **2021**,

*301* (1), 98–121. https://doi.org/10.1111/imr.12968.

(86) Thomas J. Scriba; Tameris, M.; Mansoor, N.; Smit, E.; Merwe, L. van der; Isaacs, F.; Keyser, A.; Moyo, S.; Brittain, N.; Lawrie, A.; Gelderbloem, S.; Veldsman, A.; Hatherill, M.; Hawkridge, A.; Hill, A. V. S.; Hussey, G. D.; Mahomed, H.; McShane, H.; Hanekom, W. A. Modified Vaccinia Ankara-Expressing Ag85A, a Novel Tuberculosis Vaccine, Is Safe in Adolescents and Children, and Induces Polyfunctional CD4+ T Cells. *Eur. J. Immunol.* **2010**, *40* (1), 279–290. https://doi.org/10.1002/eji.200939754.

(87) Tameris, M. D.; Hatherill, M.; Landry, B. S.; Scriba, T. J.; Snowden, M. A.; Lockhart, S.; Shea, J. E.; McClain, J. B.; Hussey, G. D.; Hanekom, W. A.; Mahomed, H.; McShane, H.; MVA85A 020 Trial Study Team. Safety and Efficacy of MVA85A, a New Tuberculosis Vaccine, in Infants Previously Vaccinated with BCG: A Randomised, Placebo-Controlled Phase 2b Trial. *Lancet* **2013**, *381* (9871), 1021–1028. https://doi.org/10.1016/S0140-6736(13)60177-4.

(88) Gopalaswamy, R., Subbian, S. An Update on Tuberculosis Vaccines. In *Vaccine Design. Methods and Protocols. Volume 1: Vaccines for Human Diseases*; Humana, New York, NY, 2022; pp 387–409. https://doi.org/10.1016/0167-7799(94)90132-5.

(89) Behr, M. A.; Kaufmann, E.; Duffin, J.; Edelstein, P. H.; Ramakrishnan, L. Latent Tuberculosis: Two Centuries of Confusion. *Am. J. Respir. Crit. Care Med.* **2021**, *204* (2), 142–148. https://doi.org/10.1164/rccm.202011-4239PP.

(90) Meeren, O. van der; Hatherill, M.; Nduba, V.; Wilkinson, R. J.; Muyoyeta, M.; Brakel, E. Van; Ayles, H. M.; Henostroza, G.; Thienemann, F.; Scriba, T. J.; Diacon, A.; Blatner, G. L.; Demoitié, M.-A.; Tameris, M.; Malahleha, M.; Innes, J. C.; Hellström, E.; Martinson, N.; Singh, T.; Akite, E. J.; Azam, A. K.; Bollaerts, A.; Ginsberg, A. M.; Evans, T. G.; Gillard, P.; Tait, D. R. Phase 2b Controlled Trial of M72/AS01$_E$ Vaccine to Prevent Tuberculosis. *N. Engl. J. Med.* **2018**, *379* (17), 1621–1634. https://doi.org/10.1056/NEJMoa1803484.

(91) Tait, D. R.; Hatherill, M.; Meeren, O. Van Der; Ginsberg, A. M.; Brakel, E. Van; Salaun, B.; Scriba, T. J.; Akite, E. J.; Ayles, H. M.; Bollaerts, A.; Demoitié, M.-A.; Diacon, A.; Evans, T. G.; Gillard, P.; Hellström, E.; Innes, J. C.; Lempicki, M.; Malahleha, M.; Martinson, N.; Vela, D. M.; Muyoyeta, M.; Nduba, V.; Pascal, T. G.; Tameris, M.; Thienemann, F.; Wilkinson, R. J.; Roman, F. Final Analysis of a Trial of M72/AS01$_E$ Vaccine to Prevent Tuberculosis. *N. Engl. J. Med.* **2019**, *381* (25), 2429–2439. https://doi.org/10.1056/NEJMoa1909953.

(92) Chaisson, R. E.; Frick, M.; Nahid, P. The Scientific Response to TB – the Other Deadly Global Health Emergency. *Int. J. Tuberc. Lung Dis.* **2022**, *26* (3), 186–189. https://doi.org/10.5588/ijtld.21.0734.

(93) Harris, R. C.; Quaife, M.; Weerasuriya, C.; Gomez, G. B.; Sumner, T.; Bozzani, F.; White, R. G. Cost-Effectiveness of Routine Adolescent Vaccination with an M72/AS01$_E$-like Tuberculosis Vaccine in South Africa and India. *Nat. Commun.* **2022**, *13* (1), 602. https://doi.org/10.1038/s41467-022-28234-7.

(94) Hinshaw, H. C.; Feldman, W. H.; Pfuetze, K. H. Treatment of Tuberculosis with Streptomycin. A Summary of Observations on One Hundred Cases. *J. Am. Med. Assoc.* **1946**, *132* (13), 778–782. https://doi.org/10.1001/jama.1946.02870480024007.

(95) Hasan, A. History of TB: Robert Koch and Beyond. In *Mycobacterium Pathogenesis, Diagnostics Infection Biology, tuberculosis: Molecular and New Interventions*; 2019; pp 3–16. https://doi.org/10.1007/978-981-32-9413-4.

(96) Daniel, T. M. Rifampin — A Major New Chemotherapeutic Agent for the Treatment of Tuberculosis. *N. Engl. J. Med.* **1969**, *280* (11), 615–616. https://doi.org/10.1056/NEJM196903132801112.

(97) Vall-Spinosa, A.; Lester, W.; Moulding, T.; Davidson, P. T.; McClatchy, J. K. Rifampin in the Treatment of Drug-Resistant *Mycobacterium tuberculosis* Infections. *N. Engl. J. Med.* **1970**, *283* (12), 616–621. https://doi.org/10.1056/NEJM197009172831202.

(98) WHO. *Guidelines for Treatment of Drug-Susceptible Tuberculosis and Patient Care*; 2017.

(99) Horsburgh, C. R.; Barry III, C. E.; Lange, C. Treatment of Tuberculosis. *N. Engl. J. Med.*

**2015**, *373* (22), 2149–2160. https://doi.org/10.1056/NEJMra1413919.

(100) Conradie, F.; Diacon, A. H.; Ngubane, N.; Howell, P.; Everitt, D.; Crook, A. M.; Mendel, C. M.; Egizi, E.; Moreira, J.; Timm, J.; McHugh, T. D.; Wills, G. H.; Bateson, A.; Hunt, R.; Niekerk, C. Van; Li, M.; Olugbosi, M.; Spigelman, M. Treatment of Highly Drug-Resistant Pulmonary Tuberculosis. *N. Engl. J. Med.* **2020**, *382* (10), 893–902. https://doi.org/10.1056/NEJMoa1901814.

(101) Kieser, K. J.; Rubin, E. J. How Sisters Grow Apart: Mycobacterial Growth and Division. *Nat. Rev. Microbiol.* **2014**, *12* (8), 550–562. https://doi.org/10.1038/nrmicro3299.

(102) Viney, K.; Linh, N. N.; Gegia, M.; Zignol, M.; Glaziou, P.; Ismail, N.; Kasaeva, T.; Mirzayev, F. New Definitions of Pre-Extensively and Extensively Drug-Resistant Tuberculosis: Update from the World Health Organization. *Eur. Respir. J.* **2021**, *57* (4), 2100361. https://doi.org/10.1183/13993003.00361-2021.

(103) Bahuguna, A.; Rawat, D. S. An Overview of New Antitubercular Drugs, Drug Candidates, and Their Targets. *Med. Res. Rev.* **2019**, *40* (1), 263–292. https://doi.org/10.1002/med.21602.

(104) Zha, B. S.; Nahid, P. Treatment of Drug-Susceptible Tuberculosis. *Clin. Chest Med.* **2019**, *40* (4), 763–774. https://doi.org/10.1016/j.ccm.2019.07.006.

(105) Mitchison, D.; Davies, G. The Chemotherapy of Tuberculosis: Past, Present and Future. *Int. J. Tuberc. Lung Dis.* **2012**, *16* (6), 724–732. https://doi.org/10.5588/ijtld.12.0083.

(106) Karumbi, J.; Garner, P. Directly Observed Therapy for Treating Tuberculosis (Review). *Cochrane Database Syst. Rev.* **2015**, *2015* (5), CD003343. https://doi.org/10.1002/14651858.CD003343.pub4.

(107) *WHO Consolidated Guidelines on Drug-Resistant Tuberculosis Treatment. Geneva: World Health Organization*; 2019.

(108) Keshavjee, S.; Farmer, P. E. Tuberculosis, Drug Resistance, and the History of Modern Medicine. *N. Engl. J. Med.* **2012**, *367* (10), 931–936. https://doi.org/10.1056/NEJMra1205429.

(109) Chakraborty, S.; Rhee, K. Y. Tuberculosis Drug Development: History and Evolution of the Mechanism-Based Paradigm. *Cold Spring Harb. Perspect. Med.* **2015**, *5* (8), a021147. https://doi.org/10.1101/cshperspect.a021147.

(110) Fox, W.; Ellard, G. A.; Mitchison, D. A. Studies on the Treatment of Tuberculosis Undertaken by the British Medical Research Council Tuberculosis Units, 1946–1986, with Relevant Subsequent Publications. *Int. J. Tuberc. Lung Dis.* **1999**, *3* (10), S231–S279.

(111) Ma, Z.; Lienhardt, C.; Mcilleron, H.; Nunn, A. J.; Wang, X. Global Tuberculosis Drug Development Pipeline: The Need and the Reality. *Lancet* **2010**, *375* (9731), 2100–2109. https://doi.org/10.1016/S0140-6736(10)60359-9.

(112) Diacon, A. H.; Donald, P. R. The Early Bactericidal Activity of Antituberculosis Drugs. *Expert Rev. Anti. Infect. Ther.* **2014**, *12* (2), 223–237. https://doi.org/10.1586/14787210.2014.870884.

(113) Connolly, L. E.; Edelstein, P. H.; Ramakrishnan, L. Why Is Long-Term Therapy Required to Cure Tuberculosis? *PLoS Med.* **2007**, *4* (3), e120. https://doi.org/10.1371/journal.pmed.0040120.

(114) Ginsberg, A. M.; Spigelman, M. Challenges in Tuberculosis Drug Research and Development. *Nat. Med.* **2007**, *13* (3), 290–294. https://doi.org/10.1038/nm0307-290.

(115) Sotgiu, G.; Tiberi, S.; D'Ambrosio, L.; Centis, R.; Alffenaar, J. W.; Caminero, J. A.; Arbex, M. A.; Guizado, V. A.; Aleksa, A.; Dore, S.; Gaga, M.; Gualano, G.; Kunst, H.; Payen, M.-C.; Arias, A. J. R.; Skrahina, A.; Solovic, I.; Sulis, G.; Tadolini, M.; Zumla, A.; Migliori, G. B. Faster for Less: The New "Shorter" Regimen for Multidrug-Resistant Tuberculosis. *Eur. Respir. J.* **2016**, *48* (5), 1503–1507. https://doi.org/10.1183/13993003.01249-2016.

(116) Mcilleron, H.; Meintjes, G.; Burman, W. J.; Maartens, G. Complications of Antiretroviral Therapy in Patients with Tuberculosis: Drug Interactions, Toxicity, and Immune Reconstitution Inflammatory Syndrome. *J. Infect. Dis.* **2007**, *196*, S63–S75. https://doi.org/10.1086/518655.

(117) Bernstein, J.; Lott, W. A.; Steinberg, B. A.; Yale, H. L. Chemotherapy of Experimental

Tuberculosis. V. Isonicotinic Acid Hydrazide (Nydrazid) and Related Compounds. *Am. Rev. Tuberc.* **1952**, *65* (4), 357–364.

(118) Meyer, H.; Mally, J. Über Hydrazinderivate Der Pyridincarbonsäuren. *Monatshefte für Chemie und verwandte Teile anderer Wissenschaften* **1912**, *33*, 393–414. https://doi.org/10.1007/BF01517946.

(119) Banerjee, A.; Dubnau, E.; Quemard, A.; Balasubramanian, V.; Um, K. S.; Wilson, T.; Collins, D.; Lisle, G. de; Jacobs Jr., W. R. InhA, a Gene Encoding a Target for Isoniazid and Ethionamide in *Mycobacterium tuberculosis*. *Science.* **1993**, *263* (5144), 227–230. https://doi.org/10.1126/science.8284673.

(120) Timmins, G. S.; Deretic, V. Mechanisms of Action of Isoniazid. *Mol. Microbiol.* **2006**, *62* (5), 1220–1227. https://doi.org/10.1111/j.1365-2958.2006.05467.x.

(121) Unissa, A. N.; Subbian, S.; Hanna, L. E.; Selvakumar, N. Overview on Mechanisms of Isoniazid Action and Resistance in *Mycobacterium tuberculosis*. *Infect. Genet. Evol.* **2016**, *45*, 474–492. https://doi.org/10.1016/j.meegid.2016.09.004.

(122) Johnsson, K.; Schultz, P. G. Mechanistic Studies of the Oxidation of Isoniazid by the Catalase Peroxidase from *Mycobacterium tuberculosis J. Am. Chem. Soc.* **1994**, *116* (16), 7425–7426. https://doi.org/10.1021/ja00095a063.

(123) Timmins, G. S.; Master, S.; Rusnak, F.; Deretic, V. Nitric Oxide Generated from Isoniazid Activation by KatG: Source of Nitric Oxide and Activity against *Mycobacterium tuberculosis*. *Antimicrob. Agents Chemother.* **2004**, *48* (8), 3006–3009. https://doi.org/10.1128/AAC.48.8.3006–3009.2004.

(124) Vilchèze, C.; Jacobs Jr., W. R. The Mechanism of Isoniazid Killing : Clarity Through the Scope of Genetics. *Annu. Rev. Microbiol.* **2007**, *61*, 35–50. https://doi.org/10.1146/annurev.micro.61.111606.122346.

(125) Isoniazid. *Tuberculosis* **2008**, *88* (2), 112–116. https://doi.org/10.1016/S1472-9792(08)70011-8.

(126) Jnawali, H. N.; Ryoo, S. First – and Second – Line Drugs and Drug Resistance. In *Tuberculosis - Current Issues in Diagnosis and Management*; Vats, B. H. M., G., M., Eds.; InTechOpen, 2013; pp 163–180. https://doi.org/10.5772/54960.

(127) Mitchison, D. A. The Action of Antituberculosis Drugs in Short-Course Chemotherapy. *Tubercle* **1985**, *66* (3), 219–225. https://doi.org/10.1016/0041-3879(85)90040-6.

(128) Zhang, Y.; Shi, W.; Zhang, W.; Mitchison, D. Mechanisms of Pyrazinamide Action and Resistance. *Microbiol. Spectr.* **2014**, *2* (4), MGM2-0023–2013. https://doi.org/10.1128/microbiolspec.MGM2-0023-2013.

(129) Falzon, D.; Schünemann, H. J.; Harausz, E.; González-angulo, L.; Lienhardt, C.; Jaramillo, E.; Weyer, K. World Health Organization Treatment Guidelines for Drug-Resistant Tuberculosis, 2016 Update. *Eur. Respir. J.* **2017**, *49* (3), 1602308. https://doi.org/10.1183/13993003.02308-2016.

(130) Rosenthal, I. M.; Zhang, M.; Williams, K. N.; Peloquin, C. A.; Tyagi, S.; Vernon, A. A.; Bishai, W. R.; Chaisson, R. E.; Grosset, J. H.; Nuermberger, E. L. Daily Dosing of Rifapentine Cures Tuberculosis in Three Months or Less in the Murine Model. *PLoS Med.* **2007**, *4* (12), e344. https://doi.org/10.1371/journal.pmed.0040344.

(131) Nuermberger, E.; Tyagi, S.; Tasneen, R.; Williams, K. N.; Almeida, D.; Rosenthal, I.; Grosset, J. H. Powerful Bactericidal and Sterilizing Activity of a Regimen Containing PA-824, Moxifloxacin, and Pyrazinamide in a Murine Model of Tuberculosis. *Antimicrob. Agents Chemother.* **2008**, *52* (4), 1522–1524. https://doi.org/10.1128/AAC.00074-08.

(132) Veziris, N.; Ibrahim, M.; Lounis, N.; Chauffour, A.; Truffot-Pernot, C.; Andries, K.; Jarlier, V. A Once-Weekly R207910-Containing Regimen Exceeds Activity of the Standard Daily Regimen in Murine Tuberculosis. *Am. J. Respir. Crit. Care Med.* **2009**, *179* (1), 75–79. https://doi.org/10.1164/rccm.200711-1736OC.

(133) Konno, K.; Feldmann, F. M.; Mcdermott, W. Pyrazinamide Susceptibility and Amidase Activity of Tubercle Bacilli. *Am. Rev. Respir. Dis.* **1966**, *95* (3), 461–469. https://doi.org/10.1164/arrd.1967.95.3.461.

(134) Scorpio, A.; Zhang, Y. Mutations in PncA, a Gene Encoding Pyrazinamidase/Nicotinamidase, Cause Resistance to the Antituberculous Drug

Pyrazinamide in Tubercle Bacillus. *Nat. Med.* **1996**, *2* (6), 662–667. https://doi.org/10.1038/nm0696-662.

(135) Shi, W.; Zhang, X.; Jiang, X.; Yuan, H.; Lee, J. S.; Barry III, C. E.; Wang, H.; Zhang, W.; Zhang, Y. Pyrazinamide Inhibits Trans-Translation in *Mycobacterium tuberculosis*. *Science*. **2011**, *333* (6049), 1630–1632. https://doi.org/10.1126/science.1208813.

(136) Zhang, S.; Chen, J.; Shi, W.; Liu, W.; Zhang, W.; Zhang, Y. Mutations in PanD Encoding Aspartate Decarboxylase Are Associated with Pyrazinamide Resistance in *Mycobacterium tuberculosis*. *Emerg. Microbes Infect.* **2013**, *2*, e34. https://doi.org/10.1038/emi.2013.38.

(137) Zhang, Y.; Mitchison, D. The Curious Characteristics of Pyrazinamide: A Review. *J. Tuberc. Lung Dis.* **2003**, *7* (1), 6–21.

(138) Zhang, Y.; Wade, M. M.; Scorpio, A.; Zhang, H.; Sun, Z. Mode of Action of Pyrazinamide: Disruption of *Mycobacterium tuberculosis* Membrane Transport and Energetics by Pyrazinoic Acid. *J. Antimicrob. Chemother.* **2003**, *52* (5), 790–795. https://doi.org/10.1093/jac/dkg446.

(139) Yee, D.; Valiquette, C.; Pelletier, M.; Parisien, I.; Rocher, I.; Menzies, D. Incidence of Serious Side Effects from First-Line Antituberculosis Drugs among Patients Treated for Active Tuberculosis. *Am. J. Respir. Crit. Care Med.* **2003**, *167*, 1472–1477. https://doi.org/10.1164/rccm.200206-626OC.

(140) Ethambutol. *Tuberculosis* **2008**, *88* (2), 102–105. https://doi.org/10.1016/S1472-9792(08)70008-8.

(141) Goude, R.; Amin, A. G.; Chatterjee, D.; Parish, T. The Arabinosyltransferase EmbC Is Inhibited by Ethambutol in *Mycobacterium tuberculosis*. *Antimicrob. Agents Chemother.* **2009**, *53* (10), 4138–4146. https://doi.org/10.1128/AAC.00162-09.

(142) Takayama, K.; Kilburn, J. Inhibition of Synthesis of Arabinogalactan by Ethambutol in *Mycobacterium smegmatis*. *Antimicrob. Agents Chemother.* **1989**, *33* (9), 1493–1499. https://doi.org/10.1128/AAC.33.9.1493.

(143) Wolucka, B. A.; McNeil, M. R.; Hoffmann, E.; Chojnacki, T.; Brennan, P. J. Recognition of the Lipid Intermediate for Arabinogalactan/Arabinomannan Biosynthesis and Its Relation to the Mode of Action of Ethambutol on Mycobacteria. *J. Biol. Chem.* **1994**, *269* (37), 23328–23335. https://doi.org/10.1016/S0021-9258(17)31657-5.

(144) Zhang, Y.; Yew, W.-W. Mechanisms of Drug Resistance in *Mycobacterium tuberculosis*: Update 2015. *Int. J. Tuberc. Lung Dis.* **2015**, *19* (11), 1276–1289. https://doi.org/10.5588/ijtld.15.0389.

(145) Palomino, J. C.; Martin, A. Drug Resistance Mechanisms in *Mycobacterium tuberculosis*. *Antibiotics* **2014**, *3*, 317–340. https://doi.org/10.3390/antibiotics3030317.

(146) *WHO Consolidated Guidelines on Tuberculosis. Module 4: Treatment - Drug-Resistant Tuberculosis Treatment; Geneva: World Health Organization, 2020*; 2020.

(147) Jager, P. de; Altena, R. van. Hearing loss and nephrotoxicity in long-term aminoglycoside treatment in patients with tuberculosis. *Int. J. Tuberc. Lung Dis.* **2002**, *6* (7), 622–627.

(148) Streptomycin. *Tuberculosis* **2008**, *88* (2), 162–163. https://doi.org/10.1016/S1472-9792(08)70027-1.

(149) Amikacin. *Tuberculosis* **2008**, *88* (2), 87–88. https://doi.org/10.1016/S1472-9792(08)70003-9.

(150) Verbist, L.; Gyselen, A. Antituberculous Activity of Rifampin *in vitro* and *in vivo* and the Concentrations Attained in Human Blood. *Am. Rev. Respir. Dis.* **1968**, *98* (6), 923–932. https://doi.org/10.1164/arrd.1968.98.6.923.

(151) Wehrli, W.; Knüsel, F.; Schmid, K.; Staehelin, M. Interaction of Rifamycin with Bacterial RNA Polymerase. *Proc. Natl. Acad. Sci.* **1968**, *61* (2), 667–673. https://doi.org/10.1073/pnas.61.2.667.

(152) Wehrli, W. Rifampin: Mechanisms of Action and Resistance. *Rev. Infect. Dis.* **1983**, *5*, S407-411. https://doi.org/10.1093/clinids/5.Supplement_3.S407.

(153) Ramaswamy, S.; Musser, J. M. Molecular Genetic Basis of Antimicrobial Agent Resistance in *Mycobacterium tuberculosis*: 1998 Update. *Tuber. Lung Dis.* **1998**, *79* (1), 3–29. https://doi.org/10.1054/tuld.1998.0002.

(154) Rifampin. *Tuberculosis* **2008**, *88* (2), 151–154. https://doi.org/10.1016/S1472-9792(08)70024-6.
(155) Steenwinkel, J. E. M. de; Knegt, G. J. de; Kate, M. T. ten; Belkum, A. van; Verbrugh, H. A.; Kremer, K.; Soolingen, D. van; Bakker-Woudenberg, I. A. J. M. Time–Kill Kinetics of Anti-Tuberculosis Drugs, and Emergence of Resistance, in Relation to Metabolic Activity of *Mycobacterium tuberculosis J. Antimicrob. Chemother.* **2010**, *65* (12), 2582–2589. https://doi.org/10.1093/jac/dkq374.
(156) Goldstein, B. P. Resistance to Rifampicin: A Review. *J. Antibiot. (Tokyo).* **2014**, *67* (9), 625–630. https://doi.org/10.1038/ja.2014.107.
(157) Semvua, H. H.; Kibiki, G. S.; Kisanga, E. R.; Boeree, M. J.; Burger, D. M.; Aarnoutse, R. Pharmacological Interactions Between Rifampicin and Antiretroviral Drugs: Challenges and Research Priorities for Resource-Limited Settings. *Ther. Drug Monit.* **2015**, *37* (1), 22–32. https://doi.org/10.1097/FTD.0000000000000108.
(158) Dheda, K.; Gumbo, T.; Maartens, G.; Dooley, K. E.; McNerney, R.; Murray, M.; Furin, J.; Nardell, E. A.; London, L.; Lessem, E.; Theron, G.; Helden, P. van; Niemann, S.; Merker, M.; Dowdy, D.; Rie, A. Van; Siu, G. K. H.; Pasipanodya, J. G.; Rodrigues, C.; Clark, T. G.; Sirgel, F. A.; Esmail, A.; Lin, H.-H.; Atre, S. R.; Schaaf, H. S.; Chang, K. C.; Lange, C.; Nahid, P.; Udwadia, Z. F.; Horsburgh Jr, C. R.; Churchyard, G. J.; Menzies, D.; Hesseling, A. C.; Nuermberger, E.; McIlleron, H.; Fennelly, K. P.; Goemaere, E.; Jaramillo, E.; Low, M.; Jara, C. M.; Padayatchi, N.; Warren, R. M. The Epidemiology, Pathogenesis, Transmission, Diagnosis, and Management of Multidrug-Resistant, Extensively Drug-Resistant, and Incurable Tuberculosis. *Lancet Respir. Med. Comm.* **2017**, *5* (4), 291–360. https://doi.org/10.1016/S2213-2600(17)30079-6.
(159) Parida, S. K.; Axelsson-Robertson, R.; Rao, M. V.; Singh, N.; Master, I.; Lutckii, A.; Keshavjee, S.; Andersson, J.; Zumla, A.; Maeurer, M. Totally Drug-Resistant Tuberculosis and Adjunct Therapies. *J. Intern. Med.* **2015**, *277* (4), 388–405. https://doi.org/10.1111/joim.12264.
(160) Mase, S. R.; Chorba, T. Treatment of Drug-Resistant Tuberculosis. *Clin. Chest Med.* **2019**, *40* (4), 775–795. https://doi.org/10.1016/j.ccm.2019.08.002.
(161) WHO. The Use of Delamanid in the Treatment of Multidrug-Resistant Tuberculosis - Interim Policy Guidance. **2014**.
(162) https://www.newtbdrugs.org/pipeline/discovery (accessed on 27th March, 2023).
(163) https://www.newtbdrugs.org/pipeline/clinical (accessed on 27th March, 2023).
(164) Degiacomi, G.; Belardinelli, J. M.; Pasca, M. R.; Rossi, E. De; Riccardi, G.; Chiarelli, L. R. Promiscuous Targets for Antitubercular Drug Discovery: The Paradigm of DprE1 and MmpL3. *Appl. Sci.* **2020**, *10* (2), 623. https://doi.org/10.3390/app10020623.
(165) Oh, S.; Trifonov, L.; Yadav, V. D.; Barry III, C. E.; Boshoff, H. I. Tuberculosis Drug Discovery: A Decade of Hit Assessment for Defined Targets. *Front. Cell. Infect. Microbiol.* **2021**, *11*, 611304. https://doi.org/10.3389/fcimb.2021.611304.
(166) Camacho, L. R.; Constant, P.; Raynaud, C.; Lanéelle, M.-A.; Triccas, J. A.; Gicquel, B.; Daffé, M.; Guilhot, C. Analysis of the Phthiocerol Dimycocerosate Locus of *Mycobacterium*. *J. Biol. Chem.* **2001**, *276* (23), 19845–19854. https://doi.org/10.1074/jbc.M100662200.
(167) Converse, S. E.; Mougous, J. D.; Leavell, M. D.; Leary, J. A.; Bertozzi, C. R.; Cox, J. S. MmpL8 Is Required for Sulfolipid-1 Biosynthesis and *Mycobacterium tuberculosis* Virulence. *Proc. Natl. Acad. Sci.* **2003**, *100* (10), 6121–6126. https://doi.org/10.1073/pnas.1030024100.
(168) Pacheco, S. A.; Hsu, F.-F.; Powers, K. M.; Purdy, G. E. MmpL11 Protein Transports Mycolic Acid-Containing Lipids to the Mycobacterial Cell Wall and Contributes to Biofilm Formation in *Mycobacterium smegmatis*. *J. Biol. Chem.* **2013**, *288* (33), 24213–24222. https://doi.org/10.1074/jbc.M113.473371.
(169) Wells, R. M.; Jones, C. M.; Xi, Z.; Speer, A.; Danilchanka, O.; Doornbos, K. S.; Sun, P.; Wu, F.; Tian, C.; Niederweis, M. Discovery of a Siderophore Export System Essential for Virulence of *Mycobacterium tuberculosis*. *PLoS Pathog.* **2013**, *9* (1), e1003120. https://doi.org/10.1371/journal.ppat.1003120.

(170) Belardinelli, J. M.; Larrouy-Maumus, G.; Jones, V.; Pedro, L.; Carvalho, S. de; McNeil, M. R.; Jackson, M. Biosynthesis and Translocation of Unsulfated Acyltrehaloses in *Mycobacterium tuberculosis*. *J. Biol. Chem.* **2014**, *289* (40), 27952–27965. https://doi.org/10.1074/jbc.M114.581199.

(171) Domenech, P.; Reed, M. B.; Barry III, C. E. Contribution of the *Mycobacterium tuberculosis* MmpL Protein Family to Virulence and Drug Resistance. *Infect. Immun.* **2005**, *73* (6), 3492–3501. https://doi.org/10.1128/IAI.73.6.3492–3501.2005.

(172) Li, W.; Obregón-Henao, A.; Wallach, J. B.; North, E. J.; Lee, R. E.; Gonzalez-Juarrero, M.; Schnappinger, D.; Jackson, M. Therapeutic Potential of the *Mycobacterium tuberculosis* Mycolic Acid Transporter, MmpL3. *Antimicrob. Agents Chemother.* **2016**, *60* (9), 5198–5207. https://doi.org/10.1128/AAC.00826-16.

(173) Belardinelli, J. M.; Yazidi, A.; Yang, L.; Fabre, L.; Li, W.; Jacques, B.; Angala, S. K.; Rouiller, I.; Zgurskaya, H. I.; Sygusch, J.; Jackson, M. Structure-Function Profile of MmpL3, the Essential Mycolic Acid Transporter from *Mycobacterium tuberculosis*. *ACS Infect. Dis.* **2016**, *2* (10), 702–713. https://doi.org/10.1021/acsinfecdis.6b00095.

(174) Carel, C.; Nukdee, K.; Cantaloube, S.; Bonne, M.; Diagne, C. T.; Laval, F.; Daffé, M.; Zerbib, D. *Mycobacterium tuberculosis* Proteins Involved in Mycolic Acid Synthesis and Transport Localize Dynamically to the Old Growing Pole and Septum. *PLoS One* **2014**, *9* (5), e97148. https://doi.org/10.1371/journal.pone.0097148.

(175) Xu, Z.; Meshcheryakov, V. A.; Poce, G.; Chng, S.-S. MmpL3 Is the Flippase for Mycolic Acids in Mycobacteria. *Proc. Natl. Acad. Sci.* **2017**, *114* (30), 7993–7998. https://doi.org/10.1073/pnas.1700062114.

(176) Zhang, B.; Li, J.; Yang, X.; Wu, L.; Zhang, J.; Yang, Y.; Zhao, Y.; Zhang, L.; Yang, X.; Yang, X.; Cheng, X.; Liu, Z.; Jiang, B.; Jiang, H.; Guddat, L. W.; Yang, H.; Rao, Z. Crystal Structures of Membrane Transporter MmpL3, an Anti-TB Drug Target. *Cell* **2019**, *176* (3), 636–648. https://doi.org/10.1016/j.cell.2019.01.003.

(177) Su, C.-C.; Klenotic, P. A.; Bolla, J. R.; Purdy, G. E.; Robinson, C. V; Yu, E. W. MmpL3 Is a Lipid Transporter That Binds Trehalose Monomycolate and Phosphatidylethanolamine. *Proc. Natl. Acad. Sci.* **2019**, *116* (23), 11241–11246. https://doi.org/10.1073/pnas.1901346116.

(178) Seeger, M. A.; Diederichs, K.; Eicher, T.; Brandstätter, L.; Schiefner, A.; Verrey, F.; Pos, K. M. The AcrB Efflux Pump: Conformational Cycling and Peristalsis Lead to Multidrug Resistance. *Curr. Drug Targets* **2008**, *9* (9), 729–749. https://doi.org/10.2174/138945008785747789.

(179) Tsukazaki, T.; Mori, H.; Echizen, Y.; Ishitani, R.; Fukai, S.; Tanaka, T.; Perederina, A.; Vassylyev, D. G.; Kohno, T.; Maturana, A. D.; Ito, K.; Nureki, O. Structure and Function of a Membrane Component SecDF That Enhances Protein Export. *Nature* **2011**, *474* (7350), 235–238. https://doi.org/10.1038/nature09980.

(180) Umare, M. D.; Khedekar, P. B.; Chikhale, R. V. Mycobacterial Membrane Protein Large 3 (MmpL3) Inhibitors: A Promising Approach to Combat Tuberculosis. *ChemMedChem* **2021**, *16* (20), 3136–3148. https://doi.org/10.1002/cmdc.202100359.

(181) Rosa, V. La; Poce, G.; Canseco, J. O.; Buroni, S.; Pasca, M. R.; Biava, M.; Raju, R. M.; Porretta, G. C.; Alfonso, S.; Battilocchio, C.; Javid, B.; Sorrentino, F.; Ioerger, T. R.; Sacchettini, J. C.; Manetti, F.; Botta, M.; Logu, A. De; Rubin, E. J.; Rossi, E. De. MmpL3 Is the Cellular Target of the Antitubercular Pyrrole Derivative BM212. *Antimicrob. Agents Chemother.* **2012**, *56* (1), 324–331. https://doi.org/10.1128/AAC.05270-11.

(182) Deidda, D.; Lampis, G.; Fioravanti, R.; Biava, M.; Porretta, G. C.; Zanetti, S.; Pompei, R. Bactericidal Activities of the Pyrrole Derivative BM212 against Multidrug-Resistant and Intramacrophagic *Mycobacterium tuberculosis* Strains. *Antimicrob. Agents Chemother.* **1998**, *42* (11), 3035–3037. https://doi.org/10.1128/AAC.42.11.3035.

(183) Tahlan, K.; Wilson, R.; Kastrinsky, D. B.; Arora, K.; Nair, V.; Fischer, E.; Barnes, S. W.; Walker, J. R.; Alland, D.; Barry III, C. E.; Boshoff, H. I. SQ109 Targets MmpL3 , a Membrane Transporter of Trehalose Monomycolate Involved in Mycolic Acid Donation to the Cell Wall Core of *Mycobacterium tuberculosis*. *Antimicrob. Agents Chemother.* **2012**, *56* (4), 1797–1809. https://doi.org/10.1128/AAC.05708-11.

(184) North, E. J.; Scherman, M. S.; Bruhn, D. F.; Scarborough, J. S.; Maddox, M. M.; Jones, V.; Grzegorzewicz, A.; Yang, L.; Hess, T.; Morisseau, C.; Jackson, M.; McNeil, M. R.; Lee, R. E. Design, Synthesis and Anti-Tuberculosis Activity of 1-Adamantyl-3-Heteroaryl Ureas with Improved *in vitro* Pharmacokinetic Properties. *Bioorg. Med. Chem.* **2013**, *21* (9), 2587–2599. https://doi.org/10.1016/j.bmc.2013.02.028.

(185) Brown, J. R.; North, E. J.; Hurdle, J. G.; Morisseau, C.; Scarborough, J. S.; Sun, D.; Korduláková, J.; Scherman, M. S.; Jones, V.; Grzegorzewicz, A.; Crew, R. M.; Jackson, M.; McNeil, M. R.; Lee, R. E. The Structure–Activity Relationship of Urea Derivatives as Anti-Tuberculosis Agents. *Bioorg. Med. Chem.* **2011**, *19* (18), 5585–5595. https://doi.org/10.1016/j.bmc.2011.07.034.

(186) Stanley, S. A.; Grant, S. S.; Kawate, T.; Iwase, N.; Shimizu, M.; Wivagg, C.; Silvis, M.; Kazyanskaya, E.; Aquadro, J.; Golas, A.; Fitzgerald, M.; Dai, H.; Zhang, L.; Hung, D. T. Identification of Novel Inhibitors of *M. tuberculosis* Growth Using Whole Cell Based High-Throughput Screening. *ACS Chem. Biol.* **2012**, *7* (8), 1377–1384. https://doi.org/10.1021/cb300151m.

(187) Raynaud, C.; Daher, W.; Johansen, M. D.; Roquet-Banères, F.; Blaise, M.; Onajole, O. K.; Kozikowski, A. P.; Herrmann, J.-L.; Dziadek, J.; Gobis, K.; Kremer, L. Active Benzimidazole Derivatives Targeting the MmpL3 Transporter in *Mycobacterium abscessus*. *ACS Infect. Dis.* **2020**, *6* (2), 324–337. https://doi.org/10.1021/acsinfecdis.9b00389.

(188) Korycka-Machała, M.; Viljoen, A.; Pawełczyk, J.; Borówka, P.; Dziadek, B.; Gobis, K.; Brzostek, A.; Kawka, M.; Blaise, M.; Strapagiel, D.; Kremer, L.; Dziadek, J. 1H-Benzo[d]Imidazole Derivatives Affect MmpL3 in *Mycobacterium tuberculosis*. *Antimicrob. Agents Chemother.* **2019**, *63* (10), e00441-19. https://doi.org/10.1128/AAC.00441-19.

(189) Rao, S. P. S.; Lakshminarayana, S. B.; Kondreddi, R. R.; Herve, M.; Camacho, L. R.; Bifani, P.; Kalapala, S. K.; Jiricek, J.; Ma, N. L.; Tan, B. H.; Ng, S. H.; Nanjundappa, M.; Ravindran, S.; Seah, P. G.; Thayalan, P.; Lim, S. H.; Lee, B. H.; Goh, A.; Barnes, W. S.; Chen, Z.; Gagaring, K.; Chatterjee, A. K.; Pethe, K.; Kuhen, K.; Walker, J.; Feng, G.; Babu, S.; Zhang, L.; Blasco, F.; Beer, D.; Weaver, M.; Dartois, V.; Glynne, R.; Dick, T.; Smith, P. W.; Diagana, T. T.; Manjunatha, U. H. Indolcarboxamide Is a Preclinical Candidate for Treating Multidrug-Resistant Tuberculosis. *Sci. Transl. Med.* **2013**, *5* (214), 214ra168. https://doi.org/10.1126/scitranslmed.3007355.

(190) Onajole, O. K.; Pieroni, M.; Tipparaju, S. K.; Lun, S.; Stec, J.; Chen, G.; Gunosewoyo, H.; Guo, H.; Ammerman, N. C.; Bishai, W. R.; Kozikowski, A. P. Preliminary Structure−Activity Relationships and Biological Evaluation of Novel Antitubercular Indolecarboxamide Derivatives Against Drug-Susceptible and Drug-Resistant *Mycobacterium tuberculosis* Strains. *J. Med. Chem.* **2013**, *56* (10), 4093–4103. https://doi.org/10.1021/jm4003878.

(191) Stec, J.; Onajole, O. K.; Lun, S.; Guo, H.; Merenbloom, B.; Vistoli, G.; Bishai, W. R.; Kozikowski, A. P. Indole-2-Carboxamide-Based MmpL3 Inhibitors Show Exceptional Antitubercular Activity in an Animal Model of Tuberculosis Infection. *J. Med. Chem.* **2016**, *59* (13), 6232–6247. https://doi.org/10.1021/acs.jmedchem.6b00415.

(192) Kondreddi, R. R.; Jiricek, J.; Rao, S. P. S.; Lakshminarayana, S. B.; Camacho, L. R.; Rao, R.; Herve, M.; Bifani, P.; Ma, N. L.; Kuhen, K.; Goh, A.; Chatterjee, A. K.; Dick, T.; Diagana, T. T.; Manjunatha, U. H.; Smith, P. W. Design, Synthesis and Biological Evaluation of Indole-2-Carboxamides, a Promising Class of Anti-Tuberculosis Agents. *J. Med. Chem.* **2013**, *56* (21), 8849–8859. https://doi.org/10.1021/jm4012774.

(193) Remuiñán, M. J.; Pérez-Herrán, E.; Rullás, J.; Alemparte, C.; Martínez-Hoyos, M.; Dow, D. J.; Afari, J.; Mehta, N.; Esquivias, J.; Jiménez, E.; Ortega-Muro, F.; Fraile-Gabaldón, M. T.; Spivey, V. L.; Loman, N. J.; Pallen, M. J.; Constantinidou, C.; Minick, D. J.; Cacho, M.; Rebollo-López, M. J.; González, C.; Sousa, V.; Angulo-Barturen, I.; Mendoza-Losana, A.; Barros, D.; Besra, G. S.; Ballell, L.; Cammack, N. Tetrahydropyrazolo[1,5-a]Pyrimidine-3-Carboxamide and *N*-Benzyl-6',7'-Dihydrospiro[Piperidine-4,4'-Thieno[3,2-*c*]Pyran] Analogues with Bactericidal Efficacy against *Mycobacterium*

*tuberculosis* Targeting MmpL3. *PLoS One* **2013**, *8* (4), e60933. https://doi.org/10.1371/journal.pone.0060933.

(194) Yokokawa, F.; Wang, G.; Chan, W. L.; Ang, S. H.; Wong, J.; Ma, I.; Rao, S. P. S.; Manjunatha, U.; Lakshminarayana, S. B.; Herve, M.; Kounde, C.; Tan, B. H.; Thayalan, P.; Ng, S. H.; Nanjundappa, M.; Ravindran, S.; Gee, P.; Tan, M.; Wei, L.; Goh, A.; Chen, P.-Y.; Lee, K. S.; Zhong, C.; Wagner, T.; Dix, I.; Chatterjee, A. K.; Pethe, K.; Kuhen, K.; Glynne, R.; Smith, P.; Bifani, P.; Jiricek, J. Discovery of Tetrahydropyrazolopyrimidine Carboxamide Derivatives As Potent and Orally Active Antitubercular Agents. *ACS Med. Chem. Lett.* **2013**, *4* (5), 451–455. https://doi.org/10.1021/ml400071a.

(195) Guardia, A.; Baiget, J.; Cacho, M.; Pérez, A.; Ortega-Guerra, M.; Nxumalo, W.; Khanye, S. D.; Rullas, J.; Ortega, F.; Jiménez, E.; Pérez-Herrán, E.; Fraile-Gabaldón, M. T.; Esquivias, J.; Fernández, R.; Francisco, E. P.-D.; Encinas, L.; Alonso, M.; Giordano, I.; Rivero, C.; Miguel-Siles, J.; Osende, J. G.; Badiola, K. A.; Rutledge, P. J.; Todd, M. H.; Remuiñán, M.; Alemparte, C. Easy-To-Synthesize Spirocyclic Compounds Possess Remarkable *in vivo* Activity against *Mycobacterium tuberculosis*. *J. Med. Chem.* **2018**, *61* (24), 11327–11340. https://doi.org/10.1021/acs.jmedchem.8b01533.

(196) Dupont, C.; Viljoen, A.; Dubar, F.; Blaise, M.; Bernut, A.; Pawlik, A.; Bouchier, C.; Brosch, R.; Guérardel, Y.; Lelièvre, J.; Ballell, L.; Herrmann, J.-L.; Biot, C.; Kremer, L. A New Piperidinol Derivative Targeting Mycolic Acid Transport in *Mycobacterium abscessus*. *Mol. Microbiol.* **2016**, *101* (3), 515–529. https://doi.org/10.1111/mmi.13406.

(197) Shetty, A.; Xu, Z.; Lakshmanan, U.; Hill, J.; Choong, M. L.; Chng, S.-S.; Yamada, Y.; Poulsen, A.; Dick, T.; Gengenbacher, M. Novel Acetamide Indirectly Targets Mycobacterial Transporter MmpL3 by Proton Motive Force Disruption. *Front. Microbiol.* **2018**, *9*, 2960. https://doi.org/10.3389/fmicb.2018.02960.

(198) Zheng, H.; Williams, J. T.; Coulson, G. B.; Haiderer, E. R.; Abramovitch, R. B. HC2091 Kills *Mycobacterium tuberculosis* by Targeting the MmpL3 Mycolic Acid Transporter. *Antimicrob. Agents Chemother.* **2018**, *62* (7), e02459-17. https://doi.org/10.1128/AAC.02459-17.

(199) Yang, X.; Hu, T.; Yang, X.; Xu, W.; Yang, H.; Guddat, L. W.; Zhang, B.; Rao, Z. Structural Basis for the Inhibition of Mycobacterial MmpL3 by NITD- 349 and SPIRO. *J. Mol. Biol.* **2020**, *432* (16), 4426–4434. https://doi.org/10.1016/j.jmb.2020.05.019.

(200) Mikušová, K.; Huang, H.; Yagi, T.; Holsters, M.; Vereecke, D.; D'Haeze, W.; Scherman, M. S.; Brennan, P. J.; McNeil, M. R.; Crick, D. C. Decaprenylphosphoryl Arabinofuranose, the Donor of the D-Arabinofuranosyl Residues of Mycobacterial Arabinan, Is Formed via a Two-Step Epimerization of Decaprenylphosphoryl Ribose. *J. Bacteriol.* **2005**, *187* (23), 8020–8025. https://doi.org/10.1128/JB.187.23.8020-8025.2005.

(201) Wolucka, B. A. Biosynthesis of D-Arabinose in Mycobacteria – a Novel Bacterial Pathway with Implications for Antimycobacterial Therapy. *FEBS J.* **2008**, *275* (11), 2691–2711. https://doi.org/10.1111/j.1742-4658.2008.06395.x.

(202) Lee, B. S.; Pethe, K. Therapeutic Potential of Promiscuous Targets in *Mycobacterium tuberculosis*. *Curr. Opin. Pharmacol.* **2018**, *42*, 22–26. https://doi.org/10.1016/j.coph.2018.06.006.

(203) Crellin, P. K.; Brammananth, R.; Coppel, R. L. Decaprenylphosphoryl-β-$_D$-Ribose 2'-Epimerase, the Target of Benzothiazinones and Dinitrobenzamides, Is an Essential Enzyme in *Mycobacterium smegmatis*. *PLoS One* **2011**, *6* (2), e16869. https://doi.org/10.1371/journal.pone.0016869.

(204) Kolly, G. S.; Boldrin, F.; Sala, C.; Dhar, N.; Hartkoorn, R. C.; Ventura, M.; Serafini, A.; Mckinney, J. D.; Manganelli, R.; Cole, S. T. Assessing the Essentiality of the Decaprenyl-Phospho-$_D$-Arabinofuranose Pathway in *Mycobacterium tuberculosis* Using Conditional Mutants. *Mol. Microbiol.* **2014**, *92* (1), 194–211. https://doi.org/10.1111/mmi.12546.

(205) Brecik, M.; Centárová, I.; Mukherjee, R.; Kolly, G. S.; Huszár, S.; Bobovska, A.; Kilacskova, E.; Mokošova, V.; Svetlíkova, Z.; Michal, S.; Neres, J.; Korduláková, J.; Cole, S. T.; Mikušová, K. DprE1 Is a Vulnerable Tuberculosis Drug Target Due to Its Cell Wall Localization. *ACS Chem. Biol.* **2015**, *10* (7), 1631–1636.

https://doi.org/10.1021/acschembio.5b00237.

(206) Batt, S. M.; Jabeen, T.; Bhowruth, V.; Quill, L.; Lund, P. A.; Eggeling, L.; Alderwick, L. J.; Fütterer, K.; Besra, G. S. Structural Basis of Inhibition of *Mycobacterium tuberculosis* DprE1 by Benzothiazinone Inhibitors. *Proc. Natl. Acad. Sci.* **2012**, *109* (28), 11354–11359. https://doi.org/10.1073/pnas.1205735109.

(207) Piton, J.; Foo, C. S.-Y.; Cole, S. T. Structural Studies of *Mycobacterium tuberculosis* DprE1 Interacting with Its Inhibitors. *Drug Discov. Today* **2017**, *22* (3), 526–533. https://doi.org/10.1016/j.drudis.2016.09.014.

(208) Campaniço, A.; Moreira, R.; Lopes, F. Drug Discovery in Tuberculosis. New Drug Targets and Antimycobacterial Agents. *Eur. J. Med. Chem.* **2018**, *150*, 525–545. https://doi.org/10.1016/j.ejmech.2018.03.020.

(209) Chikhale, R. V.; Barmade, M. A.; Murumkar, P. R.; Yadav, M. R. Overview of the Development of DprE1 Inhibitors for Combating the Menace of Tuberculosis. *J. Med. Chem.* **2018**, *61* (19), 8563–8593. https://doi.org/10.1021/acs.jmedchem.8b00281.

(210) Huszár, S.; Chibale, K.; Singh, V. The Quest for the Holy Grail: New Antitubercular Chemical Entities, Targets and Strategies. *Drug Discov. Today* **2020**, *25* (4), 772–780. https://doi.org/10.1016/j.drudis.2020.02.003.

(211) Richter, A.; Rudolph, I.; Möllmann, U.; Voigt, K.; Chung, C.-W.; Singh, O. M. P.; Rees, M.; Mendoza-Losana, A.; Bates, R.; Ballell, L.; Batt, S.; Veerapen, N.; Fütterer, K.; Besra, G.; Imming, P.; Argyrou, A. Novel Insight into the Reaction of Nitro, Nitroso and Hydroxylamino Benzothiazinones and of Benzoxacinones with *Mycobacterium tuberculosis* DprE1. *Sci. Rep.* **2018**, *8* (1), 13473. https://doi.org/10.1038/s41598-018-31316-6.

(212) Makarov, V.; Salina, E.; Reynolds, R. C.; Phyo, P.; Zin, K.; Ekins, S. Molecule Property Analyses of Active Compounds for *Mycobacterium tuberculosis*. *J. Med. Chem.* **2020**, *63* (17), 8917–8955. https://doi.org/10.1021/acs.jmedchem.9b02075.

(213) Makarov, V.; Manina, G.; Mikusova, K.; Möllmann, U.; Ryabova, O.; Saint-Joanis, B.; Dhar, N.; Pasca, M. R.; Buroni, S.; Lucarelli, A. P.; Milano, A.; Rossi, E. De; Belanova, M.; Bobovska, A.; Dianiskova, P.; Kordulakova, J.; Sala, C.; Fullam, E.; Schneider, P.; Mckinney, J. D.; Brodin, P.; Christophe, T.; Waddell, S.; Butcher, P.; Albrethsen, J.; Rosenkrands, I.; Brosch, R.; Nandi, V.; Bharath, S.; Gaonkar, S.; Shandil, R. K.; Balasubramanian, V.; Balganesh, T.; Tyagi, S.; Grosset, J.; Riccardi, G.; Cole, S. T. Benzothiazinones Kill *Mycobacterium tuberculosis* by Blocking Arabinan Synthesis. *Science*. **2009**, *324* (5928), 801–804. https://doi.org/10.1126/science.1171583.

(214) Makarov, V. A.; Cole, S. T.; Möllmann, U. Patent EP2029583 B1. *2010*.

(215) Pasca, M. R.; Degiacomi, G.; Riberio, A. L. J. L.; Zara, F.; Mori, P. De; Heym, B.; Mirrione, M.; Brerra, R.; Pagani, L.; Pucillo, L.; Troupioti, P.; Makarov, V.; Cole, S. T.; Riccardi, G. Clinical Isolates of *Mycobacterium tuberculosis* in Four European Hospitals Are Uniformly Susceptible to Benzothiazinones. *Antimicrob. Agents Chemother.* **2010**, *54* (4), 1616–1618. https://doi.org/10.1128/AAC.01676-09.

(216) Trefzer, C.; Rengifo-Gonzalez, M.; Hinner, M. J.; Schneider, P.; Makarov, V.; Cole, S. T.; Johnsson, K. Benzothiazinones: Prodrugs That Covalently Modify the Decaprenylphosphoryl-β-$_D$-Ribose 2′-Epimerase DprE1 of *Mycobacterium tuberculosis*. *J. Am. Chem. Soc.* **2010**, *132* (39), 13663–13665. https://doi.org/10.1021/ja106357w.

(217) Trefzer, C.; Škovierová, H.; Buroni, S.; Bobovská, A.; Nenci, S.; Molteni, E.; Pojer, F.; Pasca, M. R.; Makarov, V.; Cole, S. T.; Riccardi, G.; Mikušová, K.; Johnsson, K. Benzothiazinones Are Suicide Inhibitors of Mycobacterial Decaprenylphosphoryl-β-$_D$-Ribofuranose 2′-Oxidase DprE1. *J. Am. Chem. Soc.* **2012**, *134* (2), 912–915. https://doi.org/10.1021/ja211042r.

(218) Tiwari, R.; Moraski, G. C.; Krchňák, V.; Miller, P. A.; Colon-Martinez, M.; Herrero, E.; Oliver, A. G.; Miller, M. J. Thiolates Chemically Induce Redox Activation of BTZ043 and Related Potent Nitroaromatic Anti-Tuberculosis Agents. *J. Am. Chem. Soc.* **2013**, *135* (9), 3539–3549. https://doi.org/10.1021/ja311058q.

(219) Liu, R.; Krchnak, V.; Brown, S. N.; Miller, M. J. Deuteration of BTZ043 Extends the Lifetime of Meisenheimer Intermediates to the Antituberculosis Nitroso Oxidation State.

*ACS Med. Chem. Lett.* **2019**, *10* (10), 1462–1466. https://doi.org/10.1021/acsmedchemlett.9b00308.

(220) Makarov, V.; Lechartier, B.; Zhang, M.; Neres, J.; van der Sar, A. M.; Raadsen, S. A.; Hartkoorn, R. C.; Ryabova, O. B.; Vocat, A.; Decosterd, L. A.; Widmer, N.; Buclin, T.; Bitter, W.; Andries, K.; Pojer, F.; Dyson, P. J.; Cole, S. T. Towards a New Combination Therapy for Tuberculosis with next Generation Benzothiazinones. *EMBO Mol. Med.* **2014**, *6* (3), 372–383. https://doi.org/10.1002/emmm.201303575.

(221) Makarov, V.; Mikušová, K. Development of Macozinone for TB Treatment: An Update. *Appl. Sci.* **2020**, *10* (7), 2269. https://doi.org/10.3390/app10072269.

(222) https://clinicaltrials.gov/ct2/show/NCT04044001 (accessed on 14th March, 2023).

(223) https://clinicaltrials.gov/ct2/show/NCT03334734 (accessed on 17th March, 2023).

(224) Piton, J.; Vocat, A.; Lupien, A.; Foo, C. S.; Riabova, O.; Makarov, V.; Cole, S. T. Structure-Based Drug Design and Characterization of Sulfonyl- Piperazine Benzothiazinone Inhibitors of DprE1 from *Mycobacterium tuberculosis*. *Antimicrob. Agents Chemother.* **2018**, *62* (10), e00681-18. https://doi.org/10.1128/AAC.00681-18.

(225) Landge, S.; Mullick, A. B.; Nagalapur, K.; Neres, J.; Subbulakshmi, V.; Murugan, K.; Ghosh, A.; Sadler, C.; Fellows, M. D.; Humnabadkar, V.; Mahadevaswamy, J.; Vachaspati, P.; Sharma, S.; Kaur, P.; Mallya, M.; Rudrapatna, S.; Awasthy, D.; Sambandamurthy, V. K.; Pojer, F.; Cole, S. T.; Balganesh, T. S.; Ugarkar, B. G.; Balasubramanian, V.; Bandodkar, B. S.; Panda, M.; Ramachandran, V. Discovery of Benzothiazoles as Antimycobacterial Agents: Synthesis, Structure–Activity Relationships and Binding Studies with *Mycobacterium tuberculosis* Decaprenylphosphoryl-β-$_D$-Ribose 2'-Oxidase. *Bioorganic Med. Chem.* **2015**, *23* (24), 7694–7710. https://doi.org/10.1016/j.bmc.2015.11.017.

(226) Landge, S.; Ramachandran, V.; Kumar, A.; Neres, J.; Murugan, K.; Sadler, C.; Fellows, M. D.; Humnabadkar, V.; Vachaspati, P.; Raichurkar, A.; Sharma, S.; Ravishankar, S.; Guptha, S.; Sambandamurthy, V. K.; Balganesh, T. S.; Ugarkar, B. G.; Balasubramanian, V.; Bandodkar, B. S.; Panda, M. Nitroarenes as Antitubercular Agents: Stereoelectronic Modulation to Mitigate Mutagenicity. *ChemMedChem* **2016**, *11* (3), 331–339. https://doi.org/10.1002/cmdc.201500462.

(227) Christophe, T.; Jackson, M.; Jeon, H. K.; Fenistein, D.; Contreras-Dominguez, M.; Kim, J.; Genovesio, A.; Carralot, J.-P.; Ewann, F.; Kim, E. H.; Lee, S. Y.; Kang, S.; Seo, M. J.; Park, E. J.; Škovierová, H.; Pham, H.; Riccardi, G.; Nam, J. Y.; Marsollier, L.; Kempf, M.; Joly-Guillou, M.-L.; Oh, T.; Shin, W. K.; No, Z.; Nehrbass, U.; Brosch, R.; Cole, S. T.; Brodin, P. High Content Screening Identifies Decaprenyl- Phosphoribose 2' Epimerase as a Target for Intracellular Antimycobacterial Inhibitors. *PLOS Pathog.* **2009**, *5* (10), e1000645. https://doi.org/10.1371/journal.ppat.1000645.

(228) Magnet, S.; Hartkoorn, R. C.; Székely, R.; Pató, J.; Triccas, J. A.; Schneider, P.; Szántai-Kis, C.; Őrfi, L.; Chambon, M.; Banfi, D.; Bueno, M.; Turcatti, G.; Kéri, G.; Cole, S. T. Leads for Antitubercular Compounds from Kinase Inhibitor Library Screens. *Tuberculosis* **2010**, *90* (6), 354–360. https://doi.org/10.1016/j.tube.2010.09.001.

(229) Makarov, V.; Neres, J.; Hartkoorn, R. C.; Ryabova, O. B.; Kazakova, E.; Šarkan, M.; Huszár, S.; Piton, J.; Kolly, G. S.; Vocat, A.; Conroy, T. M.; Mikušová, K.; Cole, S. T. The 8-Pyrrole-Benzothiazinones Are Noncovalent Inhibitors of DprE1 from *Mycobacterium tuberculosis*. *Antimicrob. Agents Chemother.* **2015**, *59* (8), 4446–4452. https://doi.org/10.1128/AAC.00778-15.

(230) Tiwari, R.; Miller, P. A.; Chiarelli, L. R.; Mori, G.; Michal, Š.; Centárová, I.; Cho, S.; Mikušová, K.; Franzblau, S. G.; Oliver, A. G.; Miller, M. J. Design, Syntheses, and Anti-TB Activity of 1,3-Benzothiazinone Azide and Click Chemistry Products Inspired by BTZ043. *ACS J. Med. Chem.* **2016**, *7* (3), 266–270. https://doi.org/10.1021/acsmedchemlett.5b00424.

(231) Madikizela, B.; Eckhardt, T.; Goddard, R.; Richter, A.; Lins, A.; Lehmann, C.; Imming, P.; Seidel, R. W. Synthesis, Structural Characterization and Antimycobacterial Evaluation of Several Halogenated Non-Nitro Benzothiazinones. *Med. Chem. Res.* **2021**, *30* (8), 1523–1533. https://doi.org/10.1007/s00044-021-02735-4.

(232) Wang, F.; Sambandan, D.; Halder, R.; Wang, J.; Batt, S. M.; Weinrick, B.; Ahmad, I.; Yang, P.; Zhang, Y.; Kim, J.; Hassani, M.; Huszar, S.; Trefzer, C.; Ma, Z.; Kaneko, T.; Mdluli, K. E.; Franzblau, S.; Chatterjee, A. K.; Johnsson, K.; Mikusova, K.; Besra, G. S.; Fütterer, K.; Robbins, S. H.; Barnes, S. W.; Walker, J. R.; Jacobs Jr., W. R.; Schultz, P. G. Identification of a Small Molecule with Activity against Drug-Resistant and Persistent Tuberculosis. *Proc. Natl. Acad. Sci.* **2013**, *110* (27), E2510–E2517. https://doi.org/10.1073/pnas.1309171110.

(233) Chikhale, R.; Menghani, S.; Babu, R.; Bansode, R.; Bhargavi, G.; Karodia, N.; Rajasekharan, M. V.; Paradkar, A.; Khedekar, P. Development of Selective DprE1 Inhibitors: Design, Synthesis, Crystal Structure and Antitubercular Activity of Benzothiazolylpyrimidine-5-Carboxamides. *Eur. J. Med. Chem.* **2015**, *96*, 30–46. https://doi.org/10.1016/j.ejmech.2015.04.011.

(234) Mir, F.; Shafi, S.; Zaman, M. S.; Kalia, N. P.; Rajput, V. S.; Mulakayala, C.; Mulakayala, N.; Khan, I. A.; Alam, M. S. Sulfur Rich 2-Mercaptobenzothiazole and 1,2,3-Triazole Conjugates as Novel Antitubercular Agents. *Eur. J. Med. Chem.* **2014**, *76*, 274–283. https://doi.org/10.1016/j.ejmech.2014.02.017.

(235) No, Z.; Kim, J.; Brodin, P. B.; Seo, M. J.; Kim, Y. M.; Cechetto, J.; Jeon, H.; Genovesio, A.; Lee, S.; Kang, S.; Ewann, F. A.; Nam, J. Y.; Christophe, T.; Fenistein, D. P. C.; Jamung, H.; Jiyeon, J. Patent WO 2011/113606 A1, 2011.

(236) Barsanti, P. A.; Hu, C.; Jin, J.; Keyes, R.; Kucejko, R.; Lin, X.; Pan, Y.; Pfister, K. B.; Sendzik, M.; Sutton, J.; Wan, L. Patent WO 2011/085990 A1, 2011.

(237) Shirude, P. S.; Shandil, R.; Sadler, C.; Naik, M.; Hosagrahara, V.; Hameed, S.; Shinde, V.; Bathula, C.; Humnabadkar, V.; Kumar, N.; Reddy, J.; Panduga, V.; Sharma, S.; Ambady, A.; Hegde, N.; Whiteaker, J.; McLaughlin, R. E.; Gardner, H.; Madhavapeddi, P.; Ramachandran, V.; Kaur, P.; Narayan, A.; Guptha, S.; Awasthy, D.; Narayan, C.; Mahadevaswamy, J.; Vishwas, K.; Ahuja, V.; Srivastava, A.; Prabhakar, K.; Bharath, S.; Kale, R.; Ramaiah, M.; Choudhury, N. R.; Sambandamurthy, V. K.; Solapure, S.; Iyer, P. S.; Narayanan, S.; Chatterji, M. Azaindoles: Noncovalent DprE1 Inhibitors from Scaffold Morphing Efforts, Kill *Mycobacterium tuberculosis* and Are Efficacious *in vivo*. *J. Med. Chem.* **2013**, *56* (23), 9701–9708. https://doi.org/10.1021/jm401382v.

(238) Shirude, P. S.; Shandil, R. K.; Manjunatha, M. R.; Sadler, C.; Panda, M.; Panduga, V.; Reddy, J.; Saralaya, R.; Nanduri, R.; Ambady, A.; Ravishankar, S.; Sambandamurthy, V. K.; Humnabadkar, V.; Jena, L. K.; Suresh, R. S.; Srivastava, A.; Prabhakar, K. R.; Whiteaker, J.; McLaughlin, R. E.; Sharma, S.; Cooper, C. B.; Mdluli, K.; Butler, S.; Iyer, P. S.; Narayanan, S.; Chatterji, M. Lead Optimization of 1,4-Azaindoles as Antimycobacterial Agents. *J. Med. Chem.* **2014**, *57* (13), 5728–5737. https://doi.org/10.1021/jm500571f.

(239) Chatterji, M.; Shandil, R.; Manjunatha, M. R.; Solapure, S.; Ramachandran, V.; Kumar, N.; Saralaya, R.; Panduga, V.; Reddy, J.; KR, P.; Sharma, S.; Sadler, C.; Cooper, C. B.; Mdluli, K.; Iyer, P. S.; Narayanan, S.; Shirude, P. S. 1,4-Azaindole, a Potential Drug Candidate for Treatment of Tuberculosis. *Antimicrob. Agents Chemother.* **2014**, *58* (9), 5325–5331. https://doi.org/10.1128/AAC.03233-14.

(240) https://clinicaltrials.gov/ct2/show/NCT03199339 (accessed on 18th March, 2023).

(241) Manjunatha, M. R.; Shandil, R.; Panda, M.; Sadler, C.; Ambady, A.; Panduga, V.; Kumar, N.; Mahadevaswamy, J.; Sreenivasaiah, M.; Narayan, A.; Guptha, S.; Sharma, S.; Sambandamurthy, V. K.; Ramachandran, V.; Mallya, M.; Cooper, C.; Mdluli, K.; Butler, S.; Tommasi, R.; Iyer, P. S.; Narayanan, S.; Chatterji, M.; Shirude, P. S. Scaffold Morphing To Identify Novel DprE1 Inhibitors with Antimycobacterial Activity. *ACS Med. Chem. Lett.* **2019**, *10* (10), 1480–1485. https://doi.org/10.1021/acsmedchemlett.9b00343.

(242) Panda, M.; Ramachandran, S.; Ramachandran, V.; Shirude, P. S.; Humnabadkar, V.; Nagalapur, K.; Sharma, S.; Kaur, P.; Guptha, S.; Narayan, A.; Mahadevaswamy, J.; Ambady, A.; Hegde, N.; Rudrapatna, S. S.; Hosagrahara, V. P.; Sambandamurthy, V. K.; Raichurkar, A. Discovery of Pyrazolopyridones as a Novel Class of Noncovalent DprE1 Inhibitor with Potent Anti-Mycobacterial Activity. *J. Med. Chem.* **2014**, *57* (11), 4761–4771. https://doi.org/10.1021/jm5002937.

(243) Naik, M.; Humnabadkar, V.; Tantry, S. J.; Panda, M.; Narayan, A.; Guptha, S.; Panduga, V.; Manjrekar, P.; Jena, L. K.; Koushik, K.; Shanbhag, G.; Jatheendranath, S.; Manjunatha, M. R.; Gorai, G.; Bathula, C.; Rudrapatna, S.; Achar, V.; Sharma, S.; Ambady, A.; Hegde, N.; Mahadevaswamy, J.; Kaur, P.; Sambandamurthy, V. K.; Awasthy, D.; Narayan, C.; Ravishankar, S.; Madhavapeddi, P.; Reddy, J.; Prabhakar, K.; Saralaya, R.; Chatterji, M.; Whiteaker, J.; McLaughlin, B.; Chiarelli, L. R.; Riccardi, G.; Pasca, M. R.; Binda, C.; Neres, J.; Dhar, N.; Signorino-Gelo, F.; McKinney, J. D.; Ramachandran, V.; Shandil, R.; Tommasi, R.; Iyer, P. S.; Narayanan, S.; Hosagrahara, V.; Kavanagh, S.; Dinesh, N.; Ghorpade, S. R. 4-Aminoquinolone Piperidine Amides: Noncovalent Inhibitors of DprE1 with Long Residence Time and Potent Antimycobacterial Activity. *J. Med. Chem.* **2014**, *57* (12), 5419–5434. https://doi.org/10.1021/jm5005978.

(244) Neres, J.; Hartkoorn, R. C.; Chiarelli, L. R.; Gadupudi, R.; Pasca, M. R.; Mori, G.; Venturelli, A.; Savina, S.; Makarov, V.; Kolly, G. S.; Molteni, E.; Binda, C.; Dhar, N.; Ferrari, S.; Brodin, P.; Delorme, V.; Landry, V.; Ribeiro, A. L. de J. L.; Farina, D.; Saxena, P.; Pojer, F.; Carta, A.; Luciani, R.; Porta, A.; Zanoni, G.; Rossi, E. De; Costi, M. P.; Riccardi, G.; Cole, S. T. 2-Carboxyquinoxalines Kill *Mycobacterium tuberculosis* through Non-Covalent Inhibition of DprE1. *ACS Chem. Biol.* **2015**, *10* (3), 705–714. https://doi.org/10.1021/cb5007163.

(245) Ballell, L.; Bates, R. H.; Young, R. J.; Alvarez-Gomez, D.; Alvarez-Ruiz, E.; Barroso, V.; Blanco, D.; Crespo, B.; Escribano, J.; González, R.; Lozanom, S.; Huss, S.; Santos-Villarejo, A.; Martín-Plaza, J. J.; Mendoza, A.; Rebollo-Lopez, M. J.; Remuiñan-Blanco, M.; Lavandera, J. L.; Pérez-Herran, E.; Gamo-Benito, F. J.; García-Bustos, J. F.; Barros, D.; Castro, J. P.; Cammack, N. Fueling Open-Source Drug Discovery: 177 Small-Molecule Leads against Tuberculosis. *ChemMedChem* **2013**, *8* (2), 313–321. https://doi.org/10.1002/cmdc.201200428.

(246) Batt, S. M.; Izquierdo, M. C.; Pichel, J. C.; Stubbs, C. J.; Peral, L. V.-G. Del; Pérez-Herrán, E.; Dhar, N.; Mouzon, B.; Rees, M.; Hutchinson, J. P.; Young, R. J.; McKinney, J. D.; Aguirre, D. B.; Ballell, L.; Besra, G. S.; Argyrou, A. Whole Cell Target Engagement Identifies Novel Inhibitors of *Mycobacterium tuberculosis* Decaprenylphosphoryl-β-$_D$-ribose Oxidase. *ACS Infect. Dis.* **2015**, *1* (12), 615–626. https://doi.org/10.1021/acsinfecdis.5b00065.

(247) Borthwick, J. A.; Alemparte, C.; Wall, I.; Whitehurst, B. C.; Argyrou, A.; Burley, G.; Dios-Anton, P. De; Guijarro, L.; Monteiro, M. C.; Ortega, F.; Suckling, C. J.; Pichel, J. C.; Cacho, M.; Young, R. J. *Mycobacterium tuberculosis* Decaprenylphosphoryl-β-$_D$-ribose Oxidase Inhibitors: Expeditious Reconstruction of Suboptimal Hits into a Series with Potent *in vivo* Activity. *J. Med. Chem.* **2020**, *63* (5), 2557–2576. https://doi.org/10.1021/acs.jmedchem.9b01561.

(248) Oh, S.; Park, Y.; Engelhart, C. A.; Wallach, J. B.; Schnappinger, D.; Arora, K.; Manikkam, M.; Gac, B.; Wang, H.; Murgolo, N.; Olsen, D. B.; Goodwin, M.; Sutphin, M.; Weiner, D. M.; Via, L. E.; Bosho, H. I. M.; Barry III, C. E. Discovery and Structure−Activity-Relationship Study of *N*-Alkyl-5-Hydroxypyrimidinone Carboxamides as Novel Antitubercular Agents Targeting Decaprenylphosphoryl-β-$_D$-ribose 2'-Oxidase. *J. Med. Chem.* **2018**, *61* (22), 9952–9965. https://doi.org/10.1021/acs.jmedchem.8b00883.

(249) Boyd, V. A.; Mason, J.; Hanumesh, P.; Price, J.; Russell, C. J.; Webb, T. R. 2-Substituted-4,5-Dihydroxypyrimidine-6-Carboxamide Antiviral Targeted Libraries. *J. Comb. Chem.* **2009**, *11* (6), 1100–1104. https://doi.org/10.1021/cc900111u.

(250) Rogacki, M. K.; Pitta, E.; Balabon, O.; Huss, S.; Lopez-Roman, E. M.; Argyrou, A.; Blanco-Ruano, D.; Cacho, M.; Velde, C. M. L. Vande; Augustyns, K.; Ballell, L.; Barros, D.; Bates, R. H.; Cunningham, F.; Veken, P. Van der. Identification and Prof Ling of Hydantoins - A Novel Class of Potent Antimycobacterial DprE1 Inhibitors. *J. Med. Chem.* **2018**, *61* (24), 11221–11249. https://doi.org/10.1021/acs.jmedchem.8b01356.

(251) Balabon, O.; Pitta, E.; Rogacki, M. K.; Meiler, E.; Casanueva, R.; Guijarro, L.; Huss, S.; Lopez-Roman, E. M.; Santos-Villarejo, A.; Augustyns, K.; Ballell, L.; Aguirre, D. B.; Bates, R. H.; Cunningham, F.; Cacho, M.; Veken, P. Van der. Optimization of Hydantoins

as Potent Antimycobacterial Decaprenylphosphoryl-β-$_D$-Ribose Oxidase (DprE1) Inhibitors. *J. Med. Chem.* **2020**, *63* (10), 5367–5386. https://doi.org/10.1021/acs.jmedchem.0c00107.

(252) Whitehurst, B. C.; Young, R. J.; Burley, G. A.; Cacho, M.; Torres, P.; Peral, L. V.-G. del. Identification of 2-((2,3-dihydrobenzo[*b*][1,4]dioxin-6-yl)amino)-*N*-Phenylpropanamides as a Novel Class of Potent DprE1 Inhibitors. *Bioorg. Med. Chem. Lett.* **2020**, *30* (12), 127192. https://doi.org/10.1016/j.bmcl.2020.127192.

(253) Hariguchi, N.; Chen, X.; Hayashi, Y.; Kawano, Y.; Fujiwara, M.; Matsuba, M.; Shimizu, H.; Ohba, Y.; Nakamura, I.; Kitamoto, R.; Shinohara, T.; Uematsu, Y.; Ishikawa, S.; Itotani, M.; Haraguchi, Y.; Takemura, I.; Matsumoto, M. OPC-167832, a Novel Carbostyril Derivative with Potent Antituberculosis Activity as a DprE1 Inhibitor. *Antimicrob. Agents Chemother.* **2020**, *64* (6), e02020-19. https://doi.org/10.1128/AAC.02020-19.

(254) Shimizu, H.; Kawano, Y.; Ishikawa, S.; Uematsu, Y.; Shinohara, T.; Itotani, M.; Haraguchi, Y.; Takemura, I.; Kaneshige, A.; Nakai, Y.; Hariguchi, N.; Hayashi, Y.; Matsumoto, M. Patent WO/2016/031255, 2016.

(255) Young, R. J.; Green, D. V. S.; Luscombe, C. N.; Hill, A. P. Getting Physical in Drug Discovery II: The Impact of Chromatographic Hydrophobicity Measurements and Aromaticity. *Drug Discov. Today* **2011**, *16* (17–18), 822–830. https://doi.org/10.1016/j.drudis.2011.06.001.

(256) https://clinicaltrials.gov/ct2/show/NCT03678688 (accessed on 24$^{th}$ March, 2023).

(257) Robertson, G. T.; Ramey, M. E.; Massoudi, L. M.; Carter, C. L.; Zimmerman, M.; Kaya, F.; Graham, B. G.; Gruppo, V.; Hastings, C.; Woolhiser, L. K.; Scott, D. W. L.; Asay, B. C.; Eshun-Wilson, F.; Maidj, E.; Podell, B. K.; Vásquez, J. J.; Lyons, M. A.; Dartois, V.; Lenaerts, A. J. Comparative Analysis of Pharmacodynamics in the C3HeB/FeJ Mouse Tuberculosis Model for DprE1 Inhibitors TBA-7371, PBTZ169, and OPC-167832. *Antimicrob. Agents Chemother.* **2021**, *65* (11), e00583-21. https://doi.org/10.1128/AAC.00583-21.

(258) Wang, P.; Batt, S. M.; Wang, B.; Fu, L.; Qin, R.; Lu, Y.; Li, G.; Besra, G. S.; Huang, H. Discovery of Novel Thiophene-Arylamide Derivatives as DprE1 Inhibitors with Potent Antimycobacterial Activities. *J. Med. Chem.* **2021**, *64* (9), 6241–6261. https://doi.org/10.1021/acs.jmedchem.1c00263.

(259) Hu, X.; Yang, L.; Chai, X.; Lei, Y.; Shah, M. A.; Lu, L.; Shen, C.; Jiang, D.; Wang, Z.; Liu, Z.; Xu, L.; Wan, K.; Zhang, T.; Yin, Y.; Li, D.; Cao, D.; Hou, T. Discovery of Novel DprE1 Inhibitors via Computational Bioactivity Fingerprints and Structure-Based Virtual Screening. *Acta Pharmacol. Sin.* **2022**, *43* (6), 1605–1615. https://doi.org/10.1038/s41401-021-00779-1.

(260) Ezquerra-Aznárez, M.; Degiacomi, G.; Gašparovic, H.; Stelitano, G.; Sammartino, J. C.; Korduláková, J.; Governa, P.; Manetti, F.; Pasca, M. R.; Chiarelli, L. R.; Ramón-García, S. The Veterinary Anti-Parasitic Selamectin Is a Novel Inhibitor of the *Mycobacterium tuberculosis* DprE1 Enzyme. *Int. J. Mol. Sci.* **2022**, *23* (2), 771. https://doi.org/10.3390/ijms23020771.

(261) Karabanovich, G.; Dušek, J.; Savková, K.; Pavliš, O.; Pávková, I.; Korábečný, J.; Kučera, T.; Vlčková, H. K.; Huszár, S.; Konyariková, Z.; Konečná, K.; Jand'ourek, O.; Stolaříková, J.; Korduláková, J.; Vávrová, K.; Pávek, P.; Klimešová, V.; Hrabálek, A.; Mikušová, K.; Roh, J. Development of 3,5-Dinitrophenyl-Containing 1,2,4-Triazoles and Their Trifluoromethyl Analogues as Highly Efficient Antitubercular Agents Inhibiting Decaprenylphosphoryl-β-$_D$-ribofuranose 2′- Oxidase. *J. Med. Chem.* **2019**, *62* (17), 8115–8139. https://doi.org/10.1021/acs.jmedchem.9b00912.

(262) WHO. *Latent Tuberculosis Infection. Updated and Programmatic Guidelines for Consolidated Management*; 2018.

(263) Huaman, M. A.; Sterling, T. R. Treatment of Latent Tuberculosis Infection - An Update. *Clin. Chest Med.* **2019**, *40* (4), 839–848. https://doi.org/10.1016/j.ccm.2019.07.008.

(264) Getahun, H.; Matteelli, A.; Chaisson, R. E.; Raviglione, M. Latent *Mycobacterium tuberculosis* Infection. *N. Engl. J. Med.* **2015**, *372* (22), 2127–2135.

https://doi.org/10.1056/NEJMra1405427.

(265) Balcells, M. E.; Thomas, S. L.; Godfrey-Faussett, P.; Grant, A. D. Isoniazid Preventive Therapy and Risk for Resistant Tuberculosis. *Emerg. Infect. Dis.* **2006**, *12* (5), 744–751. https://doi.org/10.3201/eid1205.050681.

(266) Boon, S. den; Matteelli, A.; Getahun, H. Rifampicin Resistance after Treatment for Latent Tuberculous Infection: A Systematic Review and Meta-Analysis. *Int. J. Tuberc. Lung Dis.* **2016**, *20* (8), 1065–1071. https://doi.org/10.5588/ijtld.15.0908.

(267) Leistikow, R. L.; Morton, R. A.; Bartek, I. L.; Frimpong, I.; Wagner, K.; Voskuil, M. I. The *Mycobacterium tuberculosis* DosR Regulon Assists in Metabolic Homeostasis and Enables Rapid Recovery from Nonrespiring Dormancy. *J. Bacteriol.* **2010**, *192* (6), 1662–1670. https://doi.org/10.1128/JB.00926-09.

(268) Schnappinger, D.; Ehrt, S.; Voskuil, M. I.; Liu, Y.; Mangan, J. A.; Monahan, I. M.; Dolganov, G.; Efron, B.; Butcher, P. D.; Nathan, C.; Schoolnik, G. K. Transcriptional Adaptation of *Mycobacterium tuberculosis* within Macrophages : Insights into the Phagosomal Environment. *J. Exp. Med.* **2003**, *198* (5), 693–704. https://doi.org/10.1084/jem.20030846.

(269) Voskuil, M. I.; Schnappinger, D.; Visconti, K. C.; Harrell, M. I.; Dolganov, G. M.; Sherman, D. R.; Schoolnik, G. K. Inhibition of Respiration by Nitric Oxide Induces a *Mycobacterium tuberculosis* Dormancy Program. *J. Exp. Med.* **2003**, *198* (5), 705–713. https://doi.org/10.1084/jem.20030205.

(270) Boon, C.; Li, R.; Qi, R.; Dick, T. Proteins of *Mycobacterium bovis* BCG Induced in the Wayne Dormancy Mode. *J. Bacteriol.* **2001**, *183* (8), 2672–2676. https://doi.org/10.1128/JB.183.8.2672–2676.2001.

(271) Gautam, U. S.; McGillivray, A.; Mehra, S.; Didier, P. J.; Midkiff, C. C.; Kissee, R. S.; Golden, N. A.; Alvarez, X.; Niu, T.; Rengarajan, J.; Sherman, D. R.; Kaushal, D. DosS Is Required for the Complete Virulence of *Mycobacterium tuberculosis* in Mice with Classical Granulomatous Lesions. *Am. J. Respir. Cell Mol. Biol.* **2015**, *52* (6), 708–716. https://doi.org/10.1165/rcmb.2014-0230OC.

(272) Kumar, A.; Toledo, J. C.; Patel, R. P.; Lancaster Jr, J. R.; Steyn, A. J. C. *Mycobacterium tuberculosis* DosS Is a Redox Sensor and DosT Is a Hypoxia Sensor. *Proc. Natl. Acad. Sci.* **2007**, *104* (28), 11568–11573. https://doi.org/10.1073/pnas.0705054104.

(273) Zheng, H.; Abramovitch, R. B. Inhibiting DosRST as a New Approach to Tuberculosis Therapy. *Future Med. Chem.* **2020**, *12* (5), 457–467. https://doi.org/10.4155/fmc-2019-0263.

(274) Boon, C.; Dick, T. *Mycobacterium bovis* BCG Response Regulator Essential for Hypoxic Dormancy. *J. Bacteriol.* **2002**, *184* (24), 6760–6767. https://doi.org/10.1128/JB.184.24.6760–6767.2002.

(275) Dasgupta, N.; Kapur, V.; Singh, K. K.; Das, T. K.; Sachdeva, S.; Jyothisri, K.; Tyagi, J. S. Characterization of a Two-Component System, DevR-DevS, of *Mycobacterium tuberculosis*. *Tuber. Lung Dis.* **2000**, *80* (3), 141–159. https://doi.org/10.1054/tuld.2000.0240.

(276) Zheng, H.; Williams, J. T.; Aleiwi, B.; Ellsworth, E.; Abramovitch, R. B. Inhibiting *Mycobacterium tuberculosis* DosRST Signaling by Targeting Response Regulator DNA Binding and Sensor Kinase Heme. *ACS Chem. Biol.* **2020**, *15* (1), 52–62. https://doi.org/10.1021/acschembio.8b00849.

(277) Sousa, E. H. S.; Diógenes, I. C. N.; Lopes, L. G. F.; Moura, J. J. G. Potential Therapeutic Approaches for a Sleeping Pathogen: Tuberculosis a Case for Bioinorganic Chemistry. *JBIC J. Biol. Inorg. Chem.* **2020**, *25* (5), 685–704. https://doi.org/10.1007/s00775-020-01803-1.

(278) Roberts, D. M.; Liao, R. P.; Wisedchaisri, G.; Hol, W. G. J.; Sherman, D. R. Two Sensor Kinases Contribute to the Hypoxic Response of *Mycobacterium tuberculosis*. *J. Biol. Chem.* **2004**, *279* (22), 23082–23087. https://doi.org/10.1074/jbc.M401230200.

(279) Shiloh, M. U.; Manzanillo, P.; Cox, J. S. *Mycobacterium tuberculosis* Senses Host-Derived Carbon Monoxide during Macrophage Infection. *Cell Host Microbe* **2008**, *3* (5), 323–330. https://doi.org/10.1016/j.chom.2008.03.007.

(280) Gilles-Gonzalez, M.-A.; Gonzalez, G.; Sousa, E. H. S.; Tuckerman, J. Oxygen-Sensing Histidine-Protein Kinases : Assays of Ligand Binding and Turnover of Response-Regulator Substrates. In *Methods in Enzymology*; Elsevier Inc., 2008; Vol. 437, pp 173–189. https://doi.org/10.1016/S0076-6879(07)37010-9.

(281) Henrique, E.; Sousa, S.; Tuckerman, J. R.; Gonzalez, G.; Gilles-Gonzalez, M.-A. DosT and DevS Are Oxygen-Switched Kinases in *Mycobacterium tuberculosis*. *Protein Sci.* **2007**, *16* (8), 1708–1719. https://doi.org/10.1110/ps.072897707.

(282) Kaur, K.; Kumari, P.; Sharma, S.; Sehgal, S.; Tyagi, J. S. DevS/DosS Sensor Is Bifunctional and Its Phosphatase Activity Precludes Aerobic DevR/DosR Regulon Expression in *Mycobacterium tuberculosis*. *FEBS J.* **2016**, *283* (15), 2949–2962. https://doi.org/10.1111/febs.13787.

(283) Sivaramakrishnan, S.; Montellano, P. R. O. de. The DosS-DosT/DosR Mycobacterial Sensor System. *Biosensors* **2013**, *3* (3), 259–282. https://doi.org/10.3390/bios3030259.

(284) Barreto, G. A.; Carepo, M. S. P.; Gondim, A. C. S.; Guimarães, W. G.; Lopes, L. G. F.; Bernhardt, P. V.; Paulo, T. F.; Sousa, E. H. S.; Diógenes, I. C. N. A Spectroelectrochemical Investigation of the Heme-Based Sensor DevS from *Mycobacterium tuberculosis*: A Redox versus Oxygen Sensor. *FEBS J.* **2019**, *286* (21), 4278–4293. https://doi.org/10.1111/febs.14974.

(285) Honaker, R. W.; Leistikow, R. L.; Bartek, I. L.; Voskuil, M. I. Unique Roles of DosT and DosS in DosR Regulon Induction and *Mycobacterium tuberculosis* Dormancy. *Infect. Immun.* **2009**, *77* (8), 3258–3263. https://doi.org/10.1128/IAI.01449-08.

(286) Podust, L. M.; Ioanoviciu, A.; Montellano, P. R. O. de. 2.3 Å X-Ray Structure of the Heme-Bound GAF Domain of Sensory Histidine Kinase DosT of *Mycobacterium tuberculosis*. *Biochemistry* **2008**, *47* (47), 12523–12531. https://doi.org/10.1021/bi8012356.

(287) Cho, H. Y.; Cho, H. J.; Kim, Y. M.; Oh, J. Il; Kang, B. S. Structural Insight into the Heme-Based Redox Sensing by DosS from *Mycobacterium tuberculosis*. *J. Biol. Chem.* **2009**, *284* (19), 13057–13067. https://doi.org/10.1074/jbc.M808905200.

(288) Gautam, U. S.; Mehra, S.; Kumari, P.; Alvarez, X.; Niu, T.; Tyagi, J. S.; Kaushal, D. *Mycobacterium tuberculosis* Sensor Kinase DosS Modulates the Autophagosome in a DosR-Independent Manner. *Commun. Biol.* **2019**, *2*, 349. https://doi.org/10.1038/s42003-019-0594-0.

(289) Harper, J.; Skerry, C.; Davis, S. L.; Tasneen, R.; Weir, M.; Kramnik, I.; Bishai, W. R.; Pomper, M. G.; Nuermberger, E. L.; Jain, S. K. Mouse Model of Necrotic Tuberculosis Granulomas Develops Hypoxic Lesions. *J. Infect. Dis.* **2012**, *205* (4), 595–602. https://doi.org/10.1093/infdis/jir786.

(290) Jakkala, K.; Ajitkumar, P. Hypoxic Non-Replicating Persistent *Mycobacterium tuberculosis* Develops Thickened Outer Layer That Helps in Restricting Rifampicin Entry. *Front. Microbiol.* **2019**, *10*, 2339. https://doi.org/10.3389/fmicb.2019.02339.

(291) Reichlen, M. J.; Leistikow, R. L.; Scobey, M. S.; Born, S. E. M.; Voskuil, M. I. Anaerobic *Mycobacterium tuberculosis* Cell Death Stems from Intracellular Acidification Mitigated by the DosR Regulon. *J. Bacteriol.* **2017**, *199* (23), e00320-17. https://doi.org/10.1128/JB.00320-17.

(292) Gupta, R. K.; Thakur, T. S.; Desiraju, G. R.; Tyagi, J. S. Structure-Based Design of DevR Inhibitor Active against Nonreplicating *Mycobacterium tuberculosis*. *J. Med. Chem.* **2009**, *52* (20), 6324–6334. https://doi.org/10.1021/jm900358q.

(293) Kaur, K.; Taneja, N. K.; Dhingra, S.; Tyagi, J. S. DevR (DosR) Mimetic Peptides Impair Transcriptional Regulation and Survival of *Mycobacterium tuberculosis* under Hypoxia by Inhibiting the Autokinase Activity of DevS Sensor Kinase. *BMC Microbiol.* **2014**, *14*, 195. https://doi.org/10.1186/1471-2180-14-195.

(294) Dhingra, S.; Kaur, K.; Taneja, N. K.; Tyagi, J. S. DevR (DosR) Binding Peptide Inhibits Adaptation of *Mycobacterium tuberculosis* under Hypoxia. *FEMS Microbiol. Lett.* **2012**, *330* (1), 66–71. https://doi.org/10.1111/j.1574-6968.2012.02534.x.

(295) Zheng, H.; Colvin, C. J.; Johnson, B. K.; Kirchhoff, P. D.; Wilson, M.; Jorgensen-Muga, K.; Larsen, S. D.; Abramovitch, R. B. Inhibitors of *Mycobacterium tuberculosis* DosRST

Signaling and Persistence. *Nat. Chem. Biol.* **2017**, *13* (2), 218–225. https://doi.org/10.1038/nchembio.2259.

(296) Mak, P. A.; Rao, S. P. S.; Tan, M. P.; Lin, X.; Chyba, J.; Tay, J.; Ng, S. H.; Tan, B. H.; Cherian, J.; Duraiswamy, J.; Bifani, P.; Lim, V.; Lee, B. H.; Ma, N. L.; Beer, D.; Thayalan, P.; Kuhen, K.; Chatterjee, A.; Supek, F.; Glynne, R.; Zheng, J.; Bosho, H. I.; Barry III, C. E.; Dick, T.; Pethe, K.; Camacho, L. R. A High-Throughput Screen To Identify Inhibitors of ATP Homeostasis in Non-Replicating *Mycobacterium tuberculosis*. *ACS Chem. Biol.* **2012**, *7* (7), 1190–1197. https://doi.org/10.1021/cb2004884.

(297) Deb, C.; Lee, C.-M.; Dubey, V. S.; Daniel, J.; Abomoelak, B.; Sirakova, T. D.; Pawar, S.; Rogers, L.; Kolattukudy, P. E. A Novel *in vitro* Multiple-Stress Dormancy Model for *Mycobacterium tuberculosis* Generates a Lipid-Loaded, Drug-Tolerant, Dormant Pathogen. *PLoS One* **2009**, *4* (6), e6077. https://doi.org/10.1371/journal.pone.0006077.

(298) Hung, D. T.; Shakhnovich, E. A.; Pierson, E.; Mekalanos, J. J. Small-Molecule Inhibitor of Vibrio Cholerae Virulence and Intestinal Colonization. *Science.* **2005**, *310* (5748), 670–674. https://doi.org/10.1126/science.1116739.

(299) Shakhnovich, E. A.; Hung, D. T.; Pierson, E.; Lee, K.; Mekalanos, J. J. Virstatin Inhibits Dimerization of the Transcriptional Activator ToxT. *Proc. Natl. Acad. Sci.* **2007**, *104* (7), 2372–2377. https://doi.org/10.1073/pnas.0611643104.

(300) Morrison, C. N.; Prosser, K. E.; Stokes, R. W.; Cordes, A.; Metzler-Nolte, N.; Cohen, S. M. Expanding Medicinal Chemistry into 3D Space: Metallofragments as 3D Scaffolds for Fragment- Based Drug Discovery. *Chem. Sci.* **2020**, *11* (5), 1216–1225. https://doi.org/10.1039/c9sc05586j.

(301) Belardinelli, J. M.; Verma, D.; Li, W.; Avanzi, C.; Wiersma, C. J.; Williams, J. T.; Johnson, B. K.; Zimmerman, M.; Whittel, N.; Angala, B.; Wang, H.; Jones, V.; Dartois, V.; Moura, V. C. N. de; Gonzalez-Juarrero, M.; Pearce, C.; Schenkel, A. R.; Malcolm, K. C.; Nick, J. A.; Charman, S. A.; Wells, T. N. C.; Podell, B. K.; Vennerstrom, J. L.; Ordway, D. J.; Abramovitch, R. B.; Jackson, M. Therapeutic Efficacy of Antimalarial Drugs Targeting DosRS Signaling in *Mycobacterium abscessus*. *Sci. Transl. Med.* **2022**, *14* (633), eabj3860. https://doi.org/10.1126/scitranslmed.abj3860.

# Chapter 2

## Synthesis of 1,2,4-Trioxane-Containing Antitubercular Hybrids with Potential for Dual Mechanisms of Action

# Chapter 2

Part of the work described in this section is included in a manuscript presently under preparation:

**Amado, P. S. M**.; Woodley, C. M.; Cristiano, M. L. S.; O'Neill, P. M. Synthesis of Endoperoxide-Based Antitubercular Hybrids with Potential for Dual Mechanisms of Action. ***Manuscript in preparation.***

## CONTRIBUTIONS

Patrícia S. M. Amado (P.S.M.A) designed and carried out the synthesis and characterization of all compounds. Additionally, for the active compounds, molecular docking was performed by P.S.M.A. Shirley Leung, Prof. Paul O'Neill. Prof. Maria de Lurdes Cristiano supervised the synthetic work and revised the manuscript.

Regarding the biological studies:

- Replicating *Mtb* growth inhibition assays were carried out at the Liverpool School of Tropical Medicine by Alison Ardrey;
- *In silico* DMPK predictions were kindly provided by AstraZeneca and were obtained using their in-house predictive models;
- Experimental DMPK data was assessed through a high throughput platform provided by AstraZeneca U.K;
- *In vivo* PK cassette screening was performed by a Contract Research Organization (CRO), ChemPartner (Shanghai, China).

# 2.1. Background

## 2.1.1. Indole-2-carboxamides

In 2013, a HTS programme conducted at GSK revealed that the indole-2-carboxamide (IC) scaffold exhibits antimycobacterial activity, with compound **2.1** (**Figure 2.1**) showing a MIC of 0.47 μM.[1] In the same year, two other research groups explored and improved on this new scaffold.

The Kozikowski team (first research group) conducted a phenotypic screening of a library of 6800 compounds against *Mtb*. The compounds were selected following Lipinski's rule of five, aiming to identify drug-like compounds with antimycobacterial activity.[2] 4,6-Dimethylindole-2-carboxamide **2.2** (**Figure 2.1**) was found to exhibit an $MIC_{90}$ of 0.93 μM and an encouraging cytotoxicity profile, showing a half-maximal inhibitory concentration ($CC_{50}$) against Vero primate cells of >200 μM, thus, with an excellent selectivity index (SI).[2] An extended series of 40 new indole-carboxamide (IC) derivatives were subjected to SAR analyses to improve the drug-likeness of this series by addressing its poor physicochemical properties. It was established that other heterobiaryl rings, such as benzofuran, 5-azaindole, and benzimidazole, could not replace the indole moiety (ring A). The positioning of carboxamide function on the indole ring was also investigated. Shifting the carboxamide group to position 3 led to a significant reduction in activity, demonstrating that the carboxamide group at position 2 is critical. The loss of activity upon methylation of -NH, either of the indole or of the amide linker, revealed that the two -NH groups are essential to maintain potent antitubercular activity. When the lipophilic cyclohexane ring (ring B) was replaced by an unsubstituted phenyl ring or a nitrogen-containing heterocyclic ring, the antitubercular activity of these analogues dropped significantly.[2] The inclusion of a small ring (such as cyclopropyl) resulted in the complete loss of action, whereas bulkier substituents produced compounds with potent activity, a cyclooctane analogue **2.3** emerging as the most potent ($MIC_{90}$ = 0.013 μM, **Figure 2.1**).[2]

Another paper from the same research group revealed that a range of the saturated amide side chains was tolerated across analogues. 4,6-disubstitution with lipophilic groups proved crucial for activity, in which -F or -Cl substituents are favoured over methyl groups, which may circumvent a metabolic liability.[3] Continuous optimization resulted in the synthesis of IC compound **2.4**, bearing a 4,6-difluoro-substituted indole

and a chiral amide side chain, showing a potency of 12 nM and a superior toxicity profile, with a Vero $CC_{50}$ > 192 μM (SI ≥ 16000), together with excellent activity against MDR and XDR *Mtb* strains (**Figure 2.1)**. This compound also displayed superior ADMET properties and was shown to act in synergy with rifampicin (RIF).[3] Compounds with bulkier spiro moieties, such as ICA38 (**2.5, Figure 2.1**), retained a potent anti-TB activity, exhibiting a MIC = 0.003 μM.[3]

The Novartis team (second research group) also identified the hit **2.2** from a phenotypic HTS of a 2 million compound library, during their search for inhibitors of mycobacterial growth.[4,5] An SAR study was also conducted by this research team and similar findings were reached concerning the essentiality of the indolecarboxamide core, substituents in ring A, the indole and amide linker -NH group, and the lipophilic cycloalkyl in ring B. Their findings also indicated that 4,6-dichloro substitution on the indole ring provides superior metabolic stability, whilst the 4,4-dimethylcyclohexyl amide side chain offers a reasonable balance between metabolic stability and activity. The most advanced compounds were NITD-304 **(2.6)** and NITD-349 **(2.7)**, which demonstrated potent anti-MDR-TB activity, with MICs ranging from < 0.04 to 0.08 μM (**Figure 2.1**).[4–6] Interestingly, compound **2.4** demonstrated improved *in vivo* pharmacokinetic (PK) properties and a better dose-dependence during *in vivo* efficacy evaluation, compared to **2.7**, although having similar activity and lipophilicity.[7] Furthermore, the compounds **2.6** and **2.7** can also act synergistically with RIF.[3,8]

From research using genome sequencing to identify the molecular target and crystal structures of MmpL3 with different indolecarboxamides, MmpL3 was established as the target protein.[9,10]

The poor solubility of indole-2-carboxamides is a disadvantage. The amide-amine substitution of the incipient scaffold and the replacement of the indole ring with benzothiophene or benzoselenophene resulted in great improvements in solubility (10-20-fold higher). Without the carboxamide linker, potent activity was still achieved. However, the indole ring continues to be essential for high potency. Compound **2.8** exhibited a $MIC_{90}$ *Mtb* (**Figure 2.1**) of 0.13 μM, making it equipotent and 14-fold more soluble than its carboxamide counterpart. This compound also was shown to inhibit the mycolate transporter protein MmpL3.[11]

Since the discovery of the antitubercular properties of the IC scaffold, new IC derivatives active against *Mtb* (MIC < 10 μM) have emerged.[12–17] Additionally, many of these indole-2-carboxamide derivatives have been shown to treat nontuberculous

mycobacterial infections,[18] such those originating from *Mycobacterium abscessus*,[9,19–23] *M. massiliense*, *M. chelonae*, *M. avium* and *M. xenopi*.[23] According to the available evidence, several of these compounds exhibit activity against paediatric brain tumor cells, particularly the paediatric glioblastoma multiforme (GBM) cell line KNS42. Compound **2.9** was identified as the most potent, with dual anti-TB and cytotoxic activities against line KNS42, with a MIC of 0.62 µM and an $IC_{50}$ = 0.84 µM, respectively (**Figure 2.1**).[24]

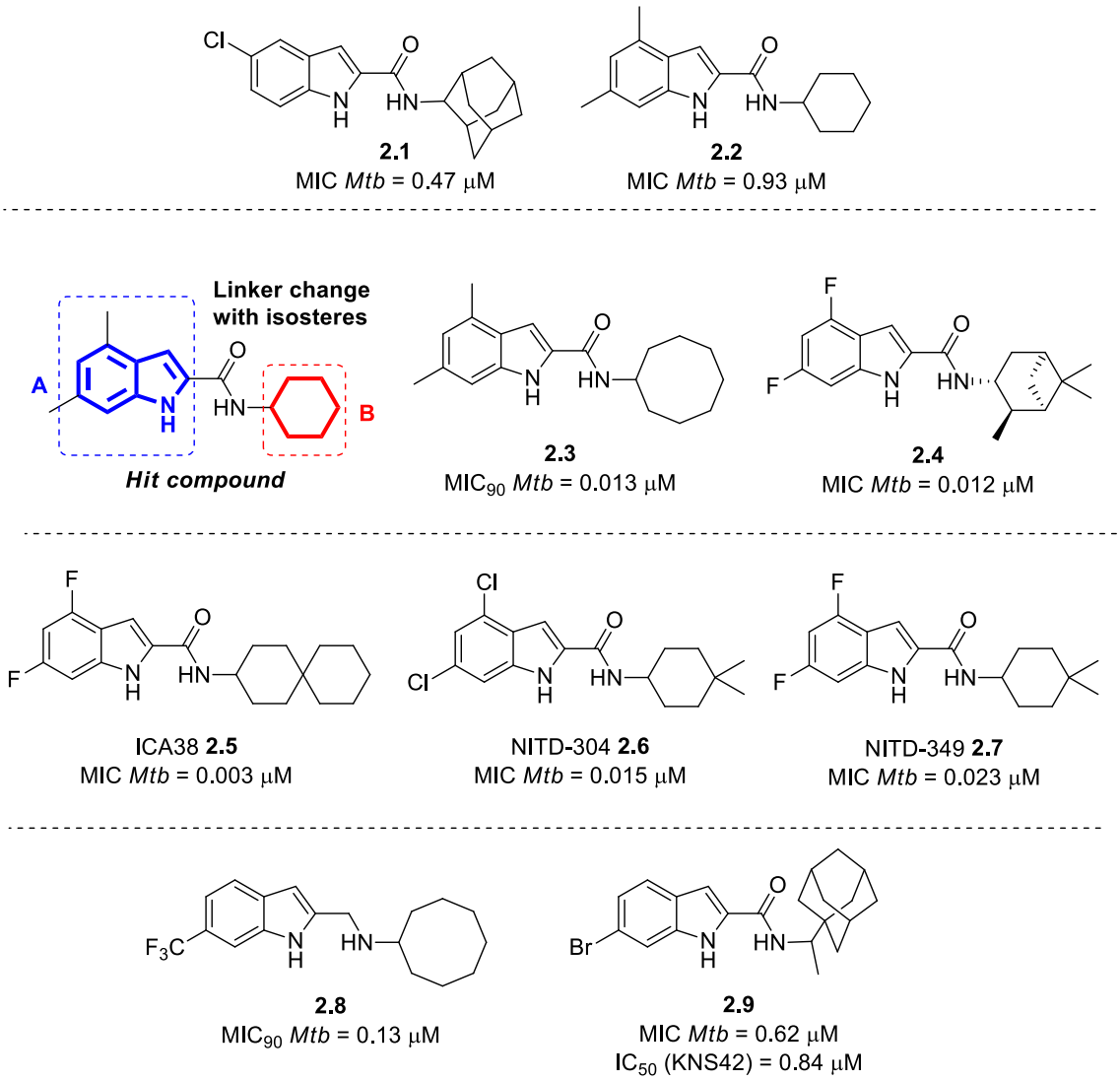


**Figure 2.1.** Structure representations of indole-2-carboxamides with potent activity as MmpL3 inhibitors.

## 2.1.2. Benzothiazinones

### 2.1.2.1. Covalent Inhibition

The flavoenzyme DprE1 was first discovered as a target of benzothiazinones (BTZ), a class of compounds known to inhibit DprE1 irreversibly through formation of a covalent adduct with the amino acid residue Cys387. Makarov and colleagues demonstrated that BTZ are capable of strongly suppressing DprE1 activity *in vitro* and *in vivo*. Compound BTZ043 (**2.10, Figure 2.2A**) is one of the most promising benzothiazinones synthesized, with a minimum inhibitory concentration (MIC) of 1 ng/mL (2.3 nM), which is significantly superior to the MICs of frontline medications such as ethambutol (EMB, 15 mg/mL) and isoniazid (INH, 0.02-0.2 mg/mL).[25–27] BTZ043 acts as a prodrug in the presence of $FADH_2$, where the nitro group linked to the BTZ core is reduced to a nitroso functionality, affording the active derivative **2.11** (which is generated by DPR). The nitroso form **2.11** reacts with the thiol group on the Cys387 residue in DprE1, producing a semi-mercaptal bond with the amino acid residue and a covalent adduct that acts as a suicide substrate, irreversibly inhibiting the enzyme (**Figure 2.2A**).

Despite its exceptional potency (MIC = 2.3 nM), BTZ043's efficacy in a mouse model of TB was lower than expected due to its poor solubility (though it has moderate hydrophobicity (logP = 2.84)).[25,28–33] Makarov and co-workers addressed these issues to improve the pharmacological properties of the benzothiazinones. As a result, substituted 2-piperazino-benzothiazinones (PBTZ) with increased lipophilicity were produced.[32] This new series yielded a variety of compounds with diverse substituents in the piperazine ring's *N*-4 position; when hydrophilic groups such as alcohols, carboxylic acids, secondary or tertiary amines were introduced, activity was reduced or eliminated, in contrast to **2.10**. The most potent blocks examined were piperidines alkyl substituted at *N*-4 position, affording PBTZ compounds with MIC values ranging from 0.41 to 1.69 nM. The most active compound was PBTZ169, also known as Macozinone (**2.12**, **Figure 2.2B**), bearing a cyclohexylmethyl group as the piperazine *N*-4 substituent. PBTZ169 produced a much more significant bactericidal effect in the lungs than **2.10**, at the same dose, reducing colony forming units (CFU) by >0.5 log units.[32,34] PBTZ169 has successfully completed Phase I clinical trials and demonstrated synergy with Bdq and PYR, establishing this combination as a viable novel tuberculosis treatment regimen.[35,36] The van der Waals interactions between the trifluoromethyl group of the molecule and the backbone of the residues are key features for potent activity, as are the interactions

involving the sulfur atom and the carbonyl group in the thiazinone ring..[25,32,33]

The clearly established essentiality of a nitro group at position 8 and its correlation in activity against DprE1 mutants C387A and C387S were taken as typical features of covalent DprE1 inhibitors.[37] Since then, more than 600 new nitrobenzothiazinones (BTZ) have been described and nearly 90% of these synthetized molecules have evidenced activity against *Mtb* (MIC < 10 µM) (**Figure 2.2C**).[26–60]

### 2.1.2.2. Non-covalent Inhibition

The nitro functional group in BTZs is critical for a covalent mechanism of inhibition. Its replacement with other functional groups with insufficient electrophilic properties for covalently binding to DprE1 resulted in a 500-fold increase in the MIC, compared to BTZ043. These modifications were made in response to concerns about the nitro group's possible mutagenicity, which have now been dismissed.[25,28] Nonetheless, progress has been made towards replacing the nitro functional group while retaining activity. Makarov *et al*.[61] proposed non-covalent benzothiazinone inhibitors (NC BTZ) in 2015, obtained by replacing the nitro group with a pyrrole ring. The MIC values for the compounds against the drug-resistant *Mtb* $H_{37}$Rv strain varied from 0.34 µM to 5.0 µM, thus less potent than the nitro-containing BTZs but still very active. Despite their *in vitro* efficacy, these compounds were ineffective against a mouse model of acute TB, demonstrating the difference in activity between non-covalent and covalent binding for BTZ-mediated TB death. PyrBTZ01 (**2.13**) and PyrBTZ02 (**2.14**) exhibited the best activity, with MIC values of 0.35 µM and 0.34 µM, respectively (**Figure 2.2D**). Tiwari *et al.* replaced the nitro group for an azide group, resulting in the non-covalent inhibitor BTZ with a MIC value of 0.47 µM (**2.15**, **Figure 2.2D**). Enzymatic experiments with recombinant DprE1 from *Mtb* revealed that BTZ-$N_3$ is an effective reversible and non-covalent inhibitor of DprE1.[62] In another investigation, Liu and co-workers demonstrated that replacing the nitro group in BTZs with halogen (Cl, Br, or I) resulted in inhibitors of the DprE1 enzyme, with DprE1 $IC_{50}$ values of 0.92-2.35 µM and MIC values of 0.03-0.063 µM against *Mtb* $H_{37}$Rv strains (**2.16-18, Figure 2.2D**).[55] All these data demonstrate how effectively the 1,3-benzothiazin-4-one scaffold inhibits enzyme activity, even in a non-covalent mode of binding.

In 2021, Madikizela *et al*. described the synthesis of halogenated non-nitro benzothiazinones, in which the 8-nitro functional group and the trifluoromethyl group at *C*-6 were replaced by H or F. *In vitro* tests against *Mycobacterium aurum* DSM 43999

and *Mtb* $H_{37}Rv$ revealed no significant inhibitory effects (**2.19** and **2.20**, MIC = 60-100 µM, **Figure 2.2D**), indicating that the 8-nitro group is required for activity in covalent inhibitors, while the elimination the -$CF_3$ at position 6 of the benzothiazinone ring significantly reduces the antimycobacterial activity in BTZ compounds designed to inhibit DprE1 non-covalently.[63]

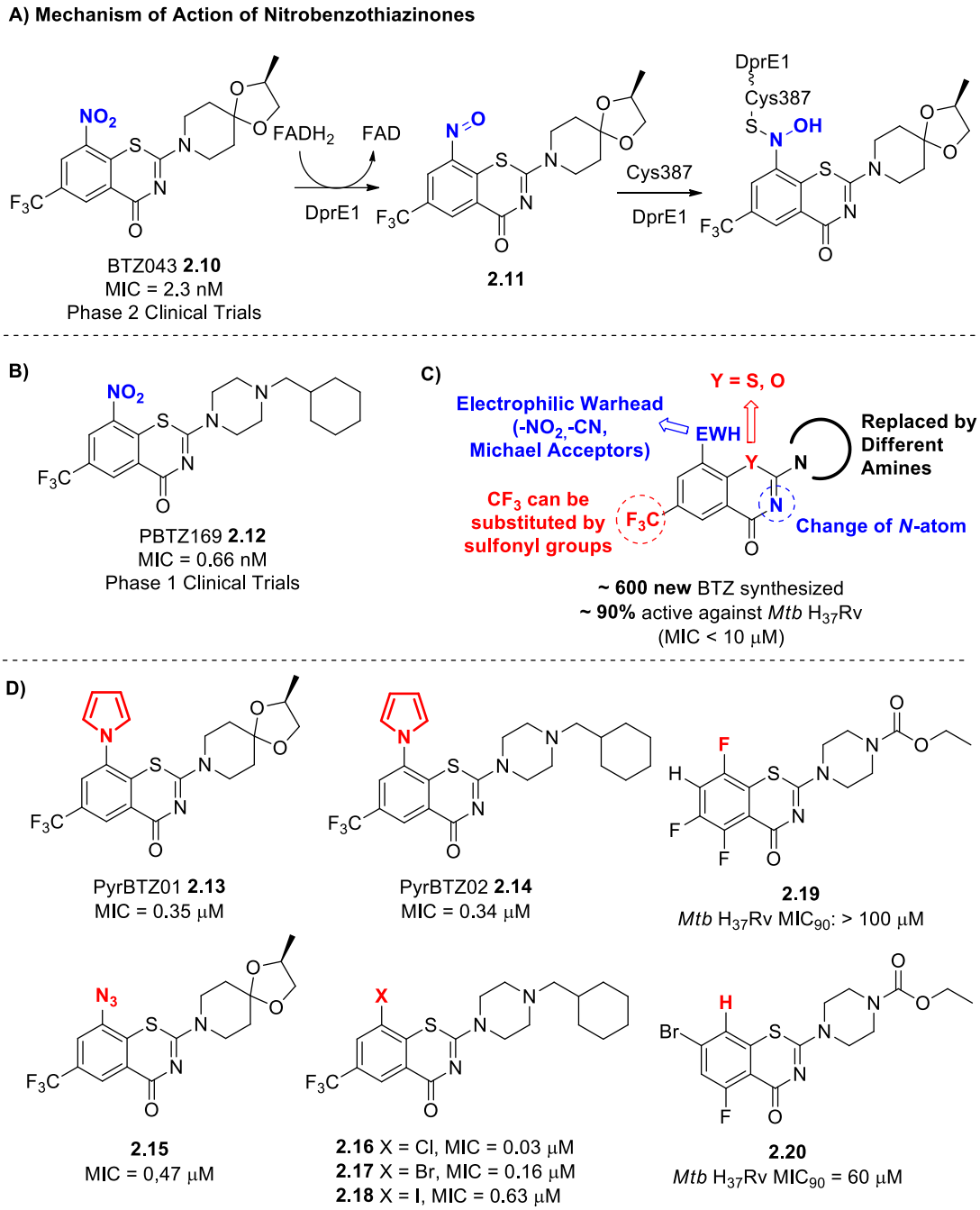


**Figure 2.2. A)** Activation of compound BTZ043 by reduction of nitro to nitroso group; **B)** PTBZ169; **C)** Allowed chemical diversity in the development of BTZs, from SAR analysis; **D)** Structure representations of non-covalent benzothiazinones.

## 2.2. The endoperoxide-hybrid approach and aim of this project.

It is widely documented that treating non-replicating persistent (NRP) tuberculosis infection is a considerable therapeutic challenge, which partially justifies the extensive anti-TB treatment regimens.[64] As described in Chapter 1 (Section 1.9.1.), the Dos regulon is controlled by the regulator protein DosR and its two heme-based histidine sensor kinases, DosS and DosT, regulating the *Mtb*'s capacity to transit into the NRP state.[65–67] Due to the NRP *Mtb*'s decreased metabolism and absorption of anti-TB drugs, many anti-TB treatments are ineffective against NRP *Mtb*.

Artemisinin (ART, **2.21**, **Figure 2.3**) downregulates DosRST-dependent proteins and reduces survival in hypoxic shift-down assays. This inhibition was attributed to the ability of ART to interact with heme in DosS and DosT, leading to inactivation. Moreover, pre-treatment with ART increases the sensitivity of NRP *Mtb* to treatment by isoniazid – a first-line anti-TB drug with no activity against NRP *Mtb*.[68] Additionally, it was discovered in 2022 that synthetic peroxides 1,2,4-trioxolane OZ277 (**2.22**) and OZ439 (**2.23**, **Figure 2.3**) could target DosS-mediated hypoxia signalling in *M. abscessus* and reproduce the DosS knock-out phenotype.[68]

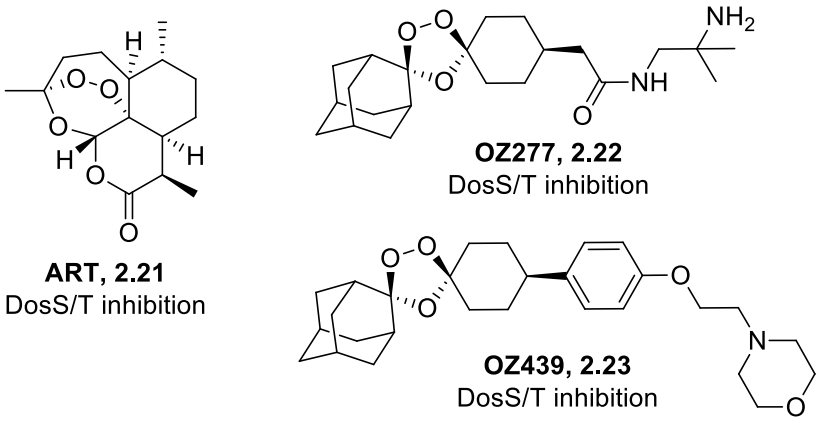


**Figure 2.3.** Structure representations of antimalarial endoperoxides with proved activity as DosRST inhibitors.

Since ART, OZ277, and OZ439 have been shown to inhibit these heme-based histidine kinases, we postulated that other synthetic endoperoxides may also interact with DosS and DosT. In addition, pursuing a dual-action small molecule capable of disrupting DosRST signaling while also inhibiting a known *Mtb* target protein appears to be a valid treatment strategy for NRP *Mtb*.

Hybrid drugs are produced when two structural or pharmacophoric moieties merge covalently to create a single molecule, with each scaffold possessing its own activity.[69] Consequently, this sort of hybrid molecules reduces the likelihood of drug resistance and can be tailored to act in different molecular targets.[70]

Endoperoxide based drug-hybrids have been extensively explored in numerous parasitic diseases, namely malaria,[71–75] schistosomiasis,[76,77] and leishmaniasis,[78] among others. Most of these hybrids are produced by linking a peroxide moiety, either a synthetic peroxide or an ART derivative, to a scaffold (e.g., aminoquinoline, pyrimidine, pyrazinoisoquinoline, pyrazole) that exhibits a different mechanism of action.

The two anti-TB drug classes explored in this section are the MmpL3 inhibitor indole-2-carboxamide scaffold and the DprE1 inhibitor benzothiazinone scaffold.

As described previously, both classes are very potent against replicating *Mtb*. For example, indole-2-carboxamide NITD-304 **(2.6)** has a MIC of 0.015 µM against replicating *Mtb,* although in the model of nonreplicating persistent TB, the molecule was found to be less effective, with a MIC >27 µM.[5] Similarly, BTZ043 **(2.10)** exhibits a very potent MIC of 0.0023 µM but was demonstrated to be less potent in starvation and auxotrophic low-metabolism in *vitro* models[25] and inactive ($MIC_{99}$ > 10 µg/mL) against the streptomycin-starved 18b strain (ss18b), a model for nonreplicating *Mtb*.[61]

Given the findings mentioned above, we propose hybridizing the two separate anti-TB classes by combining peroxide-containing moieties with the indole-2-carboxamide scaffold (MmpL3 inhibition) and the benzothiazinone scaffold (DprE1 inhibition), using the 1,2,4-trioxane moiety for this research. With this endoperoxide-based hybrid approach we aim to establish a dual mode of action, increasing *Mtb*'s sensitivity to the active anti-TB pharmacophore while also targeting the DosRST signaling.

## 2.2.1. This Project: Design of Peroxide Containing Hybrid Molecules

Synthetic endoperoxides are typically amphiphilic molecules where the peroxide-containing moiety is stabilized by a bulky aliphatic group, such as spirocyclohexyl or spiroadamantyl. Modifying the sidechain will improve the physicochemical properties for superior oral solubility and metabolic stability.[79–81]

A suitable site for peroxide moieties substitution would be in a non-polar side chain of the molecule. Both the indole-2-carboxamide ICA38 (**2.5**) and the

benzothiazinone BTZ043 (**2.10**) include amine functionalities linked to side chains in carbocyclic spiro rings, which are ideally suited for the attachment of a peroxide containing building block. In addition, coupling occurs during a final convergent step of the synthesis, allowing the peroxide core to be generated prior to its linkage to the other scaffold and thereby preventing any synthetic incompatibilities (**Scheme 2.1**).

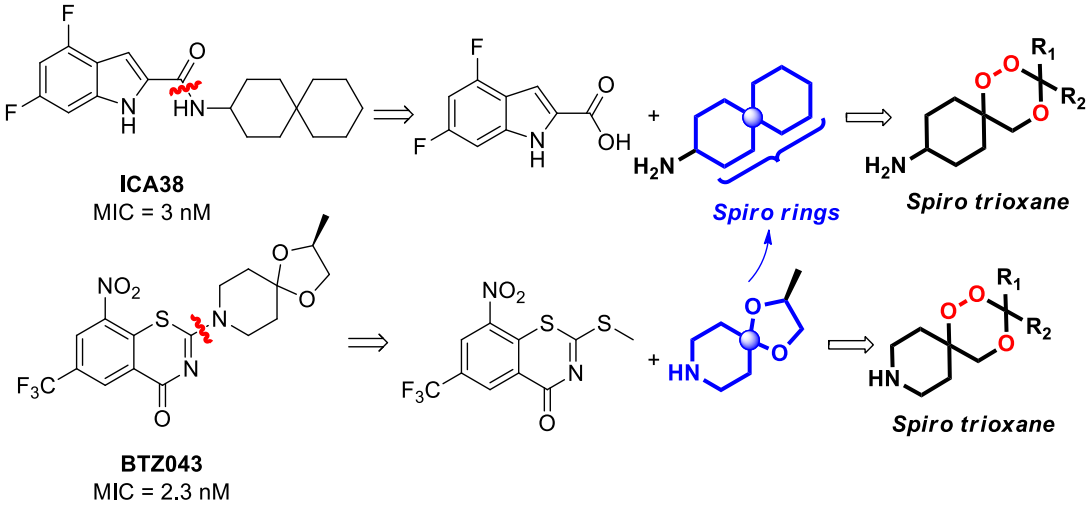


**Scheme 2.1.** Analysis for the synthesis of peroxide containing hybrids.

As described in Section 2.1.1, selected indole-2-carboxamides inhibit the transporter protein MmpL3. The structure of the complex formed between MmpL3 and ICA38 was determined, revealing that this indole-2-carboxamide recognizes the same binding pocket as the inhibitors SQ109 and AU1235 (*the reader is referred to* ***Table 1.3*** *in* ***Chapter 1*** *for the structure representations of SQ109 and AU1235*), within the pore of MmpL3, in sub-sites S3, S4 and S5 (**Figure 2.4**).[10] ICA38's bulky indole group fits neatly into the hydrophobic subsite (S3) at the top of the channel, resulting in a more extensive hydrophobic interaction. This inhibitor disrupts the two Asp-Tyr pairs involved in proton translocation upon binding. In the S4 subsite, the amide group of ICA38 forms hydrogen bonds with the side chain of Asp645, whereas the carbonyl oxygen of ICA38 establishes a non-canonical hydrogen bond with the side chain of Tyr646. The carbocyclic spiro group inserts favourably into the bulky hydrophobic subsite (S5) at the bottom of the tunnel, thereby providing an extensive network of hydrophobic interactions.[10] Notably, it has been found that the S5 pockets may tolerate a range of hydrophobic amide side chains, corroborating the pattern observed for other MmpL3 inhibitors.[17]

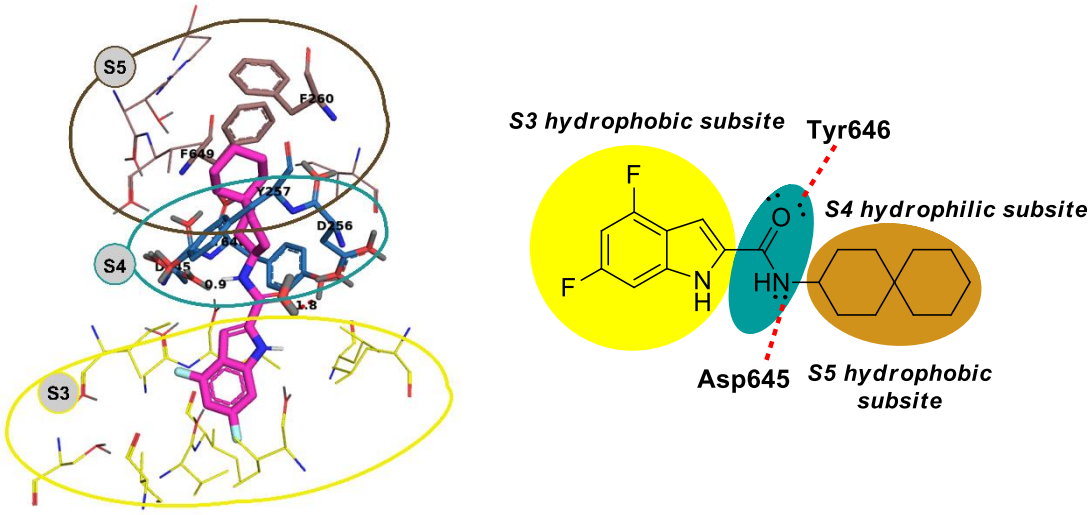


**Figure 2.4.** PyMol representation of ICA38 co-crystallised with MmpL3 (*left*, PDB: 6AJJ).[10] Structure representation and binding mode of indole-2-carboxamide ICA38 in the binding site of MmpL3 (*right*).

Regarding the proposed hybrids, the *N*-linked hydrophobic amide moiety would be replaced by a spiro endoperoxide (**Figure 2.5A)**. It is envisaged that the hydrophobic amide containing peroxide would be tolerated at the S5 site. The indole ring will be maintained in the proposed compounds, including the substituents at positions 4 and 6, which is ideal to guarantee optimal contact within subsite S3. Moreover, if permitted, it is anticipated that the binding mechanism of the peroxide side chain will not affect the hydrogen bonding interactions in the S4 pocket. Three endoperoxide classes were considered to design the corresponding hybrids (**Figure 2.5B/C)**: 1,2,4-trioxanes, 1,2,4,5-tetraoxanes and 1,2,4-trioxolanes. Trioxolane- and tetraoxane-containing analogues (**Figure 2.5B**) were synthesised by another member of the group while trioxane-containing analogues were synthesised within this PhD project. The proposed 1,2,4-trioxane-based targets (**TIC01-03**) are summarized in **Figure 2.5C**.

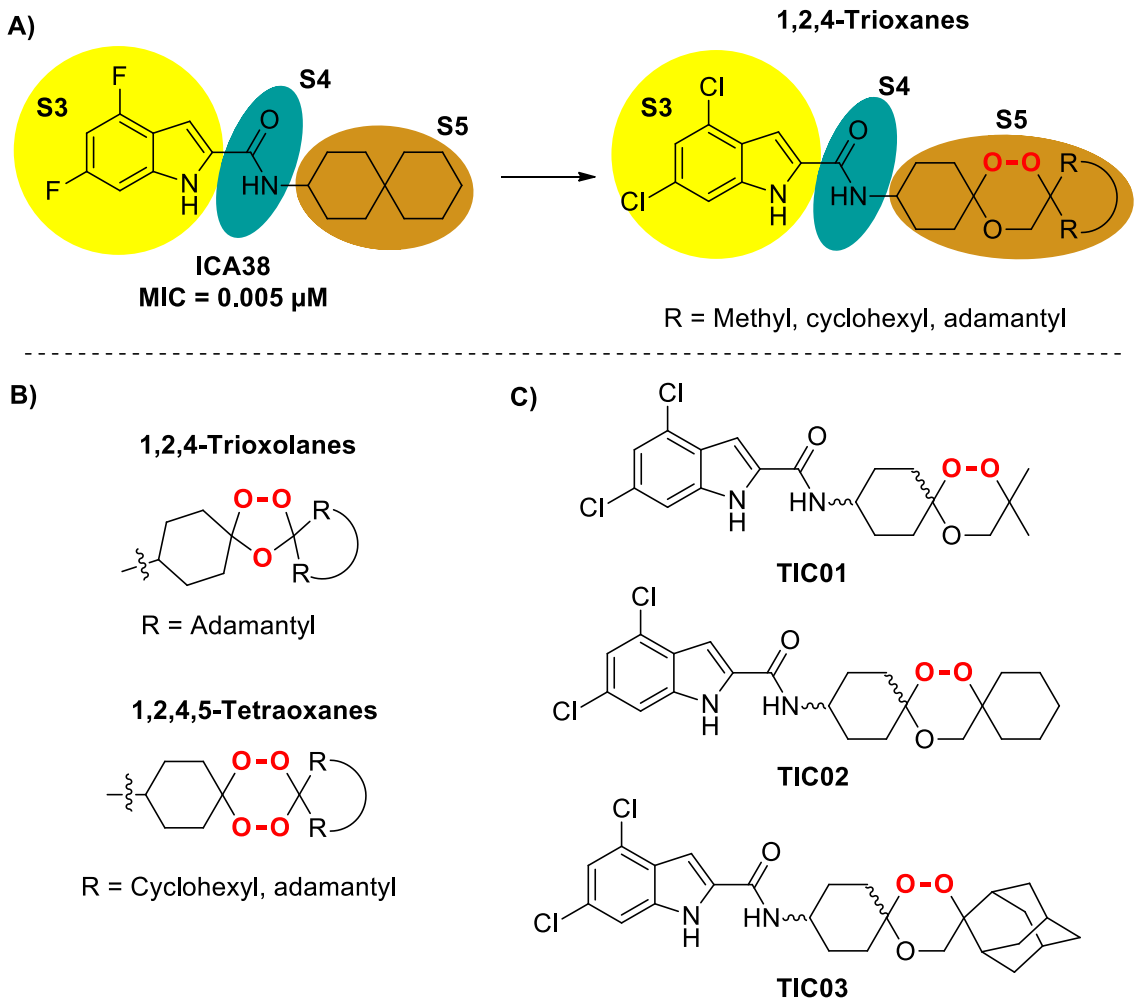


**Figure 2.5. A)** Structure representation and proposed binding mode of ICA38 and IC-trioxane hybrids, in subsites S3, S4 and S5. **B)** Structure representation of the trioxolane and tetraoxane scaffold. **C)** Structure representation of the proposed 1,2,4-trioxane containing IC-hybrid MmpL3 inhibitors prepared within this PhD project.

As described in **Section 2.1**, the DprE1 flavoenzyme displays a polar localization in *Mycobacterium tuberculosis*, in which BTZ DprE1 inhibitors bind within the binding pocket, with their hydrophobic amine side chains at position 2 extending into solvent-exposed space (**Figure 2.6A/B**).[60] This interaction profile was demonstrated using BTZ-TAMRA as a fluorescent probe in chemical biology experiments. This probe combines the BTZ core with the bulky fluorescent dye carboxytetramethylrhodamine (TAMRA) *via* an octyl linker, while maintaining a reasonable *Mtb* MIC of 6.2 µg/mL (**Figure 2.6C**).[38]

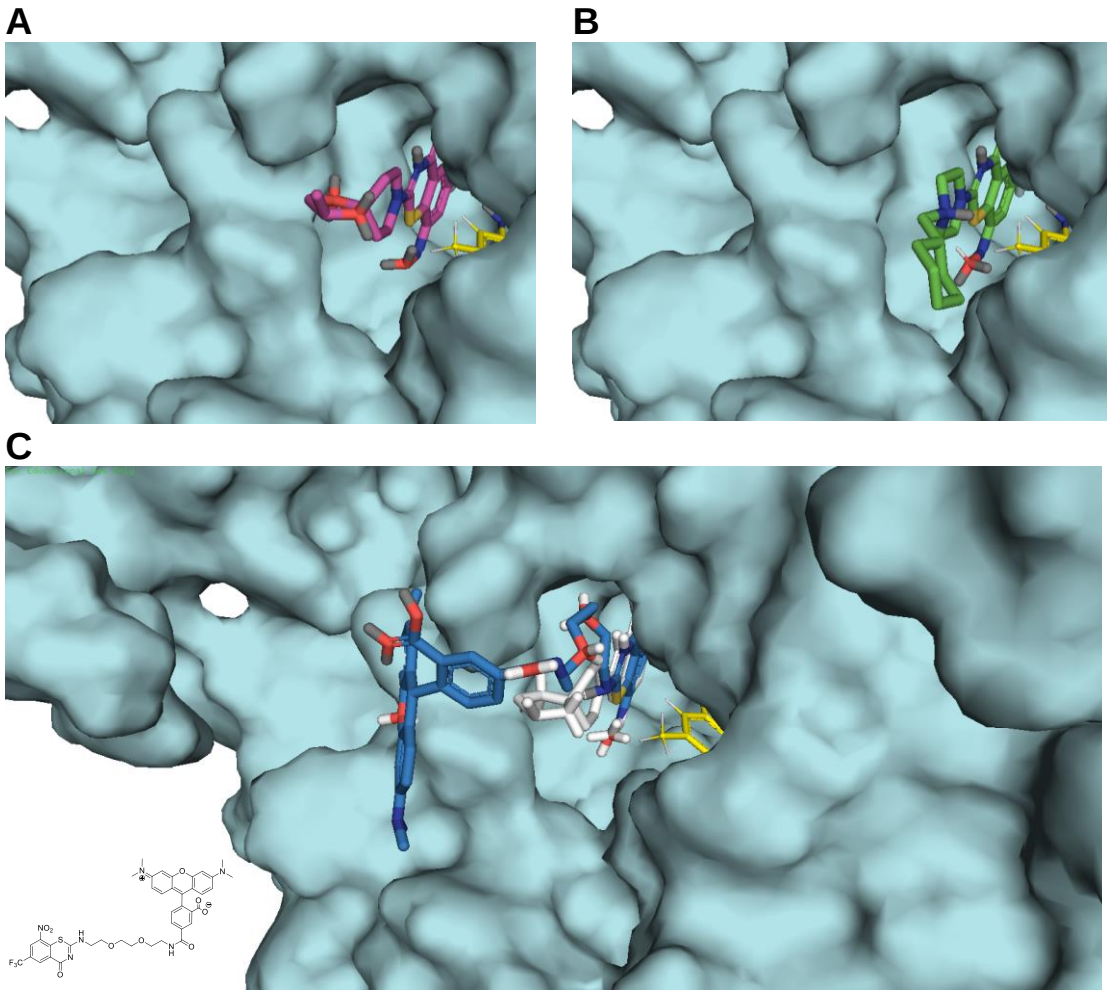


**Figure 2.6. A)** Crystal structure of BTZ403 (*dark pink*) in complex with DprE1 (PDB: 6HEZ)[82] and **B)** Crystal structure of PBTZ169 (*green*) in complex with DprE1 (PDB: 4NCR),[32] showing the side chain of both molecules in the solvent exposed space. **C)** Structure representation and overlay of docked structure of BTZ-TAMRA with the extracted reference ligand (BTZ043, *in white*).

The SAR investigations around the trifluoromethyl and nitro groups at positions 6 and 8 were found to be very restrictive, with minor modifications tolerated. In contrast, considerable diversity in the structure of the amine side chain at position 2 is possible.[37,39] These findings imply that structural changes in position 2 are a suitable spot for hybridization since side chain modifications are unlikely to impact negatively the binding interactions within the active site. Therefore, we proposed that substituting the amine side chain at position 2 of BTZ043 and PBTZ169 with peroxide-containing moieties is feasible, in which modification of the amine side chains is depicted in **Figure 2.7**. BTZ based hybrids were designed as either analogues of BTZ043 (**B1-5**) or of PBTZ169 (structures **P1-7**). Tetraoxane- (**B1** and **P1-2**) and trioxolane- (**B2** and **P3**) containing analogues were synthesised by another member of the group. Within this PhD project,

1,2,4-trioxanes **B3-B5, P4-P7** and controls **C1-C4** were synthesised.

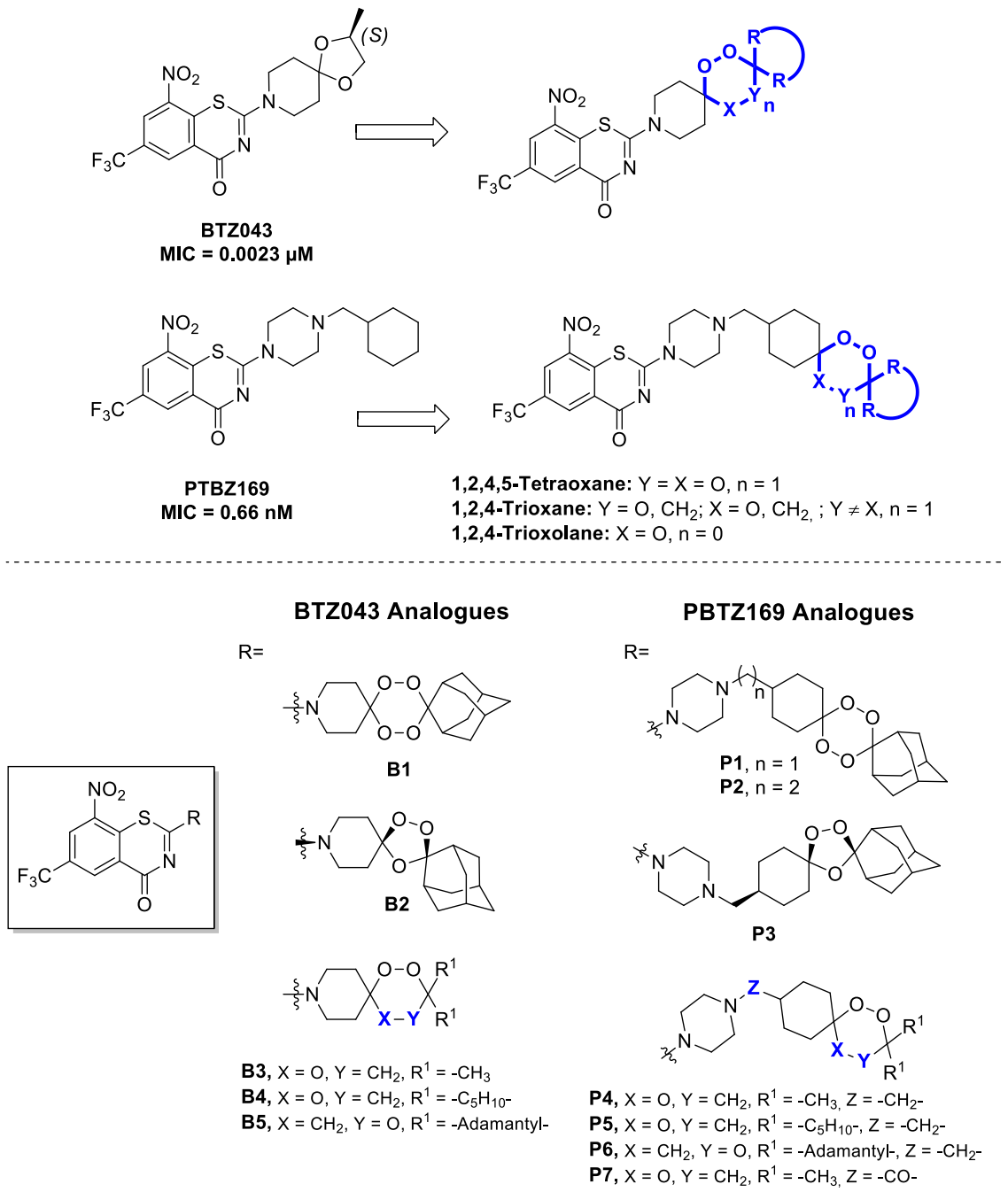


**Figure 2.7.** Proposed structure representations of BTZ043- and PBTZ169-derived peroxide hybrids.

Three classes of molecules were considered for synthesis: 1,2,4-trioxane hybrids **B3-B5** and **P4-P7** and two types of control compounds. The control compounds are divided into two categories: a) non-peroxide controls (**C1** and **C3**), enabling to compare the effect of the peroxide scaffold against the replicative and non-replicative state

in *Mtb* and b) the metabolite controls (**C2** and **C4**), which are the hypothesized products from the decomposition or metabolism of the peroxide moieties, in which these compounds would likely contribute in part to the mycobacterial activity (**Figure 2.8-A**).

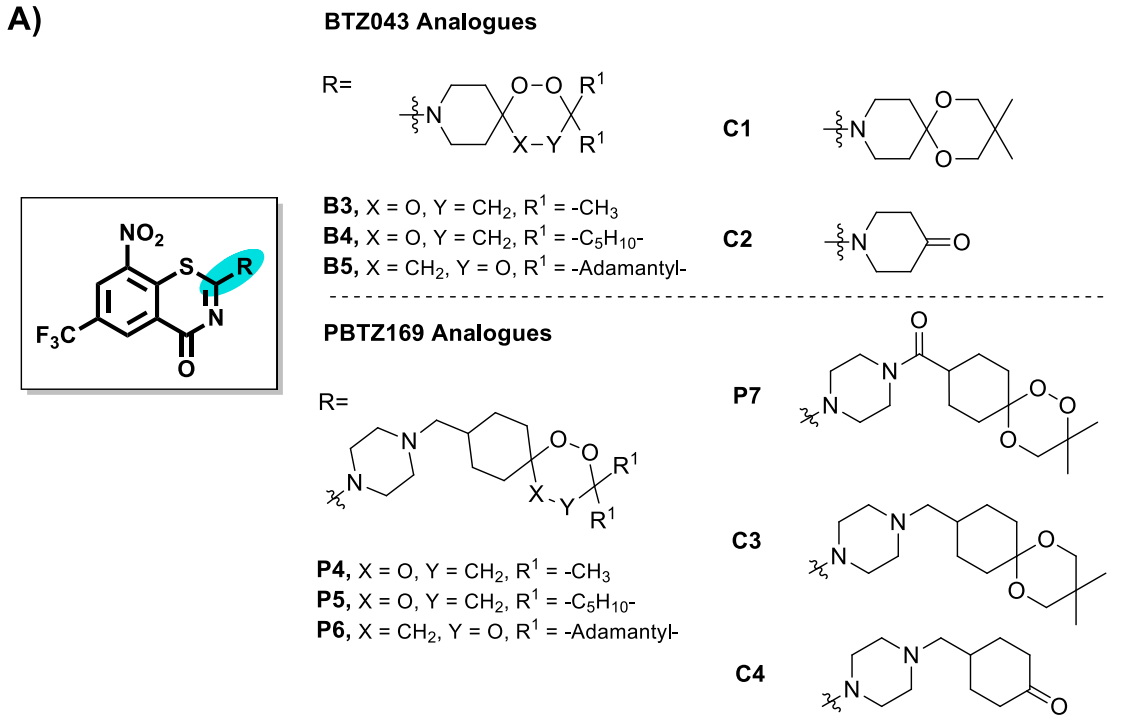


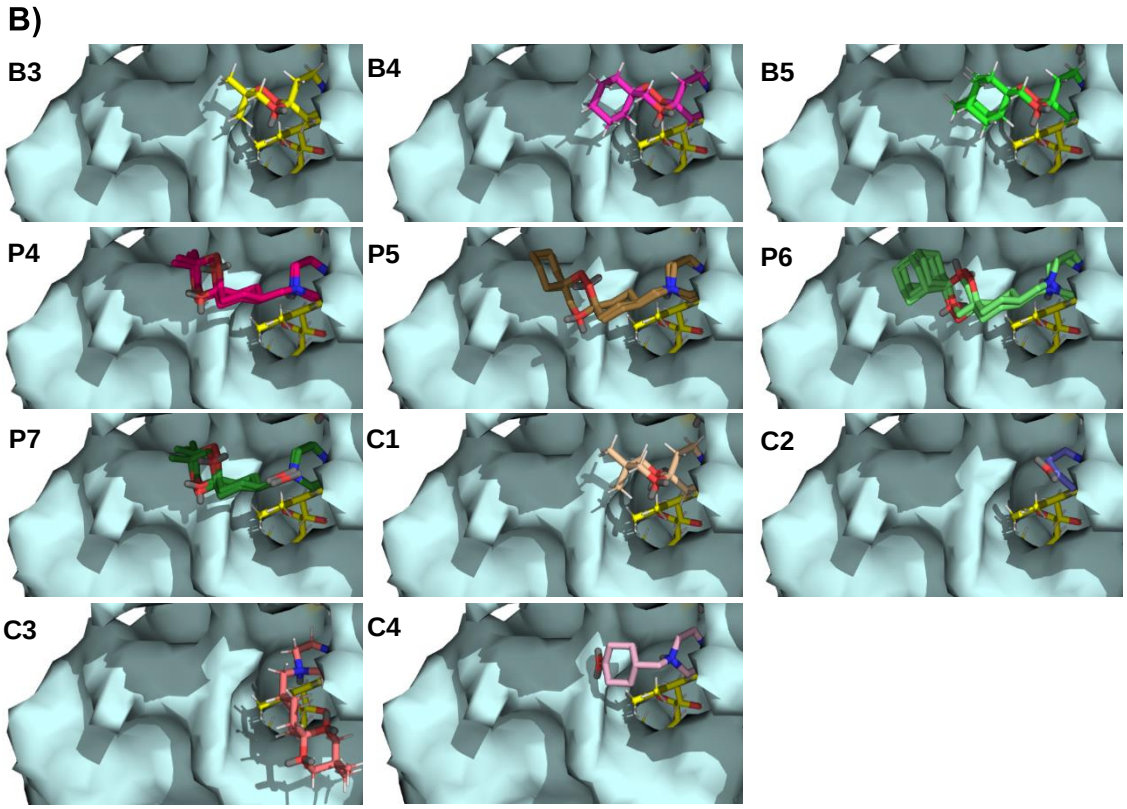


**Figure 2.8. A)** Proposed structure representations of peroxide containing BTZ-hybrid DprE1 inhibitors for this PhD project. **B)** Docked structures of 1,2,4-trioxanes **B3-B5**, **P4-P7** and controls **C1-C4.** The side chain of all molecules can be observed in the solvent exposed space.

In **Figure 2.8-B**, the docked structures of the corresponding 1,2,4-trioxanes **B3-B5**, **P4-P7** and controls **C1-C4** in the DprE1 enzyme are illustrated. Most of the side chain containing peroxide extends out of the pocket and into solvent-accessible space. Hence, replacing the side chains of BTZ043 and PBTZ169 with peroxide-containing moieties in the amine side chain at position 2 is probably to be tolerated in the active site of the flavoenzyme.

# 2.3. Results and discussion

## 2.3.1. Synthesis

### 2.3.1.1. Indole-2-Carboxamides

The preparation of the indole-2-carboxamide-trioxane hybrids involved a convergent synthetic strategy culminating in amide coupling between peroxide-containing amines and 4,6-dichloro-indole-2-carboxylic acid **2.27**. The synthetic strategies adopted are depicted in **Scheme 2.2**.

The synthesis of carboxylic acid **2.27** starts with reaction between (3,5-dichlorophenyl)hydrazine hydrochloride **2.24** and ethyl pyruvate, in acidic conditions, affording the corresponding (3,5-dichlorophenyl) hydrazone **2.25**, with 68% yield.[83] Fischer indole synthesis follows, by treating **2.25** with the Eaton's reagent, in toluene, to produce ethyl 4,6-dichloro-indole carboxylate **2.26** in moderate yield (64%). The proton corresponding to the indole ring (N-H) is evidenced at 9.31 ppm together with the singlet (-$CH_3$) disappearance at 2.11 ppm in the $^1$H NMR spectrum (in $CDCl_3$). $^{13}C\{^1H\}$ NMR also evidences characteristic carbon peaks for the indole ring at 107.10 ppm (=CH). Hydrolysis of the ester derivative **2.26** upon treatment with LiOH in THF and water (1:1) gave the free acid **2.27**, with 83% yield.

Amine derived 1,2,4-trioxanes and their corresponding intermediates were also synthesized by adapting procedures described in the literature, and the synthetic strategies are depicted in **Schemes 2.3** and **2.4**. The different methods for the synthesis of various 1,2,4-trioxane cores have been explored and are described in **Chapter 4**. For the synthesis of the dimethyl- and spirocyclohexyl-trioxane derivatives (**Scheme 2.3**), the strategy begins with Co(II)-mediated peroxysilylation of allylic alcohols **2.29** and **2.30** to generate their silyl peroxides derivatives (**HSP**), as intermediate compounds. Allylic alcohol **2.30** can be generated by reduction of the starting 1-cyclohexene-1-carboxylic acid **2.28** with $LiAlH_4$, affording the allylic alcohol in quantitative yield.

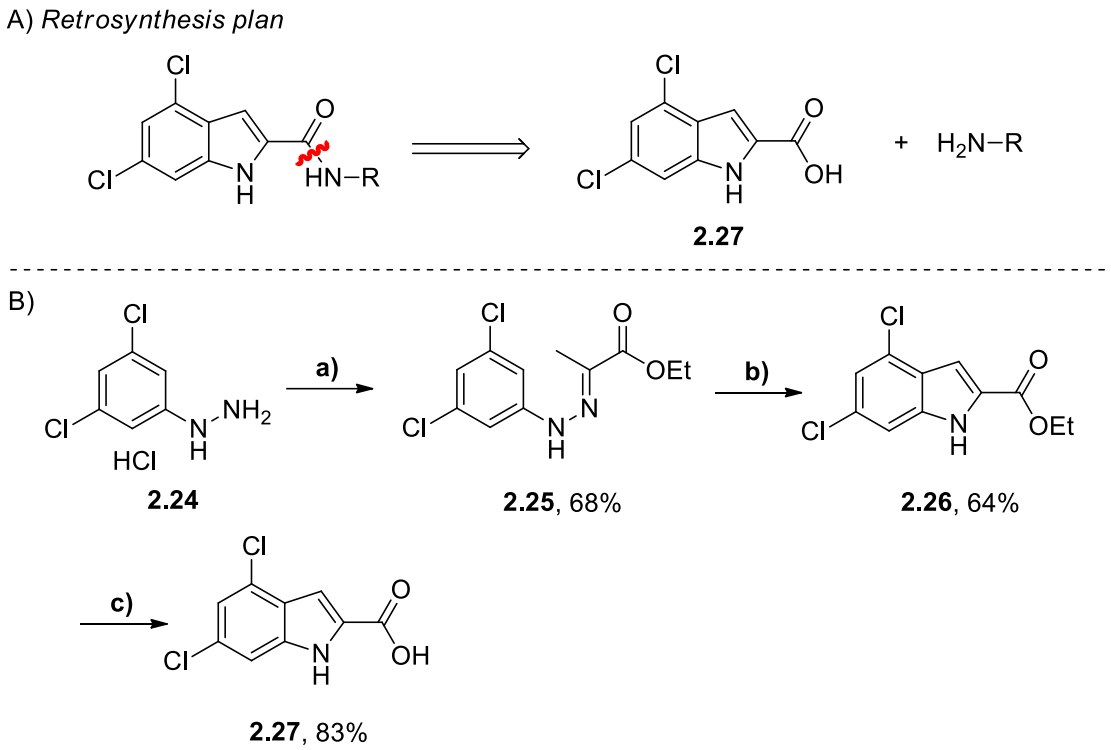


**Scheme 2.2. A)** Retrosynthesis plan for the preparation of peroxide containing 2-indole-carboxamides. **B)** Synthesis of the indole scaffold. Reagents and conditions: (a) Ethyl pyruvate, $H_2SO_4$, EtOH, 0 ºC-rt, 3 h; (b) Eaton's reagent, toluene, reflux, 2 h; (c) LiOH, THF/$H_2O$, rt, 12-16 h.

The **HSP** derivatives then underwent reaction with 2-(4-oxocyclohexyl)isoindoline 1,3-dione in the presence of heterogeneous catalyst Silica Sulfuric Acid (SSA), affording 1,2,4-trioxane- containing phthalimides **2.31** and **2.32** in moderate yields (24-56%). The phthalimido group was chosen as the protecting group for this reaction since it tolerates the strong oxidative conditions required to produce the 1,2,4-trioxane moiety. The presence of three characteristic 1,2,4-trioxane carbon peaks in their respective $^{13}C$ NMR spectra indicated the formation of the 1,2,4-trioxane cores [δ 100.67/100.56 (O-C-O), 76.92 (O-C-$CH_2$), 67.03/66.57 (-$CH_2$) ppm for **2.31** and δ 100.88 (O-C-O), 77.86 (O-C-$CH_2$), 66.43 (-$CH_2$) ppm for **2.32**, in $CDCl_3$]**.** The detection of duplicate peaks on the $^{13}C\{^1H\}$ NMR, confirmed that the peracetalization step yielded a mixture of diastereoisomers, *cis* or *trans*, in an approximately 2:1 ratio. Since separating the diastereoisomers by column chromatography or preparative TLC was unsuccessful, the synthesis was continued using the mixture. The phthalimido protecting group was removed by hydrazinolysis to give the hydrochloride salts of the desired amines (**2.33** and **2.34**) in moderate yields (72 and 81%).[84] Following the amide coupling protocol, the novel indole-2-carboxamide peroxide hybrids were efficiently

generated.[3] The 1,2,4-trioxane amines **2.33** and **2.34** were reacted with 4,6-dichloro-indole-2-carboxylic acid **2.27** under a nitrogen atmosphere, in the presence of 1-ethyl-3-(3-(dimethylamino)-propyl)carbodiimide hydrochloride (EDC·HCl) and hydroxybenzotriazole (HOBt) as coupling agents and triethylamine as a base, to obtain compounds **TIC01** and **TIC02** in reasonable yields (17-35% and 21-38%, respectively).

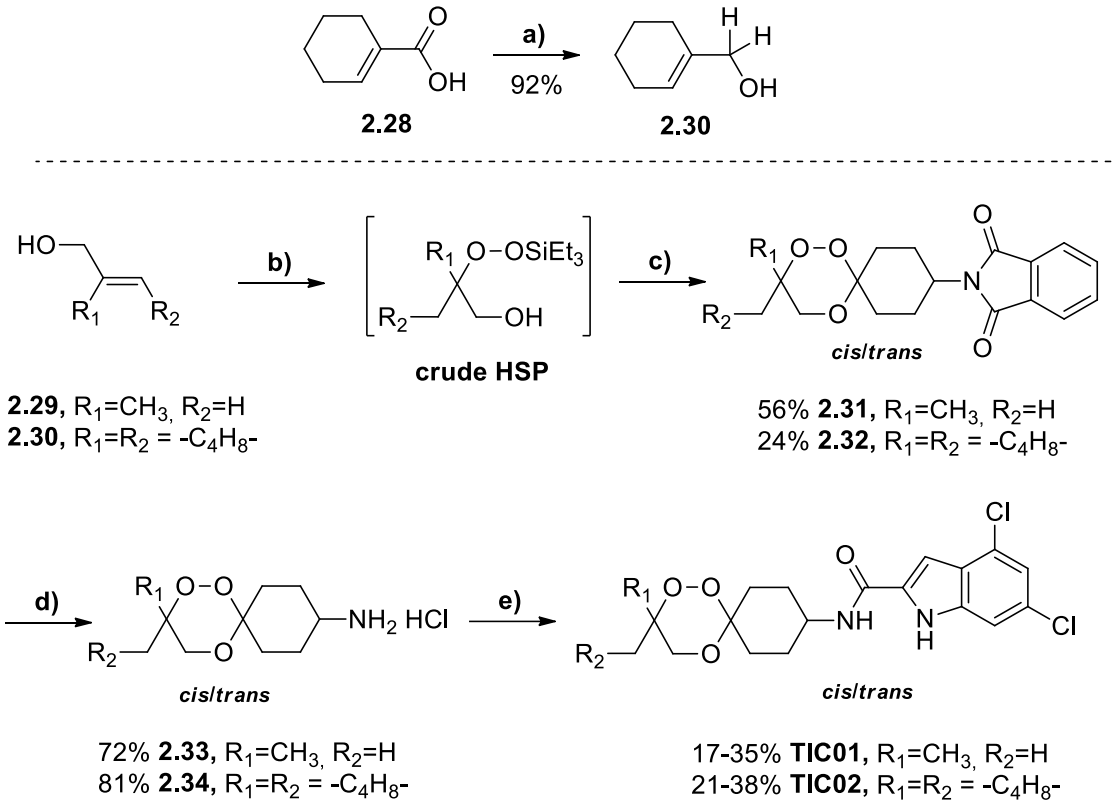


**Scheme 2.3.** Schematic representation of the general synthetic approach followed to prepare the dimethyl and cyclohexyl substituted peroxide amines for the indole-2-carboxamide-derived hybrids. Reagents and conditions: (a) 1. $LiAlH_4$, anhydrous $Et_2O$, 0ºC, 1h; 2. $H_2O$; (b) $Et_3SiH$, $Co(thd)_2$, under $O_2$, DCE, rt, o/n; (c) 2-(4-oxocyclohexyl)isoindoline-1,3-dione, SSA, anhydrous $CH_2Cl_2$, 0-rt, 1 h; (d) 1. $N_2H_4.H_2O$, $CHCl_3$/MeOH (7:3), 60 ºC, o/n; 2. 2 M HCl in $Et_2O$, 0-rt, 30 min; (e) **2.27**, EDC·HCl, HOBt, $Et_3N$, $CH_2Cl_2$, rt, o/n.

For the adamantyl-trioxane-IC hybrid (**Scheme 2.4**), the synthesis began with the preparation of the phthalimido 1,2,4-trioxane **2.37**. The process involved perhydrolysis of spiro-oxirane adamantane **2.36** to its β-hydroperoxy alcohol derivative **HPA**, then cyclocondensation with 2-(4-oxocyclohexyl)isoindoline 1,3-dione in the presence of SSA, according to a procedure described in **Chapter 4**. The phthalimido 1,2,4-trioxane **2.37** was obtained in 47% yield. The presence of three characteristic 1,2,4-trioxane

carbon peaks in the respective $^{13}C$ NMR spectra also indicated the formation of the 1,2,4-trioxane core [δ 100.69 (O-C-O), 81.44 (O-C-$CH_2$), 63.80 (-$CH_2$) ppm, in $CDCl_3$]. The spiro-epoxide **2.36** was previously obtained *via* Corey–Chaykovsky reaction, from 2-adamantan-2-one **2.35**, in 83% yield. Hydrazinolysis of 1,2,4-trioxane **2.37** to remove the phthalimido protecting group gave the free amine **2.38** as its respective hydrochloride salt in moderate yield (65%). The target 1,2,4-trioxane amine **2.38** was then coupled with 4,6-dichloro-indole-2-carboxylic acid **2.27**, in the presence of EDC·HCl and HOBt, to afford the trioxane-IC hybrid **TIC03** in low yield (18-37%, respectively).

Spectroscopic analysis proved the formation of the trioxane-IC hybrids. The main distinctive peaks in this synthesis were indole core aromatic protons, the predicted integration in the aliphatic region of the $^1H$ NMR spectra, and evidence of 1,2,4-trioxane carbons in the $^{13}C\{^1H\}$ NMR spectra. Quite interestingly, it was possible to isolate the different diastereoisomers for each 1,2,4-trioxane hybrid during purification by column chromatography.

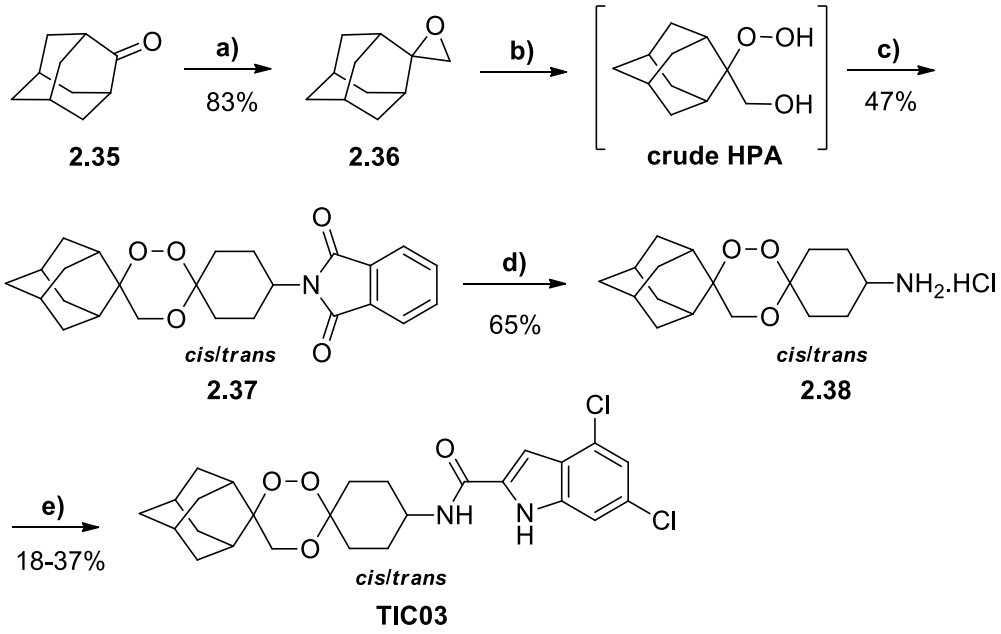


**Scheme 2.4.** Schematic representation of the synthetic approach followed to prepare the adamantyl substituted peroxide amines for the indole-2-carboxamide-derived hybrids. Reagents and conditions: (a) $(CH_3)_3S(O)I$, *t*-BuOK, 1,2-dimethoxyethane, reflux, 18 h; (b) SSA, $H_2O_2.Et_2O$, 0-rt, 1 h. (c) 2-(4-oxocyclohexyl)isoindoline-1,3-dione, SSA, anhydrous $CH_2Cl_2$, 0-rt, 1 h; (d) 1. $N_2H_4.H_2O$, $CHCl_3$/MeOH (7:3), 60 ºC, o/n; 2. 2 M HCl in $Et_2O$, 0-rt, 30 min; (e) **2.27**, EDC·HCl, HOBt, $Et_3N$, $CH_2Cl_2$, rt, o/n.

### 2.3.1.2. Benzothiazinones

Makarov's research group explored a new synthetic method for antitubercular benzothiazinone derivatives, with the improvement of linking the amine moiety to a stable 2-(alkylsulfanyl)-4*H*-1,3-benzothiazin-4-one intermediate **2.39** (**Scheme 2.5**). This method avoids derivatization of the amine substituent (*e.g.*, dithiocarbamates formation) and can be simply adapted for automatic combinatorial chemistry with varied amine moieties at position 2.[85,86] As such, we selected this method as the final step in coupling the peroxide amine derivatives to the benzothiazinone core.

The synthetic strategy (**Scheme 2.5**) for the BTZ hybrids involved the $S_NAr$ coupling of peroxide-containing amines with 2-(methylsulfanyl)-8-nitro-6-(trifluoromethyl)-4*H*-1,3-benzothiazin-4-one **2.43** as convergent point of synthesis. The common alkylsulfanyl intermediate **2.43** was synthesised by initial nitration of 2-chloro-5-trifluoromethyl benzoic acid **2.40** through treatment with concentrated $HNO_3$ and $H_2SO_4$ to afford **2.41**. 2-Chloro-3-nitro-5-(trifluoromethyl)benzoic acid **2.41** was then converted to the primary amide **2.42** *via* an intermediate acid chloride and $NH_4OH$. Treatment of **2.42** with carbon disulfide ($CS_2$) in the presence of NaOH, followed by the addition of the alkylating agent $CH_3I$, affords 2-(alkylsulfanyl)-4*H*-1,3-benzothiazin-4-one derivative **2.43** in moderate yield (42%). Synthesis of **2.43** was proved by $^1$H NMR through the presence of a characteristic peak integrating to 3 protons corresponding to the thiomethyl group (δ 2.76 ppm, in DMSO-$d_6$).

Boc-piperidone-derived 1,2,4-trioxanes and their corresponding intermediates were also synthesized by adapting procedures described in the literature, and the synthetic strategies are depicted in **Schemes 2.6** and **2.7**. The synthetic strategy begins with Co(II)-mediated peroxysilylation of allylic alcohols **2.29** and **2.30** to generate their silyl peroxide derivatives (**HSP**), followed by reaction with commercial boc-piperidone (**2.44**) under the presence of SSA, affording boc-piperidone derivative dimethyl 1,2,4-trioxane **2.45** and spirocyclohexyl 1,2,4-trioxane **2.46** in moderate yield (58 and 38%, respectively, **Scheme 2.6**). The presence of three characteristic 1,2,4-trioxane carbon peaks in their respective $^{13}$C NMR spectra also indicated the formation of the boc-piperidone derivative 1,2,4-trioxane cores [δ 100.4 (O-C-O), 77.2 (O-C-$CH_2$), 66.6 (-$CH_2$) ppm for **2.45 (**in $CDCl_3$**)** and δ 100.94 (O-C-O), 78.28 (O-C-$CH_2$), 66.04 (-$CH_2$) ppm for **2.46**, in $CD_3CN$]**.**

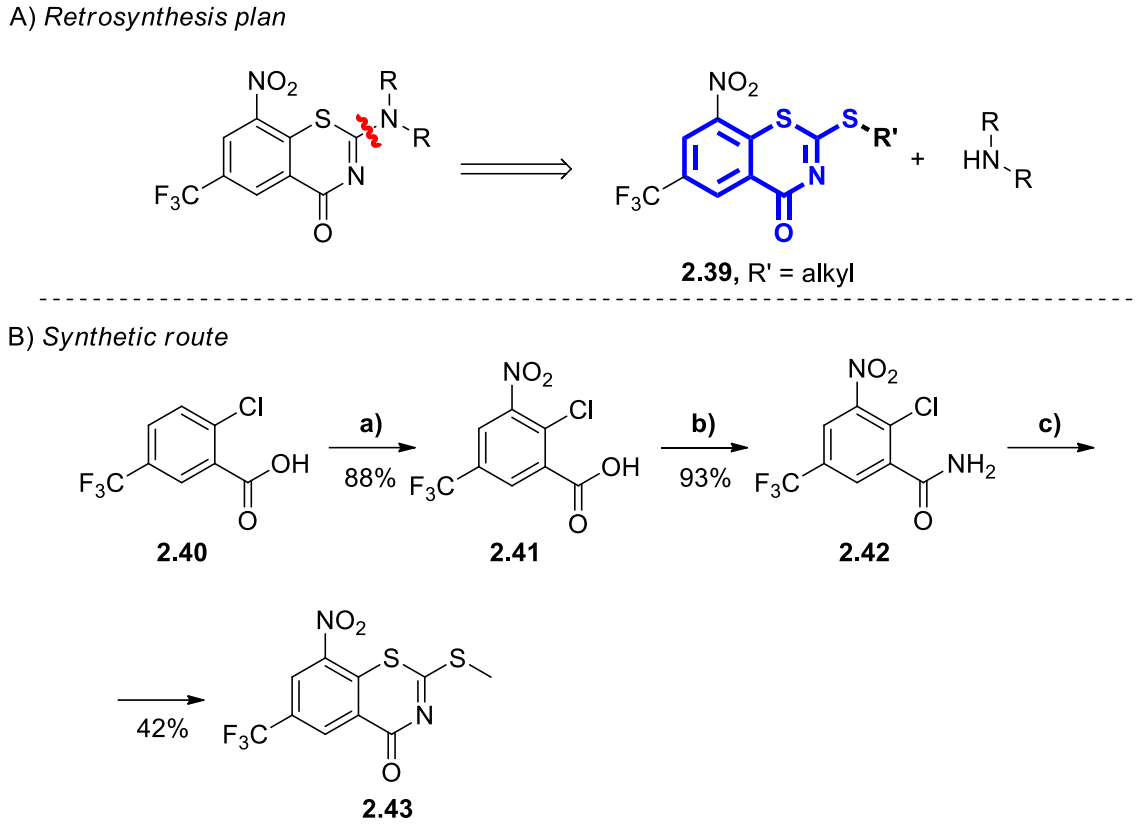


**Scheme 2.5. A)** Retrosynthesis plan for the preparation of peroxide containing benzothiazinones, through the alkylsulfanyl pathway. **B)** Synthesis of the benzothiazinone core. Reagents and conditions: (a) $HNO_3$, $H_2SO_4$, 90 ºC, 1 h; (b) 1. $SOCl_2$, toluene, reflux, o/n; 2. $NH_4OH$, $CH_3CN$, -20 ºC, 30 min; (c) 1. $CS_2$, NaOH, DMSO, 10 ºC, 1 h; 2. $CH_3I$, 10 ºC, 1 h.

Subsequent boc deprotection of **2.45** and **2.46** with HCl (2 M in diethyl ether) in methanol affords the target amines **2.47** and **2.48** as HCl salts, in 36 and 75% yield, respectively (**Scheme 2.6**). During the deprotection reaction, a disparity in yield between dimethyl- and spirocyclohexyl-substituted trioxane during boc protecting group removal was observed. The less bulky derivative (dimethyl) indicated that there was a peroxide bond susceptibility in the acidic conditions, with the detection of additional products from its degradation. In contrast, the spirocyclohexyl-trioxane exhibited greater peroxide stability, ascribed to the electron donor effect and steric hindrance of the bulky cyclohexyl ring.

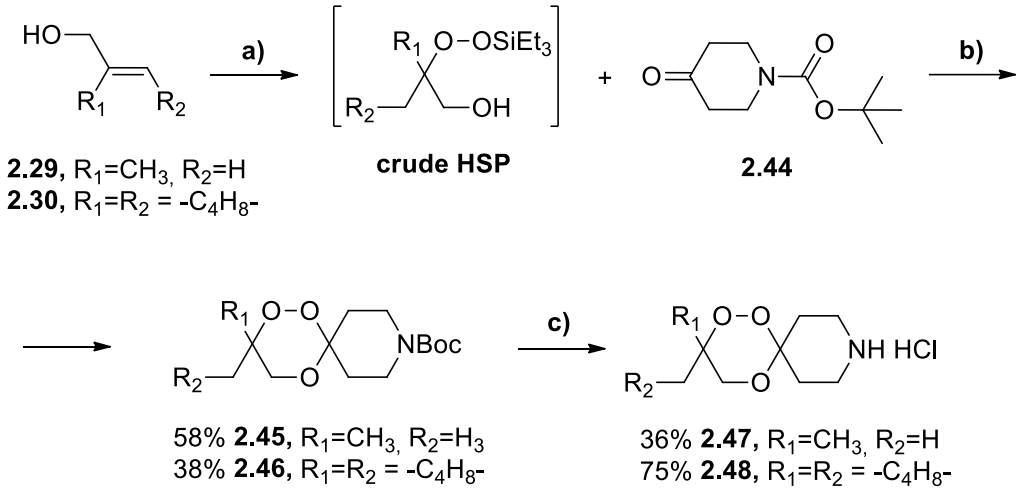


**Scheme 2.6.** Schematic representation of the general synthetic approach followed to prepare the dimethyl and cyclohexyl substituted peroxide amines for the BTZ043-derived hybrids. Reagents and conditions: (a) $Et_3SiH$, $Co(thd)_2$, under $O_2$, DCE, rt, o/n; (b) SSA, anhydrous $CH_2Cl_2$, 0 ºC-rt, 1 h; (c) 2 M HCl in $Et_2O$, rt, 48 h.

For the adamantyl-trioxane-BTZ hybrid (**Scheme 2.7**), the synthesis began with the preparation of the boc-piperidone 1,2,4-trioxane **2.50** by perhydrolysis of previously prepared boc-piperidone spiro-oxirane **2.49** to its β-hydroperoxy alcohol derivate **HPA**, followed by its cyclocondensation with adamantan-2-one **2.35** in the presence of SSA, affording **2.50** with 63% yield. The presence of three characteristic 1,2,4-trioxane carbon peaks in their respective $^{13}C$ NMR spectra also indicated the formation of this 1,2,4-trioxane core [104.62 (O-C-O), 75.67 (O-C-$CH_2$), 65.27 (-$CH_2$) ppm, in $CDCl_3$]. The boc-piperidone spiro-epoxide **2.49** was previously obtained through Corey–Chaykovsky reaction with boc-4-piperidone (**2.44**), in low yield (28%). Removal of the boc group in **2.50** with HCl (2 M) in diethyl ether affords the target amine **2.51** as the hydrochloride salt, with 72% yield. No evidence of peroxide bond degradation was observed, implying that the peroxide bond remained stable due to the protective electron donor effect of the bulky adamantyl group attached to the trioxane ring.

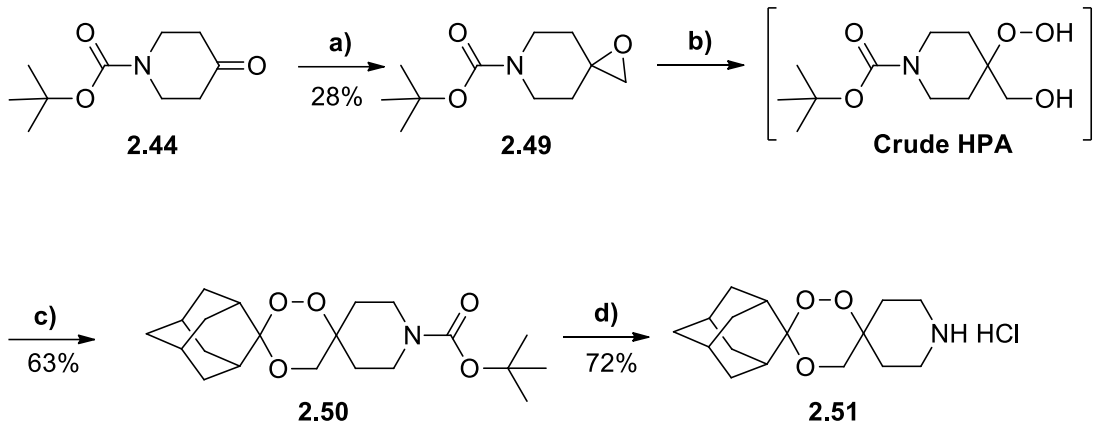


**Scheme 2.7.** Schematic representation of the synthetic approach followed to prepare the adamantyl substituted peroxide amines for the BTZ043-derived hybrids. Reagents and conditions: (a) $(CH_3)_3S(O)I$, *t*-BuOK, 1,2-dimethoxyethane, reflux, 18 h; (b) SSA, $H_2O_2$–$Et_2O$, 0 ºC-rt, 1 h. (c) Adamantan-2-one **2.35**, SSA, anhydrous $CH_2Cl_2$, 0 ºC-rt, 1 h; (d) 2 M HCl in $Et_2O$, rt, 48 h.

Concerning the synthetic path for the preparation of PBTZ169-derived trioxane hybrids, for the dimethyl-trioxane analogue (**Scheme 2.8**) it starts with initial Co(II)-mediated peroxysilylation of allylic alcohol **2.29** followed by cyclocondensation with ethyl 4-oxocyclohexanecarboxylate **2.52** in the presence of SSA, affording 1,2,4-trioxane **2.53** in moderate yield (68%). The presence of three characteristic 1,2,4-trioxane carbon peaks in their respective $^{13}C$ NMR spectra also indicated the formation of the corresponding 1,2,4-trioxane core [δ 101.16/101.06 (O-C-O), 76.96/76.92 (O-C-$CH_2$), 66.74/66.49 (-$CH_2$) ppm, in $CDCl_3$]. The detection of duplicate peaks on the $^{13}C\{^1H\}$ NMR confirmed that the peracetalization step yielded a mixture of diastereoisomers in an approximately 2:1 ratio. Since separating the diastereoisomers *cis* or *trans* by column chromatography was also unsuccessful for this series, the synthesis was resumed using the mixture of diastereoisomers. The ester derivative **2.53** was then reduced to the primary alcohol by treatment with $LiAlH_4$, affording the alcohol derivative **2.54** in 93% yield. For the synthesis of **2.57**, two synthetic routes were analyzed. The first approach for reaching the final 1,2,4-trioxane amine involved the conversion of the alcohol to its mesylate derivative, with subsequent $S_N2$ substitution with boc-piperazine. Mesylation of alcohol **2.54** occurred in 76% yield affording the mesylate derivative **2.55**, although the $S_N2$ substitution with boc-piperazine **2.56** did not occur even in the presence of sodium hydride or triethylamine. These results led us to propose an alternative approach, with oxidation of the alcohol to its corresponding aldehyde, followed by reductive amination. Oxidation of alcohol **2.54** to the aldehyde

**2.58** using pyridinium chlorochromate (PCC) was easily achieved, and **2.58** was used immediately thereafter, without further purification, to prevent further oxidation to the corresponding carboxylic acid. Subsequent reductive amination with boc-piperazine **2.56** produced compound **2.57** in 35% yield. The boc protecting group was removed by treatment with HCl (4 M in dioxane) to afford the target amine **2.59** as a dihydrochloride salt in high yield (88%). It should be highlighted that the short-timed boc deprotection reaction with HCl 4 M in dioxane prevented decomposition of the peroxide bond, allowing higher yield than when using 2 M HCl in diethyl ether.

The preparation of the spirocyclohexyl 1,2,4-trioxane **2.63** followed the same synthesis plan, previously optimized. It starts with Co(II)-mediated peroxysilylation of allylic alcohol **2.30** to generate the silyl peroxide **HSP**, followed by peroxyacetalization reaction with carbonyl **2.52** in the presence of SSA, affording diastereoisomers *cis* or *trans* of 1,2,4-trioxane **2.60** in moderate yield (40%, **Scheme 2.9**). The presence of three characteristic 1,2,4-trioxane carbon peaks in their respective $^{13}C$ NMR spectra also indicated the formation of this 1,2,4-trioxane core [δ 101.35/101.25 (O-C-O), 77.72/77.68 (O-C-$CH_2$), 66.20/65.91 (-$CH_2$) ppm, in $CDCl_3$**)],** whereas the mixture of diastereoisomers was formed in an approximately 2:1 ratio. The mixture of diastereoisomeric esters **2.60** was then reduced to the primary alcohol by treatment with $LiAlH_4$, affording **2.61** in 91% yield. The reductive amination route previously optimized was employed, whereas alcohol **2.61** was oxidized by PCC, followed by reductive amination with boc-piperazine, to afford **2.62**, in 44% yield. Boc deprotection was achieved by treatment with HCl (4 M, in dioxane) to afford the target amine **2.63** as a dihydrochloride salt.

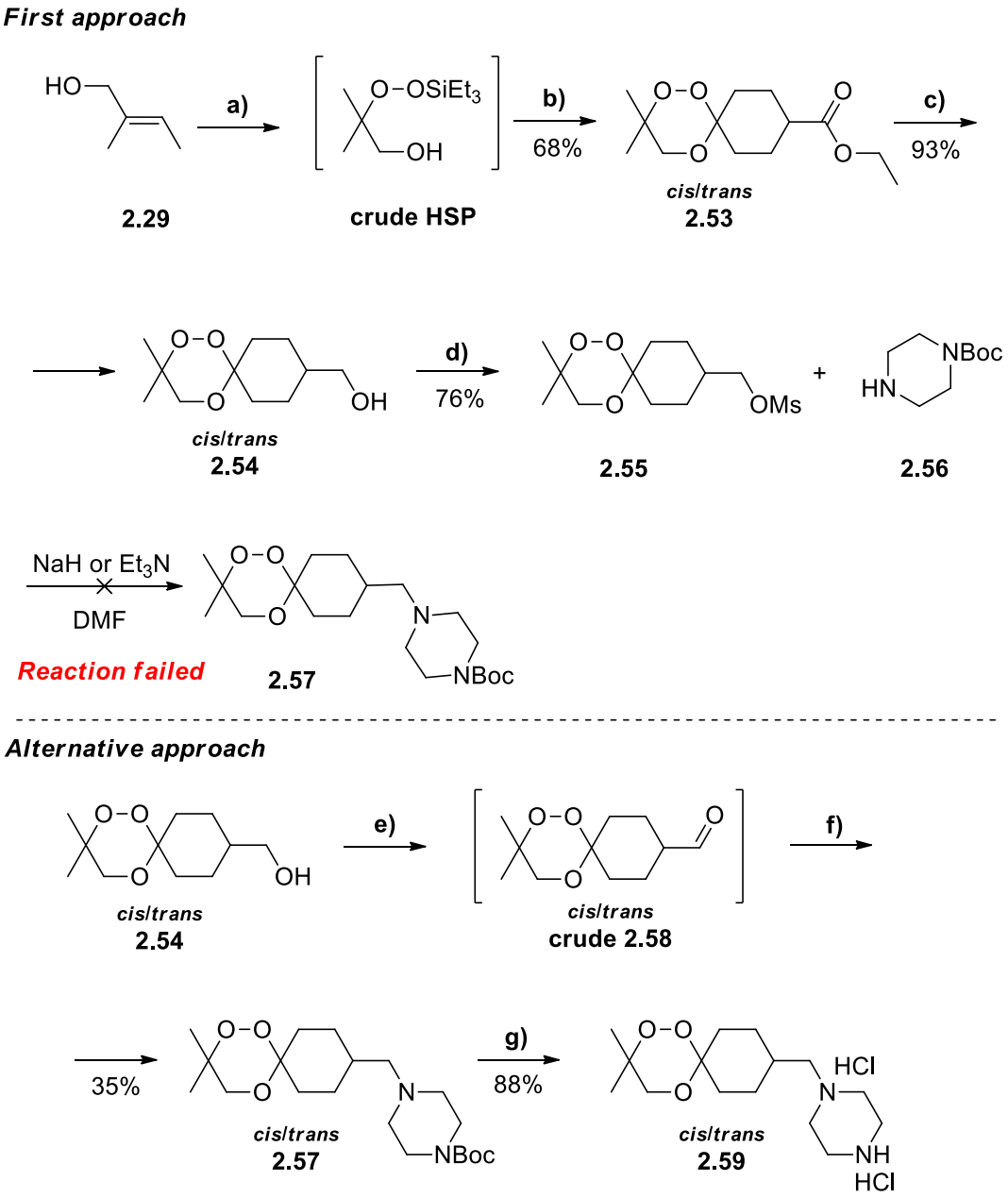


**Scheme 2.8.** Schematic representation of the synthetic strategies explored to achieve the dimethyl substituted peroxide amines for the PBTZ169-derived hybrids. Reagents and conditions**:** (a) $Et_3SiH$, $Co(thd)_2$, under $O_2$, DCE, rt, o/n; (b) ethyl 4-oxocyclohexanecarboxylate **2.52**, SSA, anhydrous $CH_2Cl_2$, 0 ºC-rt, 1 h; (c) 1. $LiAlH_4$, anhydrous $Et_2O$, 0 ºC, 1 h; 2. $H_2O$ (d) MsCl, $Et_3N$, $CH_2Cl_2$, 0 ºC-rt, 2 h; (e) PCC, $CH_2Cl_2$, 0 ºC-rt, 1 h; (f) Boc-piperazine **2.56**, AcOH, DCE, $NaBH(OAc)_3$, rt, 16 h; (g) 4 M HCl in dioxane, 0 ºC-rt, 2-4 h.

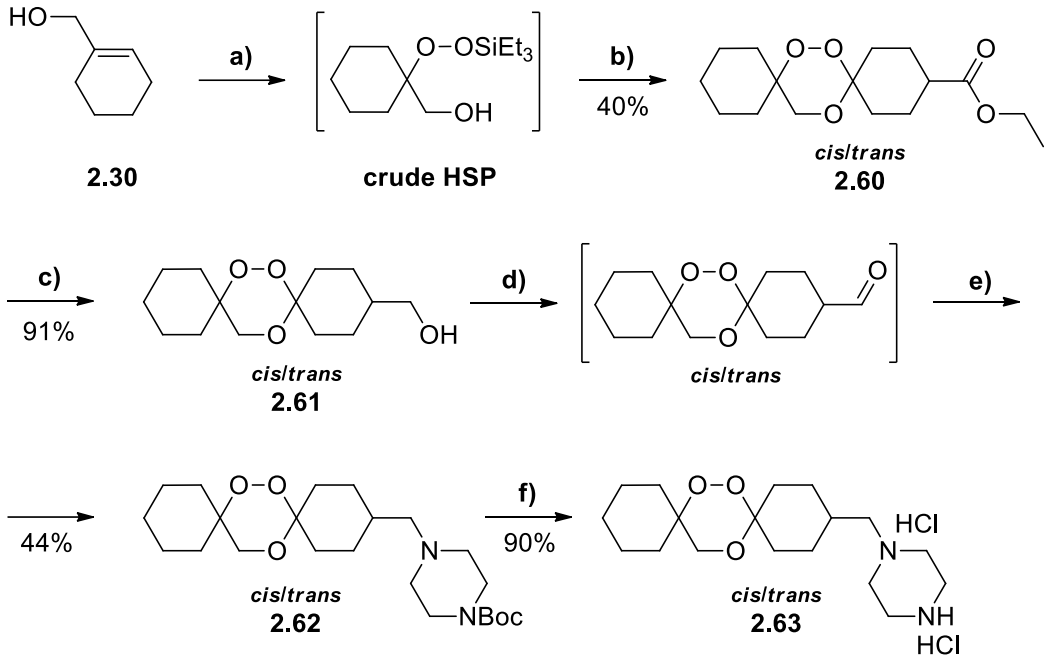


**Scheme 2.9**. Schematic representation of the synthetic approach followed to prepare the cyclohexyl substituted peroxide amines for the PBTZ169-derived hybrids. Reagents and conditions: (a) $Et_3SiH$, $Co(thd)_2$, $O_2$, DCE, rt, o/n; (b) ethyl 4-oxocyclohexanecarboxylate **2.52**, SSA, anhydrous $CH_2Cl_2$, 0 ºC-rt, 1 h; (c) 1. $LiAlH_4$, anhydrous $Et_2O$, 0 ºC, 1 h; 2. $H_2O$; (d) PCC, $CH_2Cl_2$, 0 ºC-rt, 1 h; (e) Boc-piperazine **2.56**, AcOH, DCE, $NaBH(OAc)_3$, rt, 16 h; (f) 4 M HCl in dioxane, 0 ºC-rt, 2-4 h.

As depicted in **Scheme 2.10**, the synthesis of the adamantyl derived 1,2,4-trioxane **2.65** required prior generation of spiro-epoxide **2.64**, achieved *via* Corey–Chaykovsky epoxidation reaction with **2.52**, with a yield of 24%. Perhydrolysis of spiro-oxirane **2.64** to its β-hydroperoxy alcohol derivative, followed by its cyclocondensation with adamantan-2-one **2.35**, catalysed by SSA, afforded the adamantyl derived 1,2,4-trioxane **2.65**. Isolation of analytically pure **2.65** by flash chromatography was not possible since it co-elutes with adamantan-2-one. Therefore, the product was carried forward to the next step without further purification. Hydrolysis of ester **2.65** with LiOH gave the corresponding carboxylic acid **2.66**, affording an overall yield of 17% over three steps. The presence of three characteristic 1,2,4-trioxane carbon peaks in their respective $^{13}C$ NMR spectra also indicated the formation of the adamantyl-1,2,4-trioxane core [δ 104.45 (O-C-O), 76.89 (O-C-$CH_2$), 76.89 (-$CH_2$) ppm, in $CDCl_3$]. Reduction of **2.66** with $LiAlH_4$ afforded the corresponding alcohol **2.67** in 97% yield. Oxidation of **2.67** with PCC produced the intermediate aldehyde and subsequent reductive amination with boc-piperazine **2.56** afforded the boc-piperazine derivative 1,2,4-trioxane **2.68** in 39% yield.

The boc protecting group was then removed by treatment with HCl 4 M in dioxane to afford the 1,2,4-trioxane amine **2.69** as an HCl salt, in 95% yield.

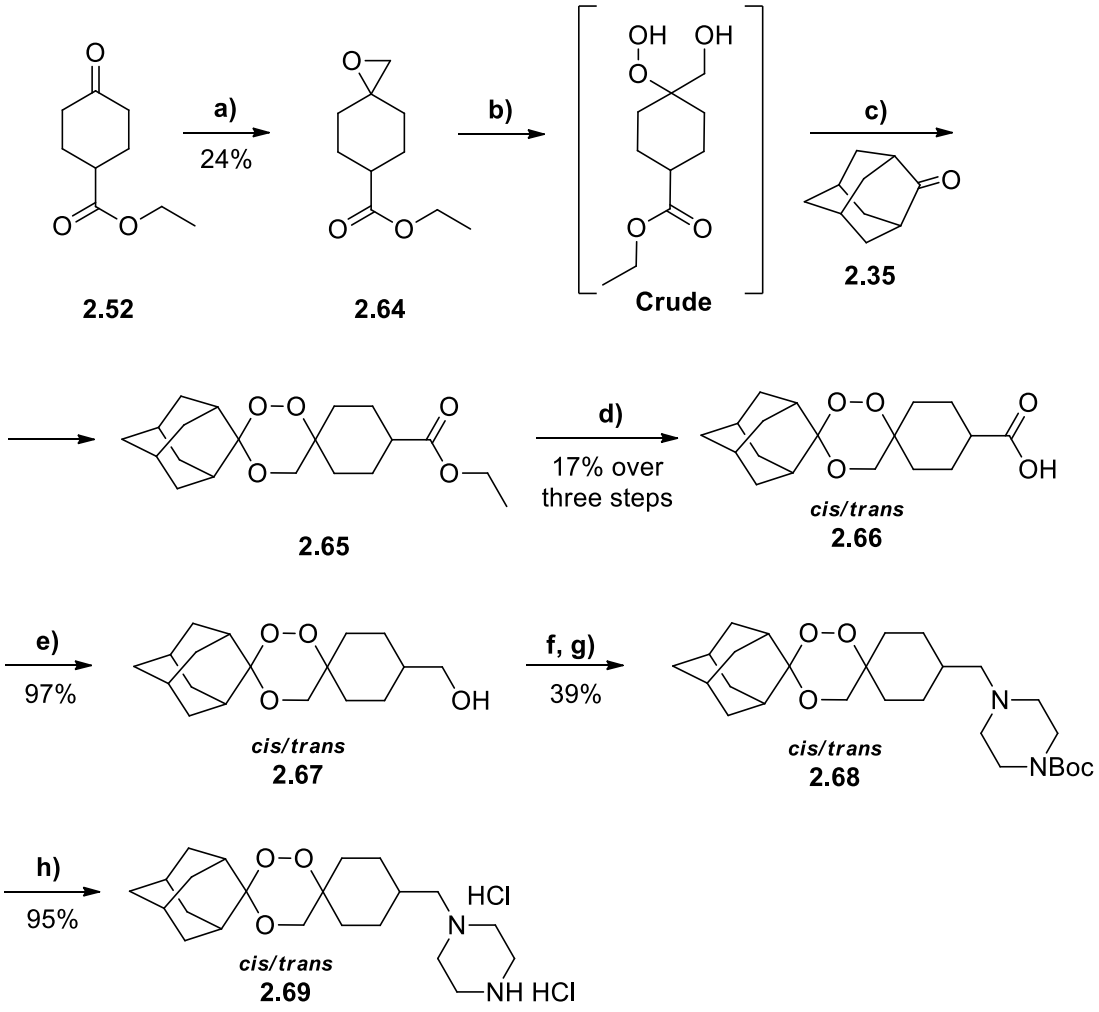


**Scheme 2.10.** Schematic representation of the synthetic approach followed to prepare the adamantyl substituted peroxide amines for the PBTZ169-derived hybrids. Reagents and conditions**:** (a) $(CH_3)_3S(O)I$, t-BuOK, THF, reflux, 18 h; (b) SSA, $H_2O_2$-$Et_2O$, 0 ºC-rt, 1 h; (c) SSA, anhydrous $CH_2Cl_2$, 0 ºC-rt, 1 h; (d) LiOH, THF/$H_2O$ (1:1), rt, 18 h; (e) 1. $LiAlH_4$, anhydrous $Et_2O$, 0 ºC, 1 h; 2. $H_2O$; (f) PCC, $CH_2Cl_2$, 0 ºC-rt, 1 h; (g) Boc-piperazine **2.56**, AcOH, DCE, $NaBH(OAc)_3$, rt, 16 h; (h) 4 M HCl in dioxane, 0 ºC-rt, 2-4 h**.**

The amide analogue of the simplest trioxane hybrid (**P7**, **Scheme 2.11**) was also synthesised, to evaluate whether an amide linker would affect the activity and stability of these BTZ hybrids. The synthesis began by a coupling reaction of boc-piperazine **2.56** with **2.43**, in the presence of triethylamine in ethanol, affording **2.70** with 79% yield. The BTZ-boc-piperazine **2.70** was then treated with HCl 4 M in dioxane, to remove the boc protecting group, affording **2.71** as the HCl salt. Hydrolysis of ester-trioxane **2.53** with

LiOH gave the corresponding carboxylic acid **2.72** in 95% yield, and **P7** was synthesised with a 65% yield by amide coupling of **2.71** with the synthesised peroxide **2.72** in the presence of HOBt and EDC hydrochloride as coupling agents.

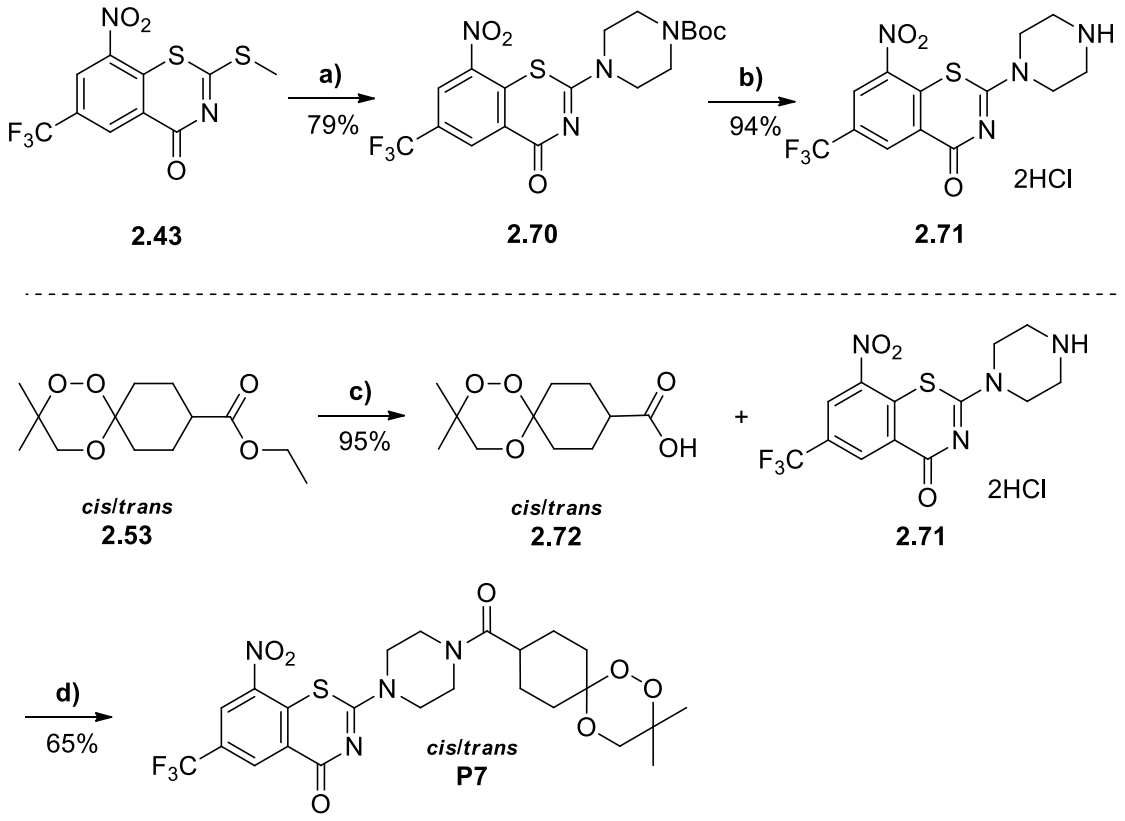


**Scheme 2.11.** Schematic representation of the general synthetic approach followed to prepare the amide analogue PBTZ169-derived hybrid **P7.** Reagents and conditions**:** (a) Boc-piperazine **2.56**, $Et_3N$, 60 ºC, 1-2 h; (b) 4 M HCl in dioxane, 0 ºC-rt, 4 h; (c) LiOH, THF/$H_2O$ (1:1), rt, 18 h; (d) EDC·HCl, HOBt, **2.71**, $Et_3N$, $CH_2Cl_2$, rt, o/n.

To evaluate and validate the role of the peroxide bond in the BTZ hybrid series, two categories of control group scaffolds were also synthesized: two non-peroxide amine moieties (**2.75** and **2.79**) and one ketone moiety (**2.83**) related to a potential degradation product of the PBTZ169-derived peroxides. The preparation of these amine analogues is depicted in **Scheme 2.12.** Synthesis of **2.75** begins by the acid-catalysed ketalization of 2,2-dimethylpropane-1,3-diol with fmoc-piperidone **2.73**, affording the ketal analogue of the fmoc-piperidone **2.74** in 91% yield, followed by removal of the Fmoc protection with diethylamine to achieve the free amine **2.75** in 45% yield. Preparation of the PBTZ169-non-peroxide analogue also proceeded by the ketalization of 2,2-dimethylpropane-1,3-diol with **2.52** to afford the ketal analogue **2.76**, and subsequent reduction with $LiAlH_4$ to the corresponding alcohol **2.77** in high yield (92%). Subsequent oxidation with PCC,

followed by reductive amination with **2.56**, afforded compound **2.78** (39% yield), from which a boc deprotection with HCl 4 M in dioxane yielded the desired amine **2.79** as HCl salt (86% yield).

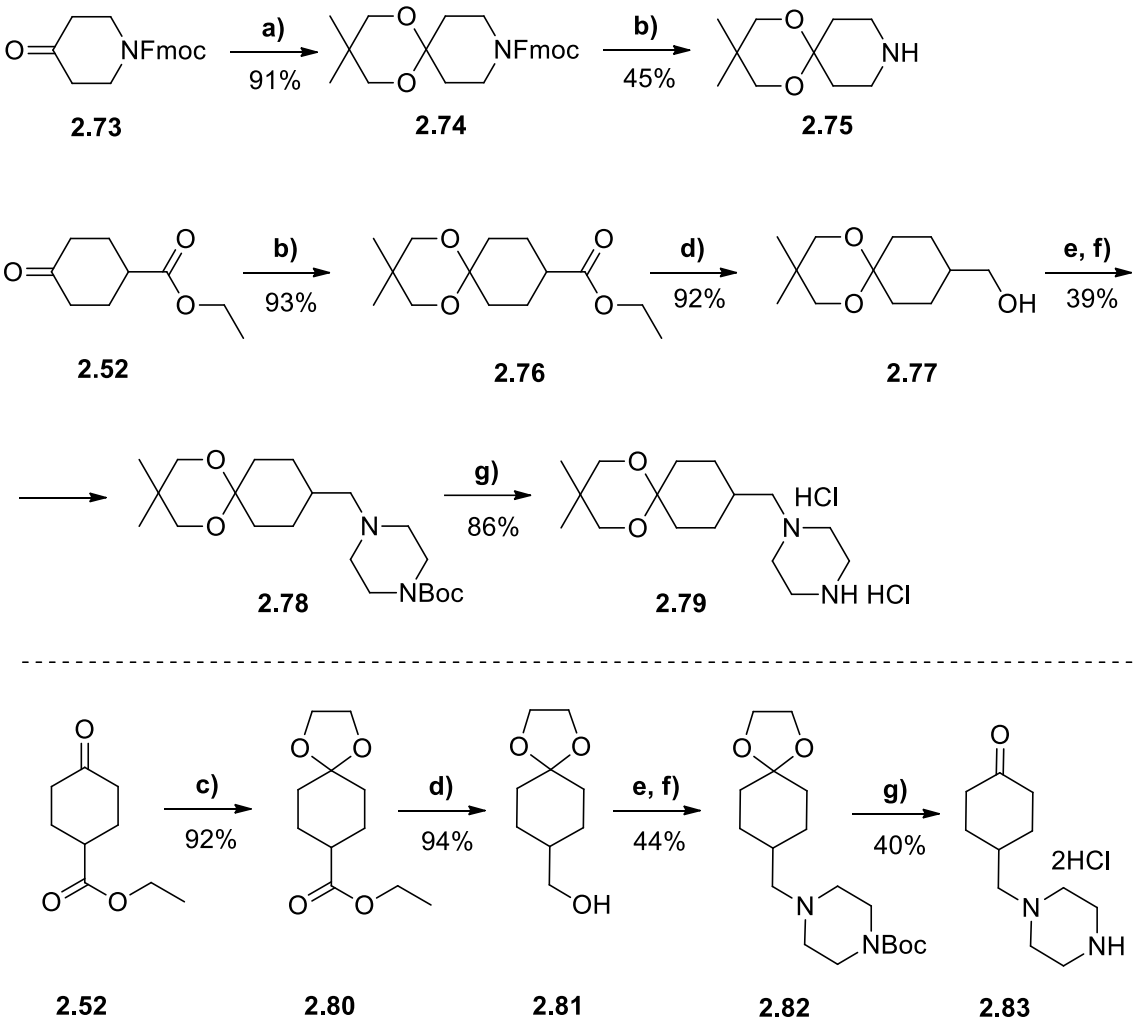


**Scheme 2.12.** Schematic representation of the general synthetic approach followed to prepare the control analogues for the BTZ043- and PBTZ169-derived hybrid series. Reagents and conditions: a) 2,2 dimethylpropane-1,3-diol (5 mmol), SSA, $CH_2Cl_2$, rt, 6 h; b) diethylamine/$CH_2Cl_2$ (1:1), rt, o/n; c) ethylene glycol, $H_2SO_4$-$SiO_2$, $CH_2Cl_2$, 0 ºC-rt, 5 h; d) 1. $LiAlH_4$, $Et_2O$, 0 ºC, 1 h; 2. $H_2O$; e) PCC, $CH_2Cl_2$, 0 ºC-rt, 1 h; f) Boc-piperazine, AcOH, DCE, $NaBH(OAc)_3$, rt, 16 h; g) 4 M HCl in dioxane, 2 h.

For synthesizing the ketone moiety **2.83** (**Scheme 2.12**), first, it was required to protect the carbonyl group to avoid incompatibilities during the synthetic route. Protection by an acid-catalysed ketalization of **2.52** with ethylene glycol afforded the corresponding ketal **2.80** in 92% yield. Reduction of the ester functional group of **2.80** with $LiAlH_4$ gave the corresponding alcohol **2.81** in 94% yield. Oxidation of **2.81** with PCC and subsequent reductive amination with boc-piperazine **2.56** afforded compound

**2.82** in 44% yield. Both Boc and ketal protecting groups were removed by treatment with HCl 4 M in dioxane, yielding the target amine **2.83** as HCl salt, in moderate yield (40%).

The peroxide-containing building blocks and their control group analogues were coupled to the BTZ core **2.43** under $S_NAr$ conditions (**Table 2.1**).[85] **C1** was synthesised by coupling **2.43** with 4-piperidone. All synthesised BTZ compounds (**B1-5, P1-7, C1-4**) were submitted to biological evaluation against replicating $H_{37}Rv$ *Mtb*.

**Table 2.1.** Summary of yields for the final coupling step.

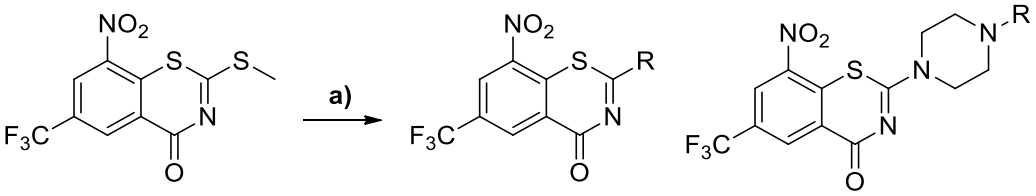


| Analogue | R | Yield (%) | Analogue | R | Yield (%) |
|---|---|---|---|---|---|
| **B3** | 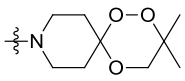 | 62 | **P6** | 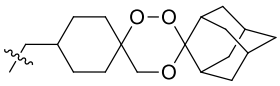 | 52 |
| **B4** | 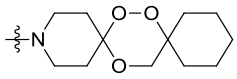 | 65 | **C1** | 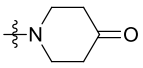 | 41 |
| **B5** | 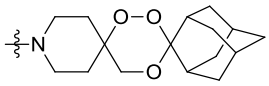 | 53 | **C2** | 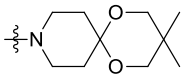 | 72 |
| **P4** | 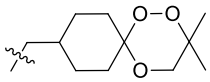 | 65 | **C3** | 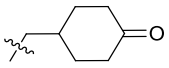 | 39 |
| **P5** | 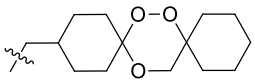 | 64 | **C4** | 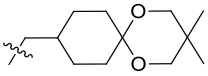 | 38 |

Reagents and conditions: a) Peroxide or control-group containing amine, $Et_3N$, EtOH, 60 ºC, 2 h.

## 2.3.2. Biological evaluation

All compounds synthesized were screened against replicating $H_{37}Rv$ *Mtb*, and the respective $IC_{50}$ values are depicted in **Tables 2.2** and **2.3**. For the IC compounds (**Table 2.2**) both the non-peroxide analogues NITD304 (**2.6**) and **2.84** displayed anti-TB activity, with the result obtained for **2.6** comparable to the literature value of 0.015 μM disclosed for this molecule.[4,5] The metabolite control compound **2.84** also displayed

moderate anti-TB activity, with an $IC_{50}$ of 5.680 µM. Of all synthesized compounds - tetraoxanes (**2.85** and **2.86**), trioxolanes **(2.87** and **2.88**) and trioxanes (**TIC01-03**) - only tetraoxane **2.86** exhibited activity against *Mtb*, with a moderate $IC_{50}$ value of 2.634 µM. A considerable decrease in activity was observed between the reference compound **2.6** and tetraoxane-IC hybrid **2.86**, suggesting that a SAR optimization in the S5 pocket is necessary. It appears that the S5 pocket cannot withstand the increase in polarity, as the switch of the spirocyclic group in template molecule **ICA38** [cLogP (spiro rings) = 5.35] to the dimethyl-1,2,4-trioxane-cyclohexyl moiety [clogP = 2.86] in **TIC01** proved incompatible for the S5 pocket. SAR exploration of the linking and terminal cyclohexyl rings by the addition of methyl substituents in **2.86** could be a proposal for structure optimization. The discrepancy in TB activity between analogues is not likely related to DMPK properties, as no trends were identified between active and inactive compounds in the predicted DMPK data (please see Section 2.3.4, for the DMPK results).

**Table 2.2.** Summary of obtained $IC_{50}$ values for peroxide containing IC MmpL3 inhibitors.

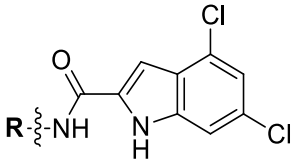


| Analogue | R | $IC_{50}$[a] (µM) | Analogue | R | $IC_{50}$[a] (µM) |
|---|---|---|---|---|---|
| **2.6** [b*] (NITD304) | 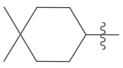 | 0.03 | **TIC01-1** | 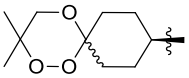 | > 10 |
| **2.84** [b*] | 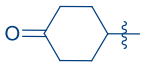 | 5.68 | **TIC01-2** | 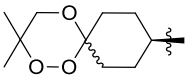 | > 10 |
| **2.85** [b*] | 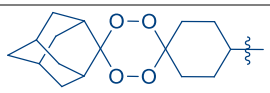 | > 10 | **TIC02-1** | 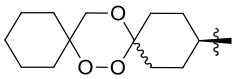 | > 10 |
| **2.86** [b*] | 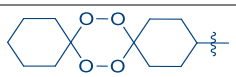 | 2.44 | **TIC02-2** | 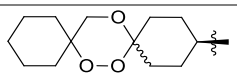 | > 10 |
| **2.87** [b*] | 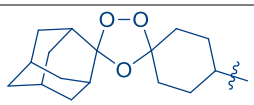 | > 10 | **TIC03-1** | 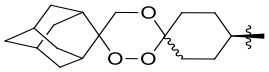 | > 10 |
| **2.88** [b*] | 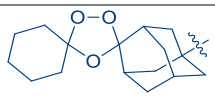 | > 10 | **TIC03-2** | 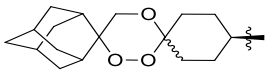 | > 10 |

[a] Tested against $H_{37}Rv$ *Mtb*, experiments were performed in triplicate. [b*] Compounds synthesized by another member of the group (***in marine blue***).

In contrast to the IC analogues, all BTZ analogues maintained potent activity against replicating $H_{37}Rv$ *Mtb* (**Table 2.3**). Compounds **B2** and **P2** require retesting at lower concentrations to determine an accurate $IC_{50}$ value. Besides carbonyl-containing compounds **P7** and **C1**, potency at low nanomolar concentrations was exhibited throughout the series. These biological findings are consistent with modelling studies and observation from the activity of BTZ-TAMRA, which demonstrated that the peroxide-containing side chain protrudes into solvent-accessible space and interacts minimally with the binding pocket of DprE1, indicating that modifications of the amine-linked peroxide-containing side chain and their control analogues can be wide-ranging.

The BTZ043 analogues **B1** and **B3** possess $IC_{50}$ values just two-fold higher than the parent molecule BTZ043, with **B5** nearly four-fold higher, thus being slightly less potent than BTZ043. Furthermore, the cyclohexyl-trioxane **B4** and BTZ043 were found to be equipotent, indicating the small contribution to binding interactions that the side chain mediates.

Of the PBTZ169 analogues **P1-3**, both the methylene linker containing analogues **P1** and **P3** showed a decrease in activity compared to PBTZ169 ($IC_{50}$ values are greater than the maximum possible MIC value), while for **P2** an accurate $IC_{50}$ value could not be recorded due to mediating near maximal inhibition at the lowest concentration measured (0.457 nM). This increase in potency compared to **P1** and **P6** may come from the additional methylene linker, allowing greater flexibility of the side chain, which avoids unfavourable steric interactions with the "entrance" of the binding pocket. Of the 1,2,4-trioxanes **P4-6**, the adamantyl analogue **P6** was the most potent – this increase in potency may be related to the high lipophilicity (LogD = 5.5) of this compound, which may impact activity through permeability, and add additional stability to the peroxide bond. **P7** was the poorest performing compound of the peroxide-containing series with an $IC_{50}$ of 423.0 nM. The position of the carbonyl group in this structure is expected to place it within the "entrance" of the DprE1 binding pocket which may experience unfavourable interactions with non-polar residues which define the shape of this region. This is supported by the poor activity of control compound **C1** ($IC_{50}$ = 870 nM), where its piperidone carbonyl would be expected to lie in a similar region of space. The potency of the carbonyl-containing **C3** (7.70 nM) supports the assumption of a structural rather than a physicochemical effect, as in this structure the carbonyl is distant from the binding pocket (Please see Section 2.3.3 for more details in the docking studies).

All control compounds **C1-4** showed slightly decreased potency compared to their parent compounds, confirming that the presence of peroxide moieties does not adversely affect the activity of these compounds.

**Table 2.3.** Summary of obtained $IC_{50}$ values for peroxide containing BTZ DprE1 inhibitors.

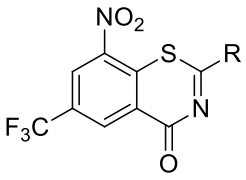

**B1-5, C1/2**

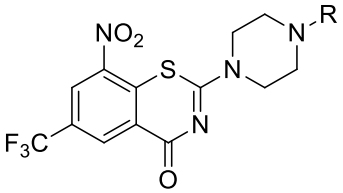

**P1-6, C3/4**

| Compd | R | $IC_{50}$[a] (nM) | Compd | R | $IC_{50}$[a] (nM) |
|---|---|---|---|---|---|
| **BTZ043** | 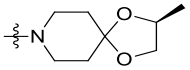 | 1.32 | **P3** [d*] | 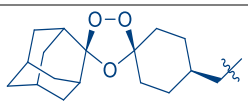 | 1.47 |
| **PBTZ169**[b] | 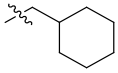 | ≤ 0.42 | **P4** | 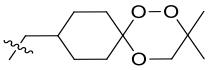 | 6.86 |
| **B1** [d*] | 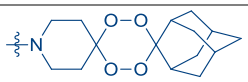 | 2.26 | **P5** | 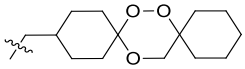 | 11.09 |
| **B2** [d*] | 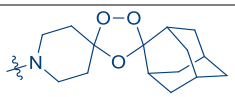 | < 80[c] | **P6** | 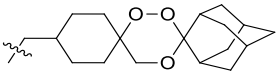 | 1.12 |
| **B3** (PA54) | 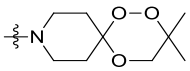 | 2.21 | **P7** | 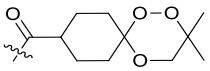 | 423 |
| **B4** | 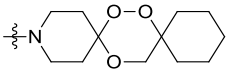 | 1.32 | **C1** | 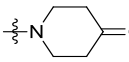 | 870 |
| **B5** | 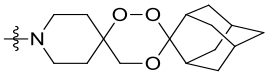 | 4.08 | **C2** (PA67) | 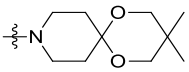 | 3.97 |
| **P1** [d*] **(CW02-9-8)** | 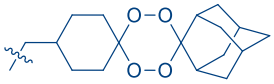 | 2.26 | **C3** | 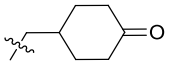 | 7.70 |
| **P2** [d*] | 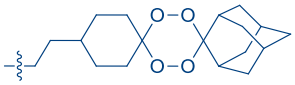 | < 0.46[c] | **C4** | 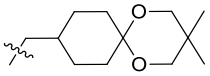 | 11.04 |

[a] Tested against $H_{37}Rv$ *Mtb*, experiments were performed in triplicate [b] Value is for MIC [c] Requires retesting at lower concentrations to determine accurate $IC_{50}$ values.[d*] Compounds synthesized by another member of the group (***in marine blue***).

## 2.3.3. Molecular Docking Studies

The publication of the crystal structures for MmpL3 and DprE1 complexed with ICs and BTZs, respectively, enabled us to perform docking studies with the synthesized peroxide hybrids.

### 2.3.3.1. MmpL3 inhibitors

Molecular docking simulations were performed to analyse the potential binding mechanism of the indole-2-carboxamide trioxane hybrids within the MmpL3 active site, given that MmpL3 is the most significant potential enzymatic target of our analogues. The crystal structure of IC compound **ICA38** in complex with *Mycobacterium smegmatis* (*Msm*) was used (PDB: 6AJJ).[10] Though the published crystal structure of the mycolic acid transporter MmpL3 complexed with **ICA38** is from *M. smegmatis*, not from *M. tuberculosis*, this crystal structure database was used to better compare the corresponding ligand with the synthesized IC peroxide hybrids. Nevertheless, despite the similarity between the two species and the conservation of the MmpL3 structure, caution must be exercised when analysing the docking studies.[10]

To confirm the docking process, the co-crystallized ligand ICA38 was re-docked into the MmpL3 binding site, following the protocol for docking depicted in **Table 2.4** and using the docking program GOLD**.**[87] This yielded 3 docked pose solutions, with the best scoring pose having a root mean square deviation (RMSD) of 0.553 Å and no pose with an RMSD greater than 0.65 Å, confirming that the docking protocol was valid (RMSD < 1.5 Å).

After validation of the docking protocol, all the IC-peroxide hybrid compounds were docked into the active site of the protein, using the docking program GOLD[87] and the docking protocol highlighted in **Table 2.4.** The binding pose with the highest GoldScore was then selected and visualised in PyMol,[88] and potential interactions were identified.

The most favourable docking pose (i.e., lowest binding energy) retained the key interactions that are observed in **ICA38** (illustrated in **Figure 2.9A**). **ICA38** inhibits MmpL3 by binding to the S3–S5 subsites of the proton transport channel, disrupting the critical components of the S4 subsite - precisely, an N-H mediated hydrogen bond to Asp645 and a hydrogen bond between the amide carbonyl and Tyr646, the two Asp-Tyr hydrogen bond pairs (Asp256-Tyr646 and Asp645-Asp257) are disrupted, thus inhibiting

the proton motive force for substrate translocation.[10]

**Table 2.4.** Docking protocol for the IC-trioxane hybrids

| Feature | Protocol |
|---|---|
| **Protein PDB** | 6AJJ |
| **Protonation** | Hydrogens added to protein |
| **Waters** | Delete remaining water molecules |
| **Ligands** | Ligands added as `.mol2` file, after energy minimization |
| **Binding Site** | IC analogues were docked using the extracted **ICA38** molecule as a reference ligand |
| **Search Efficiency** | 100% Efficiency |
| **Number of GA runs** | 10-terminated before this if 3 solutions found within 1.5 Å RMSD |
| **Lone Pairs** | Lone pairs saved |
| **Output** | Output poses saved as individual files to allow better inspection of each pose |
| **Scoring Function** | GoldScore |

The indole and spirocarboxylic groups of **ICA38** are lodged in the bulky S3 and S5 hydrophobic subsites, where they establish hydrophobic interactions with the surrounding residues. The carbocyclic spiro group shows hydrophobic interactions with the residues Phe260 and Phe649 within the S5 pocket. Regarding the S3 pocket, residues Ile253, Ile249, Ile297, Val638, Gly641, and Leu642, displayed hydrophobic contacts with the bulky indole group,[10] and SAR analyses revealed that the S3 pocket lacks tolerance for substituents in the indole ring, other than those at the 4 and 6 positions.[2]

**Figure 2.9B** reveals that **TIC01**, in the lowest docking pose, was orientated similarly to **ICA38** within the MmpL3 binding pocket. The **TIC01** docking pose is shown to be inserted in the S4 hydrophilic subsite, establishing hydrogen bonds with Asp645 (distance 1.0 Å) and Tyr646 (distance 1.9 Å) *via* the amide carbonyl. The S3 hydrophobic subsite housed the indole nucleus, whilst the spiro rings containing the 1,2,4-trioxane ring moiety were entrenched in the S5 hydrophobic subsite and overlapped with the spirocyclic group of **ICA38**. These results suggest that **TIC01** might function as an MmpL3 inhibitor, hence, exhibiting anti-TB action. However, the screening against replicating $H_{37}$Rv *Mtb* (**Table 2.2**) demonstrated that this peroxide lacked antimycobacterial activity. Even though the docking pose was favourable, it appears that

the S5 pocket cannot withstand the increase in polarity, as the switch of the spirocyclic group in **IC38** (cLogP = 5.35) to the spiro 1,2,4-trioxane (clogP = 2.86) in **TIC01** was incompatible for the S5 pocket, highlighting the limitations of the docking studies carried out.

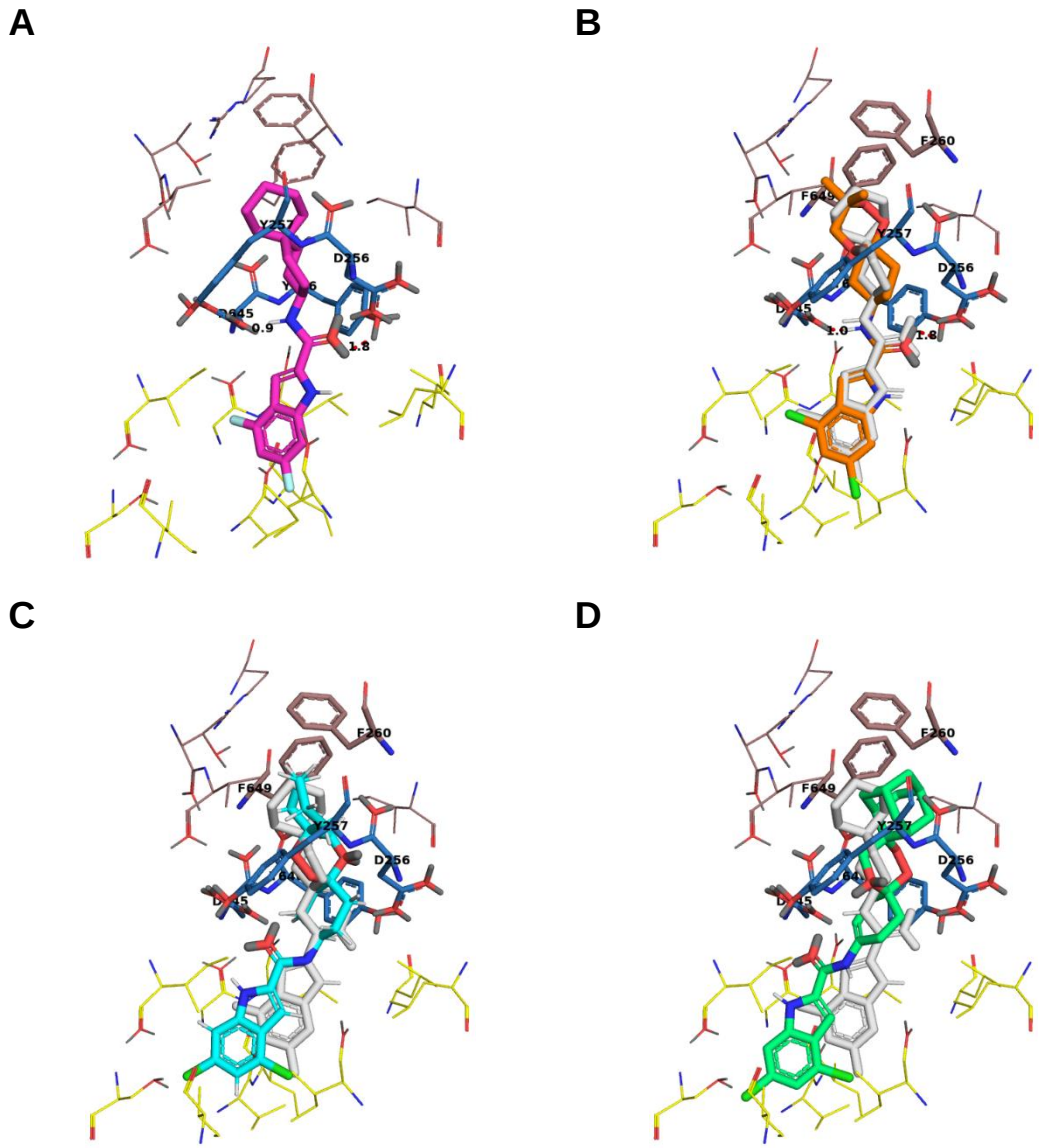


**Figure 2.9.** Molecular docking structures of IC analogues. **A)** Docked structures **ICA38** (magenta). **B-D)** Overlays of docked structures of **TIC01** (orange), **TIC02** (light blue), **TIC03** (light green), with extracted ligand **ICA38** (light grey).

In contrast, the trioxane hybrids **TIC02** and **TIC03** were shown not to be correctly aligned with the ligand **ICA38** (**Figure 2.9C/D**). A poor overlap of the indole moiety can be observed, in which the bicyclic moiety was pushed further into the S3 pocket, and the S4 hydrogen bonding motif was lost. Even Phe260 and Phe649 residues could not contain

the bulky dispiro endoperoxides because the length of the side chains exceeded the space capacity of the S5 pocket.

### 2.3.3.2. DprE1 inhibitors

Regarding DprE1 flavoenzyme docking studies, crystal structures have been reported of complexes with BTZ043 (PDB: 6HEZ)[82] and PBTZ169 (PDB: 4NCR).[32] However, for comparative purposes, it was established that all BTZ-peroxide hybrid compounds should be docked into the same crystal structure (PDB: 6HEZ). To confirm the docking process, the co-crystallized ligand BTZ043 was re-docked into the DprE1 binding site, following the protocol for docking depicted in **Table 2.5** and using the docking program GOLD.[87] This yielded 3 docked pose solutions, with the best scoring pose having an RMSD of 0.2326 Å and no pose possessing an RMSD greater than 0.3319 Å, confirming that the docking protocol was valid (RMSD < 1.5 Å.).

After validation of the docking protocol, all the BTZ-peroxide hybrid compounds were then docked into the protein's active site using the docking program GOLD[87] and the docking protocol highlighted in **Table 2.5.** The binding pose with the highest CHEMPLP score was then selected and visualised in PyMol,[88] to identify potential interactions.[88]

**Table 2.5.** Docking protocol for the BTZ-trioxane hybrids

| Feature | Protocol |
|---|---|
| **Protein PDB** | 6HEZ |
| **Protonation** | Hydrogens added to protein |
| **Waters** | Delete remaining water molecules |
| **Ligands** | Ligans added as `.mol2` file, after energy minimization |
| **Binding Site** | CYS387, identified as a residue in the binding site of BTZ043, was selected. Binding site identified within 6 Å |
| **Search Efficiency** | 100% Efficiency |
| **Number of GA runs** | 10-terminated before this if 3 solutions found within 1.5 Å RMSD |
| **Lone Pairs** | Lone pairs saved |
| **Output** | Output poses saved as individual files to allow better inspection of each pose |
| **Scoring Function** | CHEMPLP score |

BTZ043 is positioned in the substrate-binding pocket in front of the isoalloxazine ring of FAD and binds covalently to Cys387 (**Figure 2.10A/C**). The residue Lys418 is structurally close to Cys387 in the binding site of DprE1. Consequently, Lys418 can induce a protonation transformation, increasing the nucleophilicity of Cys387. Lys418 also displays a role in forming H-bonding contacts between the hydroxyl of the semimercaptal bond covalent bond between BTZ043 and Cys387 (distance 2.8 Å). The trifluoromethyl group of BTZ043 is in a hydrophobic pocket formed and displaying van der Waals and dipolar interactions by side chains of residues His132, Gly133, Lys134, Lys367, Phe369, and Asn385. The piperidine ring of BTZ043 is maintained on each side by FAD and by residues Gly117 and Val365. BTZ043's spirocyclic moiety is positioned on the protein surface, allowing for some flexibility in the protein domain. Between Leu363 and the spirocyclic moiety, there is only one van der Waals interaction.[82]

A detailed analysis at the DprE1-PBTZ169 active site (**Figure 2.10B/D**) reveals that the benzothiazinone ring interacts with the same residues as previously identified in the DprE1-BTZ043 structure, except for an additional van der Waals contact with Trp230.[32] When compared to the DprE1-BTZ043 complex structure, the cyclohexylmethyl-piperazine moiety is positioned between the isoalloxazine ring of FAD and residues Gly117, Trp230, and Leu363, with the side chains of the latter two adopting substantially different conformations.[32] Additionally, an H-bonding interaction is also observed between the hydroxyl of the semimercaptal bond in Cys387 with Lys418 (distance 2.1 Å).

The docked structures of the two BTZ-based peroxide hybrid series in association with DprE1 with the reference ligand (BZ043, white) are shown in **Figures 2.11** and **2.12.**

Docking poses demonstrate the predicted binding site, with the BTZ rings and piperidine or piperazine rings exhibiting considerable overlaps with the extracted ligand. Due to the semimercaptal bond with Cys387 and the steric restrictions of the benzothiazinone ring, the orientation of all peroxide hybrids within the active site is maintained across all compounds. There were no detectable differences in the orientation of the BTZ double-ring structure among the respective BTZ043-based peroxide hybrids. Subsequently, the trifluoromethyl group at position 6 faces residues Lys134, Gly133, His132, Lys367, and Phe369 in all compounds. Similarly, the orientation of the hydroxyl of the semimercaptal bond is not fixed, and it continually forms an H-bond interaction with Lys418 at distances between 2.7 and 3.2 Å. Most of the peroxide-containing side chain extends out of the pocket and into a solvent-accessible region. The substituents at

the 2-position generally make only a few contacts with the protein, which explains the tolerance between the amine side chains in the different peroxide hybrids.

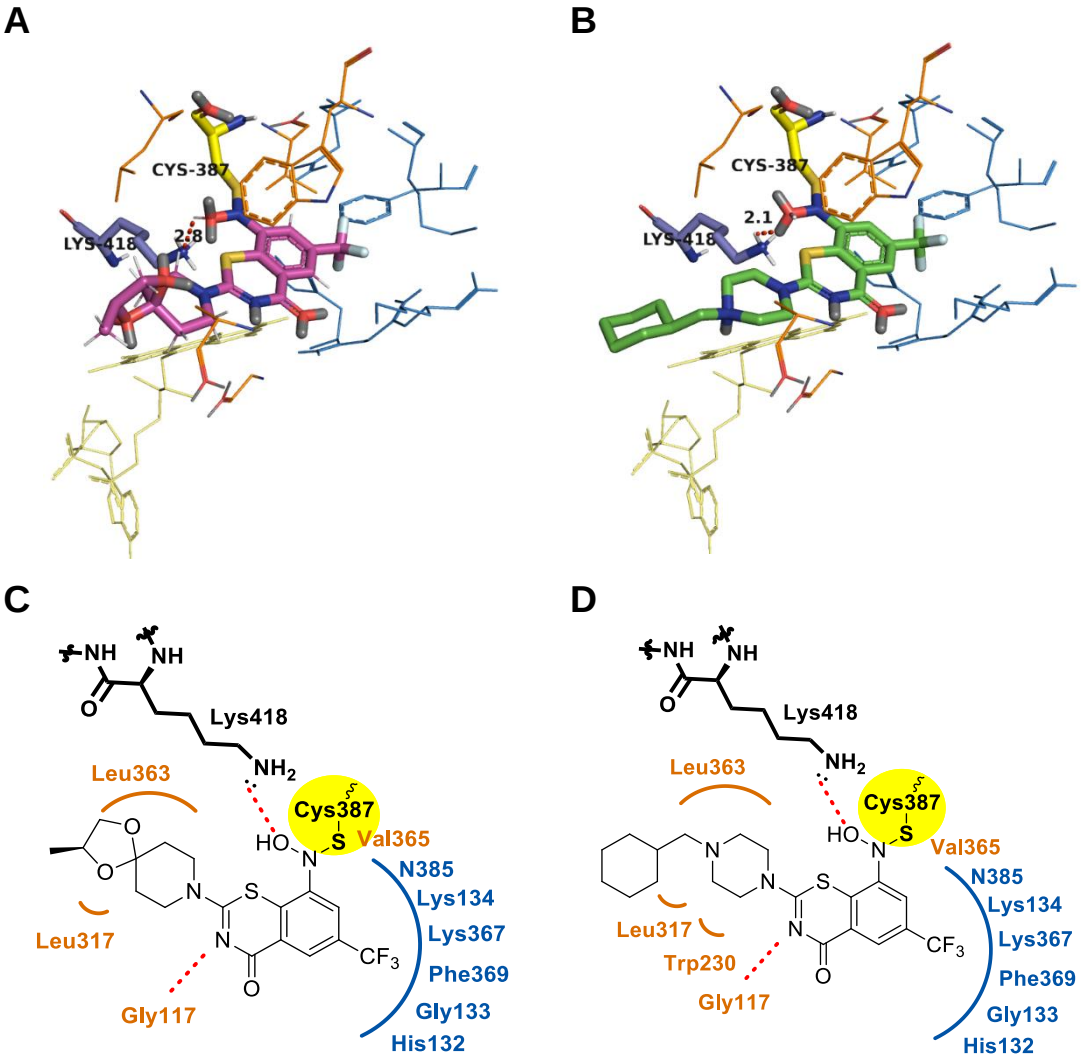


**Figure 2.10. A)** Annotated crystal structure of DprE1 in complex with BTZ043 (PDB: 6HEZ); **B)** Annotated crystal structure of DprE1 in complex with PBTZ169 (PDB: 4NCR); Structure diagram of covalent and non-covalent interactions between DprE1 with **C)** BTZ043 and **D)** PBTZ169.

As indicated in Section 2.3.2 concerning anti-TB activity, peroxide hybrid **P7** and control compound **C1** were the least active compounds of each series, with an $IC_{50}$ of 423.0 and 870 nM, respectively. Docking studies of these compounds reveal that the carbonyl group in both **P7** and **C1** are positioned within the "entrance" of the DprE1 binding pocket, close to residues Leu317 and Leu363 (**Figure 2.13A/C**). This observation shows that unfavourable interactions may occur between these non-polar residues that define the shape of this region and influence the binding of these compounds to the active

site (**Figures 2.13C-F**). The potency of carbonyl containing **C3** (7.70 nM) indicates that this effect is structural and not physicochemical, as the carbonyl is distant from the binding pocket in this molecule (**Figure 2.13B**).

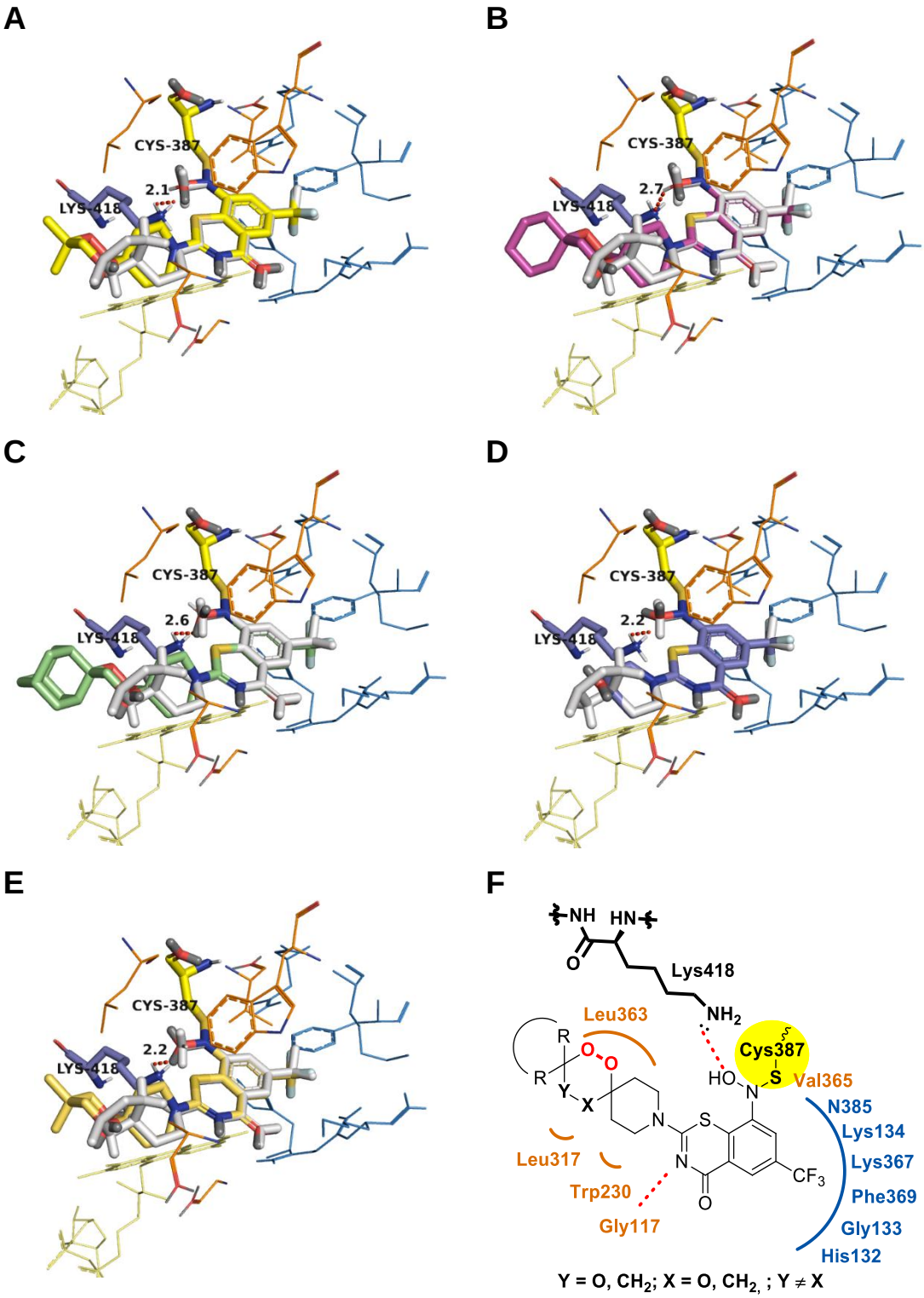


**Figure 2.11.** Molecular docking structures of BTZ043-based peroxide hybrids. **A-E)** Overlays of docked structures of **B3** (yellow), **B4** (pink), **B5** (green), **C1** (blue) and **C2**

(light brown) with the extracted reference ligand (BTZ043, white). **F)** Structure diagram of covalent and non-covalent interactions between DprE1 with peroxide hybrids.

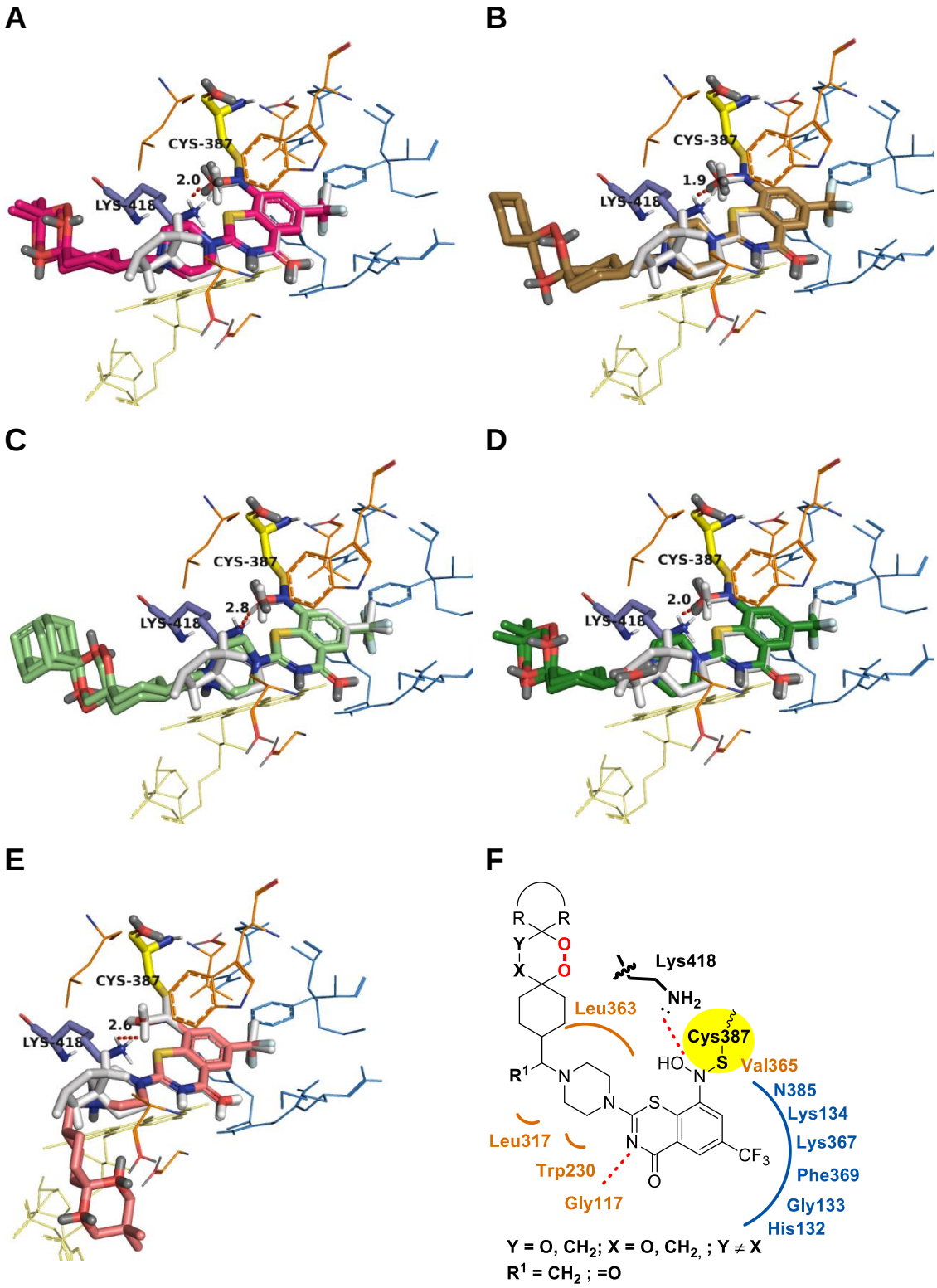


**Figure 2.12.** Molecular docking structures of PBTZ169-based peroxide hybrids. **A-E)** Overlays of docked structures of **P4** (deep pink), **P5** (brown), **P6** (light green), **P7** (dark green) and control **C4** (salmon) the extracted reference ligand (BTZ043, white). **F)**

Structure diagram of covalent and non-covalent interactions between DprE1 with peroxide hybrids.

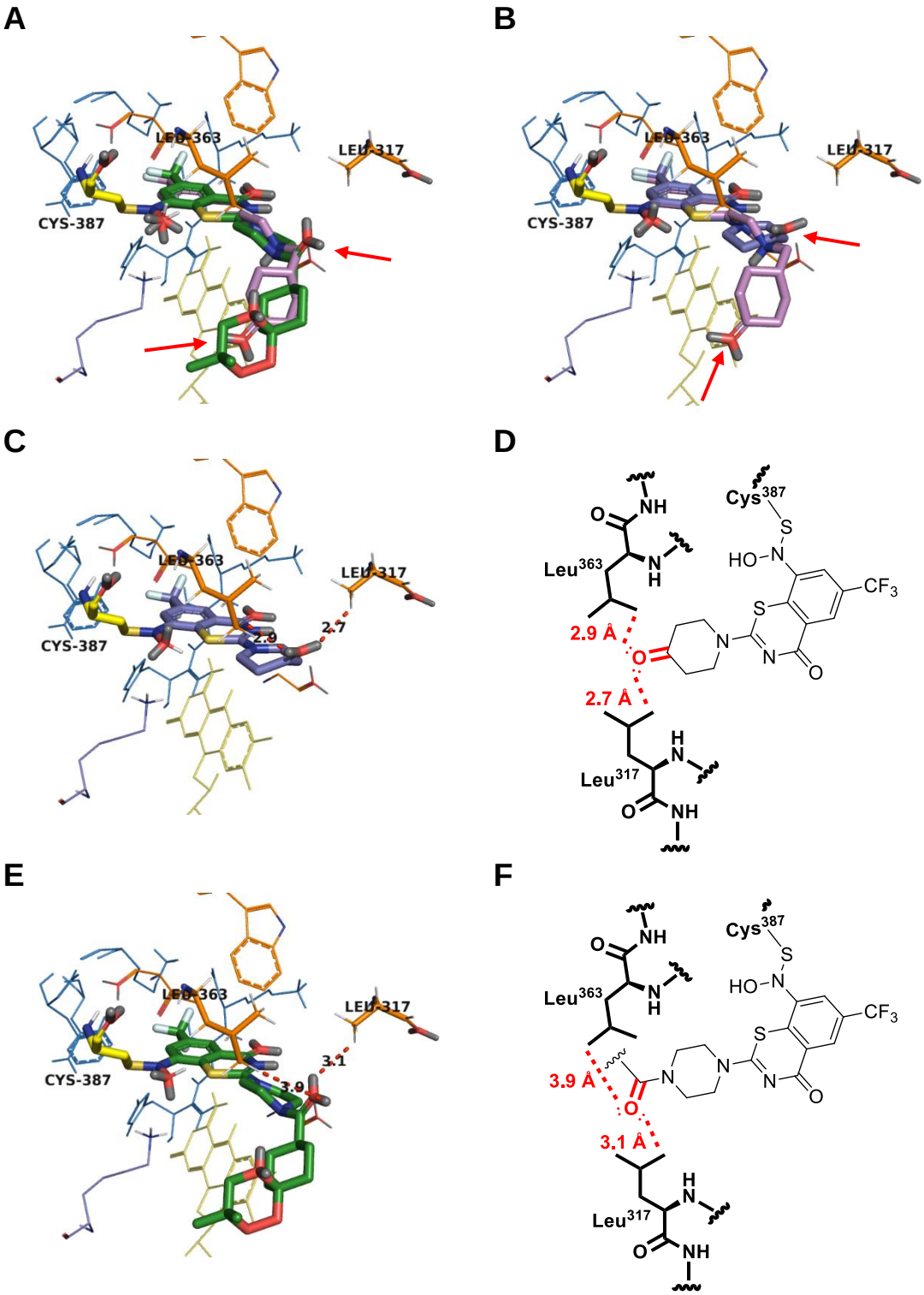


**Figure 2.13.** Molecular docking structures of **A) C1** and **P7; B) C1** and **C3; A) C1** and its interaction with residues Leu317 and Leu363 and **D) P7** its interaction with residues Leu317 and Leu363, at the DprE1 binding site. Structure diagram of non-covalent

interactions between residues Leu317 and Leu363 with **D)** control **C1** and **F)** peroxide analogue **P7.**

## 2.3.4. DMPK Data

All synthesised compounds were submitted for predicted and measured DMPK screening, provided by AstraZeneca. This screening fulfilled dual roles: 1) obtaining the measured DMPK allows to identify a molecule with appropriate properties, and 2) to compare predicted *versus* measured data. Predictive data can be combined with SAR and computational modelling to design new compounds if the values are comparable.

However, measured DMPK results could not be obtained for 1,2,4-trioxolane and 1,2,4,5-tetraoxane-containing compounds due to their incompatibility with the assay conditions. This circumstance was due to the solubility of the analogues; since the experiment was conducted under HTS conditions, it was not possible to fine-tune the conditions to measure those molecules.[89] Thus, DMPK values were only measured for 1,2,4-trioxane hybrids **TIC01-03**, **B3**, **B5**, and **P4-P6**, and the control compound **2.84**. Predicted and measured DMPK data obtained is summarised in **Tables 2.6** and **2.7**.

### 2.3.4.1. MmpL3 inhibitors

For the IC compounds, 1,2,4-trioxane hybrids **TIC01-1/2, TIC02-2, TIC03-1/2**, and the metabolite control, compound **2.84,** returned values from the DMPK assays enabling comparison between experimental and predicted values (**Table 2.6**).

For compound **2.84**, solubility was found to be over-predicted 5-fold; however, this still predicted poor solubility for this compound (12.0.73 *vs* 2 μM). The IC-trioxane hybrids **TIC01-3** were experimentally demonstrated to be similarly lipophilic and poorly soluble at pH 7.4, an anticipated property observed in indole-2-carboxamides. Dimethyl-derived trioxanes **TIC01-1** and **TIC01-2** displayed a good experimental rat hepatocyte stability (12.6 and 16.1 μl/min/mg, respectively) and good experimental stability in human liver microsomes (< 3 μl/min/mg, respectively), being in line with the predicted values. In contrast, spirocyclohexyl- and adamantyl- trioxane hybrids **TIC02** and **TIC03** were shown to have a moderate experimental rat hepatocyte stability, though these peroxide hybrids displayed high clearance values in human liver microsomes, defining these compounds as poorly stable. These results can be explained by the high metabolism suffered in the cyclo-alkyl chains of these compounds, compared to the dimethyl trioxane

analogue.

The values for plasma protein binding (PPB %free) and intrinsic clearance appear to be primarily concordant, with clearance values for rat hepatocyte clearance being set within the correct thresholds - human microsomal clearance appears to be under-anticipated by this model. Predicted or experimental values of all compounds were indicative of high protein binding properties.

**Table 2.6.** Summary of key predicted and measured DMPK values for the IC compounds – predictions kindly provided by AstraZeneca. Rat hepatocyte clearance thresholds: <30 µl/min/mg – good, 30-90 µl/min/mg – moderate; > 90 µl/min/mg – poor. Human liver microsomal clearance thresholds: <30 µl/min/mg – good, 30-90 µl/min/mg – moderate; > 90 µl/min/mg – poor.[a]

| Cmpd | ID | Type | $LogD_{7.4}$ | Aqueous solubility pH 7.4 (µM) | Human Prot. Binding (% free) | Rat hepatocyte CLint (µl/min/mg) | Human microsome CLint (µl/min/mg) |
|---|---|---|---|---|---|---|---|
| **2.6** | **1** | Pred | 5.43 | 2.837 | 0.088 | 22.44 | 41.38 |
| | | **Exp** | - | - | - | - | - |
| **2.84** | **2** | Pred | 3.17 | 12.07 | 1.134 | 13.46 | 16.29 |
| | | **Exp** | **> 3.80** | **2.000** | **1.100** | **23.80** | **40.10** |
| **2.85** | **3** | Pred | 6.057 | 0.2690 | 0.009 | 4.718 | 15.93 |
| | | **Exp** | - | - | - | - | - |
| **2.86** | **4** | Pred | 5.191 | 0.6060 | 0.037 | 6.398 | 15.55 |
| | | **Exp** | - | - | - | - | - |
| **2.87** | **5** | Pred | 6.367 | 0.2250 | 0.006 | 6.834 | 38.68 |
| | | **Exp** | - | - | - | - | - |
| **2.88** | **6** | Pred | 6.080 | 0.1920 | 0.009 | 23.37 | 66.98 |
| | | **Exp** | - | - | - | - | - |
| **TIC01-1** | **7-1** | Pred | 4.524 | 7.083 | 0.201 | 9.130 | 9.009 |
| | | **Exp** | **4.200** | **< 0.8** | **0.110** | **12.60** | **< 3** |
| **TIC01-2** | **7-2** | Pred | 4.524 | 7.083 | 0.201 | 9.130 | 9.009 |
| | | **Exp** | **3.600** | **< 1.400** | **0.350** | **16.10** | **< 3** |
| **TIC02-1** | **8-1** | Pred | 5.332 | 1.200 | 0.066 | 36.89 | 47.53 |
| | | **Exp** | - | - | - | - | - |
| **TIC02-2** | **8-2** | Pred | 5.332 | 1.200 | 0.066 | 36.89 | 47.53 |
| | | **Exp** | **3.600** | **< 2.30** | **0.050** | **51.50** | **119.0** |
| **TIC03-1** | **8-1** | Pred | 6.516 | 0.3330 | 0.015 | 30.065 | 96.46 |
| | | **Exp** | **3.400** | **< 6.80** | **< 0.31** | **22.7** | **99.20** |
| **TIC03-2** | **8-2** | Pred | 6.516 | 0.3330 | 0.015 | 30.07 | 96.46 |
| | | **Exp** | **3.400** | **< 13.1** | **< 3** | **61.60** | **89.80** |

[a] Figures in brackets represent experimentally derived values. Experimental values measured once, through a high-throughput platform provided by AstraZeneca, UK. The methods of the five assays, including $logD_{7.4}$, aqueous solubility, plasma protein binding, and microsome and hepatocyte clearance measurements, have been reported previously.[89] Values are colour coded with a traffic light system, according to how good or bad a particular value is. Green – good, amber – acceptable/medium, red – poor.

To establish a correlation between the predicted and measured/experimental values, we performed a Pearson's correlation and calculated the *R*-squared ($R^2$), a goodness-of-fit measure for evaluating linear regression models, such as those employed to predict DMPK values. The results are described in **Figure 2.14.** For the indole-2-carboxamide peroxide hybrids, Pearson's correlation analysis indicated that all parameters were not statistically significant ($p > 0.05$), except for the PPB parameter ($r$ = 0.939, $p$ = 0.018), implying that the correlation between these predicted and experimental variables cannot be determined, for this sample analysis. These observations suggest that the regression model does not explain the fitted experimental data. Consequently, the obtained results reveal that specific regression models may not be optimal for forecasting the properties of this scaffold or that software tools used to predict these DMPK parameters should be employed with caution. The opposite situation is observed for the PPB% parameter, in which the predicted and experimental value displayed a strong positive linear relationship (with $r$ = 0.939, $p$ = 0.018) and $R^2$ value of 0.882. This result shows that the PPB% predictions should be accurate and can be used to aid in the design of analogues.

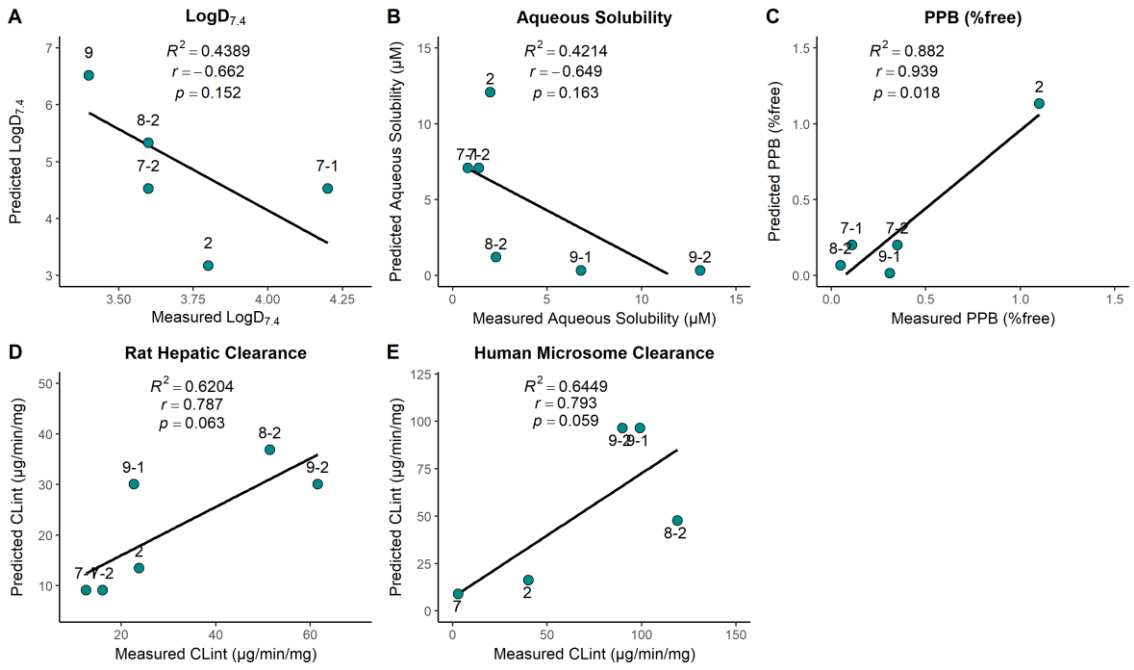


**Figure 2.14.** Scatter plots of measured *versus* predicted values for each DMPK parameter and Pearson correlation coefficient between measured *versus* predicted values for the IC-peroxide hybrids. **A)** $LogD_{7.4}$; **B)** Aqueous solubility; **C)** PPB (%free); **D)** Rat hepatic clearance; **E)** Human microsome clearance.

### 2.3.4.2. DprE1 Inhibitors

Predicted and experimental values were obtained for several endoperoxide and control compounds, enabling the evaluation of the effectiveness of the predictive models for the BTZ compounds, and the representative values are described in **Table 2.7**.

For all compounds but **C1**, where metabolic stability was vastly underestimated, metabolic stability values were correctly assigned to their threshold values. Similarly, solubility and human PPB were also underestimated for **C1,** but for all others the values were similar. LogD was also predicted to be concordant enough for use.

The BTZ043 analogues **B1**-**B2** and **B5** are very lipophilic, with logD values > 4.5, having correspondingly poor predicted and measured aqueous solubility – indicating that this may be the issue determining incompatibility with the high-throughput assay protocol. Trioxanes **B3** and **B4** were slightly less lipophilic, with $logD_{7.4}$ values of 3.2 (Exp.) and 3.9 (Pred), respectively. However, despite this, solubility remained low. The BTZ043 analogues **B1**-**2,4-5** were also predicted to have good-moderate metabolic stability, with slightly higher predicted metabolism in human liver microsomes. Curiously, trioxane **B5** displayed a poor measured rat hepatocyte stability, with a high clearance value of 139 µL/min/mg, substantially higher than the predicted value (47.1 µL/min/mg).

Meanwhile, the trioxane **B3** displayed good predicted and measured metabolic stability with a low clearance of 8.5 µL/min/mg in human liver microsomes. The PBTZ169 analogues **P1**-**3,5-6** were similarly lipophilic and poorly soluble at pH 7.4. Notably, the PBTZ series of compounds comprises a piperazine moiety, so these compounds have been observed to be more soluble in acidic media.[32] Predicted rat hepatocyte clearance for **P1**-**3** indicated good metabolic stability. However, this contrasts with the predicted human microsomal clearance, indicative of poor stability, with the trioxolane **P3** being the highest.

**P2** is predicted to be less metabolically stable than **P1,** despite differing by only an additional methylene linker, indicating that the model identified this as a marker for potential metabolism. Trioxanes **P4**-**P6** displayed good to moderate measured rat hepatocyte stability, with **P4** displaying moderate stability in human liver microsomes, in line with predicted values. In contrast, **P5** and **P6** were predicted to be poorly stable in human liver microsomes. The poor predicted human microsomal stability may be due to the substituted piperazine which may undergo *N*-demethylation – a key metabolic

pathway for other piperazine-containing drugs.[90,91] Compound **P7,** due to the presence of an additional carbonyl, was predicted to be less lipophilic and slightly more water-soluble with respect to **P4**. Similarly, **P7** has a good metabolic stability profile – predicted to be better than **P4**, which might indicate that the model predicts the methylene linker as a potential site for metabolism.

Compared to the target compounds, the control compounds **C1-3** were less lipophilic and more water-soluble than their peroxide counterparts – particularly **C1,** which had a measured LogD of 1.8 and a measured solubility of 499 µM. **C1** also had a significantly poorer metabolic profile compared to the BTZ-derived peroxides, with measured clearance in rat hepatocytes and human liver microsomes of >300 µL/min/mg and >300 µL/min/mg, respectively. Control compounds **C2-4** all exhibited moderate to good metabolic stability profiles.

To establish a correlation between the predicted and measured/experimental values we performed a Pearson's correlation and calculated the *R*-squared ($R^2$), a goodness-of-fit measure for evaluating linear regression models, such as those employed to predict DMPK values. The results are described in **Figure 2.15.** For the benzothiazinone-based peroxide hybrids, Pearson's correlation analysis revealed that all parameters were statistically significant ($p < 0.01$ or $p < 0.001$). All DMPK parameters displayed a strong positive linear relationship (with $r \geq 0.886$) and $R^2$ values ranging from 0.785 to 0.972, with the model for prediction of human microsome clearance scoring the highest, with $r = 0.986$ and $R^2 = 0.972$ ($p < 0.01$). These findings show that these DMPK models are robust and may be employed to aid in the design of novel BTZ-analogues.

**Table 2.7.** Summary of key predicted and measured DMPK values for the BTZ compounds – predictions kindly provided by AstraZeneca. Rat hepatocyte clearance thresholds: <30 µl/min/mg – good, 30-90 µl/min/mg – moderate; > 90 µl/min/mg – poor. Human liver microsomal clearance thresholds: <30 µl/min/mg – good, 30-90 µl/min/mg – moderate; > 90 µl/min/mg – poor.[a]

| Cmpd | Type | $LogD_{7.4}$ | Aqueous solubility pH 7.4 (µM) | Human Prot. Binding (% free) | Rat hepatocyte CLint (µl/min/mg) | Human microsome CLint (µl/min/mg) |
|---|---|---|---|---|---|---|
| **B1** | Pred | 4.6 | 0.55 | 0.18 | 10 | 21.2 |
| | **Exp** | - | - | - | - | - |
| **B2** | Pred | 4.7 | 0.63 | 0.19 | 38.91 | 46.8 |
| | **Exp** | - | - | - | - | - |
| **B3** | Pred | 3.1 | 12.0 | 3.5 | 16.1 | 12.8 |
| | **Exp** | **3.2** | **< 3.20** | **3.1** | **16.5** | **8.5** |
| **B4** | Pred | 3.9 | 3.6 | 1.4 | 77.1 | 59.8 |
| | **Exp** | - | - | - | - | - |
| **B5** | Pred | 4.9 | 0.53 | 0.12 | 47.1 | 81.6 |
| | **Exp** | **> 3.6** | **< 1.90** | **< 3.2** | **139** | - |
| **P1** | Pred | 5.3 | 0.17 | 0.046 | 5.8 | 48.6 |
| | **Exp** | - | - | - | - | - |
| **P2** | Pred | 5.3 | 0.13 | 0.064 | 8.5 | 64.0 |
| | **Exp** | - | - | - | - | - |
| **P3** | Pred | 5.6 | 0.15 | 0.027 | 8.7 | 117.2 |
| | **Exp** | - | - | - | - | - |
| **P4** | Pred | 3.8 | 3.3 | 0.64 | 9.4 | 33.2 |
| | **Exp** | **4.0** | **6.0** | **0.36** | **12.8** | **56.9** |
| **P5** | Pred | 4.6 | 2.1 | 0.29 | 45.2 | 161.4 |
| | **Exp** | **> 4.1** | **< 1.0** | **< 0.28** | **43.2** | - |
| **P6** | Pred | 5.5 | 0.31 | 0.075 | 50.9 | 126.5 |
| | **Exp** | - | **< 5.4** | **< 3.1** | **52.7** | - |
| **P7** | Pred | 3.4 | 13.0 | 1.4 | 8.5 | 21.6 |
| | **Exp** | - | - | - | - | - |
| **C1** | Pred | 1.9 | 29.823 | 13.4 | 92.0 | 78.5 |
| | **Exp** | **1.8** | **499** | **24** | **> 300** | **> 300** |
| **C2** | Pred | 3.4 | 4.513 | 2.2 | 33.2 | 18.1 |
| | **Exp** | **3.2** | **2.0** | **< 3.1** | **26.1** | **9.1** |
| **C3** | Pred | 2.4 | 6.214 | 7.2 | 16.9 | 31.7 |
| | **Exp** | **2.6** | **33** | **7.2** | **12.9** | **49.6** |
| **C4** | Pred | 4.0 | 1.5 | 0.62 | 20.0 | 44.4 |
| | **Exp** | **> 3.5** | **14** | **< 2.6** | **12** | - |

Experimental values measured once, through a high-throughput platform provided by AstraZeneca, UK. The methods of the five assays, including $logD_{7.4}$, aqueous solubility, plasma protein binding, and microsome and hepatocyte clearance measurements, have been reported previously.[89] Values are colour coded with a traffic light system, according to how good or bad a particular value is. Green – good, amber – acceptable/medium, red – poor.

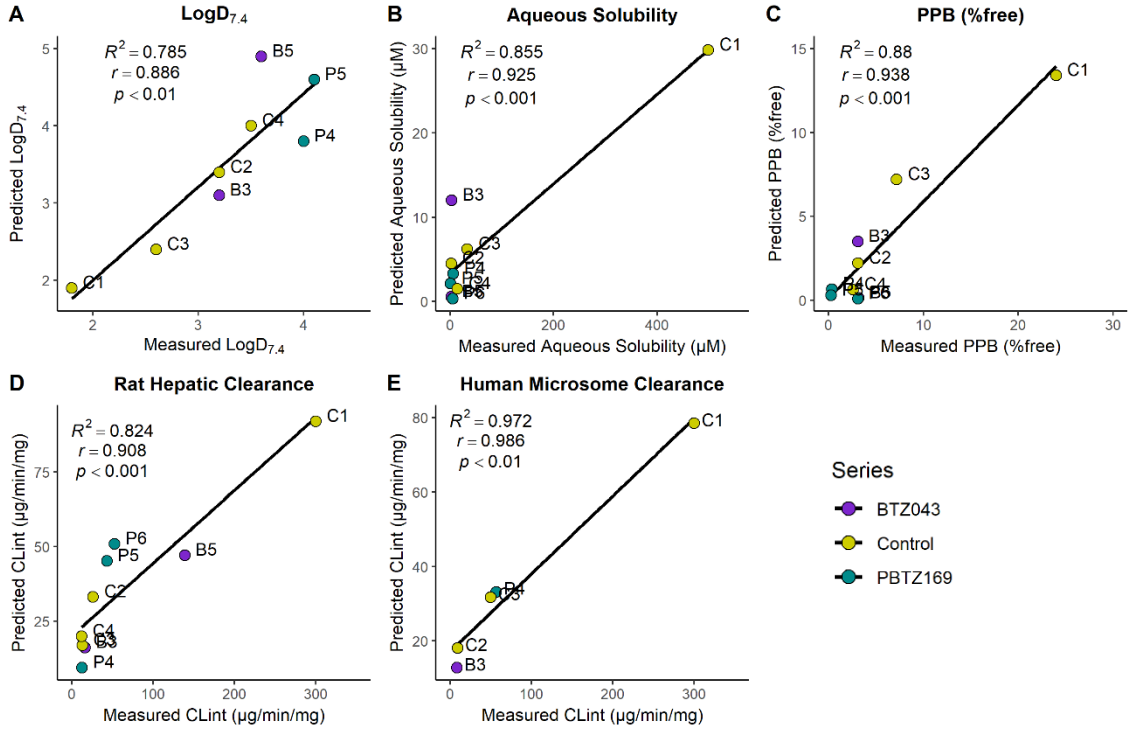


**Figure 2.15.** Scatter plots of measured *versus* predicted values for each DMPK parameter and Pearson correlation coefficient between measured *versus* predicted values, for the BTZ-peroxide hybrids. **A)** $LogD_{7.4}$; **B)** Aqueous solubility; **C)** PPB (%free); **D)** Rat hepatic clearance; **E)** Human microsome Clearance.

## 2.3.5. *In vivo* PK cassette screening results for Selected Compounds B3, P1, BTZ043 and PBTZ169

Considering the *in vitro* properties, compounds **CW02-9-8** (**P1**), **PA54-2** (**B3**), **BTZ043**, and **PBTZ169** were selected for the evaluation of *in vivo* pharmacokinetic (PK) profiles. *In vivo PK* cassette screening was carried by a Contract Research Organization (CRO), ChemPartner (Shanghai, China). PK data from studies in male CD1 mice, after single IV dosing at 1 mg/kg and after a single oral administration of 25 mg/kg, is presented in **Table 2.8**. Plots of the mean plasma concentration-time profiles of **CW02-9-8, PA54-2, BTZ043**, and **PBTZ169** are shown in **Figure 2.16.**

All compounds have exhibited a low clearance CL (0.727-2.46 mL/min/kg). Oral administration of 25 mg/kg of BTZ-peroxides resulted in rapid absorption that reached 106 ng/mL ($C_{max}$) at 4 h ($T_{max}$) for **CW02-9-8** and 595 ng/mL at 1 h for **PA54** (**Table 2.8**). Oral bioavailability was poor in the hybrids **CW02-9-8** and **PA54**, with the values F: 3.51%, F: 6.38%, respectively, which were significantly lower than those of **BTZ043** and **PTBZ169** (F: 32.3%, 47.9%). Rapid biotransformation of **CW02-9-8** was evidenced by the low half-time values ($T_{1/2}$) in both intravenous (iv) or oral (po) administration ($T_{1/2}$ = 0.291 h and 1.04 h) and $AUC_{INF}$ (i.v.) = 505 h.ng. $mL^{-1}$ and $AUC_{INF}$ (p.o.) = 432 h.ng. $mL^{-1}$. In contrast to the simpler peroxide-BTZ **PA54**, it exhibited $T_{1/2}$ values for i.v. of 0.549 h and for p.o. 2.73 h, respectively. Interestingly, oral administration $T_{1/2}$ of **PA54** is improved by 2-fold with respect to **BTZ043** ($T_{1/2}$ = 1.35 h) and is equivalent to **PBTZ169** ($T_{1/2}$ = 2.71 h). Regarding the p.o. $AUC_{INF}$ (2191 h.ng. $mL^{-1}$) for hybrid **PA54**, it was found to be 3-fold lower when compared to the **BTZ043** (6623 h.ng. $mL^{-1}$) and 2-fold lower when compared to the **PBTZ169** (4856 h.ng. $mL^{-1}$). Opposite to the i.v. $AUC_{INF}$ (1375 h.ng. $mL^{-1}$) for compound **PA54**, it was found to be ~1.5-fold higher compared to **BTZ043** (821 h.ng. $mL^{-1}$) and ~3-fold higher when compared to the **PBTZ169** (406 h.ng. $mL^{-1}$). These findings indicate that peroxide-BTZ compounds are less stable than standard BTZs, perhaps due to the labile peroxide link in their structure, which makes them susceptible to extensive metabolism. In contrast to the lead compounds, however, peroxide-BTZ **PA54** exhibited acceptable PK data.

**Table 2.8.** Mean Plasma Pharmacokinetic parameters of **CW02-9-8, PA54, BTZ043** and **PBTZ169** after single IV dosing at 1 mg/kg (4 in 1 cassette) and after single PO dosing at 25 mg/kg in male CD1 mice.

| | | **CW02-9-8** | | **PA54** | | **BTZ043** | | **PBTZ169** | |
|---|---|---|---|---|---|---|---|---|---|
| **parameters** | **unit** | **i.v.** | **p.o** | **i.v.** | **p.o** | **i.v.** | **p.o** | **i.v.** | **p.o** |
| **Dose** | **mg/kg** | **1** | **25** | **1** | **25** | **1** | **25** | **1** | **25** |
| **CL** | **L/h/kg** | 1.98 | | 0.727 | | 1.22 | | 2.46 | |
| **$V_{ss}$** | **L/kg** | 0.292 | | 0.359 | | 0.558 | | 1.86 | |
| **$T_{1/2}$** [a] | **h** | 0.291 | 1.04 | 0.549 | 2.73 | 0.585 | 1.55 | 1.35 | 2.71 |
| **$T_{max}$** | **h** | | 4.00 | | 1.00 | | 0.50 | | 1.00 |
| **$C_{max}$** | **ng/mL** | | 106 | | 595 | | 2247 | | 1400 |
| **$AUC_{last}$** | **h.ng. $mL^{-1}$** | 505 | 432 | 1371 | 2187 | 818 | 6362 | 403 | 4849 |
| **$AUC_{inf}$** | **h.ng. $mL^{-1}$** | 506 | 443 | 1375 | 2191 | 821 | 6623 | 406 | 4856 |
| **$MRT_{inf}$** [b] | **h** | 0.147 | | 0.493 | | 0.458 | | | 0.755 |
| ***F*** [c] | **%** | | 3.51 | | 6.38 | | 32.3 | | 47.9 |

[a]Plasma elimination half-life. [b]Mean residence time. [c]Oral bioavailability.

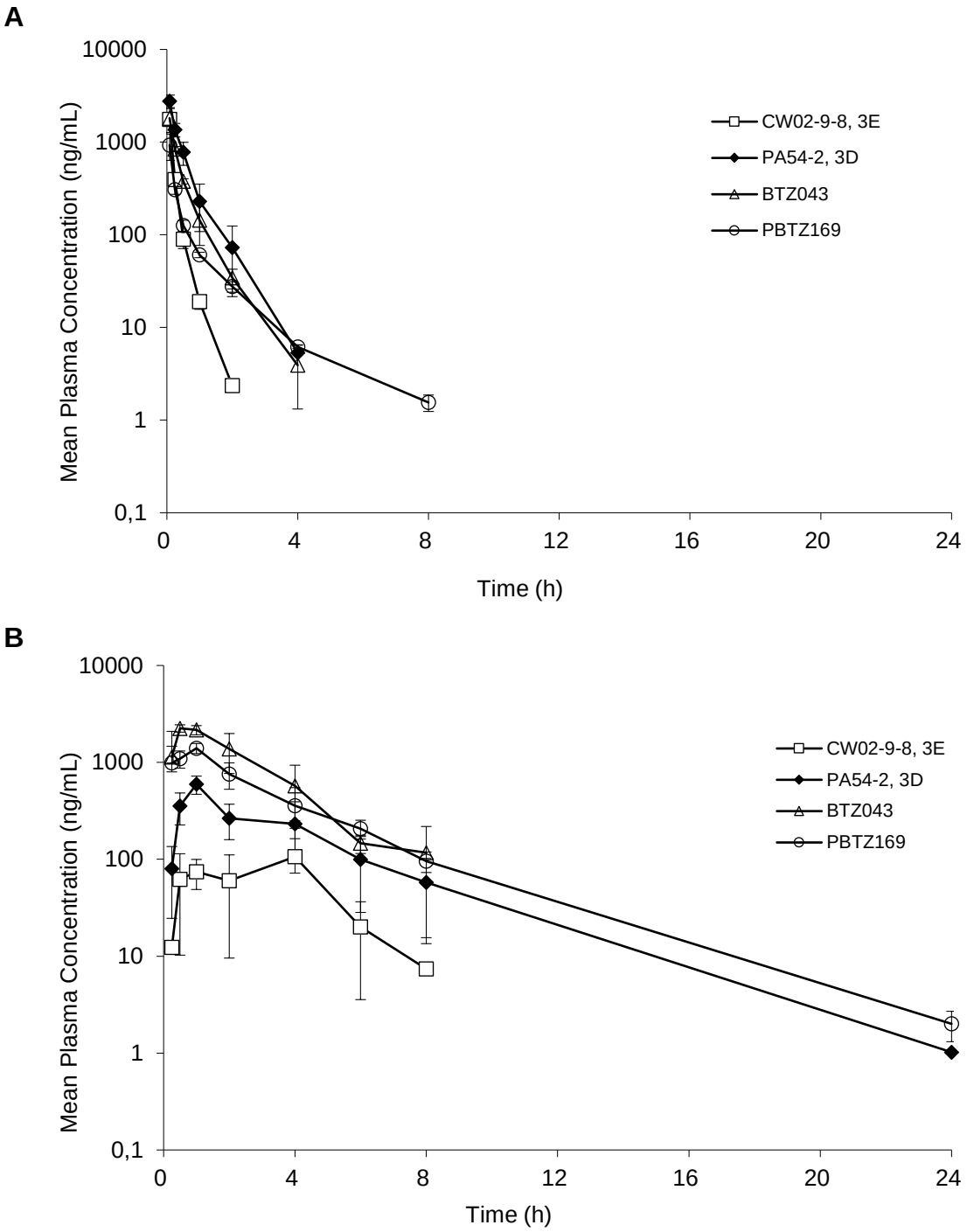


**Figure 2.16.** Mean plasma concentration-time profiles of **CW02-9-8, PA54-2, BTZ043** and **PBTZ169** after **A:** single IV dosing at 1 mg/kg in male CD1 mice and **B:** after single PO dosing at 25 mg/kg male CD1 mice.

## 2.4. Summary and Conclusions

To summarize, peroxide-based TB drug hybrids based on an indole-2-carboxamide (IC) MmpL3 inhibitor and on a benzothiazinone DprE1 inhibitor were designed and synthesized. These scaffolds were chosen due to their high potency against replicating *Mtb* but low activity against non-replicating persistent *Mtb*.

The screening of IC-based peroxide hybrids against replicating *Mtb* demonstrated poor activity for most of the compounds ($IC_{50}$ > 10 µM), although the metabolite control compound **2.84** and the tetraoxane hybrid **2.86** exhibited moderate inhibitory activity of the *Mtb* growth ($IC_{50}$ = 5.680 and 2.634 µM, respectively). Docking studies explained the poor activity of IC compounds, as IC-peroxide hybrids displayed showed poor docking results, except for IC-analogue **TIC01**. However, this peroxide hybrid was found not to be active against *Mtb*.

Fortunately, our research in BTZ analogues resulted in 16 novel BTZ-peroxide compounds and led to the identification of potent representatives in replicating *Mtb* assays, with $IC_{50}$ values in the nanomolar (1.32-870 nM) and picomolar range (< 0.457 nM). Docking studies demonstrated good overlap between the BTZ ring system of the hybrids and the reference ligand, supporting the potent sub-micromolar activity achieved by these series.

Moreover, *in silico* data were calculated for endoperoxide hybrids and compared to the *in vitro* DMPK results. Experimentally, the IC-trioxane hybrids **TIC01-03** were similarly lipophilic and poorly soluble at pH 7.4, as expected for indole-2-carboxamide compounds. The metabolic profiles of IC-based and BTZ043-based peroxide hybrids were moderate to good, whereas those derived from PBTZ169 were poor to moderate. The high cLogP values for all synthesized compounds are mirrored in the low anticipated aqueous solubility at pH 7.4.

*In vivo* pharmacokinetic profiles of **B3**, **P1**, and controls **BTZ043** and **PBTZ169**, indicate that peroxide-BTZs are less stable than standard BTZs, perhaps due to the labile peroxide link in their structure, which makes them susceptible to extensive metabolism. In contrast to the lead compounds, however, peroxide-BTZ **B3** exhibited acceptable PK data.

Selected compounds were screened against whole cell *Mtb* modified to express DosRST-dependent GFP, and the testing is still ongoing.

# 2.5. Experimental Section

## 2.5.1. General Experimental details

***Chemicals.*** All reagents and solvents used were of analytical grade and were used without further purification. When necessary, solvents were freshly distilled from appropriate drying agents prior to use. Analytical thin layer chromatography (TLC) was carried out using TLC Silica gel 60 F254 aluminium sheets (AL TLC 20x20). Column chromatography was carried out using technical grade Silica Gel 60 (0.04 – 0.063 mm).

***Analytical equipment.*** $^{1}H$ and $^{13}C$ Nuclear Magnetic Resonance (NMR) spectra were recorded using a Bruker AMX400 spectrometer or a 500 MHz JEOL system equipped with a Royal HFX probe, in solution, using the deuterated solvents described in each experimental procedure. The chemical shifts (δ) are described in parts per million (ppm), downfield from an internal standard of tetramethylsilane (TMS). Melting points (°C) were obtained on an SMP30 melting point apparatus and are uncorrected. High Resolution Mass Spectrometry (HRMS) was recorded using the analytical services within the Chemistry Department at the University of Liverpool (UoL). HRMS was conducted on a VG analytical 7070E machine, Frisons TRIO mass spectrometer, or Agilent QTOF 7200, using chemical ionisation (CI) or electrospray (ESI) (UoL). Elemental analysis (%C, %H, %N and %S where specified) were determined by the University of Liverpool Microanalysis Laboratory. HPLC was carried out using an Agilent 1200 system with a ZORBAX Eclipse Plus C18 column (4.6 mm x 100 mm, 3.5 µm) at 25°C.

***Safety.*** Organic peroxides are potentially hazardous compounds (inflammable and explosive) and must be handled carefully: 1) a safety shield should be used for all reactions involving $H_2O_2$; 2) direct exposure to strong heat or light, mechanical shock, oxidizable organic materials or transition-metal ions should be avoided.

***HPLC – Methods:*** Flow rate 1 mL/min for 17 minutes using MeCN/Water (both solvents with or without 0.1% Formic acid) with compounds dissolved in acetonitrile (with or without 0.1% Formic acid). UV detector recorded signals at 254 nm.
HPLC **Method A**: min, gradient: 2% MeCN hold to 1 min, 2-98% MeCN to 11 min, then hold at 98% MeCN to 15 min, then back to 2% MeCN until end (to 17 min).
HPLC **Method B**: min, gradient: 50% MeCN hold to 1 min, 50-98% MeCN to 12 min,

then hold at 98% MeCN to 15 min, then back to 50% MeCN until end (to 17 min).

HPLC **Method C**: min, gradient: 2% MeCN (0.1% Formic acid) hold to 1 min, 2-98% MeCN (0.1% Formic acid) in 11 min, then hold at 98% MeCN (0.1% Formic acid) to 15 min, then back to 2% MeCN (0.1% Formic acid) until end (to 17 min).

HPLC **Method D**: min, gradient: 50% MeCN (0.1% Formic acid) hold to 1 min, 50-98% MeCN (0.1% Formic acid) to 12 min, then hold at 98% MeCN (0.1% Formic acid) to 15 min, then back to 50% MeCN (0.1% Formic acid) until end (to 17 min).

HPLC **Method E**: min, gradient: 20% MeCN (0.1% Formic acid) hold to 1 min, 20-45% MeCN (0.1% Formic acid) to 12 min, then to 98% MeCN (0.1% Formic acid) to 15 min, then back to 20% MeCN (0.1% Formic acid) until end (to 17 min).

HPLC **Method F**: min, gradient: 25% MeCN (0.1% Formic acid) hold to 1 min, 25-75% MeCN (0.1% Formic acid) to 12 min, then to 98% MeCN (0.1% Formic acid) to 15 min, then back to 25% MeCN (0.1% Formic acid) until end (to 17 min).

HPLC **Method G**: min, gradient: 35% MeCN (0.1% Formic acid) hold to 1 min, 35-36% MeCN (0.1% Formic acid) to 12 min, then to 98% MeCN (0.1% Formic acid) to 15 min, then back to 35% MeCN (0.1% Formic acid) until end (to 17 min).

## 2.5.2. General Procedures

**General Procedure 1: Synthesis of 1,2,4-trioxanes *via* hydroperoxysilylation of allylic alcohols, followed by cyclocondensation to 1,2,4-trioxane**. *The procedure with the catalyst silica sulfuric acid (SSA) was used, which is described in detail in **Chapter 4**. **Step 1**: **Hydroperoxysilylation of allylic alcohols***. To a solution of allylic alcohol (1 mmol) in anhydrous1,2-dichloroethane (DCE, 10 mL) was added $Co(thd)_2$ (0.03 mmol), at room temperature, and the solution allowed to stir, while bubbling with oxygen for 5 min. Triethylsilane (2 mmol) was then added and the reactants were allowed to react under an oxygen atmosphere. The original purple/brown solution became green, and the reaction was followed by TLC until completion. The reaction mixture was then filtered through a plug of celite in a sinter funnel, under reduced pressure. The celite was further washed with ethyl acetate and the resulting combined filtrate was then concentrated under reduced pressure to give the semi-crude peroxysilyl alcohol, which was used immediately in the next step without further purification. ***Step 2*: *Cyclocondensation of the peroxysilyl alcohol to 1,2,4-trioxanes***. The peroxysilyl alcohol semi-crude (1 mmol) and the carbonyl compound (1.5 mmol) were dissolved in anhydrous dichloromethane (5 mL). The mixture

was cooled to below 5°C and then silica sulfuric acid (SSA, 2 mmol) was added. The final mixture was then warmed and allowed to stir at room temperature until completion of the reaction (reaction followed by TLC, usually 30-60 min). The resulting solution was then filtered, rinsed with dichloromethane, and concentrated under reduced pressure. Purification by flash chromatography using a mixture of EtOAc/Hexane (unless specified differently) gave the pure product.

**General Procedure 2: Synthesis of 1,2,4-trioxanes via perhydrolysis of spiro-oxiranes, followed by cyclocondensation to 1,2,4-trioxanes**. *The procedure with SSA was used, which is described in detail in* ***Chapter 4,*** or adapted the procedure from An *et al.*[92] ***Step 1*****:** To a spiro-oxirane (1 mmol) in solution of $MgSO_4$ dried $H_2O_2$–$Et_2O$ (15 mL, see note below), SSA (2 mmol) or bis(acetylacetonato)dioxomolybdenum(VI) ($MoO_2(acac)_2$, 0.05 mmol)[92] was added, at 0°C. The reaction mixture was then allowed to warm at room temperature and stirred until completion (usually 1 h). The final mixture was then washed with water (1 × 100 ml) and brine (1 × 100 mL). *In the event of using the SSA method, prior filtration to remove the SSA catalyst and rinsing with $CH_2Cl_2$ is required*. The combined aqueous layers were extracted with $CH_2Cl_2$ (2 × 75 mL). The combined organic layers were concentrated under *vacuum*, affording the β-hydroperoxy alcohol crude, which was immediately used in the next step without any further purification. **Step 2: Cyclocondensation of the β-hydroperoxy alcohol to 1,2,4-trioxanes.** The β-hydroperoxy alcohol semi-crude (1 mmol) and the carbonyl compound (1.5 mmol) were dissolved in anhydrous dichloromethane (5 mL). The mixture was cooled to below 5°C and then SSA (2 mmol) was added. The mixture was then warmed and allowed to stir at room temperature, until completion of the reaction (usually 1-2 h). The resulting solution was then filtered, rinsed with dichloromethane, and concentrated under *vacuum*. Purification by flash chromatography using a EtOAc−hexane gradient (unless specified differently) gave the pure 1,2,4-trioxane compound.

**General Procedure 3: Reduction with $LiAlH_4$**. The procedure described by Kwiatkowski and *et al.*[93] was followed, with slight modifications. A solution of the carboxylic acid or ester (1 mmol) in anhydrous diethyl ether (5 mL) was added dropwise to a suspension of $LiAlH_4$ (3 mmol) in anhydrous diethyl ether (5 mL), at 0ºC. The reaction mixture was allowed to stir at 0°C for 60 min. Then it was quenched successively with $H_2O$ (2 mL) and 6 M NaOH (1.0 mL) and was allowed to warm to room temperature

while stirring. Anhydrous $Na_2SO_4$ was added, and the mixture was stirred for 30 min, then filtered over a pad of celite. The filtrate was washed with EtOAc (3x15 mL). The combined organic layers were concentrated under reduced pressure to afford the desired product.

**General Procedure 4: Corey–Chaykovsky epoxidation.** The procedure described by Sabbani *et al.*[94] was followed, with slight modifications. A suspension of potassium *tert*-butoxide (1.5 mmol) in anhydrous 1,2-dimethoxyethane or tetrahydrofuran (5 mL) was treated with trimethylsulfoxonium iodide (1.5 mmol), and the mixture was allowed to stir at reflux temperature, under nitrogen, for 2 h. The mixture was then cooled to room temperature and treated dropwise over 2 min with a solution (2 mL) of the corresponding ketone (1 mmol) and left stirring under reflux overnight, or until completion. The final mixture was cooled to room temperature and then quenched with water. The aqueous layer was extracted with dichloromethane (3 x 15 mL), the combined organic layers were dried over anhydrous $MgSO_4$, filtered and concentrated under reduced pressure. Purification by flash chromatography using a 0-5% EtOAc−hexane gradient (unless specified differently) gave the pure spiro-epoxide.

**General Procedure 5: Deprotection of the phthalimide group.** The procedure described by Lobo *et al.*[84] was followed, with slight modifications. A solution of trioxane-phthalimide (1 mmol) and hydrazine monohydrate (6 mmol) in chloroform:methanol (7:3, 6 mL) was heated at 60 ºC, overnight. The reaction mixture was then cooled down to room temperature and filtered to remove solid by-products, then washed with dichloromethane and the organic phase concentrated under reduced pressure. The crude was dissolved in methanol (1 mL), cooled down to 0 ºC, then a 2 M ethereal HCl solution (5 mL) was added dropwise. The solid obtained was filtered and washed with diethyl ether and hexane to give the desired trioxane hydrochloride salt.

**General Procedure 6: Synthesis of the 1,2,4-trioxane-carboxamide hybrids**. The procedure described by Stec *et al.*[3] was followed, with slight modifications. 4,6-Dichloro-1*H*-indole-2-carboxylic acid (**2.27**, 1 mmol) was dissolved in anhydrous dichloromethane (5 mL/mmol) at room temperature. To the solution was added hydroxybenzotriazole (HOBt, 1.5 mmol) and 1-ethyl-3-(3-(dimethylamino)propyl)-carbodiimide hydrochloride (EDC·HCl, 1.5 mmol), under a nitrogen atmosphere. After stirring for 1 h, the appropriate

trioxane-amine (1.1 mmol) and triethylamine (2 mmol) were added, and the resulting reaction mixture was allowed to stir at room temperature until disappearance of the starting material (followed by TLC, usually overnight). Water was added to the resulting solution and the final mixture was extracted with dichloromethane (3 × 15 mL) and EtOAc (3 x 15 mL). The organic layers were combined, washed with brine, dried over anhydrous $MgSO_4$, filtered, and concentrated under reduced pressure. The residue was purified by flash chromatography using a 0-40% EtOAc−hexane gradient (unless specified differently) to obtain the required peroxide hybrid.

**General Procedure 7: *N*-Boc removal;**

**(i)** ***2 M HCl in diethyl ether method.*** The procedure described by Sabbani *et al.*[94] was followed, with slight modifications. Anhydrous HCl–$Et_2O$ (2 M, 9 mL) was added to a solution of *N*-Boc-protected starting material (1 mmol) in anhydrous $Et_2O$ (1.8 mL) and the reaction mixture was allowed to stir at room temperature under a nitrogen atmosphere, until completion (usually 24-48 h). The white precipitate was filtrated and washed with anhydrous $Et_2O$ and hexane to give the desired hydrochloride salt.

***(ii) 4 M HCl in 1,4-dioxane method.*** The procedure described by Han *et al.*[95] was followed with slight modifications. The *N*-Boc-protected starting material (1 mmol) was added to a solution of 4 M HCl/dioxane (20 mL), under stirring over an ice-water bath, under an atmosphere of nitrogen. The reaction mixture was then allowed to warm to room temperature and left to stir until completion (usually 2-4 h). Diethyl ether (20 mL) was added, the white solid formed was filtered, then washed with $Et_2O$ and hexane to give the desired hydrochloride salt.

**General Procedure 8: Synthesis of the 1,2,4-trioxane-benzothiazinone hybrids.** The procedure was adapted from Makarov *et al*.[85] A suspension of 2-(methylthio)-8-nitro-6-(trifluoromethyl)-*4H*-benzo[*e*][1,3]thiazin-4-one (**2.43**, 1 mmol) and the respective 1,2,4-trioxane amine (1.5 mmol), in 15 mL of ethanol, was treated with 3 mmol of triethylamine, at room temperature. The reaction mixture was heated to 60°C until completion (usually for 30-60 minutes). The solvent was removed by evaporation under reduced pressure and the residue was dissolved in dichloromethane (20 mL) and washed with brine (2x20 mL). The organic layer was dried over anhydrous $MgSO_4$, filtered, and concentrated under reduced pressure. Purification by recrystallization with methanol or

through flash chromatography, using a EtOAc−hexane gradient (unless specified differently), yielded the peroxide hybrids.

**General Procedure 9: Ketal formation**. The procedure was adapted from Jin *et al.*[96] Microwaves were not used in this procedure. A simpler procedure was proposed for the ketal formation with SSA: the carbonyl compound (1.1 mmol) and corresponding alcohol (in excess, 5 mmol) were dissolved in anhydrous dichloromethane (5 mL), and SSA (2 mmol) was added. The mixture was left to stir at room temperature until completion (usually overnight). The resulting solution was filtered, rinsed with dichloromethane and concentrated under reduced pressure. Purification by flash chromatography using a mixture of EtOAc/Hexane gave the pure compound.

**General Procedure 10: Oxidation to aldehyde.** The procedure from Opsenica *et al.*[97] was followed, with slight modifications. Pyridinium chlorochromate (PCC, 2.5 mmol) was added to a solution of alcohol (1 mmol) in anhydrous $CH_2Cl_2$ (5 mL), and the resulting suspension was allowed to stir overnight at room temperature. The crude product was filtered through a plug of silica using a mixture of 3/7 EtOAc/hexane as eluent. Such obtained aldehyde was used immediately thereafter, without further purification.

**General Procedure 11: Reductive amination with Boc-piperazine**

The procedure by Lobo *et al.*[84] was followed, with slight modifications. The corresponding crude aldehyde (1 mmol) and amine Boc-piperazine (1.5 mmol) were dissolved in dichloroethane (DCE, 10 mL) and glacial acetic acid (1.1 mmol) was added. The mixture was allowed to stir at room temperature for 30 minutes, followed by addition of sodium triacetoxyborohydride (2.5 mmol), then left to stir for 16 hours. The reaction mixture was washed with aqueous NaOH (5 M; 2 x 10 mL) and dichloromethane (2 x 20 mL). The combined organic layers were dried over $MgSO_4$, filtered, and the solvent removed under reduced pressure. The residue was purified by flash chromatography using a 0−40% EtOAc−hexane gradient (unless specified differently) to obtain desired product.

## 2.5.3. Synthesis

### Preparation of (E)-ethyl 2-(2-(3,5-dichlorophenyl)-hydrazono)propanoate (2.25)

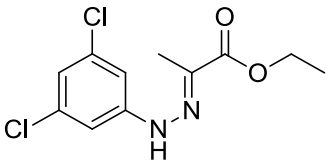

The procedure described by Jiricek *et al.*[83] was followed. 3,5-Dichlorophenylhydrazine hydrochloride **2.24** (2.50 g, 11.71 mmmol) and ethyl pyruvate (1.30 mL, 11.71 mmol) was dissolved in ethanol (15 mL). Concentrated Sulfuric acid (2 mL) was added slowly to the reaction mixture, at 0 ºC. The mixture was then warmed to room temperature and allowed to stir for 2 hours. The solvent was removed under reduced pressure, the residue dissolved in ethyl acetate (EtOAc) (50 mL) and allowed to stir with 1 M NaOH solution. The organic phase was then washed with brine (2×50 mL) and dried over with $MgSO_4$. Purification through flash chromatography (EtOAc: hexane, 20:80, *v/v*) yielded the desired product (2.2 g, 68%) as a white powder (m.p.=137-139 ºC). $^1$H NMR (400 MHz, $CDCl_3$): δ 7.66 (s, 1H), 7.11 (d, *J* = 1.8 Hz, 2H), 6.94 (s, 1H), 4.33 (q, *J* = 7.1 Hz, 2H), 2.11 (s, 3H), 1.39 (t, *J* = 7.1 Hz, 3H). $^{13}$C{$^1$H} NMR (101 MHz, $CDCl_3$): δ 164.77, 145.03, 135.73, 135.08, 121.75, 112.54, 61.59, 14.30, 10.55. HRMS (ESI, *m/z*) calcd for $C_{11}H_{12}Cl_2N_2O_2Na$ $[M+Na]^+$: 297.0168; found 297.0173. Diff: -1.84 ppm.

### Preparation of ethyl 4,6-dichloro-*1H*-indole-2-carboxylate (2.26)

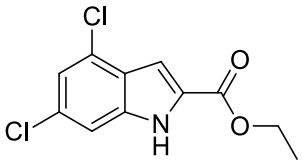

This compound was synthesised following the procedure by Jiricek *et al.*[83] (*E*)-ethyl 2-(2-(3,5-dichloro-phenyl)hydrazono)propanoate **2.25** (1 g, 3.63 mmol) was dissolved in toluene (20 mL) and added Eaton's reagent (5 mL). The reaction mixture was then allowed to stir under reflux for 2 hours. The solution was left to cool down and it was added EtOAc and 1 M NaOH solution until a pH of 11 was reached. Aqueous phase was then washed 3 times with EtOAc. The combined organic layers were washed with brine

and dried over with anhydrous $MgSO_4$. Filtered and concentrated under reduced pressure. Recrystalization with hexane and EtOAc, gave the desired product **2.26** (0.61 g, 64%) as a white solid (m.p. 184-185 ºC). $^1$H NMR (400 MHz, $CDCl_3$): δ 9.31 (s, 1H), 7.34 (s, 1H), 7.28 (d, *J* = 1.8 Hz, 1H), 7.17 (d, *J* = 1.6 Hz, 1H), 4.45 (q, *J* = 7.1 Hz, 2H), 1.44 (t, *J* = 7.1 Hz, 3H). $^{13}$C{$^1$H} NMR (101 MHz, $CDCl_3$): δ 161.62, 137.07, 131.07, 128.53, 128.43, 125.37, 121.33, 110.53, 107.10, 61.56, 14.35. HRMS (CI, *m/z*) calcd for $C_{11}H_{10}Cl_2NO_2$ $[M+H]^+$: 258.0083; found 258.0085. Diff: -0.80 ppm.

## Preparation of 4,6-dichloro-*1H*-indole-2-carboxylic acid (2.27)

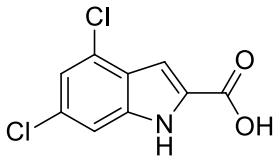


Procedure adapted from Jiricek *et al.*[83] LiOH (0.139 g, 5.81 mmol) was added to a solution of ethyl 4,6-dichloro-*1H*-indole-2-carboxylate **2.26** (0.50 g, 1.94 mmol) in THF:$H_2O$ (1:1) (20 mL). The reaction mixture was allowed to stir until completion (followed by TLC), at room temperature. THF was removed under reduced pressure, the remaining mixture was diluted with water and acidified with 1 M HCl. The aqueous layer was extracted with EtOAc (3 x 30 mL) and the extracts washed with brine (2 x 30 mL) and dried over with anhydrous $MgSO_4$. The organic phase then was filtered and concentrated under reduced pressure. The solid obtained was crushed with cold hexane and dichloromethane ($CH_2Cl_2$), filtered and washed with both solvents, giving the desired product **2.27** (0.37 g, 83%) as a light brown solid (m.p. 234-236 ºC). $^1$H NMR (400 MHz, DMSO-$d_6$): δ 12.30 (s, 1H), 7.44 (m, 1H), 7.27 (d, *J* = 1.7 Hz, 1H), 7.07 (d, *J* = 2.1 Hz, 1H). $^{13}$C{$^1$H} NMR (101 MHz, DMSO-$d_6$): δ 162.51, 137.93, 130.88, 129.19, 127.23, 124.97, 120.29, 111.76, 105.40. HRMS (ESI, *m/z*) calcd for $C_9H_4Cl_2NO_2$ $[M-H]^-$: 227.9625; found 227.9626. Diff: -0.78 ppm.

## Preparation of cyclohex-1-enyl-methanol (2.30)

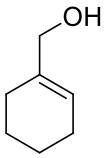


Compound **2.30** was synthesized in accordance with **general procedure 3**, from cyclohexene-1-carboxylic acid **2.28**. Obtained as a colourless oil (92% yield). $^{1}$H NMR (400 MHz, $CDCl_3$): δ 5.71 – 5.65 (m, 1H), 3.97 (s, 2H), 2.07 – 1.97 (m, 4H), 1.80 – 1.53 (m, 5H). $^{13}C\{^{1}H\}$ NMR (101 MHz, $CDCl_3$): δ 137.55, 123.08, 67.74, 25.62, 24.92, 22.54, 22.44. HRMS (CI, *m/z*) calcd for $C_7H_{12}O$ $[M+NH_4]^+$: 112.1121; found 112.1124. Diff: -2.88 ppm.

## Preparation of 1-oxaspiro[2.5]octane

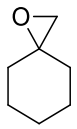


This compound was synthesised following the **general procedure 4**, from cyclohexanone and 1,2-dimethoxyethane as the solvent. Purification through flash chromatography (EtOAc: hexane, 1:99, *v/v*) yielded 1-oxaspiro[2.5]octane as a colourless oil (37% yield). $^{1}$H NMR (400 MHz, $CDCl_3$): δ 2.59 (s, 2H), 1.79 – 1.70 (m, 2H), 1.64 – 1.46 (m, 8H). $^{13}C\{^{1}H\}$ NMR (101 MHz, $CDCl_3$): δ 59.03, 54.51, 33.67, 25.27, 24.91. HRMS (CI, *m/z*) calcd for $C_7H_{16}NO$ $[M+NH_4]^+$: 112.1121; found 112.1121. Diff: -0.61 ppm.

## Preparation of 2-(3,3-dimethyl-1,2,5-trioxa-9-spiro[5.5]undecyl)-1,3-isoindolinedione (2.31)

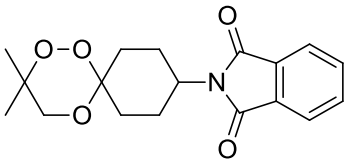


Compound **2.31** was synthesised following the **general procedure 1**, from 2-methylprop-2-en-1-ol (**2.29**) and 2-(4-oxocyclohexyl)isoindoline-1,3-dione. Purification through

flash chromatography (EtOAc: hexane, 5:95, *v/v*) yielded **2.31** as a white solid (56% yield). $^{1}$H NMR (400 MHz, $CDCl_3$): δ 7.82 (m, 2H), 7.70 (td, *J* = 5.4, 3.0 Hz, 2H), 4.20 (tt, *J* = 12.4, 4.0 Hz, 1H), 3.93 – 3.39 (m, 2H), 3.18 – 2.37 (m, 3H), 1.84 – 1.03 (m, 11H). $^{13}$C{$^{1}$H} NMR (101 MHz, $CDCl_3$): δ 168.22, 168.10, 133.88, 133.80, 132.00, 131.98, 123.11, 100.67, 100.56, 76.92, 67.03, 66.57, 49.92, 49.89, 33.27, 27.43, 25.54, 25.14, 22.33. Duplicate peaks on $^{13}$C{$^{1}$H} NMR were observed and are due to the mixture of isomers *cis* or *trans.* HRMS (ESI, *m/z*) calcd for $C_{18}H_{21}NO_5Na$ $[M+Na]^+$: 354.1312; found 354.1319. Diff: -1.39 ppm. Anal. Calcd for $C_{18}H_{21}NO_5$: C, 65.24; H, 6.39; N, 4.23, found: C, 65.14; H, 6.37; N, 4.22.

## Preparation of 2-(7,8,15-trioxa-12-dispiro[5.2.5.2]hexadecyl)-1,3-isoindolinedione (2.32)

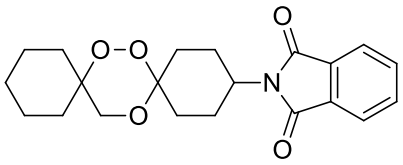

Compound **2.32** was synthesised following the **general procedure 1**, from **2.30** and 2-(4-oxocyclohexyl)isoindoline-1,3-dione, or following the **general procedure 2** (SSA Method), from 1-oxaspiro[2.5]octane and 2-(4-oxocyclohexyl)isoindoline-1,3-dione. Purification through flash chromatography (EtOAc: hexane, 5:95, *v/v*) followed by recrystallization with acetone yielded **2.32** as a white solid (24% yield). $^{1}$H NMR (400 MHz, $CDCl_3$): δ 7.85 – 7.78 (m, 2H), 7.74 – 7.66 (m, 2H), 4.19 (ddt, *J* = 12.2, 7.8, 4.0 Hz, 1H), 3.64 (s, 2H), 3.09 – 2.31 (m, 3H), 2.00 – 1.64 (m, 4H), 1.63 – 1.27 (m, 11H). $^{13}$C{$^{1}$H} NMR (101 MHz, $CDCl_3$): δ 168.23, 168.13, 133.87, 133.80, 132.02, 132.00, 123.12, 100.88, 77.86, 77.65, 66.43, 66.01, 50.04, 49.91, 31.07, 30.14, 25.93, 25.17, 21.31. Duplicate peaks on $^{13}$C{$^{1}$H} NMR were observed and are due to the mixture of isomers *cis* or *trans.* HRMS (ESI, *m/z*) calcd $C_{21}H_{25}NO_5Na$ $[M+Na]^+$: 394.1625; found 394.1626. Diff: -0.24 ppm. Anal Calcd for $C_{21}H_{25}NO_5$: C, 67.91; H, 6.78; N, 3.77, found: C, 67.51; H, 7.03; N, 3.58.

## Preparation of 3,3-dimethyl-1,2,5-trioxa-9-spiro[5.5]undecylamine hydrochloride (2.33)

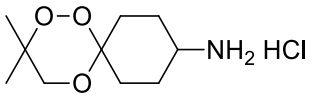


Compound **2.33** was synthesised following the **general procedure 5**, from 2-(3,3-dimethyl-1,2,5-trioxa-9-spiro[5.5]undecyl)-1,3-isoindolinedione **2.31**. Obtained as a colourless solid (81% yield). $^{1}$H NMR (400 MHz, $CD_3OD$): δ 3.96 – 3.43 (m, 2H), 3.27 – 2.80 (m, 2H), 2.00 – 0.93 (m, 13H). $^{13}C\{^{1}H\}$ NMR (101 MHz, DMSO-*d*$_6$): δ 100.58, 100.45, 77.23, 77.20, 66.21, 65.88, 48.47, 48.41, 31.49, 26.47, 26.22, 22.27. Duplicate peaks on $^{13}C\{^{1}H\}$ NMR were observed and are due to the mixture of isomers *cis* or *trans.* HRMS (ESI, *m/z*) calcd $C_{10}H_{20}NO_3$ $[M+H]^+$: 202.1438; found 202.1442. Diff: -2.33 ppm.

## Preparation of 7,8,15-trioxa-12-dispiro[5.2.5.2]hexadecylamine hydrochloride (2.34)

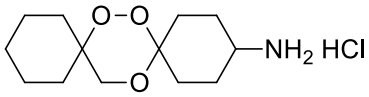


Compound **2.34** was synthesised following the **general procedure 5**, from 2-(7,8,15-trioxa-12-dispiro[5.2.5.2]hexadecyl)-1,3-isoindolinedione **2.32**. Obtained as a colourless solid (72% yield). $^{1}$H NMR (400 MHz, $CD_3OD$): δ 3.81 – 3.47 (m, 2H), 3.26 – 3.17 (m, 1H), 2.92 (br s, 1H), 2.40 (br s, 1H), 2.03 – 1.94 (m, 2H), 1.87 – 1.34 (m, 16H). $^{13}C\{^{1}H\}$ NMR (101 MHz, DMSO-*d*$_6$): δ 101.42, 77.53, 65.56, 65.18, 49.05, 32.29, 30.81, 28.40, 25.85, 21.28. Duplicate peaks on $^{13}C\{^{1}H\}$ NMR were observed and are due to the mixture of isomers *cis* or *trans.* HRMS (ESI, *m/z*) calcd $C_{13}H_{24}NO_3$ $[M+H]^+$: 242.1751; found 242.1758. Diff: -2.81 ppm.

## Preparation of spiro[adamantane-2,2'-oxirane] (2.36)

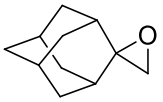


Compound **2.36** was synthesised following the **general procedure 4**, from adamantan-2-one **2.35** and 1,2-dimethoxyethane as the solvent. Purification through flash chromatography (EtOAc: hexane, 1:99, *v/v*) yielded a colourless solid (83% yield). $^{1}$H NMR (400 MHz, $CDCl_3$): δ 2.64 (s, 2H), 2.05 – 1.75 (m, 12H), 1.40 (t, *J* = 3.1 Hz, 2H). $^{13}C\{^{1}H\}$ NMR (101 MHz, $CDCl_3$): δ 64.60, 54.82, 37.07, 36.85, 35.89, 35.06, 27.12, 26.98. HRMS (CI, *m/z*) calcd for $C_{11}H_{17}O$ $[M+H]^+$: 165.1274; found 165.1275. Diff: -0.36 ppm.

## Preparation of 2-(dispiro[cyclohexane-1,3'-[1,2,4]trioxane-6',2''-tricyclo[3.3.1.1$^{3,7}$]decan]-4-yl)-1,3-isoindolinedione (2.37)

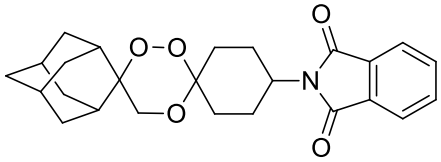


Compound **2.37** was synthesized following the **general procedure 2** (SSA Method), from **2.36** and 2-(4-oxocyclohexyl)isoindoline-1,3-dione. Purification through flash chromatography (EtOAc: hexane, 5:95, *v/v*) followed by recrystallization with acetone yielded a colourless solid (47% yield). $^{1}$H NMR (400 MHz, $CDCl_3$): δ 7.83 (dd, *J* = 5.5, 3.0 Hz, 2H), 7.70 (dd, *J* = 5.5, 3.0 Hz, 2H), 4.20 (tt, *J* = 12.4, 4.0 Hz, 1H), 3.70 (br s, 1H), 3.03 (br s, 1H), 2.77 – 2.00 (m, 5H), 1.94 – 1.38 (m, 17H). $^{13}C\{^{1}H\}$ NMR (101 MHz, $CDCl_3$): δ 168.23, 133.86, 132.00, 123.12, 100.69, 81.44, 63.80, 49.93, 37.76, 33.73, 31.97, 27.52, 27.43, 24.74. HRMS (ESI, *m/z*) calcd $C_{25}H_{29}NO_5Na$ $[M+Na]^+$: 446.1938; found 446.1925. Diff: -2.79 ppm.

## Preparation of dispiro[cyclohexane-1,3'-[1,2,4]trioxane-6',2''-tricyclo[3.3.1.1$^{3,7}$]decan]-4-ylamine hydrochloride (2.38)

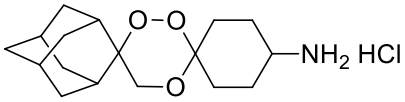


Compound **2.38** was synthesised following the **general procedure 5**, from 2-(dispiro[cyclohexane-1,3'-[1,2,4]trioxane-6',2''-tricyclo[3.3.1.1$^{3,7}$]decan]-4-yl)-1,3-isoindolinedione **2.37**. Obtained as a colourless solid (65% yield). $^{1}$H NMR (400 MHz, $CDCl_3$): δ 4.00 (br s, 1H), 3.64 (br s, 1H), 2.94 – 2.39 (m, 3H), 2.07 (br s, 2H), 1.84 – 1.65 (m, 12H), 1.55 – 1.19 (m, 8H). $^{13}$C{$^{1}$H} NMR (101 MHz, $CDCl_3$): δ 101.33, 101.18, 81.26, 81.23, 64.06, 63.66, 49.65, 49.37, 37.76, 34.03, 31.96, 31.27, 27.51, 27.41. Duplicate peaks on $^{13}$C{$^{1}$H} NMR were observed and are due to the mixture of isomers *cis* or *trans*. HRMS (ESI, *m/z*) calcd $C_{17}H_{28}NO_3$ $[M+H]^+$: 294.2064; found 294.2061. Diff: 0.89 ppm.

## Preparation of (4,6-dichloro-*1H*-indol-2-yl)(3,3-dimethyl-1,2,5-trioxa-9-spiro[5.5]undecylamino)-formaldehyde (TIC01)

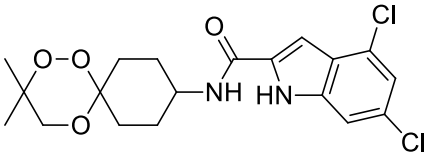


**TIC01** was synthesised following the **general procedure 6**, from 3,3-dimethyl-1,2,5-trioxa-9-spiro[5.5]undecylamine hydrochloride **2.33**. Purification by flash chromatography (EtOAc: hexane, 15:85, *v/v*) yielded two colourless solids:

**- Isomer 1 (*cis* or *trans*):** 17% yield. M.p = 212-214 ºC. $^{1}$H NMR (400 MHz, DMSO-$d_6$): δ 12.05 (s, 1H), 8.50 (d, *J* = 7.9 Hz, 1H), 7.42 (dd, *J* = 1.7, 0.9 Hz, 1H), 7.35 (s, 1H), 7.22 (d, *J* = 1.7 Hz, 1H), 3.93 (br s, 1H), 3.71 (br s, 1H), 2.72 (br d, *J* = 26.7 Hz, 1H), 1.76 – 0.86 (m, 14H). $^{13}$C{$^{1}$H} NMR (101 MHz, DMSO-$d_6$): δ 159.96, 137.21, 133.98, 128.06, 126.77, 125.29, 119.83, 111.55, 101.29, 101.09, 77.10, 65.90, 47.40, 32.22, 27.87, 22.20. HRMS (ESI, *m/z*) calcd $C_{19}H_{22}Cl_2N_2O_4Na$ $[M+Na]^+$: 435.0849; found 435.0849. Diff: -1.79 ppm. Purity HPLC (Method A): 90.63%, *Rt* = 11.64 min.

**- Isomer 2 (*cis* or *trans*):** 35% yield. M.p = 200-202 ºC. $^{1}$H NMR (400 MHz, DMSO-

$d_6$): δ 12.05 (s, 1H), 8.49 (d, *J* = 7.9 Hz, 1H), 7.42 (t, *J* = 1.2 Hz, 1H), 7.34 (s, 1H), 7.22 (d, *J* = 1.7 Hz, 1H), 3.94 (br s, 1H), 3.77 (br s, 1H), 2.90 – 2.69 (m, 1H), 1.82 – 1.05 (m, 14H). $^{13}C\{^1H\}$ NMR (101 MHz, DMSO-$d_6$): δ 159.96, 137.24, 134.03, 128.03, 126.76, 125.29, 119.81, 111.56, 101.28, 100.95, 77.14, 66.24, 47.39, 28.18, 22.46, 18.95. HRMS (ESI, *m/z*): calcd $C_{19}H_{22}Cl_2N_2O_4Na$ $[M+Na]^+$: 435.0849; found 435.0849. Diff: 0.03 ppm. Purity HPLC (Method C): 92.51%, *Rt* = 11.66 min.

## Preparation of (4,6-dichloro-1H-indol-2-yl)(7,8,15-trioxa-12-dispiro[5.2.5.2]hexadecylamino)formaldehyde (TIC02)

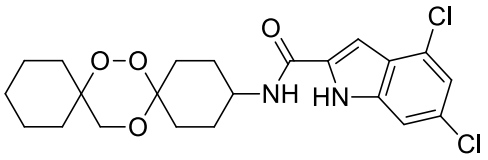


**TIC02** was synthesised following the general **procedure 6**, from 7,8,15-trioxa-12-dispiro[5.2.5.2]hexadecylamine hydrochloride **2.34**. Purification by flash chromatography (EtOAc: hexane, 15:85, *v/v*) yielded two colourless solids:

**- Isomer 1 (*cis* or *trans*):** 21% yield. M.p = 195-197 ºC. $^1H$ NMR (400 MHz, $CDCl_3$): δ 10.22 (s, 1H), 7.38 (s, 1H), 7.16 (d, *J* = 1.6 Hz, 1H), 6.87 (d, *J* = 2.2 Hz, 1H), 6.13 (d, *J* = 8.1 Hz, 1H), 4.20 – 4.07 (m, 1H), 3.76 (br s, 1H), 3.55 (br s, 1H), 2.95 (br s, 1H), 2.40 (br s, 1H), 2.12 – 1.66 (m, 5H), 1.62 – 1.16 (m, 11H). $^{13}C\{^1H\}$ NMR (101 MHz, DMSO-$d_6$): δ 159.97, 137.20, 133.98, 128.06, 126.77, 125.29, 119.83, 111.55, 101.29, 100.14, 77.61, 65.26, 47.41, 37.19, 35.06, 27.89, 25.85, 21.44. HRMS (ESI, *m/z*) calcd $C_{22}H_{26}Cl_2N_2O_4Na$ $[M+Na]^+$: 475.1162; found 475.1159. Diff: 1.21 ppm. Purity HPLC (Method C): 90.44%, *Rt* = 12.77 min.

**- Isomer 2 (*cis* or *trans*):** 38% yield. M.p = 192-194 ºC. $^1H$ NMR (400 MHz, $CDCl_3$): δ 10.24 (s, 1H), 7.38 (s, 1H), 7.16 (d, *J* = 1.6 Hz, 1H), 6.87 (d, *J* = 2.2 Hz, 1H), 6.13 (d, *J* = 8.1 Hz, 1H), 4.20 – 4.07 (m, 1H), 3.76 (br s, 1H), 3.55 (br s, 1H), 2.95 (br s, 1H), 2.40 (br s, 1H), 2.12 – 1.66 (m, 5H), 1.62 – 1.16 (m, 11H). $^{13}C\{^1H\}$ NMR (101 MHz, $CDCl_3$): δ 160.47, 136.78, 131.69, 130.10, 127.59, 125.42, 121.03, 110.79, 100.89, 100.43, 77.92, 77.34, 77.22, 66.39, 48.06, 28.54, 25.88, 20.96. HRMS (ESI, *m/z*) calcd $C_{22}H_{26}Cl_2N_2O_4Na$ $[M+Na]^+$: 475.1162; found 475.1158. Diff: 0.91 ppm. Purity HPLC (Method C): 92.48%, *Rt* = 12.82 min.

## Preparation of (4,6-dichloro-*1H*-indol-2-yl)(dispiro[cyclohexane-1,3'-[1,2,4]trioxane-6',2''-tricyclo [3.3.1.1$^{3,7}$]decan]-4-ylamino)-formaldehyde (TIC03)

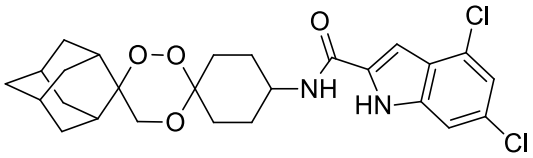


**TIC03** was synthesised following the general **procedure 6**, from dispiro[cyclohexane-1,3'-[1,2,4]trioxane-6',2''-tricyclo[3.3.1.1$^{3,7}$]decan]-4-ylamine hydrochloride **2.38**. Purification by flash chromatography (EtOAc: hexane, 15:85, *v/v*) yielded two colourless solids:

**- Isomer 1 (*cis* or *trans*):** 18% yield. M.p = 200-203 ºC. $^{1}$H NMR (400 MHz, $CDCl_3$): δ 10.19 (s, 1H), 7.38 (d, *J* = 1.6 Hz, 1H), 7.16 (d, *J* = 1.6 Hz, 1H), 6.90 (dd, *J* = 2.3, 0.9 Hz, 1H), 6.17 (d, *J* = 8.0 Hz, 1H), 4.20 – 3.98 (m, 2H), 3.68 (br s, 1H), 2.75 (br s, 1H), 2.23 – 1.68 (m, 18H), 1.61 – 1.42 (m, 3H). $^{13}$C{$^{1}$H} NMR (101 MHz $CDCl_3$): δ 160.45, 136.76, 131.72, 130.15, 127.53, 125.40, 121.05, 110.81, 100.75, 100.41, 81.40, 63.80, 47.87, 37.72, 34.16, 31.95, 28.20, 27.50, 27.39. HRMS (ESI, *m/z*) calcd $C_{26}H_{30}Cl_2N_2O_4Na$ $[M+Na]^+$: 527.1475; found 527.1473. Diff: 0.40 ppm. Purity HPLC (Method A): 95.99%, *Rt* = 13.96 min.

**- Isomer 2 (*cis* or *trans*):** 37% yield. M.p = 215-217 ºC. $^{1}$H NMR (400 MHz, DMSO-$d_6$): δ 12.05 (s, 1H), 8.47 (d, *J* = 8.1 Hz, 1H), 7.42 (s, 1H), 7.32 (s, 1H), 7.20 (s, 1H), 4.10 (br s, 1H), 3.94 (br s, 1H), 3.69 (br s, 2H), 2.93 – 2.59 (m, 2H), 2.00 – 1.50 (m, 19H). $^{13}$C{$^{1}$H} NMR (101 MHz, DMSO-$d_6$): δ 159.91, 137.23, 134.01, 128.04, 126.76, 125.28, 119.79, 111.54, 101.23, 101.00, 81.03, 63.48, 47.30, 37.68, 34.91, 33.62, 32.00, 29.16, 28.21, 27.37. HRMS (ESI, *m/z*) calcd $C_{26}H_{30}Cl_2N_2O_4Na$ $[M+Na]^+$: 527.1475; found 527.1473. Diff: 0.41 ppm. Purity HPLC (Method D): 99.87%, *Rt* = 11.99 min.

## Preparation of 2-chloro-3-nitro-5-(trifluoromethyl)benzoic acid (2.41)

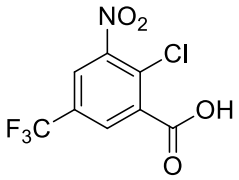


The procedure was adapted from Cooper *et al.*[98] 2-Chloro-5-trifluoromethylbenzoic acid **2.40** (5g, 22.27 mmol) was added to a solution of sulfuric acid (17.7 mL) and nitric acid (2.5 mL), under vigorous stirring. The mixture was warmed to 90 ºC, over 25 min, then a further 7.8 mL of sulfuric acid was added to the thick mixture and vigorous stirring was continued. After 45 min at 90 ºC the mixture was cooled to room temperature and poured over crushed ice, then rinsing forward with icy water. The product was isolated by vacuum filtration, washed with cold water and dried under reduced pressure to give the desired product **2.41** as a white solid (5.3 g, 88% yield). $^{1}$H NMR (400 MHz, $CD_3OD$): δ 8.42 (d, *J* = 2.2 Hz, 1H), 8.36 (d, *J* = 1.7 Hz, 1H). $^{13}C\{^{1}H\}$ NMR (101 MHz, $CD_3OD$): δ 164.46, 150.31, 135.20, 131.74, 130.27, 129.92, 129.82 (q, *J* = 3.6 Hz), 129.57, 129.22, 128.44, 126.44, 123.78 (q, *J* = 3.2, 2.7 Hz), 121.03, 118.32. HRMS (ESI, *m/z*) calcd for $C_8H_3ClF_3NO_4$ $[M-H]^-$: 267.9630; found 267.9629. Diff: 0.51 ppm.

## Preparation of 2-chloro-3-nitro-5-(trifluoromethyl)benzamide (2.42)

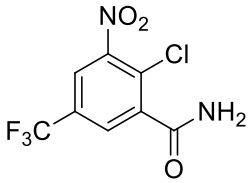


The procedure was adapted from Cooper *et al.*[98], with slight modifications. 2-chloro-3-nitro-5-(trifluoromethyl)benzoic acid **2.41** (5.00 g, 18.55 mmol) was dissolved in toluene (90 mL), $SOCl_2$ (4.00 mL, 55.60 mmol) was added and the reaction mixture was refluxed overnight. The solvent was then evaporated under reduced pressure and the corresponding benzoylchloride was dried under reduced pressure for several minutes. The crude was dissolved in 15 mL acetonitrile and 74 mL aq. $NH_4OH$ were added slowly, at -20 °C. After 10 min, 50 mL EtOAc were added. The aqueous layer was washed with EtOAc (3 x 30 mL) and with brine (30 mL). The organic layer was dried over anhydrous $MgSO_4$, filtered, and concentrated under reduced pressure, giving the final product **2.42** (4.65 g,

93%). $^{1}$H NMR (400 MHz, $CD_3OD$): δ 8.27 (dd, *J* = 2.1, 0.8 Hz, 1H), 7.97 (dd, *J* = 2.1, 0.8 Hz, 1H). $^{13}C\{^{1}H\}$ NMR (101 MHz, $CD_3OD$): δ 167.29, 149.39, 140.32, 130.03 (q, *J* = 34.9 Hz), 127.85 (q, *J* = 3.7 Hz), 126.65, 123.83, 122.67 (q, *J* = 3.8 Hz), 121.12, 118.42. HRMS (CI, *m/z*) calcd for $C_8H_5ClF_3N_2O_3$ $[M+H]^+$: 268.9935; found 268.9945. Diff: -3.45 ppm.

## Preparation of 2-(methylthio)-8-nitro-6-(trifluoromethyl)-*4H*-benzo[*e*][1,3]thiazin-4-one (BTZ) (2.43)

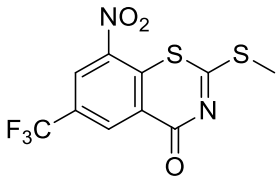


Procedure adapted from Makarov *et al*.[85], with slight modifications. To a solution of 2-chloro-3-nitro-5-(trifluoromethyl)benzamide **2.42** (4.00 g, 14.89 mmol) in anhydrous DMSO (60 mL) was added carbon disulfide (3.15 mL, 52.13 mmol), at 10 °C. Sodium hydroxide (1.34 g, 33.51 mmol), in powder, was added to the reaction mixture, and the final mixture was allowed to stand for 1 hour. Subsequently, iodomethane (3.25 mL, 52.13 mmol) was added. The reaction mixture was allowed to stand for another 2 hours, then 100 mL of ice water was added. The resulting yellow-orange solid was separated by filtration and washed with ice water. Recrystallization from methanol yielded the pure product **2.43** (2.01 g, 42% yield) as yellow crystals.

$^{1}$H NMR (400 MHz, DMSO-$d_6$): δ 8.96 (d, *J* = 2.2 Hz, 1H), 8.84 (d, *J* = 2.4 Hz, 1H), 2.77 (s, 3H). $^{13}C\{^{1}H\}$ NMR (101 MHz, DMSO-$d_6$): δ 181.74, 163.57, 143.77, 136.66, 133.02, 132.98, 129.15, 128.81, 127.22, 127.19, 126.37, 124.27, 121.56, 14.98. HRMS (CI, *m/z*) calcd for $C_{10}H_6F_3N_2O_3S_2$ $[M+H]^+$: 322.9766; found 322.9765. Diff: 0.35 ppm.

## Preparation of *tert*-butyl 3,3-dimethyl-1,2,5-trioxa-9-aza-9-spiro[5.5]undecanecarboxylate (2.45)

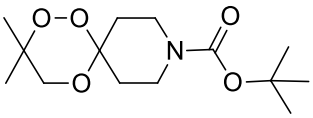

Compound **2.45** was synthesised following the **general procedure 1**, using **2.29** and boc-4-piperidone (**2.44**). Purification by flash chromatography (EtOAc: hexane, 5:95, *v/v*) yielded **2.45** as a colourless solid (58% yield). M.p = 69-70 ºC. $^{1}$H NMR (400 MHz, $CDCl_3$): δ 3.96 – 3.57 (m, 2H), 3.56 – 3.20 (m, 4H), 2.42 – 1.71 (m, 3H), 1.59 – 1.02 (m, 16H). $^{13}$C{$^{1}$H} NMR (101 MHz, $CDCl_3$): δ 154.6, 100.4, 80.0, 77.2, 66.6, 40.3, 34.4, 28.4, 22.6. HRMS (ESI, *m/z*) calcd $C_{14}H_{25}NO_5Na$ $[M+Na]^+$: 310.1625; found 310.1627. Diff: -0.75 ppm.

## Preparation of *tert*-butyl 7,8,16-trioxa-3-aza-3-dispiro[5.2.5.2]hexadecanecarboxylate (2.46)

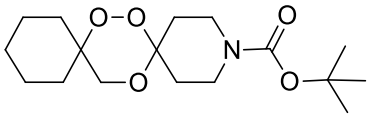

Compound **2.46** was synthesised following the **general procedure 1**, from **2.30** and 1-boc-4-piperidone (**2.44**), or following the **general procedure 2** (SSA Method), from 1-oxaspiro[2.5]octane and **2.44**. Purification by flash chromatography (EtOAc: hexane, 5:95, *v/v*) yielded **2.46** as a colourless solid (38% yield). $^{1}$H NMR (400 MHz, $CD_3CN$): δ 3.87−3.48 (m, 2H), 3.48−3.26 (m, 4H), 2.37 – 2.16 (m, 1H), 1.86 – 1.43 (m, 9H), 1.42 (s, 9H), 1.40 – 1.13 (m, 4H).$^{13}$C{$^{1}$H} NMR (101 MHz, $CD_3CN$): δ 154.89, 100.94, 79.57, 78.28, 66.04, 40.82, 34.52, 32.15, 30.47, 28.13, 26.14, 21.63. HRMS (ESI, *m/z*) calcd $C_{17}H_{29}NO_5Na$ $[M+Na]^+$:350.1938 found 350.1942. Diff: -1.17 ppm.

## Preparation of 3,3-dimethyl-1,2,5-trioxa-9-azaspiro[5.5]undecane hydrochloride (2.47)

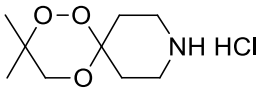


Compound **2.47** was synthesised following the **general procedure 7** (2 M HCl-$Et_2O$ method), from *tert*-butyl 3,3-dimethyl-1,2,5-trioxa-9-aza-9-spiro[5.5]undecanecarboxylate **2.45**. Yielded **2.47** as a colourless solid (36% yield). $^1$H NMR (400 MHz, DMSO-$d_6$): δ 3 3.72 (br s, 1H), 3.42 (br s, 1H), 2.84 – 2.62 (m, 3H), 2.49 – 0.89 (m, 11H). $^{13}$C{$^1$H} NMR (101 MHz, DMSO-$d_6$): δ 100.59, 77.07, 65.77, 42.71, 35.36, 29.77, 22.42. HRMS (ESI, *m/z*) calcd $C_9H_{18}NO_3$ $[M+H]^+$: 188.1281; found 188.1285. Diff: -2.27 ppm.

## Preparation of 7,8,16-trioxa-3-azadispiro[5.2.5.2]hexadecane hydrochloride (2.48)

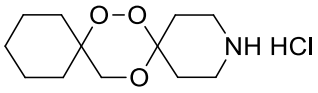


Compound **2.48** was synthesised following the **general procedure 7** (2 M HCl-$Et_2O$ method), from *tert*-butyl 7,8,16-trioxa-3-aza-3-dispiro[5.2.5.2]hexadecanecarboxylate **2.46**. Yielded **2.48** as a colourless solid (75% yield). $^1$H NMR (400 MHz, $CD_3OD$): δ 3.66 (br s, 1H), 3.53 (br s, 1H), 3.17 – 3.07 (m, 4H), 2.43 – 1.20 (m, 15H). $^{13}$C{$^1$H} NMR (101 MHz, $CD_3OD$): δ 97.57, 78.05, 65.85, 41.07, 30.88, 29.51, 25.45, 20.79. HRMS (ESI, *m/z*) calcd $C_{12}H_{22}NO_3$ $[M+H]^+$: 228.1594; found 228.1587. Diff: 3.33 ppm.

## Preparation of *tert*-butyl 1-oxa-6-azaspiro[2.5]octane-6-carboxylate (2.49)

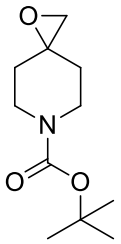

Compound **2.49** was synthesised following the **general procedure 4**, from 1-boc-4-piperidone (**2.44**) and 1,2-dimethoxyethane as the solvent. Purification by flash chromatography (EtOAc:hexane, 5:95, *v/v*) yielded **2.49** as a colourless solid (28% yield). $^{1}$H NMR (400 MHz, $CDCl_3$): δ 3.72 (s, 2H), 3.43 (ddd, *J* = 13.3, 9.4, 3.7 Hz, 2H), 2.69 (s, 2H), 1.80 (td, *J* = 9.4, 4.7 Hz, 2H), 1.48 (s, 9H), 1.44 (d, *J* = 4.9 Hz, 2H). $^{13}$C{$^{1}$H} NMR (101 MHz, $CDCl_3$): δ 154.77, 79.75, 57.17, 53.75, 42.55, 32.95, 28.43. HRMS (ESI, *m/z*) calcd for $C_{11}H_{19}NO_3Na$ $[M+Na]^+$: 236.1257; found 236.1256. Diff: 0.55 ppm.

## Preparation of *tert*-butyl dispiro[piperidine-4,3'-[1,2,4]trioxane-6',2''-tricyclo[3.3.1.1$^{3,7}$]decane]-1-carboxylate (2.50)

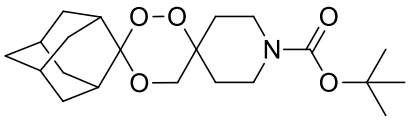

Compound **2.50** was synthesised following the **general procedure 2** ($MoO_2(acac)_2$ Method), from *tert*-butyl 1-oxa-6-azaspiro[2.5]octane-6-carboxylate **2.49** and adamantan-2-one **2.35**. Purification by flash chromatography (EtOAc:hexane, 4:96, *v/v*) yielded **2.50** as a colourless solid (63% yield). $^{1}$H NMR (400 MHz, $CDCl_3$): δ 3.75 (br s, 3H), 3.53−2.36 (m, 4H), 2.21−1.62 (m, 14H), 1.58−1.47 (m, 3H), 1.45 (s, 9H). $^{13}$C{$^{1}$H} NMR (101 MHz, $CDCl_3$): δ 154.76, 104.62, 79.57, 75.67, 65.27, 39.26, 37.14, 34.86, 33.35, 28.45, 27.13, 27.11, 27.04. HRMS (ESI, *m/z*) calcd $C_{21}H_{33}NO_5Na$ $[M+Na]^+$: 402.2251; found 402.2254. Diff: -0.64 ppm.

## Preparation of dispiro[piperidine-4,6'-[1,2,4]trioxane-3',2''-tricyclo[3.3.1.1$^{3,7}$]decane] hydrochloride (2.51)

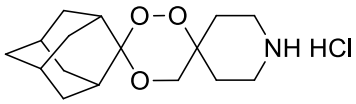


Compound **2.51** was synthesised following the **general procedure 7** (2M HCl-$Et_2O$ method), from *tert*-butyl dispiro[piperidine-4,3'-[1,2,4]trioxane-6',2''-tricyclo[3.3.1.1$^{3,7}$]decane]-1-carboxylate **2.50**. Yielded **2.51** as a colourless solid (72% yield). $^1$H NMR (400 MHz, $CD_3OD$): 3.88 (br s, 1H), 3.54 (br s, 1H), 3.33 – 2.81 (m, 6H), 2.23 – 1.54 (m, 17H). $^{13}C\{^1H\}$ NMR (101 MHz, $CD_3OD$): δ 104.67, 73.22, 64.15, 36.74, 34.49, 32.92, 32.05, 27.18, 27.17. HRMS (ESI, *m/z*) calcd $C_{16}H_{26}NO_3$ $[M+H]^+$: 280.1907; found 280.191. Diff: -0.84 ppm.

## Preparation of ethyl 3,3-dimethyl-1,2,5-trioxa-9-spiro[5.5]undecanecarboxylate (2.53)

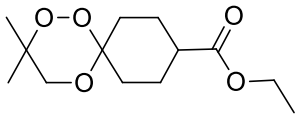


Compound **2.53** was synthesised following the **general procedure 1**, from **2.29** and ethyl 4-oxocyclohexanecarboxylate **2.52**. Purification by flash chromatography (EtOAc: hexane, 5:95, *v/v*) yielded **2.53** as a colourless solid (68% yield).

$^1$H NMR (400 MHz, $CDCl_3$): δ 4.12 (d, *J* = 7.1 Hz, 2H), 3.91 – 3.36 (m, 2H), 2.85 – 2.28 (m, 2H), 1.94 – 1.68 (m, 5H), 1.61 – 1.27 (m, 6H), 1.27 – 1.22 (m, 3H), 1.21 – 1.06 (m, 2H). $^{13}C\{^1H\}$ NMR (101 MHz, $CDCl_3$): δ 175.03, 174.94, 101.16, 101.06, 76.96, 76.92, 66.74, 66.49, 60.33, 60.31, 60.23, 42.12, 41.71, 35.24, 27.10, 26.38, 26.07, 24.76, 24.44, 22.00, 14.23, 14.20. Duplicate peaks on $^{13}C\{^1H\}$ NMR were observed and are due to the mixture of isomers *cis* or *trans*. HRMS (ESI, *m/z*) calcd $C_{13}H_{22}O_5Na$ $[M+Na]^+$: 281.1359; found 281.1361. Diff: -0.51 ppm.

## Preparation of (3,3-dimethyl-1,2,5-trioxa-9-spiro[5.5]undecyl)methanol (2.54)

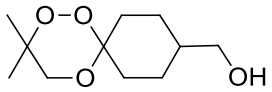


Compound **2.54** was synthesised following the **general procedure 3**, from ethyl 3,3-dimethyl-1,2,5-trioxa-9-spiro[5.5]undecanecarboxylate **2.53**. Yielded **2.54** as a colourless oil (93% yield). $^{1}$H NMR (400 MHz, $CDCl_3$): δ 3 3.95 – 3.37 (m, 4H), 3.32 – 2.48 (m, 1H), 1.96 – 1.66 (m, 3H), 1.63 – 1.08 (m, 12H). $^{13}C\{^{1}H\}$ NMR (101 MHz, $CDCl_3$): δ 102.01, 101.93, 76.91, 76.87, 67.71, 67.52, 66.72, 66.48, 39.58, 34.18, 27.12, 25.19, 22.71. Duplicate peaks on $^{13}C\{^{1}H\}$ NMR were observed and are due to the mixture of isomers *cis* or *trans*. HRMS (CI, *m/z*) calcd $C_{11}H_{21}O_4$ $[M+H]^+$: 217.1434, found 217.1439. Diff: -2.04 ppm.

## Preparation of (3,3-dimethyl-1,2,5-trioxaspiro[5.5]undecan-9-yl)methyl methanesulfonate (2.55)

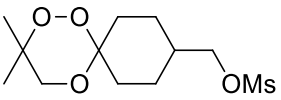


The procedure was adapted from Tang *et al.*[99] with slight modifications. To a solution of **2.54** (0.50 g, 2.31 mmol) and triethylamine (0.97 mL, 6.94 mmol) in $CH_2Cl_2$ (12 mL) at 0 ºC was added dropwise a solution of methanesulfonyl chloride (0.27 mL, 3.49 mmol) in $CH_2Cl_2$ (2.5 mL). The mixture was allowed to stir at rt, for 1 h, before being quenched with water (20 mL). After separation of the aqueous layer, the organic layer was washed with water (20 mL) and brine (20 mL), dried over $MgSO_4$, filtered, and concentrated to afford **2.55** (0.68 g, 76%), without further purification, as a colourless solid. $^{1}$H NMR (400 MHz, $CDCl_3$): δ 4.06 (dd, *J* = 11.4, 6.4 Hz, 2H), 4.01 – 3.13 (m, 2H), 3.01 (d, *J* = 4.4 Hz, 3H), 2.96 – 2.16 (m, 1H), 1.93 – 1.67 (m, 4H), 1.65 – 0.95 (m, 10H). $^{13}C\{^{1}H\}$ NMR (101 MHz, $CDCl_3$): δ 101.42, 76.97, 73.73, 73.55, 66.75, 66.51, 37.29, 37.27, 36.65, 36.57, 26.79, 24.90, 24.89, 24.52, 22.40. Duplicate peaks on $^{13}C\{^{1}H\}$ NMR were observed and are due to the mixture of isomers *cis* or *trans*. HRMS (ESI, *m/z*) calcd for $C_{12}H_{22}O_6SNa$ $[M+Na]^+$: 317.1029; found 317.1030. Diff: -0.31 ppm.

## Preparation of *tert*-butyl 4-{(3,3-dimethyl-1,2,5-trioxa-9-spiro[5.5]undecyl)methyl}-1-piperazine-carboxylate (2.57)

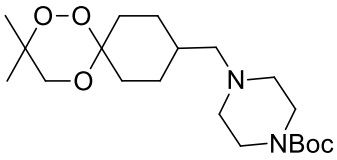


Compound **2.57** was synthesised following the **general procedures 10** and **11**, from (3,3-dimethyl-1,2,5-trioxa-9-spiro[5.5]undecyl)methanol **2.54** and 1-boc-piperazine **2.56**. Purification by flash chromatography (EtOAc: hexane, 25:75, *v/v*) yielded **2.57** as a colourless solid (35% yield).$^{1}$H NMR (400 MHz, $CDCl_3$): δ 3.96 – 3.14 (m, 6H), 2.91 – 2.19 (m, 5H), 2.18 – 2.12 (dd, *J* = 9.6, 7.1 Hz, 2H), 1.80 – 1.47 (m, 7H), 1.46 – 1.44 (s, 9H), 1.42 – 1.01 (m, 7H). $^{13}$C{$^{1}$H} NMR (101 MHz, $CDCl_3$): δ 154.82, 102.18, 102.08, 79.51, 79.49, 76.86, 76.84, 66.73, 66.47, 64.50, 64.27, 53.49, 47.22, 41.84, 34.29, 34.11, 28.44, 27.19, 26.78, 22.23. Duplicate peaks on $^{13}$C{$^{1}$H} NMR were observed and are due to the mixture of isomers *cis* or *trans*. HRMS (ESI, *m/z*) calcd for $C_{20}H_{37}N_2O_5$ $[M+H]^+$: 385.2697; found 385.2703. Diff: -1.66 ppm.

## Preparation of 3,3-dimethyl-9-[(1-piperazinyl)methyl]-1,2,5-trioxaspiro[5.5]undecane dihydrochloride (2.59)

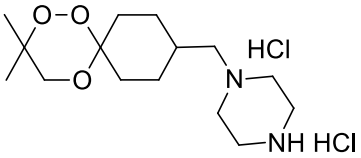


Compound **2.59** was synthesised following the **general procedure 7** (4M in 1,4-dioxane method), from *tert*-butyl 4-{(3,3-dimethyl-1,2,5-trioxa-9-spiro[5.5]undecyl)-methyl}-1-piperazine-carboxylate **2.57**. Yielded **2.59** as a colourless solid (88% yield). $^{1}$H NMR (400 MHz, $CD_3OD$): 4.19 – 3.33 (m, 11H), 3.29 – 3.15 (dd, *J* = 7.0, 3.2 Hz, 2H), 2.95 (br s, 1H), 2.26 – 0.89 (m, 14H). $^{13}$C{$^{1}$H} NMR (101 MHz, $CD_3OD$): δ 100.77, 100.66, 76.68, 76.66, 66.15, 65.94, 62.18, 62.08, 48.75, 48.73, 40.29, 31.55, 31.50, 30.90, 26.62, 26.24, 25.85, 19.47. Duplicate peaks on $^{13}$C{$^{1}$H} NMR were observed and are due to the mixture of isomers *cis* or *trans*. HRMS (ESI, *m/z*) calcd for $C_{15}H_{29}N_2O_3$ $[M+H]^+$: 285.2173; found 285.2177. Diff: -1.59 ppm.

## Preparation of ethyl 7,8,15-trioxa-12-dispiro[5.2.5.2]hexadecanecarboxylate (2.60)

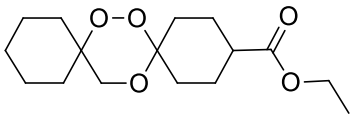

Compound **2.60** was synthesised following the **general procedure 1**, from **2.30** and **2.52**, or following the **general procedure 2** (SSA Method), from 1-oxaspiro[2.5]octane and **2.52**. Purification by chromatography (EtOAc: hexane, 5:95, *v/v*) yielded a white solid (40% yield). $^{1}$H NMR (400 MHz, $CDCl_3$): δ 4.12 (qd, *J* = 7.1, 5.4 Hz, 2H), 3.84 – 3.34 (m, 2H), 2.86 – 2.30 (m, 2H), 1.93 – 1.27 (m, 17H), 1.24 (td, *J* = 7.1, 5.6 Hz, 3H). $^{13}$C{$^{1}$H} NMR (101 MHz, $CDCl_3$): δ 175.04, 174.94, 101.35, 101.25, 77.72, 77.68, 66.20, 65.91, 60.32, 60.29, 42.18, 41.70, 32.92, 29.93, 25.91, 25.89, 24.77, 24.44, 21.28, 14.22. Duplicate peaks on $^{13}$C{$^{1}$H} NMR were observed and are due to the mixture of isomers *cis* or *trans.* HRMS (ESI, *m/z*) calcd for $C_{16}H_{26}O_5Na$ $[M+Na]^+$: 321.1672; found 321.1676. Diff: -1.09 ppm.

## Preparation of (7,8,15-trioxa-12-dispiro[5.2.5.2]hexadecyl)methanol (2.61)

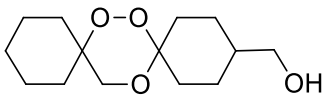

Compound **2.61** was synthesised following the **general procedure 3**, from ethyl 7,8,15-trioxa-12-dispiro[5.2.5.2]hexadecanecarboxylate **2.60**. Yielded **2.61** as a colourless solid (91% yield). $^{1}$H NMR (400 MHz, $CDCl_3$): δ 3.97 – 3.51 (m, 2H), 3.51 – 3.38 (m, 2H), 3.01 – 2.00 (m, 2H), 2.00 – 1.05 (m, 17H). $^{13}$C{$^{1}$H} NMR (101 MHz, $CDCl_3$): δ 102.20, 102.12, 77.66, 77.64, 67.74, 67.54, 66.22, 65.89, 39.63, 39.58, 34.32, 32.06, 30.04, 27.53, 25.93, 25.90, 25.21, 24.84, 21.29. Duplicate peaks on $^{13}$C{$^{1}$H} NMR were observed and are due to the mixture of isomers *cis* or *trans.* HRMS (CI, *m/z*) calcd $C_{14}H_{25}O_4$ $[M+H]^+$: 257.1747, found 257.1735. Diff: 4.94 ppm.

## Preparation of *tert*-butyl 4-{(7,8,15-trioxa-12-dispiro[5.2.5.2]hexadecyl)ethyl}-1-piperazinecarboxylate (2.62)

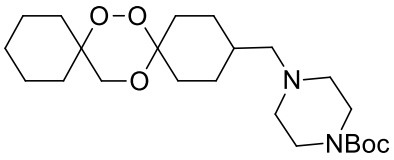


Compound **2.62** was synthesised following the **general procedures 10** and **11**, from (3,3-dimethyl-1,2,5-trioxa-9-spiro[5.5]undecyl)methanol **2.61** and 1-boc-piperazine **2.56**. Purification by flash chromatography (EtOAc: hexane, 25:75, *v/v*) yielded **2.62** as a colourless solid (44% yield). $^{1}$H NMR (400 MHz, $CDCl_3$): δ 3.92 – 3.25 (m, 6H), 2.96 – 2.19 (m, 5H), 2.15 (t, *J* = 7.6 Hz, 2H), 1.76 – 1.46 (m, 11H), 1.45 (s, 9H), 1.44 – 1.14 (m, 7H). $^{13}$C{$^{1}$H} NMR (101 MHz, $CDCl_3$): δ 154.82, 102.39, 102.28, 79.50, 79.48, 77.61, 66.21, 65.90, 64.52, 64.27, 53.49, 43.92, 36.89, 34.31, 34.11, 32.18, 29.78, 28.44, 27.19, 26.79, 25.94, 25.91, 21.25. Duplicate peaks on $^{13}$C{$^{1}$H} NMR were observed and are due to the mixture of isomers *cis* or *trans.* HRMS (ESI, *m/z*) calcd for $C_{23}H_{41}N_2O_5$ $[M+H]^+$: 425.3010; found 425.3015. Diff: -1.14 ppm.

## Preparation of 12-[(1-piperazinyl)methyl]-7,8,15-trioxadispiro[5.2.5.2]hexadecane dihydrochloride (2.63)

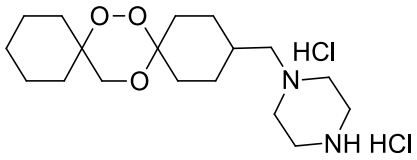


Compound **2.63** was synthesised following the **general procedure 7** (4 M in 1,4-dioxane method), from *tert*-butyl 4-{(7,8,15-trioxa-12-dispiro[5.2.5.2]hexadecyl) ethyl}-1-piperazinecarboxylate **2.62**. Yielded **2.63** as a colourless solid (90% yield). $^{1}$H NMR (400 MHz, $D_2O$): δ 3.93 – 3.36 (m, 11H), 3.18 – 3.08 (m, 2H), 2.01 – 1.05 (m, 18H). $^{13}$C{$^{1}$H} NMR (101 MHz, $D_2O$): δ 102.63, 102.46, 79.44, 79.38, 65.59, 65.27, 62.03, 61.90, 48.73, 40.43, 30.87, 30.84, 25.70, 25.31, 25.08, 20.75. Duplicate peaks on $^{13}$C{$^{1}$H} NMR were observed and are due to the mixture of isomers *cis* or *trans.* HRMS (ESI, *m/z*) calcd for $C_{18}H_{33}N_2O_3$ $[M+H]^+$: 325.2486; found 325.2489. Diff: -1.06 ppm.

## Preparation of ethyl 1-oxaspiro[2.5]octane-6-carboxylate (2.64)

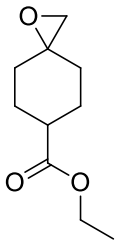

Compound **2.64** was synthesised following the **general procedure 4**, from ethyl 4-oxocyclohexanecarboxylate **2.52** and tetrahydrofuran as the solvent. Purification yielded **2.64** as a colourless oil (24% yield).

$^{1}$H NMR (400 MHz, $CDCl_3$): δ 4.16 (q, *J* = 7.1 Hz, 2H), 2.64 (d, *J* = 11.5 Hz, 2H), 2.45 – 2.34 (m, 1H), 2.13 – 1.98 (m, 1H), 1.97 – 1.91 (m, 1H), 1.90 – 1.85 (m, 2H), 1.84 – 1.70 (m, 2H), 1.53 – 1.37 (m, 2H), 1.26 (t, *J* = 7.1 Hz, 3H). $^{13}$C{$^{1}$H} NMR (101 MHz, $CDCl_3$) δ 175.11, 60.36, 57.49, 53.85, 41.89, 31.96, 26.50, 14.23. HRMS (ESI, *m/z*) calcd $C_{10}H_{16}O_3Na$ $[M+Na]^+$: 207.0992; found 207.0994. Diff: -0.93 ppm.

## Preparation of ethyl dispiro[cyclohexane-1,6'-[1,2,4]trioxane-3',2''-tricyclo[3.3.1.1$^{3,7}$]decane]-4-carboxylate (2.65)

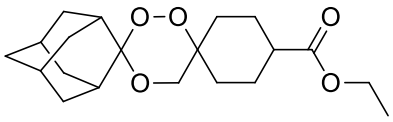

Compound **2.65** was synthesised following the general **procedure 2** (SSA Method), from ethyl 1-oxaspiro[2.5]octane-6-carboxylate **2.64** and adamantan-2-one. Isolation of analytically pure product by flash chromatography on silica gel was not possible since it co-elutes with adamantan-2-one. Therefore, the product was carried forward to the next step. MS (ESI) $[M+Na]^+$: 373.2 (100).

## Preparation of dispiro[cyclohexane-1,6'-[1,2,4]trioxane-3',2''-tricyclo[3.3.1.1$^{3,7}$]decane]-4-carboxylic acid (2.66)

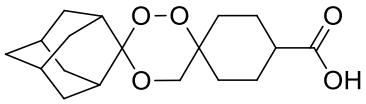

The procedure by Jiricek *et al.*[83] was followed, using ethyl dispiro[cyclohexane-1,6'-[1,2,4]trioxane-3',2''-tricyclo[3.3.1.1$^{3,7}$]decane]-4-carboxylate **2.65**. Purification by flash chromatography (gradient eluent EtOAc: hexane, 50-100%:50-0%, *v/v*) yielded **2.66** as a colourless solid (17% yield over 3 steps). $^{1}$H NMR (400 MHz, $CDCl_3$): δ 3.92 – 3.52 (m, 2H), 2.93 (br s, 1H), 2.56 (dt, *J* = 7.5, 3.6 Hz, 1H), 2.27 – 1.62 (m, 19H), 1.51 – 1.12 (m, 2H). $^{13}$C{$^{1}$H} NMR (101 MHz, $CDCl_3$): δ 180.95, 104.45, 76.89, 64.03, 40.47, 37.17, 36.24, 33.38, 30.14, 27.15, 24.05, 23.28. HRMS (ESI, *m/z*) calcd $C_{18}H_{25}O_5$ $[M-H]^-$: 321.1701; found 321.1706. Diff: 0.60 ppm.

## Preparation of (dispiro[cyclohexane-1,6'-[1,2,4]trioxane-3',2''-tricyclo[3.3.1.1$^{3,7}$]decan]-4-yl)methanol (2.67)

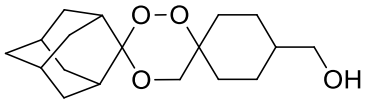

Compound **2.67** was synthesised following the **general procedure 3**, from dispiro[cyclohexane-1,6'-[1,2,4]trioxane-3',2''-tricyclo[3.3.1.1$^{3,7}$]decane]-4-carboxylic acid **2.66**. Yielded **2.67** as a colourless foam (97% yield). $^{1}$H NMR (400 MHz, $CDCl_3$): δ 3.75 (s, 2H), 3.50 (d, *J* = 6.4 Hz, 2H), 3.12 – 2.27 (m, 2H), 2.10 – 1.74 (m, 10H), 1.67 – 1.45 (m, 8H), 1.41 – 0.92 (m, 4H). $^{13}$C{$^{1}$H} NMR (101 MHz, $CDCl_3$): δ 104.34, 78.08, 67.16, 62.67, 40.25, 37.19, 36.21, 33.92, 31.03, 28.91, 27.16, 25.10. HRMS (ESI, *m/z*) calcd for $C_{18}H_{28}O_4Na$ $[M+Na]^+$: 331.1880; found 331.1887. Diff: -2.03 ppm.

## Preparation of *tert*-butyl 4-{(dispiro[cyclohexane-1,6'-[1,2,4]trioxane-3',2''-tricyclo[3.3.1.1$^{3,7}$]de-can]-4-yl)methyl}-1-piperazinecarboxylate (2.68)

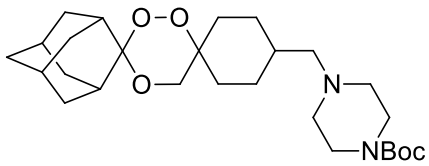


Compound **2.68** was synthesised following the **general procedure 10** and **11**, from (dispiro[cyclohexane-1,6'-[1,2,4]trioxane-3',2''-tricyclo[3.3.1.1$^{3,7}$]decan]-4-yl)methanol **2.67** and 1-boc-piperazine. Purification by flash chromatography (EtOAc: hexane, 25:75, *v/v*) yielded **2.68** as a colourless solid (39% yield). $^{1}$H NMR (400 MHz, $CDCl_3$): δ 3.74 (s, 2H), 3.40 (t, *J* = 5.0 Hz, 4H), 3.05 – 2.27 (m, 5H), 2.19 – 2.13 (m, 2H), 2.11 – 1.68 (m, 10H), 1.67 – 1.49 (m, 7H), 1.48 – 1.44 (s, 9H), 1.45 (m, 3H), 1.13 – 0.81 (m, 2H). $^{13}$C{$^{1}$H} NMR (101 MHz, $CDCl_3$): δ 154.80, 104.30, 79.53, 78.23, 63.97, 62.75, 53.48, 43.57, 37.22, 37.19, 34.09, 33.39, 28.44, 27.18, 27.16. HRMS (ESI, *m/z*) calcd for $C_{27}H_{45}N_2O_5$ $[M+H]^+$: 477.3323; found 477.3329. Diff: -1.32 ppm.

## Preparation of 4-[(1-piperazinyl)methyl]dispiro[cyclohexane-1,6'-[1,2,4]trioxane-3',2''-tricyclo-[3.3.1.1$^{3,7}$]decane] dihydrochloride (2.69)

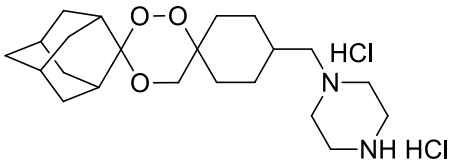


Compound **2.69** was synthesised following the **general procedure 7** (4 M in 1,4-dioxane method), from *tert*-butyl 4-{(dispiro[cyclohexane-1,6'-[1,2,4]trioxane-3',2''-tricyclo[3.3.1.1$^{3,7}$]decan]-4-yl)methyl}-1-pipe-razinecarboxylate **2.68**. Yielded **2.69** as a colourless solid (95% yield). $^{1}$H NMR (400 MHz, $D_2O$): δ 3.91 – 3.36 (m, 11H), 3.15 (dd, *J* = 14.0, 7.0 Hz, 2H), 2.06 – 0.98 (m, 22H). $^{13}$C{$^{1}$H} NMR (101 MHz, $D_2O$): δ 106.18, 78.67, 61.99, 61.42, 48.73, 40.45, 36.26, 32.83, 31.31, 30.70, 26.55, 24.65. HRMS (ESI, *m/z*) calcd for $C_{22}H_{37}N_2O_3$ $[M+H]^+$: 377.2799; found 377.2807. Diff: -2.21 ppm.

## Preparation of *tert*-butyl 4-[8-nitro-4-oxo-6-(trifluoromethyl)-1,3-benzothiazin-2-yl]-1-piperazine-carboxylate (2.70)

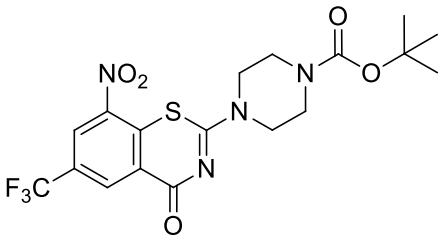

This compound was synthesised following the **general procedure 8**, from 1-boc-piperazine **2.56** and 2-(methylthio)-8-nitro-6-(trifluoromethyl)-*4H*-benzo[*e*][1,3]thiazin-4-one **2.43**. Recrystallization from methanol gave the pure product **2.70** as a yellow solid (79% yield).

$^{1}$H NMR (400 MHz, $CDCl_3$): δ 9.11 (d, *J* = 2.2 Hz, 1H), 8.79 (d, *J* = 2.1 Hz, 1H), 4.03 (br s, 4H), 3.60 (s, 4H), 1.50 (s, 9H). $^{13}C\{^{1}H\}$ NMR (101 MHz, $CDCl_3$): δ 166.37, 162.63, 154.26, 143.91, 133.78, 133.50, 130.11, 126.68, 126.17, 126.13, 123.69, 81.07, 46.21, 43.20, 28.34. HRMS (ESI, *m/z*) calcd for $C_{18}H_{19}F_3N_4O_5SNa$ $[M+Na]^+$: 483.092; found 483.0922. Diff: -0.33 ppm.

## Preparation of 8-nitro-2-(1-piperazinyl)-6-(trifluoromethyl)-1,3-benzothiazin-4-one dihydrochloride (2.71)

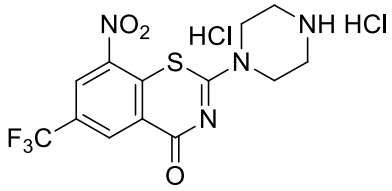

Compound **2.71** was synthesised following the **general procedure 7** (4 M in 1,4-dioxane method), from *tert*-butyl 4-[8-nitro-4-oxo-6-(trifluoromethyl)-1,3-benzo-thiazin-2-yl]-1-piperazinecarboxylate **2.70**. Obtained as a pale-yellow solid (94% yield). $^{1}$H NMR (400 MHz, $CD_3OD$): δ 8.89 (dd, *J* = 2.2, 0.7 Hz, 1H), 8.84 – 8.82 (m, 1H), 4.19 (t, *J* = 5.4 Hz, 4H), 3.35 (t, *J* = 5.4 Hz, 4H). $^{13}C\{^{1}H\}$ NMR (101 MHz, DMSO-$d_6$): δ 165.86, 163.09, 144.90, 138.33, 134.51, 131.92, 128.26, 127.92, 126.90, 126.89, 126.43, 124.41, 121.70, 43.20, 42.09. HRMS (ESI, *m/z*) calcd for $C_{13}H_{12}F_3N_4O_3S$ $[M+H]^+$: 361.0577; found 361.0579. Diff: -0.55 ppm.

## Preparation of 3,3-dimethyl-1,2,5-trioxa-9-spiro[5.5]undecanecarboxylic acid (2.72)

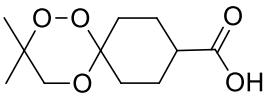

The procedure by Jiricek *et al.*[83] was followed, using ethyl 3,3-dimethyl-1,2,5-trioxa-9-spiro[5.5]undecanecarboxylate **2.53**. White solid (95% yield). $^{1}$H NMR (400 MHz, $CDCl_3$): δ 3.91 – 3.38 (m, 2H), 2.85 – 2.39 (m, 1H), 2.00 – 0.76 (m, 14H). $^{13}C\{^{1}H\}$ NMR (101 MHz, $CDCl_3$): δ 181.11, 180.98, 101.04, 100.95, 76.96, 66.74, 66.49, 41.67, 41.29, 35.09, 27.12, 27.08, 24.51, 24.18, 22.59, 22.21. Duplicate peaks on $^{13}C\{^{1}H\}$ NMR, it is due to the mixture of isomers *cis* or *trans*. HRMS (ESI, *m/z*) calcd $C_{11}H_{17}O_5$ $[M-H]^-$: 229.1081; found 229.1082. Diff: -0.40 ppm.

## Preparation of (9*H*-fluoren-9-yl)methyl 3,3-dimethyl-1,5-dioxa-9-aza-9-spiro[5.5]undecanecarboxylate (2.74)

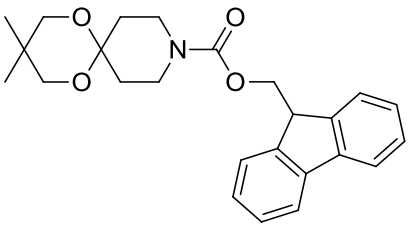

This compound was synthesised following the general **procedure 9**, from Fmoc-piperidone **2.73** and 2,2-dimethylpropane-1,3-diol. Purification by flash chromatography (EtOAc: hexane, 25:75, *v/v*) yielded a white solid (91% yield). $^{1}$H NMR (400 MHz, $CDCl_3$): δ 7.76 (d, *J* = 7.5 Hz, 2H), 7.57 (dd, *J* = 7.6, 1.1 Hz, 2H), 7.39 (td, *J* = 7.5, 1.2 Hz, 2H), 7.31 (td, *J* = 7.5, 1.2 Hz, 2H), 4.42 (d, *J* = 6.9 Hz, 2H), 4.24 (t, *J* = 6.8 Hz, 1H), 3.55 – 3.46 (m, 8H), 1.88 – 1.76 (m, 4H), 1.02 – 0.94 (m, 6H). $^{13}C\{^{1}H\}$ NMR (101 MHz, $CDCl_3$): δ 155.12, 144.08, 141.35, 127.68, 127.05, 124.99, 119.99, 95.96, 70.03, 67.28, 53.44, 47.38, 40.76, 32.77, 31.81, 30.26, 22.66. HRMS (ESI, *m/z*) calcd $C_{25}H_{29}NO_4Na$ $[M+Na]^+$: 430.1989, found 430.1988. Diff: 0.30 ppm.

## Preparation of 3,3-dimethyl-1,5-dioxa-9-azaspiro[5.5]undecane (2.75)

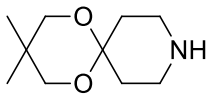


The procedure by Sureshbabu *et al.*[100] was followed, with slight modifications. To a solution of (*9H*-fluoren-9-yl)methyl 3,3-dimethyl-1,5-dioxa-9-aza-9-spiro[5.5]-undecanecarboxylate **2.74** (1 mmol) in dry $CH_2Cl_2$ (2 mL) was added diethylamine (2 mL) and the mixture was allowed to stir at room temperature overnight. The solvent was concentrated under reduced pressure, then purified by flash chromatography (MeOH: $CH_2Cl_2$:$NH_4OH$, 10:90:1, *v/v*), and yielded a white solid (45% yield). $^1$H NMR (400 MHz, $CDCl_3$): δ 3.48 (br s, 4H), 3.24 (t, *J* = 5.7 Hz, 4H), 2.21 – 2.15 (m, 4H), 0.97 (s, 6H). $^{13}C\{^1H\}$ NMR (101 MHz, $CDCl_3$): δ 93.68, 70.09, 41.02, 30.20, 29.38, 22.52. HRMS (ESI, *m/z*) calcd $C_{10}H_{20}NO_2$ $[M+H]^+$: 186.1489; found 186.1487. Diff: 0.62 ppm.

## Preparation of ethyl 3,3-dimethyl-1,5-dioxa-9-spiro[5.5]undecanecarboxylate (2.76)

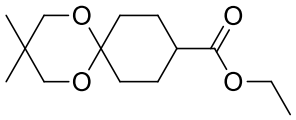


This compound was synthesised following the general **procedure 9**, from **2.52** and 2,2-dimethylpropane-1,3-diol. Purification by flash chromatography (EtOAc: hexane, 25:75, *v/v*) yielded a colourless oil (93% yield). $^1$H NMR (400 MHz, $CDCl_3$): δ 4.12 (q, *J* = 7.1 Hz, 2H), 3.51 (s, 2H), 3.47 (s, 2H), 2.33 (tt, *J* = 10.7, 4.1 Hz, 1H), 2.19 (d, *J* = 13.1 Hz, 2H), 1.84 (m, 2H), 1.73 (m, 2H), 1.45 (td, *J* = 12.8, 4.3 Hz, 2H), 1.24 (t, *J* = 7.1 Hz, 3H), 0.96 (s, 6H). $^{13}C\{^1H\}$ NMR (101 MHz, $CDCl_3$): δ 175.33, 96.88, 70.07, 69.82, 60.23, 42.17, 31.16, 30.18, 24.88, 22.72, 14.23. HRMS (ESI, *m/z*) calcd for $C_{14}H_{25}O_4$ $[M+H]^+$: 257.1747; found 257.1751. Diff: -1.38 ppm.

## Preparation of (3,3-dimethyl-1,5-dioxa-9-spiro[5.5]undecyl)methanol (2.77)

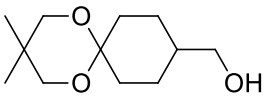


This compound was synthesised following the **general procedure 3**, from ethyl 3,3-dimethyl-1,5-dioxa-9-spiro[5.5]undecanecarboxylate **2.76**. Colourless oil (92% yield). $^{1}$H NMR (400 MHz, $CDCl_3$): δ 3.54 (s, 2H), 3.48 (br s, 4H), 2.30 – 2.23 (m, 2H), 1.73 – 1.66 (m, 2H), 1.60 – 1.46 (m, 2H), 1.37 (td, *J* = 13.3, 3.9 Hz, 2H), 1.25 – 1.15 (m, 2H), 0.96 (s, 6H). $^{13}$C{$^{1}$H} NMR (101 MHz, $CDCl_3$): δ 97.75, 70.04, 69.83, 67.79, 39.74, 31.52, 30.19, 25.24, 22.73. HRMS (CI, *m/z*) calcd for $C_{12}H_{23}O_3$ $[M+H]^+$: 215.1642; found 215.1646. Diff: -1.82 ppm.

## Preparation of *tert*-butyl 4-{(3,3-dimethyl-1,5-dioxa-9-spiro[5.5]undecyl)methyl}-1-piperazinecarboxylate (2.78)

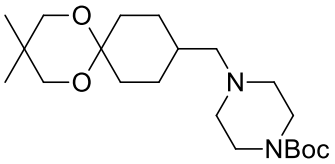


This compound was synthesised following the **general procedures 10** and **11**, from (3,3-dimethyl-1,5-dioxa-9-spiro[5.5]undecyl)methanol **2.77** and 1-boc-piperazine **2.56**. Purification by flash chromatography (EtOAc: hexane, 25:75, *v/v*) yielded a white solid (39% yield). $^{1}$H NMR (400 MHz, $CDCl_3$): δ 3.52 (s, 2H), 3.46 (s, 2H), 3.41 (t, *J* = 5.1 Hz, 4H), 2.32 (t, *J* = 5.0 Hz, 4H), 2.26 – 2.19 (m, 2H), 2.15 (d, *J* = 7.1 Hz, 2H), 1.71 – 1.66 (m, 2H), 1.53 (ddt, *J* = 11.1, 7.4, 3.7 Hz, 1H), 1.46 (s, 9H), 1.34 (td, *J* = 13.4, 4.0 Hz, 2H), 1.14 (dt, *J* = 16.4, 11.5 Hz, 2H), 0.97 (s, 6H). $^{13}$C{$^{1}$H} NMR (101 MHz, $CDCl_3$): δ 154.82, 97.91, 79.48, 70.05, 69.81, 64.57, 53.50, 43.67, 34.29, 31.71, 30.19, 28.44, 27.24, 22.75. HRMS (ESI, *m/z*) calcd for $C_{21}H_{39}N_2O_4$ $[M+H]^+$: 383.2904; found 383.2908. Diff: -0.91 ppm.

## Preparation of 1-{(3,3-dimethyl-1,5-dioxa-9-spiro[5.5]undecyl)methyl}piperazine dihydrochloride (2.79)

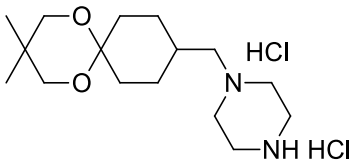


This compound was synthesised following the **general procedure 7** (4 M in 1,4-dioxane method), from *tert*-butyl 4-{(dispiro[cyclohexane-1,6'-[1,2,4]trioxane-3',2''-tricyclo[3.3.1.1$^{3,7}$]decan]-4-yl)methyl}-1-piperazinecarboxylate **2.78**. White solid (86% yield). $^{1}$H NMR (400 MHz, $D_2O$): δ 3.66 – 3.48 (m, 13H), 3.11 (d, *J* = 7.9 Hz, 2H), 2.48 – 2.14 (m, 2H), 1.93 – 1.47 (m, 3H), 1.38 (td, *J* = 13.5, 3.8 Hz, 2H), 1.28 (q, *J* = 13.0 Hz, 2H), 0.90 (s, 6H). $^{13}$C{$^{1}$H} NMR (101 MHz, $D_2O$): δ 98.17, 69.57, 69.41, 68.01, 48.69, 40.41, 39.07, 30.93, 29.23, 25.66, 21.42. HRMS (ESI, *m/z*) calcd for $C_{16}H_{31}N_2O_2$ $[M+H]^+$: 283.2380; found 283.2382. Diff: -0.82 ppm.

## Preparation of ethyl 1,4-dioxaspiro[4.5]decane-8-carboxylate (2.80)

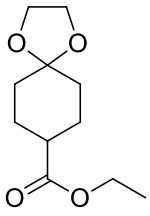


Compound **2.80** was synthesised following the general **procedure 9**, from **2.52** and ethylene glycol. Purification by flash chromatography (EtOAc: hexane, 25:75, *v/v*) yielded a colourless oil (92% yield). $^{1}$H NMR (400 MHz, $CDCl_3$): δ 4.13 (q, *J* = 7.1 Hz, 2H), 3.94 (s, 4H), 2.33 (tt, *J* = 10.4, 3.9 Hz, 1H), 1.98 – 1.89 (m, 2H), 1.86 – 1.74 (m, 4H), 1.55 (td, *J* = 12.4, 11.7, 4.2 Hz, 2H), 1.25 (t, *J* = 7.1 Hz, 3H). $^{13}$C{$^{1}$H} NMR (101 MHz, $CDCl_3$): δ 175.20, 108.10, 64.30, 60.26, 41.62, 33.74, 26.29, 14.22. HRMS (ESI, *m/z*) calcd $C_{11}H_{18}O_4$ $[M+H]^+$: 215.1278; found 215.1273. Diff: 2.06 ppm.

## Preparation of (1,4-dioxa-8-spiro[4.5]decyl)methanol (2.81)

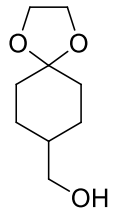


Compound **2.81** was synthesised following the **general procedure 3**, from ethyl 1,4 dioxaspiro[4.5]decane-8-carboxylate **2.80**. Colourless oil (94% yield). $^{1}$H NMR (400 MHz, $CDCl_3$): 3.94 (s, 4H), 3.51 – 3.45 (m, 2H), 1.82 – 1.75 (m, 4H), 1.60 – 1.48 (m, 4H), 1.34 – 1.20 (m, 2H). $^{13}C\{^{1}H\}$ NMR (101 MHz, $CDCl_3$): δ 109.04, 67.71, 64.24, 39.11, 34.11, 26.64. HRMS (CI, *m/z*) calcd for $C_9H_{17}O_3$ $[M+H]^+$: 173.1172; found 173.1174. Diff: -0.85 ppm.

## Preparation of *tert*-butyl 4-{(1,4-dioxa-8-spiro[4.5]decyl)methyl}-1-piperazinecarboxylate (2.82)

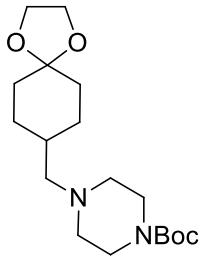


This compound was synthesised following the **general procedure 10** and **11**, from (1,4-dioxa-8-spiro[4.5]decyl)methanol **2.81** and 1-boc-piperazine **2.56**. Purification by flash chromatography (EtOAc: hexane, 25:75, *v/v*) yielded a white solid (44% yield).
$^{1}$H NMR (400 MHz, $CDCl_3$): δ 3.94 (s, 4H), 3.40 (t, *J* = 5.1 Hz, 4H), 2.32 (t, *J* = 5.1 Hz, 4H), 2.15 (d, *J* = 7.2 Hz, 2H), 1.82 – 1.71 (m, 4H), 1.56 – 1.47 (m, 3H), 1.45 (s, 9H), 1.28 – 1.14 (m, 2H). $^{13}C\{^{1}H\}$ NMR (101 MHz, $CDCl_3$): δ 154.82, 109.21, 79.48, 64.49, 64.22, 53.50, 44.22, 34.32, 33.70, 28.65, 28.44**.** HRMS (ESI, *m/z*) calcd for $C_{18}H_{33}N_2O_4$ $[M+H]^+$: 341.2435; found 341.2446. Diff: -3.33 ppm.

## Preparation of 4-[(1-piperazinyl)methyl]cyclohexanone dihydrochloride (2.83)

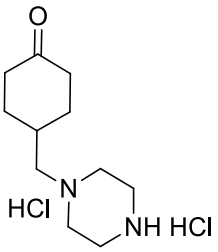


Compound **2.83** was synthesised following the **general procedure 7** (4 M in 1,4-dioxane method), from *tert*-butyl 4-{(1,4-dioxa-8-spiro[4.5]decyl)methyl}-1-piperazine-carboxylate **2.82**. Colourless solid (40% yield). $^{1}$H NMR (400 MHz, $D_2O$): δ 3.61 (br s, 8H), 3.24 (d, *J* = 7.1 Hz, 2H), 2.47 (td, *J* = 14.4, 13.8, 5.9 Hz, 2H), 2.39 – 2.30 (m, 2H), 2.12 – 1.87 (m, 2H), 1.85 – 1.16 (m, 3H). $^{13}$C{$^{1}$H} NMR (101 MHz, $D_2O$): δ 217.14, 61.50, 48.83, 40.44, 39.05, 30.01, 29.21. HRMS (ESI, *m/z*) calcd for $C_{11}H_{21}N_2O$ $[M+H]^+$: 197.1648; found 197.1649. Diff: -0.07 ppm.

## Preparation of 2-(3,3-dimethyl-1,2,5-trioxa-9-aza-9-spiro[5.5]undecyl)-8-nitro-6-(trifluorome-thyl)-1,3-benzothiazin-4-one (B3)

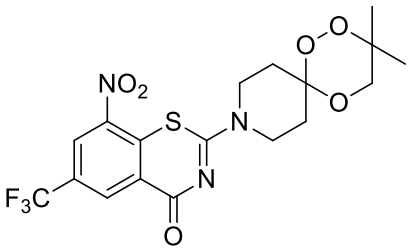


**B3** was synthesised following the **general procedure 8**, from 3,3-dimethyl-1,2,5-trioxa-9-azaspiro[5.5]undecane **2.47** and **2.43**. Recrystallization from methanol gave the pure product as a pale green solid (62% yield). M.p = 204-206 ºC. $^{1}$H NMR (400 MHz, $CDCl_3$): δ 9.10 (d, *J* = 2.1 Hz, 1H), 8.77 (d, *J* = 2.1 Hz, 1H), 4.69 – 3.40 (m, 6H), 2.72 – 1.78 (m, 4H), 1.53 (s, 3H), 1.16 (s, 3H). $^{13}$C{$^{1}$H} NMR (101 MHz, $CDCl_3$): δ 166.52, 161.96, 143.93, 134.03, 133.43, 133.40, 129.93, 129.58, 126.63, 126.08, 126.05, 123.72, 121.01, 99.61, 77.61, 66.95, 42.96, 34.36, 21.90. HRMS (ESI, *m/z*) calcd $C_{18}H_{18}F_3N_3O_6SNa$ $[M+Na]^+$: 484.0761; found 484.0759. Diff: 0.27 ppm. Anal. Calcd for $C_{18}H_{18}F_3N_3O_6S$: C, 46.85; H, 3.93; N, 9.11, found: C, 46.73; H, 3.88; N, 9.16.

## Preparation of 8-nitro-6-(trifluoromethyl)-2-(7,8,16-trioxa-3-aza-3-dispiro[5.2.5.2]hexadecyl)-1,3-benzothiazin-4-one (B4)

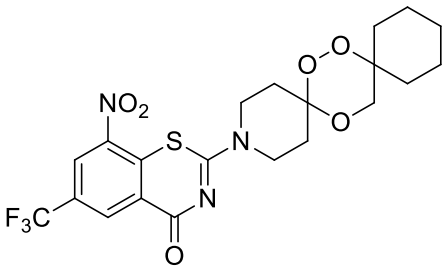


**B4** was synthesised following the **general procedure 8**, from 7,8,16-trioxa-3-azadispiro[5.2.5.2]hexadecane **2.48** and **2.43**. Recrystallization from methanol gave the pure product as a pale green solid (65% yield). M.p = 205-207 ºC. $^{1}$H NMR (400 MHz, $CDCl_3$): δ 9.02 (d, *J* = 2.1 Hz, 1H), 8.69 (d, *J* = 2.1 Hz, 1H), 4.43 – 3.48 (m, 6H), 2.71 – 2.21 (m, 2H), 2.09 – 1.74 (m, 3H), 1.59 – 1.17 (m, 9H). $^{13}$C{$^{1}$H} NMR (101 MHz, $CDCl_3$): δ 166.50, 161.92, 143.92, 134.04, 133.41, 133.38, 130.25, 129.90, 129.55, 129.20, 126.63, 126.07, 126.03, 123.72, 121.01, 99.78, 78.40, 66.40, 43.16, 34.44, 32.10, 29.97, 25.76, 21.21. HRMS (ESI, *m/z*) calcd $C_{21}H_{22}F_3N_3O_6SNa$ $[M+Na]^+$: 524.1074; found 524.108. Diff: -1.22 ppm. Anal. Calcd for $C_{21}H_{22}F_3N_3O_6S$: C, 50.30; H, 4.42; N, 8.38, found: C, 50.44; H, 4.35; N, 8.40.

## Preparation of 2-(dispiro[piperidine-4,6'-[1,2,4]trioxane-3',2''-tricyclo[3.3.1.1$^{3,7}$]decan]-1-yl)-8-nitro-6-(trifluoro-methyl)-1,3-benzothiazin-4-one (B5)

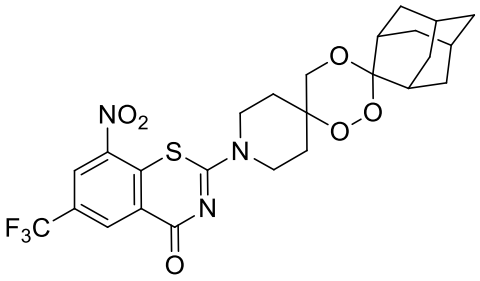


**B5** was synthesised in accordance with **general procedure 8**, using dispiro[piperidine-4,6'-[1,2,4]trioxane-3',2''-tricyclo[3.3.1.1$^{3,7}$]decane] **2.51** and **2.43**. Recrystallization from methanol gave the pure product as a pale green solid (53% yield).

M.p = 198-200 ºC. $^{1}$H NMR (400 MHz, $CDCl_3$): δ 9.12 (s, 1H), 8.77 (s, 1H), 5.08 (br s, 1H), 4.20 (br s, 1H), 3.92 – 3.31 (m, 4H), 2.97 (br s, 2H), 2.09 – 1.62 (m, 16H). $^{13}$C{$^{1}$H} NMR (101 MHz, $CDCl_3$): δ 166.53, 161.84, 143.93, 134.10, 133.40, 133.36, 130.40 – 129.71 (q, *J* = 35.5, 35.0 Hz), 126.69, 126.05, 126.01, 123.73, 121.02, 118.31, 105.13, 75.33, 64.96, 42.64, 37.05, 36.05, 33.33, 30.33, 28.41, 27.06. HRMS (ESI, *m/z*) calcd $C_{25}H_{26}F_3N_3O_6SNa$ $[M+Na]^+$: 576.1387; found 576.1387. Diff: 0.01 ppm. Anal. Calcd for $C_{25}H_{26}F_3N_3O_6S$: C, 54.24; H, 4.73; N, 7.59, found: C, 54.52; H, 4.66; N, 7.64.

## Preparation of 8-nitro-2-(4-oxo-1-piperidyl)-6-(trifluoromethyl)-1,3-benzothiazin-4-one (C1)

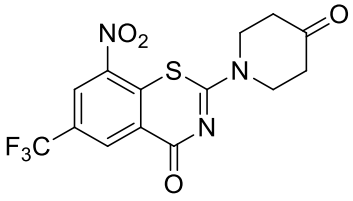


Compound **C1** was synthesised following the **general procedure 8**, from piperidone hydrochloride and **2.43**. Purification by flash chromatography (EtOAc: hexane, 20:80, *v/v*) yielded a yellow solid (41% yield). M.p = 223-226 ºC. $^{1}$H NMR (400 MHz, $CDCl_3$): δ 9.13 (s, 1H), 8.80 (s, 1H), 4.32 (br s, 4H), 2.73 (t, *J* = 6.3 Hz, 4H). $^{13}$C{$^{1}$H} NMR (101 MHz, $CDCl_3$): δ 204.25, 166.29, 162.71, 143.93, 133.66, 133.62,

133.59, 133.55, 130.63, 130.28, 129.93, 129.57, 126.47, 126.30, 126.27, 126.23, 126.19, 123.65, 120.94, 118.22, 44.33, 39.94. HRMS (CI, *m/z*) calcd $C_{14}H_{11}F_3N_3O_4S$ $[M+H]^+$: 374.0417, found 374.0421**.** Diff: -1.16 ppm. Purity HPLC (Method B): 96.47%, *Rt* = 2.77 min.

## Preparation of 2-(3,3-dimethyl-1,5-dioxa-9-aza-9-spiro[5.5]undecyl)-8-nitro-6-(trifluoromethyl)-1,3-benzothiazin-4-one (C2)

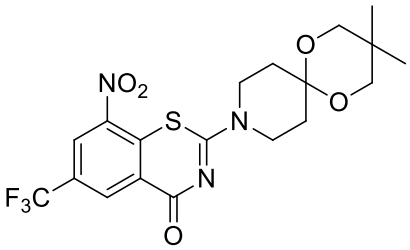


This compound was synthesised following the **general procedure 8**, from 3,3-dimethyl-1,5-dioxa-9-azaspiro[5.5]undecane **2.75** and **2.43**. Recrystallization from methanol gave the pure product as a pale green solid (72% yield). M.p = 264-266 ºC. $^1$H NMR (400 MHz, $CDCl_3$): δ 9.11 (d, *J* = 2.1 Hz, 1H), 8.75 (d, *J* = 2.1 Hz, 1H), 4.16 (br s, 2H), 3.90 (br s, 2H), 3.57 (s, 4H), 2.03 (t, *J* = 5.7 Hz, 4H), 1.02 (s, 6H). $^{13}$C{$^1$H} NMR (101 MHz, $CDCl_3$): δ 166.58, 161.82, 143.94, 134.17, 133.40, 133.36, 129.85, 129.50, 126.67, 126.04, 126.01, 123.74, 121.03, 95.41, 70.29, 43.68, 33.36, 31.64, 30.31, 22.56. HRMS (ESI, *m/z*) calcd $C_{19}H_{20}F_3N_3O_5SNa$ $[M+Na]^+$: 482.0968, found 482.0974. Diff: -1.27 ppm. Anal. Calcd for $C_{19}H_{20}F_3N_3O_5S$: C, 49.67; H, 4.39; F, 12.41; N, 9.15; found: C, 49.38; H, 4.33; N, 9.07.

## Preparation of 8-nitro-2-{4-[(4-oxocyclohexyl)methyl]-1-piperazinyl}-6-(trifluoromethyl)-1,3-benzo-thiazin-4-one (C3)

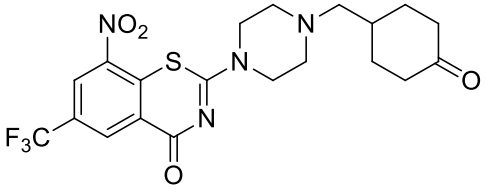


Compound **C3** was synthesised following the **general procedure 8**, from 4-[(1-piperazinyl)methyl]cyclohexanone dihydrochloride **2.83** and **2.43**. Purification by flash

chromatography (100% EtOAc) gave the pure product as a dark yellow solid (39% yield). M.p = 200-202 ºC. $^{1}$H NMR (400 MHz, $CDCl_3$): δ 9.11 (d, *J* = 2.2 Hz, 1H), 8.77 (d, *J* = 2.1 Hz, 1H), 4.25 – 3.81 (m, 4H), 2.62 (br s, 4H), 2.47 – 2.29 (m, 6H), 2.21 – 2.12 (m, 2H), 1.98 (ddq, *J* = 11.0, 7.2, 3.7 Hz, 1H), 1.39 (tt, *J* = 12.4, 6.5 Hz, 2H). $^{13}$C{$^{1}$H} NMR (101 MHz, $CDCl_3$): δ 211.67, 166.47, 162.11, 143.92, 134.02, 133.44, 133.41, 129.94, 129.58, 129.22, 126.74, 126.07, 126.03, 123.72, 121.01, 63.11, 53.09, 46.50, 40.51, 33.46, 30.89. HRMS (ESI, *m/z*) calcd for $C_{20}H_{22}F_3N_4O_4S$ $[M+H]^+$: 471.1308; found 471.1311. Diff: -0.52 ppm. Calcd for $C_{20}H_{21}F_3N_4O_4S$: C, 51.06; H, 4.50; N, 11.91, found: C, 50.69; H, 4.48; N, 11.75.

## Preparation of 2-(4-{(3,3-dimethyl-1,5-dioxa-9-spiro[5.5]undecyl)methyl}-1-piperazinyl)-8-nitro-6-(trifluoromethyl)-1,3-benzothiazin-4-one (C4)

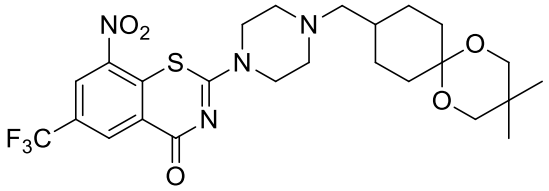


This compound was synthesised following the **general procedure 8** using 1-{(3,3-dimethyl-1,5-dioxa-9-spiro[5.5]undecyl)methyl}piperazine dihydrochloride **2.79** and **2.43**. Purification by flash chromatography (EtOAc: hexane, 70:30, *v/v* followed by recrystallization from acetone gave the pure product as a yellow solid (38% yield). M.p = 230-232 ºC. $^{1}$H NMR (400 MHz, $CDCl_3$): 9.10 (d, *J* = 2.1 Hz, 1H), 8.76 (d, *J* = 2.2 Hz, 1H), 4.13 (br s, 2H), 3.90 (br s, 2H), 3.53 (s, 2H), 3.47 (s, 2H), 2.55 (br s, 4H), 2.28 – 2.20 (m, 4H), 1.74 – 1.66 (m, 2H), 1.55 (ddt, *J* = 11.0, 7.3, 3.9 Hz, 1H), 1.37 (td, *J* = 13.3, 3.8 Hz, 2H), 1.22 – 1.12 (m, 2H), 0.97 (s, 6H). $^{13}$C{$^{1}$H} NMR (101 MHz, $CDCl_3$): δ 166.47, 162.01, 143.91, 134.10, 133.41, 129.86, 129.51, 126.78, 126.02, 125.98, 123.74, 120.94, 97.79, 70.07, 69.86, 64.01, 53.09, 46.59, 34.30, 31.64, 30.21, 27.12, 22.74. HRMS (ESI, *m/z*) calcd for $C_{25}H_{32}F_3N_4O_5S$ $[M+H]^+$: 557.2040; found 557.2044. Diff: -0.75 ppm. Anal. Calcd for $C_{25}H_{31}F_3N_4O_5S$: C, 53.95; H, 5.61; N, 10.07, found: C, 53.64; H, 5.59; N, 9.92.

## Preparation of 2-(4-((3,3-dimethyl-1,2,5-trioxa-9-spiro[5.5]undecyl)methyl)-1-piperazinyl)-8-nitro -6-(trifluoromethyl)-1,3-benzothiazin-4-one (P4)

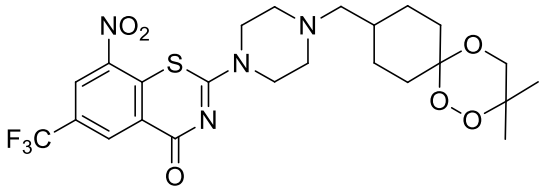

**P4** was synthesised following the **general procedure 8**, from 3,3-dimethyl-9-[(1-piperazinyl)methyl]-1,2,5-trioxaspiro[5.5]undecane dihydrochloride **2.59** and **2.43**. Recrystallization from methanol gave the pure product as a yellow solid (65% yield). M.p = 199-201 ºC. $^{1}$H NMR (400 MHz, $CDCl_3$): δ 9.10 (d, *J* = 2.1 Hz, 1H), 8.73 (d, *J* = 2.1 Hz, 1H), 4.26 – 3.36 (m, 6H), 2.95 – 2.30 (m, 5H), 2.29 – 2.18 (dd, *J* = 9.6, 7.1 Hz, 2H), 2.13 – 1.63 (m, 3H), 1.61 – 1.01 (m, 11H). $^{13}$C{$^{1}$H} NMR (101 MHz, $CDCl_3$): δ 166.46, 162.02, 143.91, 134.09, 133.41, 133.37, 129.79, 129.51, 126.77, 126.02, 125.99, 123.60, 121.02, 102.05, 101.95, 76.93, 76.88, 66.75, 66.50, 63.94, 63.72, 53.08, 46.59, 34.28, 34.12, 27.05, 26.66, 21.96. Duplicate peaks on $^{13}$C{$^{1}$H} NMR were observed and are due to the mixture of isomers *cis* or *trans*. HRMS (ESI, *m/z*) calcd $C_{24}H_{30}F_3N_4O_6S$ $[M+H]^+$: 559.1833; found 559.1839. Diff: -1.09 ppm. Anal. Calcd for $C_{24}H_{29}F_3N_4O_6S$: C, 51.61; H, 5.23; N, 10.03, found: C, 51.36; H, 5.19; N, 10.00. Purity HPLC (Method E): Purity HPLC (Method E): diastereomer 1: 31.45%, *Rt* = 9.67 min; diastereomer 2: 64.09%, *Rt* = 9.80. Differentiation of *cis*/*trans* isomers was not determined.

## Preparation of 8-nitro-6-(trifluoromethyl)-2-(4-{(7,8,15-trioxa-12-dispiro[5.2.5.2]hexadecyl)me-thyl}-1-piperazinyl)-1,3-benzothiazin-4-one (P5)

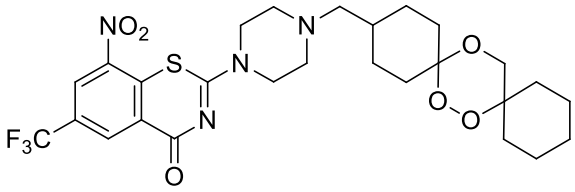


**P5** was synthesised following the **general procedure 8**, from 12-[(1-piperazinyl)methyl]-7,8,15-trioxadispiro[5.2.5.2]hexadecane dihydrochloride **2.63** and **2.43**. Recrystallization from methanol gave the pure product as a yellow solid (64% yield). M.p = 187-189 ºC. $^{1}$H NMR (400 MHz, $CDCl_3$): δ 9.10 (d, *J* = 2.1 Hz, 1H), 8.76 (d, *J* = 2.1 Hz, 1H), 4.12 (br s, 2H), 3.89 (br s, 2H), 3.75 – 3.30 (m, 2H), 2.83 (br s, 1H), 2.56 (s, 4H), 2.45 – 2.29 (m, 1H), 2.23 (t, *J* = 7.8 Hz, 2H), 1.81 – 1.62 (m, 5H), 1.59 – 1.14 (m, 12H). $^{13}$C{$^{1}$H} NMR (101 MHz, $CDCl_3$): δ 166.46, 162.02, 143.91, 134.09, 133.41, 133.37, 129.86, 129.50, 126.77, 126.02, 125.98, 123.74, 121.02, 102.25, 102.15, 77.69, 77.65, 66.22, 65.93, 63.96, 63.72, 53.08, 46.48, 34.30, 34.11, 27.08, 26.68, 25.92, 21.29. Duplicate peaks on $^{13}$C{$^{1}$H} NMR were observed and are due to the mixture of isomers *cis* or *trans*. HRMS (ESI, *m/z*) calcd $C_{27}H_{34}F_3N_4O_6S$ $[M+H]^+$: 599.2146; found 599.2153. Diff: -1.23 ppm. Anal. Calcd for $C_{27}H_{33}F_3N_4O_6S$: C, 54.17; H, 5.56; N, 9.36, found: C, 53.89; H, 5.44; N, 9.36. Purity HPLC (Method G): diastereomer 1: 33.70%, *Rt* = 8.18 min; diastereomer 2: 64.95%, *Rt* = 9.11. Differentiation of *cis*/*trans* isomers was not determined.

## Preparation of 2-(4-{(dispiro[cyclohexane-1,6'-[1,2,4]trioxane-3',2''-tricyclo[3.3.1.1$^{3,7}$]decan]-4-yl)methyl}-1-piperazinyl) -8-nitro-6-(trifluoromethyl)-1,3-benzothiazin-4-one (P6)

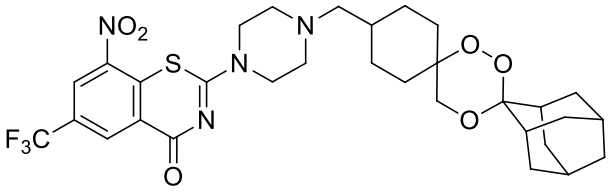

Compound **P6** was synthesised following the **general procedure 8**, from 4-[(1-piperazinyl)methyl]dispiro[cyclohexane-1,6'-[1,2,4]trioxane-3',2''-tricyclo[3.3.1.1$^{3,7}$]decane] dihydrochloride **2.69** and **2.43**. Recrystallization from methanol gave the pure product as a yellow solid (52% yield). M.p = 185-187 ºC. $^{1}$H NMR (400 MHz, $CDCl_3$): δ 9.10 (d, *J* = 2.1 Hz, 1H), 8.76 (d, *J* = 2.1 Hz, 1H), 4.12 (br s, 2H), 3.90 (br s, 2H), 3.75 (br s, 2H), 2.96 (br s, 1H), 2.67 – 2.45 (m, 5H), 2.24 (d, *J* = 7.2 Hz, 2H), 1.98 (br d, *J* = 12.7 Hz, 4H), 1.88 – 1.79 (m, 5H), 1.67 – 1.56 (m, 7H), 1.56 – 0.94 (m, 5H). $^{13}$C{$^{1}$H} NMR (101 MHz, $CDCl_3$): δ 166.47, 162.03, 143.91, 134.07, 133.41, 129.58, 129.27, 129.12, 126.77, 126.00, 123.54, 120.54, 104.37, 78.10, 63.37, 62.79, 53.09, 46.37, 37.18, 34.02, 33.39, 27.17, 27.15. HRMS (ESI, *m/z*) calcd $C_{31}H_{38}F_3N_4O_6S$ $[M+H]^+$: 651.2459; found 651.2460. Diff: -0.27 ppm. Anal. Calcd for $C_{31}H_{37}F_3N_4O_6S$: C, 57.22; H, 5.73; F, 8.61; N, 9.15; found: C, 56.92; H, 5.70 N, 8.62.

## Preparation of 2-(4-{(3,3-dimethyl-1,2,5-trioxa-9-spiro[5.5]undecyl)carbonyl}-1-piperazinyl)-8-nitro-6-(trifluoromethyl)-1,3-benzothiazin-4-one (P7)

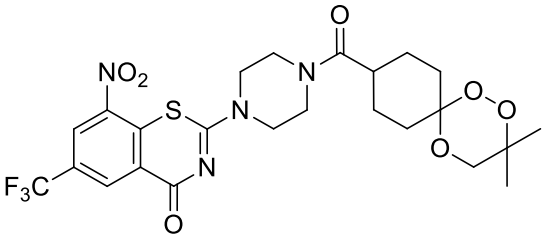

Compound **P7** was synthesised following the **general procedure 6**, from 8-nitro-2-(1-piperazinyl)-6-(trifluoromethyl)-1,3-benzothiazin-4-one dihydrochloride **2.71** and 3,3-dimethyl-1,2,5-trioxa-9-spiro[5.5]undecanecarboxylic acid **2.72**. Purification by flash chromatography (methanol:dichloromethane, 2.5:97.5, *v/v*) followed by recrystallization from methanol gave the pure product as a light green solid (65% yield). M.p = 210-212 ºC. $^{1}$H NMR (400 MHz, $CDCl_3$): δ 9.11 (d, *J* = 2.1 Hz, 1H), 8.79 (d, *J* = 2.2 Hz, 1H), 4.38 – 3.89 (m, 4H), 3.87 – 3.62 (m, 5H), 3.57 – 3.30 (m, 1H), 3.18 – 2.39 (m, 2H), 2.14 – 1.77 (m, 3H), 1.73 – 1.63 (m, 2H), 1.60 – 1.01 (m, 8H). $^{13}$C{$^{1}$H} NMR (101 MHz, DMSO-$d_6$): δ 173.71, 165.63, 162.46, 144.85, 134.66, 131.90, 128.13, 127.79, 126.73, 126.71, 126.58, 124.44, 121.72, 101.19, 101.04, 77.08, 77.06, 66.08, 65.88, 46.39, 44.17, 38.42, 38.34, 27.44, 25.41, 25.08, 22.27. Duplicate peaks on $^{13}$C{$^{1}$H} NMR were observed and are due to the mixture of isomers *cis* or *trans*. HRMS (ESI, *m/z*) calcd for $C_{24}H_{27}F_3N_4O_7SNa$ $[M+Na]^+$: 595.1445; found 595.1440. Diff: 0.75 ppm. Anal. Calcd for $C_{24}H_{27}F_3N_4O_7S$: C, 50.35; H, 4.75; N, 9.79, found: C, 49.36; H, 4.69; N, 9.50. Purity HPLC (Method F, UV254 nm): diastereomer 1: 36.71%, *Rt* = 10.12 min; diastereomer 2: 57.69%, *Rt* = 10.33. Differentiation of *cis*/*trans* isomers was not determined.

## 2.5.4. Computational Details

All structures were built using the molecular modelling software Spartan18[101] and energy minimised by molecular mechanics at the MMFF level. For covalent BTZ based compounds, structures were built as semithioacetal addition products and manually aligned with the extracted Cys387 sulfur. Molecular docking simulations were carried out using the molecular docking package GOLD[87] and the interface Hermes, as part of the

GOLD suite.

IC based structures were docked into the binding site of *Msm* MmpL3, using an obtained crystal structure of MMPL3 co-crystallised with ICA38 (PDB: 6AJJ).[10] IC analogues were docked using the extracted ICA38 molecule as a reference ligand. Genetic algorithm runs were carried out at a search efficiency of 100% and structures were scored by the GoldScore scoring function and RMSD.

BTZ based structures were docked into the binding site of DprE1 using an obtained crystal structure of DprE1 co-crystallised with BTZ043 (PDB: 6HEZ).[82] BTZ-based analogues were docked covalently at Cys387, using the extracted BTZ043 as a reference ligand. Genetic algorithm runs were carried out using default settings and structures were scored by the ChemPLP scoring function and RMSD.

## 2.5.5. Replicating *Mtb* Growth Inhibition Assays

Replicating *Mtb* growth inhibition assays were carried out at the Liverpool School of Tropical Medicine by Alison Ardrey using a microplate AlamarBlue assay (MABA), as described previously.[102] Serial dilutions of compounds to be tested (50 μl, 10 μM – 0.457 nM, in DMSO and *Mtb* culture media) were co-incubated with replicating Mtb inoculum prepared by diluting 2-3 week old Mtb culture (1 mL, OD 0.3) with Mtb culture media (29 mL). MABA was carried out after incubation at 37°C for 7 days. Absorption at 570 and 600 nm were recorded using an Opsys MR plate reader and $IC_{50}$ values were calculated for the inhibitors.

## 2.5.6. DMPK Assays and Predictions

Where experimentally determined, DMPK data was available as indicated in **Tables 2.6** and **2.7**. Compounds were assessed through a high throughput platform kindly provided by AstraZeneca U.K. The methods of the three assays, including aqueous solubility in pH 7.4 PBS buffer, microsome and hepatocyte clearance measurements, have been reported previously.[89] *In silico* DMPK predictions were kindly provided by AstraZeneca, and were obtained using their in-house predictive models.

## 2.5.7. Statistical Analysis

Graphics and statistical analysis were generated with manual R scripts in RStudio

(Version 2022.07.2), using `ggplot2` libraries for the graphic figures.

## 2.6. References


(1) Ballell, L.; Bates, R. H.; Young, R. J.; Alvarez-Gomez, D.; Alvarez-Ruiz, E.; Barroso, V.; Blanco, D.; Crespo, B.; Escribano, J.; González, R.; Lozanom, S.; Huss, S.; Santos-Villarejo, A.; Martín-Plaza, J. J.; Mendoza, A.; Rebollo-Lopez, M. J.; Remuiñan-Blanco, M.; Lavandera, J. L.; Pérez-Herran, E.; Gamo-Benito, F. J.; García-Bustos, J. F.; Barros, D.; Castro, J. P.; Cammack, N. Fueling Open-Source Drug Discovery: 177 Small-Molecule Leads against Tuberculosis. *ChemMedChem* **2013**, *8* (2), 313–321. https://doi.org/10.1002/cmdc.201200428.

(2) Onajole, O. K.; Pieroni, M.; Tipparaju, S. K.; Lun, S.; Stec, J.; Chen, G.; Gunosewoyo, H.; Guo, H.; Ammerman, N. C.; Bishai, W. R.; Kozikowski, A. P. Preliminary Structure−Activity Relationships and Biological Evaluation of Novel Antitubercular Indolecarboxamide Derivatives Against Drug-Susceptible and Drug-Resistant *Mycobacterium tuberculosis* Strains. *J. Med. Chem.* **2013**, *56* (10), 4093–4103. https://doi.org/10.1021/jm4003878.

(3) Stec, J.; Onajole, O. K.; Lun, S.; Guo, H.; Merenbloom, B.; Vistoli, G.; Bishai, W. R.; Kozikowski, A. P. Indole-2-Carboxamide-Based MmpL3 Inhibitors Show Exceptional Antitubercular Activity in an Animal Model of Tuberculosis Infection. *J. Med. Chem.* **2016**, *59* (13), 6232–6247. https://doi.org/10.1021/acs.jmedchem.6b00415.

(4) Kondreddi, R. R.; Jiricek, J.; Rao, S. P. S.; Lakshminarayana, S. B.; Camacho, L. R.; Rao, R.; Herve, M.; Bifani, P.; Ma, N. L.; Kuhen, K.; Goh, A.; Chatterjee, A. K.; Dick, T.; Diagana, T. T.; Manjunatha, U. H.; Smith, P. W. Design, Synthesis and Biological Evaluation of Indole-2- Carboxamides, a Promising Class of Anti-Tuberculosis Agents. *J. Med. Chem.* **2013**, *56* (21), 8849–8859. https://doi.org/10.1021/jm4012774.

(5) Rao, S. P. S.; Lakshminarayana, S. B.; Kondreddi, R. R.; Herve, M.; Camacho, L. R.; Bifani, P.; Kalapala, S. K.; Jiricek, J.; Ma, N. L.; Tan, B. H.; Ng, S. H.; Nanjundappa, M.; Ravindran, S.; Seah, P. G.; Thayalan, P.; Lim, S. H.; Lee, B. H.; Goh, A.; Barnes, W. S.; Chen, Z.; Gagaring, K.; Chatterjee, A. K.; Pethe, K.; Kuhen, K.; Walker, J.; Feng, G.; Babu, S.; Zhang, L.; Blasco, F.; Beer, D.; Weaver, M.; Dartois, V.; Glynne, R.; Dick, T.; Smith, P. W.; Diagana, T. T.; Manjunatha, U. H. Indolcarboxamide Is a Preclinical Candidate for Treating Multidrug-Resistant Tuberculosis. *Sci. Transl. Med.* **2013**, *5* (214), 214ra168. https://doi.org/10.1126/scitranslmed.3007355.

(6) Yang, X.; Hu, T.; Yang, X.; Xu, W.; Yang, H.; Guddat, L. W.; Zhang, B.; Rao, Z. Structural Basis for the Inhibition of Mycobacterial MmpL3 by NITD- 349 and SPIRO. *J. Mol. Biol.* **2020**, *432* (16), 4426–4434. https://doi.org/10.1016/j.jmb.2020.05.019.

(7) Lun, S.; Tasneen, R.; Chaira, T.; Stec, J.; Onajole, O. K.; Yang, T. J.; Cooper, C. B.; Mdluli, K.; Converse, P. J.; Nuermberger, E. L.; Raj, V. S.; Kozikowski, A.; Bishai, W. R. Advancing the Therapeutic Potential of Indoleamides for Tuberculosis. *Antimicrob. Agents Chemother.* **2019**, *63* (7), e00343-19. https://doi.org/10.1128/AAC.00343-19.

(8) Li, W.; Sanchez-Hidalgo, A.; Jones, V.; Moura, V. C. N. de; North, E. J.; Jackson, M. Synergistic Interactions of MmpL3 Inhibitors with Antitubercular Compounds *in vitro*. *Antimicrob. Agents Chemother.* **2017**, *61* (4), e02399-16. https://doi.org/10.1128/AAC.02399-16.

(9) Lun, S.; Guo, H.; Onajole, O. K.; Pieroni, M.; Gunosewoyo, H.; Chen, G.; Tipparaju, S. K.; Ammerman, N. C.; Kozikowski, A. P.; Bishai, W. R. Indoleamides Are Active against Drug-Resistant *Mycobacterium tuberculosis*. *Nat. Commun.* **2013**, *4*, 2907. https://doi.org/10.1038/ncomms3907.

(10) Zhang, B.; Li, J.; Yang, X.; Wu, L.; Zhang, J.; Yang, Y.; Zhao, Y.; Zhang, L.; Yang, X.; Yang, X.; Cheng, X.; Liu, Z.; Jiang, B.; Jiang, H.; Guddat, L. W.; Yang, H.; Rao, Z. Crystal Structures of Membrane Transporter MmpL3, an Anti-TB Drug Target. *Cell* **2019**, *176* (3), 636–648. https://doi.org/10.1016/j.cell.2019.01.003.

(11) Tan, Y. J.; Li, M.; Gunawan, G. A.; Nyantakyi, S. A.; Dick, T.; Go, M.-L.; Lam, Y. Amide−Amine Replacement in Indole-2-Carboxamides Yields Potent Mycobactericidal Agents with Improved Water Solubility. *ACS Med. Chem. Lett.* **2020**, *12* (5), 704–712. https://doi.org/10.1021/acsmedchemlett.0c00588.

(12) Alsayed, S. S. R.; Lun, S.; Luna, G.; Beh, C. C.; Payne, A. D.; Foster, N.; Bishai, W. R.; Gunosewoyo, H. Design, Synthesis, and Biological Evaluation of Novel Arylcarboxamide Derivatives as Anti-Tubercular Agents. *RSC Adv.* **2020**, *10* (13), 7523–7540. https://doi.org/10.1039/c9ra10663d.

(13) Alsayed, S. S. R.; Lun, S.; Payne, A.; Bishai, W. R.; Gunosewoyo, H. Design, Synthesis and Antimycobacterial Evaluation of Novel Adamantane and Adamantanol Analogues Effective against Drug-Resistant Tuberculosis. *Bioorg. Chem.* **2021**, *106*, 104486. https://doi.org/10.1016/j.bioorg.2020.104486.

(14) Ray, R.; Birangal, S. R.; Fathima, F.; Boshoff, H. I.; Forbes, H. E.; Hariharapura, R. C.; Shenoy, G. G. Molecular Insights into Mmpl3 Lead to the Development of Novel Indole-2-Carboxamides as Antitubercular Agents. *Mol. Syst. Des. Eng.* **2022**, *7* (6), 592–606. https://doi.org/10.1039/d1me00122a.

(15) Bhakhar, K. A.; Vaghela, P. V.; Varakala, S. D.; Chudasma, S. J.; Gajjar, N. D.; Nagar, P. R.; Sriram, D.; Dhameliya, T. M. Indole-2-Carboxamides as New Anti-Mycobacterial Agents: Design, Synthesis, Biological Evaluation and Molecular Modeling against MmpL3. *ChemistrySelect* **2022**, *7* (26), e202201813. https://doi.org/10.1002/slct.202201813.

(16) Umare, M. D.; Khedekar, P. B.; Chikhale, R. V. Mycobacterial Membrane Protein Large 3 (MmpL3) Inhibitors: A Promising Approach to Combat Tuberculosis. *ChemMedChem* **2021**, *16* (20), 3136–3148. https://doi.org/10.1002/cmdc.202100359.

(17) Shao, M.; McNeil, M.; Cook, G. M.; Lu, X. MmpL3 Inhibitors as Antituberculosis Drugs. *Eur. J. Med. Chem.* **2020**, *200*, 112390. https://doi.org/10.1016/j.ejmech.2020.112390.

(18) Sethiya, J. P.; Sowards, M. A.; Jackson, M.; North, E. J. MmpL3 Inhibition: A New Approach to Treat Nontuberculous Mycobacterial Infections. *Int. J. Mol. Sci.* **2020**, *21* (17), 6202. https://doi.org/10.3390/ijms21176202.

(19) Kozikowski, A. P.; Onajole, O. K.; Stec, J.; Dupont, C.; Viljoen, A.; Richard, M.; Chaira, T.; Lun, S.; Bishai, W.; Raj, V. S.; Ordway, D.; Kremer, L. Targeting Mycolic Acid Transport by Indole-2-Carboxamides for the Treatment of *Mycobacterium abscessus* Infections. *J. Med. Chem.* **2017**, *60* (13), 5876–5888. https://doi.org/10.1021/acs.jmedchem.7b00582.

(20) Pandya, A. N.; Prathipati, P. K.; Hegde, P.; Li, W.; Graham, K. F.; Mandal, S.; Drescher, K. M.; Destache, C. J.; Ordway, D.; Jackson, M.; North, E. J. Indole-2-Carboxamides Are Active against *Mycobacterium abscessus* in a Mouse Model of Acute Infection. *Antimicrob. Agents Chemother.* **2019**, *63* (3), e02245-18. https://doi.org/10.1128/AAC.02245-18.

(21) Raynaud, C.; Daher, W.; Roquet-Banères, F.; Johansen, M. D.; Stec, J.; Onajole, O. K.; Ordway, D.; Kozikowski, A. P.; Kremer, L. Synergistic Interactions of Indole-2-Carboxamides and β-Lactam Antibiotics against *Mycobacterium abscessus*. *Antimicrob. Agents Chemother.* **2020**, *64* (5), e02548-19. https://doi.org/10.1128/AAC.02548-19.

(22) Viljoen, A.; Herrmann, J.-L.; Onajole, O. K.; Stec, J.; Kozikowski, A. P.; Kremer, L. Controlling Extra- and Intramacrophagic Mycobacterium Abscessus by Targeting Mycolic Acid Transport. *Front. Cell. Infect. Microbiol.* **2017**, *7*, 388. https://doi.org/10.3389/fcimb.2017.00388.

(23) Franz, N. D.; Belardinelli, J. M.; Kaminski, M. A.; Dunn, L. C.; de Moura, V. C. N.; Blaha, M. A.; Truong, D. D.; Li, W.; Jackson, M.; North, E. J. Design, Synthesis and Evaluation of Indole-2-Carboxamides with Pan Anti-Mycobacterial Activity. *Bioorg. Med. Chem.* **2017**, *25* (14), 3746–3755. https://doi.org/10.1016/j.bmc.2017.05.015.

(24) Alsayed, S. S. R.; Lun, S.; Bailey, A. W.; Suri, A.; Huang, C.-C.; Mocerino, M.; Payne, A.; Sredni, S. T.; Bishai, W. R.; Gunosewoyo, H. Design, Synthesis and Evaluation of Novel Indole-2-Carboxamides for Growth Inhibition of *Mycobacterium tuberculosis* and Paediatric Brain Tumour Cells. *RSC Adv.* **2021**, *11* (26), 15497–15511.

https://doi.org/10.1039/d0ra10728j.

(25) Makarov, V.; Manina, G.; Mikusova, K.; Möllmann, U.; Ryabova, O.; Saint-Joanis, B.; Dhar, N.; Pasca, M. R.; Buroni, S.; Lucarelli, A. P.; Milano, A.; Rossi, E. De; Belanova, M.; Bobovska, A.; Dianiskova, P.; Kordulakova, J.; Sala, C.; Fullam, E.; Schneider, P.; Mckinney, J. D.; Brodin, P.; Christophe, T.; Waddell, S.; Butcher, P.; Albrethsen, J.; Rosenkrands, I.; Brosch, R.; Nandi, V.; Bharath, S.; Gaonkar, S.; Shandil, R. K.; Balasubramanian, V.; Balganesh, T.; Tyagi, S.; Grosset, J.; Riccardi, G.; Cole, S. T. Benzothiazinones Kill *Mycobacterium tuberculosis* by Blocking Arabinan Synthesis. *Science (80-. ).* **2009**, *324* (5928), 801–804. https://doi.org/10.1126/science.1171583.

(26) Makarov, V. A.; Cole, S. T.; Möllmann, U. Patent EP2029583 B1. *2010*.

(27) Pasca, M. R.; Degiacomi, G.; Riberio, A. L. J. L.; Zara, F.; Mori, P. De; Heym, B.; Mirrione, M.; Brerra, R.; Pagani, L.; Pucillo, L.; Troupioti, P.; Makarov, V.; Cole, S. T.; Riccardi, G. Clinical Isolates of *Mycobacterium tuberculosis* in Four European Hospitals Are Uniformly Susceptible to Benzothiazinones. *Antimicrob. Agents Chemother.* **2010**, *54* (4), 1616–1618. https://doi.org/10.1128/AAC.01676-09.

(28) Trefzer, C.; Rengifo-Gonzalez, M.; Hinner, M. J.; Schneider, P.; Makarov, V.; Cole, S. T.; Johnsson, K. Benzothiazinones: Prodrugs That Covalently Modify the Decaprenylphosphoryl-β-$_D$-Ribose 2′-Epimerase DprE1 of *Mycobacterium tuberculosis*. *J. Am. Chem. Soc.* **2010**, *132* (39), 13663–13665. https://doi.org/10.1021/ja106357w.

(29) Trefzer, C.; Škovierová, H.; Buroni, S.; Bobovská, A.; Nenci, S.; Molteni, E.; Pojer, F.; Pasca, M. R.; Makarov, V.; Cole, S. T.; Riccardi, G.; Mikušová, K.; Johnsson, K. Benzothiazinones Are Suicide Inhibitors of Mycobacterial Decaprenylphosphoryl-β-$_D$-Ribofuranose 2′-Oxidase DprE1. *J. Am. Chem. Soc.* **2012**, *134* (2), 912–915. https://doi.org/10.1021/ja211042r.

(30) Tiwari, R.; Moraski, G. C.; Krchňák, V.; Miller, P. A.; Colon-Martinez, M.; Herrero, E.; Oliver, A. G.; Miller, M. J. Thiolates Chemically Induce Redox Activation of BTZ043 and Related Potent Nitroaromatic Anti-Tuberculosis Agents. *J. Am. Chem. Soc.* **2013**, *135* (9), 3539–3549. https://doi.org/10.1021/ja311058q.

(31) Liu, R.; Krchnak, V.; Brown, S. N.; Miller, M. J. Deuteration of BTZ043 Extends the Lifetime of Meisenheimer Intermediates to the Antituberculosis Nitroso Oxidation State. *ACS Med. Chem. Lett.* **2019**, *10* (10), 1462–1466. https://doi.org/10.1021/acsmedchemlett.9b00308.

(32) Makarov, V.; Lechartier, B.; Zhang, M.; Neres, J.; van der Sar, A. M.; Raadsen, S. A.; Hartkoorn, R. C.; Ryabova, O. B.; Vocat, A.; Decosterd, L. A.; Widmer, N.; Buclin, T.; Bitter, W.; Andries, K.; Pojer, F.; Dyson, P. J.; Cole, S. T. Towards a New Combination Therapy for Tuberculosis with next Generation Benzothiazinones. *EMBO Mol. Med.* **2014**, *6* (3), 372–383. https://doi.org/10.1002/emmm.201303575.

(33) Batt, S. M.; Jabeen, T.; Bhowruth, V.; Quill, L.; Lund, P. A.; Eggeling, L.; Alderwick, L. J.; Fütterer, K.; Besra, G. S. Structural Basis of Inhibition of *Mycobacterium tuberculosis* DprE1 by Benzothiazinone Inhibitors. *Proc. Natl. Acad. Sci.* **2012**, *109* (28), 11354–11359. https://doi.org/10.1073/pnas.1205735109.

(34) Makarov, V.; Mikušová, K. Development of Macozinone for TB Treatment: An Update. *Appl. Sci.* **2020**, *10* (7), 2269. https://doi.org/10.3390/app10072269.

(35) https://clinicaltrials.gov/ct2/show/NCT04044001.

(36) Piton, J.; Foo, C. S.-Y.; Cole, S. T. Structural Studies of *Mycobacterium tuberculosis* DprE1 Interacting with Its Inhibitors. *Drug Discov. Today* **2017**, *22* (3), 526–533. https://doi.org/10.1016/j.drudis.2016.09.014.

(37) Piton, J.; Vocat, A.; Lupien, A.; Foo, C. S.; Riabova, O.; Makarov, V.; Cole, S. T. Structure-Based Drug Design and Characterization of Sulfonyl- Piperazine Benzothiazinone Inhibitors of DprE1 from *Mycobacterium tuberculosis*. *Antimicrob. Agents Chemother.* **2018**, *62* (10), e00681-18. https://doi.org/10.1128/AAC.00681-18.

(38) Sommer, R.; Neres, J.; Piton, J.; Dhar, N.; Sar, A. van der; Raju, M.; Laroche, T.; Dyson, P. J.; Mckinney, J. D.; Bitter, W.; Makarov, V.; Cole, S. T. Fluorescent Benzothiazinone Analogues Efficiently and Selectively Label DprE1 in Mycobacteria and Actinobacteria. *ACS Chem. Biol.* **2018**, *13* (11), 3184–3192.

https://doi.org/10.1021/acschembio.8b00790.

(39) Karoli, T.; Becker, B.; Zuegg, J.; Möllmann, U.; Ramu, S.; Huang, J. X.; Cooper, M. A. Identification of Antitubercular Benzothiazinone Compounds by Ligand-Based Design. *J. Med. Chem.* **2012**, *55* (17), 7940–7944. https://doi.org/10.1021/jm3008882.

(40) Gao, C.; Ye, T.-H.; Wang, N.-Y.; Zeng, X.-X.; Zhang, L.-D.; Xiong, Y.; You, X.-Y.; Xia, Y.; Xu, Y.; Peng, C.-T.; Zuo, W.-Q.; Wei, Y.; Yu, L.-T. Synthesis and Structure–Activity Relationships Evaluation of Benzothiazinone Derivatives as Potential Anti-Tubercular Agents. *Bioorg. Med. Chem. Lett.* **2013**, *23* (17), 4919–4922. https://doi.org/10.1016/j.bmcl.2013.06.069.

(41) Tiwari, R.; Miller, P. A.; Cho, S.; Franzblau, S. G.; Miller, M. J. Syntheses and Antituberculosis Activity of 1,3-Benzothiazinone Sulfoxide and Sulfone Derived from BTZ043. *ACS Med. Chem. Lett.* **2015**, *6* (2), 128–133. https://doi.org/10.1021/ml5003458.

(42) Gao, C.; Peng, C.; Shi, Y.; You, X.; Ran, K.; Xiong, L.; Ye, T.-H.; Zhang, L.; Wang, N.; Zhu, Y.-X.; Liu, K.; Zuo, W.; Yu, L.; Wei, Y. Benzothiazinethione Is a Potent Preclinical Candidate for the Treatment of Drug-Resistant Tuberculosis. *Sci. Rep.* **2016**, *6*, 29717. https://doi.org/10.1038/srep29717.

(43) Zhang, R.; Lv, K.; Wang, B.; Li, L.; Wang, B.; Liu, M.; Guo, H.; Wanga, A.; Lu, Y. Design, Synthesis and Antitubercular Evaluation of Benzothiazinones Containing an Oximido or Amino Nitrogen Heterocycle Moiety. *RSC Adv.* **2017**, *7* (3), 1480–1483. https://doi.org/10.1039/C6RA25712G.

(44) Wang, A.; Lv, K.; Tao, Z.; Gu, J.; Fu, L.; Liu, M.; Wan, B.; Franzblau, S. G.; Ma, C.; Ma, X.; Han, B.; Wang, A.; Xu, S.; Lu, Y. Identification of Benzothiazinones Containing an Oxime Functional Moiety as New Anti-Tuberculosis Agents. *Eur. J. Med. Chem.* **2019**, *181*, 111595. https://doi.org/10.1016/j.ejmech.2019.111595.

(45) Peng, C.-T.; Gao, C.; Wang, N.-Y.; You, X.-Y.; Zhang, L.-D.; Zhu, Y.-X.; Xv, Y.; Zuo, W.-Q.; Ran, K.; Deng, H.-X.; Lei, Q.; Xiao, K.-J.; Yu, L.-T. Synthesis and Antitubercular Evaluation of 4-Carbonyl Piperazine Substituted 1,3-Benzothiazin-4-One Derivatives. *Bioorganic Med. Chem. Lett.* **2015**, *25* (7), 1373–1376. https://doi.org/10.1016/j.bmcl.2015.02.061.

(46) Xiong, L.; Gao, C.; Shi, Y.-J.; Tao, X.; Rong, J.; Liu, K.-L.; Peng, C.-T.; Wang, N.-Y.; Lei, Q.; Zhang, Y.-W.; Yu, L.-T.; Wei, Y.-Q. Identification of a New Series of Benzothiazinone Derivatives with Excellent Antitubercular Activity and Improved Pharmacokinetic Profile. *RSC Adv.* **2018**, *8* (20), 11163–11176. https://doi.org/10.1039/c8ra00720a.

(47) Li, P.; Wang, B.; Zhang, X.; Batt, S. M.; Besra, G. S.; Zhang, T.; Ma, C.; Zhang, D.; Lin, Z.; Li, G.; Huang, H.; Lu, Y. Identification of Novel Benzothiopyranone Compounds against *Mycobacterium tuberculosis* through Scaffold Morphing from Benzothiazinones. *Eur. J. Med. Chem.* **2018**, *160*, 157–170. https://doi.org/10.1016/j.ejmech.2018.09.042.

(48) Lv, K.; Tao, Z.; Liu, Q.; Yang, L.; Wang, B.; Wu, S.; Wang, A.; Huang, M.; Liu, M.; Lu, Y. Design, Synthesis and Antitubercular Evaluation of Benzothiazinones Containing a Piperidine Moiety. *Eur. J. Med. Chem.* **2018**, *151*, 1–8. https://doi.org/10.1016/j.ejmech.2018.03.060.

(49) Zhang, G.; Howe, M.; Aldrich, C. C. Spirocyclic and Bicyclic 8-Nitrobenzothiazinones for Tuberculosis with Improved Physicochemical and Pharmacokinetic Properties. *ACS Med. Chem. Lett.* **2019**, *10* (3), 348–351. https://doi.org/10.1021/acsmedchemlett.8b00634.

(50) Lv, K.; You, X.; Wang, B.; Wei, Z.; Chai, Y.; Wang, B.; Wang, A.; Huang, G.; Liu, M.; Lu, Y. Identification of Better Pharmacokinetic Benzothiazinone Derivatives as New Antitubercular Agents. *ACS Med. Chem. Lett.* **2017**, *8* (6), 636–641. https://doi.org/10.1021/acsmedchemlett.7b00106.

(51) Lv, K.; Wang, A.; Tao, Z.; Fu, L.; Liu, H.; Wang, B.; Ma, C.; Wang, H.; Ma, X.; Han, B.; Wang, A.; Zhang, K.; Liu, M.; Lu, Y. HERG Optimizations of IMB1603, Discovery of Alternative Benzothiazinones as New Antitubercular Agents. *Eur. J. Med. Chem.* **2019**, *179*, 208–217. https://doi.org/10.1016/j.ejmech.2019.06.053.

(52) Ma, X.; Han, B.; Wang, A.; Yang, L.; Huang, M.; Chowdhury, K.; Gu, J.; Zhang, K.; Lv,

K. Identification of Benzothiazones Containing a Hexahydropyrrolo[3,4-c]Pyrrol Moiety as Antitubercular Agents against MDR-MTB. *RSC Adv.* **2020**, *10* (24), 14410–14414. https://doi.org/10.1039/d0ra00750a.

(53) Wang, A.; Ma, C.; Chai, Y.; Liu, X.; Lv, K.; Fu, L.; Wang, B.; Jia, X.; Liu, M.; Lu, Y. Identification of Benzothiazinones Containing 2-Benzyl-2,7-Diazaspiro [3.5]Nonane Moieties as New Antitubercular Agents. *Eur. J. Med. Chem.* **2020**, *200*, 112409. https://doi.org/10.1016/j.ejmech.2020.112409.

(54) Wang, A.; Lu, Y.; Lv, K.; Ma, C.; Xu, S.; Wang, B.; Wang, A.; Xia, G.; Liu, M. Design, Synthesis and Antimycobacterial Activity of New Benzothiazinones Inspired by Rifampicin/Rifapentine. *Bioorg. Chem.* **2020**, *102*, 104135. https://doi.org/10.1016/j.bioorg.2020.104135.

(55) Liu, L.; Kong, C.; Fumagalli, M.; Savková, K.; Xu, Y.; Huszár, S.; Sammartino, J. C.; Fan, D.; Chiarelli, L. R.; Mikušová, K.; Sun, Z.; Qiao, C. Design, Synthesis and Evaluation of Covalent Inhibitors of DprE1 as Antitubercular Agents. *Eur. J. Med. Chem.* **2020**, *208*, 112773. https://doi.org/10.1016/j.ejmech.2020.112773.

(56) Wang, A.; Xu, S.; Chai, Y.; Xia, G.; Wang, B.; Lv, K.; Ma, C.; Wang, D.; Wang, A.; Qin, X.; Liu, M.; Lu, Y. Design, Synthesis and Biological Activity of N-(Amino)Piperazine-Containing Benzothiazinones against *Mycobacterium tuberculosis*. *Eur. J. Med. Chem.* **2021**, *218*, 113398. https://doi.org/10.1016/j.ejmech.2021.113398.

(57) Zhang, G.; Sheng, L.; Hegde, P.; Li, Y.; Aldrich, C. C. 8-Cyanobenzothiazinone Analogs with Potent Antitubercular Activity. *Med. Chem. Res.* **2021**, *30* (2), 449–458. https://doi.org/10.1007/s00044-020-02676-4.

(58) Fan, D.; Wang, B.; Stelitano, G.; Savková, K.; Shi, R.; Huszár, S.; Han, Q.; Mikušová, K.; Chiarelli, L. R.; Lu, Y.; Qiao, C. Structural and Activity Relationships of 6-Sulfonyl-8-Nitrobenzothiazinones as Antitubercular Agents. *J. Med. Chem.* **2021**, *64* (19), 14526–14539. https://doi.org/10.1021/acs.jmedchem.1c01049.

(59) Li, P.; Wang, B.; Fu, L.; Guo, K.; Ma, C.; Wang, B.; Lin, Z.; Li, G.; Huang, H.; Lu, Y. Identification of Novel Benzothiopyranones with Ester and Amide Motifs Derived from Active Metabolite as Promising Leads against *Mycobacterium tuberculosis*. *Eur. J. Med. Chem.* **2021**, *222*, 113603. https://doi.org/10.1016/j.ejmech.2021.113603.

(60) Neres, J.; Pojer, F.; Molteni, E.; Chiarelli, L. R.; Dhar, N.; Boy-Röttger, S.; Buroni, S.; Fullam, E.; Degiacomi, G.; Lucarelli, A. P.; Read, R. J.; Zanoni, G.; Edmondson, D. E.; Rossi, E. De; Pasca, M. R.; Mckinney, J. D.; Dyson, P. J.; Riccardi, G.; Mattevi, A.; Cole, S. T.; Binda, C. Structural Basis for Benzothiazinone-Mediated Killing of *Mycobacterium tuberculosis*. *Sci. Transl. Med.* **2012**, *4* (150), 150ra121. https://doi.org/10.1126/scitranslmed.3004395.

(61) Makarov, V.; Neres, J.; Hartkoorn, R. C.; Ryabova, O. B.; Kazakova, E.; Šarkan, M.; Huszár, S.; Piton, J.; Kolly, G. S.; Vocat, A.; Conroy, T. M.; Mikušová, K.; Cole, S. T. The 8-Pyrrole-Benzothiazinones Are Noncovalent Inhibitors of DprE1 from *Mycobacterium tuberculosis*. *Antimicrob. Agents Chemother.* **2015**, *59* (8), 4446–4452. https://doi.org/10.1128/AAC.00778-15.

(62) Tiwari, R.; Miller, P. A.; Chiarelli, L. R.; Mori, G.; Michal, Š.; Centárová, I.; Cho, S.; Mikušová, K.; Franzblau, S. G.; Oliver, A. G.; Miller, M. J. Design, Syntheses, and Anti-TB Activity of 1,3-Benzothiazinone Azide and Click Chemistry Products Inspired by BTZ043. *ACS J. Med. Chem.* **2016**, *7* (3), 266–270. https://doi.org/10.1021/acsmedchemlett.5b00424.

(63) Madikizela, B.; Eckhardt, T.; Goddard, R.; Richter, A.; Lins, A.; Lehmann, C.; Imming, P.; Seidel, R. W. Synthesis, Structural Characterization and Antimycobacterial Evaluation of Several Halogenated Non-Nitro Benzothiazinones. *Med. Chem. Res.* **2021**, *30* (8), 1523–1533. https://doi.org/10.1007/s00044-021-02735-4.

(64) Ying, Z.; Wai, Y. W.; Barer, M. R. Targeting Persisters for Tuberculosis Control. *Antimicrob. Agents Chemother.* **2012**, *56* (5), 2223–2230. https://doi.org/10.1128/AAC.06288-11.

(65) Leistikow, R. L.; Morton, R. A.; Bartek, I. L.; Frimpong, I.; Wagner, K.; Voskuil, M. I. The *Mycobacterium tuberculosis* DosR Regulon Assists in Metabolic Homeostasis and

Enables Rapid Recovery from Nonrespiring Dormancy. *J. Bacteriol.* **2010**, *192* (6), 1662–1670. https://doi.org/10.1128/JB.00926-09.

(66) Kumar, A.; Toledo, J. C.; Patel, R. P.; Lancaster Jr, J. R.; Steyn, A. J. C. *Mycobacterium tuberculosis* DosS Is a Redox Sensor and DosT Is a Hypoxia Sensor. *Proc. Natl. Acad. Sci.* **2007**, *104* (28), 11568–11573. https://doi.org/10.1073/pnas.0705054104.

(67) Boon, C.; Dick, T. *Mycobacterium bovis* BCG Response Regulator Essential for Hypoxic Dormancy. *J. Bacteriol.* **2002**, *184* (24), 6760–6767. https://doi.org/10.1128/JB.184.24.6760–6767.2002.

(68) Belardinelli, J. M.; Verma, D.; Li, W.; Avanzi, C.; Wiersma, C. J.; Williams, J. T.; Johnson, B. K.; Zimmerman, M.; Whittel, N.; Angala, B.; Wang, H.; Jones, V.; Dartois, V.; Moura, V. C. N. de; Gonzalez-Juarrero, M.; Pearce, C.; Schenkel, A. R.; Malcolm, K. C.; Nick, J. A.; Charman, S. A.; Wells, T. N. C.; Podell, B. K.; Vennerstrom, J. L.; Ordway, D. J.; Abramovitch, R. B.; Jackson, M. Therapeutic Efficacy of Antimalarial Drugs Targeting DosRS Signaling in *Mycobacterium abscessus*. *Sci. Transl. Med.* **2022**, *14* (633), eabj3860. https://doi.org/10.1126/scitranslmed.abj3860.

(69) Uddin, A.; Chawla, M.; Irfan, I.; Mahajan, S.; Shailja, S.; Mohammad, A. Medicinal Chemistry Updates on Quinoline- and Endoperoxide-Based Hybrids with Potent Antimalarial Activity. *RSC Med. Chem.* **2021**, *12* (1), 24–42. https://doi.org/10.1039/d0md00244e.

(70) Alkhzem, A. H.; Woodman, T. J.; Blagbrough, I. S. Design and Synthesis of Hybrid Compounds as Novel Drugs and Medicines. *RSC Adv.* **2022**, *12* (30), 19470–19484. https://doi.org/10.1039/d2ra03281c.

(71) Oliveira, R.; Guedes, R. C.; Meireles, P.; Albuquerque, I. S.; Gonçalves, L. M.; Pires, E.; Bronze, M. R.; Gut, J.; Rosenthal, P. J.; Prudêncio, M.; Moreira, R.; O'Neill, P. M.; Lopes, F. Tetraoxane−Pyrimidine Nitrile Hybrids as Dual Stage Antimalarials. *J. Med. Chem.* **2014**, *57* (11), 4916–4923. https://doi.org/10.1021/jm5004528.

(72) Capela, R.; Magalhães, J.; Miranda, D.; Machado, M.; Sanches-Vaz, M.; Albuquerque, I. S.; Sharma, M.; Gut, J.; Rosenthal, P. J.; Frade, R.; Perry, M. J.; Moreira, R.; Prudêncio, M.; Lopes, F. Endoperoxide-8-Aminoquinoline Hybrids as Dual-Stage Antimalarial Agents with Enhanced Metabolic Stability. *Eur. J. Med. Chem.* **2018**, *149*, 69–78. https://doi.org/10.1016/j.ejmech.2018.02.048.

(73) Coslédan, F.; Fraisse, L.; Pellet, A.; Guillou, F.; Mordmüller, B.; Kremsner, P. G.; Moreno, A.; Mazier, D.; Maffrand, J.-P.; Meunier, B. Selection of a Trioxaquine as an Antimalarial Drug Candidate. *Proc. Natl. Acad. Sci.* **2008**, *105* (45), 17579–17584. https://doi.org/10.1073/pnas.0804338105.

(74) Garah, F. B.; Claparols, C.; Benoit-Vical, F.; Meunier, B.; Robert, A. The Antimalarial Trioxaquine DU1301 Alkylates Heme in Malaria-Infected Mice. *Antimicrob. Agents Chemother.* **2008**, *52* (8), 2966–2969. https://doi.org/10.1128/AAC.00165-08.

(75) Wang, N.; Wicht, K. J.; Shaban, E.; Ngoc, T. A.; Wang, M.-Q.; Hayashi, I.; Hossain, M. I.; Takemasa, Y.; Kaiser, M.; El Tantawy El Sayed, I.; Egan, T. J.; Inokuchi, T. Synthesis and Evaluation of Artesunate–Indoloquinoline Hybrids as Antimalarial Drug Candidates. *Medchemcomm* **2014**, *5* (7), 927–931. https://doi.org/10.1039/C4MD00091A.

(76) Laurent, S. A.-L.; Boissier, J.; Coslédan, F.; Gornitzka, H.; Robert, A.; Meunier, B. Synthesis of "Trioxaquantel"® Derivatives as Potential New Antischistosomal Drugs. *European J. Org. Chem.* **2008**, *2008* (5), 895–913. https://doi.org/10.1002/ejoc.200700975.

(77) Miranda, D.; Capela, R.; Albuquerque, I. S.; Meireles, P.; Paiva, I.; Nogueira, F.; Amewu, R.; Gut, J.; Rosenthal, P. J.; Oliveira, R.; Mota, M. M.; Moreira, R.; Marti, F.; Prudeîncio, M.; O'Neill, P. M.; Lopes, F. Novel Endoperoxide-Based Transmission-Blocking Antimalarials with Liver- and Blood-Schizontocidal Activities. *ACS Med. Chem. Lett.* **2014**, *5* (2), 108–112. https://doi.org/10.1021/ml4002985.

(78) Amado, P. S. M.; Costa, I. C. C.; Paixão, J. A.; Mendes, R. F.; Cortes, S.; Cristiano, M. L. S. Synthesis, Structure and Antileishmanial Evaluation of Endoperoxide–Pyrazole Hybrids. *Molecules* **2022**, *27* (17), 5401. https://doi.org/10.3390/molecules27175401.

(79) Woodley, C. M.; Amado, P. S. M.; Cristiano, M. L. S.; O'Neill, P. M. Artemisinin Inspired

Synthetic Endoperoxide Drug Candidates: Design, Synthesis, and Mechanism of Action Studies. *Med. Res. Rev.* **2021**, *41* (6), 3062–3095. https://doi.org/10.1002/med.21849.

(80) Vennerstrom, J. L.; Arbe-Barnes, S.; Brun, R.; Charman, S. A.; Chiu, F. C. K.; Chollet, J.; Dong, Y.; Dorn, A.; Hunziker, D.; Matile, H.; McIntosh, K.; Padmanilayam, M.; Santo Tomas, J.; Scheurer, C.; Scorneaux, B.; Tang, Y.; Urwyler, H.; Wittlin, S.; Charman, W. N. Identification of an Antimalarial Synthetic Trioxolane Drug Development Candidate. *Nature* **2004**, *430* (7002), 900–904. https://doi.org/10.1038/nature02779.

(81) O'Neill, P. M.; Amewu, R. K.; Charman, S. A.; Sabbani, S.; Gnädig, N. F.; Straimer, J.; Fidock, D. A.; Shore, E. R.; Roberts, N. L.; Wong, M. H.-L.; Hong, W. D.; Pidathala, C.; Riley, C.; Murphy, B.; Aljayyoussi, G.; Gamo, F. J.; Sanz, L.; Rodrigues, J.; Cortes, C. G.; Herreros, E.; Angulo-Barturén, I.; Jiménez-Díaz, M. B.; Bazaga, S. F.; Martínez-Martínez, M. S.; Campo, B.; Sharma, R.; Ryan, E.; Shackleford, D. M.; Campbell, S.; Smith, D. A.; Wirjanata, G.; Noviyanti, R.; Price, R. N.; Marfurt, J.; Palmer, M. J.; Copple, I. M.; Mercer, A. E.; Ruecker, A.; Delves, M. J.; Sinden, R. E.; Siegl, P.; Davies, J.; Rochford, R.; Kocken, C. H. M.; Zeeman, A.-M.; Nixon, G. L.; Biagini, G. A.; Ward, S. A. A Tetraoxane-Based Antimalarial Drug Candidate That Overcomes PfK13-C580Y Dependent Artemisinin Resistance. *Nat. Commun.* **2017**, *8*, 15159. https://doi.org/10.1038/ncomms15159.

(82) Richter, A.; Rudolph, I.; Möllmann, U.; Voigt, K.; Chung, C.-W.; Singh, O. M. P.; Rees, M.; Mendoza-Losana, A.; Bates, R.; Ballell, L.; Batt, S.; Veerapen, N.; Fütterer, K.; Besra, G.; Imming, P.; Argyrou, A. Novel Insight into the Reaction of Nitro, Nitroso and Hydroxylamino Benzothiazinones and of Benzoxacinones with *Mycobacterium tuberculosis* DprE1. *Sci. Rep.* **2018**, *8* (1), 13473. https://doi.org/10.1038/s41598-018-31316-6.

(83) Jiricek, J.; Kondreddi, R. R.; Smith, P. W. International Patent WO2014037900A1.

(84) Lobo, L.; Cabral, L. I. L.; Sena, M. I.; Guerreiro, B.; Rodrigues, A. S.; de Andrade-Neto, V. F.; Cristiano, M. L. S.; Nogueira, F. New Endoperoxides Highly Active *in vivo* and *in vitro* against Artemisinin-Resistant *Plasmodium falciparum*. *Malar. J.* **2018**, *17* (1), 145. https://doi.org/10.1186/s12936-018-2281-x.

(85) Makarov, V. A. WO2011132070A1, 2011.

(86) Richter, A.; Narula, G.; Rudolph, I.; Seidel, R. W.; Wagner, C.; Av-Gay, Y.; Imming, P. Efficient Synthesis of Benzothiazinone Analogues with Activity against Intracellular *Mycobacterium tuberculosis*. *ChemMedChem* **2022**, *17* (6), e202100733. https://doi.org/10.1002/cmdc.202100733.

(87) CCDC, GOLD Suite v5.3. 2014.

(88) Schrodinger LCC. The PyMOL Molecular Graphics System V2.3.3. 2018.

(89) Wernevik, J.; Bergström, F.; Novén, A.; Hulthe, J.; Fredlund, L.; Addison, D.; Holmgren, J.; Strömstedt, P.-E.; Rehnström, E.; Lundbäck, T. A Fully Integrated Assay Panel for Early Drug Metabolism and Pharmacokinetics Profiling. *Assay Drug Dev. Technol.* **2020**, *18* (4), 157–179. https://doi.org/10.1089/adt.2020.970.

(90) Faulkner, J. K.; Smith, K. J. A. Dealkylation and *N*-Oxidation in the Metabolism of I-Diethylcarbamyl-4-Methylpiperazine in the Rat. *Xenobiotica* **1972**, *2* (1), 59–68. https://doi.org/10.3109/00498257209036234.

(91) Hyland, R.; Roe, E. G. H.; Jones, B. C.; Smith, D. A. Identification of the Cytochrome P450 Enzymes Involved in the *N*-Demethylation of Sildenafil. *Br. J. Clin. Pharmacol.* **2001**, *51* (3), 239–248. https://doi.org/10.1046/j.1365-2125.2001.00318.x.

(92) An, X.; Zha, Q.; Wu, Y. Perhydrolysis in Ethereal $H_2O_2$ Mediated by $MoO_2(Acac)_2$: Distinct Chemoselectivity between Ketones, Ketals, and Epoxides. *Org. Lett.* **2019**, *21* (5), 1542–1546. https://doi.org/10.1021/acs.orglett.9b00425.

(93) Kwiatkowski, M. R.; Alexanian, E. J. Synthetic Methods Nickel-Catalyzed Mizoroki – Heck-Type Reactions of Unactivated Alkyl Bromides. *Angew. Chemie - Int. Ed.* **2018**, *57* (51), 16857–16860. https://doi.org/10.1002/anie.201810757.

(94) Sabbani, S.; Stocks, P. A.; Ellis, G. L.; Davies, J.; Hedenstrom, E.; Ward, S. A.; Neill, P. M. O. Piperidine Dispiro-1,2,4-Trioxane Analogues. *Bioorg. Med. Chem. Lett.* **2008**, *18* (21), 5804–5808. https://doi.org/10.1016/j.bmcl.2008.09.052.

(95) Han, G.; Tamaki, M.; Hruby, V. J. Fast, Efficient and Selective Deprotection of the Tert-Butoxycarbonyl (Boc) Group Using HCl/Dioxane (4 M). *J. Pept. Res.* **2001**, *58* (4), 338–341. https://doi.org/10.1034/j.1399-3011.2001.00935.x.

(96) Jin, T.-S.; Wang, H.-X.; Wang, K.-F.; Li, T.-S. Synthesis of Diacetals from Aldehydes and Ketones with Pentaerythritol Catalyzed by Silica Sulfate Under Microwave Irradiation. *Synth. Commun.* **2004**, *34* (16), 2993–2999. https://doi.org/10.1081/SCC-200026658.

(97) Opsenica, I.; Opsenica, D.; Lanteri, C. A.; Anova, L.; Milhous, W. K.; Smith, K. S.; Šolaja, B. A. New Chimeric Antimalarials with 4-Aminoquinoline Moiety Linked to a Tetraoxane Skeleton. *J. Med. Chem.* **2008**, *51* (19), 6216–6219. https://doi.org/10.1021/jm8006905.

(98) Cooper, M.; Zuegg, J.; Becker, B.; Tomislav, K. AU2012310242A1. 2011.

(99) Tang, Y.; Dong, Y.; Karle, J. M.; DiTusa, C. A.; Vennerstrom, J. L. Synthesis of Tetrasubstituted Ozonides by the Griesbaum Coozonolysis Reaction: Diastereoselectivity and Functional Group Transformations by Post-Ozonolysis Reactions. *J. Org. Chem.* **2004**, *69* (19), 6470–6473. https://doi.org/10.1021/jo040171c.

(100) Sureshbabu, V. V; Venkataramanarao, R.; Naik, S. A.; Chennakrishnareddy, G. Synthesis of Tetrazole Analogues of Amino Acids Using Fmoc Chemistry : Isolation of Amino Free Tetrazoles and Their Incorporation into Peptides. *Tetrahedron Lett.* **2007**, *48* (39), 7038–7041. https://doi.org/10.1016/j.tetlet.2007.07.129.

(101) Spartan18. Wavefunction inc.: Irvine, CA 2019.

(102) Hong, W. D.; Gibbons, P. D.; Leung, S. C.; Amewu, R.; Stocks, P. A.; Stachulski, A.; Horta, P.; Cristiano, M. L. S.; Shone, A. E.; Moss, D.; Ardrey, A.; Sharma, R.; Warman, A. J.; Bedingfield, P. T. P.; Fisher, N. E.; Aljayyoussi, G.; Mead, S.; Caws, M.; Berry, N. G.; Ward, S. A.; Biagini, G. A.; O'Neill, P. M.; Nixon, G. L. Rational Design, Synthesis, and Biological Evaluation of Heterocyclic Quinolones Targeting the Respiratory Chain of *Mycobacterium tuberculosis*. *J. Med. Chem.* **2017**, *60* (9), 3703–3726. https://doi.org/10.1021/acs.jmedchem.6b01718.

# Chapter 3

## Computational Analysis of Physicochemical and ADMET Properties of DprE1 Inhibitors and Development of Predictive Classification Models

# Chapter 3

Part of the work described in this section was included in the following publication:

**Amado**, **P. S. M.**; Woodley, C., J. A.; Cristiano, M. L. S. and O'Neill P. M. Recent advances of DprE1 Inhibitors against *Mycobacterium tuberculosis:* Computational Analysis of Physicochemical and ADMET Properties. *ACS Omega.* **2022**, 7, 40659–40681. https://doi.org/10.1021/acsomega.2c05307

## CONTRIBUTIONS

Patrícia S. M. Amado collected all the data, designed, and developed the protocols for the computational studies. Prof. Maria de Lurdes Cristiano, Prof. Neil Berry, and Prof. Paul O'Neill supervised the work and revised the manuscript.

Additionally, the unpublished part of the work described in this section will be included in a manuscript presently under preparation:

**Amado**, **P. S. M**.; Cristiano, M. L. S.; O'Neill, P. M. Classification models on DprE1 inhibitors using machine learning methods. ***Manuscript in preparation.***

# 3.1. Background

DprE1, also known as decaprenylphosphoryl-β-$_D$-ribose 2′-epimerase, is an indispensable flavoenzyme involved in forming the *Mtb* cell wall.[1] It catalyses the two-step epimerization of decaprenyl-phospho-ribose (DPR) to decaprenyl-phospho-arabinose (DPA), the precursor for arabinogalactan and lipoarabinomannan synthesis, in conjunction with decaprenylphosphoryl-$_D$-2-keto erythro pentose reductase (DprE2, **Figure 3.1, A**).[1–3] DprE1 initiates the first step of the epimerization process, where DPR is oxidized to the intermediate decaprenyl-phospho-2'-keto-$_D$-arabinose (DPX), co-factored by flavin adenine dinucleotide (FAD), yielding $FADH_2$. DprE2, which is NADH-dependent, subsequently converts DPX to DPA.[4–6] The epimerization occurs in the periplasmic region, which explains DprE1's vulnerability as a target,[6] making this flavoenzyme a promising target for developing novel therapeutic candidates to tackle TB. The druggable yet promiscuous nature of DprE1 has led to a significant number of DprE1 inhibitors with diverse molecular scaffolds and pharmacological profiles[7–12], as evidenced by an increasing number of publications on the subject. Twenty-three new classes of DprE1 inhibitors with antimycobacterial activity were identified, which are divided into two types, according to their mechanism of action (MoA): (1) covalent binders, where five classes have been shown to irreversibly inhibit DprE1 by generating a covalent adduct with the C387 residue, and (2) non-covalent binders, in which seventeen reported classes were experimentally confirmed to act as competitive inhibitors (**Figure 3.1-B**). Several review articles focusing DprE1 inhibitors have emerged during the last decade, covering both scaffold and docking studies.[7–11,13,14]

In this Chapter, we present an in-depth examination of the physicochemical (PC) properties, to provide a different perspective on creating novel compounds targeting DprE1. Moreover, we produced a total of 105 models. seeking to identify predictive models to discover DprE1 inhibitors by combining a range of molecular fingerprints as descriptors with the construction of classification models with five different modelling algorithms.

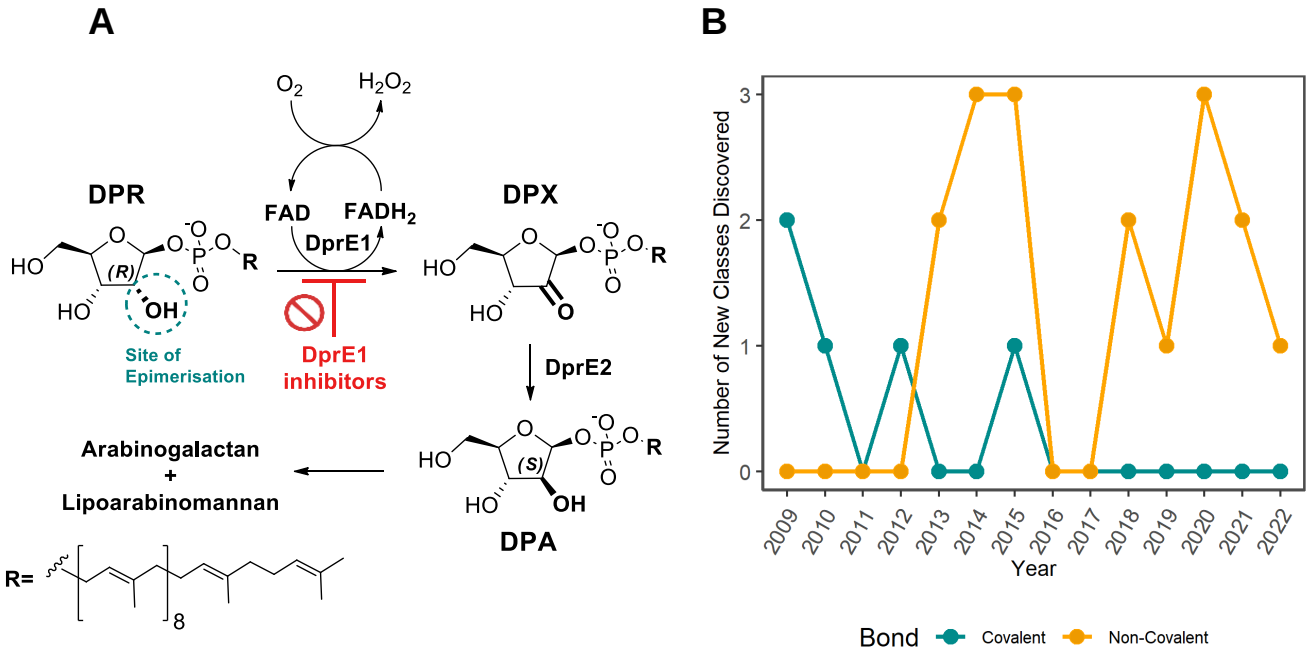


**Figure 3.1. A:** The DPA biosynthetic pathway: in the presence of the co-factor FAD, the DprE1 and DprE2 enzymes catalyse the epimerization of the 2'-OH group in DPR to form DPA. **B**: Timeline of the discovery of the different DprE1 classes.

## 3.2. Physicochemical and ADMET Properties of DprE1 inhibitors

Numerous research groups have examined the connections between small molecules' physicochemical (PC) descriptors, potency, and ADMET profile.[15–17] PC descriptors can affect efficacy, safety, or metabolism. Numerous molecular descriptors have been shown to be useful in predicting ADMET characteristics and have been used to characterize a variety of molecular properties, including lipophilicity, molecular flexibility, hydrogen bonding ability, and molecular weight.[16,18] Additionally, small molecules' based pharmacological candidates must be sufficiently soluble to allow experimental testing, as well as capable to cross through membranes, reach their site of action and activate their main targets, for which the PC descriptors are critical.[19] Research on the chemical space exploration of DprE1 inhibitors found a significant lipophilic character, establishing a different cluster from currently available tuberculosis medicines, as shown by principal component analysis from their physicochemical descriptors analysis.[20] Thus, further research focused on correlations between small molecules' physicochemical (PC) descriptors, potency and ADMET profile is essential to gain new insights for the design and development of highly active covalent and non-

covalent DprE1 inhibitors and guiding hit and lead optimization to produce non-hazardous small molecules' based treatments against *Mtb*.

## 3.2.1. Methods

### 3.2.1.1. Data Collection and Pre-Processing.

To investigate the molecular diversity and ADMET properties of the DprE1 inhibitors disclosed in the literature, for the chemical classes covered in the previous section, we collected a dataset of a total 1519 structurally diverse molecules by reviewing the literature from the year 2009 to April 2022.[21-104]

The dataset was split into two subsets, covalent (Cov) and non-covalent (NCov) binders, and then each compound was classified as active (MIC < 10 μM, **Act**) or not active (MIC ≥ 10 μM, **NAct**), following the MIC cut-off criteria adapted by the report of Makarov *et al.*[13] The PC descriptors considered were molecular weight (MW), lipophilicity through calculated partition coefficient (ClogP), distribution coefficient at pH=7.4 (ClogD), intrinsic aqueous solubility (logS), hydrogen bond acceptors and donors (HBAs and HBDs), topological polar surface area (TPSA), number of rotatable bonds (ROTBS) and Flexibility Index (FInd), which were computed by StarDrop v7.2.0.32905.[105] The Median (Md), Mean (Mn), Standard Deviation (SD), Student *t*-test analyses were implemented and analysed. Known drug design oriented rules such as Lipinski's Rule of 5 (Ro5),[106] GSK's 4/400 rule,[107] and Pfizer's 3/75 rule[108] were also explored in this work. The ADMET predictions, CYP inhibition and metabolism, blood-brain barrier (BBB) penetration, plasma protein binding (PPB), P-glycoprotein (P-gp) substrate classification, and Pan-Assay INterference compoundS (PAINS) count were obtained with StarDrop v7.2.0.32905,[105,109–111] and structure alerts were processed through ChemBioServer 2.0.[112] The generated raw data was then analysed using manual R scripts in RStudio (Version 1.4.1106). Prior to processing, any observation with missing values was removed using `na.omit()` function, and the graphic figures were produced using the `ggplot2` package.

### 3.2.1.2. QSAR Metrics to Evaluate Model Performance

When appropriate, an analysis of the predictive model was conducted in which numerous model performance metrics for a classification model were calculated. Internally, we used four measures: (1) accuracy (Q), (2) precision, (3) sensitivity, and (4) specificity. The following equations show their corresponding definitions:[113]

$$Accuracy\ (Q) = \frac{TP + TN}{TP + TN + FP + FN} \quad (1)$$

$$Precision\ (P) = \frac{TP}{TP + FP} \quad (2)$$

$$Sensitivity\ (SE) = \frac{TP}{TP + FN} \quad (3)$$

$$Specificity\ (SP) = \frac{TN}{TN + FP} \quad (4)$$

where TP are true positives, TN are true negatives, FP are false positives, and FN are false negatives (**Table 3.1**).[113]

**Table 3.1.** An outline of a confusion matrix for a classification model

| | | **Observation** | | |
|---|---|---|---|---|
| | | **Positive** | **Negative** | |
| **Prediction** | **Positive** | True Positive (TP) | False Positive (FP) | **Positive (P)** |
| | **Negative** | False Negative (FN) | True Negative (TN) | **Negative (N)** |
| | | True (T) | False (F) | **Total** |

## 3.2.2. Results and Discussion

### 3.2.2.1. Correlations of MIC with $IC_{50}$ DprE1 and with $CC_{50}$

To establish a correlation between the DprE1 enzyme inhibition and the subsequent MIC between the different classes of inhibitors, we performed a Pearson's correlation (between the experimental $pIC_{50}$ DprE1 and pMIC values), and the results are described in **Figure 3.2-A**. A moderate to strong positive correlation is observed between DprE1 $pIC_{50}$ and *Mtb* pMIC for both types of binders, with statistical analyses of our results showing a significant correlation ($p < 0.0001$), whereas non-covalent inhibitors display a higher positive correlation coefficient ($n = 420$, $r = 0.647$) than the covalent binders ($n = 47$, $r = 0.539$). These results reveal conclusively that antimycobacterial

efficacy significantly depends on the inhibition of the flavoenzyme DprE1. Several of these inhibitors were investigated for cytotoxicity in various human cell lines, including A549,[59,72,76,83,84] HeLa,[24,26] HepG2,[28,56,66,69,72,74,87,88,90-92,109,111] J-774,[62] THP-1,[114] and Vero cell lines.[24-29,31,35-37,39,40,53,64,98,100] A small negative correlation ($r$ = -0.291, $p$ = 0.011, **Figure 3.2-B**) was found between the experimental cytotoxic concentrations ($CC_{50}$) and MIC, for covalent binders. This observation suggests that even the most effective covalent binders appear to display a safe profile, encouraging the ongoing search for novel inhibitors. In contrast, Pearson's correlation analysis did not reveal the existence of a correlation between $pCC_{50}$ and pMIC (not statistically significant, $n$ = 42, $r$ = 0.221, $p$ = 0.161, **Figure 3.2-B**) for the non-covalent binders.

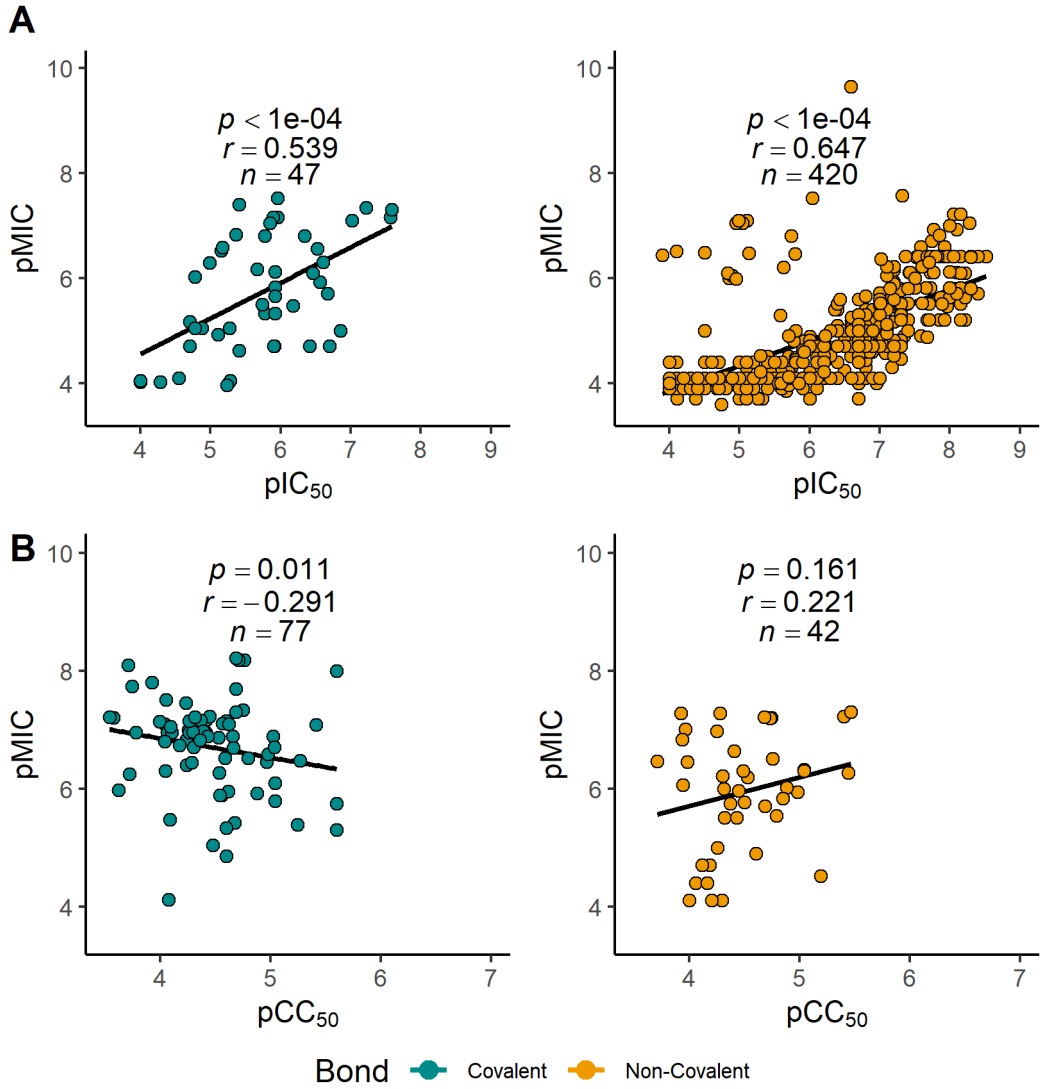


**Figure 3.2. A:** Scatter plot of DprE1 $pIC_{50}$ ($-\log_{10}[IC_{50}$ (molar)]) versus pMIC ($-\log_{10}$[MIC (molar)]) against Mtb for covalent (*left*) and non-covalent (*right*) inhibitors, and Pearson correlation coefficient between DprE1 $pIC_{50}$ and pMIC. **B:** Scatter plot of cytotoxicity $pCC_{50}$ ($-\log_{10}[CC_{50}$ (molar)]) versus pMIC for covalent (*left*) and non-covalent (*right*) inhibitors, and Pearson correlation coefficient between $pCC_{50}$ and pMIC.

### 3.2.2.2. The Impact of Nine Molecular Properties

The nine molecular properties for the active (≤ 10 μM, **Act**) and not active classes (> 10 μM, **Nact**), considering separately the covalent and non-covalent ones, are represented in **Figure 3.3.** We evaluated the significance of the difference between the means by a two-sided Student's *t*-test.

• **Molecular Weight.** The molecular weight (MW) is a critical property in the development of small-molecule drugs.[115,116] It has the potential to influence a variety of molecular processes, including absorption, blood-brain barrier (BBB) penetration, bile elimination rate and interactions with biological targets, being frequently investigated as part of the process for compounds optimization.[117,118]

***Covalent inhibitors.*** The MW values for most of the drugs varied from 361.3 Da ($10^{th}$ percentile) to 558.5 Da ($90^{th}$ percentile), with a median MW value of 480.4 Da. Non-active compounds generally had a lower molecular weight, with most molecules ranging from 332.9 Da ($10^{th}$ percentile) to 525.8 Da ($90^{th}$ percentile) and a median MW value of 408.4 Da. Comparison of the MW for active and non-active candidates also showed that the set of actives had a higher mean MW (474.5 Da) than the set of non-actives (424.4 Da) by 50.1 Da, which proved statistically significant ($p < 0.0001$).

***Non-covalent inhibitors.*** The MW values for most of the compounds varied from 373.4 Da ($10^{th}$ percentile) to 500.2 Da ($90^{th}$ percentile), with a median MW value of 435.6 Da. Non-active molecules had a lower molecular weight, with most of the molecules ranging from 333.1 Da ($10^{th}$ percentile) to 452.7 Da ($90^{th}$ percentile) and a median MW value of 383.3 Da. Comparison of the MW for active and non-active candidates also showed that the set of active molecules had a higher mean MW (436.0 Da) than the set of non-active ones (391.7 Da) by 44.3 Da, which was statistically significant ($p < 0.0001$).

• **Lipophilicity**. Lipophilicity, as indicated by the ClogP and ClogD values obtained here, is critical in defining key ADMET characteristics and potency. For instance, when lipophilicity levels are high, metabolism and solubility are more susceptible to being impaired, while low lipophilicity may increase permeability.[119]

***Covalent inhibitors.*** Covalent molecules in the active set displayed a similar ClogP range, though right-shifted to higher lipophilicity, with $10^{th}$ to $90^{th}$ percentile values of 2.40 to 5.03 and a higher mean value of 3.77 ($p < 0.0001$), *versus* 3.28 for the non-active counterparts (1.87 for the $10^{th}$ percentile, 4.71 for the $90^{th}$ percentile). Regarding the ClogD values, the covalent binders in the active set showed a similar ClogD range to the

non-active counterparts, with 10$^{th}$ to 90$^{th}$ percentile values of 2.18 to 3.77 and a slightly higher mean value of 2.99 ($p$ = 0.002), *versus* 2.73 for the not active counterparts (1.83 for the 10$^{th}$ percentile, 3.60 for the 90$^{th}$ percentile).

***Non-covalent inhibitors.*** An opposite situation is observed in the non-covalent binders set, although in this case there was no statistically significant difference in both ClogP ($p$ = 0.298) and ClogD ($p$ = 0.633) properties.

• **Intrinsic Aqueous Solubility (logS)**. The intrinsic aqueous solubility (logS) of an ionizable molecule is defined as its concentration in saturated aqueous solution at a particular temperature.[120]

***Covalent inhibitors.*** Comparison of logS for active and non-active inhibitors showed that the active set had a lower mean of logS (0.58) than the non-active set (1.24, $p < 0.0001$).

***Non-covalent inhibitors.*** In contrast, assessment of logS values for the non-covalent inhibitors were not significantly different between active and non-active sets ($p$ = 0.057).

• **Hydrogen Bond Acceptors and Donors**. HBAs and HBDs are additional significant descriptors for drug discovery that relate to the polarity and permeability of compounds.[117,121] For example, it was revealed that while HBA and MW have increased considerably over time, HBDs and lipophilicity have remained rather consistent.[122] These data suggest that counting HBDs may be more significant for drug development than counting HBAs, since a higher number of HBDs can lead to very poor solubility, permeability, and bioavailability.[123]

***Covalent inhibitors.*** The active covalent inhibitors set displayed more HBAs (from 7 (10$^{th}$ percentile) to 10 (90$^{th}$ percentile) with a median HBAs value of 8), compared to the non-active counterparts (from 5 (10$^{th}$ percentile) to 10 (90$^{th}$ percentile) with a median of 7). The higher mean value of 8.26 to the active compounds was shown to be statistically significant against the non-active ($\overline{x}$ = 7.43, $p$ = 0.0007). The covalent active and non-active inhibitors had a minimal number of HBDs, with the median value being 0 for active and 1 for the non-active sets. Comparison of the HBDs for active and non-active candidates also showed that the active set had a lower mean HBD (0.27) than the non-active set (0.66, $p < 0.0001$). A more significant number of HBAs in the active set is likely attributable to the enthalpic aspect of the binding process, in which H-bonding plays a crucial role in aligning the molecule/warhead to facilitate interaction with the active nucleophile site. Regarding the effect of HBDs leading to molecules with poor solubility, permeability, and bioavailability, the observation of a reduced number of HBDs in active compounds can be explained to avoid a self-reaction of the molecules

with their covalent warhead and the corresponding hydrogen bond donor (e.g., -OH/NH/SH groups).

***Non-covalent inhibitors.*** The non-covalent active set displayed higher values of HBAs, from 5 ($10^{th}$ percentile) to 9 ($90^{th}$ percentile) with a median HBA value of 7, compared to the non-active set (5, $10^{th}$ percentile; 8, $90^{th}$ percentile; 6, median). The higher mean value of 7.25 for the active compounds was shown to be statistically significant against the non-active ($\overline{x} = 6.23$, $p < 0.0001$). Unlike for the covalent binders, the non-covalent inhibitors showed a higher number of HBD, with a median value of 2 for the active set and 1 for the non-active. Comparison of the HBD for active and non-active sets also showed that the active set had a higher mean HBD ($\overline{x} = 1.69$) than the non-active set ($\overline{x} = 1.24$, $p < 0.0001$). This result is expected given that the H-bonding potential via HBD or HBA would be greater in non-covalent analogues for active versus inactive sets. The analysis shows that increasing HBA/HBD for non-covalent inhibitors can be a strategy to increase potency by increasing a stronger binding *via* H-bonding on the binding site rather than increasing lipophilicity (ClogP values were found to be non-statistically significant in the non-covalent set).

• **Topological Surface Area**. The topological surface area (TPSA) is another descriptor of importance in permeability and oral bioavailability estimates connected to hydrogen bonding (N and O atom count).[124]

***Covalent inhibitors.*** TPSA values ranged from about 82.3 $Å^2$ ($10^{th}$ percentile) to 137.7 $Å^2$ ($90^{th}$ percentile), with a median value of 100.6 $Å^2$ for the actives set. Non-actives are left-shifted to lower value of TPSA, with values varying from 60.2 $Å^2$ ($10^{th}$ percentile) to 138.0 $Å^2$ ($90^{th}$ percentile) and a median TPSA value of 94.3 $Å^2$. Comparison of the TPSA for active and non-active candidates also showed a higher mean TPSA value of 104.4 $Å^2$ for the actives set, compared to the non-active set (97.1 $Å^2$, $p = 0.027$).

***Non-covalent inhibitors.*** TPSA values varied from about 61.8 $Å^2$ ($10^{th}$ percentile) to 130.7 $Å^2$ ($90^{th}$ percentile) with a median value of 85.4 $Å^2$ for the actives set. Non-actives are left shifted to a lower value of TPSA, with values varying from 50.5 $Å^2$ ($10^{th}$ percentile) to 112.6 $Å^2$ ($90^{th}$ percentile), with a median TPSA value of 79.4 $Å^2$. Comparison of the TPSA for active and non-active candidates also showed that the actives set had a higher mean TPSA value (93.0 $Å^2$) than the non-active set (79.4 $Å^2$, $p < 0.0001$). Non-covalent binders have lower TPSA values than covalent inhibitors, both active and inactive. This result is likely due to the existing electrophilic warhead in the covalent binders (acrylamide or nitro), which increases this PC descriptor. Similarly demonstrated

with HBAs and HBDs, we can observe the H-bonding role in affecting the potency of the different types of inhibitors.

• **Flexibility Index**. The flexibility index (FInd) is described as the ratio of rotatable bonds to total bonds. No statistically significant difference was observed between the active and non-active sets, for the covalent inhibitors ($p$ = 0.34). The non-covalent active set displayed values of FInd, from 0.12 ($10^{th}$ percentile) to 0.30 ($90^{th}$ percentile) with a median FInd value of 0.19, compared to the non-active set (0.14, $10^{th}$ percentile; 0.23, $90^{th}$ percentile; 0.19, median). The higher mean value of 0.20 for the active compounds was shown to be statistically significant against the non-actives ($\overline{x}$ = 0.19, $p$ = 0.0002).

• **Number of Rotatable Bonds.** Similarly, ROTBS for the covalent inhibitors were not significantly different between active and non-active sets ($p$ = 0.13), even though the means were quite similar between inhibitors ($\overline{x}$ = 6.02) and non-inhibitors ($\overline{x}$ = 5.65). In contrast, for the non-covalent inhibitors the means for the ROTBS were statistically significant ($p < 0.0001$), with values of 6.62 for the active vs. 5.56 for the non-active sets. ROTBS values for most of the inhibitors set varied from 4 ($10^{th}$ percentile) to 10 ($90^{th}$ percentile) with a median ROTBS value of 6.

The analysis described above indicates that, for inactive covalent DprE1 inhibitors, it may be necessary to optimize the compounds by increasing MW, ClogP, ClogD, HBA, and TPSA while reducing logS and HBD, to match more closely the active set's corresponding properties. Concerning reducing HBD, the presence of a hydrogen bond donor in a core with a chemically reactive warhead could lead to drug instability through self-reactivity (though less likely for *in situ* bio-reductively activated warheads such as nitro-substituted heterocycles), so this needs to be considered in line with the analysis. For active non-covalent DprE1 inhibitors, the study indicates that compound optimization may benefit from increasing MW, HBA, HBD, TPSA, FInd, and ROTBS. This step-change in properties will drive the enthalpic component of binding by enhancing hydrogen bonding and improving the ligand conformation for optimal fit.

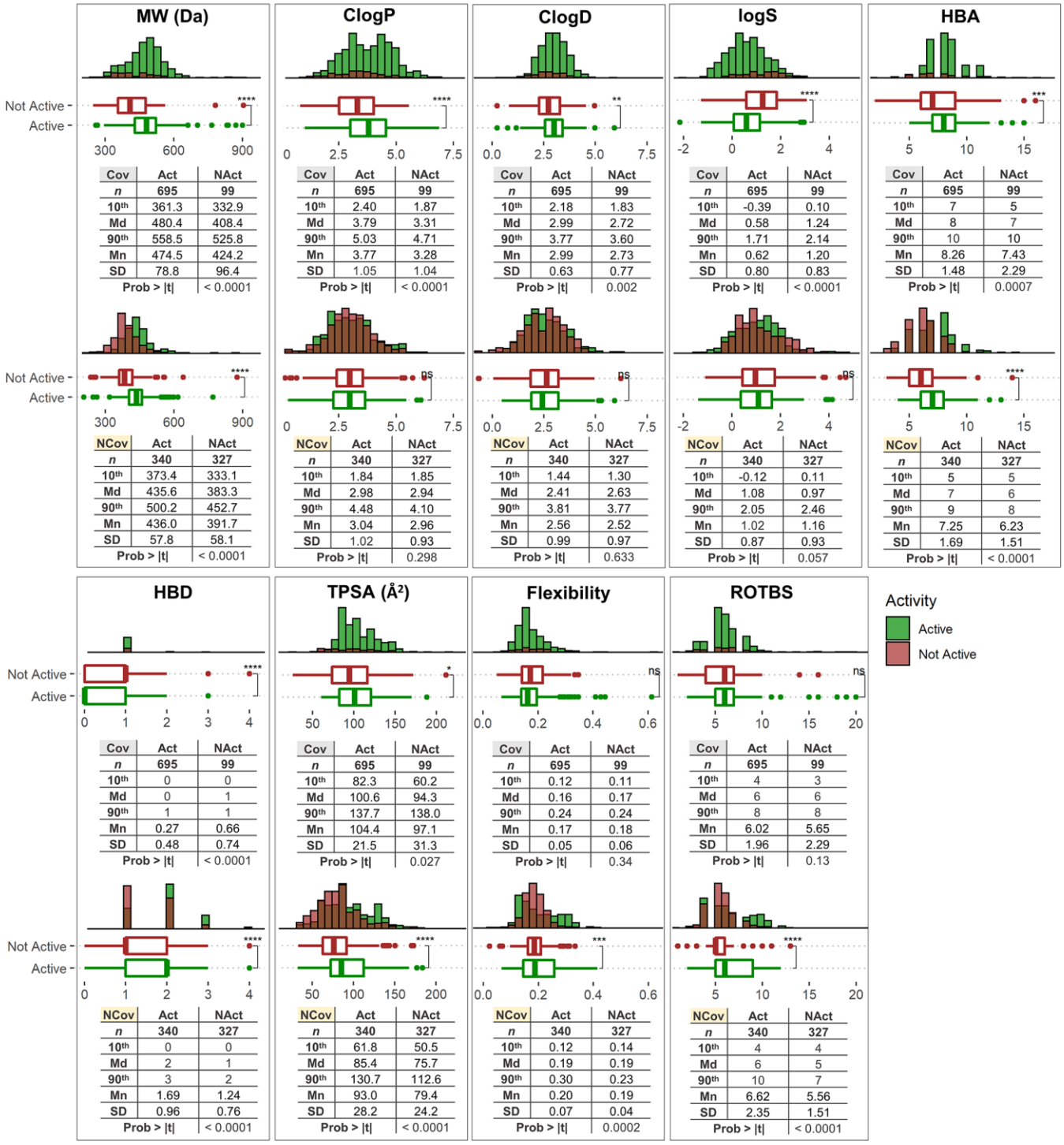


**Figure 3.3.** Physicochemical property distribution and statistics of the inhibitor (**Act**, *in green*) and non-inhibitor (**NAct**, *in red*) classes. Each corresponding binding type (covalent (Cov) upper and non-covalent (NCov) above) is shown for MW, ClogP, ClogD, log S, HBA, HBD, TPSA, Flexibility, and ROTBS. *N* indicates the total number of compounds considered in each analysis. The two-sided Student's *t*-test was used to determine the statistical significance of active and inactive compounds, among those classified as covalent or non-covalent inhibitors and the *p*-values were evaluated (ns: *p*-value > 0.05, * *p*-value < 0.05, ** *p*-value < 0.01, *** *p*-value < 0.001, **** *p*-value < 0.0001; Md = Median, Mn = Mean).

### 3.2.2.3. Impact of Physicochemical Properties of DprE1 inhibitors on Oral Absorption

Lipinski's Rule of 5 (Ro5) indicates that if a molecule meets the criteria log P ≤ 5; MW ≤ 500 Da; HBAs (O + N atom count) ≤ 10 and HBDs (OH + NH count) ≤ 5, the compound is more likely to benefit from membrane permeability and hence be more readily absorbed in the human digestive system via passive diffusion.[106,125] These set limits were chosen to cover around 90% of the range for the four estimated PC descriptors and the Ro5 is compromised when two or more criteria are exceeded.[106,125] Our analysis reveals that 65.1% of active DprE1 inhibitors (*n* = 674/1035, MIC < 10 μM) do not show violations of the Ro5. Among the covalent binders only 54.8% (381/695) fall inside the chemical space of Ro5, while a larger proportion is seen among the non-covalent binders [86.2% (293/340)] (**Figure 3.4-B**). Within the covalent dataset, both NBTO, NQ, and NTZ score 100% for no Ro5 violations, while DNB and BTZ score 80.4% and 48.2%, respectively. The non-covalent dataset proved more diverse, with 4-AQ, AZA, BI, BD, HYD, NAHPC and PTD showing no violations (100%), BTO (96.3%) > MP (96.2%) > CD (88.6%) > TPA (88.1%) > NMDS (80.0%) > PP (77.8%). 2-CQ and NC BTZ were the classes with a lower score of no violation (37.5, 27.3%) (**Figure 3.4-A**). If we analyse both binding subsets which scored with one violation (25.6%, 265/1035), among covalent (33.4%, 232/695) and non-covalent (9.7%, 33/340) inhibitors, the classes of the covalent category were BTZ (38.6%) > DNB (12.8%) and those of the non-covalent were 2-CQ (62.5%) > NC BTZ (54.5%) > 2-S-BTO (33.3%) > PP (22.2%) > NMDS (20%) > CD (11.4%) > TPA (10.4%) > MP (3.8%) and BTO (3.7%) (**Figure 3.4-A**). The main descriptor involved in Ro5 violations is MW, with a prevalence of 55.4% for the covalent and 42.6% for the non-covalent binders (**Figure 3.4-C**). While analysing the two subsets which scored at least two violations, we obtained for the covalent 11.8% (82/695) and for non-covalent 4.1% (14/340) (**Figure 3.4-B**). The classes for the covalent inhibitors were BTZ (13.2%) > DNB (6.9%) and for the non-covalent counterparts, AVMT (100%) > 2-S-BTO (66.7%) > NC BTZ (18.2%) and TPA (1.5%), respectively (**Figure 3.4-A**). The most frequently used pair of PC descriptors in two Ro5 violations is MW-ClogP for the covalent binders, with a frequency of 15.9%, and MW-HBA for non-covalent binders, 21.3%. The set MW-ClogP-HBA was found to be the most frequently violated for the compounds with three violations, with a score of 1.0% for the covalent binders (**Figure 3.4-C**). This finding was consistent with our PC descriptors analysis; nevertheless, covalent inhibitors exhibit higher molecular weight values and are more lipophilic than

non-covalent binders. This property may impair oral bioavailability and should be considered during drug optimization.

**Mapping bRo5 and eRo5 Space.** Lipinski's rules delineate chemical space with compounds that "are more likely to be orally absorbed" as one way to describe chemical space, whereas "possible to be orally absorbed" is regarding the extended Ro5 (eRo5) and beyond Ro5 (bRo5). Understanding the precise boundaries of this chemical space will increase the likelihood of creating cell-permeable and orally accessible ligands for more difficult targets.[117,126,127] Of the 1035 active compounds in this study, a large proportion (23.9%, *n* = 247/1035) cluster into what can be considered as an extension of Ro5 space ($0 \leq \log P \leq 7.5$; 500 Da < MW ≤ 700 Da; HBDs (OH + NH count) ≤ 5; TPSA ≤ 200 $Å^2$; ROTBS ≤ 20) and a natural tail of the distribution of compounds is based on Ro5 properties. Among these, 32.1% (223/695) are from the covalent class while only 7.1% (24/340) are from the non-covalent class. For the covalent and non-covalent inhibitors, only 4.7% (33/695) and 2.9% (10/340), respectively, were observed in oral bRo5 space ($0 < \log P$ or $> 7.5$; 700 Da < MW ≤ 3000 Da; HBDs (OH + NH count) > 5; TPSA > 200 $Å^2$; ROTBS > 20). A small proportion of DprE1 inhibitors, 6.9% (71/1035), did not fall into any Ro5 chemical space, with the highest proportion, 8.3% (58/695), for covalent and 3.8% (13/340) for the non-covalent binders (**Figure 3.4-D**).

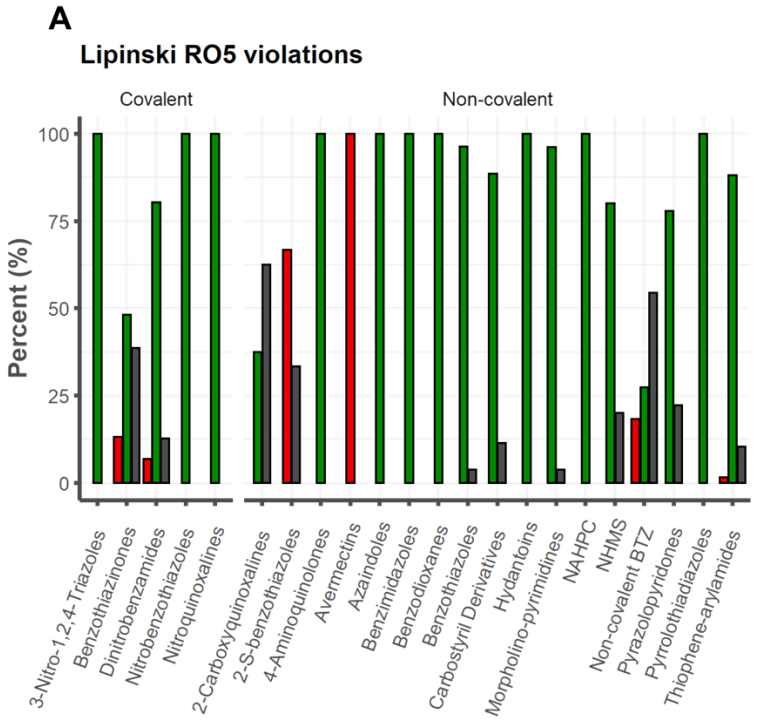


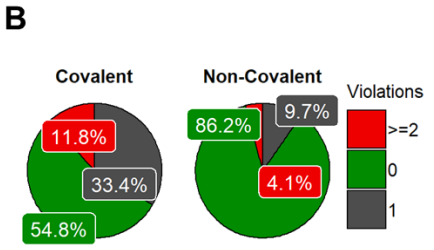


C

| Binding | Violations | Type | *N* | % |
|---|---|---|---|---|
| Covalent | ≥2 | MW-HBA | 29 | 9.2 |
| | | MW-LogP | 50 | 15.9 |
| | | MW-LogP-HBA | 3 | 1.0 |
| | 1 | HBA | 31 | 9.9 |
| | | LogP | 27 | 8.6 |
| | | MW | 174 | 55.4 |
| Non-covalent | ≥2 | MW-HBA | 10 | 21.3 |
| | | MW-LogP | 4 | 8.5 |
| | 1 | HBA | 1 | 2.1 |
| | | LogP | 12 | 25.5 |
| | | MW | 20 | 42.6 |

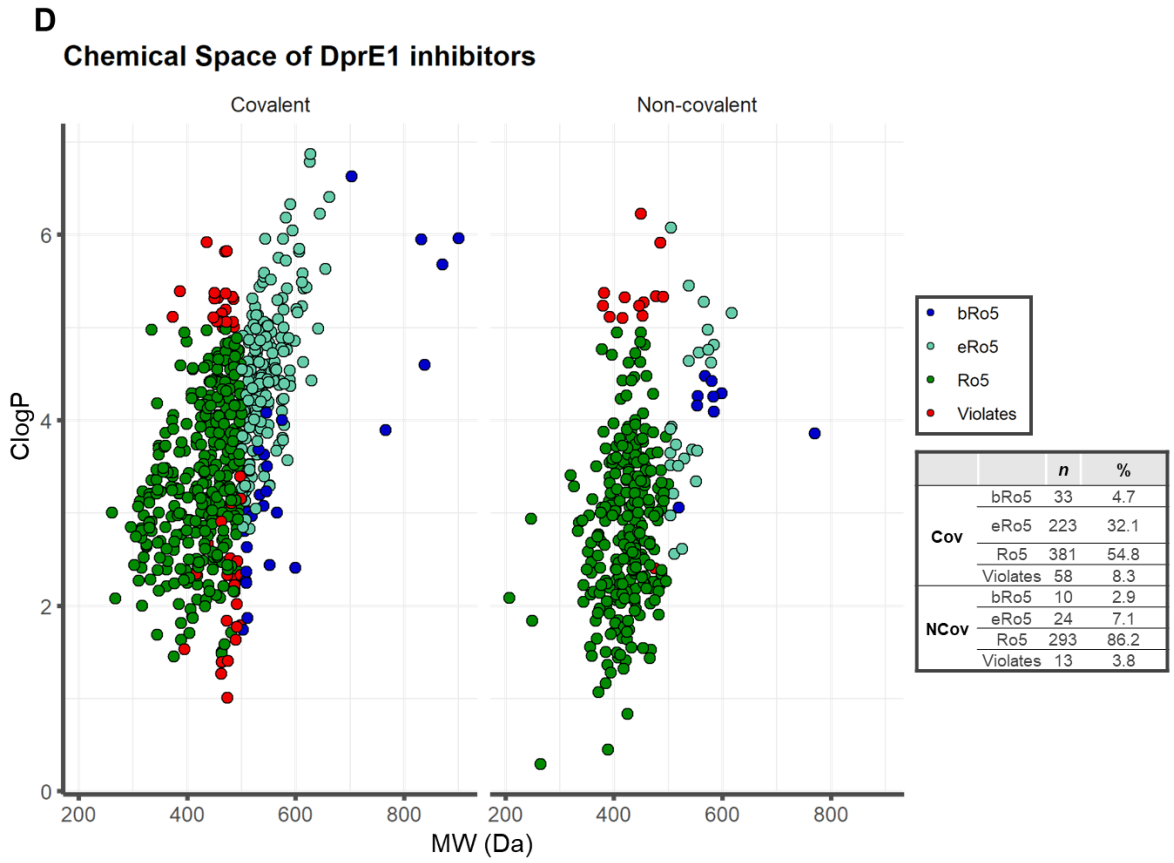


| | | *n* | % |
|---|---|---|---|
| Cov | bRo5 | 33 | 4.7 |
| | eRo5 | 223 | 32.1 |
| | Ro5 | 381 | 54.8 |
| | Violates | 58 | 8.3 |
| NCov | bRo5 | 10 | 2.9 |
| | eRo5 | 24 | 7.1 |
| | Ro5 | 293 | 86.2 |
| | Violates | 13 | 3.8 |

**Figure 3.4.** Lipinski's Rule of 5 (Ro5): Distribution of the number of Lipinski Ro5 violations for **A**) each class of DprE1 inhibitors and **B**) for the covalent and non-covalent category binders. **C:** Ro5 violation types. **D**: Physicochemical Property Space of covalent and non-covalent DprE1 inhibitors, with CLogP as a function of MW.

### 3.2.2.4. Distribution

The term "drug distribution" refers to how a substance is distributed across the body's compartments. Certain factors, such as penetration through the central nervous system (CNS) or BBB, P-gp efflux, and PPB can be adequately studied *in silico*. Additionally, since only the unbound (free) drug can interact with the target protein, the interaction of the drug with plasma proteins must be evaluated throughout the drug development process.[128]

#### 3.2.2.4.1 Central Nervous System Penetration

For CNS therapeutic targets good penetration is an essential requirement, but for non-CNS targets the BBB penetration rate should be minimized to reduce potential neurotoxicity or adverse pharmacological events.[129] StarDrop software uses the random forest classification model to classify if a molecule is a crossing or non-crossing of the BBB, while one that employs descriptors compatible with the common fact that neutral molecules tend to penetrate the CNS more effectively than charged compounds and that cations normally permeate the CNS more effectively than anions.[105,109,110] The predictive accuracy of BBB+ ranges from 80% to 100% while that of BBB- ranges from 65% to 87%.[105,109,110] Close to ~99% of the total DprE1 inhibitors were predicted not to penetrate the CNS, with 100% within the covalent set and 96.8% for the non-covalent binders. Only 3.2% of the non-covalent inhibitors were found to have some BBB penetration, respectively NC BTZ 27.3% (3/11) > NHMS 20% (1/5) > MP 7.7 % (2/26) > CD 6.8 % (3/44) > AZA 5.3% (2/38) (**Figure 3.5-A**).

#### 3.2.2.4.2. P-gp Efflux System

P-gp is one of the most widely studied drug transporters to date, given the evidence of its presence in the majority of cells, including those of the intestinal mucosa and the BBB.[107] We used the statistical model built-in to StarDrop v7.2.0.32905 to predict which DprE1 inhibitors could behave as P-gp substrates. It employs a random forest classification approach to classify compounds as probable or unlikely to be P-gp substrates. The model's performance was evaluated on an independent test set of 51 chemicals, with 82% of non-substrates and 79% of substrates accurately categorized.[109] A higher frequency of P-gp binders is predicted among the covalent inhibitors (80.4%), compared to the non-covalent class (65%). For the covalent inhibitors set, predictions point to P-gp substrates among the BTZ (88%) > NBTO (50%) > DNB (48%) and no P-

gp substrates for the NTZ, NQ datasets (0%). For the non-covalent inhibitors set, predictions identify P-gp substrates among the AVMT, NC BTZ, PP, PTD (100%) > MP (92.3%) > 4-AQ (91.7%) > CD (90.9%) > 2-S-BTO (86.7%) > TPA (85.1%) > BTO (63%) > 2-CQ (50%) > BI (44.4%) > NHMS (40%) > AZA (23.7%) > NAHPC (11.1%) > HYD (7.9%), and no P-gp substrates for the BD (0%) (**Figure 3.5-B**).

#### 3.2.2.4.3. Plasma Protein Binding

The extent to which a drug binds to plasma proteins substantially affects its pharmacokinetic and pharmacodynamic effects. The drug's efficacy will be proportional to the quantity of unbound drug in plasma. Additionally, the bound drug in plasma can operate as a reservoir for free drug clearance via various elimination pathways, lengthening the duration of action.[130,131] From a QSAR model integrated into StarDrop v7.2.0.32905, **Figure 3.5-C** categorizes and forecasts human PPB% (Hu PPB%) values for both covalent and non-covalent datasets. The model is a random forest that classifies the extent of plasma protein binding of test set substances as either "high" or "low" about the threshold above. Low binding molecules are those that are less than 90% bound, and high binding molecules are those that are more than 90% bound.[105,109,110] It can be observed that both types of inhibitors display high binding capacity, with the non-covalent inhibitors scoring around 84.1% while the covalent inhibitors scored around 77.1%. For the covalent set, all inhibitors belonging to the NQ class displayed high binding capacity (100%), this high tendency holding for DNB and BTZ classes (80.4% and 78.8%), while NBTO scores only around 18.2% and NTZ is predicted to have an irrelevant protein binding capacity (0%). For the non-covalent inhibitors, nine classes (2-CQ, 2-S-BTO, BD, BTO, BI, NAHPC, CD, NHMS, PP) were predicted to have a high binding capacity (100%), followed by 4-AQ (87.5%) > AZA (86.8%) > NC BTZ (81.8%) > PTD (75%) > HYD (71.1%) > TPA (67.2%) > MP (65.4%). AVMT is predicted to have an irrelevant protein binding capacity.

A comparison of the experimental PPB% values for covalent and non-covalent binders with the results obtained from the StarDrop model was performed, and the corresponding datasets are depicted in **Tables 3.2** and **3.3**. Regarding the covalent inhibitors, the literature examination returned a total of 21 compounds, including 16 BTZ[31,132] and 5 NBTO[59] molecules. The compounds with experimental data were employed to evaluate the performance metrics of the classification model from StarDrop, and the results and confusion matrix are displayed in **Table 3.2**. The obtained accuracy

(Q) rating of 81% indicates that the classification of ~8 of every 10 molecules is correct. According to the StarDrop manual, the accuracy of the Plasma Protein Binding Classification (90%) model is 81%, which is consistent with the obtained predictions using covalent inhibitors. The precision value of 100% indicates that all the molecules predicted with high PPB% were correctly identified, and a sensitivity value of 80% reveals that 20% of the molecules with high PPB% were lost during the model application. The specificity value of 100% indicates that all molecules with low PPB% were accurately labelled.

Regarding the non-covalent inhibitors, the literature analysis provided a total of 18 compounds, including 10 AZA,[78,79] 6 PP[84] and 2 BI[82] molecules. These compounds with experimental data were also employed to evaluate the performance metrics of the classification model from StarDrop, the results and confusion matrix being displayed in **Table 3.3**. The obtained accuracy (Q) rating of 78% indicates that the classification of ~8 of every 10 molecules is correct, with a similar accuracy value reported from StarDrop's manual (81%). The precision value (73%) indicates that 73% of the molecules predicted with high PPB% were correctly identified, and a sensitivity value of 100% reveals that no false negative value was predicted. The specificity value of 43% indicates that 57% molecules with low PPB% were mis-labelled as high PPB% (False Positive).

High plasma protein binding restricts the distribution of xenobiotics from the blood to tissues, impacting their metabolism, also holding a significant role in drug-drug interactions. Therefore, a reasonable predictive model with high sensitivity is required to avoid losing high PPB molecules during prediction and a high precision is also required to prevent excess false-positive results. Both model analyses for the experimental data of each class exhibited high sensitivity (Cov= 0.80 and Ncov = 1), together with high Precision (Cov= 1 and Ncov = 0.73). Even though the sample size is relatively small in both testing sets [*N* (Cov) = 21 and *N* (Ncov) = 18], this study using experimental data reveals that the StarDrop model can predict plasma protein binding reasonably, for both covalent and non-covalent binders, thus representing a fairly reliable tool in the development of DprE1 inhibitors.

To summarize this section, our computed analysis, along with literature values, indicate that both covalent and non-covalent DprE1 inhibitors are projected to be non-permeable to the blood-brain barrier and to have a moderate to high plasma protein binding affinity. Covalent DprE1 inhibitors are more likely to be possible substrates (80.4%) for P-gp substrate transporters than their non-covalent counterparts (65%).

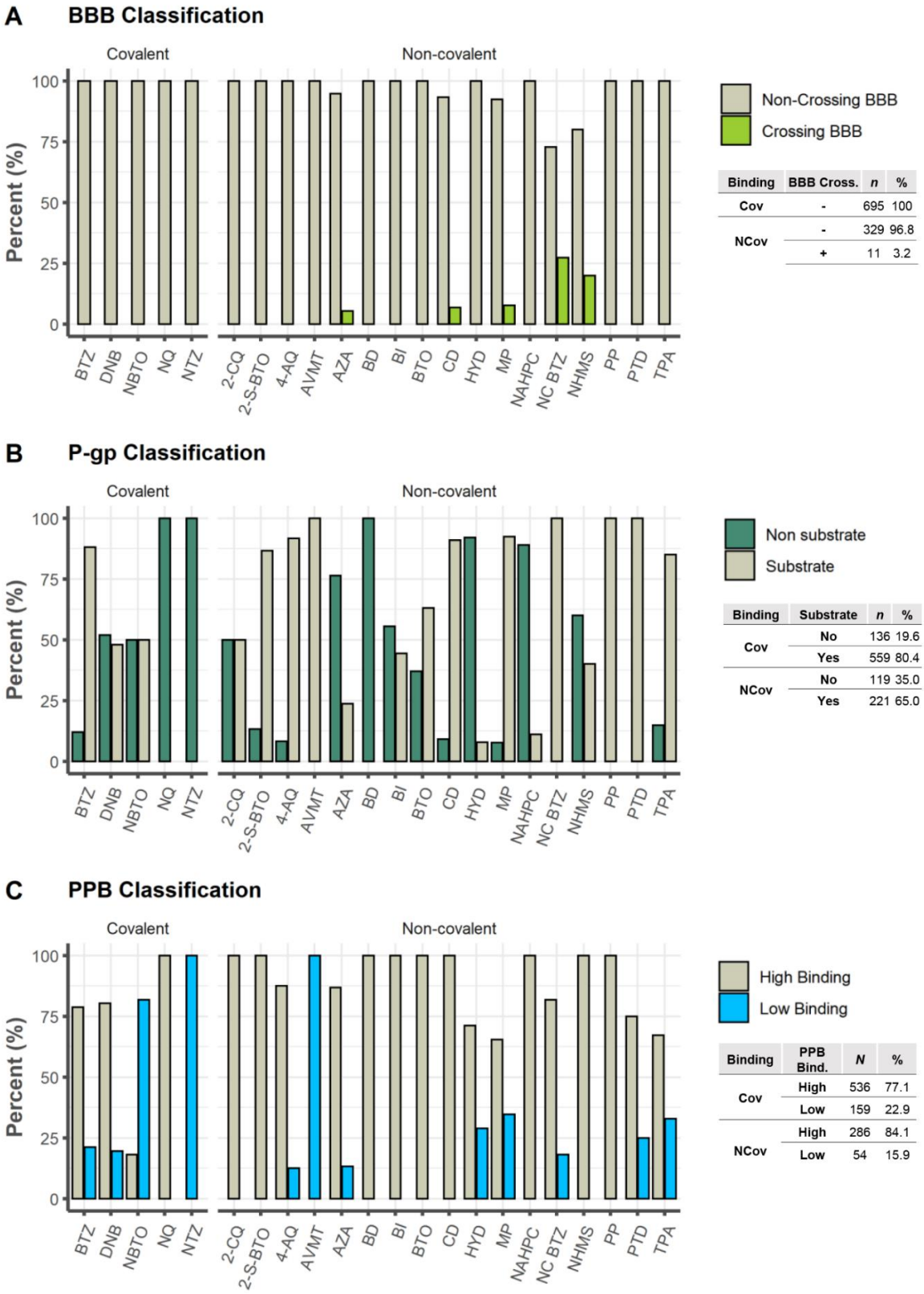


| Binding | BBB Cross. | *n* | % |
|---|---|---|---|
| Cov | - | 695 | 100 |
| NCov | - | 329 | 96.8 |
| | + | 11 | 3.2 |

| Binding | Substrate | *n* | % |
|---|---|---|---|
| Cov | No | 136 | 19.6 |
| | Yes | 559 | 80.4 |
| NCov | No | 119 | 35.0 |
| | Yes | 221 | 65.0 |

| Binding | PPB Bind. | *N* | % |
|---|---|---|---|
| Cov | High | 536 | 77.1 |
| | Low | 159 | 22.9 |
| NCov | High | 286 | 84.1 |
| | Low | 54 | 15.9 |

**Figure 3.5.** Analysis of some properties related to distribution. **A**: Blood-brain-barrier (BBB) penetration classification; **B**: P-gp inhibitors classification. **C**: Plasma protein binding (PPB) classification.

**Table 3.2.** Experimental and the corresponding predicted plasma protein binding (PPB**)** data, confusion matrix and performance metrics evaluating the PPB data for covalent inhibitors.

**Benzothiazinones**

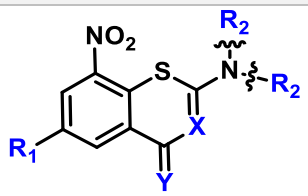

| X | Y | $R_1$ | $R_2$ | PPB (%) | Pred PPB[a] |
|---|---|---|---|---|---|
| N | O | $CF_3$ | 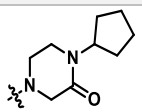 | 90.7 | High |
| N | O | $CF_3$ | 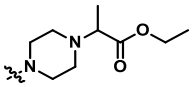 | 92.5 | Low |
| N | O | $CF_3$ | 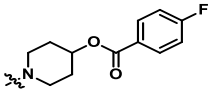 | 99.8 | high |
| N | O | $CF_3$ | 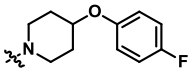 | >99 | high |
| N | O | $CF_3$ | 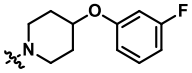 | >99 | high |
| N | O | $CF_3$ | 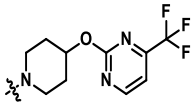 | 99.4 | high |
| N | O | $CF_3$ | 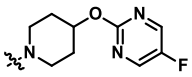 | 98.6 | high |
| N | O | $CF_3$ | 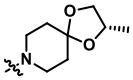 | 99.4 | high |
| N | O | $CF_3$ | 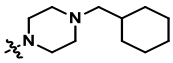 | 99.6 | high |
| N | S | $CF_3$ | 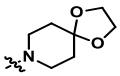 | 99.4 | low |
| N | O |  | 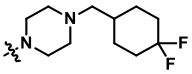 | 97.9 | high |
| N | O |  | 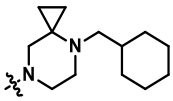 | 98.4 | high |
| N | O | $CF_3$ | 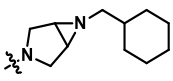 | 99.5 | high |
| N | O | $CF_3$ | 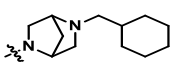 | 99.6 | high |
| N | O | $CF_3$ | 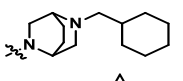 | 99.9 | high |
| N | O | $CF_3$ | 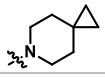 | 99.4 | high |

**Nitrobenzothiazoles**

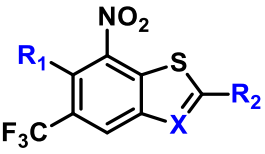

| Structure | PPB (%) | Pred PPB[a] |
|---|---|---|
| 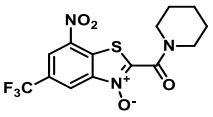 | 89.7 | Low |
| 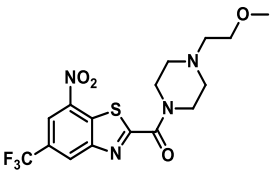 | 93.9 | Low |
| 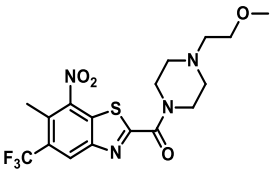 | 95.7 | Low |
| 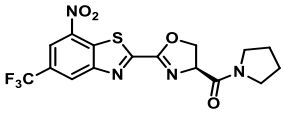 | 94 | high |
| 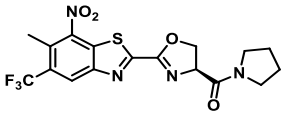 | 93.7 | high |

**Confusion matrix**

| PPB | H | L | T |
|---|---|---|---|
| H | 16 | 4 | 20 |
| L | 0 | 1 | 1 |
| T | 16 | 5 | 21 |

| | |
|---|---|
| **Q** | 0.81 |
| **Precision** | 1.00 |
| **Sensitivity** | 0.80 |
| **Specificity** | 1.00 |
| **Q Model** | **0.81** |

[a]Pred PPB: Predicted plasma protein binding computed by StarDrop v7.2.0.32905. Legend: H: High (*in green*); L: Low (*in yellow*).

**Table 3.3.** Experimental and the corresponding predicted PPB data, confusion matrix and performance metrics evaluating the PPB data for non-covalent inhibitors.

| 1,4-Azaindoles | | | | | Pyrazolopyridones | | | | |
|---|---|---|---|---|---|---|---|---|---|
| 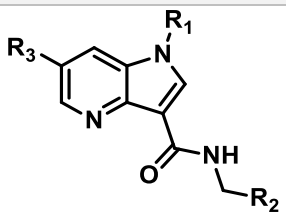 | | | | | 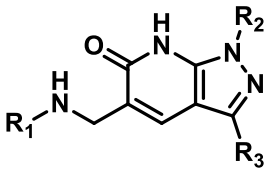 | | | | |
| $R_1$ | $R_2$ | $R_3$ | PPB (%) | Pred PPB[a] | $R_1$ | $R_2$ | $R_2$ | PPB (%) | Pred PPB[a] |
| 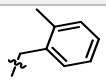 |  | -H | >99 | high | 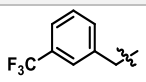 |  |  | 99 | high |
| 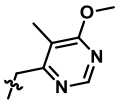 |  | -H | 90.2 | high | 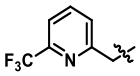 |  |  | 98.9 | high |
| 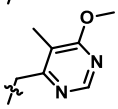 |  | -H | 95 | high | 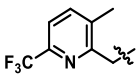 |  |  | >99 | high |
| 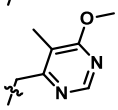 |  | $-CH_3$ | 95 | high | 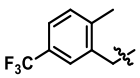 |  |  | >99 | high |
| 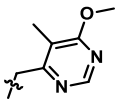 |  | $-CH_3$ | 78 | high | 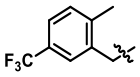 |  |  | >99 | high |
| 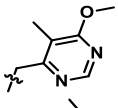 |  | $-CH_3$ | 95 | high | 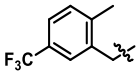 |  |  | >99 | high |
| 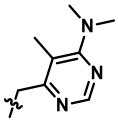 |  | $-CH_3$ | 70 | low | | | | | |
| 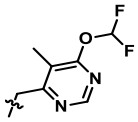 |  | $-CH_3$ | 70 | high | **Benzimidazoles** | | | | |
| | | | | | **Structures** | | | PPB (%) | Pred PPB |
| 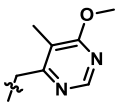 |  | $-OCH_3$ | 83 | Low | 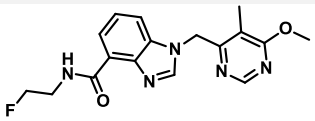 | | | 68 | high |
| 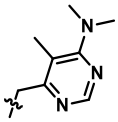 |  | $-OCH_3$ | 70 | Low | 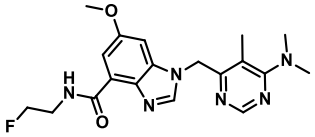 | | | 69 | high |

**Confusion matrix**

| | PPB | | |
|---|---|---|---|
| | H | L | T |
| H | 11 | 0 | 11 |
| L | 4 | 3 | 7 |
| T | 15 | 3 | 18 |

| | |
|---|---|
| **Q** | 0.78 |
| **Precision** | 0.73 |
| **Sensitivity** | 1.00 |
| **Specificity** | 0.43 |
| **Q Model** | **0.81** |

[a]Pred PPB: Predicted plasma protein binding computed by StarDrop v7.2.0.32905. Legend: H: High (*in green*); L: Low (*in yellow*).

### 3.2.2.5. Cytochromes P450 Metabolism.

Six alleles of the cytochromes P450 are particularly important in drug metabolism: CYP1A2, CYP2C9, CYP2C19, CYP2D6, CYP2E1, and CYP3A4. They catalyse the oxidative metabolism of about 90% of human drugs and are the main determinants of the systemic clearance and bioavailability of the molecules.[133,134] To evaluate which compounds in our dataset might be CYP binders we used the StarDrop WhichP450 module. Predictions of CYPs isoforms metabolism for each class of inhibitors are displayed in **Figure 3.6**. Calculations were conducted to determine the drug's mean probability of being metabolized by related isoforms, indicating that it could be a candidate substrate. The computed predictions suggest that the DprE1 inhibitors would be metabolized mainly by the 3A4 isoform, with mean values of 54.4% and 47.6% of metabolism prediction for covalent and non-covalent binders, respectively, followed by the isoforms 2D6, 2C19, 2C9 (13.21, 9.53, and 8.86%) for the covalent inhibitors, and 2C9, 2D6, 2C19 (15.09, 12.16, and 11.61%) for the non-covalent inhibitors. This set of molecules reveals a low proportion of metabolism by the 1A2, 2C8, and 2E1 isoforms (6.84, 6.28 and 0.83% for covalent inhibitors, and 7.16, 5.72 and 0.66% for non-covalent inhibitors; **Figure 3.6-A**). Regarding the corresponding moiety class for each isoform: AVMT was found to be the class with highest prediction to be metabolized by the 3A4 isoform (83.0%) and BD the lowest (34.3%); NQ scored the highest prediction to be metabolized by the 1A2 isoform (19.67%) and AVMT the lowest (2.2%). CD showed the highest metabolism prediction (8.03%) for the 2C8 isoform, and NQ the lowest (0.93%). HYD was the class with highest probability to be metabolized by the 2C9 isoform (28.9%) and AVMT the lowest (3.0%). Regarding the 2C19 isoform, the HYD class was predicted to have the highest probability (15.7%), and AVMT the lowest (3.6%). For the 2D6 isoform, PP displayed the highest value (25.3%), and AVMT the lowest (1.4%). For the 2E1 isoform, NQ had the highest metabolism prediction (2.53%) and BI the lowest (0.13%, **Figure 3.6-B**). These findings should be interpreted cautiously, as building appropriate prediction models is challenging due to the complicated chemical mechanisms underlying CYP metabolism[128], but they allow for a broad comparison of the various classes of compounds. These predictions contribute to our understanding of the role of the CYP superfamily in the metabolic stability of DprE1 inhibitors.

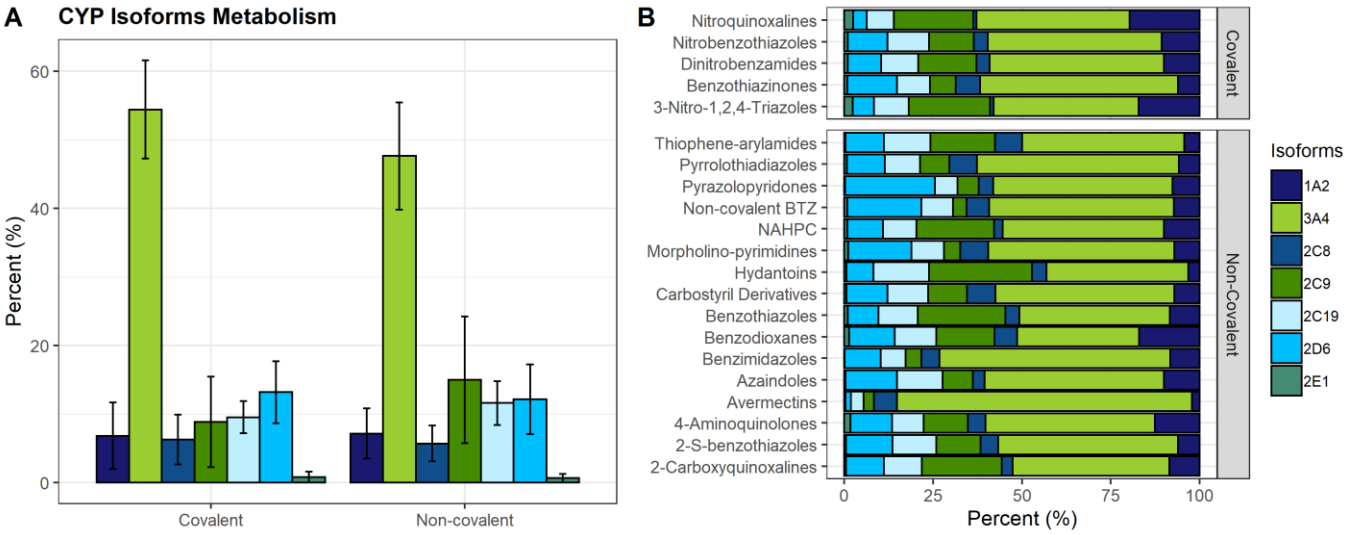


**Figure 3.6.** CYP isoforms metabolism for **A:** all covalent and non-covalent inhibitors; **B:** each corresponding class of the covalent and non-covalent inhibitor.

### 3.2.2.6. Safety Profile

In addition to bioavailability, the safety profile is important since it details the harmful consequences associated to the chemical substances under study. The analysis of the logP versus MW, GSK's 4/400 rule (logP ≤ 4 and MW ≤ 400Da)[107] for evaluation of ADMET liabilities, shows that 17.1% (*n* = 177/1035) of the active inhibitors fall in the more desirable category, with 15.7% for the covalent (*n* = 109/695) and 20.0% (*n* = 68/340) for non-covalent inhibitors (**Figure 3.7-A1**). Prevalence of adverse toxicological outcomes can be assessed using Pfizer's 3/75 rule,[108] where logP > 3 and TPSA < 75 Å$^2$ are related to the adverse effect of chemical compounds. Application to our dataset reveals that 2.4% (*n* = 17/695) of the covalent and 22.9% (*n* = 78/340) of the non-covalent binders do not comply with the Pfizer 3/75 rule, meaning that they may exhibit increased toxicity (**Figure 3.7-A2**). It is worth highlighting that the Pfizer 3/75 rule does not take into consideration the possible presence of mutagenic functional groups. For instance, nitro groups are often present in DprE1 covalent inhibitors, although drugs containing nitro groups have been linked to mutagenicity and genotoxicity.[135] Noteworthy, various reports indicate that nitro-containing DprE1 inhibitors exhibit favourable metabolic, microsomal, and plasma stability, and reduced toxicity.[24]

### 3.2.2.7. hERG Inhibition

Throughout the drug development process, one of the most common undesirable side effects that contribute to a medicine's failure is cardiac arrhythmias.[136] Numerous forms of cardiovascular toxicity must be taken into account, the promiscuous blocking of hERG cardiac potassium channels by small molecules posing a significant therapeutic challenge, with severe consequences for human health.[137–139]

The model implemented in StarDrop v7.2.0.32905 predicts that covalent DprE1 inhibitors exhibit the highest potential for hERG inhibition, with a mean $pIC_{50}$ of 6.16, with values ranging from 5.01 ($10^{th}$ percentile) to 7.21 ($90^{th}$ percentile) for most drugs, while the non-covalent binders varied from 4.28 ($10^{th}$ percentile) to 6.30 ($90^{th}$ percentile), with a lower mean of 5.26. In general, an experimental binding assay is indicated if the score is larger than 5, since the molecules are likely to display some toxicity linked to these cardiac potassium channels.[137–139] We present a categorization histogram (**Figure 3.7-B**) where it is shown that 90.4% of the covalent and 55.0% of the non-covalent inhibitors have a $pIC_{50} > 5$. Both subsets also scored 58.7% (Cov) and 25.0% (NCov) of compounds with $pIC_{50} > 6$. Within the covalent inhibitors, 99.3% of the benzothiazinones have a $pIC_{50} > 5$, with 70.7% showing $pIC_{50} > 6$ and 28.6% between 5-6. hERG inhibitions in BTZ have been observed previously and, following SAR studies, optimizations of three moieties (benzene ring, linker, and *N*-heterocycle) on the C-2 side chain of the BTZ scaffold have been performed, allowing identification of new lead compounds with reduced hERG liability [inhibition rate (IR) < 50% at 10 μM], without sacrificing antimycobacterial potency.[37,42] The DNB class showed a smaller proportion for a predicted $pIC_{50} > 6$ (6.9%). A $pIC_{50}$ of 5-6 is predicted for 100% of the inhibitors in both NQ and NTZ classes, followed by 68.2% for NBTO and 38.2% for DNB. Values of $pIC_{50}$ below 5 are predicted for DNB (54.9%) > NBTO (31.8%) > BTZ (0.8%) inhibitors. Among the covalent binders, the NBTO class emerges as the one with lower predicted hERG inhibition. Predictions within the non-covalent inhibitors are: $pIC_{50} > 6$, NC BTZ (81.8%) > 2-S-BTO (80%) > PTD (75%) > MP (65.4%) > CD (59.1%) > PP (55.6%) > 4-AQ (50%) > NHMS (20%). For $pIC_{50}$ values in the range 5-6: AVMT, BI (100%) > BD (80%) > NHMS (60%) > AZA (57.9%) > 4-AQ (50%) > PP (44.4%) > CD (40.9%) > 2-CQ (37.5%) > MP (34.6%) > PTD (25%) > NAHPC (22.2%) > 2-S-BTO (20%) > NC BTZ (18.2%) > TPA (9.0%) > HYD (5.3%) > BTO (3.7%). $pIC_{50}$ values below 5 are predicted for BTO (96.3%) > HYD (94.7%) > TPA (91.0%) > NAHPC (77.8%) > 2-CQ

(62.5%) > AZA (42.1%) > BD, NHMS (20%).

1,4-Azaindoles scored 57.9% for $pIC_{50}$ in the range 5-6 and 42.1% for $pIC_{50}$ <5. Reported hERG assays for this class have shown no inhibition of the hERG channel at up to 33 μM ($pIC_{50}$ < 4.48) concentrations,[76,79] displaying a calculated absolute error ($\overline{x} \pm \sigma$) of 0.40 ± 0.11 log $IC_{50}$ comparing to the predicted values (**Table 3.4**). Although the hydantoin heterocycle is linked to potential cardiotoxicity,[91,103] predictions for this scaffold point to 5.3% with $pIC_{50}$ between 5-6 and 94.7% with $pIC_{50}$ < 5. The calculated absolute error ($\overline{x} \pm \sigma$) for HYD compounds, between the experimental and predicted data, was in the range of 0.26 ± 0.14 log $IC_{50}$ (**Table 3.4**). Thiophene-arylamide compounds showed a high proportion of predicted $pIC_{50}$ < 5 (91.0%), which is in keeping with literature reports. In contrast, selected TPA compounds exhibited low inhibition profiles of the hERG channel [$IC_{50}$ >20 μM ($pIC_{50}$ < 4.70)] across the series, indicating a low risk of blocking the cardiac potassium channel and causing QT prolongation.[98] The calculated absolute error ($\overline{x} \pm \sigma$) between the experimental and predicted data was in the range of 0.26 ± 0.14 log $IC_{50}$, for the TPA compounds (**Table 3.4**). Predictions for the BI series placed 100% of the compounds within a $pIC_{50}$ range of 5-6, though hERG channel assays indicated no major safety liabilities, with values of $IC_{50}$ >33 μM ($pIC_{50}$ < 4.48).[82] The calculated absolute error ($\overline{x} \pm \sigma$) between the experimental and predicted data for the BI class was in the range of 0.80 ± 0.11 log $IC_{50}$, displaying the highest relative error (15.1 ± 1.8%) whilst using the predictive model (**Table 3.4**). For the benzothiazole group, an hERG assay showed that TCA1 (**Table 3.4**) has no activity at $IC_{50}$ >30 μM ($pIC_{50}$ < 4.52),[52] in keeping with the prediction of 96.3% for $pIC_{50}$ values below 5, for the BTO class. As for an evaluation of the prediction model between the non-covalent binders, it shows that it appears to vary between the different scaffolds, with the HYD class scoring the best predicted values and BI the poorest.

### 3.2.2.8. AMES Mutagenicity

The AMES test is a biological assay used to determine the mutagenic potential of a chemical compound,[140,141] which entails the activation of promutagens via mammalian metabolism.[142,143] AMES mutagenicity predictions were computed using StarDrop modules' toxicity models. Results yielded a high score of 96.0% (667/695) for covalent inhibitors, whereas the non-covalent binders only scored 32.5% (109/340) as an AMES positive prediction. The high value computed for covalent inhibitors was somewhat

expected, since nitro-aromatics are generally associated to mutagenicity[135,144] and the nitro-aromatic moiety is a common motif in covalent DprE1 inhibitors. The results revealed predictions of AMES mutagenicity for NBTO and NQ (100%), followed by BTZ (98.8%) > DNB (80.4%) and, lastly, predicted the non-mutagenic nature of NTZ (0%). All tested experimental NBTOs were found to be AMES positive[60], in keeping with the predictions. This liability of the NBTOs was circumvented by the addition of a methyl group adjacent to the nitro group, affording crowded benzothiazoles (cBTs), which tested AMES negative. Although the experimental work has shown no indication of mutagenic or nitro-active gene expression profiles following treatment with BTZ043, chemical proteomics showed evidence for induction of 60 genes, which was expected, as BTZs specifically target cell wall biogenesis. Therefore, concerns on the mutagenicity of the nitro group proved unfounded.[49] The AMES test demonstrated that the DNPT did not generate mutations in *S. typhimurium* TA98 and TA100 strains, even with metabolic activation.[71] For the non-covalent dataset the scored mutagenicity was 34.9%, with 2-S-BTO (100%) > HYD (76.3%) > MP (69.2%) > BD (60%) > BI (55.6%) > PTD (50%) > NC BTZ (36.4%) > AZA (31.6%) > PP (22.2%) > BTO (18.5%) > CD (15.9%) > TPA (10.4%) > 4-AQ, AVMT, NAHPC (0%) (**Figure 3.7-C**).

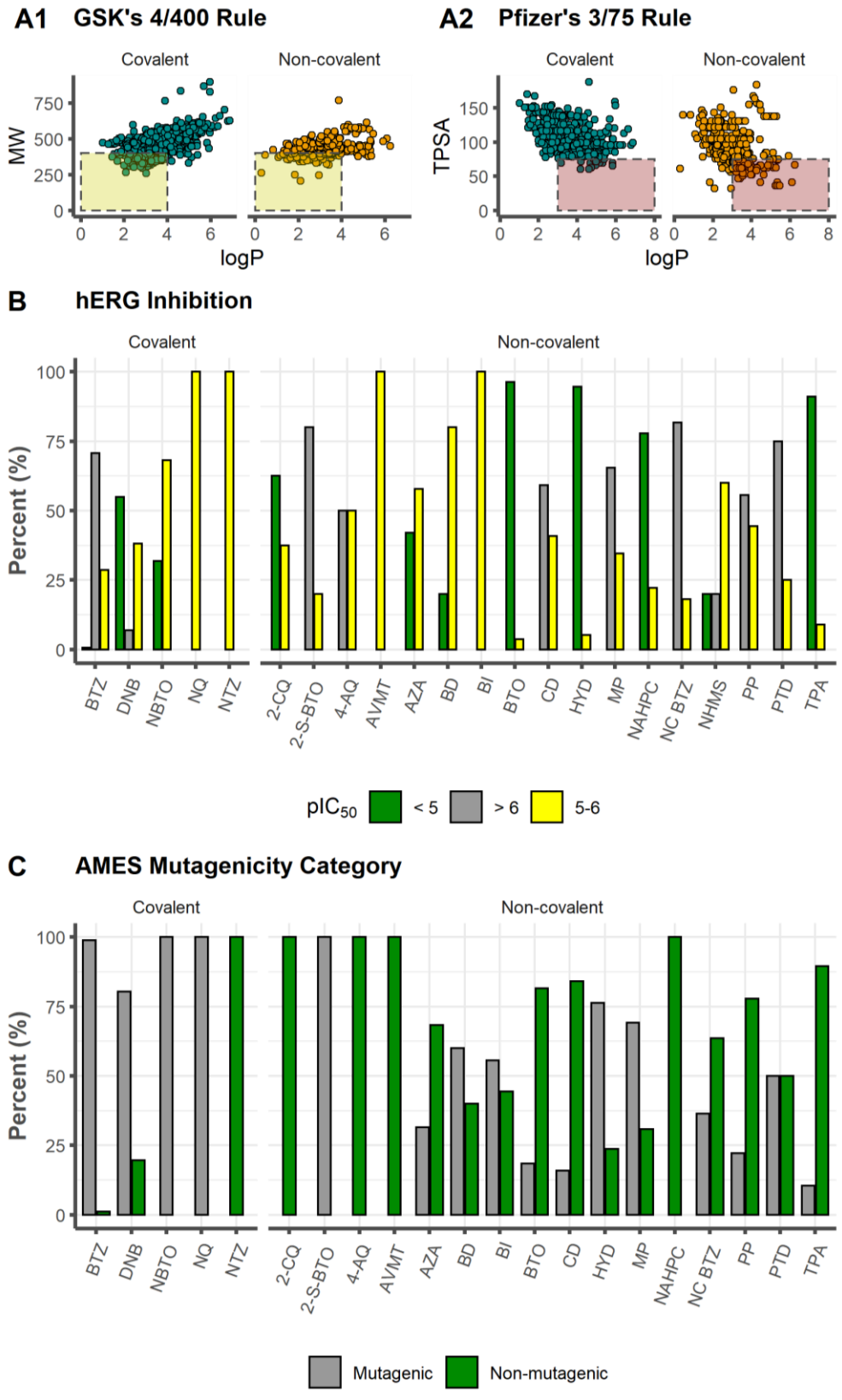


**Figure 3.7. A1:** MW as a function of cLogP. The yellow area indicates conformity by GSK's 4/400 Rule. **A2**: TPSA as a function of cLogP. The red area indicates the molecules that failed on Pfizer's 3/75 Rule. **B**: hERG Inhibition. **C:** AMES Mutagenicity Category.

**Table 3.4.** Experimental and the corresponding predicted hERG $pIC_{50}$ data of the non-covalent inhibitors.

**Hydantoins**

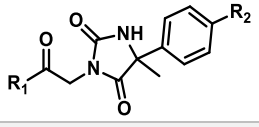

| $R_1$ | $R_2$ | $pIC_{50}$ | Pred $pIC_{50}$[a] |
|---|---|---|---|
| 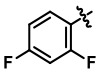 | -CN | **4.6** | **4.69** |
| 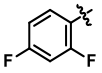 | $-OCH_3$ | **<4.3** | **4.57** |
| 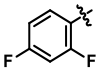 | $-OCHF_2$ | **5.3** | **4.94** |
| 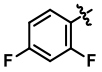 |  | **5.2** | **4.79** |
| 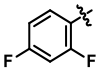 |  | **<4.3** | **4.68** |
| 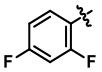 | $-SO_2CH_3$ | **<4.3** | **4.68** |
| 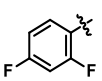 | $-NHSO_2CH_3$ | **4.4** | **5.14** |
| 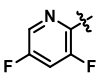 | -CN | **<4.3** | **4.44** |
| 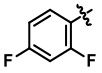 | $-SO_2NH_2$ | **<4.3** | **4.64** |
| 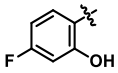 | $-SO_2NH_2$ | **<4.3** | **4.10** |
| 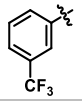 | $-SO_2NH_2$ | **<4.3** | **4.36** |
| 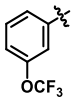 | $-SO_2NH_2$ | **<4.3** | **4.49** |
|  | $-SO_2NH_2$ | **<4.3** | **4.20** |
| 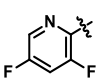 | $-SO_2NH_2$ | **<4.3** | **4.39** |
|  | $-SO_2NH_2$ | **<4.3** | **4.11** |

**1,4-Azaindoles**

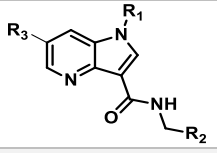

| $R_1$ | $R_2$ | $R_3$ | $pIC_{50}$ | Pred $pIC_{50}$[a] |
|---|---|---|---|---|
| 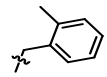 |  | -H | **4.55** | **5.14** |
| 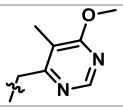 |  | -H | **<4.48** | **4.91** |
| 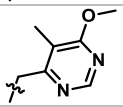 |  | -H | **<4.48** | **5.00** |
| 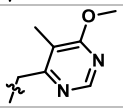 |  | $-CH_3$ | **<4.48** | **4.93** |
| 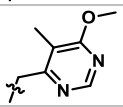 |  | $-CH_3$ | **<4.48** | **4.63** |
| 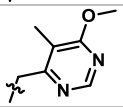 |  | $-CH_3$ | **<4.48** | **4.98** |
| 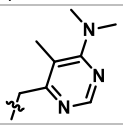 |  | $-CH_3$ | **<4.48** | **4.91** |
| 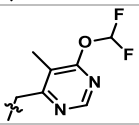 |  | $-CH_3$ | **<4.48** | **4.87** |
| 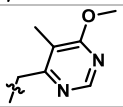 |  | $-OCH_3$ | **<4.48** | **4.61** |
| 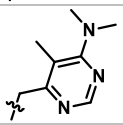 |  | $-OCH_3$ | **<4.48** | **4.88** |

**Thiophene-arylamides**

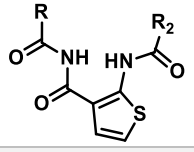

| $R_1$ | $R_2$ | $pIC_{50}$ | Pred $pIC_{50}$[a] |
|---|---|---|---|
|  | 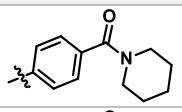 | **5.57** | **4.59** |
|  | 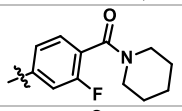 | **<4.52** | **4.59** |
|  | 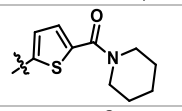 | **4.55** | **4.24** |
|  | 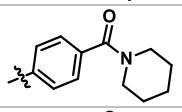 | **4.65** | **4.35** |
|  | 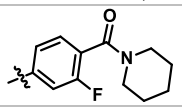 | **<4.52** | **4.47** |
|  | 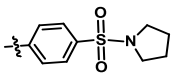 | **<4.52** | **4.47** |
| 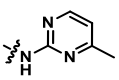 | 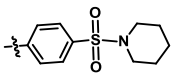 | **5.77** | **5.64** |
|  | 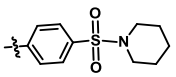 | **5.05** | **4.33** |

**Benzimidazoles**

| Structures | $pIC_{50}$ | Pred $pIC_{50}$ |
|---|---|---|
| 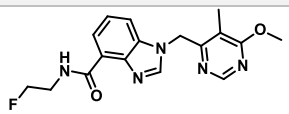 | **<4.48** | **5.17** |
| 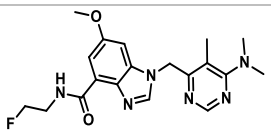 | **<4.48** | **5.39** |

**Benzothiazoles**

| | Structures | $pIC_{50}$ | Pred $pIC_{50}$ |
|---|---|---|---|
| TCA1 | 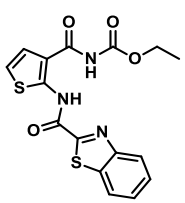 | **4.74** | **4.23** |

[a]Pred $pIC_{50}$: predicted hERG $pIC_{50}$ computed by StarDrop v7.2.0.32905

### 3.2.2.9. PAINS and Structural Alerts

Substructural warnings have become a common feature of the triage process in biological screening campaigns to identify Pan-Assay INterference compoundS (PAINS). PAINS generate false-positive assay responses as a result of their reactivity under assay circumstances,[145] which may include covalent modification, metal chelation, autofluorescence, aggregation, redox reactivity, among others.[146–149] Certain structural motifs ("Structural Alerts", SA) may result in covalent alteration of proteins or DNA, inducing negative effects (hepatotoxicity, CYP inhibition, *in vitro* genotoxicity, carcinogenicity).[146–149] We screened our dataset for PAINS count with StarDrop that embeds the original PAINS definitions, and we show that only 7.5% (52/695) of the covalent inhibitors scored for detected PAINS, with DNB having the highest percentage (29.4%), followed by the BTZ class (3.9%). The identified Structural Alerts (SA) for the covalent subset were Anil_Di_alk_E (3.45%) > Catechol (2.01%) > Hydroquinone (1.01%) > Anil_Di_alk_C (0.86%) > Aminothiazole (0.43%) > Benzodioxane, Azo_A (0.14%). The non-covalent set scored a higher proportion than the covalent set for PAINS, with 13.4% (45/340). The classes that contained SA were 2-S-BTO, BD (100%) > BTO (74.1%) > PTD (25%) > NC BTZ (9.1%) > CD (4.5%) > HYD (2.6%). Aminothiazole (11.48%) was the most frequent SA detected, followed by catechol (3.29%), then some residual Anil_Di_alk_E and hydroquinone (0.60%), together with anil_Di_alk_C, azide, benzodioxane (0.30%) (**Figure 3.8**). It is important to emphasize that, like for PC descriptors, PAINS substructures searches must be used cautiously when picking candidates, as there have been numerous observed deviations to these principles.

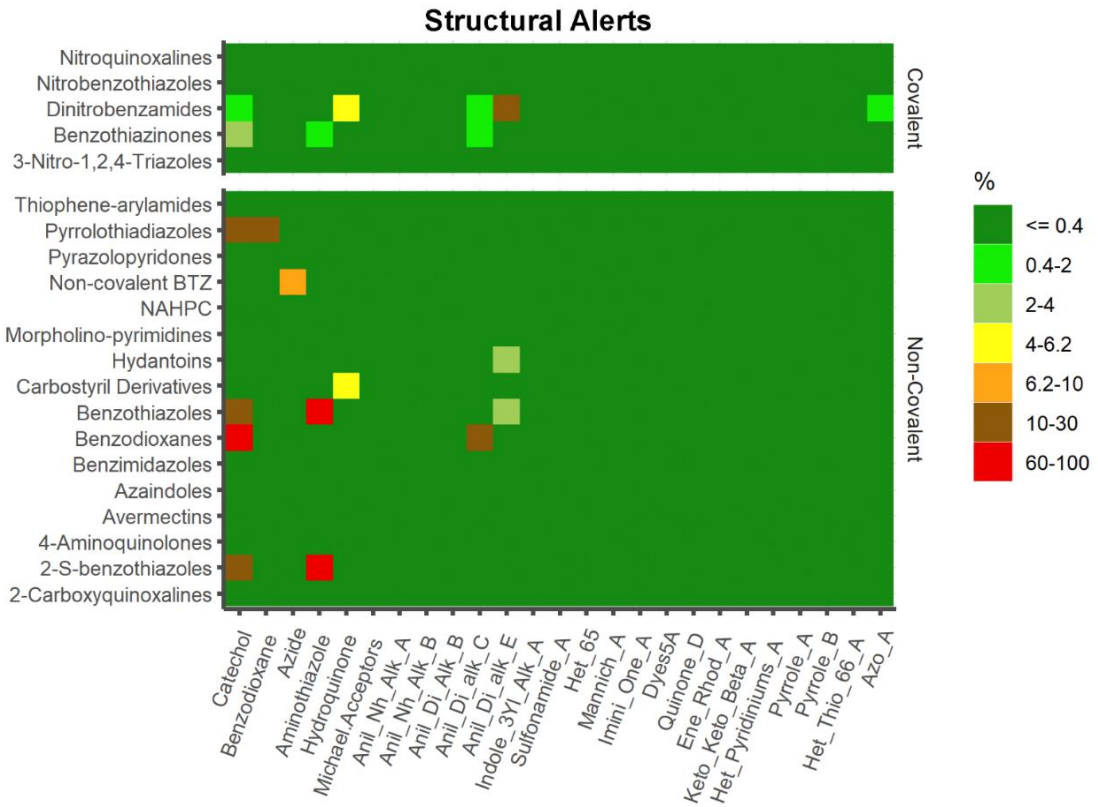


**Figure 3.8.** Matrix plot of Structural Alerts computed by ChemBioServer 2.0.

## 3.2.3. Conclusions for this section

DprE1 has been established as a potential therapeutic target for inhibiting mycobacterial cell wall biosynthesis. This enzyme is a highly druggable target against *M. tuberculosis* and various chemical scaffolds have been developed since its discovery. Twenty-three distinct chemical classes have been found to exhibit a high affinity for this enzyme, which are endowed with varying antimycobacterial activity and DMPK profiles. These inhibitor scaffolds are divided into covalent and non-covalent binders.

The design of DprE1 inhibitors can be challenging, therefore prediction of PC descriptors and ADMET properties for these molecules may aid in the design of new lead compounds. Extensive PC descriptor analysis indicates that for inactive covalent DprE1 to match the active set's corresponding properties more closely it may be necessary to optimize the compounds by increasing MW, ClogP, ClogD, HBA and TPSA, while reducing logS and HBD. In contrast, for inactive non-covalent DprE1 inhibitors it may be required to optimize the compounds by increasing MW, HBA, HBD, TPSA, FInd and ROTBS. All these changes are likely to increase the enthalpic component of drug binding through enhanced hydrogen bonding contacts with the enzyme. Covalent DprE1

inhibitors tend to violate the Ro5 more frequently than their non-covalent counterparts. However, only a small proportion fails the criteria by two or more violations, indicating that the DprE1 inhibitors are more likely to benefit from membrane permeability and hence be more readily absorbed in the human digestive system via passive diffusion. Almost all DprE1 inhibitors were predicted to have no CNS penetration, with the entire covalent subgroup scoring no CNS penetration and a residual value for non-covalent binders, reducing the possibility of side effects on the CNS. On the other hand, DprE1 inhibitors, particularly covalent binders, may act as P-gp substrates, which must be closely evaluated during drug optimization.

CYP3A4 was the major predicted isoform to metabolise DprE1 inhibitors, followed by the isoforms 2D6 > 2C19 > 2C9 for the covalent inhibitors, and 2C9 > 2D6 > 2C19 for the non-covalent inhibitors. These predictions contribute to our understanding of the role of the CYP superfamily in the metabolic stability of DprE1 inhibitors.

Toxicity endpoints were also examined and the cardiovascular toxicity of the DprE1 inhibitors *via* hERG inhibition was observed to be higher in the covalent than in the non-covalent subset, this observation holding for a cardiotoxicity investigation. Experimental data shows that optimizations can be made to improve this feature, as seen in the case of the hydantoin class. Noteworthy, other data with BTZ and TPA have shown no inhibition of the hERG potassium channel. Covalent inhibitors have scored in a higher proportion for mutagenic warnings than the non-covalent binders. This computed high value was expected since nitro-aromatic molecules are known to be mutagenic. In terms of undesirable structural motifs (Structural Alerts and PAINS), DprE1 inhibitors have a small number of these substructures, with the non-covalent set scoring higher for PAINS than the covalent set.

In conclusion, several molecular properties known as relevant for drug performance were analysed for the classes of DprE1 inhibitors described in the literature, comparing predicted and experimental values, when available. Our study provided information that should facilitate the design and optimization of future DprE1 inhibitors, allowing for the development of novel compounds targeting *M. tuberculosis.* As a mere aside, we would like to emphasize that our study comparing predicted and experimental values reveal that software tools employed to predict specific DMPK parameters must be used with caution while optimizing a drug class.

# 3.3. Machine learning in Medicinal Chemistry

From biological screening to hit-to-lead investigations and lead optimization, candidate drugs generate a great amount of experimental data. Most pharmaceutical company data is proprietary, although chemical activity data is rapidly becoming available. Chemoinformatics uses compound data for many chemical applications, including machine learning (ML) methodologies, to develop predictive models to find new active molecules.[150,151] Using predictive models to predict which compounds will have the best activity and those that should be prioritized, so that only the most promising are synthesized, would save time and resources.

To predict and identify potent DprE1 inhibitors, we built classification models of DprE1, a standard method for predicting the activity of a compound through its structural descriptors. The previously collected dataset of DprE1 inhibitors (Section 3.2.1.1.) was used to develop the classification models using molecular fingerprints MACCS, ECFP, and FCFP.

## 3.3.1. Molecular Fingerprints

Molecular fingerprints encode information about molecular properties and structure as sets of features that are mostly ordered bit strings and are one of the most used tools for similarity searches. They serve a crucial role in QSAR analysis, virtual screening, similarity-based compound search, ranking of target molecules, and drug ADMET prediction, among other drug discovery processes. In recent decades, numerous fingerprints have been produced for molecular feature encoding. Most fingerprints are 2D and can be retrieved from molecular connection tables without needing 3D structure information.[152-154]

There are four primary types of 2D fingerprints: substructure key-based fingerprints, circular fingerprints, topological or path-based fingerprints, and pharmacophore fingerprints.[154,155]

Substructure key-based fingerprints are bit strings that indicate the existence of particular substructures or fragments from a given set of structural keys in the compound. Molecular ACCess System (MACCS) keys are one of the most widely used key-based substructure fingerprinting techniques (**Figure 3.9**).[152]

Circular fingerprints are also hashed topological fingerprints, but instead of searching for routes in a molecule, they record the surroundings of each atom within a

predetermined radius. A well-known example of this class is the extended-connectivity fingerprint (ECFP, **Figure 3.9**), and the variant termed FCFP, the functional-class fingerprints (FCFP, **Figure 3.9**).[153] ECFPs are intended to capture precise atom environment substructural properties and employ a particular atom type as initial atom identifier, while FCFPs are designed to capture the broad functional roles of atoms and abstract-specific identifiers into one of several general atomic classes (e.g., hydrogen-bond donor, acceptor, halogen, aromatic).[153,156]

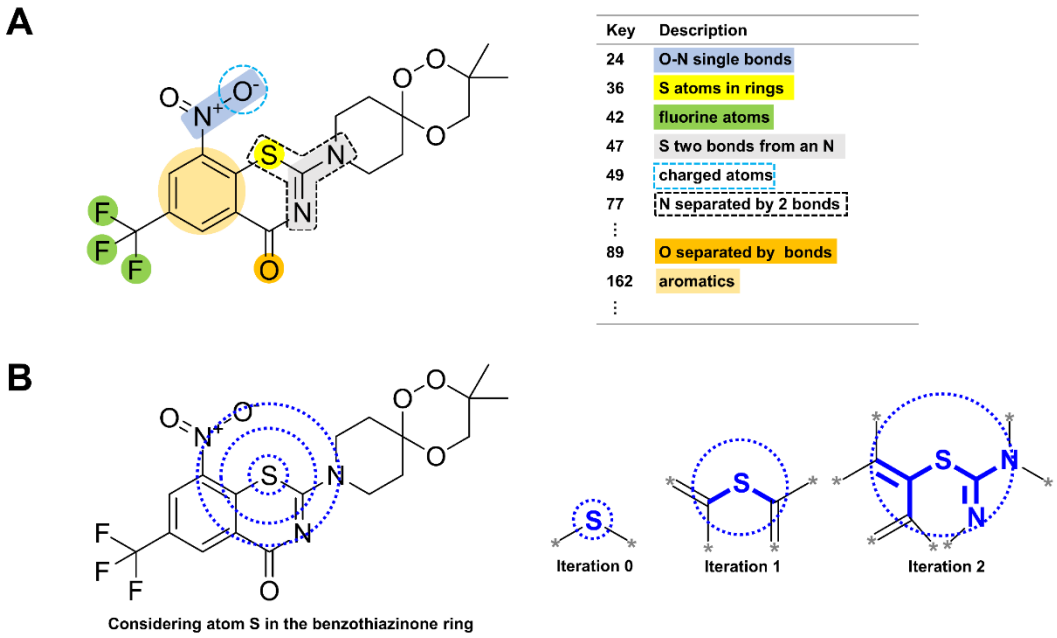


**Figure 3.9.** Illustrative example of the fingerprints for BTZ hybrid **PA54**: A) MACCS substructural keys. The molecule is shown with eight highlighted substructural features corresponding to the MACCS keys. B) Circular fingerprints consider local structural information. *Note that just a few of the molecule's fingerprints are represented in this example*. The binary fingerprint detects the absence or presence of those features in a compound, indicated by bit settings of 0 or 1, respectively.

## 3.3.2. Design of Classification Models for DprE1 inhibitors

Based on molecular fingerprints, we built a series of classification models by the machine learning methods of K-nearest neighbours (KNN),[157] support vector machine (SVM),[158] stochastic gradient boosting (GBM),[159] random forest (RF),[160] and extreme gradient boosting (XGB),[161] ranging from simpler and more interpretable models for establishing the best-performing methods for predicting DprE1 inhibitors. These algorithms are frequently used in QSAR studies.[162] **Figure 3.10** illustrates the protocol used for generating the different classification models. The protocol used was adapted from the reports of Li *et al*.[163] and Chu *et al*.[164]

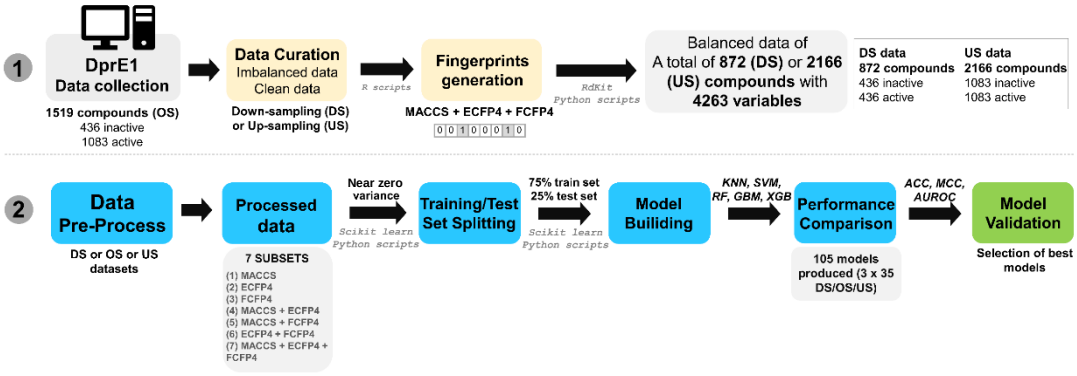


**Figure 3.10.** Schematic representation of the protocol used for generating the different classification models.

### 3.3.2.1. Data Preparation, compilation, and pre-processing

The dataset [data collection is explained in Section 3.2.1.1, and it is defined as original sample (OS)] was split into two subsets, a binary active (MIC < 10 μM, **1**) and not active (MIC ≥ 10 μM, **0**), following the MIC cut-off criteria adopted by the report of Makarov *et al.*[13] For this study, the separation of covalent and non-covalent inhibitors was not considered. We chose to produce a more general model for detecting new DprE1 inhibitors, regardless of the type of binding. The generated raw data was then prepared using manual R scripts in RStudio (Version 1.4.1106). Before processing, any observation with missing values was removed using `na.omit()` function,[165] and any duplicates across the data collection were identified and removed using the `duplicated()` function.[166]

The original sample (OS) dataset contained 1519 compounds corresponding to 1083 inhibitors and 463 non-inhibitors. By calculating the molecular fingerprints, the dataset was represented as a binary matrix (0 for absence of the fingerprint and 1 for the presence of the corresponding fingerprint), with the columns corresponding to the fingerprint length and the rows corresponding to the number of molecules in the data set. The RDKit toolkit (2022.9.3) was used to obtain the following molecular fingerprints: MACCS fingerprints, extended connectivity fingerprints[153] (ECFP4, diameter = 4, 2048 bits), and functional-class fingerprints[153] (FCFP4, diameter = 4, 2048 bits). A detailed description of the calculation of each fingerprint type can be found in the RDKit documentation.[167]

Note that the dataset was imbalanced, with 1083 active molecules *versus* 436 non-active molecules. In supervised machine learning, it is important to train an estimator on

balanced data, allowing the model to be equally informed in all classes.[168] Therefore, we used two different functions available in R to solve this situation: (1) `downSample()` function,[169] which will randomly sample a data set so that the frequency of all classes equals that of the minority class, hence producing a final down-sampling dataset (DS) of 872 molecules with 4263 variables (167 MACCS + 2048 ECFP4 + 2048 FCFP4) or (2) `upSample()` function,[170] which uses random up-sampling to adjust group sizes to the largest group within the data frame, therefore producing a final up-sampling dataset (US) of 2070 molecules with 4263 variables (167 MACCS + 2048 ECFP4 + 2048 FCFP4). Various compilations of these generated predictors sets were exported as separate .csv files, resulting in seven predictor data sets (**Table 3.5)**:

1. MACCS: 167 MACCS fingerprints only (total of 167, M);
2. ECFP: 2048 bits of extended connectivity fingerprints only (total of 2048, E);
3. FCFP: 2048 bits of functional-class fingerprints only (total of 2048, F);
4. MACCS + ECFP, the combination of 167 MACS fingerprints and 2048 bits of extended connectivity fingerprints (total of 2215, ME);
5. MACCS + FCFP, the combination of 167 MACS fingerprints and 2048 bits of functional-class fingerprints (total of 2215, MF);
6. ECFP + FCFP: the combination of 2048 bits of extended connectivity fingerprints and 2048 bits of functional-class fingerprints (total of 4096, EF);
7. MACCS + ECFP + FCFP: the combination of 167 MACCS fingerprints, 2048 bits of extended connectivity fingerprints, and 2048 bits of functional-class fingerprints (total of 4263, MEF).

The datasets of 872 (DS), 1519 (OS), and 2070 (US) available compounds were also pre-processed by R scripts. Pre-processing was employed, using the library `caret`, in which the `nearZeroVar()` function was used to identify predictors with one unique value (i.e., zero variance predictors) or predictors with both of the following criteria: they have a small number of unique values compared to the number of samples and a high ratio between the frequency of the most frequent value and the frequency of the second most frequent value.[171] Using near zero variance function afforded the final number of predictors for each subset, as shown in **Table 3.5**. The pre-processed subsets were then divided into a training set and a test set, at a ratio of 3:1, by employing `train_test_split()` function,[172] with the defined parameter `random_state=789`. Subsequently, the training sets were employed for model

construction and the test sets were used to evaluate the constructed model's classification performance.

**Table 3.5.** Number of predictors generated within the RDKit package and after data pre-processing using R.

| | | | After pre-processing | | |
|---|---|---|---|---|---|
| **ID** | Data set | **Original number of predictors** | **DS** | **OS** | **US** |
| **M** | MACCS | 167 | 112 | 110 | 111 |
| **E** | ECFP4 | 2048 | 350 | 342 | 345 |
| **F** | FCFP4 | 2048 | 291 | 291 | 280 |
| **ME** | MACCS + ECFP4 | 2215 | 461 | 451 | 455 |
| **MF** | MACCS + FCFP4 | 2215 | 402 | 400 | 390 |
| **EF** | ECFP4 + FCFP4 | 4096 | 615 | 632 | 624 |
| **MEF** | MACCS + ECFP4 + FCFP4 | 4263 | 751 | 741 | 734 |

### 3.3.2.2. Algorithm selection

Five machine learning algorithms were used to build the best classification model: KNN, SVM, RF, GBM, and XGB models, in which these models were built with the scikit-learn package (`sklearn` libraries, version 1.0.2)[173] and XGB with the `xgboost` library.[174] These algorithms are frequently used in QSAR studies.[162] Before training with the various datasets, the selected algorithms (described in the following paragraphs) underwent slight hyperparameter tuning, employing the US dataset incorporating all fingerprints.

#### 3.3.2.2.1. K-Nearest Neighbours

K-nearest neighbours (KNN) is a non-parametric, supervised learning classifier that employs proximity to classify or predict how a particular data point will be clustered.[157] KNN construction relies solely on data from the training set; therefore, the model cannot sufficiently summarize it. The number of k-closest samples observed in each class determines the class probability of a new sample in classification.[164] For our KNN model building, the hyperparameter `n_neighbors` was set to 3, using the `KNeighborsClassifier()` function, while other parameters were default values.[175]

#### 3.3.2.2.2. Support Vector Machines

Support vector machines (SVM) look for the best hyperplane in an N-dimensional space (N is the number of features) to categorize the data points distinctly.[176] The support

vectors used to determine the class probability for the new samples are training points that define the greatest margin that the optimal hyperplane would have.[176,177] SVM uses the so-called kernel functions to map the sample to a high-dimensional feature space using nonlinear mapping to perform nonlinear classification accurately, allowing calculation without the need to transform the predictors.[158,176,177] Within this study, the function `svm.svc()` was used to create the SVM model, in which it was set the parameter `probability=True`, the radial basis function as the kernel function (`'rbf'`). The remaining parameters were set to the default values.[178]

#### 3.3.2.2.3. Random Forest

For classification, regression, and other tasks, the ensemble learning method, known as random forest (RF), assembles a large number of classification trees during training, being able to produce accurate models without the need for input data preparation. When using decision trees as classifiers, this method improves predictive accuracy while avoiding over-fitting.[160]

Within this study, the function `RandomForestClassifier()` was used for the random forest models, in which four training parameters were optimized in the evaluation criteria when splitting nodes: `criterion`, set to `'entropy'`; the number of decision trees in the forest (`n_estimators`), set to 120; the maximum number of leaf nodes (`max_leaf_nodes`), set to 150, and the parameter `random_state=0`, while other parameters were default values.[179]

#### 3.3.2.2.4. Stochastic Gradient Boosting

In gradient boosting machines (GBMs), the learning mechanism successively fits new models to provide an increasingly accurate estimate of the response variable.[180] Based on the previously assembled trees, this algorithm aims to generate new base learners that are maximally associated with the loss function's negative gradient.[159] GBM shares similarities to RF, where both are ensembles of tree models, although the tree models within GBM are generated using a randomly selected fraction of the input data at each iteration, relying on previously computed trees.[113] Within this study, the function `GradientBoostingClassifier` was used to build the GBM model, in which all the parameters were set to default values, except for the parameter `random_state`, which was set to 123.[181]

#### 3.3.2.2.5. Extreme Gradient Boosting

Extreme gradient boosting (XGB) is an ensemble learner based on gradient boosting that incorporates additional regularisation parameters to aid in the control of over-fitting, resulting in potentially improved performance.[182] The function `XGBClassifier()` was used to build the XGB model, where twenty training parameters were manually set (Please see **Table S5**, in the *Appendix*, for more information).[183,184]

### 3.3.2.3. Model evaluation

Following model construction using `sklearn` libraries with the default tuning parameters outlined previously, five- and ten-fold (5 and 10-fold) cross-validation on the training set for each predictor data set were performed. Cross-validation enables us to validate which models do not overfit, particularly those displaying high accuracy values in the training set.[113] The generated models were then tested using the test set.

The performance of classification models was assessed using a variety of metrics: (1) accuracy (Q), (2) precision (P), (3) sensitivity (SE), (4) specificity (SP), (5) Matthews correlation coefficient (MCC), and (6) f1 score. The following equations express their corresponding definitions,[113]

$$Accuracy\ (Q) = \frac{TP + TN}{TP + TN + FP + FN} \tag{1}$$

$$Precision\ (P) = \frac{TP}{TP + FP} \tag{2}$$

$$Sensitivity\ (SE) = \frac{TP}{TP + FN} \tag{3}$$

$$Specificity\ (SP) = \frac{TN}{TN + FP} \tag{4}$$

$$MCC = \frac{TP\ \times TN - FP\ \times\ FN}{\sqrt{(TP + FP)(TP + FN)(TN + FP)(TN + FN)}} \tag{5}$$

$$f1\ score = \frac{2\ \times (Precision\ \times sensitivity)}{(Precision + sensitivity)}\ or$$

$$f1\ score = \frac{TP}{TP + \frac{1}{2}(FP + FN)} \tag{6}$$

where TP are true positives, TN are true negatives, FP are false positives, FN are false negatives.[113]

Accuracy provides a global measure of how effectively the model predicts the full data set.[113]

Precision, also known as positive predictive value, is the proportion of true positives among positive samples, and it ranges from 0 to 1.[113]

Sensitivity, also known as recall, is the ratio of true positives to all positives, and it ranges from 0 to 1.[113]

The f1 score is the weighted mean of recall and precision. It ranges between 0 and 1 and takes both false negatives and false positives into account. This metric is particularly useful when the data set is imbalanced.[113,185]

MCC analyses the performance of the models based on the confusion metrics. Among these evaluations, the MCC is the most relevant indicator for measuring binary classification performance and is considered the primary parameter for selecting a prediction model. Overall, the higher the MCC value, the superior the classification performance.[184,185] When MCC equals −1, it shows a total disagreement between observed and predicted classes. A value of 0 shows no better than a random prediction whereas a coefficient of +1 shows a perfect prediction.[186,187]

The area under the Receiver Operating Characteristic Curve (AUROC, or AUC or ROC) can assess how much better the model prediction is, over a random guess, and it was also calculated and plotted.[188]

## 3.3.3. Results and discussions

### 3.3.3.1. Diversity of DprE1 inhibitors

For similarity searches with molecular fingerprints, one must additionally quantify the overlap between two fingerprints, enabling the chemical diversity of these molecules to be characterized. Different structure similarity coefficients can be employed for this purpose (e.g. Cosine, Hamming, Tanimoto),[155] in which we calculated the Tanimoto coefficient (TC) based on the ECFP4 fingerprints for each pair of compounds. The TC can be used to measure pairwise structural similarity.[189] These metrics attempt to establish a correlation between the number of typically set bits, returning similarity values between 0 and 1, where 1 indicates a perfect match. The TC was calculated against each molecule (combination: $C_2^n$), with $n$ =1519 for the whole dataset, $n$ = 852 for the covalent inhibitors, and $n$ = 667 for the non-covalent ones. The distribution profile of TC for the different datasets is depicted in **Figure 3.11.** For all DprE1 inhibitors (**Figure 3.11A**) a mean of TC of 0.144 ± 0.118 was obtained, indicating a chemical diversity over the DprE1 inhibitors class. Curiously, when analysing the covalent and non-covalent binders separately, the covalent class has a higher TC mean value of 0.242 ± 0.147 (**Figure 3.11B1**), versus 0.125 ± 0.107 (**Figure 3.11B2**), a nearly two-fold increase compared to the non-covalent binders. This result can be explained, since in our covalent subset there are only 5 types of covalent binders (compared to 17 types in the non-covalent binders subset), and approximately ~74% of the covalent subset is composed of benzothiazinone-based compounds, which differ mostly in the amine chain at position 2.

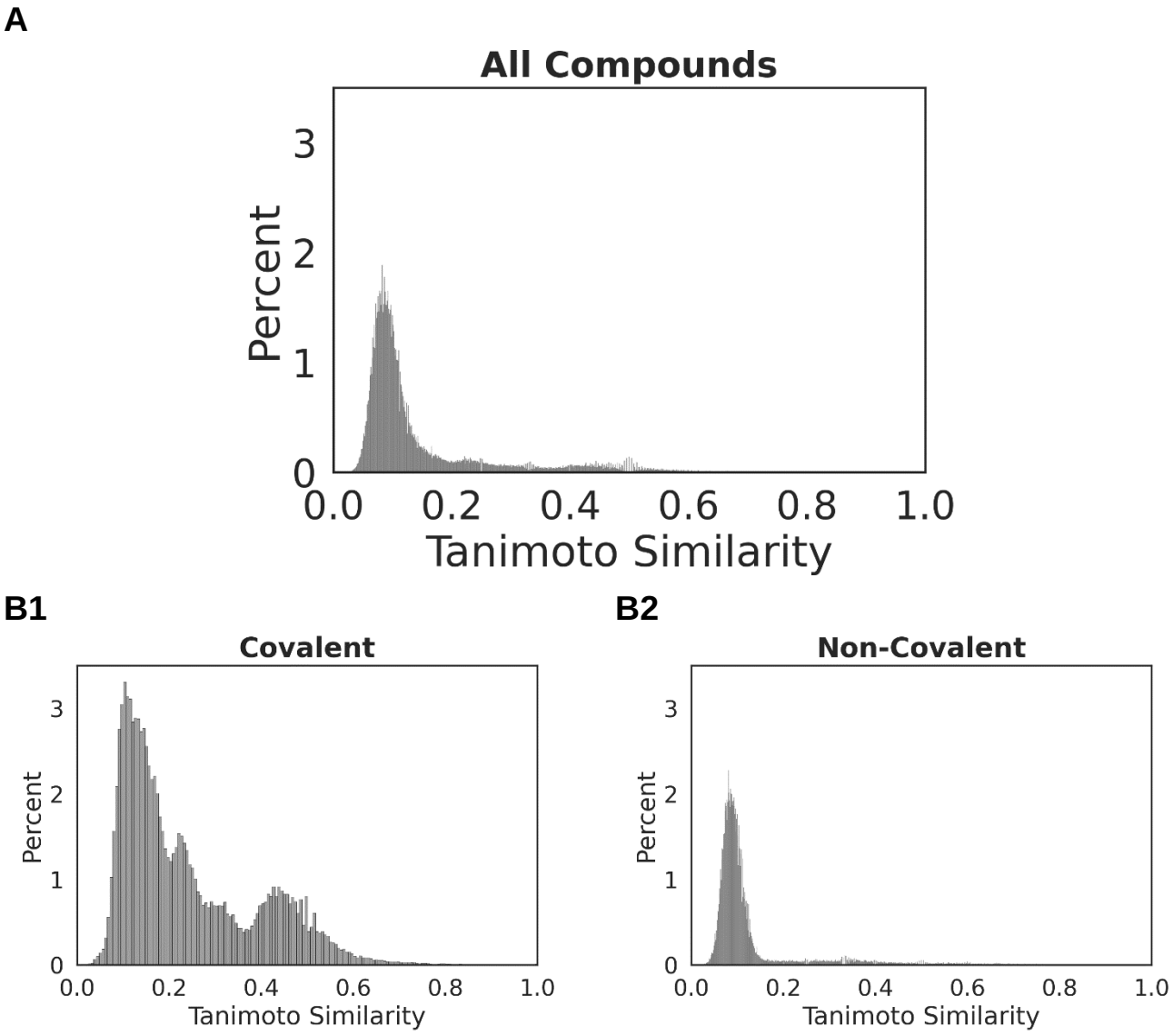


**Figure 3.11.** Frequency distribution of topological similarity (Tanimoto coefficient, TC) of DprE1 inhibitors based on ECFP4 fingerprints for **A)** all compounds (Covalent + Non-covalent), **B1)** covalent and **B2)** non-covalent inhibitors.

### 3.3.3.2. Performance of optimal models identified by 5 and 10-fold cross-validation.

In this study, a total of 105 binary classification models were constructed using the combination of five algorithms with three variations of the sample set (DS, OS, US) for each of the seven predictor subsets. The binary classification prediction models were developed using three types of fingerprints (MACCS, ECFP4, and FCFP4) with five classification machine learning methods: KNN, SVM, GBM, RF, and XGB, and their performances are depicted in **Tables S1-5** (see in the *Appendix*). When training the models, fivefold cross-validation (CV-5) and tenfold cross-validation (CV-10) were

employed on the training set. All the models were tested and measured by Q, P, SE, SP, MCC, and f1-score, to assess of the model performance.

The detailed performances of the optimal model for each algorithm are shown in **Table 3.6.** Afterward, we further analysed the AUROC curve of the best model for each algorithm (**Figure 3.12**).

**Table 3.6.** Performance metrics of the best model for each algorithm (KNN, SVM, GBM, RF, XGB).

| Model | Subset | FPS | Training set | | | | Test set | | | | | | |
|---|---|---|---|---|---|---|---|---|---|---|---|---|---|
| | | | Q | MCC | 5-CV | 10-CV | Q | P | SE | SP | MCC | AUC | f1 |
| **KNN16** | **US** | **E** | 0.947 | 0.895 | 0.883 ± 0.010 | 0.886 ± 0.017 | 0.895 | 0.896 | 0.895 | 0.895 | 0.791 | 0.895 | 0.895 |
| **SVM19** | **US** | **M + F** | 0.903 | 0.807 | 0.873 ± 0.016 | 0.878 ± 0.019 | 0.887 | 0.888 | 0.887 | 0.888 | 0.775 | 0.887 | 0.887 |
| **GBM18** | **US** | **M + E** | 0.936 | 0.873 | 0.892 ± 0.015 | 0.896 ± 0.020 | 0.900 | 0.900 | 0.900 | 0.900 | 0.801 | 0.900 | 0.900 |
| **RF21** | **US** | **M + E + F** | 0.972 | 0.945 | 0.928 ± 0.008 | 0.929 ± 0.016 | 0.921 | 0.921 | 0.921 | 0.921 | 0.842 | 0.921 | 0.921 |
| **XGB21** | **US** | **M + E + F** | 0.997 | 0.994 | 0.933 ± 0.014 | 0.939 ± 0.016 | 0.941 | 0.941 | 0.941 | 0.941 | 0.882 | 0.941 | 0.941 |

As depicted in **Tables S1-5**, it was determined that the 35 generated models for the DS subset show a good performance, with accuracy >0.78, precision >0.78, sensitivity >0.78, specificity >0.78, MCC >0.57, AUROC >0.78, and f1 score >0.78. Regarding the 35 constructed models for the US subset, these models showed the best performance among the subsets, with accuracy >0.85, precision >0.85, sensitivity >0.85, specificity >0.85, MCC >0.71, AUROC >0.85, and f1 score >0.85. In comparison to the balanced subsets, the performance of the 35 generated models for the original subset (OS) was inferior, with an accuracy >0.80, precision >0.77, sensitivity >0.80, specificity >0.63, MCC >0.51, AUROC >0.72, and f1 score >0.75. When examining the different metrics, it can be shown that the OS subset had the lowest metric specificity (>0.63) compared to the DS (>0.78) and US (>0.85) subsets. A specificity value of 0.63 means that 63% of the inactive compounds were labelled accurately. This result is expected, given that the original sample comprises only ~30% inactive molecules ($n$ = 463/1519) and, during model training, the model is less likely to identify the inactive compounds precisely. Evidently, this reduced specificity value will impact the MCC metric used to evaluate the performance model. This result provides a clear example for the need to prepare a balanced dataset during pre-processing. The specificity metric improves when the sample is balanced by down-sampling or up-sampling, with the US subset exhibiting the highest value (>0.85). Lastly, ECFP4 and FCFP4 fingerprints outperformed MACCS in

differentiating between active and inactive DprE1 inhibitors in models with only one fingerprint type.

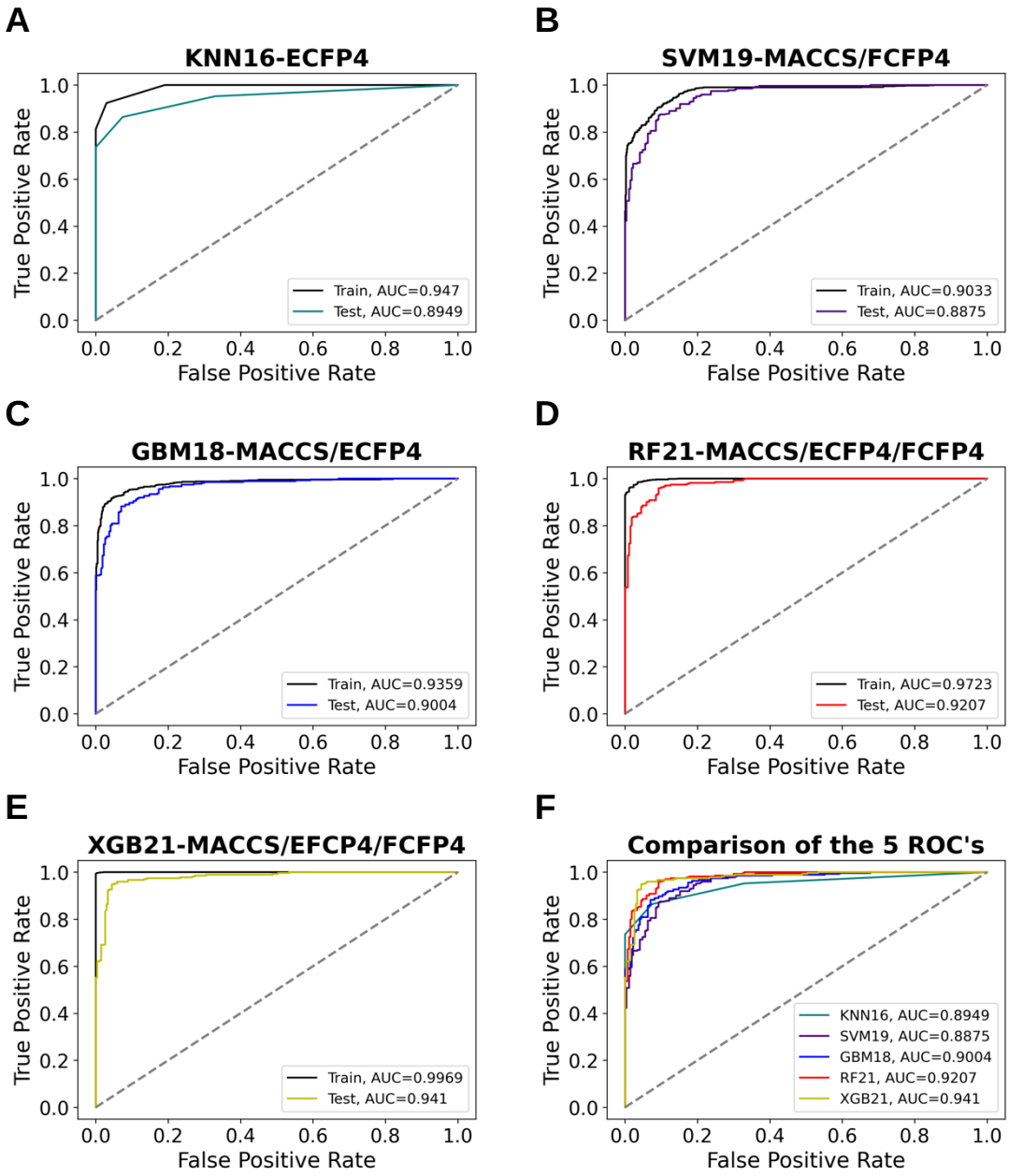


**Figure 3.12.** Receiver operating characteristics (AUROC, or AUC, or ROC) curves of 5 models were optimal for each algorithm. **(A)** KNN16-ECFP4, **(B)** SVM19-MACCS/FCFP4, **(C)** GBM18-MACCS/ECFP4, **(D)** RF21-MACCS/ECFP4/FCFP4, **(E)** XGB21-MACCS/EFCP4 /FCFP4. **(F)** Comparison of the ROC curves between the 5 best models.

Regarding the KNN models, MCC values on the test set exceeded >0.53, which showed that the 21 KNN models had moderate to good predictive performance. The models built with DS or OS exhibited MCC values of >0.57 (good) and >0.53 (moderate),

whereas all models built with US subsets surpassed >0.73 (good). F1 scores increased when assessing predictions on balanced sets, with an f1 score ranging from 0.81 ± 0.01 for DS and an f1 score ranging from 0.88 ± 0.01 for the US dataset, while for the OS, it had an f1 score between 0.77 ± 0.01. The best performed KNN model was KNN16, using the US subset built with solely ECFP4 fingerprints. It gave a prediction accuracy of 0.947 on the training set, 0.895 on the test set, with MCC = 0.791, precision = 0.896, sensitivity = 0.895, and specificity = 0.895 on the test set. The training and test sets' AUROC values (**Figure 3.12A**) were 0.947 and 0.895, respectively. ECFP4 fingerprints are more suitable for the KNN algorithm to classify DprE1 inhibitors than the other three types of molecular fingerprints. Detailed results for each KNN model are given in **Table S1**.

For the SVM models, MCC values on the test set exceeded >0.53, which showed that the 21 SVM models had moderate to good predictive performance. The models built with DS or OS exhibited MCC values of >0.63 (good) and >0.53 (moderate), whereas all models built with the US subset exceeded >0.71 (good). As expected, F1 scores also increased when assessing predictions on balanced subsets for this algorithm, with an f1 score ranging from 0.84 ± 0.01 for the DS and from 0.88 ± 0.01 for the US datasets, while for the OS it showed an f1 score between 0.78 ± 0.02. The best performed SVM model was SVM19, using the US subset built with MACCS and FCFP4 fingerprints. It gave a prediction accuracy of 0.903 on the training set, 0.887 on the test set, with MCC = 0.775, precision = 0.888, sensitivity = 0.887, and specificity = 0.888 on the test set. The AUROC values (**Figure 3.12B**) of the training and test sets were 0.903 and 0.888. MACCS and FCFP4 fingerprints are more suitable for the SVM algorithm to classify DprE1 inhibitors than the other three types of molecular fingerprints. Detailed results for SVM algorithm with each model are given in **Table S2**.

Within the GBM models, the MCC values on the test set exceeded >0.56, which showed that the 21 GBM models had moderate to good predictive performance. The models built with DS or OS exhibited MCC values of >0.61 (good) and >0.56 (moderate), whereas all models built with the US subset exceeded >0.73 (good). F1 scores also increased when assessing predictions on balanced sets for this algorithm, with an f1 score ranging from 0.83 ± 0.01 for the DS and from 0.89 ± 0.01 for the US datasets, while for the OS, it had an f1 score between 0.81 ± 0.02. The best performed GBM model was GBM18, using a US subset built with MACCS and ECFP4 fingerprints. It gave a prediction accuracy of 0.936 on the training set, 0.900 on the test set, and an MCC = 0.801, precision = 0.900, sensitivity = 0.900, and specificity = 0.900 on the test set. The

training and test sets' AUROC values (**Figure 3.12C**) were 0.936 and 0.900. MACCS and ECFP4 fingerprints are more suitable for the GBM algorithm to classify DprE1 inhibitors than the other three types of molecular fingerprints combined. Detailed results for each GBM model are given in **Table S3**.

The MCC values of all the RF models on the test set exceeded >0.53, which showed that the 21 RF models had moderate to good predictive performance. The models built with DS or OS exhibited MCC values of >0.59 (good) and >0.53 (moderate), whereas all models built with the US subset exceeded >0.78 (good). Using this approach, the models constructed from US subsets ensure an increase in performance. F1 scores only increased when assessing predictions on the balanced US sample, with an f1 score ranging from 0.91 ± 0.01 for the US dataset, while for the OS f1 score ranged between 0.83 ± 0.02 and for the DS also ranged from 0.83 ± 0.01. The best performed RF model was Model RF21, built with three types of fingerprints, MACCS, ECFP4, and FCFP4. It gave a prediction accuracy of 0.972 on the training set, 0.921 on the test set, with MCC = 0.842, precision = 0.921, sensitivity = 0.921, and specificity = 0.921 on the test set on the test set. The training and test sets' AUROC values (**Figure 3.12D**) were 0.972 and 0.921. Detailed results for each RF model are given in **Table S4**.

For the XGBoost models, MCC values on the test set exceeded >0.51, which showed that the 21 XGB models had moderate to good predictive performance. The models built with DS or OS exhibited MCC values of >0.57 (moderate) and >0.51 (moderate), whereas all models built with the US subset exceeded >0.81 (very good). The f1 scores only increased when assessing predictions on the balanced US sample, with an f1 score ranging from 0.93 ± 0.01 for the US dataset, while for the OS and DS datasets the f1 score ranged between 0.83 ± 0.02. The best performed one in XGB models or even in all the generated models was XGB21, using the US subset, built with MACCS, ECFP4, and FCFP4 fingerprints. It gave a prediction accuracy of 0.997 on the training set and 0.941 on the test set, with MCC = 0.882, precision = 0.941, sensitivity = 0.941, specificity = 0.941 and f1 score = 0.941 on the test set. The training and test sets' AUROC values (**Figure 3.12E**) were 0.997 and 0.941. Detailed results are given in **Table S5**.

Our results, as measured by the MCC and f1 score, clearly demonstrate that imbalanced data impacts greatly the performance of the models. Even balancing the dataset can be difficult, as evidenced by the fact that the US dataset appeared to be the most effective at avoiding this problem, as it provided higher MCC and f1 scores for all algorithms.

The results of five- and ten-fold cross-validation for each of the five optimal models confirmed that the models did not appear to overfit, particularly in the ensemble tree models (RF and XGB), which displayed very high accuracy values in the training set (**Table 3.6**).

### 3.3.3.3. The overall importance of the fingerprints within the SVM, RF and XGB models

Having successfully constructed the predictive models, we chose to investigate the effect of molecular fingerprints on the model's output to interpret the importance of the relevant features. The variable importance of the predictors for the best models was provided by the fitted attribute `feature_importances_` from the scikit-learn library.[190] **Figure 3.13** shows the property importance for the best models GBM, RF, and XGB. These fingerprints are ranked based on their significance in accurately predicting the activity of a compound.

Regarding the best model for the algorithm GBM, the MACCS key 63 is the most important property, and it is related to the N atoms in double bonds with O (**Figure 3.13A**). This probably indicates a nitro or nitroso group (N=O). For the algorithm RF, the most important property was the MACCS key 49, which is related to charged atoms (**Figure 3.13B**). When analysing our dataset, it is likely to be an N-**O**$^{-}$ function for the nitro group (**Figure 3.13C**). Concerning the XGB model, the most important property was the FCFP4 key 16, and considering as an example for the benzothiazinone BTZ043, it is related to the $N^{+}$, belonging to the distinct nitro group present in these molecules.

The results clearly show a pattern across all models: the presence or absence of a nitro group is the most important factor in determining whether a molecule inhibits or does not inhibit the DprE1 enzyme. Thus, it suggests that models may be better suited to recognise covalent binders. This observation indicates that tuning these models to enable a more effective selection of non-covalent binders ought to be addressed. A potential solution could be to split the collected dataset into covalent and non-covalent binder subsets. It is not always possible to map fingerprints onto molecular fragments, but the approach's value comes from virtual screening and prioritization of molecules. From these new data, new classification models can be produced. The models' performance should then be evaluated with external validation data.

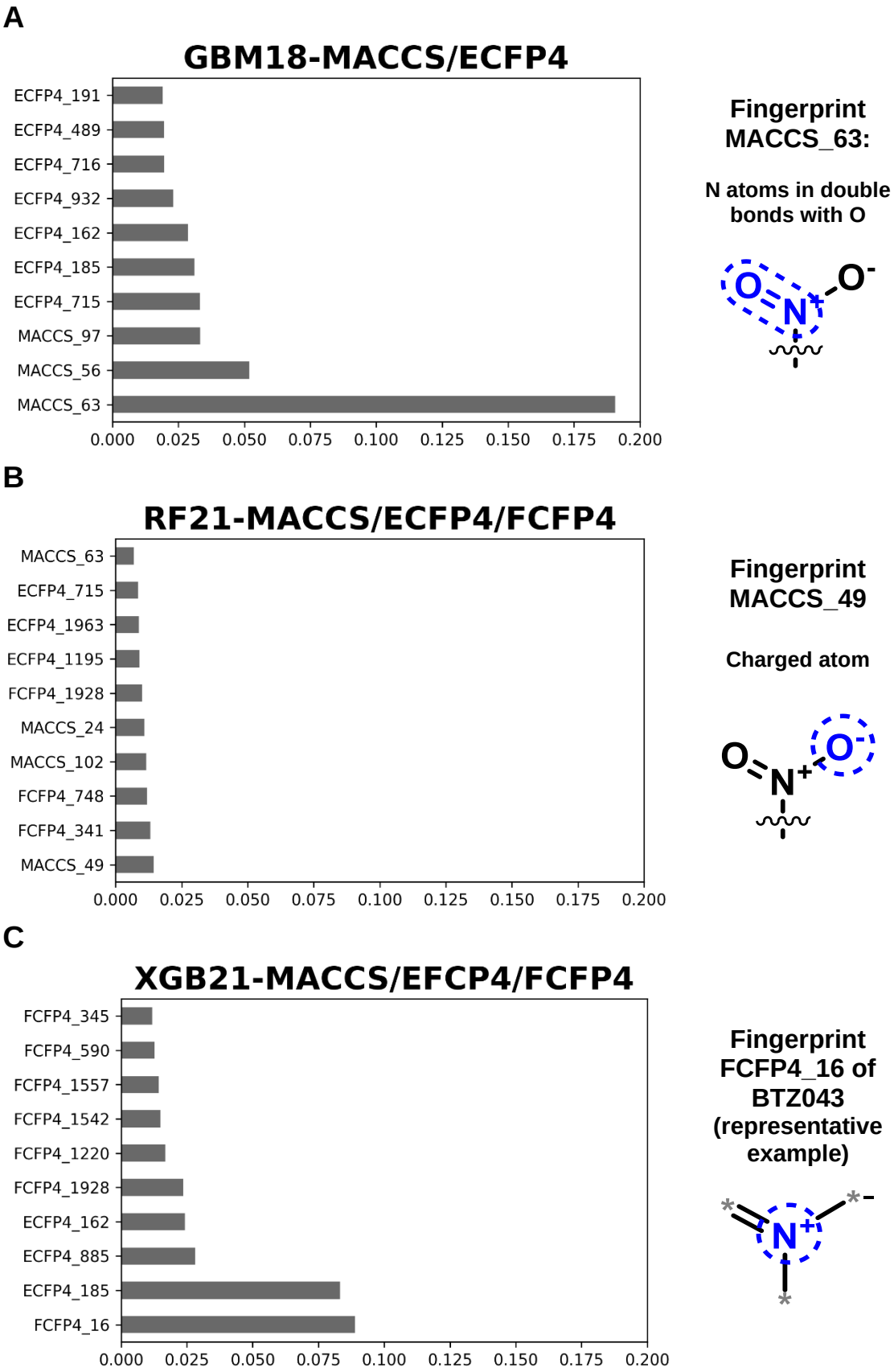


**Figure 3.13.** Property importance for the best models: A) GBM18, B) RF21 and C) XGB21.

### 3.3.3.4. Evaluation of the performance in classifying the profile in the synthesized 1,2,4-trioxane hybrids

Following the general calculations of the performance metrics of the models, we used the best model for each algorithm to assess the classification as active or inactive for the 1,2,4-trioxane hybrids that were synthesized throughout this PhD project. The small sample of the hybrids comprised the three IC-trioxane MmpL3 inhibitors, which should be classified as not active (or non-inhibitor of DprE1), and eleven BTZ-trioxane hybrids, which should be classified as active (or inhibitor of DprE1). Confusion matrices for algorithms KNN, SVM, GBM, RF, and XGB are depicted in **Figure 3.14**. Only the KNN16 model could not appropriately classify IC-trioxane hybrids as non-inhibitors or inactive molecules, as evidenced by the confusion matrix, and with an MCC value of 0.531 (**Figure 3.14A** and **F**). Except for model KNN16, the remaining algorithms correctly identified the corresponding compounds as active, for the BTZ peroxide hybrids, and inactive, for IC peroxide hybrids. Since all models seem to be better suited to classify potential covalent inhibitors, this result of high predictive performance was somewhat anticipated. To effectively evaluate these classification models, more validation data should be employed.

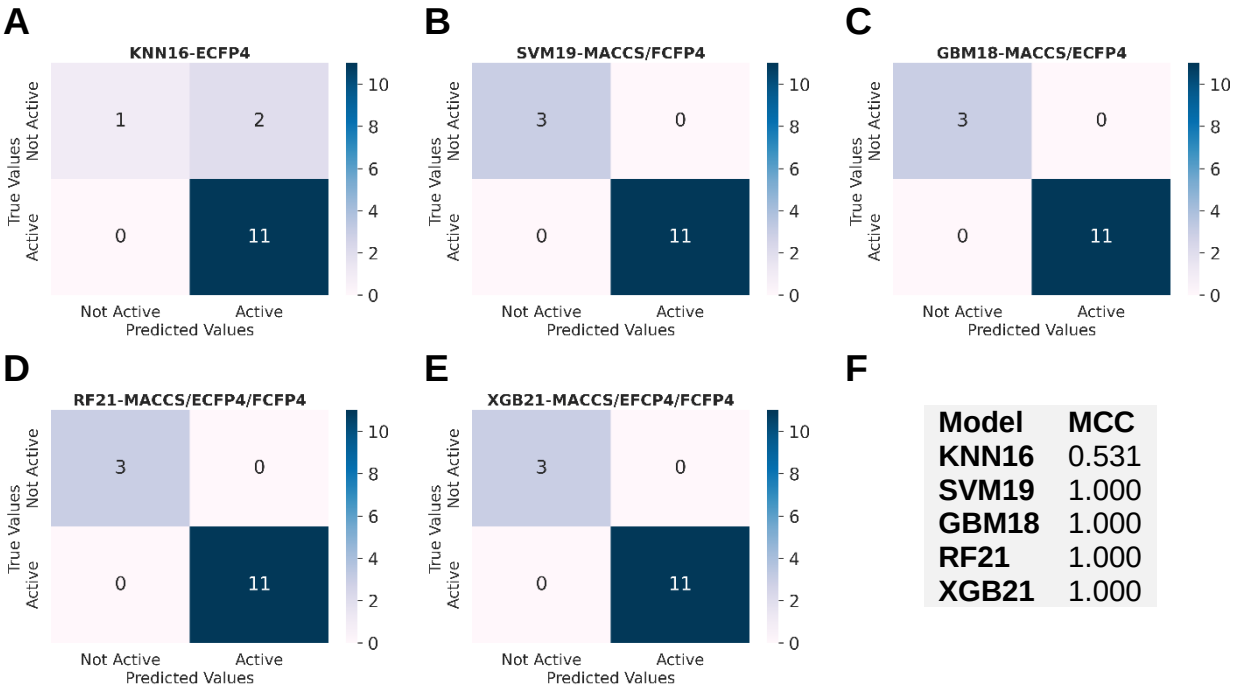


**Figure 3.14.** Confusion matrices for **(A)** KNN16, **(B)** SVM19, **(C)** GBM18, **(D)** RF21, and **(E)** XGB21 during predictions of activity class of the 1,2,4-trioxane hybrids compounds.

There is the question regarding whether these molecules fall inside the "applicability domain" (AD) in these models. The purpose of the AD is to identify the limitations of a model's applicability and offer reliable and accurate predictions.[191] Different approaches can be performed to assess the AD. For our compounds, we evaluate the Tanimoto coefficient of the BTZ-hybrids and IC-hybrids towards the complete dataset (covalent and non-covalent inhibitors), the covalent and non-covalent sets separately and the results are shown in **Figure 3.15A-C**.

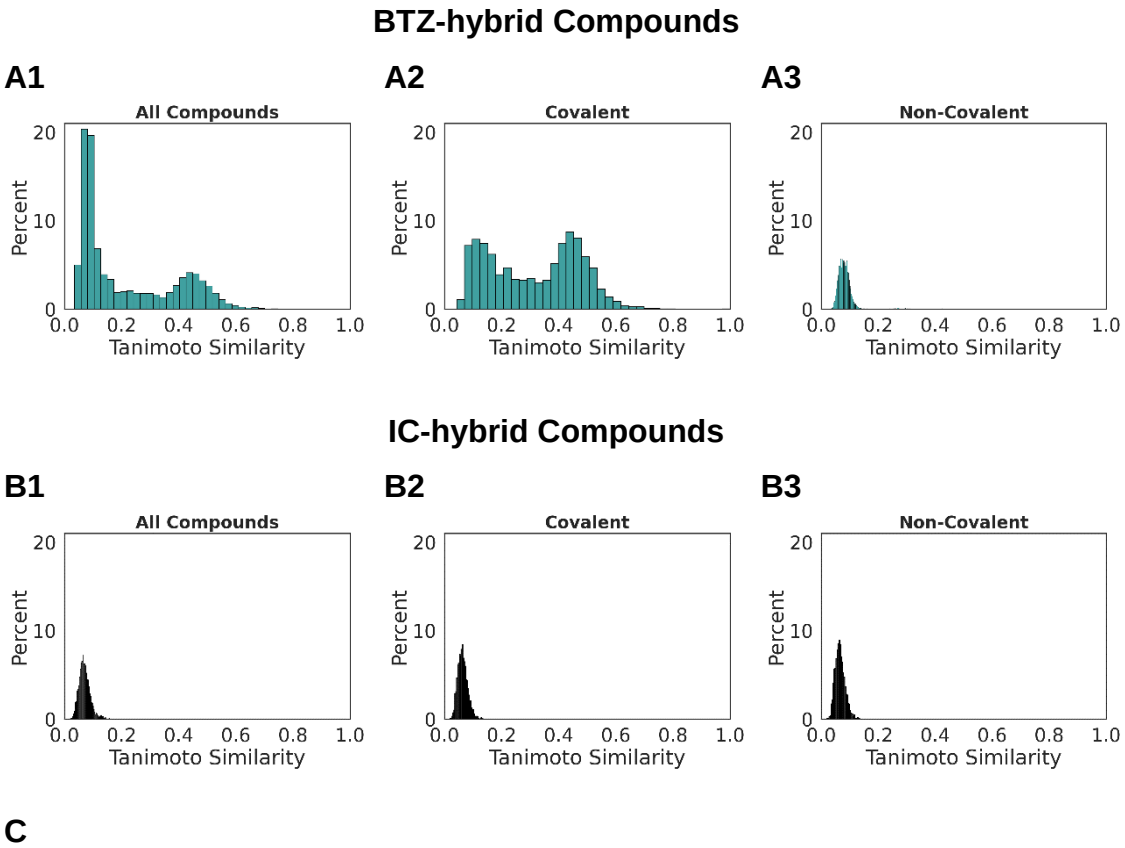


**C**

| | Tanimoto Similarity |
|---|---|
| **BTZs vs every compound** | 0.213 ± 0.167 |
| **BTZs vs covalent** | 0.315 ± 0.158 |
| **BTZs vs non-covalent** | 0.084 ± 0.037 |
| **ICs vs every compound** | 0.070 ± 0.019 |
| **ICs vs covalent** | 0.064 ± 0.017 |
| **ICs vs non-covalent** | 0.066 ± 0.017 |

**Figure 3.15.** Frequency distribution of topological similarity (Tanimoto coefficient, TC) of the 1,2,4-hybrids synthesized (A) BTZs and **B)** ICs) screened against the DprE1 dataset of **A/B1)** all compounds (Covalent + Non-covalent), **A/B2)** covalent and **A/B3)** non-covalent inhibitors. C. Median and standard deviation for each Tanimoto similarity.

Regarding the BTZ-hybrids, comparing with the dataset with all compounds (**Figure 3.15A1**), a mean TC of 0.213 ± 0.167 was obtained, indicating a chemical diversity of the BTZ-hybrids over the DprE1 inhibitors class. When analysing the covalent and non-covalent binders separately, the covalent class has a higher TC mean value of 0.315 ± 0.158 (**Figure 3.15A2**) *versus* 0.084 ± 0.037 (**Figure 3.15A3**), a nearly four-fold increase compared to the non-covalent binders. This result is expected since ~74% of the covalent subset comprises benzothiazinone-based compounds, which differ mostly in the amine chain at position 2. Regarding the IC-hybrid compounds (experimentally defined as not active against TB), all datasets displayed similar means of TC for every dataset, with 0.070 ± 0.019 for the complete dataset (**Figure 3.15B1**), 0.064 ± 0.017 for covalent binders (**Figure 3.15B2**), and 0.066 ± 0.017 (**Figure 3.15B3**), explaining why these compounds failed acting as TB drugs.

In analysing larger datasets, these results should provide additional information for tracking the required property similarity to choose molecules with possible TB activity with greater accuracy. Improvement of the applicability domain should also be addressed to optimise the reliability and decidability of these models.

## 3.3.4. Conclusions for this section and Future Work

Within this work, we obtained a dataset containing 1519 DprE1 inhibitors and computed three types of molecular fingerprints (MACCS, ECFP4, and FCFP4) to evaluate the molecular structural properties. According to the Tanimoto coefficients calculation, our dataset was shown to have chemical diversity; however, this was more pronounced for non-covalent than for covalent binders.

We attempted to build models with good performance, to predict DprE1 inhibitors. We used the original dataset, with 1519 molecules, and another two modified datasets, with down or up-sampling pre-processing, to balance the active and inactive molecules in the sample.

A total of 105 models using five different algorithms (KNN, SVM, GBM, RF, and XGB) were built, in which the best models for each algorithm produced MCC values of 0.791, 0.775, 0.801, 0.842, 0.882 on the test set, respectively when using the up-sampling balanced subset. It was determined that the 35 generated models for the DS subset had a good performance, with accuracy >0.78, precision >0.78, sensitivity >0.78, specificity >0.78, MCC >0.57, AUROC >0.78, and f1 score >0.78. Regarding the 35 constructed

models for the US subset, these models had the best performance among the subsets, with accuracy >0.85, precision >0.85, sensitivity >0.85, specificity >0.85, MCC >0.71, AUROC >0.85, and f1 score >0.85. In comparison to the balanced subsets, the performance of the 35 generated models for the original subset was inferior, with an accuracy >0.80, precision >0.77, sensitivity >0.80, specificity >0.63, MCC >0.51, AUROC >0.72, and f1 score >0.75. When examining the different metrics, it can be shown that the OS subset has the lowest metric specificity (>0.63) compared to the DS (>0.78) and US (>0.85) subsets, and this result was due to the imbalanced dataset between inactive and active compounds. The XGB models had the best performance across most data sets during the 5 and 10-fold cross-validation training, in which the best model was model XGB21, using the US subset built with MACCS, ECFP4, and FCFP4 fingerprints.

MACCS and FCFP4 fingerprints were the most important features in GBM, RF, and XGB models. For each algorithm, such important properties feature the presence or absence of a nitro group that appears in determining whether a molecule inhibits or does not inhibit the enzyme DprE1. Therefore, models are better trained to identify covalent binders. Evaluation of peroxide hybrids in the best models for each algorithm was also performed. Only model KNN16 could not appropriately classify IC-trioxane hybrids as non-inhibitors or inactive molecules. The remaining algorithms correctly identified the corresponding compounds as active, for the BTZ peroxide hybrids, and inactive, for IC peroxide hybrids. This result of high predictive performance was expected since the models seem to be better trained for identifying covalent binders. More external validation data should be used to evaluate better these produced models.

In future work, refinement of these models is necessary to allow for a more efficient selection of non-covalent binders. Splitting the collected dataset into subsets for covalent and non-covalent binders is a potential solution for this issue. Ensuring that overfitting does not occur is another crucial aspect to validation, in future models to improve performance. In addition, developing regression (quantitative) models should be investigated since they will allow us to predict a molecule's MIC value instead of merely classifying it as active or inactive. Improvement of the applicability domain should also be addressed to optimise the reliability and decidability of these models.

Since there is a strong correlation between DprE1 inhibition and anti-TB activity, we were able to develop classification models that could identify either DprE1 inhibitors or new anti-TB drugs in this study.

# 3.4. References


(1) Mikušová, K.; Huang, H.; Yagi, T.; Holsters, M.; Vereecke, D.; D'Haeze, W.; Scherman, M. S.; Brennan, P. J.; McNeil, M. R.; Crick, D. C. Decaprenylphosphoryl Arabinofuranose, the Donor of the D-Arabinofuranosyl Residues of Mycobacterial Arabinan, Is Formed via a Two-Step Epimerization of Decaprenylphosphoryl Ribose. *J. Bacteriol.* **2005**, *187* (23), 8020–8025. https://doi.org/10.1128/JB.187.23.8020-8025.2005.

(2) Wolucka, B. A. Biosynthesis of D-Arabinose in Mycobacteria – a Novel Bacterial Pathway with Implications for Antimycobacterial Therapy. *FEBS J.* **2008**, *275* (11), 2691–2711. https://doi.org/10.1111/j.1742-4658.2008.06395.x.

(3) Lee, B. S.; Pethe, K. Therapeutic Potential of Promiscuous Targets in *Mycobacterium tuberculosis*. *Curr. Opin. Pharmacol.* **2018**, *42*, 22–26. https://doi.org/10.1016/j.coph.2018.06.006.

(4) Crellin, P. K.; Brammananth, R.; Coppel, R. L. Decaprenylphosphoryl-β-D-Ribose 2'-Epimerase, the Target of Benzothiazinones and Dinitrobenzamides, Is an Essential Enzyme in *Mycobacterium smegmatis*. *PLoS One* **2011**, *6* (2), e16869. https://doi.org/10.1371/journal.pone.0016869.

(5) Kolly, G. S.; Boldrin, F.; Sala, C.; Dhar, N.; Hartkoorn, R. C.; Ventura, M.; Serafini, A.; Mckinney, J. D.; Manganelli, R.; Cole, S. T. Assessing the Essentiality of the Decaprenyl-Phospho-D-Arabinofuranose Pathway in *Mycobacterium tuberculosis* Using Conditional Mutants. *Mol. Microbiol.* **2014**, *92* (1), 194–211. https://doi.org/10.1111/mmi.12546.

(6) Brecik, M.; Centárová, I.; Mukherjee, R.; Kolly, G. S.; Huszár, S.; Bobovska, A.; Kilacskova, E.; Mokošova, V.; Svetlíkova, Z.; Michal, S.; Neres, J.; Korduláková, J.; Cole, S. T.; Mikušová, K. DprE1 Is a Vulnerable Tuberculosis Drug Target Due to Its Cell Wall Localization. *ACS Chem. Biol.* **2015**, *10* (7), 1631–1636. https://doi.org/10.1021/acschembio.5b00237.

(7) Piton, J.; Foo, C. S.-Y.; Cole, S. T. Structural Studies of *Mycobacterium tuberculosis* DprE1 Interacting with Its Inhibitors. *Drug Discov. Today* **2017**, *22* (3), 526–533. https://doi.org/10.1016/j.drudis.2016.09.014.

(8) Campaniço, A.; Moreira, R.; Lopes, F. Drug Discovery in Tuberculosis. New Drug Targets and Antimycobacterial Agents. *Eur. J. Med. Chem.* **2018**, *150*, 525–545. https://doi.org/10.1016/j.ejmech.2018.03.020.

(9) Chikhale, R. V.; Barmade, M. A.; Murumkar, P. R.; Yadav, M. R. Overview of the Development of DprE1 Inhibitors for Combating the Menace of Tuberculosis. *J. Med. Chem.* **2018**, *61* (19), 8563–8593. https://doi.org/10.1021/acs.jmedchem.8b00281.

(10) Degiacomi, G.; Belardinelli, J. M.; Pasca, M. R.; Rossi, E. De; Riccardi, G.; Chiarelli, L. R. Promiscuous Targets for Antitubercular Drug Discovery: The Paradigm of DprE1 and MmpL3. *Appl. Sci.* **2020**, *10* (2), 623. https://doi.org/10.3390/app10020623.

(11) Huszár, S.; Chibale, K.; Singh, V. The Quest for the Holy Grail: New Antitubercular Chemical Entities, Targets and Strategies. *Drug Discov. Today* **2020**, *25* (4), 772–780. https://doi.org/10.1016/j.drudis.2020.02.003.

(12) Richter, A.; Rudolph, I.; Möllmann, U.; Voigt, K.; Chung, C.-W.; Singh, O. M. P.; Rees, M.; Mendoza-Losana, A.; Bates, R.; Ballell, L.; Batt, S.; Veerapen, N.; Fütterer, K.; Besra, G.; Imming, P.; Argyrou, A. Novel Insight into the Reaction of Nitro, Nitroso and Hydroxylamino Benzothiazinones and of Benzoxacinones with *Mycobacterium tuberculosis* DprE1. *Sci. Rep.* **2018**, *8* (1), 13473. https://doi.org/10.1038/s41598-018-31316-6.

(13) Makarov, V.; Salina, E.; Reynolds, R. C.; Phyo, P.; Zin, K.; Ekins, S. Molecule Property Analyses of Active Compounds for *Mycobacterium tuberculosis*. *J. Med. Chem.* **2020**, *63* (17), 8917–8955. https://doi.org/10.1021/acs.jmedchem.9b02075.

(14) Oh, S.; Trifonov, L.; Yadav, V. D.; Barry III, C. E.; Boshoff, H. I. Tuberculosis Drug Discovery: A Decade of Hit Assessment for Defined Targets. *Front. Cell. Infect. Microbiol.* **2021**, *11*, 611304. https://doi.org/10.3389/fcimb.2021.611304.

(15) Ertl, P.; Rohde, B.; Selzer, P. Fast Calculation of Molecular Polar Surface Area as a Sum of Fragment-Based Contributions and Its Application to the Prediction of Drug Transport Properties. *J. Med. Chem.* **2000**, *43* (20), 3714–3717. https://doi.org/10.1021/jm000942e.

(16) Gola, J.; Obrezanova, O.; Champness, E.; Segall, M. ADMET Property Prediction : The State of the Art and Current Challenges. *QSAR Comb. Sci.* **2006**, *25* (12), 1172–1180. https://doi.org/10.1002/qsar.200610093.

(17) Lagorce, D.; Douguet, D.; Miteva, M. A.; Villoutreix, B. O. Computational Analysis of Calculated Physicochemical and ADMET Properties of Protein- Protein Interaction Inhibitors. *Sci. Rep.* **2017**, *7*, 46277. https://doi.org/10.1038/srep46277.

(18) Beresford, A. P.; Selick, H. E.; Tarbit, M. H. The Emerging Importance of Predictive ADME Simulation in Drug Discovery. *Drug Discov. Today* **2002**, *7* (2), 109–116. https://doi.org/10.1016/S1359-6446(01)02100-6.

(19) Waring, M. J. Defining Optimum Lipophilicity and Molecular Weight Ranges for Drug Candidates—Molecular Weight Dependent Lower LogD Limits Based on Permeability. *Bioorg. Med. Chem. Lett.* **2009**, *19* (10), 2844–2851. https://doi.org/10.1016/j.bmcl.2009.03.109.

(20) Chhabra, S.; Kumar, S.; Parkesh, R. Chemical Space Exploration of DprE1 Inhibitors Using Chemoinformatics and Artificial Intelligence. *ACS Omega* **2021**, *6* (22), 14430–14441. https://doi.org/10.1021/acsomega.1c01314.

(21) Makarov, V.; Manina, G.; Mikusova, K.; Möllmann, U.; Ryabova, O.; Saint-Joanis, B.; Dhar, N.; Pasca, M. R.; Buroni, S.; Lucarelli, A. P.; Milano, A.; Rossi, E. De; Belanova, M.; Bobovska, A.; Dianiskova, P.; Kordulakova, J.; Sala, C.; Fullam, E.; Schneider, P.; Mckinney, J. D.; Brodin, P.; Christophe, T.; Waddell, S.; Butcher, P.; Albrethsen, J.; Rosenkrands, I.; Brosch, R.; Nandi, V.; Bharath, S.; Gaonkar, S.; Shandil, R. K.; Balasubramanian, V.; Balganesh, T.; Tyagi, S.; Grosset, J.; Riccardi, G.; Cole, S. T. Benzothiazinones Kill *Mycobacterium tuberculosis* by Blocking Arabinan Synthesis. *Science.* **2009**, *324* (5928), 801–804. https://doi.org/10.1126/science.1171583.

(22) Makarov, V. A.; Cole, S. T.; Möllmann, U. Patent EP2029583 B1. *2010*.

(23) Sommer, R.; Neres, J.; Piton, J.; Dhar, N.; Sar, A. van der; Raju, M.; Laroche, T.; Dyson, P. J.; Mckinney, J. D.; Bitter, W.; Makarov, V.; Cole, S. T. Fluorescent Benzothiazinone Analogues Efficiently and Selectively Label DprE1 in Mycobacteria and Actinobacteria. *ACS Chem. Biol.* **2018**, *13* (11), 3184–3192. https://doi.org/10.1021/acschembio.8b00790.

(24) Karoli, T.; Becker, B.; Zuegg, J.; Möllmann, U.; Ramu, S.; Huang, J. X.; Cooper, M. A. Identification of Antitubercular Benzothiazinone Compounds by Ligand-Based Design. *J. Med. Chem.* **2012**, *55* (17), 7940–7944. https://doi.org/10.1021/jm3008882.

(25) Gao, C.; Ye, T.-H.; Wang, N.-Y.; Zeng, X.-X.; Zhang, L.-D.; Xiong, Y.; You, X.-Y.; Xia, Y.; Xu, Y.; Peng, C.-T.; Zuo, W.-Q.; Wei, Y.; Yu, L.-T. Synthesis and Structure–Activity Relationships Evaluation of Benzothiazinone Derivatives as Potential Anti-Tubercular Agents. *Bioorg. Med. Chem. Lett.* **2013**, *23* (17), 4919–4922. https://doi.org/10.1016/j.bmcl.2013.06.069.

(26) Tiwari, R.; Miller, P. A.; Cho, S.; Franzblau, S. G.; Miller, M. J. Syntheses and Antituberculosis Activity of 1,3-Benzothiazinone Sulfoxide and Sulfone Derived from BTZ043. *ACS Med. Chem. Lett.* **2015**, *6* (2), 128–133. https://doi.org/10.1021/ml5003458.

(27) Gao, C.; Peng, C.; Shi, Y.; You, X.; Ran, K.; Xiong, L.; Ye, T.-H.; Zhang, L.; Wang, N.; Zhu, Y.-X.; Liu, K.; Zuo, W.; Yu, L.; Wei, Y. Benzothiazinethione Is a Potent Preclinical Candidate for the Treatment of Drug-Resistant Tuberculosis. *Sci. Rep.* **2016**, *6*, 29717. https://doi.org/10.1038/srep29717.

(28) Zhang, R.; Lv, K.; Wang, B.; Li, L.; Wang, B.; Liu, M.; Guo, H.; Wanga, A.; Lu, Y. Design, Synthesis and Antitubercular Evaluation of Benzothiazinones Containing an Oximido or Amino Nitrogen Heterocycle Moiety. *RSC Adv.* **2017**, *7* (3), 1480–1483. https://doi.org/10.1039/C6RA25712G.

(29) Wang, A.; Lv, K.; Tao, Z.; Gu, J.; Fu, L.; Liu, M.; Wan, B.; Franzblau, S. G.; Ma, C.; Ma, X.; Han, B.; Wang, A.; Xu, S.; Lu, Y. Identification of Benzothiazinones Containing an Oxime Functional Moiety as New Anti-Tuberculosis Agents. *Eur. J. Med. Chem.* **2019**, *181*, 111595. https://doi.org/10.1016/j.ejmech.2019.111595.

(30) Peng, C.-T.; Gao, C.; Wang, N.-Y.; You, X.-Y.; Zhang, L.-D.; Zhu, Y.-X.; Xv, Y.; Zuo, W.-Q.; Ran, K.; Deng, H.-X.; Lei, Q.; Xiao, K.-J.; Yu, L.-T. Synthesis and Antitubercular Evaluation of 4-Carbonyl Piperazine Substituted 1,3-Benzothiazin-4-One Derivatives. *Bioorganic Med. Chem. Lett.* **2015**, *25* (7), 1373–1376. https://doi.org/10.1016/j.bmcl.2015.02.061.

(31) Xiong, L.; Gao, C.; Shi, Y.-J.; Tao, X.; Rong, J.; Liu, K.-L.; Peng, C.-T.; Wang, N.-Y.; Lei, Q.; Zhang, Y.-W.; Yu, L.-T.; Wei, Y.-Q. Identification of a New Series of Benzothiazinone Derivatives with Excellent Antitubercular Activity and Improved Pharmacokinetic Profile. *RSC Adv.* **2018**, *8* (20), 11163–11176. https://doi.org/10.1039/c8ra00720a.

(32) Li, P.; Wang, B.; Zhang, X.; Batt, S. M.; Besra, G. S.; Zhang, T.; Ma, C.; Zhang, D.; Lin, Z.; Li, G.; Huang, H.; Lu, Y. Identification of Novel Benzothiopyranone Compounds against *Mycobacterium tuberculosis* through Scaffold Morphing from Benzothiazinones. *Eur. J. Med. Chem.* **2018**, *160*, 157–170. https://doi.org/10.1016/j.ejmech.2018.09.042.

(33) Pasca, M. R.; Degiacomi, G.; Riberio, A. L. J. L.; Zara, F.; Mori, P. De; Heym, B.; Mirrione, M.; Brerra, R.; Pagani, L.; Pucillo, L.; Troupioti, P.; Makarov, V.; Cole, S. T.; Riccardi, G. Clinical Isolates of *Mycobacterium tuberculosis* in Four European Hospitals Are Uniformly Susceptible to Benzothiazinones. *Antimicrob. Agents Chemother.* **2010**, *54* (4), 1616–1618. https://doi.org/10.1128/AAC.01676-09.

(34) Lv, K.; Tao, Z.; Liu, Q.; Yang, L.; Wang, B.; Wu, S.; Wang, A.; Huang, M.; Liu, M.; Lu, Y. Design, Synthesis and Antitubercular Evaluation of Benzothiazinones Containing a Piperidine Moiety. *Eur. J. Med. Chem.* **2018**, *151*, 1–8. https://doi.org/10.1016/j.ejmech.2018.03.060.

(35) Zhang, G.; Howe, M.; Aldrich, C. C. Spirocyclic and Bicyclic 8-Nitrobenzothiazinones for Tuberculosis with Improved Physicochemical and Pharmacokinetic Properties. *ACS Med. Chem. Lett.* **2019**, *10* (3), 348–351. https://doi.org/10.1021/acsmedchemlett.8b00634.

(36) Lv, K.; You, X.; Wang, B.; Wei, Z.; Chai, Y.; Wang, B.; Wang, A.; Huang, G.; Liu, M.; Lu, Y. Identification of Better Pharmacokinetic Benzothiazinone Derivatives as New Antitubercular Agents. *ACS Med. Chem. Lett.* **2017**, *8* (6), 636–641. https://doi.org/10.1021/acsmedchemlett.7b00106.

(37) Lv, K.; Wang, A.; Tao, Z.; Fu, L.; Liu, H.; Wang, B.; Ma, C.; Wang, H.; Ma, X.; Han, B.; Wang, A.; Zhang, K.; Liu, M.; Lu, Y. HERG Optimizations of IMB1603, Discovery of Alternative Benzothiazinones as New Antitubercular Agents. *Eur. J. Med. Chem.* **2019**, *179*, 208–217. https://doi.org/10.1016/j.ejmech.2019.06.053.

(38) Ma, X.; Han, B.; Wang, A.; Yang, L.; Huang, M.; Chowdhury, K.; Gu, J.; Zhang, K.; Lv, K. Identification of Benzothiazones Containing a Hexahydropyrrolo[3,4-c]Pyrrol Moiety as Antitubercular Agents against MDR-MTB. *RSC Adv.* **2020**, *10* (24), 14410–14414. https://doi.org/10.1039/d0ra00750a.

(39) Wang, A.; Ma, C.; Chai, Y.; Liu, X.; Lv, K.; Fu, L.; Wang, B.; Jia, X.; Liu, M.; Lu, Y. Identification of Benzothiazinones Containing 2-Benzyl-2,7-Diazaspiro [3.5]Nonane Moieties as New Antitubercular Agents. *Eur. J. Med. Chem.* **2020**, *200*, 112409. https://doi.org/10.1016/j.ejmech.2020.112409.

(40) Wang, A.; Lu, Y.; Lv, K.; Ma, C.; Xu, S.; Wang, B.; Wang, A.; Xia, G.; Liu, M. Design, Synthesis and Antimycobacterial Activity of New Benzothiazinones Inspired by Rifampicin/Rifapentine. *Bioorg. Chem.* **2020**, *102*, 104135. https://doi.org/10.1016/j.bioorg.2020.104135.

(41) Liu, L.; Kong, C.; Fumagalli, M.; Savková, K.; Xu, Y.; Huszár, S.; Sammartino, J. C.; Fan, D.; Chiarelli, L. R.; Mikušová, K.; Sun, Z.; Qiao, C. Design, Synthesis and Evaluation of Covalent Inhibitors of DprE1 as Antitubercular Agents. *Eur. J. Med. Chem.* **2020**, *208*, 112773. https://doi.org/10.1016/j.ejmech.2020.112773.

(42) Wang, A.; Xu, S.; Chai, Y.; Xia, G.; Wang, B.; Lv, K.; Ma, C.; Wang, D.; Wang, A.; Qin, X.; Liu, M.; Lu, Y. Design, Synthesis and Biological Activity of N-(Amino)Piperazine-Containing Benzothiazinones against *Mycobacterium tuberculosis*. *Eur. J. Med. Chem.* **2021**, *218*, 113398. https://doi.org/10.1016/j.ejmech.2021.113398.

(43) Zhang, G.; Sheng, L.; Hegde, P.; Li, Y.; Aldrich, C. C. 8-Cyanobenzothiazinone Analogs with Potent Antitubercular Activity. *Med. Chem. Res.* **2021**, *30* (2), 449–458. https://doi.org/10.1007/s00044-020-02676-4.

(44) Neres, J.; Pojer, F.; Molteni, E.; Chiarelli, L. R.; Dhar, N.; Boy-Röttger, S.; Buroni, S.; Fullam, E.; Degiacomi, G.; Lucarelli, A. P.; Read, R. J.; Zanoni, G.; Edmondson, D. E.; Rossi, E. De; Pasca, M. R.; Mckinney, J. D.; Dyson, P. J.; Riccardi, G.; Mattevi, A.; Cole, S. T.; Binda, C. Structural Basis for Benzothiazinone-Mediated Killing of *Mycobacterium tuberculosis*. *Sci. Transl. Med.* **2012**, *4* (150), 150ra121. https://doi.org/10.1126/scitranslmed.3004395.

(45) Fan, D.; Wang, B.; Stelitano, G.; Savková, K.; Shi, R.; Huszár, S.; Han, Q.; Mikušová, K.; Chiarelli, L. R.; Lu, Y.; Qiao, C. Structural and Activity Relationships of 6-Sulfonyl-8-Nitrobenzothiazinones as Antitubercular Agents. *J. Med. Chem.* **2021**, *64* (19), 14526–14539. https://doi.org/10.1021/acs.jmedchem.1c01049.

(46) Li, P.; Wang, B.; Fu, L.; Guo, K.; Ma, C.; Wang, B.; Lin, Z.; Li, G.; Huang, H.; Lu, Y. Identification of Novel Benzothiopyranones with Ester and Amide Motifs Derived from Active Metabolite as Promising Leads against *Mycobacterium tuberculosis*. *Eur. J. Med. Chem.* **2021**, *222*, 113603. https://doi.org/10.1016/j.ejmech.2021.113603.

(47) Shi, R.; Wang, B.; Stelitano, G.; Wu, X.; Shan, Y.; Wu, Y.; Wang, X.; Chiarelli, L. R.; Lu, Y.; Qiao, C. Development of 6-Methanesulfonyl-8-Nitrobenzothiazinone Based Antitubercular Agents. *ACS Med. Chem. Lett.* **2022**, *13* (4), 593–598. https://doi.org/10.1021/acsmedchemlett.1c00652.

(48) Schieferdecker, S.; Bernal, F. A.; Wojtas, K. P.; Keiff, F.; Li, Y.; Dahse, H.-M.; Kloss, F. Development of Predictive Classification Models for Whole Cell Antimycobacterial Activity of Benzothiazinones. *J. Med. Chem.* **2022**, *65* (9), 6748–6763. https://doi.org/10.1021/acs.jmedchem.2c00098.

(49) Makarov, V.; Neres, J.; Hartkoorn, R. C.; Ryabova, O. B.; Kazakova, E.; Šarkan, M.; Huszár, S.; Piton, J.; Kolly, G. S.; Vocat, A.; Conroy, T. M.; Mikušová, K.; Cole, S. T. The 8-Pyrrole-Benzothiazinones Are Noncovalent Inhibitors of DprE1 from *Mycobacterium tuberculosis*. *Antimicrob. Agents Chemother.* **2015**, *59* (8), 4446–4452. https://doi.org/10.1128/AAC.00778-15.

(50) Tiwari, R.; Miller, P. A.; Chiarelli, L. R.; Mori, G.; Michal, Š.; Centárová, I.; Cho, S.; Mikušová, K.; Franzblau, S. G.; Oliver, A. G.; Miller, M. J. Design, Syntheses, and Anti-TB Activity of 1,3-Benzothiazinone Azide and Click Chemistry Products Inspired by BTZ043. *ACS J. Med. Chem.* **2016**, *7* (3), 266–270. https://doi.org/10.1021/acsmedchemlett.5b00424.

(51) Madikizela, B.; Eckhardt, T.; Goddard, R.; Richter, A.; Lins, A.; Lehmann, C.; Imming, P.; Seidel, R. W. Synthesis, Structural Characterization and Antimycobacterial Evaluation of Several Halogenated Non-Nitro Benzothiazinones. *Med. Chem. Res.* **2021**, *30* (8), 1523–1533. https://doi.org/10.1007/s00044-021-02735-4.

(52) Wang, F.; Sambandan, D.; Halder, R.; Wang, J.; Batt, S. M.; Weinrick, B.; Ahmad, I.; Yang, P.; Zhang, Y.; Kim, J.; Hassani, M.; Huszar, S.; Trefzer, C.; Ma, Z.; Kaneko, T.; Mdluli, K. E.; Franzblau, S.; Chatterjee, A. K.; Johnsson, K.; Mikusova, K.; Besra, G. S.; Fütterer, K.; Robbins, S. H.; Barnes, S. W.; Walker, J. R.; Jacobs Jr., W. R.; Schultz, P. G. Identification of a Small Molecule with Activity against Drug-Resistant and Persistent Tuberculosis. *Proc. Natl. Acad. Sci.* **2013**, *110* (27), E2510–E2517. https://doi.org/10.1073/pnas.1309171110.

(53) Liu, R.; Lyu, X.; Batt, S. M.; Hsu, M.-H.; Harbut, M. B.; Vilcheze, C.; Cheng, B.; Ajayi, K.; Yang, B.; Yang, Y.; Guo, H.; Lin, C.; Gan, F.; Wang, C.; Franzblau, S. G.; Jacobs Jr., W. R.; Besra, G. S.; Johnson, E. F.; Petrassi, M.; Chatterjee, A. K.; Fütterer, K.; Wang, F. Determinants of the Inhibition of DprE1 and CYP2C9 by Antitubercular Thiophenes. *Angew. Chemie - Int. Ed.* **2017**, *56* (42), 13011–13015. https://doi.org/10.1002/anie.201707324.

(54) Mir, F.; Shafi, S.; Zaman, M. S.; Kalia, N. P.; Rajput, V. S.; Mulakayala, C.; Mulakayala, N.; Khan, I. A.; Alam, M. S. Sulfur Rich 2-Mercaptobenzothiazole and 1,2,3-Triazole Conjugates as Novel Antitubercular Agents. *Eur. J. Med. Chem.* **2014**, *76*, 274–283.

https://doi.org/10.1016/j.ejmech.2014.02.017.

(55) Trefzer, C.; Rengifo-Gonzalez, M.; Hinner, M. J.; Schneider, P.; Makarov, V.; Cole, S. T.; Johnsson, K. Benzothiazinones: Prodrugs That Covalently Modify the Decaprenylphosphoryl-β-$_D$-Ribose 2′-Epimerase DprE1 of *Mycobacterium tuberculosis*. *J. Am. Chem. Soc.* **2010**, *132* (39), 13663–13665. https://doi.org/10.1021/ja106357w.

(56) Chikhale, R.; Menghani, S.; Babu, R.; Bansode, R.; Bhargavi, G.; Karodia, N.; Rajasekharan, M. V.; Paradkar, A.; Khedekar, P. Development of Selective DprE1 Inhibitors: Design, Synthesis, Crystal Structure and Antitubercular Activity of Benzothiazolylpyrimidine-5-Carboxamides. *Eur. J. Med. Chem.* **2015**, *96*, 30–46. https://doi.org/10.1016/j.ejmech.2015.04.011.

(57) Gawad, J.; Bonde, C. Design, Synthesis and Biological Evaluation of Some 2-(6-Nitrobenzo[d]Thiazol-2-Ylthio)-N-Benzyl-N-(6-Nitrobenzo[d]Thiazol-2-Yl)Acetamide Derivatives as Selective DprE1 Inhibitors. *Synth. Commun.* **2019**, *49* (20), 2696–2708. https://doi.org/10.1080/00397911.2019.1639756.

(58) Liu, J.; Dai, H.; Wang, B.; Liu, H.; Tian, Z.; Zhang, Y. Exploring Disordered Loops in DprE1 Provides a Functional Site to Combat Drug-Resistance in *Mycobacterium* Strains. *Eur. J. Med. Chem.* **2021**, *227*, 113932. https://doi.org/10.1016/j.ejmech.2021.113932.

(59) Landge, S.; Mullick, A. B.; Nagalapur, K.; Neres, J.; Subbulakshmi, V.; Murugan, K.; Ghosh, A.; Sadler, C.; Fellows, M. D.; Humnabadkar, V.; Mahadevaswamy, J.; Vachaspati, P.; Sharma, S.; Kaur, P.; Mallya, M.; Rudrapatna, S.; Awasthy, D.; Sambandamurthy, V. K.; Pojer, F.; Cole, S. T.; Balganesh, T. S.; Ugarkar, B. G.; Balasubramanian, V.; Bandodkar, B. S.; Panda, M.; Ramachandran, V. Discovery of Benzothiazoles as Antimycobacterial Agents: Synthesis, Structure–Activity Relationships and Binding Studies with *Mycobacterium tuberculosis* Decaprenylphosphoryl-β-$_D$-Ribose 2'-Oxidase. *Bioorganic Med. Chem.* **2015**, *23* (24), 7694–7710. https://doi.org/10.1016/j.bmc.2015.11.017.

(60) Landge, S.; Ramachandran, V.; Kumar, A.; Neres, J.; Murugan, K.; Sadler, C.; Fellows, M. D.; Humnabadkar, V.; Vachaspati, P.; Raichurkar, A.; Sharma, S.; Ravishankar, S.; Guptha, S.; Sambandamurthy, V. K.; Balganesh, T. S.; Ugarkar, B. G.; Balasubramanian, V.; Bandodkar, B. S.; Panda, M. Nitroarenes as Antitubercular Agents: Stereoelectronic Modulation to Mitigate Mutagenicity. *ChemMedChem* **2016**, *11* (3), 331–339. https://doi.org/10.1002/cmdc.201500462.

(61) Christophe, T.; Jackson, M.; Jeon, H. K.; Fenistein, D.; Contreras-Dominguez, M.; Kim, J.; Genovesio, A.; Carralot, J.-P.; Ewann, F.; Kim, E. H.; Lee, S. Y.; Kang, S.; Seo, M. J.; Park, E. J.; Škovierová, H.; Pham, H.; Riccardi, G.; Nam, J. Y.; Marsollier, L.; Kempf, M.; Joly-Guillou, M.-L.; Oh, T.; Shin, W. K.; No, Z.; Nehrbass, U.; Brosch, R.; Cole, S. T.; Brodin, P. High Content Screening Identifies Decaprenyl- Phosphoribose 2' Epimerase as a Target for Intracellular Antimycobacterial Inhibitors. *PLOS Pathog.* **2009**, *5* (10), e1000645. https://doi.org/10.1371/journal.ppat.1000645.

(62) Munagala, G.; Yempalla, K. R.; Aithagani, S. K.; Kalia, N. P.; Ali, F.; Ali, I.; Rajput, V. S.; Rani, C.; Chib, R.; Mehra, R.; Nargotra, A.; Khan, I. A.; Vishwakarma, R. A.; Singh, P. P. Synthesis and Biological Evaluation of Substituted N-Alkylphenyl-3,5-Dinitrobenzamide Analogs as Anti-TB Agents. *Med. Chem. Commun* **2014**, *5* (4), 521–527. https://doi.org/10.1039/c3md00366c.

(63) Li, L.; Lv, K.; Yang, Y.; Sun, J.; Tao, Z.; Wang, A.; Wang, B.; Wang, H.; Geng, Y.; Liu, M.; Guo, H.; Lu, Y. Identification of N-Benzyl 3,5-Dinitrobenzamides Derived from PBTZ169 as Antitubercular Agents. *ACS Med. Chem. Lett.* **2018**, *9* (7), 741–745. https://doi.org/10.1021/acsmedchemlett.8b00177.

(64) Wang, H.; Lv, K.; Li, X.; Wang, B.; Wang, A.; Tao, Z.; Geng, Y.; Wang, B.; Huang, M.; Liu, M.; Guo, H.; Lu, Y. Design, Synthesis and Antimycobacterial Activity of Novel Nitrobenzamide Derivatives. *Chinese Chem. Lett.* **2019**, *30* (2), 413–416. https://doi.org/10.1016/j.cclet.2018.08.005.

(65) Hu, X.; Yang, L.; Chai, X.; Lei, Y.; Shah, M. A.; Lu, L.; Shen, C.; Jiang, D.; Wang, Z.; Liu, Z.; Xu, L.; Wan, K.; Zhang, T.; Yin, Y.; Li, D.; Cao, D.; Hou, T. Discovery of Novel DprE1 Inhibitors via Computational Bioactivity Fingerprints and Structure-Based Virtual

Screening. *Acta Pharmacol. Sin.* **2022**, *43* (6), 1605–1615. https://doi.org/10.1038/s41401-021-00779-1.

(66) Trefzer, C.; Škovierová, H.; Buroni, S.; Bobovská, A.; Nenci, S.; Molteni, E.; Pojer, F.; Pasca, M. R.; Makarov, V.; Cole, S. T.; Riccardi, G.; Mikušová, K.; Johnsson, K. Benzothiazinones Are Suicide Inhibitors of Mycobacterial Decaprenylphosphoryl-β-$_D$-Ribofuranose 2′-Oxidase DprE1. *J. Am. Chem. Soc.* **2012**, *134* (2), 912–915. https://doi.org/10.1021/ja211042r.

(67) Stanley, S. A.; Grant, S. S.; Kawate, T.; Iwase, N.; Shimizu, M.; Wivagg, C.; Silvis, M.; Kazyanskaya, E.; Aquadro, J.; Golas, A.; Fitzgerald, M.; Dai, H.; Zhang, L.; Hung, D. T. Identification of Novel Inhibitors of M. Tuberculosis Growth Using Whole Cell Based High-Throughput Screening. *ACS Chem. Biol.* **2012**, *7* (8), 1377–1384. https://doi.org/10.1021/cb300151m.

(68) Goldman, R. C.; Laughon, B. E. Discovery and Validation of New Antitubercular Compounds as Potential Drug Leads and Probes. *Tuberculosis* **2009**, *89* (5), 331–333. https://doi.org/10.1016/j.tube.2009.07.007.

(69) Ananthan, S.; Faaleolea, E. R.; Goldman, R. C.; Hobrath, J. V.; Kwong, C. D.; Laughon, B. E.; Maddry, J. A.; Mehta, A.; Rasmussen, L.; Reynolds, R. C.; Secrist III, J. A.; Shindo, N.; Showe, D. N.; Sosa, M. I.; Suling, W. J.; White, E. L. High-Throughput Screening for Inhibitors of *Mycobacterium tuberculosis* H37Rv. *Tuberculosis* **2009**, *89* (5), 334–353. https://doi.org/10.1016/j.tube.2009.05.008.

(70) Maddry, J. A.; Ananthan, S.; Goldman, R. C.; Hobrath, J. V.; Kwong, C. D.; Maddox, C.; Rasmussen, L.; Reynolds, R. C.; Secrist III, J. A.; Sosa, M. I.; White, E. L.; Zhang, W. Antituberculosis Activity of the Molecular Libraries Screening Center Network Library. *Tuberculosis* **2009**, *89* (5), 354–363. https://doi.org/10.1016/j.tube.2009.07.006.

(71) Karabanovich, G.; Dušek, J.; Savková, K.; Pavliš, O.; Pávková, I.; Korábečný, J.; Kučera, T.; Vlčková, H. K.; Huszár, S.; Konyariková, Z.; Konečná, K.; Jand'ourek, O.; Stolaříková, J.; Korduláková, J.; Vávrová, K.; Pávek, P.; Klimešová, V.; Hrabálek, A.; Mikušová, K.; Roh, J. Development of 3,5-Dinitrophenyl-Containing 1,2,4-Triazoles and Their Trifluoromethyl Analogues as Highly Efficient Antitubercular Agents Inhibiting Decaprenylphosphoryl-β-$_D$-ribofuranose 2′- Oxidase. *J. Med. Chem.* **2019**, *62* (17), 8115–8139. https://doi.org/10.1021/acs.jmedchem.9b00912.

(72) Magnet, S.; Hartkoorn, R. C.; Székely, R.; Pató, J.; Triccas, J. A.; Schneider, P.; Szántai-Kis, C.; Őrfi, L.; Chambon, M.; Banfi, D.; Bueno, M.; Turcatti, G.; Kéri, G.; Cole, S. T. Leads for Antitubercular Compounds from Kinase Inhibitor Library Screens. *Tuberculosis* **2010**, *90* (6), 354–360. https://doi.org/10.1016/j.tube.2010.09.001.

(73) Neres, J.; Hartkoorn, R. C.; Chiarelli, L. R.; Gadupudi, R.; Pasca, M. R.; Mori, G.; Venturelli, A.; Savina, S.; Makarov, V.; Kolly, G. S.; Molteni, E.; Binda, C.; Dhar, N.; Ferrari, S.; Brodin, P.; Delorme, V.; Landry, V.; Ribeiro, A. L. de J. L.; Farina, D.; Saxena, P.; Pojer, F.; Carta, A.; Luciani, R.; Porta, A.; Zanoni, G.; Rossi, E. De; Costi, M. P.; Riccardi, G.; Cole, S. T. 2-Carboxyquinoxalines Kill *Mycobacterium tuberculosis* through Non-Covalent Inhibition of DprE1. *ACS Chem. Biol.* **2015**, *10* (3), 705–714. https://doi.org/10.1021/cb5007163.

(74) No, Z.; Kim, J.; Brodin, P. B.; Seo, M. J.; Kim, Y. M.; Cechetto, J.; Jeon, H.; Genovesio, A.; Lee, S.; Kang, S.; Ewann, F. A.; Nam, J. Y.; Christophe, T.; Fenistein, D. P. C.; Jamung, H.; Jiyeon, J. Patent WO 2011/113606 A1, 2011.

(75) Barsanti, P. A.; Hu, C.; Jin, J.; Keyes, R.; Kucejko, R.; Lin, X.; Pan, Y.; Pfister, K. B.; Sendzik, M.; Sutton, J.; Wan, L. Patent WO 2011/085990 A1, 2011.

(76) Shirude, P. S.; Shandil, R.; Sadler, C.; Naik, M.; Hosagrahara, V.; Hameed, S.; Shinde, V.; Bathula, C.; Humnabadkar, V.; Kumar, N.; Reddy, J.; Panduga, V.; Sharma, S.; Ambady, A.; Hegde, N.; Whiteaker, J.; McLaughlin, R. E.; Gardner, H.; Madhavapeddi, P.; Ramachandran, V.; Kaur, P.; Narayan, A.; Guptha, S.; Awasthy, D.; Narayan, C.; Mahadevaswamy, J.; Vishwas, K.; Ahuja, V.; Srivastava, A.; Prabhakar, K.; Bharath, S.; Kale, R.; Ramaiah, M.; Choudhury, N. R.; Sambandamurthy, V. K.; Solapure, S.; Iyer, P. S.; Narayanan, S.; Chatterji, M. Azaindoles: Noncovalent DprE1 Inhibitors from Scaffold Morphing Efforts, Kill *Mycobacterium tuberculosis* and Are Efficacious in Vivo. *J. Med.*

*Chem.* **2013**, *56* (23), 9701–9708. https://doi.org/10.1021/jm401382v.

(77) Tiwari, R.; Moraski, G. C.; Krchňák, V.; Miller, P. A.; Colon-Martinez, M.; Herrero, E.; Oliver, A. G.; Miller, M. J. Thiolates Chemically Induce Redox Activation of BTZ043 and Related Potent Nitroaromatic Anti-Tuberculosis Agents. *J. Am. Chem. Soc.* **2013**, *135* (9), 3539–3549. https://doi.org/10.1021/ja311058q.

(78) Shirude, P. S.; Shandil, R. K.; Manjunatha, M. R.; Sadler, C.; Panda, M.; Panduga, V.; Reddy, J.; Saralaya, R.; Nanduri, R.; Ambady, A.; Ravishankar, S.; Sambandamurthy, V. K.; Humnabadkar, V.; Jena, L. K.; Suresh, R. S.; Srivastava, A.; Prabhakar, K. R.; Whiteaker, J.; McLaughlin, R. E.; Sharma, S.; Cooper, C. B.; Mdluli, K.; Butler, S.; Iyer, P. S.; Narayanan, S.; Chatterji, M. Lead Optimization of 1,4-Azaindoles as Antimycobacterial Agents. *J. Med. Chem.* **2014**, *57* (13), 5728–5737. https://doi.org/10.1021/jm500571f.

(79) Chatterji, M.; Shandil, R.; Manjunatha, M. R.; Solapure, S.; Ramachandran, V.; Kumar, N.; Saralaya, R.; Panduga, V.; Reddy, J.; KR, P.; Sharma, S.; Sadler, C.; Cooper, C. B.; Mdluli, K.; Iyer, P. S.; Narayanan, S.; Shirude, P. S. 1,4-Azaindole, a Potential Drug Candidate for Treatment of Tuberculosis. *Antimicrob. Agents Chemother.* **2014**, *58* (9), 5325–5331. https://doi.org/10.1128/AAC.03233-14.

(80) https://clinicaltrials.gov/ct2/show/NCT03199339 (accessed on 19th February, 2023).

(81) Bodige, S.; Ravula, P.; Gulipalli, K. C.; Endoori, S.; Cherukumalli, P. K. R.; Sharath, N. S. C. J.; Seelam, N. Design, Synthesis, Antitubercular and Antibacterial Activities of Pyrrolo[3,2-b]Pyridine-3-Carboxamide Linked 2-Methoxypyridine Derivatives and in Silico Docking Studies. *Synth. Commun.* **2019**, *49* (17), 2219–2234. https://doi.org/10.1080/00397911.2019.1618874.

(82) Manjunatha, M. R.; Shandil, R.; Panda, M.; Sadler, C.; Ambady, A.; Panduga, V.; Kumar, N.; Mahadevaswamy, J.; Sreenivasaiah, M.; Narayan, A.; Guptha, S.; Sharma, S.; Sambandamurthy, V. K.; Ramachandran, V.; Mallya, M.; Cooper, C.; Mdluli, K.; Butler, S.; Tommasi, R.; Iyer, P. S.; Narayanan, S.; Chatterji, M.; Shirude, P. S. Scaffold Morphing To Identify Novel DprE1 Inhibitors with Antimycobacterial Activity. *ACS Med. Chem. Lett.* **2019**, *10* (10), 1480–1485. https://doi.org/10.1021/acsmedchemlett.9b00343.

(83) Naik, M.; Humnabadkar, V.; Tantry, S. J.; Panda, M.; Narayan, A.; Guptha, S.; Panduga, V.; Manjrekar, P.; Jena, L. K.; Koushik, K.; Shanbhag, G.; Jatheendranath, S.; Manjunatha, M. R.; Gorai, G.; Bathula, C.; Rudrapatna, S.; Achar, V.; Sharma, S.; Ambady, A.; Hegde, N.; Mahadevaswamy, J.; Kaur, P.; Sambandamurthy, V. K.; Awasthy, D.; Narayan, C.; Ravishankar, S.; Madhavapeddi, P.; Reddy, J.; Prabhakar, K.; Saralaya, R.; Chatterji, M.; Whiteaker, J.; McLaughlin, B.; Chiarelli, L. R.; Riccardi, G.; Pasca, M. R.; Binda, C.; Neres, J.; Dhar, N.; Signorino-Gelo, F.; McKinney, J. D.; Ramachandran, V.; Shandil, R.; Tommasi, R.; Iyer, P. S.; Narayanan, S.; Hosagrahara, V.; Kavanagh, S.; Dinesh, N.; Ghorpade, S. R. 4-Aminoquinolone Piperidine Amides: Noncovalent Inhibitors of DprE1 with Long Residence Time and Potent Antimycobacterial Activity. *J. Med. Chem.* **2014**, *57* (12), 5419–5434. https://doi.org/10.1021/jm5005978.

(84) Panda, M.; Ramachandran, S.; Ramachandran, V.; Shirude, P. S.; Humnabadkar, V.; Nagalapur, K.; Sharma, S.; Kaur, P.; Guptha, S.; Narayan, A.; Mahadevaswamy, J.; Ambady, A.; Hegde, N.; Rudrapatna, S. S.; Hosagrahara, V. P.; Sambandamurthy, V. K.; Raichurkar, A. Discovery of Pyrazolopyridones as a Novel Class of Noncovalent DprE1 Inhibitor with Potent Anti-Mycobacterial Activity. *J. Med. Chem.* **2014**, *57* (11), 4761–4771. https://doi.org/10.1021/jm5002937.

(85) Ballell, L.; Bates, R. H.; Young, R. J.; Alvarez-Gomez, D.; Alvarez-Ruiz, E.; Barroso, V.; Blanco, D.; Crespo, B.; Escribano, J.; González, R.; Lozanom, S.; Huss, S.; Santos-Villarejo, A.; Martín-Plaza, J. J.; Mendoza, A.; Rebollo-Lopez, M. J.; Remuiñan-Blanco, M.; Lavandera, J. L.; Pérez-Herran, E.; Gamo-Benito, F. J.; García-Bustos, J. F.; Barros, D.; Castro, J. P.; Cammack, N. Fueling Open-Source Drug Discovery: 177 Small-Molecule Leads against Tuberculosis. *ChemMedChem* **2013**, *8* (2), 313–321. https://doi.org/10.1002/cmdc.201200428.

(86) Batt, S. M.; Izquierdo, M. C.; Pichel, J. C.; Stubbs, C. J.; Peral, L. V.-G. Del; Pérez-Herrán,

E.; Dhar, N.; Mouzon, B.; Rees, M.; Hutchinson, J. P.; Young, R. J.; McKinney, J. D.; Aguirre, D. B.; Ballell, L.; Besra, G. S.; Argyrou, A. Whole Cell Target Engagement Identifies Novel Inhibitors of *Mycobacterium tuberculosis* Decaprenylphosphoryl-β-$_D$-ribose Oxidase. *ACS Infect. Dis.* **2015**, *1* (12), 615–626. https://doi.org/10.1021/acsinfecdis.5b00065.

(87) Borthwick, J. A.; Alemparte, C.; Wall, I.; Whitehurst, B. C.; Argyrou, A.; Burley, G.; Dios-Anton, P. De; Guijarro, L.; Monteiro, M. C.; Ortega, F.; Suckling, C. J.; Pichel, J. C.; Cacho, M.; Young, R. J. *Mycobacterium tuberculosis* Decaprenylphosphoryl-β-$_D$-ribose Oxidase Inhibitors: Expeditious Reconstruction of Suboptimal Hits into a Series with Potent in Vivo Activity. *J. Med. Chem.* **2020**, *63* (5), 2557–2576. https://doi.org/10.1021/acs.jmedchem.9b01561.

(88) Liu, R.; Krchnak, V.; Brown, S. N.; Miller, M. J. Deuteration of BTZ043 Extends the Lifetime of Meisenheimer Intermediates to the Antituberculosis Nitroso Oxidation State. *ACS Med. Chem. Lett.* **2019**, *10* (10), 1462–1466. https://doi.org/10.1021/acsmedchemlett.9b00308.

(89) Oh, S.; Park, Y.; Engelhart, C. A.; Wallach, J. B.; Schnappinger, D.; Arora, K.; Manikkam, M.; Gac, B.; Wang, H.; Murgolo, N.; Olsen, D. B.; Goodwin, M.; Sutphin, M.; Weiner, D. M.; Via, L. E.; Bosho, H. I. M.; Barry III, C. E. Discovery and Structure−Activity-Relationship Study of N-Alkyl-5-Hydroxypyrimidinone Carboxamides as Novel Antitubercular Agents Targeting Decaprenylphosphoryl- β-$_D$-ribose 2'-Oxidase. *J. Med. Chem.* **2018**, *61* (22), 9952–9965. https://doi.org/10.1021/acs.jmedchem.8b00883.

(90) Boyd, V. A.; Mason, J.; Hanumesh, P.; Price, J.; Russell, C. J.; Webb, T. R. 2-Substituted-4,5-Dihydroxypyrimidine-6-Carboxamide Antiviral Targeted Libraries. *J. Comb. Chem.* **2009**, *11* (6), 1100–1104. https://doi.org/10.1021/cc900111u.

(91) Balabon, O.; Pitta, E.; Rogacki, M. K.; Meiler, E.; Casanueva, R.; Guijarro, L.; Huss, S.; Lopez-Roman, E. M.; Santos-Villarejo, A.; Augustyns, K.; Ballell, L.; Aguirre, D. B.; Bates, R. H.; Cunningham, F.; Cacho, M.; Veken, P. Van der. Optimization of Hydantoins as Potent Antimycobacterial Decaprenylphosphoryl- β-$_D$-Ribose Oxidase (DprE1) Inhibitors. *J. Med. Chem.* **2020**, *63* (10), 5367–5386. https://doi.org/10.1021/acs.jmedchem.0c00107.

(92) Whitehurst, B. C.; Young, R. J.; Burley, G. A.; Cacho, M.; Torres, P.; Peral, L. V.-G. del. Identification of 2-((2,3-Dihydrobenzo[b][1,4]Dioxin-6-Yl)Amino)-N-Phenylpropanamides as a Novel Class of Potent DprE1 Inhibitors. *Bioorg. Med. Chem. Lett.* **2020**, *30* (12), 127192. https://doi.org/10.1016/j.bmcl.2020.127192.

(93) Hill, A. P.; Young, R. J. Getting Physical in Drug Discovery: A Contemporary Perspective on Solubility and Hydrophobicity. *Drug Discov. Today* **2010**, *15* (15–16), 648–655. https://doi.org/10.1016/j.drudis.2010.05.016.

(94) Young, R. J.; Green, D. V. S.; Luscombe, C. N.; Hill, A. P. Getting Physical in Drug Discovery II: The Impact of Chromatographic Hydrophobicity Measurements and Aromaticity. *Drug Discov. Today* **2011**, *16* (17–18), 822–830. https://doi.org/10.1016/j.drudis.2011.06.001.

(95) Hariguchi, N.; Chen, X.; Hayashi, Y.; Kawano, Y.; Fujiwara, M.; Matsuba, M.; Shimizu, H.; Ohba, Y.; Nakamura, I.; Kitamoto, R.; Shinohara, T.; Uematsu, Y.; Ishikawa, S.; Itotani, M.; Haraguchi, Y.; Takemura, I.; Matsumoto, M. OPC-167832, a Novel Carbostyril Derivative with Potent Antituberculosis Activity as a DprE1 Inhibitor. *Antimicrob. Agents Chemother.* **2020**, *64* (6), e02020-19. https://doi.org/10.1128/AAC.02020-19.

(96) Shimizu, H.; Kawano, Y.; Ishikawa, S.; Uematsu, Y.; Shinohara, T.; Itotani, M.; Haraguchi, Y.; Takemura, I.; Kaneshige, A.; Nakai, Y.; Hariguchi, N.; Hayashi, Y.; Matsumoto, M. Patent WO/2016/031255, 2016.

(97) https://Clinicaltrials.Gov/Ct2/Show/NCT03678688 (accessed on 20$^{th}$ February, 2023).

(98) Wang, P.; Batt, S. M.; Wang, B.; Fu, L.; Qin, R.; Lu, Y.; Li, G.; Besra, G. S.; Huang, H. Discovery of Novel Thiophene-Arylamide Derivatives as DprE1 Inhibitors with Potent Antimycobacterial Activities. *J. Med. Chem.* **2021**, *64* (9), 6241–6261. https://doi.org/10.1021/acs.jmedchem.1c00263.

(99) Makarov, V.; Lechartier, B.; Zhang, M.; Neres, J.; van der Sar, A. M.; Raadsen, S. A.; Hartkoorn, R. C.; Ryabova, O. B.; Vocat, A.; Decosterd, L. A.; Widmer, N.; Buclin, T.; Bitter, W.; Andries, K.; Pojer, F.; Dyson, P. J.; Cole, S. T. Towards a New Combination Therapy for Tuberculosis with next Generation Benzothiazinones. *EMBO Mol. Med.* **2014**, *6* (3), 372–383. https://doi.org/10.1002/emmm.201303575.

(100) Qin, R.; Wang, P.; Wang, B.; Fu, L.; Batt, S. M.; Besra, G. S.; Wu, C.; Wang, Y.; Huang, H.; Lu, Y.; Li, G. Identification of Thiophene-Benzenesulfonamide Derivatives for the Treatment of Multidrug-Resistant Tuberculosis. *Eur. J. Med. Chem.* **2022**, *231*, 114145. https://doi.org/10.1016/j.ejmech.2022.114145.

(101) Ezquerra-Aznárez, M.; Degiacomi, G.; Gašparovic, H.; Stelitano, G.; Sammartino, J. C.; Korduláková, J.; Governa, P.; Manetti, F.; Pasca, M. R.; Chiarelli, L. R.; Ramón-García, S. The Veterinary Anti-Parasitic Selamectin Is a Novel Inhibitor of the *Mycobacterium tuberculosis* DprE1 Enzyme. *Int. J. Mol. Sci.* **2022**, *23* (2), 771. https://doi.org/10.3390/ijms23020771.

(102) Piton, J.; Vocat, A.; Lupien, A.; Foo, C. S.; Riabova, O.; Makarov, V.; Cole, S. T. Structure-Based Drug Design and Characterization of Sulfonyl- Piperazine Benzothiazinone Inhibitors of DprE1 from *Mycobacterium tuberculosis*. *Antimicrob. Agents Chemother.* **2018**, *62* (10), e00681-18. https://doi.org/10.1128/AAC.00681-18.

(103) Rogacki, M. K.; Pitta, E.; Balabon, O.; Huss, S.; Lopez-Roman, E. M.; Argyrou, A.; Blanco-Ruano, D.; Cacho, M.; Velde, C. M. L. Vande; Augustyns, K.; Ballell, L.; Barros, D.; Bates, R. H.; Cunningham, F.; Veken, P. Van Der. Identification and Profiling of Hydantoins-A Novel Class of Potent Antimycobacterial DprE1 Inhibitors. *J. Med. Chem.* **2018**, *61*, 11221–11249. https://doi.org/10.1021/acs.jmedchem.8b01356.

(104) Batt, S. M.; Jabeen, T.; Bhowruth, V.; Quill, L.; Lund, P. A.; Eggeling, L.; Alderwick, L. J.; Fütterer, K.; Besra, G. S. Structural Basis of Inhibition of *Mycobacterium tuberculosis* DprE1 by Benzothiazinone Inhibitors. *Proc. Natl. Acad. Sci.* **2012**, *109* (28), 11354–11359. https://doi.org/10.1073/pnas.1205735109.

(105) StarDrop v7.2.0.32905. 2022.

(106) Lipinski, C. A.; Lombardo, F.; Dominy, B. W.; Feeney, P. J. Experimental and Computational Approaches to Estimate Solubility and Permeability in Drug Discovery and Development Settings. *Adv. Drug Deliv. Rev.* **1997**, *23* (1–3), 3–25. https://doi.org/10.1016/S0169-409X(96)00423-1.

(107) Gleeson, M. P. Generation of a Set of Simple, Interpretable ADMET Rules of Thumb. *J. Med. Chem.* **2008**, *51* (4), 817–834. https://doi.org/10.1021/jm701122q.

(108) Hughes, J. D.; Blagg, J.; Price, D. A.; Bailey, S.; Decrescenzo, G. A.; Devraj, R. V.; Ellsworth, E.; Fobian, Y. M.; Gibbs, M. E.; Gilles, R. W.; Greene, N.; Huang, E.; Krieger-Burke, T.; Loesel, J.; Wager, T.; Whiteley, L.; Zhang, Y. Physiochemical Drug Properties Associated with in Vivo Toxicological Outcomes. *Bioorg. Med. Chem. Lett.* **2008**, *18* (17), 4872–4875. https://doi.org/10.1016/j.bmcl.2008.07.071.

(109) ADME Models Reference. In *Optibrium Ltd.*; 2011.

(110) StarDrop TM Reference Guide. *Optibrium Ltd V6.3*. 2016.

(111) Toxicity Prediction in StarDrop. *Optibrium Ltd.* 2011.

(112) Athanasiadis, E.; Cournia, Z.; Spyrou, G. ChemBioServer: A Web-Based Pipeline for Filtering, Clustering and Visualization of Chemical Compounds Used in Drug Discovery. *Bioinformatics* **2012**, *28* (22), 3002–3003. https://doi.org/10.1093/bioinformatics/bts551.

(113) Kuhn, M.; Johnson, K. *Applied Predictive Modeling*; 2013. https://doi.org/10.1007/978-1-4614-6849-3.

(114) Richter, A.; Narula, G.; Rudolph, I.; Seidel, R. W.; Wagner, C.; Av-Gay, Y.; Imming, P. Efficient Synthesis of Benzothiazinone Analogues with Activity against Intracellular *Mycobacterium tuberculosis*. *ChemMedChem* **2022**, *17* (6), e202100733. https://doi.org/10.1002/cmdc.202100733.

(115) Meanwell, N. A. Improving Drug Candidates by Design: A Focus on Physicochemical Properties As a Means of Improving Compound Disposition and Safety. *Chem. Res. Toxicol.* **2011**, *24* (9), 1420–1456. https://doi.org/10.1021/tx200211v.

(116) Leeson, P. D. Molecular Inflation, Attrition and the Rule of Five. *Adv. Drug Deliv. Rev.*

**2016**, *101*, 22–33. https://doi.org/10.1016/j.addr.2016.01.018.
(117) Matsson, P.; Doak, B. C.; Over, B.; Kihlberg, J. Cell Permeability beyond the Rule of 5. *Adv. Drug Deliv. Rev.* **2016**, *101*, 42–61. https://doi.org/10.1016/j.addr.2016.03.013.
(118) Tinworth, C. P.; Young, R. J. Facts, Patterns, and Principles in Drug Discovery: Appraising the Rule of 5 with Measured Physicochemical Data. *J. Med. Chem.* **2020**, *63* (18), 10091–10108. https://doi.org/10.1021/acs.jmedchem.9b01596.
(119) Waring, M. J. Lipophilicity in Drug Discovery. *Expert Opin. Drug Discov.* **2010**, *5* (3), 235–248. https://doi.org/10.1517/17460441003605098.
(120) Palmer, D. S.; Llinàs, A.; Morao, I.; Day, G. M.; Goodman, J. M.; Glen, R. C.; Mitchell, J. B. O. Predicting Intrinsic Aqueous Solubility by a Thermodynamic Cycle. *Mol. Pharm.* **2008**, *5* (2), 266–279. https://doi.org/10.1021/mp7000878.
(121) Alex, A.; Millan, D. S.; Perez, M.; Wakenhut, F.; Whitlock, G. A. Intramolecular Hydrogen Bonding to Improve Membrane Permeability and Absorption in beyond Rule of Five Chemical Space. *Medchemcomm* **2011**, *2* (7), 669–674. https://doi.org/10.1039/c1md00093d.
(122) Leeson, P. D.; Davis, A. M. Time-Related Differences in the Physical Property Profiles of Oral Drugs. *J. Med. Chem.* **2004**, *47* (25), 6338–6348. https://doi.org/10.1021/jm049717d.
(123) Wenlock, M. C.; Austin, R. P.; Barton, P.; Davis, A. M.; Leeson, P. D. A Comparison of Physiochemical Property Profiles of Development and Marketed Oral Drugs. *J. Med. Chem.* **2003**, *46* (7), 1250–1256. https://doi.org/10.1021/jm021053p.
(124) Lipinski, C. A. Rule Offive in 2015 and beyond: Target and Ligand Structural Limitations, Ligand Chemistry Structure and Drug Discovery Project Decisions. *Adv. Drug Deliv. Rev.* **2016**, *101*, 34–41. https://doi.org/10.1016/j.addr.2016.04.029.
(125) Lipinski, C. A. Drug-like Properties and the Causes of Poor Solubility and Poor Permeability. *J. Pharmacol. Toxicol. Methods* **2001**, *44* (1), 235–249. https://doi.org/10.1016/S1056-8719(00)00107-6.
(126) Doak, B. C.; Zheng, J.; Dobritzsch, D.; Kihlberg, J. How Beyond Rule of 5 Drugs and Clinical Candidates Bind to Their Targets. *J. Med. Chem.* **2015**, *59* (6), 2312–2327. https://doi.org/10.1021/acs.jmedchem.5b01286.
(127) Doak, B. C.; Over, B.; Giordanetto, F.; Kihlberg, J. Oral Druggable Space beyond the Rule of 5: Insights from Drugs and Clinical Candidates. *Chem. Biol.* **2014**, *21* (9), 1115–1142. https://doi.org/10.1016/j.chembiol.2014.08.013.
(128) Moroy, G.; Martiny, V. Y.; Vayer, P.; Villoutreix, B. O.; Miteva, M. A. Toward in Silico Structure-Based ADMET Prediction in Drug Discovery. *Drug Discov. Today* **2012**, *17* (1–2), 44–55. https://doi.org/10.1016/j.drudis.2011.10.023.
(129) Jeffrey, P.; Summerfield, S. Assessment of the Blood – Brain Barrier in CNS Drug Discovery. *Neurobiol. Dis.* **2010**, *37* (1), 33–37. https://doi.org/10.1016/j.nbd.2009.07.033.
(130) Vallner, J. J. Binding of Drugs by Albumin and Plasma Protein. *J. Pharm. Sci.* **1977**, *66* (4), 447–465. https://doi.org/10.1002/jps.2600660402.
(131) Lambrinidis, G.; Vallianatou, T.; Tsantili-Kakoulidou, A. In Vitro, in Silico and Integrated Strategies for the Estimation of Plasma Protein Binding. A Review. *Adv. Drug Deliv. Rev.* **2015**, *86*, 27–45. https://doi.org/10.1016/j.addr.2015.03.011.
(132) Xiong, L.; Gao, C.; Shi, Y.-J.; Tao, X.; Peng, C.-T.; Rong, J.; Liu, K.-L.; Lei, Q.; Zhang, Y.-W.; Wang, N.-Y.; Yu, L.-T. Metabolism of SKLB-TB1001, a Potent Antituberculosis Agent, in Animals. *Antimicrob. Agents Chemother.* **2018**, *62* (7), e02375-17. https://doi.org/10.1128/AAC.02375-17.
(133) Zanger, U. M.; Schwab, M. Cytochrome P450 Enzymes in Drug Metabolism: Regulation of Gene Expression, Enzyme Activities, and Impact of Genetic Variation. *Pharmacol. Ther.* **2013**, *138* (1), 103–141. https://doi.org/10.1016/j.pharmthera.2012.12.007.
(134) Isvoran, A.; Louet, M.; Vladoiu, D. L.; Craciun, D.; Loriot, M.-A.; Villoutreix, B. O.; Miteva, M. A. Pharmacogenomics of the Cytochrome P450 2C Family: Impacts of Amino Acid Variations on Drug Metabolism. *Drug Discov. Today* **2017**, *22* (2), 366–376. https://doi.org/10.1016/j.drudis.2016.09.015.
(135) Nepali, K.; Lee, H.-Y.; Liou, J.-P. Nitro-Group-Containing Drugs. *J. Med. Chem.* **2019**,

*62* (6), 2851–2893. https://doi.org/10.1021/acs.jmedchem.8b00147.
(136) Garrido, A.; Lepailleur, A.; Mignani, S. M.; Dallemagne, P.; Rochais, C. HERG Toxicity Assessment: Useful Guidelines for Drug Design Amanda. *Eur. J. Med. Chem.* **2020**, *195*, 112290. https://doi.org/10.1016/j.ejmech.2020.112290.
(137) Cavalli, A.; Poluzzi, E.; Ponti, F. De; Recanatini, M. Toward a Pharmacophore for Drugs Inducing the Long QT Syndrome: Insights from a CoMFA Study of HERG K+ Channel Blockers. *J. Med. Chem.* **2002**, *45* (18), 3844–3853. https://doi.org/10.1021/jm0208875.
(138) Aronov, A. M.; Goldman, B. B. A Model for Identifying HERG K+ Channel Blockers. *Bioorg. Med. Chem.* **2004**, *12* (9), 2307–2315. https://doi.org/10.1016/j.bmc.2004.02.003.
(139) Raschi, E.; Ceccarini, L.; Ponti, F. De; Recanatini, M. HERG-Related Drug Toxicity and Models for Predicting HERG Liability and QT Prolongation. *Expert Opin. Drug Metab. Toxicol.* **2009**, *5* (9), 1005–1021. https://doi.org/10.1517/17425250903055070.
(140) Modi, S.; Li, J.; Malcomber, S.; Moore, C.; Scott, A.; White, A.; Carmichael, P. Integrated in Silico Approaches for the Prediction of Ames Test Mutagenicity. *J. Comput. Aided. Mol. Des.* **2012**, *26* (9), 1017–1033. https://doi.org/10.1007/s10822-012-9595-5.
(141) Benfenati, E.; Golbamaki, A.; Raitano, G.; Roncaglioni, A.; Manganelli, S.; Lemke, F.; Norinder, U.; Piparo, E. L.; Honma, M.; Manganaro, A.; Gini, G.; Golbamaki, A.; Raitano, G.; Roncaglioni, A.; Manganelli, S. A Large Comparison of Integrated SAR / QSAR Models of the Ames Test for Mutagenicity Ames Test for Mutagenicity$. *SAR QSAR Environ. Res.* **2018**, *29* (8), 591–611. https://doi.org/10.1080/1062936X.2018.1497702.
(142) Hengstler, J. G.; Oesch, F. Ames Test. In *Encyclopedia of Genetics*; 2001; pp 51–54. https://doi.org/10.1006/rwgn.2001.1543.
(143) Föllmann, W.; Degen, G.; Oesch, F.; Hengstler, J. G. Ames Test. In *Brenner's Encyclopedia of Genetics (Second Edition)*; Elsevier Inc., 2013; pp 104–107. https://doi.org/10.1016/B978-0-12-374984-0.00048-6.
(144) Purohit, V.; Basu, A. K. Mutagenicity of Nitroaromatic Compounds. *Chem. Res. Toxicol.* **2000**, *13* (8), 673–692. https://doi.org/10.1021/tx000002x.
(145) Jasial, S.; Hu, Y.; Bajorah, J. How Frequently Are Pan-Assay Interference Compounds Active? Large-Scale Analysis of Screening Data Reveals Diverse Activity Profiles, Low Global Hit Frequency, and Many Consistently Inactive Compounds. *J. Med. Chem.* **2017**, *60* (9), 3879–3886. https://doi.org/10.1021/acs.jmedchem.7b00154.
(146) Baell, J. B.; Holloway, G. A. New Substructure Filters for Removal of Pan Assay Interference Compounds (PAINS) from Screening Libraries and for Their Exclusion in Bioassays. *J. Med. Chem.* **2010**, *53* (7), 2719–2740. https://doi.org/10.1021/jm901137j.
(147) Baell, J. B.; Nissink, J. W. M. Seven Year Itch: Pan-Assay Interference Compounds (PAINS) in 2017 - Utility and Limitations. *ACS Chem. Biol.* **2018**, *13* (1), 36–44. https://doi.org/10.1021/acschembio.7b00903.
(148) Baell, J. B. Broad Coverage of Commercially Available Lead-like Screening Space with Fewer than 350,000 Compounds. *J. Chem. Inf. Model.* **2013**, *53* (1), 39–55. https://doi.org/10.1021/ci300461a.
(149) Capuzzi, S. J.; Muratov, E. N.; Tropsha, A. Phantom PAINS: Problems with the Utility of Alerts for Pan-Assay INterference CompoundS. *J. Chem. Inf. Model.* **2017**, *57* (3), 417–427. https://doi.org/10.1021/acs.jcim.6b00465.
(150) Rodríguez-Pérez, R.; Miljković, F.; Bajorath, J. Machine Learning in Chemoinformatics and Medicinal Chemistry. *Annu. Rev. Biomed. Data Sci.* **2022**, *5* (1), 43–65. https://doi.org/10.1146/annurev-biodatasci-122120-124216.
(151) Panteleev, J.; Gao, H.; Jia, L. Recent Applications of Machine Learning in Medicinal Chemistry. *Bioorganic Med. Chem. Lett.* **2018**, *28* (17), 2807–2815. https://doi.org/10.1016/j.bmcl.2018.06.046.
(152) Durant, J. L.; Leland, B. A.; Henry, D. R.; Nourse, J. G. Reoptimization of MDL Keys for Use in Drug Discovery. *J. Chem. Inf. Comput. Sci.* **2002**, *42* (6), 1273–1280. https://doi.org/10.1021/ci010132r.
(153) Rogers, D.; Hahn, M. Extended-Connectivity Fingerprints. *J. Chem. Inf. Model.* **2010**, *50* (5), 742–754. https://doi.org/10.1021/ci100050t.
(154) Gao, K.; Nguyen, D. D.; Sresht, V.; Mathiowetz, A. M.; Tu, M.; Wei, G.-W. Are 2D

Fingerprints Still Valuable for Drug Discovery? *Phys. Chem. Chem. Phys.* **2020**, *22* (16), 8373–8390. https://doi.org/10.1039/d0cp00305k.
(155) Willett, P. Similarity-Based Virtual Screening Using 2D Fingerprints. *Drug Discov. Today* **2006**, *11* (23–24), 1046–1053. https://doi.org/10.1016/j.drudis.2006.10.005.
(156) Rogers, D.; Brown, R. D.; Hahn, M. Using Extended-Connectivity Fingerprints with Laplacian-Modified Bayesian Analysis in High-Throughput Screening Follow-Up. *J. Biomol. Screen.* **2005**, *10* (7), 682–686. https://doi.org/10.1177/1087057105281365.
(157) Cunningham, P.; Delany, S. J. K-Nearest Neighbour Classifiers - A Tutorial. *ACM Comput. Surv.* **2021**, *54* (6), 1–25. https://doi.org/10.1145/3459665.
(158) Harrington, P. D. B. Support Vector Machine Classification Trees. *Anal. Chem.* **2015**, *87* (21), 11065–11071. https://doi.org/10.1021/acs.analchem.5b03113.
(159) Friedman, J. H. Stochastic Gradient Boosting. *Comput. Stat. Data Anal.* **2002**, *38* (4), 367–378. https://doi.org/10.1016/S0167-9473(01)00065-2.
(160) Biau, G. Analysis of a Random Forests Model. *J. Mach. Learn. Res.* **2012**, *13*, 1063–1095.
(161) Sheridan, R. P.; Wang, W. M.; Liaw, A.; Ma, J.; Gifford, E. M. Extreme Gradient Boosting as a Method for Quantitative Structure− Activity Relationships. *J. Chem. Inf. Model.* **2016**, *56* (12), 2353–2360. https://doi.org/10.1021/acs.jcim.6b00591.
(162) Polishchuk, P. G. Interpretation of Quantitative Structure–Activity Relationship Models: Past, Present, and Future. *J. Chem. Inf. Model.* **2017**, *57* (11), 2618–2639. https://doi.org/10.1021/acs.jcim.7b00274.
(163) Li, R.; Tian, Y.; Yang, Z.; Ji, Y.; Ding, J.; Yan, A. Classification Models and SAR Analysis on HDAC1 Inhibitors Using Machine Learning Methods. *Mol. Divers.* **2022**. https://doi.org/10.1007/s11030-022-10466-w.
(164) Chu, C. S. M.; Simpson, J. D.; O'Neill, P. M.; Berry, N. G. Journal of Molecular Graphics and Modelling Machine Learning – Predicting Ames Mutagenicity of Small Molecules. *J. Mol. Graph. Model.* **2021**, *109*, 108011. https://doi.org/10.1016/j.jmgm.2021.108011.
(165) https://www.rdocumentation.org/packages/photobiology/versions/0.10.6/topics/na.omit (accessed on 15th February, 2023).
(166) https://www.rdocumentation.org/packages/base/versions/3.6.2/topics/duplicated (accessed on 17th February, 2023).
(167) Landrum G. Rdkit: open-source cheminformatics (2012). www.rdkit.org (accessed on 27th February, 2023).
(168) Moreira, L.; Dantas, C.; Oliveira, L.; Soares, J.; Ogasawara, E. On Evaluating Data Preprocessing Methods for Machine Learning Models for Flight Delays. In *2018 International Joint Conference on Neural Networks (IJCNN)*; IEEE, 2018. https://doi.org/10.1109/IJCNN.2018.8489294.
(169) https://www.rdocumentation.org/packages/caret/versions/6.0-93/topics/downSample. (accessed on 7th March, 2023).
(170) https://www.rdocumentation.org/packages/groupdata2/versions/1.1.2/topics/upsample. (accessed on 8h March, 2023).
(171) https://www.rdocumentation.org/packages/caret/versions/6.0-92/topics/nearZeroVar. (accessed on 10th March, 2023).
(172) https://scikit-learn.org/stable/modules/generated/sklearn.model_selection.train_test_split.html. (accessed on 10th March, 2023).
(173) https://scikit-learn.org/ (accessed on 15th March, 2023)
(174) XGBoost. https://pypi.org/project/xgboost/ (accessed on 7th March, 2023)
(175) https://scikit-learn.org/stable/modules/generated/sklearn.neighbors.KNeighborsClassifier.html. (accessed on 10th March, 2023).
(176) Cortes, C.; Vapnik, V. Support-Vector Networks. *Mach. Learn.* **1995**, *20*, 273–297. https://doi.org/10.1007/BF00994018.
(177) Kinnings, S. L.; Liu, N.; Tonge, P. J.; Jackson, R. M.; Xie, L.; Bourne, P. E. A Machine Learning-Based Method To Improve Docking Scoring Functions and Its Application to Drug Repurposing. *J. Chem. Inf. Model.* **2011**, *51* (2), 408–419.

(178) https://Scikit-Learn.Org/Stable/Modules/Generated/Sklearn.Svm.SVC.Html. (accessed on 10th March, 2023).
(179) https://scikit-learn.org/stable/modules/generated/sklearn.ensemble.RandomForestClassifier.html. (accessed on 15th March, 2023).
(180) Natekin, A.; Knoll, A. Gradient Boosting Machines, a Tutorial. *Front. Neurorobot.* **2013**, *7*. https://doi.org/10.3389/fnbot.2013.00021.
(181) https://Scikit-Learn.Org/Stable/Modules/Generated/Sklearn.Ensemble.GradientBoostingClassifier.Html. (accessed on 16th March, 2023).
(182) Chen, T.; Guestrin, C. XGBoost: A Scalable Tree Boosting System. In *Proceedings of the 22nd ACM SIGKDD International Conference on Knowledge Discovery and Data Mining*; 2016; pp 785–794. https://doi.org/10.1145/2939672.2939785.
(183) https://scikit-learn.org/stable/modules/generated/sklearn.ensemble.GradientBoostingClassifier.html. (accessed on 22nd March, 2023).
(184) https://xgboost.readthedocs.io/en/stable/.(accessed on 24th March, 2023).
(185) Korkmaz, S. Deep Learning-Based Imbalanced Data Classification for Drug Discovery. *J. Chem. Inf. Model.* **2020**, *60* (9), 4180–4190. https://doi.org/10.1021/acs.jcim.9b01162.
(186) Yao, J.; Shepperd, M. Assessing Software Defection Prediction Performance: Why Using the Matthews Correlation Coefficient Matters. In *EASE '20: Proceedings of the Evaluation and Assessment in Software Engineering*; 2020; pp 120–129. https://doi.org/10.1145/3383219.3383232.
(187) Li, Y.; Tian, Y.; Qin, Z.; Yan, A. Classification of HIV-1 Protease Inhibitors by Machine Learning Methods. *ACS Omega* **2018**, *3* (11), 15837–15849. https://doi.org/10.1021/acsomega.8b01843.
(188) Walsh, I.; Fishman, D.; Garcia-Gasulla, D.; Titma, T.; Pollastri, G.; ELIXIR Machine Learning Focus Group; Harrow, J.; Psomopoulos, F. E.; Tosatto, S. C. E. DOME: Recommendations for Supervised Machine Learning Validation in Biology. *Nat. Methods* **2021**, *18* (10), 1122–1144. https://doi.org/10.1038/s41592-021-01205-4.
(189) Chung, N. C.; Miasojedow, B.; Startek, M.; Gambin, A. Jaccard/Tanimoto Similarity Test and Estimation Methods for Biological Presence-Absence Data. *BMC Bioinformatics* **2019**, *20*, 644. https://doi.org/10.1186/s12859-019-3118-5.
(190) https://scikit-learn.org/stable/auto_examples/ensemble/plot_forest_importances.html (accessed on 19th March, 2023).
(191) Hanser, T.; Barber, C.; Marchaland, J. F.; Werner, S. Applicability Domain: Towards a More Formal Definition. *SAR QSAR Environ. Res.* **2016**, *27* (11), 893–909. https://doi.org/10.1080/1062936X.2016.1250229.

# Chapter 4

## Synthesis of Non-Symmetrical Dispiro 1,2,4,5-Tetraoxanes and 1,2,4-Trioxanes Catalyzed by Silica Sulfuric Acid

# Chapter 4

The work described in this section was included in the following publication:

**Amado, P. S. M**.; Frija, L. M. T.; Coelho, J. A. S.; O'Neill, P. M.; Cristiano, M. L. S. Synthesis of Non-Symmetrical Dispiro-1,2,4,5-Tetraoxanes and Dispiro-1,2,4-Trioxanes Catalyzed by Silica Sulfuric Acid. *J. Org. Chem.* **2021**, *86* (15), 10608–10620. https://doi.org/10.1021/acs.joc.1c01258

Literature Review submitted as a book chapter:

**Amado, P. S. M**.; Frija, L. M. T.; O'Neill, P. M.; Cristiano, M. L. S. Synthesis of Non-Symmetrical 1,2,4,5-Tetraoxanes: Past and Current Routes. *To be published by World Scientific*. *Submitted on 17th February 2022. In editorial Revision.*

***A small part of the book chapter is described in this Chapter.***

**CONTRIBUTIONS**

Patrícia S. M. Amado designed and carried out the synthesis and characterization of all compounds. Density functional theory (DFT) calculations were performed by Luís M. T. Frija and Jaime A. S. Coelho (Centro de Química Estrutural (CQE), University of Lisbon). Prof. Maria de Lurdes Cristiano and Prof. Paul O'Neill supervised the work and revised the manuscript. All authors have contributed to the discussion of the results and have written the manuscript.

## 4.1. Summary

This chapter presents a novel protocol for the preparation of non-symmetrical 1,2,4,5-tetraoxanes and 1,2,4-trioxanes, promoted by the heterogeneous Silica Sulfuric Acid (SSA) catalyst. Different ketones react under mild conditions with *gem*-dihydroperoxides or peroxysilyl alcohols/β-hydroperoxy alcohols, to generate the corresponding endoperoxides in good yields. Our mechanistic proposal, assisted by molecular orbital calculations, at the ωB97XD/def2-TZVPP/PCM(DCM)//B3LYP/6-31G(d) level of theory, enhances the role of SSA in the cyclocondensation step. This novel procedure differs from previously reported methods by using readily available and inexpensive reagents, with recyclable properties, therefore establishing a valid alternative approach for the synthesis of new biologically active endoperoxides.

## 4.2. Synthetic 1,2,4,5-tetraoxanes and 1,2,4-trioxanes: an introduction

Organic peroxides are found in various natural products, biologically active compounds, and chemical reactions, as intermediates.[1] Among organic peroxides, six-membered cyclic 1,2,4-trioxanes and 1,2,4,5-tetraoxanes have gained considerable interest in medicinal chemistry due to their potential for treating various diseases, including malaria.[2–5] The interest in cyclic organic peroxides is mainly driven by the fact that an endoperoxide moiety is the pharmacophore in ART and its derivatives, which demonstrate excellent antimalarial activity (**Figure 4.1**).[6] There are some drawbacks to using ART and its semisynthetic counterparts, including their restricted availability and high cost due to the extraction process.[7–9] As such, there is an urgent need to expand the arsenal of endoperoxide-based medicines, among which synthetic 1,2,4-trioxanes and 1,2,4,5-tetraoxanes are undoubtedly a promising approach for the development of novel alternatives to ART.[10]

Besides the impressive antimalarial activity, especially against the deadly parasite *Plasmodium falciparum (Pf)*[7–9,11], selected 1,2,4-trioxanes and 1,2,4,5-tetraoxanes also exhibit other biological activities: anticancer[12–19], antimycobacterial[20,21], antiparasitic against *Leishmania spp.*[22–24], *Trypanosoma cruzi*[24], *Toxoplasma gondii*[15], trematodes as *Fasciola hepatica*[25–28], *Echinostoma caproni*[26], *Schistosoma japonicum*[27,29], *Schistosoma mansoni (Sm)*[27,30–32], and acting as an antifungal, for crop protection[33] (a few notable

examples are depicted in **Figure 4.1**). 1,2,4,5-Tetraoxane-containing compounds were also found to act as elicitors in plants. It was observed in two species belonging to the genus *Nepeta* that tetraoxanes induce the production of specific secondary metabolites with essential properties that can be used in the pharmaceutical, cosmetic, and food industries.[34]

This chapter describes our work on the improvement of methodologies for the preparation of six-membered peroxides to facilitate the expansion of their libraries, hence allowing the discovery of novel drug candidates. There have been a few reviews covering the 1,2,4-trioxane and 1,2,4,5-tetraoxane chemistry, namely those by McCullough *et al.*[35], Dong *et al.*[36], Antonovskii *et al.*[37], Tang *et al.*[38], Opsenica *et al.*[39], Kumar *et al.*[40], Jorge *et al.*[41], Yadav *et al.*[42], Terent'ev *et al.*[43] and Yaremenko *et al.*[44]

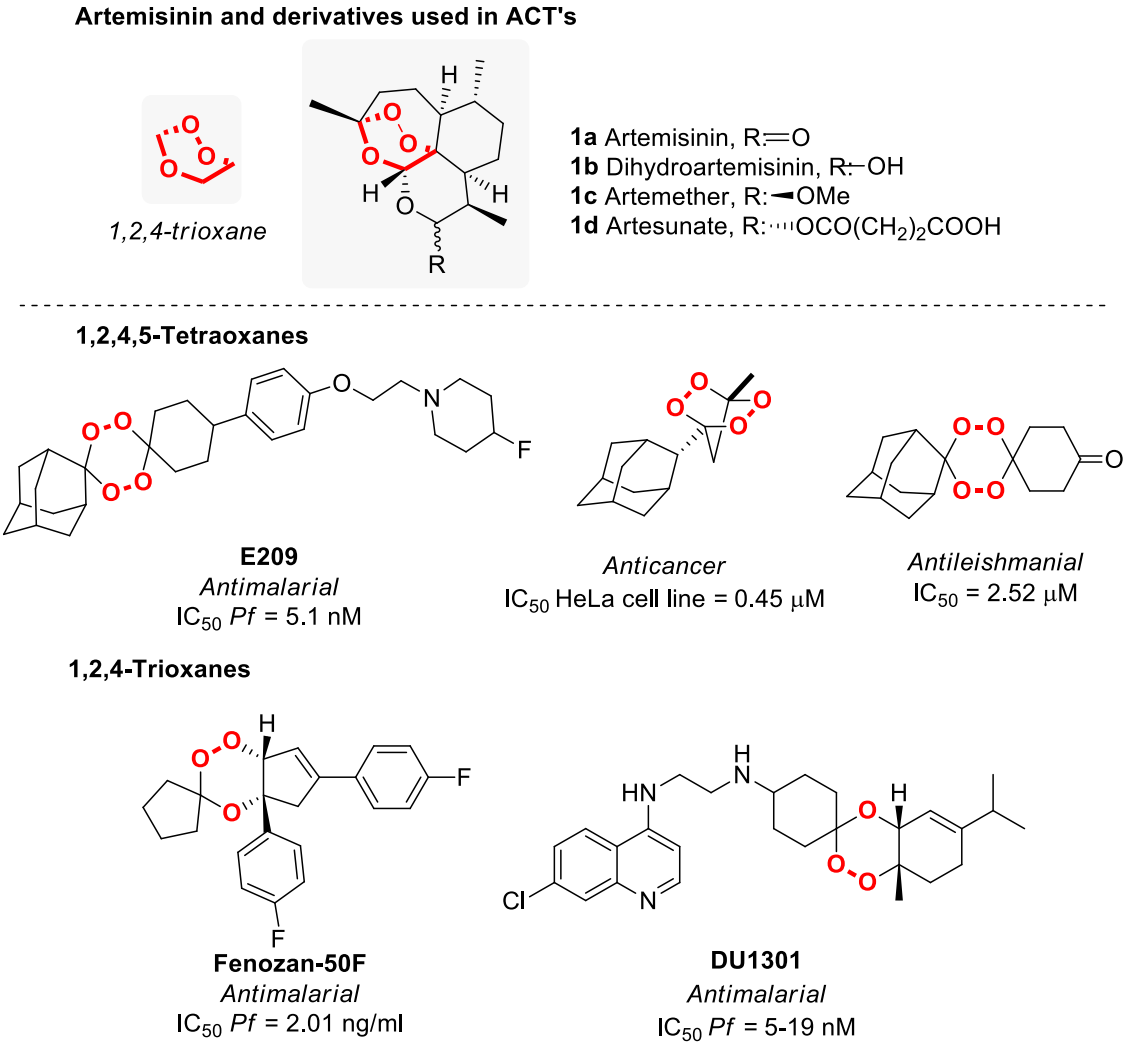


**Figure 4.1**. Structure representation of artemisinin, its derivatives and selected examples of synthetic non-symmetric 1,2,4-trioxanes and 1,2,4,5-tetraoxanes that evidenced very relevant biological activities and therapeutic potential.

## 4.3. Stereoelectronic analysis

1,2,4-Trioxanes and 1,2,4,5-tetraoxanes are remarkably stable compared to the parent trioxolanes. The singular thermodynamic stability observed in these cyclic peroxides was addressed by Gomes *et al.*[45], to understand why multiple O–O bonds in one molecule could induce stabilization of the six-membered heterocycle and not the opposite. Results of theoretical calculations, established on stereoelectronic analysis, indicated that the comparatively high thermodynamic stability of bis-peroxides (1,2,4,5-tetraoxanes) is due to the reactivation of anomeric effect caused by strong $n_O \rightarrow \sigma^*_{C–O}$ interactions. The interaction (hyperconjugation) between the unshared electron pair on the oxygen (from the peroxide bond) and the antibonding σ* orbital of the C–O bond lowers the overall energy of the ring system. Thus, the antibonding $\sigma^*_{C–O}$ orbital appears to be the true source of stabilization, which improves when the ring adopts a boat conformation. Based on these observations, 1,2,4,5-tetraoxanes can be compared stereoelectronically to bis-acetals, while 1,2,4-trioxanes may be viewed as mono-acetals. As observed in **Figure 4.2**, the addition of a second O–O bond results in negative values for both ΔE (-3.8 kcal/mol) and ΔG (-4.2 kcal/mol), the molecule becomes thermodynamically more stable than the parent monoperoxide bearing a similar membered-ring system (1,2,4-trioxane, ΔG= -2.2 kcal/mol, ΔG= -2.4 kcal/mol; removing one oxygen atom decreases the stabilization by half). Addition of one carbon in the bridge that separates the two peroxides proved to induce loss of stabilization, the molecule becoming a "true" bis-peroxide, with positive values for ΔE (+6.1 kcal/mol) and ΔG (+7.9 kcal/mol) indicating a decrease in the system's stability.[45–47] The stereoelectronic stabilizing effects on the O–O bond can be increased by introducing strong sigma acceptors (C–F, C–O, or C–N).[45–47] Compared to the monocyclic system, [2.2.1] bicyclic tetraoxanes are stabilized by 4–5 kcal/mol. Each of the four symmetry-equivalent $n_O \rightarrow \sigma^*_{C–O}$ interactions has a stabilizing effect of 16.4 kcal, implying an even more favourable configuration of the donor and acceptor orbitals when the 1,2,4,5-tetraoxane boat conformation is adopted/imposed.[45]

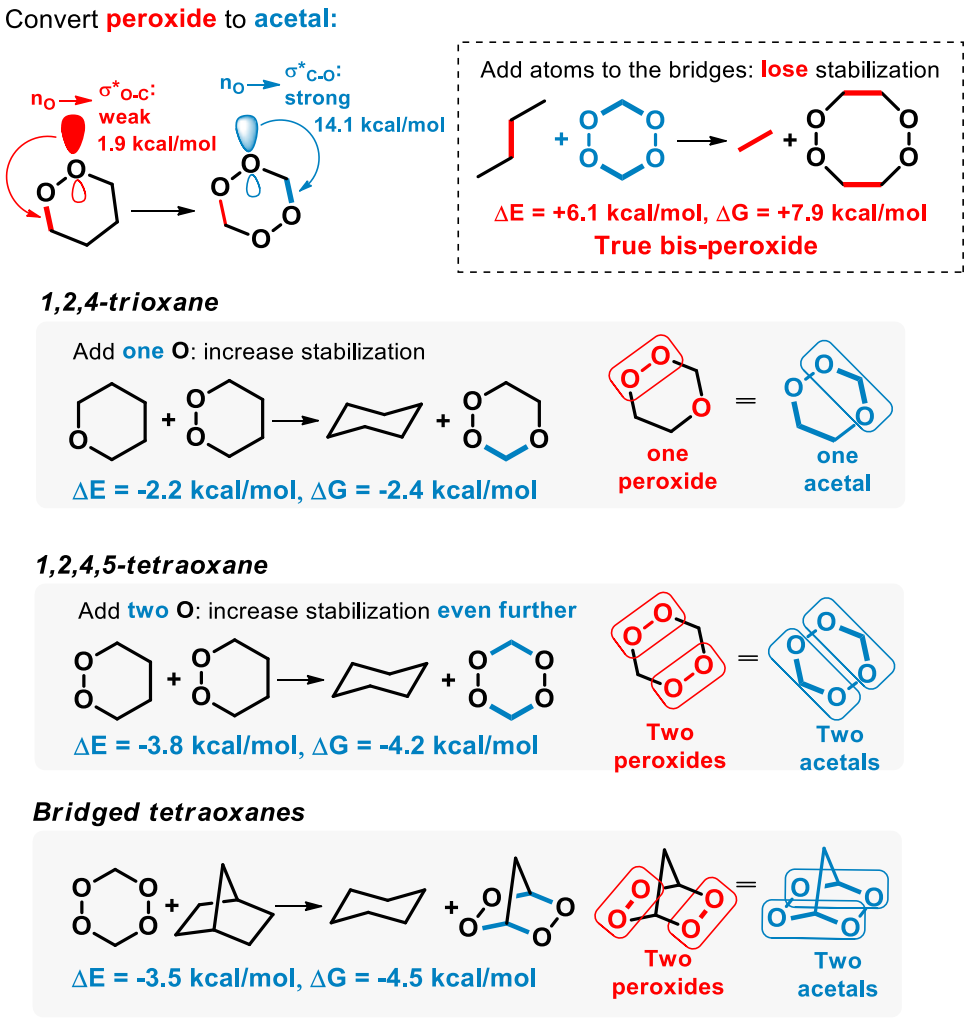


**Figure 4.2.** Clarification of the unexpected stability of cyclic six-membered peroxides, as 1,2,4-trioxanes, 1,2,4,5-tetraoxanes, and bridged tetraoxanes. Adapted from Gomes *et al.*[45] and Alabugin *et al.*[47]

## 4.4. Chemical synthesis of 1,2,4,5-tetraoxanes

Several methods for preparing 1,2,4,5-tetraoxanes have been developed in the last three decades. The 1,2,4,5-tetraoxane core can be synthesized *via* ozonolysis (**Figure 4.3-A**), followed by dimerization of zwitterions produced during the decomposition of ozonides prepared from alkenes **4.1**,[48–50] *O*-methyloximes **4.2**,[51,52] or vinyl ethers **4.3**.[53–56] The most common and widely used method to afford non-symmetrical 1,2,4,5-tetraoxanes **4.4** is the peroxyacetalization/peracetalization of *gem*-dihydroperoxides (DHP) with aldehydes/ketones or acetals. The DHPs can be easily generated through peroxidation of carbonyl compounds (aldehydes/ketones) or acetals with hydrogen peroxide ($H_2O_2$), in the presence of a catalyst, such as a Brønsted acid, a Lewis acid (LA), a metal ($M^{n+}$), or a zeolite/silica-supported catalyst. Understanding the different mechanisms involved in generating DHPs is critical for developing novel methods for synthesizing non-symmetric 1,2,4,5-tetraoxanes. *For a more comprehensive review of acyclic geminal bis-peroxides, including DHPs, the reader is referred to reference* 57. An alternative route for the synthesis of alkoxy-substituted 1,2,4,5-tetraoxanes **4.5** involves cyclocondensation with aliphatic and aromatic orthoesters ($R_3C(OR)_3$) as carbonyl sources, using different catalysts (**Figure 4.3-B**). The synthesis of bridged 1,2,4,5-tetraoxanes **4.6** is usually achieved through Brønsted acid- or heteropolyacid-catalyzed condensation of β-diketones with $H_2O_2$ (**Figure 4.3-C**).

In the development of the 1,2,4,5-tetraoxane chemotype, considerable attention has been directed to the synthesis of non-symmetric 1,2,4,5-tetraoxanes, which are particularly interesting from a pharmacological perspective since they offer more flexibility for various functional groups linked to the tetraoxane scaffold. However, these molecules are more difficult to synthesize than their symmetrical counterparts.[58] This chapter will focus mostly on the synthetic approach **B** for the preparation of non-symmetrical 1,2,4,5-tetraoxanes.

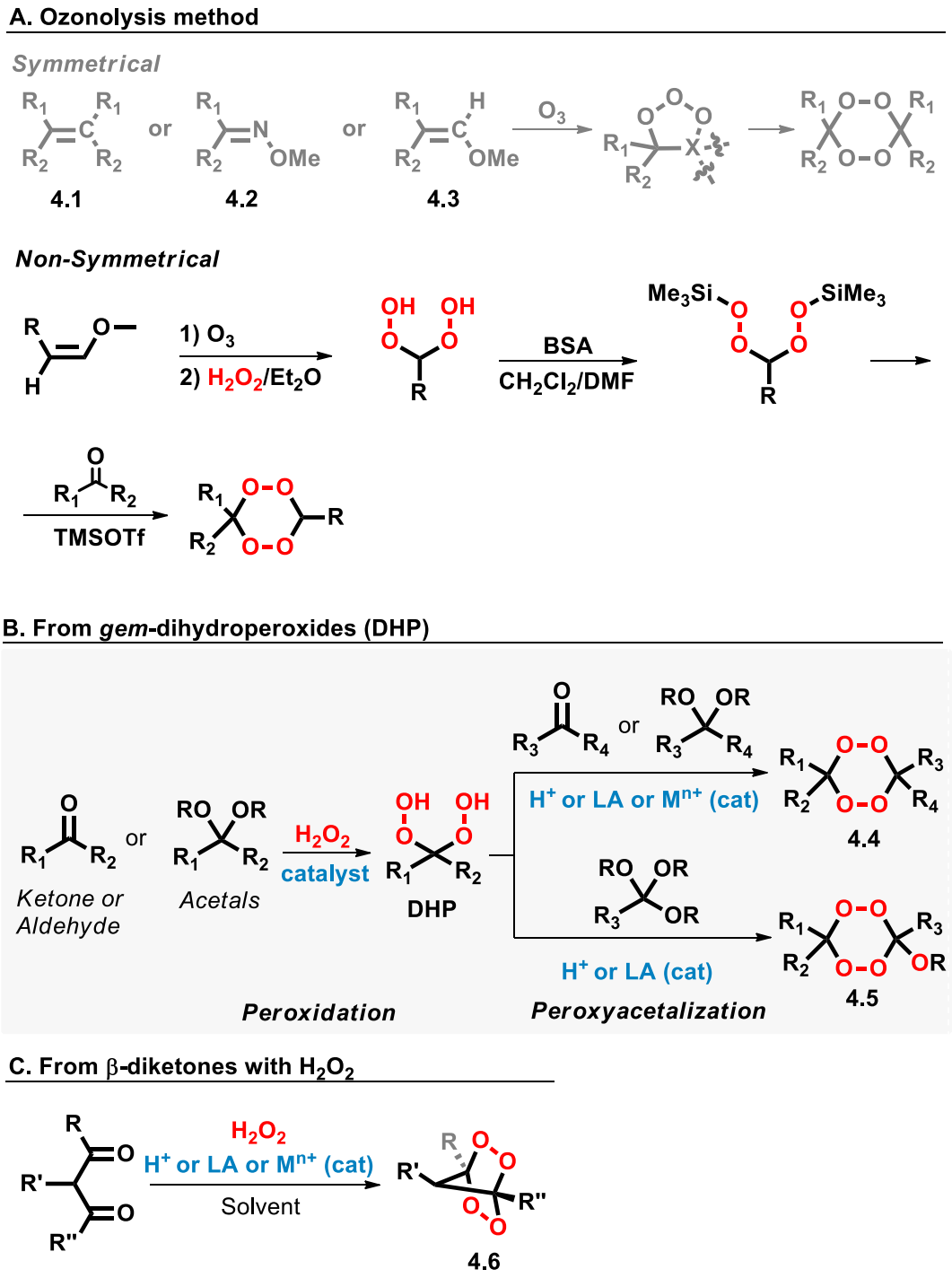


**Figure 4.3.** General trends for the generation of non-symmetrical 1,2,4,5-tetraoxanes. *[This chapter will focus particularly on the synthetic approach B for the preparation of 1,2,4,5-tetraoxanes (in grey)].*

## 4.5. Chemical synthesis of 1,2,4-trioxanes

A vast number of methods for preparing 1,2,4-trioxanes have been developed in the last three decades. The most common and widely used method to afford 1,2,4-trioxanes is the peroxyacetalization/peracetalization of β-hydroxy hydroperoxide alcohols (HPA) with aldehydes/ketones or acetals, in the presence of a Brønsted acid ($H^+$), a Lewis acid (LA), or a metal catalyst ($M^{n+}$). HPAs can be produced through photooxygenation of allylic alcohols, which relies on the generation of singlet oxygen $^1O_2$ from oxygen in the presence of a photosensitizer (**Figure 4.4-A**), and through ring-opening of epoxides with $H_2O_2$, promoted by a suitable catalyst (**Figure 4.4-C).**[59,60] Understanding the different mechanisms involved in producing HPAs is critical for developing novel methods for synthesizing 1,2,4-trioxanes. *For a more comprehensive review of β-Hydroxy Hydroperoxides alcohols (HPA), the reader is referred to references 59 and 60*. Isayama-Mukaiyama peroxysilylation of unsaturated alcohols can also deliver hydroxy silyl peroxides (HSP), which can undergo peroxyacetalization with aldehydes/ketones to afford 1,2,4-trioxanes, in the presence of a Brønsted acid ($H^+$), a LA or a $M^{n+}$ catalyst **(Figure 4.4-D**). Other methodologies for the synthesis of 1,2,4-trioxanes have been reported, namely [4 + 2]-cycloaddition of singlet oxygen to 2*H*-pyrans **(Figure 4.4-B**).[61–64] The synthesis of bridged 1,2,4-trioxanes can be achieved through a Kobayashi modified method (**Figure 4.4-E**)[65,66] and also by Brønsted acid- or heteropolyacid-catalyzed condensation of γ,δ-unsaturated ketones with $H_2O_2$ (**Figure 4.4-F**).[67] This chapter will focus particularly on the synthetic approaches **C** and **D** for the preparation of 1,2,4-trioxanes.

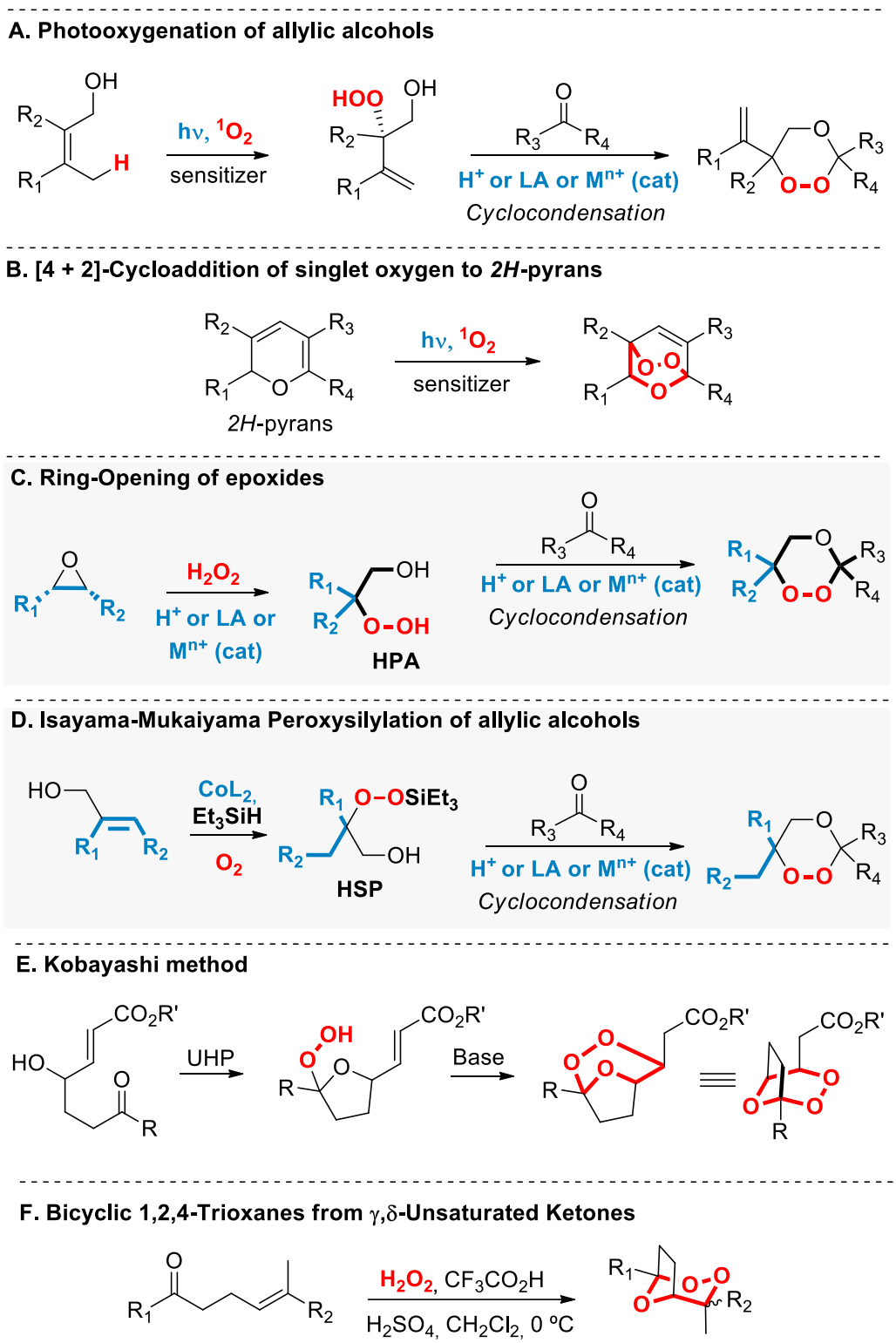


**Figure 4.4.** General trends for the generation of 1,2,4-trioxanes. *[This chapter will focus particularly on the synthetic approaches C and D for the preparation of 1,2,4-trioxanes (in grey)].*

## 4.6. Use of Silica Sulfuric Acid as a catalyst

ART combination therapies (ACTs) have been used as the first-line treatment against *Plasmodium falciparum* malaria during the last decades.[68–73] Disturbingly, the rise of resistance to ART and its semi-synthetic derivatives in South East Asia and the synthetic limitations of the ART scaffold have pushed the course of research towards the development of entirely synthetic endoperoxide-based antimalarials.[2,74–76] Several classes of synthetic endoperoxides have been scrutinized in this context, including 1,2-dioxanes, 1,2,4-trioxanes, 1,2,4-trioxolanes, and 1,2,4,5-tetraoxanes.[38,40,77] Among these classes, 1,2,4-trioxolanes and 1,2,4,5-tetraoxanes were extensively explored, notably yielding four antimalarial candidates [ozonides OZ277[78] (**4.7**) and OZ439[79,80] (**4.8**); 1,2,4,5-tetraoxanes RKA182[7] (**4.9**) and E209[8] (**4.10**, **Figure 4.5**)].

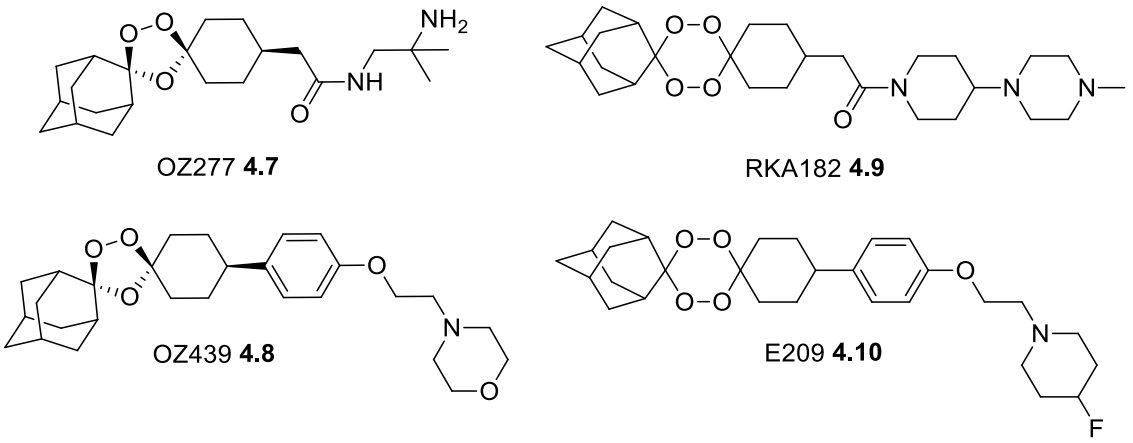


**Figure 4.5.** Representative endoperoxide-based antimalarial candidates 1,2,4-trioxolanes OZ277 (**4.7**), OZ439 (**4.8**); and 1,2,4,5-tetraoxanes RKA182 (**4.9**) and E209 (**4.10**).

The O'Neill's group reported E209 **4.10**,[8] the newest 1,2,4,5-tetraoxane antimalarial under development. This candidate displays superior pharmacokinetic and pharmacodynamic properties, together with potent nanomolar efficacy against multiple strains of *P. falciparum* and *P. vivax*, *in vitro* and *in vivo*. Furthermore, **4.10** also shows reduced cross-resistance with the C580Y mutation in transgenic parasites expressing variant forms of K13, known as the primary liability for artemisinin resistance.[81]

Notwithstanding the promising properties shown by the novel antimalarial candidate E209, the synthetic approach to its preparation demands improvement (**Scheme 4.1**). Preparation of E209 involves a six step-synthesis comprising the generation of the 1,2,4,5-tetraoxane core present in precursor **4.13a**, which requires the use of moisture-sensitive catalysts such as $Re_2O_7$[82] or $Bi(OTf)_3$[83] affording a maximum yield of around

61% (when using $Bi(OTf)_3$)[8] (**Scheme 4.1a**).

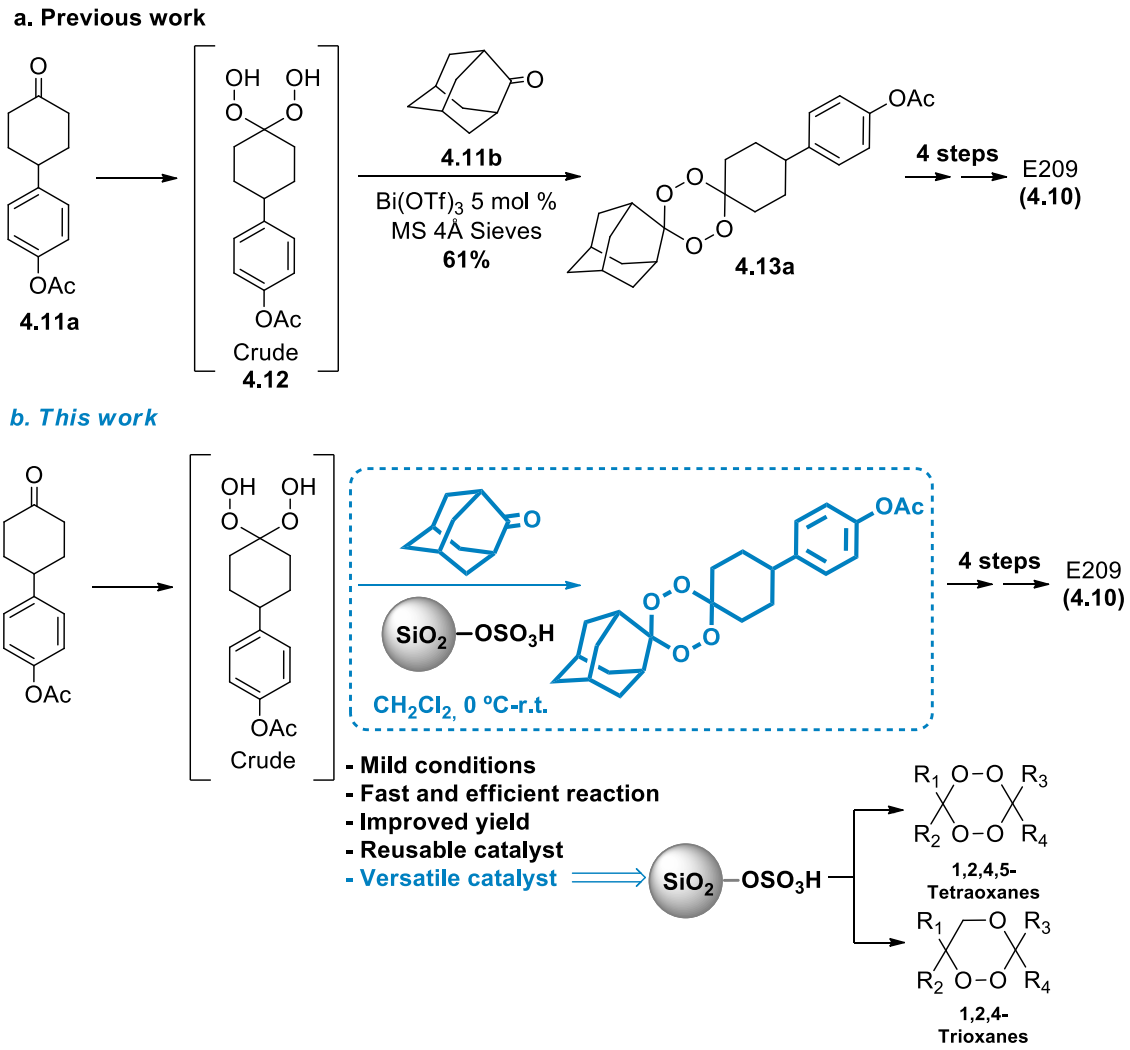


**Scheme 4.1.** (a) Synthetic approach and conditions used in previous preparation of E209; (b) Improved conditions proposed in this work.

During attempts to improve this synthetic step we successfully explored a new methodology for synthesizing the 1,2,4,5-tetraoxane subunit, involving the use of readily available and low-cost silica sulfuric acid (SSA) as a catalyst. Silica-supported catalysts have attracted attention recently due to their promising reactivity and recoverable and reusable properties, leading to economic and environmental benefits.[84,85] Silica sulfuric acid was reported by Azarifar *et al.*[86] as an effective catalyst for the preparation of DHP. Peroxyacetalization is the first step in the most broadly used method for synthesizing 1,2,4,5-tetraoxanes, which involves the acid-catalyzed cyclocondensation of a ketone or aldehyde with an active DHP intermediate prepared *in situ*. Generally, DHP is generated

from the reaction of a carbonyl compound with hydrogen peroxide (30 or 50 *wt* %) in the presence of a catalyst.[42] Given the attractive properties of SSA, we decided to explore the potential of silica-supported catalysts to promote the cyclocondensation of the 1,2,4,5-tetraoxane ring. Our methodology involves a 'two-pot' procedure, whereby the DHP generated immediately reacts with the partner carbonyl compound to achieve the cyclocondensation step (**Scheme 4.1b**).

## 4.6.1. Results and discussion

This section features the successes and limitations of applying the heterogeneous silica sulfuric acid (SSA) catalyst to synthesize non-symmetrical 1,2,4,5-tetraoxanes and 1,2,4-trioxanes. The fundamental steps governing the cyclocondensation pathway through were evaluated through molecular orbital calculations, using the DFT method, at the ωB97XD/def2-TZVPP/PCM(DCM)//B3LYP/6-31G(d) level of approximation. This novel procedure differs from previously reported methods by using readily available and inexpensive reagents with recyclable properties, providing a valid alternative approach for the synthesis of new biologically active endoperoxides.

### 4.6.1.1. Preparation of the Silica Sulfuric Acid catalyst

Concerning the preparation of the SSA catalysts, different proportions of sulfuric acid were used [SSA-(**A-D**): 1, 2, 3, and 4 mL of $H_2SO_4$ (> 95%), respectively]. The procedure for preparing each catalyst was identical (**Figure 4.6**) and is described in detail in the Experimental Section. The molarity of sulfuric acid adsorbed on the silica gel was determined by acid-base titration. The results, summarized in **Figure 4.7-A**, indicate that in both SSA-**(A)** and SSA-**(B)** the amount of $H_2SO_4$ adsorbed by the silica appears to be directly proportional to the amount of $H_2SO_4$ added (3.85 ± 0.04 and 6.10 ± 0.03 mmol in 1 g of SSA, respectively), in contrast to what was observed in SSA-**(C)** and SSA-**(D)** (7.54 ± 0.04 and 8.40 ± 0.04 mmol in 1 g of SSA), demonstrating a saturation tendency on the silica gel surface after continuous addition of $H_2SO_4$.

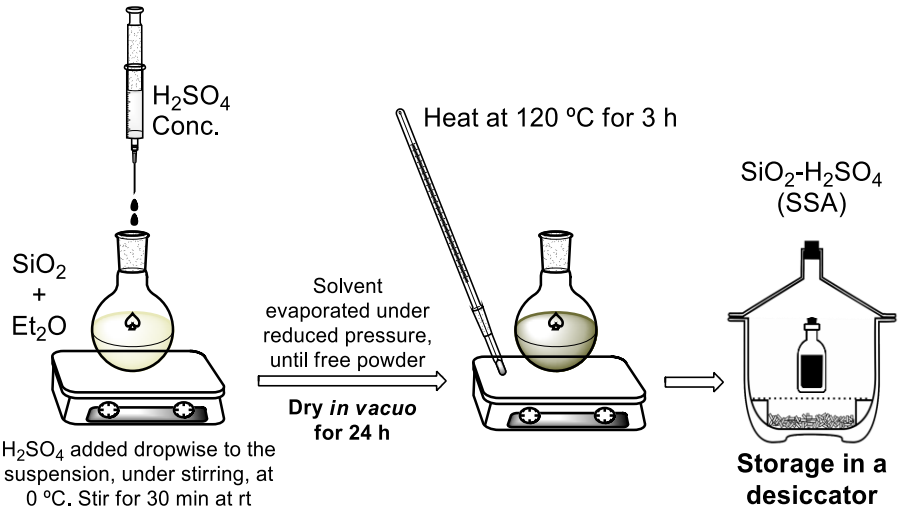


**Figure 4.6.** Representation of the procedure followed for the preparation of the SSA-(**A-D**) catalysts.

### 4.6.1.2. Optimization of reaction conditions

The preparation of the intermediate DHP **4.12** followed the method reported by Azarifar *et al.*[86], with some adjustments. Typically, 4-(4-oxocyclohexyl)phenyl acetate **4.11a** was reacted with aqueous hydrogen peroxide (50% w/w) in acetonitrile (4:1 molar ratio of $H_2O_2$ to the starting ketone), in the presence of the SSA catalyst, at room temperature (**Table 4.1**). A solvent extraction workup was followed to remove excess $H_2O_2$, intended for the safety and overall yield optimization.

The reaction of the crude DHP **4.12** with adamantan-2-one **4.11b**, in the presence of the SSA catalyst, was selected as the model to find the optimized reaction conditions for the cyclocondensation step. The factors analyzed were the nature of the solvent, the amount and the type of catalyst, namely the ratio of $H_2SO_4$:$SiO_2$ [SSA-(**A-D**) (see **Table 4.1**)]. Analysis of the data shows that, at room temperature, when using a 2:1 molar ratio of SSA-**(C)** to 4-(4-oxocyclohexyl)phenyl acetate **4.11a**, in anhydrous dichloromethane, *p*-(dispiro[cyclohexane-1,3'-[1,2,4,5]tetraoxane-6',2''-tricyclo-[3.3.1.1$^{3,7}$]decan]-4yl)phenyl acetate **4.13a** is selectively produced with the highest observed yield (67%), after 60 min (**Table 4.1**, entry 19). Increasing the reaction time (12h, **Table 4.1**, entry 20) and using a higher molar ratio of SSA-**(C)** (3 equivalents, **Table 4.1**, entry 21) did not improve the efficacy of the model reaction. SSA-**(C)** seemed to outperform in efficiency, compared to the other SSA batches, in the same equivalency (**Table 4.1**, entries 4-7). Conduction of the model reaction using silica gel, or in the absence of catalyst, did not lead to **4.13a,** even when extending the reaction time for 48 h, showing the importance of

SSA for the reaction's success (**Table 4.1**, entries 1, 2). Conduction of the model reaction with $H_2SO_4$ (1 equivalent) afforded the desired 1,2,4,5-tetraoxane **4.13a**, though in a much lower yield (13%) than the silica-supported-$H_2SO_4$ catalyst (**Table 4.1**, entry 3). Solvent effects were also investigated. As shown from the data presented in **Table 4.1**, anhydrous dichloromethane preformed as the most efficient solvent. The reaction failed when solvents DMSO and DMF were used (**Table 4.1**, entries 16 and 17), which was ascribed to their hygroscopic nature. The presence of moisture in the reaction mixture could entail the following results: 1) water may affect the $SiO_2$-$H_2SO_4$ ⇔ $SiO_2$-$H_2O$ conversion equilibrium, altering the catalytic capabilities of SSA by adsorbing on its surface, interfering with the cyclocondensation step, and promoting the hydrolysis of the intermediate DHP, with the regeneration of the corresponding starting ketone; 2) water itself may also hydrolyze the DHP, regenerating its starting ketone. Even though DMSO and DMF had a commercial purity of >98%, these solvents were not freshly distilled prior to use. The use of ethereal solvents such as diethyl ether or 1,4-dioxane strongly inhibited the ability of SSA to promote cyclocondensation to the tetraoxane core (**Table 4.1**, entries 15 and 18). The yield decreased considerably when the reaction was performed under non-anhydrous conditions (**Table 4.1**, entries 11-14), revealing that anhydrous conditions favor the cyclocondensation of the 1,2,4,5-tetraoxane core by avoiding decomposition of the DHP to its starting material. The cyclocondensation was achieved even with minimal amounts of SSA-**(C)**, such as 0.01 equivalent, although with 11% yield (**Table 4.1**, entry 24), demonstrating its catalytic capacity.

**Table 4.1.** Screening of reaction parameters for the formation of 1,2,4,5-tetraoxane **4.13a**

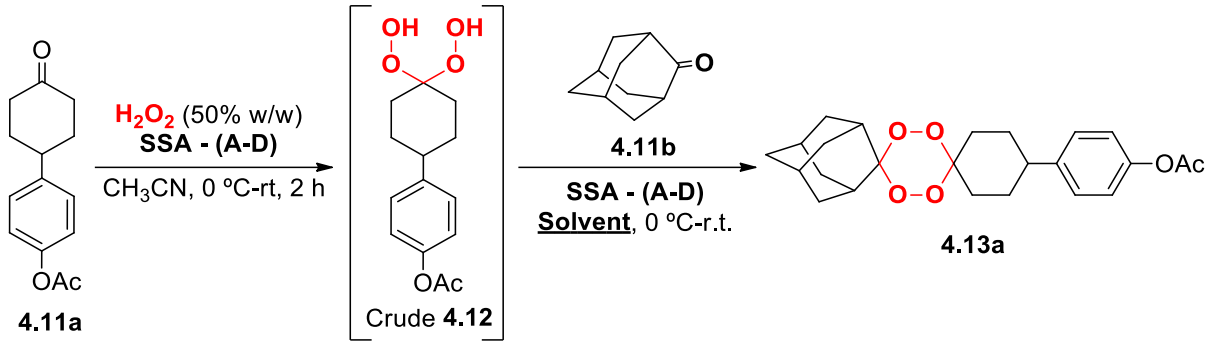


| Entry | Catalyst | Solvent | Molar ratio SSA/ST[a] | *t* (min) | Yield (%) |
|---|---|---|---|---|---|
| 1 | None | $CH_2Cl_2$ | - | 48h | nr |
| 2 | $SiO_2$ | $CH_2Cl_2$ | 1[d] | 48h | nr |
| 3 | $H_2SO_4$ | $CH_2Cl_2$ | 1[d] | 12h | 13 |
| 4 | SSA - **(A)** | $CH_2Cl_2$ | 1 | 60 | 48 |
| 5 | SSA - **(B)** | $CH_2Cl_2$ | 1 | 60 | 58 |
| 6 | SSA - **(C)** | $CH_2Cl_2$ | 1 | 60 | 62 |
| 7 | SSA - **(D)** | $CH_2Cl_2$ | 1 | 60 | 53 |
| 8 | SSA - **(C)**[b] | $CH_2Cl_2$ | 1 | 60 | 56 |
| 9 | SSA - **(C)** | $CH_3CN$ | 1 | 75 | 51 |
| 10 | SSA - **(C)** | $CH_3CN/CH_2Cl_2$ (1:1) | 1 | 75 | 53 |
| 11 | SSA - **(C)** | $CH_2Cl_2$[c] | 1 | 75 | 52 |
| 12 | SSA - **(C)** | $CH_3CN$[c] | 1 | 90 | 48 |
| 13 | SSA - **(C)** | $CH_3CN/CH_2Cl_2$ (1:1)[c] | 1 | 90 | 52 |
| 14 | SSA - **(C)** | $CH_3CO_2Et$[c] | 1 | 120 | 24 |
| 15 | SSA - **(C)** | $Et_2O$ | 1 | 180 | 12 |
| 16 | SSA - **(C)** | DMSO | 1 | 48h | nr |
| 17 | SSA - **(C)** | DMF | 1 | 48h | nr |
| 18 | SSA - **(C)** | 1,4-Dioxane | 1 | 48h | nr |
| ***19*** | ***SSA - (C)*** | ***$CH_2Cl_2$*** | ***2*** | ***60*** | ***67*** |
| 20 | SSA - **(C)** | $CH_2Cl_2$ | 2 | 12h | 63 |
| 21 | SSA - **(C)** | $CH_2Cl_2$ | 3 | 60 | 62 |
| 22 | SSA - **(C)** | $CH_2Cl_2$ | 0.5 | 60 | 57 |
| 23 | SSA - **(C)** | $CH_2Cl_2$ | 0.1 | 120 | 34 |
| 24 | SSA - **(C)** | $CH_2Cl_2$ | 0.01 | 12h | 11 |
| | $Re_2O_7$ | $CH_2Cl_2$ | - | 60 | 46[18] |
| | $Bi(OTf)_3$ | $CH_2Cl_2$ | - | 120 | 61[18] |

[a]*ST*: Starting material; [b]Formic acid used in the first step, instead of SSA-(C); [c]Not anhydrous; [d]1 equivalent of $SiO_2$ or $H_2SO_4$; nr = no reaction; SSA-(**A-D**): 1, 2, 3, and 4 mL of $H_2SO_4$ (> 95%), respectively).

### 4.6.1.3. Evaluation of the substrate scope

A library of 1,2,4,5-tetraoxanes **4.13a-g** was synthesized using the optimal conditions (**Table 4.1**, entry 19), thereby demonstrating the methodology's tolerance to a range of functional groups and structural features (**Table 4.2**). We also applied the methodology to the synthesis of non-symmetrical 1,2,4,5-tetraoxanes, and, under heterogeneous conditions, the required compounds were generated with yields ranging from 5 to 67%. The reactions, performed in the presence of two equivalents of SSA-**(C)** and using an excess of the second ketone (1.5 mmol) relative to the starting one, were usually completed in the period of 1 to 6 hours. Homodimeric byproducts were occasionally formed during the cyclocondensation step, especially during the preparation of **4.13g**. The symmetric 1,2,4,5-tetraoxane byproduct could be differentiated by TLC and was obtained in lower proportion for ketones in which both structures varied substantially from each other, in polarity or composition. These circumstances could be avoided by isolating the DHP through column chromatography and then reacting it with an excess of the second ketone (2 mmol) in the cyclocondensation step. 1,2,4,5-Tetraoxane **4.13e** was generated in very low yield (5%), which may be ascribed to the use of a very bulky ketone, adamantan-2-one **4.11b**, which preferentially undergoes a Baeyer-Villiger rearrangement during the cyclocondensation step, originating its corresponding lactone. In fact, 4-oxahomoadamantan-5-one was isolated in a higher amount than the desired 1,2,4,5-tetraoxane **4.13e**. Hydroperoxidation of aromatic ketone **4.11c** was achieved easily with SSA-**(C)** during the first step. Although cyclocondensation with **4.11b** was observed, the DHP decomposed back to **4.11c**, suggesting some instability of the DHP in the reaction medium. An attempt to generate the corresponding tetraoxane from 4,4-difluorocyclohexanone (**4.11d)** and **4.11b** was disrupted during purification. It appears that strong electron withdrawing groups (EWG) close to the tetraoxane ring, such as the fluorine, favour its instability, promoting decomposition (**Table 4.2**).

**Table 4.2.** Scope evaluation in the SSA-promoted formation of 1,2,4,5-tetraoxanes.

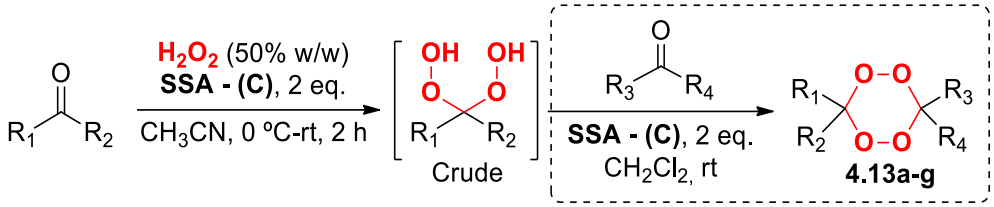


| Entry | Ketone 1 | Ketone 2 | Product (reaction time, yield) |
|---|---|---|---|
| 1 | 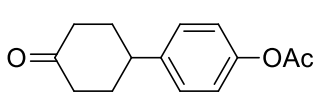 **4.11a** | 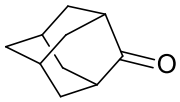 **4.11b** | 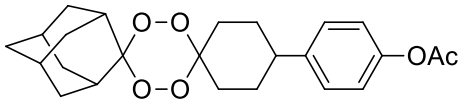 **4.13a** (1 h, 67%) |
| 2 | 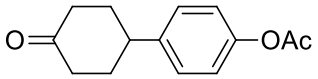 | 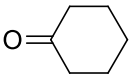 | 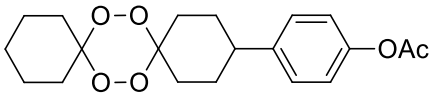 **4.13b** (1.5 h, 57%) |
| 3 | 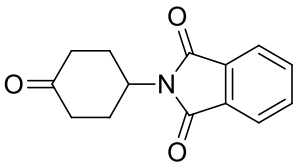 | 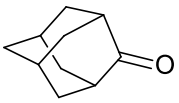 | 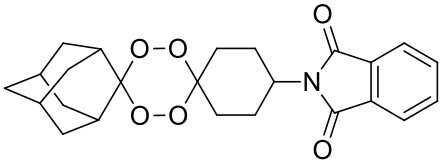 **4.13c** (1 h, 63%) |
| 4 | 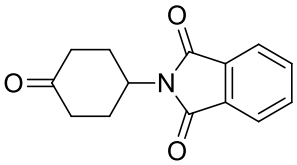 | 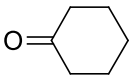 | 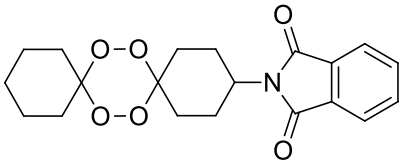 **4.13d** (1 h, 47%) |
| 5 | 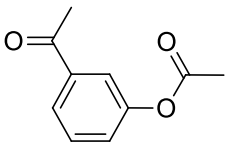 **4.11c** | 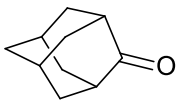 | (Mostly unreacted **4.11c**) |
| 6 | 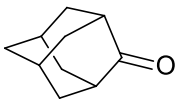 | 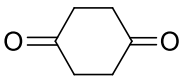 | 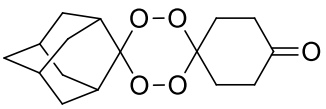 **4.13e** (4 h, 5%) |
| 7 | 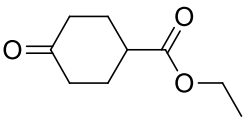 | 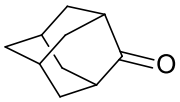 | 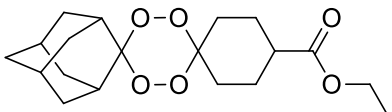 **4.13f** (6 h, 51%) |
| 8 | 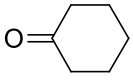 | 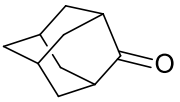 | 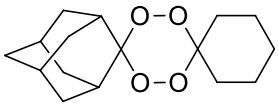 **4.13g** (2 h, 64%) |
| 9 | 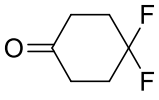 **4.11d** | 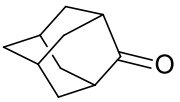 | (Decomposition during purification) |

A one-pot approach to synthesize the 1,2,4,5-tetraoxanes was also carried out to understand if the performance would match the two-step protocol. The procedure involved the addition of two equivalents of SSA-**(C)** and 50% aqueous $H_2O_2$ (4 mmol) to a solution of the starting ketone (1.0 mmol), in acetonitrile. After consumption of the starting material, adamantan-2-one (1.5 mmol) was added and the final mixture was left stirring overnight (**Scheme 4.2**). Under these conditions, the desired 1,2,4,5-tetraoxane was obtained in poor yields (8%). Evaporation of the solvent after the peroxidation step was not considered because it would lead to a dangerous concentration of free hydrogen peroxide, highly explosive.

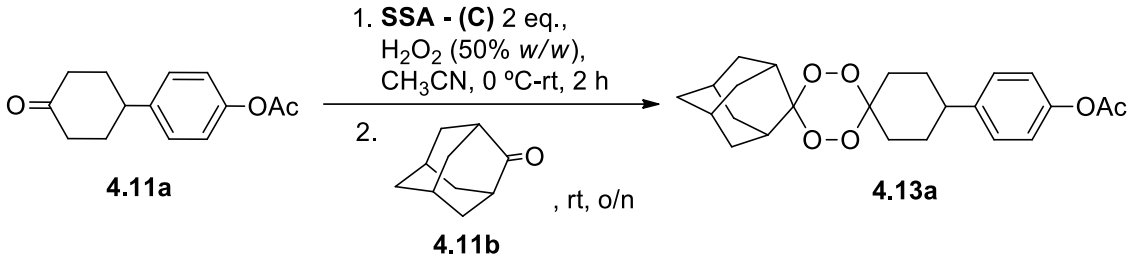


**Scheme 4.2.** Conditions for one-pot synthesis of 1,2,4,5-tetraoxanes, using SSA-**(C)**.

### 4.6.1.4. Evaluation of the recycling properties

The recycling properties of SSA were also thoroughly analyzed. Following each run of the cyclocondensation step of **4.13a**, SSA-(**C**) was removed from the reaction mixture by filtration and rinsed several times with dichloromethane to remove contaminants adsorbed on the surface of SSA and subsequently dried in a vacuum oven at 60 °C, for 24 h. The recovered SSA-(**C**) was reused in the next run. Analysis of the results displayed in **Figure 4.7-B** shows that the catalyst SSA-(**C**) can be used up to two times with only a slight loss in the yield of **4.13a** (67% to 62%). When using the catalyst in the synthesis of **4.13a** for five consecutive times, we observed that the yield decreased considerably from the third, the fourth, and fifth runs (41%, 27%, and 12%, respectively), which was ascribed to the gradual catalyst contamination by the starting materials and byproducts and the slow loss of $H_2SO_4$. To confirm this hypothesis, the amount of sulfuric acid loaded on the recovered SSA-**(C)** was also evaluated using the acid-base titration method to understand better the molarity exchanges that occurred during the reaction and recovery process of the compound. **Figure 4.7-B** shows that, indeed, the molarity of $H_2SO_4$ on the silica surface decreases in the recovered catalyst with each run (**run 1**: 7.54 ± 0.04; **run 2**: 4.20 ± 0.08; **run 3**: 3.17 ± 0.06; **run 4**: 1.14 ± 0.05 and **run 5:** 0.53 ± 0.01

mmol in 1 g of SSA) and this decrease is directly related to the corresponding run's yield of 1,2,4,5-tetraoxane (**Figure 4.7-C**, $r = 0.921$, $p < 0.001$).

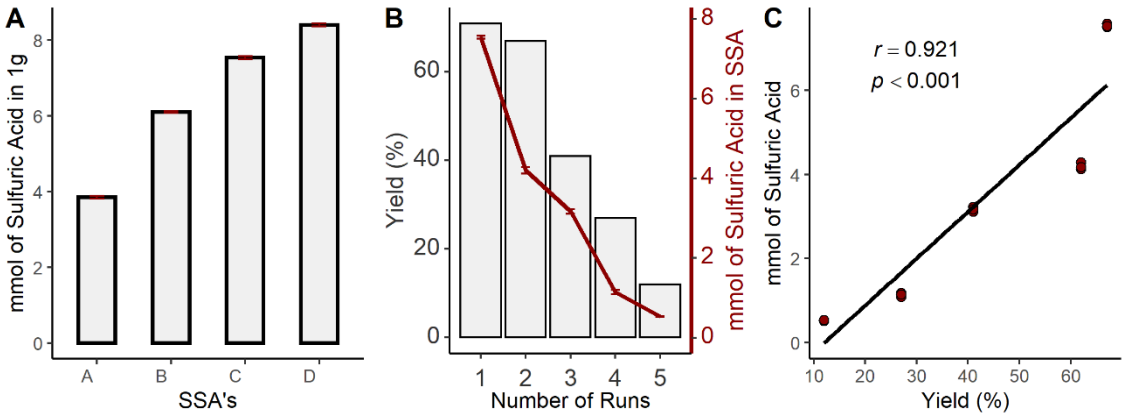


**Figure 4.7.** A) Molarity of $H_2SO_4$ in SSA-(**A-D**). Bars represent mean values of molarity of $H_2SO_4$ triplicates ± standard deviation (SD); (B) Reusability SSA-(**C**) in the generation of **4.13a** (***red line*** corresponds to the molarity of $H_2SO_4$ in 1 g of SSA, in each run); (C) Pearson correlation coefficient between the yield of each run and the molarity of $H_2SO_4$, in 1g of SSA.

### 4.6.1.5. Mechanistic study for the formation of 1,2,4,5-tetraoxanes

The role of SSA as an acid promoter was investigated by density functional theory (DFT) calculations at the ωB97XD/def2-TZVPP/PCM(DCM)//B3LYP/6-31G(d) level of theory. A mechanism proposal for the formation of 1,2,4,5-tetraoxanes is provided in **Figure 4.8**. In this study, adamantan-2-one (**4.11b**) and 1,1-cyclohexanediyl dihydroperoxide (**4.12g**) were selected as model substrates, and two molecules of $Si(OH)_3(SO_3H)$ were considered to mimic the SSA. Calculations predict a thermodynamically favoured process, globally. The proposed mechanism involves protonation of the carbonyl group of **4.11b** by SSA; followed by 1,2-addition of a hydroperoxide of **4.12g** to the protonated ketone, with concomitant proton abstraction by SSA, *via* TS1 (11.4 kcal $mol^{-1}$); then protonation of the hydroxyl moiety by SSA; and, finally, an $S_N1$-type reaction to form the 1,2,4,5-tetraoxane **4.13g**. The $S_N1$ reaction occurs *via* water dissociation (TS2, rate-limiting step, 12.4 kcal $mol^{-1}$) to form a tertiary carbocation that reacts with the second hydroperoxide of **4.12g** (TS3, 10.5 kcal $mol^{-1}$), generating **4.13g** after proton abstraction by SSA. The calculations also suggest that all steps are reversible, except the last one (TS3), the dissociation of the product **4.13g** from SSA-$H_2O$ being thermodynamically favoured.

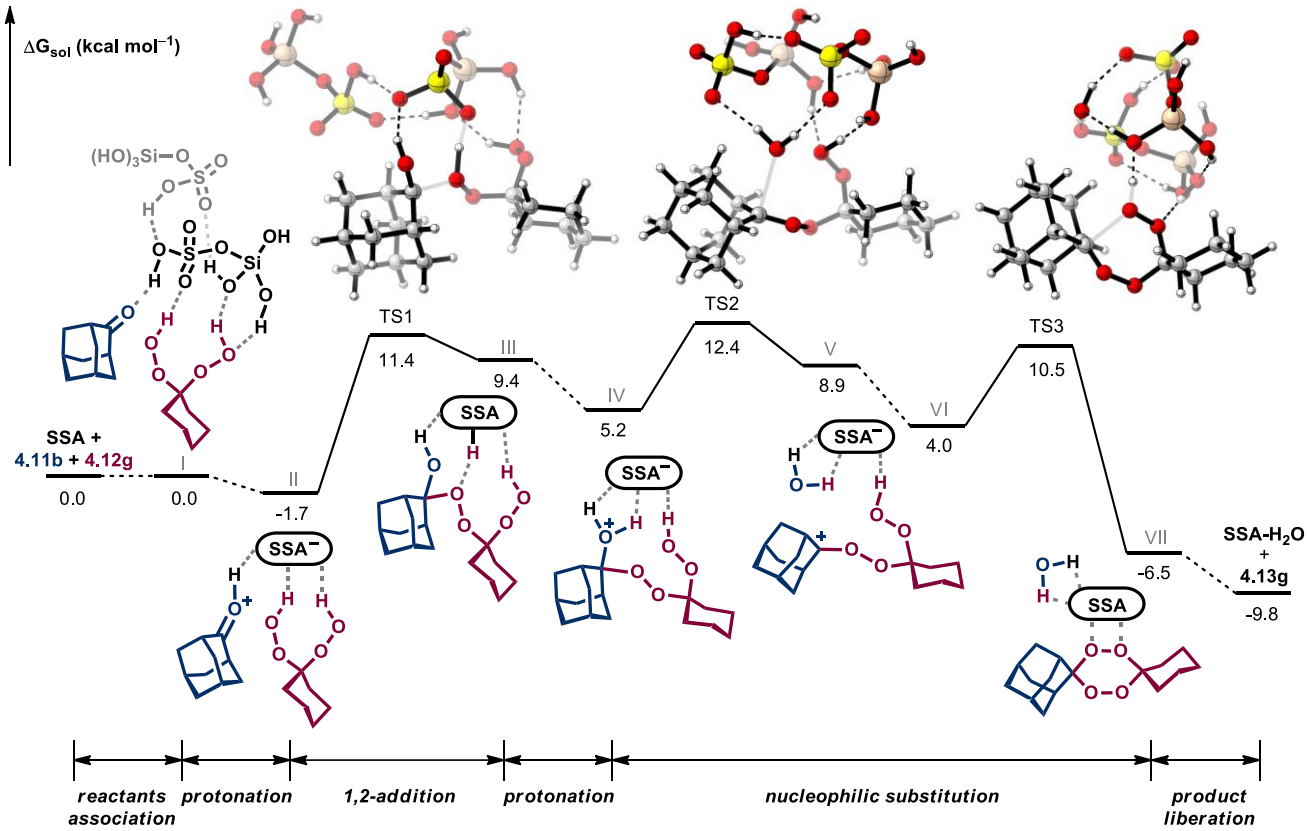


**Figure 4.8.** Free energy profile for **the formation of** 1,2,4,5-tetraoxane **4.13g** promoted by SSA (modelled by two molecules of $Si(OH)_3(SO_3H)$)**.** DFT calculations were performed at the ωB97XD/Def2-TZVPP/PCM(DCM)//B3LYP/6-31G(d) level of theory (energy values in kcal mol$^{-1}$).

### 4.6.1.6. SSA-catalysed synthesis of 1,2,4-trioxanes

Inspired by the results obtained for the synthesis of 1,2,4,5-tetraoxanes, we decided to evaluate the SSA catalyst's potential in the cyclocondensation process to generate 1,2,4-trioxanes. Two methods were used: (A) hydroperoxysilylation of allylic alcohols and (B) perhydrolysis of spiro-oxiranes, followed by cyclocondensation to 1,2,4-trioxanes, through reaction with the corresponding ketones, at room temperature, in the presence of SSA.

### A) *Via* Hydroperoxysilylation of allylic alcohols, followed by cyclocondensation to 1,2,4-trioxanes

The Co(II)-mediated hydroperoxysilylation of allylic alcohols was initially reported by Oh *et al.*[87], following an investigation to generate seven-membered 1,2,4-trioxepane systems. This chemistry was later applied to the synthesis of asymmetric six-membered 1,2,4-trioxanes by O'Neill and co-workers.[88] A 1,2,4-trioxane moiety could be easily built by a milder approach, in the sequence of a Co(II)-mediated peroxysilylation of allylic alcohols **4.14** [through an Isayama and Mukaiyama hydroperoxysilylation (*See Section 4.5. for more information regarding this method*)] and subsequent reaction with a carbonyl compound, in a one-pot procedure, with the support of a catalyst. For this project, we used the $Co(thd)_2$ method in the hydroperoxysilylation step, to generate the hydroxy silyl peroxide **4.15** (**Scheme 4.3**). The $Co(thd)_2$ catalyst was synthesised in a convenient one-step reaction, from cobalt (II) chloride and 2,2,6,6-tetramethyl-3,5-heptanedionate (**thd**), in basic conditions (**Scheme 4.3).**

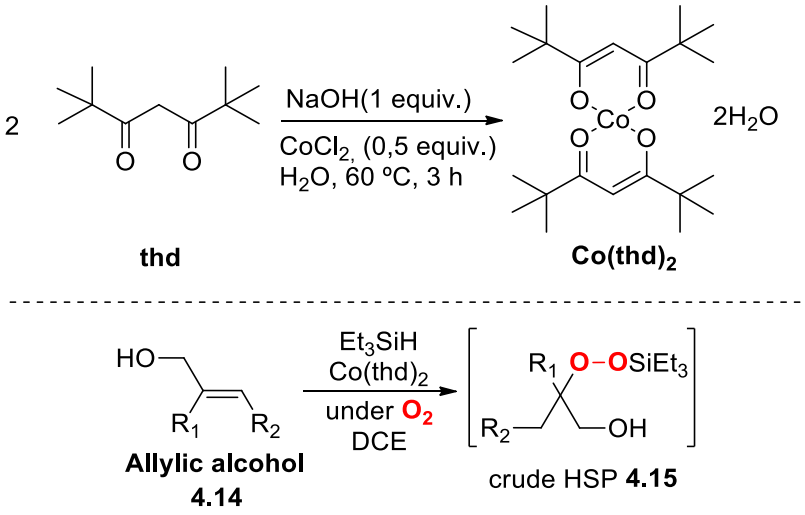


**Scheme 4.3.** Synthesis of $Co(thd)_2$ (*top*) and representative example of a Co(II)-mediated hydroperoxysilylation of allylic alcohols (*bottom*).

The hydroperoxysilylation of allylic alcohols **4.14** using the catalyst bis(2,2,6,6-tetramethyl-3,5-heptanedionate)cobalt(II) ($Co(thd)_2$)[88] generates the HSP **4.15**. The HSP crude is used immediately, without further purification, in the cyclocondensation step with the corresponding ketone, to afford the non-symmetrical 1,2,4-trioxanes. For the cyclocondensation step we successfully explored the new SSA-catalysed methodology for construction of the 1,2,4-trioxane core. The 1,2,4-trioxane moiety (**4.16a-f**) could be

easily built in moderate yields (38-68%, **Table 4.3**), through a milder approach, in the sequence of a Co(II)-mediated peroxysilylation of allylic alcohols.

The reactions, performed in the presence of two equivalents of SSA-**(C)** and using an excess of the second ketone (1.5 mmol) relative to the starting one, were usually completed in the period of 1 to 2 hours. The yields of 1,2,4-trioxanes **4.16a-c** were significantly different from those of **4.16d-f**. The sole difference between these molecules is the allylic alcohol used in the peroxysilylation reaction. The bulky cyclohexyl group in the allylic alcohol **4.14a** seemed to interfere with the reactivity during this step, affording a more impure semi-crude HSP (observed by TLC and NMR spectra). This situation was not encountered during the peroxysilylation of allylic alcohol **4.14b**, which explains why the cyclocondensation reaction with crude **4.14b**-derived HSP produced 1,2,4-trioxanes with higher yields.

**B) *Via* perhydrolysis of spiro-oxiranes, followed by cyclocondensation to 1,2,4-trioxanes**

We also explored SSA as a potential catalyst for the perhydrolysis step since it has been previously reported as a promoter in the alcoholysis and hydrolysis of epoxides[89] and regioselective ring-opening of epoxides by the thiocyanate anion to yield thiocyanohydrins[90] (*See Section 4.5. for more information regarding perhydrolysis of epoxides*). Perhydrolysis of spiro-oxiranes **4.17a-b** was achieved with SSA, in the presence of ethereal $H_2O_2$. A simple solvent extraction workup was performed to remove the excess $H_2O_2$, and the crude *β*-hydroperoxy alcohols were used immediately in the next step, without further purification. Subsequent cyclocondensation with the corresponding ketones yielded the 1,2,4-trioxanes **4.18a-b** in reasonable yields (47-63%, **Table 4.4**). These results highlight the versatility of SSA for promoting selective cyclocondensation to different six-membered endoperoxide core structures.

**Table 4.3.** Hydroperoxysilylation of allylic alcohols, followed by SSA mediated cyclocondensation to 1,2,4-trioxanes.

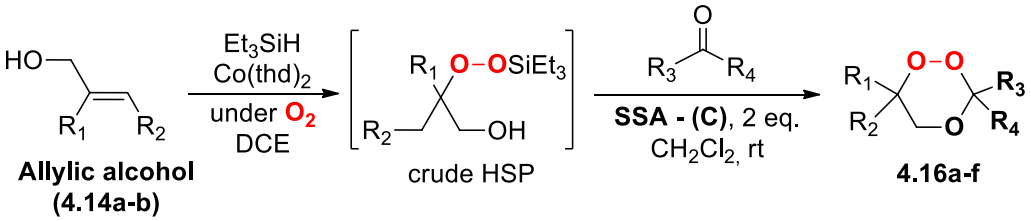


**Allylic alcohol (4.14a-b)** — crude HSP — **4.16a-f**

| Entry | Allylic Alcohol | Ketone | Product (reaction time, yield) |
|---|---|---|---|
| 1 | 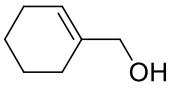 **4.14a** | 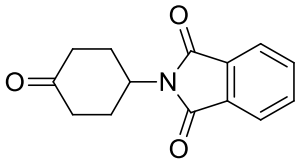 | 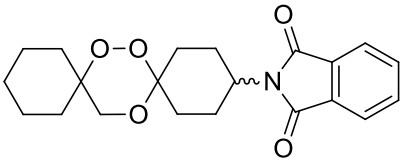 **4.16a** (2 h, 46%) |
| 2 | 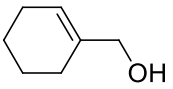 **4.14a** | 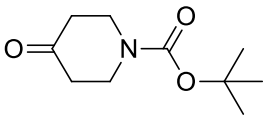 | 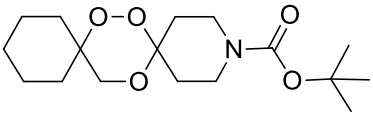 **4.16b** (2 h, 38%) |
| 3 | 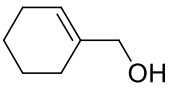 **4.14a** | 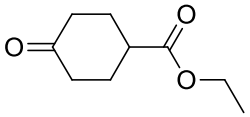 | 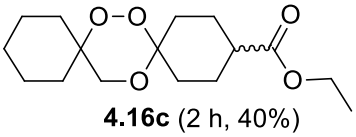 **4.16c** (2 h, 40%) |
| 4 | 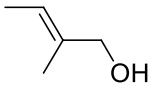 **4.14b** | 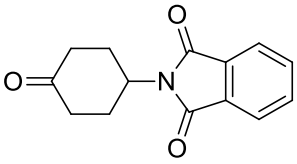 | 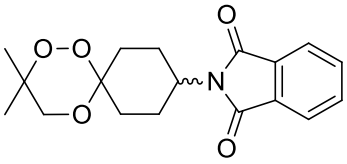 **4.16d** (1 h, 62%) |
| 5 | 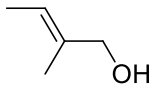 **4.14b** | 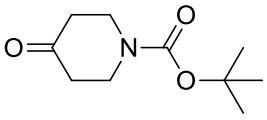 | 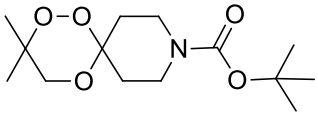 **4.16e** (1 h, 58%) |
| 6 | 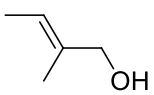 **4.14b** | 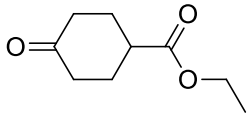 | 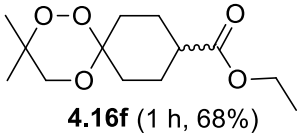 **4.16f** (1 h, 68%) |

**Table 4.4**. Perhydrolysis of spiro-oxiranes, followed by SSA-mediated cyclocondensation to 1,2,4-trioxanes.

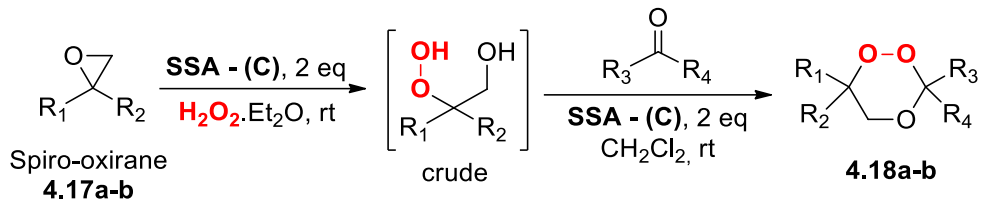


| Entry | Spiro-oxirane | Ketone | Product (reaction time*, yield) |
|---|---|---|---|
| 1 | 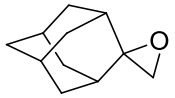 **4.17a** | 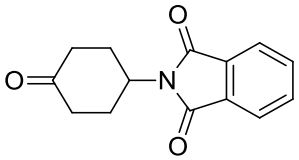 | 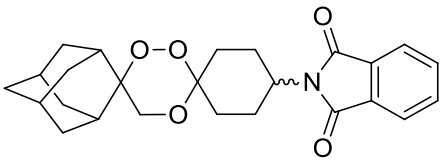 **4.18a** (2/1 h, 47%) |
| 2 | 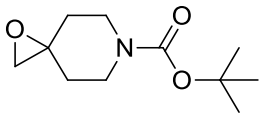 **4.17b** | 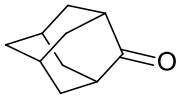 | 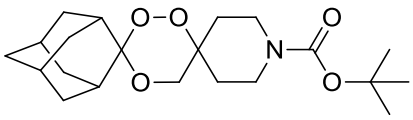 **4.18b** (2/2 h, 63%) |

*Reaction time (Step 1/Step 2, hours)

## 4.6.2. Conclusions

The cyclocondensation of a representative library of ketones with *gem*-dihydroperoxides or peroxysilyl alcohols/β-hydroperoxy alcohols to afford the corresponding unsymmetrical 1,2,4,5-tetraoxanes or 1,2,4-trioxanes, mediated by the SSA catalyst, was systematically investigated. The elementary steps governing the cyclocondensation pathway were investigated through molecular orbital calculations, using the DFT method, at the ωB97XD/def2-TZVPP/PCM(DCM)//B3LYP/6-31G(d) level of approximation. The results support a mechanistic proposal that highlights the catalytic role of SSA, where SSA's initial protonation of the ketone carbonyl group emerges as a key step in the mechanism.

This novel approach involving the silica-supported catalyst offers several advantages, namely tolerance to a wide range of substrates. In addition, easy preparation, recyclability, and eco-friendly properties of the SSA catalyst are features that make this method an appealing tool in broadening the design of new biologically active endoperoxides. This improved methodology was successfully applied to the preparation of *p*-(dispiro[cyclohexane-1,3'-[1,2,4,5]tetraoxane-6',2''-tricyclo[3.3.1.1$^{3,7}$]decan]-4-yl)-

phenyl acetate, a crucial 1,2,4,5-tetraoxane intermediate scaffold for the synthesis of the antimalarial candidate E209.

## 4.7. Experimental and computational details

***Chemicals.*** All reagents and solvents used were of analytical grade and were used without further purification. Adamantan-2-one (**4.11b**), 4,4-difluorocyclohexanone (**4.11d**) and 2-methylprop-2-en-1-ol (**4.14b**) were purchased and used without additional purification. When necessary, solvents were freshly distilled from appropriate drying agents prior to use. Analytical thin layer chromatography (TLC) was carried out using TLC Silica gel 60 F254 aluminium sheets (AL TLC 20x20). Column chromatography was carried out using technical grade Silica Gel 60 (0.04 – 0.063 mm).

***Analytical equipment.*** $^{1}H$ and $^{13}C$ Nuclear Magnetic Resonance (NMR) spectra were recorded using a Bruker AMX400 spectrometer or a 500 MHz JEOL system equipped with a Royal HFX probe, in solution, using the deuterated solvents described in each experimental procedure. The chemical shifts (δ) are described in parts per million (ppm), downfield from an internal standard of tetramethylsilane (TMS). Melting points (°C) were obtained on an SMP30 melting point apparatus and are uncorrected. High Resolution Mass Spectrometry (HRMS) was recorded using the analytical services within the Chemistry Department at the University of Liverpool (UoL), and within the Centre of Marine Sciences (CCMar). HRMS was conducted on a VG analytical 7070E machine, Frisons TRIO mass spectrometer, or Agilent QTOF 7200, using chemical ionisation (CI) or electrospray (ESI) (UoL), and on Thermo Scientific High Resolution Mass Spectrometer (HRMS), model Orbitrap Elite, capable of MSn, n up to 10 (CCMar). Elemental analysis (%C, %H, %N and %S where specified) were determined by the University of Liverpool Microanalysis Laboratory.

***Safety.*** Organic peroxides are potentially hazardous compounds (inflammable and explosive) and must be handled carefully: 1) a safety shield should be used for all reactions involving $H_2O_2$; 2) direct exposure to strong heat or light, mechanical shock, oxidizable organic materials or transition-metal ions should be avoided.

***Computational Details.*** Density functional theory (DFT) calculations were performed using the Gaussian 09 software package[91] and structural representations were generated with *CYLview*.[92] All the geometry optimizations were carried out using the standard B3LYP functional and the valence double-zeta 6-31G(d) basis set. All the optimized geometries were verified by frequency computations as minima (zero imaginary frequencies) or transition states (a single imaginary frequency corresponding to the desired reaction coordinate). Single-point energy calculations on the optimized geometries were then evaluated using the long-range corrected hybrid functional ωB97XD developed by Head-Gordon and co-workers[93] and the valence triple-zeta Def2-TZVPP basis set, with solvent effects (dichloromethane) calculated by means of the Polarizable Continuum Model (PCM) initially devised by Tomasi and co-workers,[94–97] with radii and non-electrostatic terms of the SMD solvation model, developed by Truhler and co-workers.[98] The free energy values presented along the chapter and appendix were derived from the electronic energy values obtained at the ωB97XD/Def2-TZVPP//B3LYP/6-31G(d) level, including solvent effects, and corrected by using the thermal and entropic corrections based on structural and vibration frequency data calculated at the B3LYP/6-31G(d) level.

***Statistical Analysis.*** The values in this study are expressed as means ± SD. The Shapiro–Wilk test was used for verification of the normality of the data. Graphics and statistical analysis were generated with manual R scripts in RStudio (Version 1.4.1106), using ggplot2 libraries for the graphic figures.

## 4.7.1. General procedures

**General procedure for preparation of silica sulfuric acid (SSA):** Adapted from Roy *et al.*[99], with slight modifications. To a slurry of silica gel (10 g, 230–400 mesh, pore size 60 Å) in dry diethyl ether (50 mL) was added concentrated $H_2SO_4$ (>95%, 3 mL) under strong stirring, for 30 min, at 0 °C. The solvent was evaporated under reduced pressure, resulting in free-flowing silica sulfuric acid that was dried *in vacuo* for 24 hours. Then, it was heated at 120 °C for 3 h (using a hot plate), affording the catalyst **SSA-(C).** The prepared catalyst was stored inside a desiccator. The molarity of sulfuric acid adsorbed on the silica gel was determined by the acid−base titration method. 10 mL of purified water was added to 0.01 g of SSA, and the mixture was stirred for 1 hour at room temperature. The suspension was then titrated with a solution of NaOH (0.0025 M).

**Procedure for catalyst regeneration.** Following the cyclocondensation process with SSA, the catalyst was filtered out of the reaction mixture and washed several times with dichloromethane to remove any remaining organic contaminants (5 x 25 mL). Drying in a vacuum oven at 60 °C for 24 h regenerates the catalyst.

**General procedure 1: Synthesis of 1,2,4,5-tetraoxanes (4.13a-g).** ***Step 1:*** Carbonyl compound (1 mmol) was dissolved in acetonitrile (3 mL), and **SSA-(C)** (2 mmol) was added to the mixture. Hydrogen peroxide 50 wt. % in $H_2O$ (4 mmol) was slowly added over an ice bath, then the mixture was left to stir at room temperature until consumption of the starting material. To this mixture was added distilled water, then the catalyst was filtered and rinsed with $CH_2Cl_2$. The filtrate was extracted with $CH_2Cl_2$ (3 × 30 mL), dried over with $MgSO_4$, and concentrated under reduced pressure at low temperature (30-35 °C), to obtain the *gem*-dihydroperoxide semi-crude, which was used immediately without further purification. ***Step 2:*** The *gem*-dihydroperoxide semi-crude was dissolved in anhydrous $CH_2Cl_2$ (5 mL), followed by adding the second carbonyl compound (1.5 mmol). The mixture was cooled over an ice bath prior to the addition of **SSA-(C)** (2 mmol). The mixture was then warmed and left to stir at room temperature until consumption of the starting material. The resulting solution was then filtered, rinsed with $CH_2Cl_2$, and concentrated under reduced pressure. The residue was purified by flash chromatography using an EtOAc−hexane gradient (unless specified differently) to afford pure 1,2,4,5-tetraoxanes.

**General procedure 2: Synthesis of 1,2,4-trioxanes (4.16a-f), *via* hydroperoxysilylation of allylic alcohols, followed by cyclocondensation to 1,2,4-trioxane.** ***Step 1: hydroperoxysilylation of allylic alcohols.*** Procedure as described by O'Neill *et al.*[88] To a solution of allylic alcohol (1 mmol) in 1,2-dichloroethane (DCE) (10 mL) was added $Co(thd)_2$ (0.03 mmol) at room temperature, and the solution allowed to stir, while bubbling with oxygen. After a couple of minutes, triethylsilane (2 mmol) was added and the reactants were allowed to react under an oxygen atmosphere. The original purple/brown solution became green, and the reaction was followed by TLC until completion. The reaction mixture was then filtered through a plug of celite in a sinter funnel, under pressure. The celite was washed with ethyl acetate and the resulting filtrate was then concentrated under reduced pressure to give the semi-crude peroxysilyl alcohol,

which was used immediately in the next step without further purification. ***Step 2:*** ***Cyclocondensation of the peroxysilyl alcohol to 1,2,4-trioxanes.*** The peroxysilyl alcohol semi-crude (1 mmol) and the carbonyl compound (1.5 mmol) were dissolved in anhydrous dichloromethane (5 mL). The mixture was cooled to below 5 °C and then **SSA-(C)** (2 mmol) was added. The mixture was then warmed and left to stir at room temperature until completion of the reaction (usually 30-60 min). The resulting solution was then filtered, rinsed with dichloromethane, and concentrated under reduced pressure. Purification by flash chromatography using a mixture of EtOAc/Hexane (unless specified differently), gave the pure product.

**Preparation of the $Co(thd)_2.H_2O$ catalyst.** Procedure as described by O'Neill *et al.*[88] To an aq. solution (95 mL) of NaOH (0.43g, 10 mmol) and 2,2,6,6-tetramethyl-3,5-heptanedione (thd, 4.0 mL, 19.17 mmol) was slowly added a solution (15 mL) of cobalt (II) chloride (1.34 g, 10.35 mmol). After stirring for 3 hours at 60 °C (using an oil bath), and filtering, the product was washed with water and stored under reduced pressure as a purple powder (3.55 g, 40%). The prepared catalyst was stored inside in a desiccator.

**General procedure 3: Synthesis of 1,2,4-trioxanes (4.18a and 4.18b): *Via* perhydrolysis of spiro-oxiranes, followed by cyclocondensation to 1,2,4-trioxanes**. ***Step 1:*** To a spiro-oxirane (1 mmol) solution of $MgSO_4$ dried $H_2O_2$–$Et_2O$ (15 mL, see note below), **SSA-(C)** (2 mmol) was added, at 0 °C. The reaction mixture was then allowed to warm at room temperature and stirred until completion (usually 1 h). The reaction mixture was then washed with water (1 × 100 ml) and brine (1 × 100 mL). The combined aqueous layers were extracted with $CH_2Cl_2$ (2 × 75 mL). The combined organic layers were concentrated under *vacuum*, affording the *β*-hydroperoxy alcohol crude, which was immediately used in the next step without any further purification. ***Step 2:*** ***Cyclocondensation of the β-hydroperoxy alcohol to 1,2,4-trioxanes*.** The *β*-hydroperoxy alcohol semi-crude (1 mmol) and the carbonyl compound (1.5 mmol) were dissolved in anhydrous dichloromethane (5 mL). The mixture was cooled to below 5 °C and then **SSA-(C)** (2 mmol) was added. The mixture was then warmed and left to stir at room temperature until completion or the reaction (usually 30-60 min). The resulting solution was then filtered, rinsed with dichloromethane, and concentrated under *vacu*um. Purification by flash chromatography using a EtOAc−hexane gradient (unless specified differently), gave the pure 1,2,4-trioxane compound.

**Method to dry $H_2O_2$–$Et_2O$**. Procedure as described by Sabbani *et al.*[100] At 0 °C, hydrogen peroxide peroxide ($H_2O_2$, 42 mL, 50 wt% in $H_2O$) was dissolved in anhydrous diethyl ether (395 mL). Constant stirring was used to add anhydrous $MgSO_4$ until a thick white slurry sank to the bottom of the flask. The supernatant was then decanted and dried with anhydrous $MgSO_4$ and filtered again, producing an ethereal solution of $H_2O_2$ with a concentration of approximately 1.5 M. The solution was used immediately thereafter. The solution cannot be stored for later use, due to safety hazards.

## 4.7.2. Synthesis

### Preparation of 4-(4-oxocyclohexyl)phenyl) acetate (4.11a)

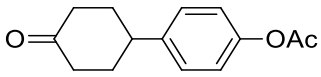


Procedure adapted from by O'Neill *et al.*[8] with slight modifications. To a stirred solution of 4-(4-hydroxyphenyl)cyclohexanone (2.00 g, 10.51 mmol) and triethylamine (2.90 mL, 20.8 mmol) in anhydrous dichloromethane (20 mL) was added acetic anhydride (3.00 mL, 31.74 mmol), dropwise, at 0 °C. The reaction mixture was then allowed to warm to room temperature and stirred for 3 hours, until reaction's completion. The final reaction mixture was washed with water (3 × 20 mL), sodium bicarbonate (3 × 20 mL) and brine (20 mL). The organic layer was dried with $MgSO_4$, filtered and then concentrated under reduced pressure. Recrystallization of the solid residue from acetone gave the ester (2.20 g, 90% yield) as a white solid. M.p. = 101-103 °C. Spectral data are in accordance with the reported in the literature.[8] $^1$H-NMR (400 MHz, $CDCl_3$): δ 7.25 (d, *J* = 8.5 Hz, 2H), 7.04 (d, *J* = 8.6 Hz, 2H), 3.08 – 2.98 (m, 1H), 2.50 (dd, *J* = 10.6, 4.6 Hz, 4H), 2.29 (s, 3H), 2.22 (dt, *J* = 14.6, 3.0 Hz, 2H), 1.93 (dt, *J* = 22.7, 10.6 Hz, 2H) ppm. $^{13}C\{^1H\}$ NMR (101 MHz, $CDCl_3$): δ 210.9, 169.6, 149.2, 142.3, 127.7, 121.6, 42.2, 41.3, 34.0, 21.1 ppm. HRMS (ESI, *m/z*) calcd $C_{14}H_{16}O_3Na$ $[M+Na]^+$: 255.0992; found 255.0992.

## Preparation of 3-acetylphenyl acetate (4.11c)

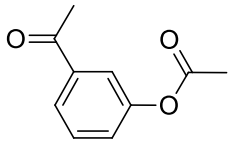

This compound was synthesised following the procedure described previously by O'Neill *et al.*[8], using 3′-hydroxyacetophenone. Colourless solid (1.12 g, 86% yield). M.p. = 43 – 44 °C. Spectral data are in accordance with the reported in the literature.[101] $^{1}$H NMR (500 MHz, $CDCl_3$): δ 7.83 (ddd, *J* = 7.8, 1.6, 1.1 Hz, 1H), 7.67 (t, *J* = 2.0 Hz, 1H), 7.48 (t, *J* = 7.9 Hz, 1H), 7.30 (ddd, *J* = 8.0, 2.4, 1.0 Hz, 1H), 2.60 (s, 3H), 2.32 (s, 3H). $^{13}$C{$^{1}$H} NMR (126 MHz, $CDCl_3$): δ 197.1, 169.4, 151.0, 138.6, 129.8, 126.6, 125.9, 121.6, 26.8, 21.2. HRMS (ESI, *m/z*) calcd for $C_{10}H_{10}O_3Na$ $[M+Na]^+$: 201.05222; found 201.05185.

## Preparation of *p*-(dispiro[cyclohexane-1,3'-[1,2,4,5]tetraoxane-6',2''-tricyclo[3.3.1.1$^{3,7}$]decan]-4-yl)-phenyl acetate (4.13a)

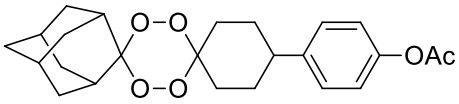


This compound was synthesised in accordance with general procedure 1 using 4-(4-oxocyclohexyl)phenyl acetate **4.11a** (for the peroxidation step) and adamantan-2-one **4.11b** (for the cyclocondensation step). Purification by flash chromatography (EtOAc: hexane, 2.5:97.5, *v/v*) provided a white solid (278 mg, 67% yield). M.p. = 195-197°C. Spectral data are in accordance with the reported in the literature.[8] $^{1}$H NMR (500 MHz, $CDCl_3$): δ 7.15 (d, *J* = 8.6 Hz, 2H), 6.93 (d, *J* = 8.5 Hz, 2H), 3.35 – 2.94 (m, 2H), 2.54 (tt, *J* = 12.0, 3.7 Hz, 1H), 2.22 (s, 3H), 2.08 – 1.66 (m, 14H), 1.65 – 1.49 (m, 6H). $^{13}$C{$^{1}$H} NMR (126 MHz, $CDCl_3$): δ 169.8, 149.0, 143.5, 127.9, 121.5, 110.6, 107.6, 43.2, 37.0, 34.4, 33.3, 32.0, 30.2, 29.8, 27.2, 21.3. HRMS (ESI, *m/z*) calcd $C_{24}H_{30}O_6Na$ $[M+Na]^+$ : 437.19346; found 437.19229.

## Preparation of *p*-(7,8,15,16-tetraoxa-3-dispiro [5.2.5.2]hexadecyl)phenyl acetate (4.13b)

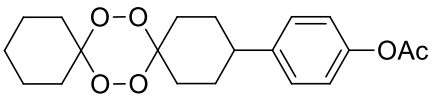


This compound was synthesised in accordance with general procedure 1 using **4.11a** (for the peroxidation step) and cyclohexanone (for the cyclocondensation step). Purification by flash chromatography (EtOAc: hexane, 2.5:97.5, *v/v*) provided a white solid (207 mg, 57% yield). M.p. = 93-95 °C. $^{1}$H NMR (500 MHz, $CDCl_3$): δ 7.20 (d, *J* = 8.5 Hz, 2H), 6.98 (d, *J* = 8.5 Hz, 2H), 3.25 (s, 1H), 2.59 (tt, *J* = 12.0, 3.7 Hz, 1H), 2.32 (d, *J* = 22.7 Hz, 1H), 2.27 (s, 3H), 1.87 – 1.55 (m, 13H), 1.53 – 1.39 (m, 3H). $^{13}$C{$^{1}$H} NMR (126 MHz, $CDCl_3$): δ 169.8, 149.0, 143.5, 127.9, 121.5, 108.5, 107.7, 43.2, 31.9, 31.7, 29.6, 25.5, 22.4, 21.2. HRMS (ESI, *m/z*) calcd $C_{20}H_{26}O_6Na$ $[M+Na]^+$: 385.16216; found 385.16165.

## Preparation of 2-(dispiro[cyclohexane-1,3'-[1,2,4,5]tetraoxane-6',2''-tricyclo[3.3.1.1$^{3,7}$]decan]-4-yl)-1,3-isoindolinedione (4.13c)

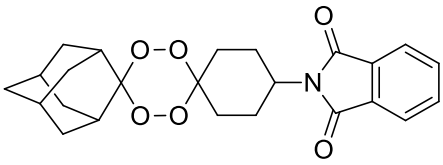


This compound was synthesised in accordance with general procedure 1 using 2-(4-oxocyclohexyl)isoindoline-1,3-dione (for the peroxidation step) and **4.11b** (for the cyclocondensation step). Purification by flash chromatography (EtOAc: hexane, 5:95, *v/v*) provided a white solid (268 mg, 63% yield). M.p. = 174-176 °C. $^{1}$H NMR (500 MHz, $CDCl_3$): δ 7.84 (dd, *J* = 5.4, 3.0 Hz, 2H), 7.70 (dd, *J* = 5.4, 3.0 Hz, 2H), 4.22 (tt, *J* = 12.5, 3.8 Hz, 1H), 3.25 (br d, 2H), 2.55 (s, 2H), 2.15 – 1.84 (m, 8H), 1.79 – 1.61 (m, 10H). $^{13}$C{$^{1}$H} NMR (126 MHz, $CDCl_3$): δ 168.2, 134.0, 132.0, 123.3, 110.7, 106.7, 49.8, 37.0, 34.4, 33.2, 31.2, 30.2, 29.0, 27.2, 25.6, 24.8. HRMS (ESI, *m/z*) calcd $C_{24}H_{27}NO_6Na$ $[M+Na]^+$: 448.17306; found 448.17273.

## Preparation of 2-(7,8,15,16-tetraoxa-3-dispiro[5.2.5.2]hexadecyl)-1,3-isoindolinedione (4.13d)

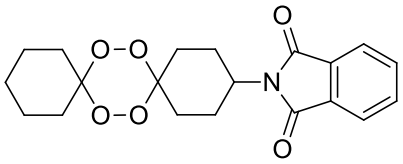

This compound was synthesised in accordance with general procedure 1 using 2-(4-oxocyclohexyl)isoindoline-1,3-dione (for the peroxidation step) and cyclohexanone (for the cyclocondensation step). Purification by flash chromatography (EtOAc: hexane, 5:95, *v/v*) provided a white solid (175 mg, 47% yield). M.p. = 177-179 °C. $^{1}$H NMR (500 MHz, $CDCl_3$): δ 7.82 (dd, *J* = 5.4, 3.0 Hz, 2H), 7.69 (dd, *J* = 5.5, 3.0 Hz, 2H), 4.21 (tt, *J* = 12.5, 3.8 Hz, 1H), 3.30 (s, 1H), 2.53 (s, 2H), 2.30 (d, *J* = 31.9 Hz, 2H), 1.90 (s, 1H), 1.79 – 1.61 (m, 6H), 1.60 – 1.42 (m, 6H). $^{13}$C{$^{1}$H} NMR (126 MHz, $CDCl_3$): δ 168.2, 134.0, 132.0, 123.3, 108.6, 106.9, 49.7, 31.9, 31.2, 29.6, 28.8, 25.5, 24.7, 22.3, 21.9. HRMS (ESI, *m/z*) calcd $C_{20}H_{23}NO_6Na$ $[M+Na]^+$: 396.14176; found 396.14148.

## Preparation of dispiro[cyclohexane-1,3'-[1,2,4,5]tetraoxane-6',2''-tricyclo[3.3.1.1$^{3,7}$]decan]-4-one (4.13e)

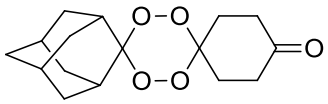

This compound was synthesised in accordance with general procedure 1 using **4.11b** (for the peroxidation step) and 1,4-cyclohexanedione (for the cyclocondensation step). Purification by flash chromatography (EtOAc: hexane, 2.5:97.5, *v/v*) provided a white solid (14.7 mg, 5% yield). M.p = 156-158 ºC. Spectral data are in accordance with the reported in the literature.[102] $^{1}$H NMR (500 MHz, $CDCl_3$): δ 3.20 (br s, 1H), 2.72 (s, 2H), 2.48 (br d, 4H), 2.10 – 1.86 (m, 9H), 1.82 – 1.59 (m, 6H). $^{13}$C{$^{1}$H} NMR (126 MHz, $CDCl_3$): δ 209.4, 111.1, 106.7, 37.0, 36.5, 35.7, 34.4, 33.2, 30.5, 30.2, 28.0, 27.1. HRMS (ESI, *m/z*) calcd $C_{16}H_{22}O_5Na$ $[M+Na]^+$: 317.13594; found 317.13599.

## Preparation of ethyl dispiro[cyclohexane-1,3'-[1,2,4,5]tetraoxane-6',2''-tricyclo[3.3.1.1$^{3,7}$]decane]-4-carboxylate (4.13f)

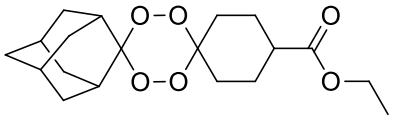

This compound was synthesised in accordance with general procedure 1 using 2-ethyl 4-oxocyclohexanecarboxylate (for the peroxidation step) and **4.11b** (for the cyclocondensation step). Purification by flash chromatography (EtOAc: hexane, 1:99, *v/v*) provided a white solid (178 mg, 51% yield). M.p. = 67-69 °C. Spectral data are in accordance with the reported in the literature.[103] $^{1}$H NMR (500 MHz, $CDCl_3$): 4.12 (q, *J* = 7.1 Hz, 2H), 3.02 (br d, *J* = 118.6 Hz, 2H), 2.41 – 2.34 (m, 1H), 2.08 – 1.60 (m, 19H), 1.50 (s, 1H), 1.23 (t, *J* = 7.1 Hz, 3H). $^{13}$C{$^{1}$H} NMR (126 MHz, $CDCl_3$): δ 174.8, 110.6, 107.3, 60.5, 41.8, 39.4, 37.0, 34.4, 33.2, 30.2, 30.2, 28.3, 27.1, 24.8, 23.9, 14.3. HRMS (ESI, *m/z*) calcd $C_{19}H_{28}O_6Na$ $[M+Na]^+$: 375.17781; found 375.17725.

## Preparation of dispiro[cyclohexane-1,3'-[1,2,4,5]tetraoxane-6',2''-tricyclo[3.3.1.1$^{3,7}$]decane] (4.13g)

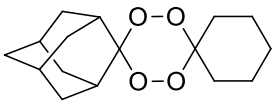

This compound was synthesised in accordance with general procedure 1 using cyclohexanone (for the peroxidation step) and **4.11b** (cyclocondensation step). Purification by flash chromatography (hexane, 100%, *v/v*) provided a white solid (179 mg, 64% yield). M.p = 57-59 ºC. Spectral data are in accordance with the reported in the literature[28]. $^{1}$H NMR (500 MHz, $CDCl_3$): δ 3.17 (s, 1H), 2.30 (s, 2H), 2.04 – 1.44 (m, 21H). $^{13}$C{$^{1}$H} NMR (126 MHz, $CDCl_3$): δ 110.4, 108.1, 37.1, 37.1, 34.4, 33.3, 33.2, 31.9, 30.2, 29.7, 27.2, 25.5, 22.4. HRMS (MALDI-TOF, *m/z*) calcd for $C_{16}H_{24}O_4K$ $[M+K]^+$: 318,1311; found 318.3302.

## Preparation of cyclohex-1-enyl-methanol (4.14a)

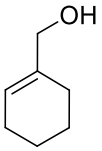


The synthesis for compound **4.14a** is described in Chapter 2, section 2.5.3 (compound **2.30**).

## Preparation of 2-(7,8,15-trioxa-12-dispiro[5.2.5.2]hexadecyl)-1,3-isoindolinedione (4.16a)

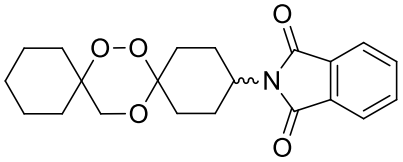


The synthesis for compound **4.16a** is described in Chapter 2, section 2.5.3 (compound **2.32**).

## Preparation of tert-butyl 7,8,16-trioxa-3-aza-3-dispiro[5.2.5.2] hexadecanecarboxylate (4.16b)

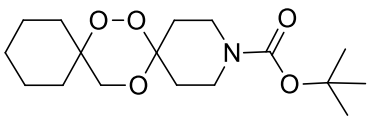


The synthesis for compound **4.16b** is described in Chapter 2, section 2.5.3 (compound **2.46**).

## Preparation of ethyl 7,8,15-trioxa-12-dispiro[5.2.5.2] hexadecanecarboxylate (4.16c)

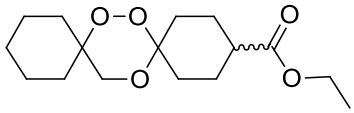

The synthesis for compound **4.16c** is described in Chapter 2, section 2.5.3 (compound **2.60**).

## Preparation of 2-(3,3-dimethyl-1,2,5-trioxa-9-spiro[5.5]undecyl)-1,3-isoindolinedione (4.16d)

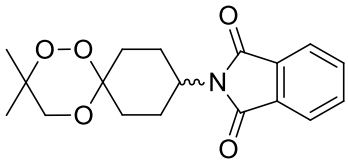

The synthesis for compound **4.16d** is described in Chapter 2, section 2.5.3 (compound **2.31**).

## Preparation of *tert*-butyl 3,3-dimethyl-1,2,5-trioxa-9-aza-9-spiro[5.5]undecanecarboxylate (4.16e)

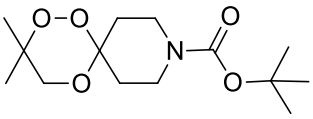

The synthesis for compound **4.16e** is described in Chapter 2, section 2.5.3 (compound **2.45**).

## Preparation of ethyl 3,3-dimethyl-1,2,5-trioxa-9-spiro[5.5] undecanecarboxylate (4.16f)

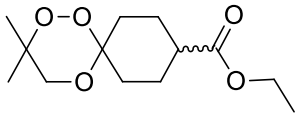

The synthesis for compound **4.16f** is described in Chapter 2, section 2.5.3 (compound **2.53**).

## Preparation spiro[adamantane-2,2'-oxirane] (4.17a)

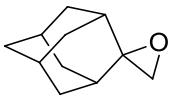

The synthesis for compound **4.17a** is described in Chapter 2, section 2.5.3 (compound **2.36**).

## Preparation of *tert*-butyl 1-oxa-6-azaspiro[2.5]octane-6-carboxylate (4.17b)

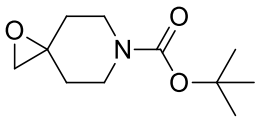

The synthesis for compound **4.17b** is described in Chapter 2, section 2.5.3 (compound **2.49**).

### Preparation of 2-(dispiro[cyclohexane-1,3'-[1,2,4]trioxane-6',2''-tricyclo[3.3.1.1$^{3,7}$]decan]-4-yl)-1,3-isoindolinedione (4.18a)

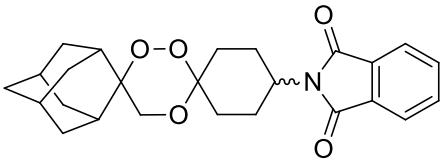

The synthesis for compound **4.18a** is described in Chapter 2, section 2.5.3 (compound **2.37**).

### Preparation of tert-butyl dispiro[piperidine-4,3'-[1,2,4]trioxane-6',2''-tricyclo[3.3.1.1$^{3,7}$]decane]-1-carboxylate (4.18b)

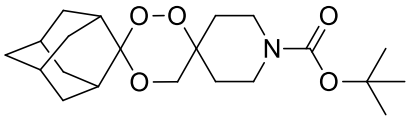

The synthesis for compound **4.18b** is described in Chapter 2, section 2.5.3 (compound **2.50**).

## 4.8. References

(1) Klussmann, M. Alkenyl and Aryl Peroxides. *Chem. - A Eur. J.* **2017**, *24* (18), 4480–4496. https://doi.org/10.1002/chem.201703775.

(2) Ashley, E. A.; Dhorda, M.; Fairhurst, R. M.; Amaratunga, C.; Lim, P.; Suon, S.; Sreng, S.; Anderson, J. M.; Mao, S.; Sam, B.; Sopha, C.; Chuor, C. M.; Nguon, C.; Sovannaroth, S.; Pukrittayakamee, S.; Jittamala, P.; Chotivanich, K.; Chutasmit, K.; Suchatsoonthorn, C.; Runcharoen, R.; Hien, T. T.; Thuy-Nhien, N. T.; Thanh, N. V.; Phu, N. H.; Htut, Y.; Han, K.-T.; Aye, K. H.; Mokuolu, O. A.; Olaosebikan, R. R.; Folaranmi, O. O.; Mayxay, M.; Khanthavong, M.; Hongvanthong, B.; Newton, P. N.; Onyamboko, M. A.; Fanello, C. I.; Tshefu, A. K.; Mishra, N.; Valecha, N.; Phyo, A. P.; Nosten, F.; Poravuth Yi, R. T.; Borrmann, S.; Bashraheil, M.; Peshu, J.; Faiz, M. A.; Ghose, A.; Hossain, M. A.; Samad, R.; Rahman, M. R.; Hasan, M. M.; Islam, A.; Miotto, O.; Amato, R.; MacInnis, B.; Stalker, J.; Kwiatkowski, D. P.; Bozdech, Z.; Jeeyapant, A.; Cheah, P. Y.; Sakulthaew, T.; Chalk, J.; Intharabut, B.; Silamut, K.; Lee, S. J.; Vihokhern, B.; Kunasol, C.; Imwong, M.; Tarning, J.; Taylor, W. J.; Yeung, S.; Woodrow, C. J.; Flegg, J. A.; Das, D.; Smith, J.; Venkatesan, M.; Plowe, C. V; Stepniewska, K.; Guerin, P. J.; Dondorp, A. M.; Day, N. P.; White, N. J.; Tracking Resistance to Artemisinin Collaboration (TRAC). Spread of Artemisinin Resistance in *Plasmodium falciparum* Malaria. *N. Engl. J. Med.* **2014**, *371*

(5), 411–423. https://doi.org/10.1056/NEJMoa1314981.

(3) Dondorp, A. M.; Ringwald, P. Artemisinin Resistance Is a Clear and Present Danger. *Trends Parasitol.* **2013**, *29* (8), 359–360. https://doi.org/10.1016/j.pt.2013.05.005.

(4) Kumar, N.; Khan, S. I.; Beena; Rajalakshmi, G.; Kumaradhas, P.; Rawat, D. S. Synthesis, Antimalarial Activity and Cytotoxicity of Substituted 3,6-Diphenyl-[1,2,4,5]Tetraoxanes. *Bioorg. Med. Chem.* **2009**, *17* (15), 5632–5638. https://doi.org/10.1016/j.bmc.2009.06.020.

(5) Haldar, K.; Bhattacharjee, S.; Safeukui, I. Drug Resistance in *Plasmodium*. *Nat. Rev. Microbiol.* **2018**, *16* (3), 156–170. https://doi.org/10.1038/nrmicro.2017.161.

(6) Abiodun, O. O.; Brun, R.; Wittlin, S. *In vitro* Interaction of Artemisinin Derivatives or the Fully Synthetic Peroxidic Anti-Malarial OZ277 with Thapsigargin in *Plasmodium falciparum* Strains. *Malar. J.* **2013**, *12*, 43. https://doi.org/10.1186/1475-2875-12-43.

(7) O'Neill, P. M.; Amewu, R. K.; Nixon, G. L.; ElGarah, F. B.; Mungthin, M.; Chadwick, J.; Shone, A. E.; Vivas, L.; Lander, H.; Barton, V.; Muangnoicharoen, S.; Bray, P. G.; Davies, J.; Park, B. K.; Wittlin, S.; Brun, R.; Preschel, M.; Zhang, K.; Ward, S. A. Identification of a 1,2,4,5-Tetraoxane Antimalarial Drug-Development Candidate (RKA 182) with Superior Properties to the Semisynthetic Artemisinins. *Angew. Chemie - Int. Ed.* **2010**, *49* (33), 5693–5697. https://doi.org/10.1002/anie.201001026.

(8) O'Neill, P. M.; Sabbani, S.; Nixon, G. L.; Schnaderbeck, M.; Roberts, N. L.; Shore, E. R.; Riley, C.; Murphy, B.; McGillan, P.; Ward, S. A.; Davies, J.; Amewu, R. K. Optimisation of the Synthesis of Second Generation 1,2,4,5 Tetraoxane Antimalarials. *Tetrahedron* **2016**, *72* (40), 6118–6126. https://doi.org/10.1016/j.tet.2016.08.043.

(9) Woodley, C. M.; Amado, P. S. M.; Cristiano, M. L. S.; O'Neill, P. M. Artemisinin Inspired Synthetic Endoperoxide Drug Candidates: Design, Synthesis, and Mechanism of Action Studies. *Med. Res. Rev.* **2021**, *41* (6), 3062–3095. https://doi.org/10.1002/med.21849.

(10) Li, Y.; Hao, H.-D.; Zhang, Q.; Wu, Y. A Broadly Applicable Mild Method for the Synthesis of *Gem*-Diperoxides from Corresponding Ketones or 1,3-Dioxolanes. *Org. Lett.* **2009**, *11* (7), 1615–1618. https://doi.org/10.1021/ol900262t.

(11) Amit, C.; Manish, S.; Arti, D.; Shammy, J.; Kamya, G. A Review on Antimalarial 1,2,4-Trioxane Derivatives. *J. Drug Deliv. Ther.* **2020**, *10* (4-S), 240–253. https://doi.org/10.22270/jddt.v10i4-s.4268.

(12) Crespo-Ortiz, M. P.; Wei, M. Q. Antitumor Activity of Artemisinin and Its Derivatives: From a Well-Known Antimalarial Agent to a Potential Anticancer Drug. *J. Biomed. Biotechnol.* **2012**, *2012*, 247597. https://doi.org/10.1155/2012/247597.

(13) Amewu, R. K.; Chadwick, J.; Hussain, A.; Panda, S.; Rinki, R.; Janneh, O.; Ward, S. A.; Miguel, C.; Burrell-Saward, H.; Vivas, L.; O'Neill, P. M. Synthesis and Evaluation of the Antimalarial, Anticancer, and Caspase 3 Activities of Tetraoxane Dimers. *Bioorg. Med. Chem.* **2013**, *21* (23), 7392–7397. https://doi.org/10.1016/j.bmc.2013.09.047.

(14) Yaremenko, I. A.; Syroeshkin, M. A.; Levitsky, D. O.; Fleury, F.; Terent'ev, A. O. Cyclic Peroxides as Promising Anticancer Agents: *In vitro* Cytotoxicity Study of Synthetic Ozonides and Tetraoxanes on Human Prostate Cancer Cell Lines. *Med. Chem. Res.* **2017**, *26* (1), 170–179. https://doi.org/10.1007/s00044-016-1736-2.

(15) Opsenica, D. M.; Radivojevic, J.; Matić, I. Z.; Štajner, T.; Kneževic-Ušaj, S.; Djurkovic-Djakovic, O.; Šolaja, B. A. Tetraoxanes as Inhibitors of Apicomplexan Parasites *Plasmodium falciparum* and *Toxoplasma gondii* Growth and Anti-Cancer Molecules. *J. Serbian Chem. Soc.* **2015**, *80* (11), 1339–1359. https://doi.org/10.2298/JSC150430063O.

(16) Gangadhar, B.; Khongsti, K.; Das, B.; Bez, G. 1,2,3-Triazole Tethered 1,2,4-Trioxanes: Studies on Their Synthesis and Effect on Osteopontin Expression in MDA-MB-435 Breast Cancer Cell. *Eur. J. Med. Chem.* **2020**, *186*, 111908. https://doi.org/10.1016/j.ejmech.2019.111908.

(17) Vil', V. A.; Yaremenko, I. A.; Fomenkov, D. I.; Levitsky, D. O.; Fleury, F.; Terent'ev, A. O. Ion Exchange Resin-Catalyzed Synthesis of Bridged Tetraoxanes Possessing *in vitro* Cytotoxicity against HeLa Cancer Cells. *Chem. Heterocycl. Compd.* **2020**, *56* (6), 722–726. https://doi.org/10.1007/s10593-020-02722-4.

(18) Yaremenko, I. A.; Coghi, P.; Prommana, P.; Qiu, C.; Radulov, P. S.; Qu, Y.; Belyakova,

Y. Y.; Zanforlin, E.; Kokorekin, V. A.; Wu, Y. Y. J.; Fleury, F.; Uthaipibull, C.; Wong, V. K. W.; Terent'ev, A. O. Synthetic Peroxides Promote Apoptosis of Cancer Cells by Inhibiting P-Glycoprotein ABCB5. *ChemMedChem* **2020**, *15* (13), 1118–1127. https://doi.org/10.1002/cmdc.202000042.

(19) Coghi, P.; Yaremenko, I. A.; Prommana, P.; Radulov, P. S.; Syroeshkin, M. A.; Wu, Y. J.; Gao, J. Y.; Gordillo-Martinez, F. M.; Mok, S.; Wong, V. K. W.; Uthaipibull, C.; Terent'ev, A. O. Novel Peroxides as Promising Anticancer Agents with Unexpected Depressed Antimalarial Activity. *ChemMedChem* **2018**, *13* (9), 902–908. https://doi.org/10.1002/cmdc.201700804.

(20) Šolaja, B. A.; Terzić, N.; Pocsfalvi, G.; Gerena, L.; Tinant, B.; Opsenica, D.; Milhous, W. K. Mixed Steroidal 1,2,4,5-Tetraoxanes: Antimalarial and Antimycobacterial Activity. *J. Med. Chem.* **2002**, *45* (16), 3331–3336. https://doi.org/10.1021/jm020891g.

(21) Opsenica, I.; Opsenica, D.; Lanteri, C. A.; Anova, L.; Milhous, W. K.; Smith, K. S.; Šolaja, B. A. New Chimeric Antimalarials with 4-Aminoquinoline Moiety Linked to a Tetraoxane Skeleton. *J. Med. Chem.* **2008**, *51* (19), 6216–6219. https://doi.org/10.1021/jm8006905.

(22) Cabral, L. I. L.; Pomel, S.; Cojean, S.; Amado, P. S. M.; Loiseau, P. M.; Cristiano, M. L. S. Synthesis and Antileishmanial Activity of 1,2,4,5-Tetraoxanes against *Leishmania donovani*. *Molecules* **2020**, *25* (3), 465. https://doi.org/10.3390/molecules25030465.

(23) Antolínez, I. V.; Barbosa, L. C. A.; Borgati, T. F.; Baldaia, A.; Ferreira, S. R.; Almeida, R. M.; Fujiwara, R. T. Tetraoxanes as New Agents Agains *Leishmania amazonensis*. *Chem. Biodivers.* **2020**, *17* (6), e2000142. https://doi.org/10.1002/cbdv.202000142.

(24) Medrán, N. S.; Sayé, M.; Pereira, C. A.; Tekwani, B. L.; La-Venia, A.; Labadie, G. R. Expanding the Scope of Synthetic 1,2,4-Trioxanes towards *Trypanosoma cruzi* and *Leishmania donovani*. *Bioorg. Med. Chem. Lett.* **2020**, *30* (20), 127491. https://doi.org/10.1016/j.bmcl.2020.127491.

(25) Wang, X.; Zhao, Q.; Vargas, M.; Dong, Y.; Sriraghavan, K.; Keiser, J.; Vennerstrom, J. L. The Activity of Dispiro Peroxides against *Fasciola hepatica*. *Bioorganic Med. Chem. Lett.* **2011**, *21* (18), 5320–5323. https://doi.org/10.1016/j.bmcl.2011.07.024.

(26) Kirchhofer, C.; Vargas, M.; Braissant, O.; Dong, Y.; Wang, X.; Vennerstrom, J. L.; Keiser, J. Activity of OZ78 Analogues against *Fasciola hepatica* and *Echinostoma caproni*. *Acta Trop.* **2011**, *118* (1), 56–62. https://doi.org/10.1016/j.actatropica.2011.02.003.

(27) Vil', V. A.; Yaremenko, I. A.; Ilovaisky, A. I.; Terent'ev, A. O. Peroxides with Anthelmintic, Antiprotozoal, Fungicidal and Antiviral Bioactivity: Properties, Synthesis and Reactions. *Molecules* **2017**, *22* (11), 1881. https://doi.org/10.3390/molecules22111881.

(28) Kirchhofer, C.; Vargas, M.; Huwyler, J.; Keiser, J. Pharmacokinetics of the Fasciocidal Drug Candidates MT04 and OZ78 in Uninfected Rats and *in vitro* Pharmacodynamic Studies. *Int. J. Parasitol. Drugs Drug Resist.* **2012**, *2*, 121–125. https://doi.org/10.1016/j.ijpddr.2012.03.003.

(29) Duan, W.-W.; Qiu, S.-J.; Zhao, Y.; Sun, H.; Qiao, C.; Xia, C.-M. Praziquantel Derivatives Exhibit Activity against Both Juvenile and Adult *Schistosoma japonicum*. *Bioorganic Med. Chem. Lett.* **2012**, *22* (4), 1587–1590. https://doi.org/10.1016/j.bmcl.2011.12.133.

(30) Cowan, N.; Yaremenko, I. A.; Krylov, I. B.; Terent'ev, A. O.; Keiser, J. Elucidation of the *in vitro* and *in vivo* Activities of Bridged 1,2,4-Trioxolanes, Bridged 1,2,4,5-Tetraoxanes, Tricyclic Monoperoxides, Silyl Peroxides, and Hydroxylamine Derivatives against *Schistosoma Mansoni*. *Bioorg. Med. Chem.* **2015**, *23* (16), 5175–5181. https://doi.org/10.1016/j.bmc.2015.02.010.

(31) Ingram, K.; Yaremenko, I. A.; Krylov, I. B.; Hofer, L.; Terent'ev, A. O.; Keiser, J. Identification of Antischistosomal Leads by Evaluating Bridged 1,2,4,5-Tetraoxanes, Alphaperoxides, and Tricyclic Monoperoxides. *J. Med. Chem.* **2012**, *55* (20), 8700–8711. https://doi.org/10.1021/jm3009184.

(32) Portela, J.; Boissier, J.; Gourbal, B.; Pradines, V.; Collière, V.; Coslédan, F.; Meunier, B.; Robert, A. Antischistosomal Activity of Trioxaquines: *In vivo* Efficacy and Mechanism of Action on *Schistosoma mansoni*. *PLoS Negl. Trop. Dis.* **2012**, *6* (2), e1474. https://doi.org/10.1371/journal.pntd.0001474.

(33) Yaremenko, I. A.; Radulov, P. S.; Belyakova, Y. Y.; Demina, A. A.; Fomenkov, D. I.; Barsukov, D. V.; Subbotina, I. R.; Fleury, F.; Terent'ev, A. O. Catalyst Development for the Synthesis of Ozonides and Tetraoxanes under Heterogeneous Conditions. Disclosure of an Unprecedented Class of Fungicides for Agricultural Application. *Chem. - A Eur. J.* **2020**, *26* (21), 4734–4751. https://doi.org/10.1002/chem.201904555.

(34) Dmitrović, S.; Skorić, M.; Boljević, J.; Aničić, N.; Božić, D.; Mišić, D.; Filipović, V.; Opsenica, D. Elicitation Effects of a Synthetic 1,2,4,5-Tetraoxane and a 2,5-Diphenylthiophene in Shoot Cultures of Two *Nepeta* Species. *J. Serbian Chem. Soc.* **2016**, *81* (9), 999–1012. https://doi.org/10.2298/JSC160226054D.

(35) McCullough, K. J. Synthesis and Use of Cyclic Peroxides. *Contemp. Org. Synth.* **1995**, *2* (4), 225–249. https://doi.org/10.1039/CO9950200225.

(36) Dong, Y. Synthesis and Antimalarial Activity of 1,2,4,5-Tetraoxanes. *Mini-Reviews Med. Chem.* **2002**, *2* (2), 113–123. https://doi.org/https://doi.org/10.2174/1389557024605537.

(37) Antonovskii, V. L.; Khursan, S. L. Thermolysis of Organic Peroxides in Solution. *Russ. Chem. Rev.* **2003**, *72* (11), 939–963. https://doi.org/10.1070/RC2003v072n11ABEH000749.

(38) Tang, Y.; Dong, Y.; Vennerstrom, J. L. Synthetic Peroxides as Antimalarials. *Med. Res. Rev.* **2004**, *24* (4), 425–448. https://doi.org/10.1002/med.10066.

(39) Opsenica, D. M.; Šolaja, B. A. Antimalarial Peroxides. *J. Serbian Chem. Soc.* **2009**, *74* (11), 1155–1193. https://doi.org/10.2298/JSC0911155.

(40) Kumar, N.; Singh, R.; Rawat, D. S. Tetraoxanes: Synthetic and Medicinal Chemistry Perspective. *Med. Res. Rev.* **2012**, *32* (3), 581–610. https://doi.org/10.1002/med.20223.

(41) Jorge, N. L.; Hernández-Laguna, A.; Castro, E. A. Some Recent Developments on the Synthesis, Chemical Reactivity, and Theoretical Studies of Tetroxanes. *Int. J. Chemoinformatics Chem. Eng.* **2013**, *3* (1), 48–73. https://doi.org/10.4018/ijcce.2013010105.

(42) Yadav, N.; Sharma, C.; Awasthi, S. Diversification in the Synthesis of Antimalarial Trioxane and Tetraoxane Analogs. *RSC Adv.* **2014**, *4* (11), 5469–5498. https://doi.org/10.1039/c3ra42513d.

(43) Terent'ev, A. O.; Borisov, D. A.; Vil', V. A.; Dembitsky, V. M. Synthesis of Five- and Six-Membered Cyclic Organic Peroxides: Key Transformations into Peroxide Ring-Retaining Products. *Beilstein J. Org. Chem.* **2014**, *10*, 34–114. https://doi.org/10.3762/bjoc.10.6.

(44) Yaremenko, I. A.; Radulov, P. S.; Belyakova, Y. Y.; Fomenkov, D. I.; Tsogoeva, S. B.; Terent'ev, A. O. Lewis Acids and Heteropoly Acids in the Synthesis of Organic Peroxides. *Pharmaceuticals* **2022**, *15* (4), 472. https://doi.org/10.3390/ph15040472.

(45) Gomes, G. dos P.; Vil', V.; Terent'ev, A.; Alabugin, I. V. Stereoelectronic Source of the Anomalous Stability of Bis-Peroxides. *Chem. Sci.* **2015**, *6* (12), 6783–6791. https://doi.org/10.1039/C5SC02402A.

(46) Juaristi, E.; Gomes, G. dos P.; Terent'ev, A. O.; Notario, R.; Alabugin, I. V. Stereoelectronic Interactions as a Probe for the Existence of the Intramolecular α-Effect. *J. Am. Chem. Soc.* **2017**, *139* (31), 10799–10813. https://doi.org/10.1021/jacs.7b05367.

(47) Alabugin, I. V.; Kuhn, L.; Medvedev, M. G.; Krivoshchapov, N. V.; Vil', V. A.; Yaremenko, I. A.; Mehaffy, P.; Yarie, M.; Terent'ev, A. O.; Zolfigol, M. A. Stereoelectronic Power of Oxygen in Control of Chemical Reactivity: The Anomeric Effect Is Not Alone. *Chem. Soc. Rev.* **2021**, *50* (18), 10253–10345. https://doi.org/10.1039/d1cs00386k.

(48) Chiang, C.-Y.; Butler, W.; Kuczkowski, R. L. The Synthesis, X-Ray Structural Analysis, and Anomeric Effect in Trans-3,6-Dimethoxy-1,2,4,5-Tetroxane. *J. Chem. Soc. Chem. Commun.* **1988**, No. 7, 465–466. https://doi.org/10.1039/C39880000465.

(49) Murray, R. W.; Kong, W.; Rajadhyaksha, S. N. The Ozonolysis of Tetramethylethylene. Concentration and Temperature Effects. *J. Org. Chem.* **1993**, *58* (2), 315–321. https://doi.org/10.1021/jo00054a010.

(50) Kukovinets, O. S.; Zvereva, T. I.; Kabalnova, N. N.; Kasradze, V. G.; Salimova, E. V.; Khalitova, L. R.; Abdullin, M. I.; Spirikhin, L. V. Ozonolysis of Verbenone in Aprotic

Solvents. *Mendeleev Commun.* **2009**, *19* (2), 106–107. https://doi.org/10.1016/j.mencom.2009.03.019.

(51) Ito, Y.; Yokoya, H.; Umehara, Y.; Matsuura, T. Formation of Ketone Diperoxides from Ozonation of *O*-Methyloximes. *Bull. Chem. Soc. Jpn.* **1980**, *53* (8), 2407–2408. https://doi.org/10.1246/bcsj.53.2407.

(52) Dong, Y.; Vennerstrom, J. L. Dispiro-1,2,4,5-Tetraoxanes via Ozonolysis of Cycloalkanone *O*-Methyl Oximes: A Comparison with the Peroxidation of Cycloalkanones in Acetonitrile-Sulfuric Acid Media. *J. Org. Chem.* **1998**, *63* (23), 8582–8585. https://doi.org/10.1021/jo981261i.

(53) Nakamura, N.; Nojima, M.; Kusabayashi, S. Ozonolysis of Vinyl Ethers. Evidence for Intramolecular Oxygen Transfer from a Carbonyl Oxide Moiety to a Methoxyvinyl Group. *J. Am. Chem. Soc.* **1987**, *109* (16), 4969–4973. https://doi.org/10.1021/ja00250a034.

(54) Wojciechowski, B. J.; Pearson, W. H.; Kuczkowski, R. L. Stereochemical Effects in the Ozololysis of (E)- and (Z)-1-Ethoxypropene. *J. Org. Chem.* **1989**, *54* (1), 115–121. https://doi.org/10.1021/jo00262a027.

(55) Griesbaum, K.; Kim, W. S. Ozonolyses of Selected Vinyl Ethers. *J. Org. Chem.* **1992**, *57* (21), 5574–5577. https://doi.org/10.1021/jo00047a007.

(56) Sugiyama, T.; Yamakoshi, H.; Nojima, M. Ozonolysis of β-(Alkoxycarbonyl)- and β-Acyl-Substituted Vinyl Ethers. Cycloaddition Chemistry of the Derived α-Keto Ester O-Oxides and α-Diketone O-Oxides. *J. Org. Chem.* **1993**, *58* (16), 4212–4218. https://doi.org/10.1021/jo00068a014.

(57) Bityukov, O. V.; Vil', V. A.; Terent'ev, A. O. Synthesis of Acyclic Geminal Bis-Peroxides. *Russ. J. Org. Chem.* **2021**, *57* (6), 853–878. https://doi.org/10.1134/S1070428021060014.

(58) Terent'ev, A. O.; Borisov, D. A.; Yaremenko, I. A. General Methods for the Preparation of 1,2,4,5-Tetraoxanes - Key Structures for the Development of Peroxidic Antimalarial Agents. *Chem. Heterocycl. Compd.* **2012**, *48* (1), 55–58. https://doi.org/10.1007/s10593-012-0969-3.

(59) Louvel, D.; Miguel, T. D. D.; Vu, N. D.; Duguet, N. The Chemistry of β-Hydroxy Hydroperoxides. *European J. Org. Chem.* **2021**, *2021* (21), 2990–3014. https://doi.org/10.1002/ejoc.202100343.

(60) Bordier, C.; Escande, V.; Darcel, C. Past and Current Routes to β-Hydroxy Hydroperoxides: A Functional Group with High Potential in Organic Synthesis. *Tetrahedron* **2021**, *97* (78), 132379. https://doi.org/10.1016/j.tet.2021.132379.

(61) Etoh, H.; Ina, K.; Iguchi, M. Photosensitized Oxygenation of α-Pyran Derived from β-Ionone. *Agric. Biol. Chem.* **1973**, *37* (10), 2241–2244. https://doi.org/10.1080/00021369.1973.10860982.

(62) Huber, S. N.; Mischne, M. P. A Simple and Efficient Approach for the Synthesis of a 1,2,4-Trioxane Related to Artemisinin. *Nat. Prod. Lett.* **1995**, *7* (1), 37–41. https://doi.org/10.1080/10575639508043185.

(63) Singh, R.; Ishar, M. P. S. UV Irradiation of Arylidene-β-Ionones in the Presence of Dioxygen: Regioselective Formation of Stable Endoperoxides. *Tetrahedron Lett.* **2003**, *44* (9), 1943–1945. https://doi.org/10.1016/S0040-4039(03)00086-8.

(64) Cole, K. P.; Hsung, R. P. Unique Structural Topology and Reactivities of the ABD Tricycle in Phomactin A. *Chem. Commun.* **2005**, No. 46, 5784–5786. https://doi.org/10.1039/b511338e.

(65) Zhang, Q.; Jin, H.-X.; Wu, Y. A Facile Access to Bridged 1,2,4-Trioxanes. *Tetrahedron* **2006**, *62* (50), 11627–11634. https://doi.org/10.1016/j.tet.2006.09.061.

(66) Zhang, Q.; Wu, Y. Further Explorations on Bridged 1,2,4-Trioxanes. *Tetrahedron* **2007**, *63* (41), 10189–10201. https://doi.org/10.1016/j.tet.2007.07.090.

(67) Ramirez, A. P.; Thomas, A. M.; Woerpel, K. A. Preparation of Bicyclic 1,2,4-Trioxanes from γ,δ-Unsaturated Ketones. *Org. Lett.* **2009**, *11* (2), 507–510. https://doi.org/10.1021/ol8022853.

(68) Abdulla, S.; Sagara, I. Dispersible Formulation of Artemether/Lumefantrine: Specifically Developed for Infants and Young Children. *Malar. J.* **2009**, *8* (Suppl 1), S7.

https://doi.org/10.1186/1475-2875-8-S1-S7.

(69) Abdulla, S.; Sagara, I.; Borrmann, S.; D'Alessandro, U.; González, R.; Hamel, M.; Ogutu, B.; Mårtensson, A.; Lyimo, J.; Maiga, H.; Sasi, P.; Nahum, A.; Bassat, Q.; Juma, E.; Otieno, L.; Björkman, A.; Beck, H. P.; Andriano, K.; Cousin, M.; Lefèvre, G.; Ubben, D.; Premji, Z. Efficacy and Safety of Artemether-Lumefantrine Dispersible Tablets Compared with Crushed Commercial Tablets in African Infants and Children with Uncomplicated Malaria: A Randomised, Single-Blind, Multicentre Trial. *Lancet* **2008**, *372* (9652), 1819–1827. https://doi.org/10.1016/S0140-6736(08)61492-0.

(70) Djimdé, A. A.; Tekete, M.; Abdulla, S.; Lyimo, J.; Bassat, Q.; Mandomando, I.; Lefèvre, G.; Borrmann, S.; B2303 Study Group. Pharmacokinetic and Pharmacodynamic Characteristics of a New Pediatric Formulation of Artemether-Lumefantrine in African Children with Uncomplicated *Plasmodium falciparum* Malaria. *Antimicrob. Agents Chemother.* **2011**, *55* (9), 3994–3999. https://doi.org/10.1128/AAC.01115-10.

(71) John, C. C. Primaquine plus Artemisinin Combination Therapy for Reduction of Malaria Transmission: Promise and Risk. *BMC Med.* **2016**, *14*, 65. https://doi.org/10.1186/s12916-016-0611-9.

(72) WHO. *Guidelines for the Treatment of Malaria, 2nd Edition*; 2010.

(73) Rawe, S. L. Artemisinin and Artemisinin-Related Agents. In *Antimalarial Agents*; Elsevier Ltd, 2020; pp 99–132. https://doi.org/10.1016/B978-0-08-101210-9.00004-4.

(74) Dondorp, A. M.; Nosten, F.; Yi, P.; Das, D.; Phyo, A. P.; Tarning, J.; Lwin, K. M.; Ariey, F.; Hanpithakpong, W.; Lee, S. J.; Ringwald, P.; Silamut, K.; Imwong, M.; Chotivanich, K.; Lim, P.; Herdman, T.; An, S. S.; Yeung, S.; Singhasivanon, P.; Day, N. P. J.; Lindegardh, N.; Socheat, D.; White, N. J. Artemisinin Resistance in *Plasmodium falciparum* Malaria. *N. Engl. J. Med.* **2009**, *361* (5), 455–467. https://doi.org/10.1056/NEJMoa0808859.

(75) WHO. Status Report on Artemisinin and ACT Resistance (April 2017).

(76) Rosenthal, M. R.; Ng, C. L. *Plasmodium falciparum* Artemisinin Resistance: The Effect of Heme, Protein Damage, and Parasite Cell Stress Response. *ACS Infect. Dis.* **2020**, *6* (7), 1599–1614. https://doi.org/10.1021/acsinfecdis.9b00527.

(77) Neill, P. M. O.; Posner, G. H. Perspective A Medicinal Chemistry Perspective on Artemisinin and Related Endoperoxides. *J. Med. Chem.* **2004**, *47* (12), 2945–2964. https://doi.org/10.1021/jm030571c.

(78) Vennerstrom, J. L.; Arbe-Barnes, S.; Brun, R.; Charman, S. A.; Chiu, F. C. K.; Chollet, J.; Dong, Y.; Dorn, A.; Hunziker, D.; Matile, H.; McIntosh, K.; Padmanilayam, M.; Santo Tomas, J.; Scheurer, C.; Scorneaux, B.; Tang, Y.; Urwyler, H.; Wittlin, S.; Charman, W. N. Identification of an Antimalarial Synthetic Trioxolane Drug Development Candidate. *Nature* **2004**, *430* (7002), 900–904. https://doi.org/10.1038/nature02779.

(79) Charman, S. A.; Arbe-Barnes, S.; Bathurst, I. C.; Brun, R.; Campbell, M.; Charman, W. N.; Chiu, F. C. K.; Chollet, J.; Craft, J. C.; Creek, D. J.; Dong, Y.; Matile, H.; Maurer, M.; Morizzi, J.; Nguyen, T.; Papastogiannidis, P.; Scheurer, C.; Shackleford, D. M.; Sriraghavan, K.; Stingelin, L.; Tang, Y.; Urwyler, H.; Wang, X.; White, K. L.; Wittlin, S.; Zhou, L.; Vennerstrom, J. L. Synthetic Ozonide Drug Candidate OZ439 Offers New Hope for a Single-Dose Cure of Uncomplicated Malaria. *Proc. Natl. Acad. Sci. U. S. A.* **2011**, *108* (11), 4400–4405. https://doi.org/10.1073/pnas.1015762108.

(80) Phyo, A. P.; Jittamala, P.; Nosten, F. H.; Pukrittayakamee, S.; Imwong, M.; White, N. J.; Duparc, S.; Macintyre, F.; Baker, M.; Möhrle, J. J. Antimalarial Activity of Artefenomel (OZ439), a Novel Synthetic Antimalarial Endoperoxide, in Patients with *Plasmodium falciparum* and *Plasmodium vivax* Malaria: An Open-Label Phase 2 Trial. *Lancet Infect. Dis.* **2016**, *16* (1), 61–69. https://doi.org/10.1016/S1473-3099(15)00320-5.

(81) O'Neill, P. M.; Amewu, R. K.; Charman, S. A.; Sabbani, S.; Gnädig, N. F.; Straimer, J.; Fidock, D. A.; Shore, E. R.; Roberts, N. L.; Wong, M. H.-L.; Hong, W. D.; Pidathala, C.; Riley, C.; Murphy, B.; Aljayyoussi, G.; Gamo, F. J.; Sanz, L.; Rodrigues, J.; Cortes, C. G.; Herreros, E.; Angulo-Barturén, I.; Jiménez-Díaz, M. B.; Bazaga, S. F.; Martínez-Martínez, M. S.; Campo, B.; Sharma, R.; Ryan, E.; Shackleford, D. M.; Campbell, S.; Smith, D. A.; Wirjanata, G.; Noviyanti, R.; Price, R. N.; Marfurt, J.; Palmer, M. J.; Copple,

I. M.; Mercer, A. E.; Ruecker, A.; Delves, M. J.; Sinden, R. E.; Siegl, P.; Davies, J.; Rochford, R.; Kocken, C. H. M.; Zeeman, A.-M.; Nixon, G. L.; Biagini, G. A.; Ward, S. A. A Tetraoxane-Based Antimalarial Drug Candidate That Overcomes PfK13-C580Y Dependent Artemisinin Resistance. *Nat. Commun.* **2017**, *8*, 15159. https://doi.org/10.1038/ncomms15159.

(82) Ghorai, P.; Dussault, P. H. Broadly Applicable Synthesis of 1,2,4,5-Tetraoxanes. *Org. Lett.* **2009**, *11* (1), 213–216. https://doi.org/10.1021/ol8023874.

(83) Sashidhara, K. V.; Avula, S. R.; Ravithej Singh, L.; Palnati, G. R. A Facile and Efficient Bi(III) Catalyzed Synthesis of 1,1-Dihydroperoxides and 1,2,4,5-Tetraoxanes. *Tetrahedron Lett.* **2012**, *53* (36), 4880–4884. https://doi.org/10.1016/j.tetlet.2012.07.001.

(84) Das, B.; Thirupathi, P. A Highly Selective and Efficient Acetylation of Alcohols and Amines with Acetic Anhydride Using NaHSO4·SiO2 as a Heterogeneous Catalyst. *J. Mol. Catal. A Chem.* **2007**, *269* (1–2), 12–16. https://doi.org/10.1016/j.molcata.2006.12.029.

(85) Sardarian, A. R.; Inaloo, I. D.; Modarresi-Alam, A. R.; Kleinpeter, E.; Schilde, U. Metal-Free Regioselective Monocyanation of Hydroxy - , Alkoxy- , and Benzyloxyarenes by Potassium Thiocyanate and Silica Sulfuric Acid as a Cyanating Agent. *J. Org. Chem.* **2019**, *84* (4), 1748–1756. https://doi.org/10.1021/acs.joc.8b02191.

(86) Azarifar, D.; Najminejad, Z.; Khosravi, K. Synthesis of Gem-Dihydroperoxides from Ketones and Aldehydes Using Silica Sulfuric Acid as Heterogeneous Reusable Catalyst. *Synth. Commun.* **2013**, *43* (6), 826–836. https://doi.org/10.1080/00397911.2011.610549.

(87) Oh, C. H.; Kang, J. H. A Convenient Synthesis of Substituted 1,2,4-Trioxepanes via Co(II) Catalyzed Oxygenation of Cinnamyl Alcohol. *Tetrahedron Lett.* **1998**, *39* (18), 2771–2774. https://doi.org/10.1016/S0040-4039(98)00335-9.

(88) O'Neill, P. M.; Hindley, S.; Pugh, M. D.; Davies, J.; Bray, P. G.; Park, B. K.; Kapu, D. S.; Ward, A.; Stocks, P. A. $Co(Thd)_2$: A Superior Catalyst for Aerobic Epoxidation and Hydroperoxysilylation of Unactivated Alkenes: Application to the Synthesis of Spiro-1,2,4-Trioxanes. *Tetrahedron Lett.* **2003**, *44* (44), 8135–8138. https://doi.org/10.1016/j.tetlet.2003.09.033.

(89) Taylor, P.; Salehi, P.; Dabiri, M.; Zolfigol, A.; Fard, A. B. Silica Sulfuric Acid; An Efficient and Reusable Catalyst for Regioselective Ring Opening of Epoxides by Alcohols and Water. *Phosphorus, Sulfur, and Silicon* **2004**, *179* (6), 1113–1121. https://doi.org/10.1080/10426500490459722.

(90) Kiasat, A. R.; Fallah-Mehrjardi, M. B(HSO4)3 : A Novel and Efficient Solid Acid Catalyst for the Regioselective Conversion of Epoxides to Thiocyanohydrins under Solvent-Free Conditions. *J. Braz. Chem. Soc.* **2008**, *19* (8), 1595–1599. https://doi.org/10.1590/S0103-50532008000800020.

(91) Frisch, M. J.; Trucks, G. W.; Schlegel, H. B.; Scuseria, G. E.; Robb, M. A.; Cheeseman, J. R.; Scalmani, G.; Barone, V.; Mennucci, B.; Petersson, G. A.; Nakatsuji, H.; Caricato, M.; Li, X.; Hratchian, H. P.; Izmaylov, A. F.; Bloino, J.; Zheng, G.; Sonnenberg, J. L.; Hada, M.; Ehara, M.; Toyota, K.; Fukuda, R.; Hasegawa, J.; Ishida, M.; Nakajima, T.; Honda, Y.; Kitao, O.; Nakai, H.; Vreven, T.; Jr., J. A. M.; Peralta, J. E.; Ogliaro, F.; Bearpark, M.; Heyd, J. J.; Brothers, E.; Kudin, K. N.; Staroverov, V. N.; Kobayashi, R.; Normand, J.; Raghavachari, K.; Rendell, A.; Burant, J. C.; Iyengar, S. S.; Tomasi, J.; Cossi, M.; Rega, N.; Millam, J. M.; Klene, M.; Knox, J. E.; Cross, J. B.; Bakken, V.; Adamo, C.; Jaramillo, J.; Gomperts, R.; Stratmann, R. E.; Yazyev, O.; Austin, A. J.; Cammi, R.; Pomelli, C.; Ochterski, J. W.; Martin, R. L.; Morokuma, K.; Zakrzewski, V. G.; Voth, G. A.; Salvador, P.; Dannenberg, J. J.; Dapprich, S.; Daniels, A. D.; Ö. Farkas; Foresman, J. B.; Ortiz, J. V.; Cioslowski, J.; Fox, D. J. GAUSSIAN 09 (Revision D.01), Gaussian, Inc.: Wallingford CT, 2009.

(92) CYLview, 1.0b; Legault, C. Y., Université de Sherbrooke, 2009 (http://www.cylview.org)

(93) Chai, J.-D.; Head-Gordon, M. Long-Range Corrected Hybrid Density Functionals with Damped Atom–Atom Dispersion Corrections. *Phys. Chem. Chem. Phys.* **2008**, *10* (44), 6615–6620. https://doi.org/10.1039/b810189b.

(94) Cancès, E. A New Integral Equation Formalism for the Polarizable Continuum Model: Theoretical Background and Applications to Isotropic and Anisotropic Dielectrics. *J.*

*Chem. Phys.* **1997**, *107* (8), 3032–3041. https://doi.org/10.1063/1.474659.

(95) Cossi, M.; Barone, V.; Mennucci, B.; Tomasi, J. *Ab Initio* Study of Ionic Solutions by a Polarizable Continuum Dielectric Model. *Chem. Phys. Lett.* **1998**, *286* (3–4), 253–260. https://doi.org/10.1016/S0009-2614(98)00106-7.

(96) Mennucci, B.; Tomasi, J. Continuum Solvation Models: A New Approach to the Problem of Solute's Charge Distribution and Cavity Boundaries. *J. Chem. Phys.* **1997**, *106* (12), 5151–5158. https://doi.org/10.1063/1.473558.

(97) Tomasi, J.; Mennucci, B.; Cammi, R. Quantum Mechanical Continuum Solvation Models. *Chem. Rev.* **2005**, *105* (8), 2999–3094. https://doi.org/10.1021/cr9904009.

(98) Marenich, A. V; Cramer, C. J.; Truhlar, D. G. Universal Solvation Model Based on Solute Electron Density and on a Continuum Model of the Solvent Defined by the Bulk Dielectric Constant and Atomic Surface Tensions. *J. Phys. Chem.* **2009**, *113* (18), 6378–6396. https://doi.org/10.1021/jp810292n.

(99) Roy, B.; Mukhopadhyay, B. Sulfuric Acid Immobilized on Silica: An Excellent Catalyst for Fischer Type Glycosylation. *Tetrahedron Lett.* **2007**, *48* (22), 3783–3787. https://doi.org/10.1016/j.tetlet.2007.03.165.

(100) Sabbani, S.; Stocks, P. A.; Ellis, G. L.; Davies, J.; Hedenstrom, E.; Ward, S. A.; Neill, P. M. O. Piperidine Dispiro-1,2,4-Trioxane Analogues. *Bioorg. Med. Chem. Lett.* **2008**, *18* (21), 5804–5808. https://doi.org/10.1016/j.bmcl.2008.09.052.

(101) Li, W.-R.; Yo, Y.-C.; Lin, Y.-S. Efficient One-Pot Formation of Amides from Benzyl Carbamates: Application to Solid-Phase Synthesis. *Tetrahedron* **2000**, *56* (45), 8867–8875. https://doi.org/10.1016/S0040-4020(00)00850-4.

(102) Marti, F.; Chadwick, J.; Amewu, R. K.; Burrell-Saward, H.; Srivastava, A.; Ward, S. A.; Sharma, R.; Berry, N.; O'Neill, P. M. Second Generation Analogues of RKA182: Synthetic Tetraoxanes with Outstanding *in vitro* and *in vivo* antimalarial Activities. *Med. Chem. Commun* **2011**, *2* (7), 661–665. https://doi.org/10.1039/c1md00102g.

(103) Oliveira, R.; Newton, A. S.; Guedes, R. C.; Miranda, D.; Amewu, R. K.; Srivastava, A.; Gut, J.; Rosenthal, P. J.; O'Neill, P. M.; Ward, S. A.; Lopes, F.; Moreira, R. An Endoperoxide-Based Hybrid Approach to Deliver Falcipain Inhibitors Inside Malaria Parasites. *ChemMedChem* **2013**, *8* (9), 1528–1536. https://doi.org/10.1002/cmdc.201300202.

# Chapter 5

## Unravelling the structure of peroxides with antiparasitic activity: relative impact of a trioxolane or a tetraoxane pharmacophore on the overall molecular structure

# Chapter 5

Part of the work described in this section was included in the following publication:

**Amado, P. S. M.;** Jesus, A. J..; Paixão, J. A.; Fausto, R. and Cristiano, M. L. S. Unravelling the structure of peroxides with antiparasitic activity: relative impact of a trioxolane or a tetraoxane pharmacophore on the overall molecular structure. *ChemPlusChem.* **2022,** *87* (8), e202200207. https://doi.org/10.1002/cplu.202200207

**CONTRIBUTIONS**

Patrícia S. M. Amado designed and carried out the synthesis and characterization of all compounds. DFT calculations and Hirshfeld surface analysis were performed by Prof. António J. L. Jesus (CQC-IMS, Faculty of Pharmacy, University of Coimbra) and Prof. Rui Fausto (CQC-IMS, Department of Chemistry, University of Coimbra). X-ray crystallographic studies were performed by Prof. José A. Paixão (CFisUC, Department of Physics, University of Coimbra). Prof. Maria de Lurdes Cristiano designed the investigation, supervised the work, and revised the manuscript. All authors have contributed to the discussion of the results and participated in writing the manuscript.

## 5.1. Summary

This chapter presents a general overview of the results obtained from our investigations on the structure of two endoperoxide building blocks used in the synthesis of the antimalarial candidates **OZ439** and **E209,** which incorporate the pharmacophoric moieties trioxolane and tetraoxane, respectively. By combining X-ray crystallography and vibrational spectroscopy, along with Hirshfeld surface analysis and calculations (CE-B3LYP/6-31G(d,p)) of pairwise interaction energies of intermolecular contacts existing in the crystal structure, this structural study allowed us to deepen the understanding of the relative reactivity and the properties of the two endoperoxide classes.

## 5.2. Introduction

The rise and spread of *Plasmodium falciparum* resistance to artemisinin-based combination therapy in Southeast Asia stimulated the search for novel plasmodial "fast killers". Endoperoxide-derived compounds have been shown to offer alternative solutions to ARTs.[1,2] Selected synthetic 1,2,4-trioxolanes[3,4] and 1,2,4,5-tetraoxanes[5–7] proved particularly promising in this context, exhibiting anti-malarial activity similar or higher than ARTs.[8] Besides their impressive antimalarial activity,[7–9] 1,2,4-trioxolanes and 1,2,4,5-tetraoxanes revealed other biological activities, namely anticancer,[10–16] antimycobacterial,[17,18] antiprotozoan,[13,19–21] and antiparasitic.[22–28]

Meanwhile, synthetic routes have been developed for both compound classes, enabling the preparation of a chemically diverse range of analogues for the selection of leads, optimization, and development into anti-malarial drugs or drug candidates. This approach has yielded the ozonide **OZ439** (artefenomel, **Figure 5.1**),[29] which is currently on Phase IIb of clinical trials,[30,31] and the 1,2,4,5-tetraoxane **E209** (**Figure 5.1**),[7] a superior next-generation endoperoxide with combined pharmacokinetic and pharmacodynamic features that overcome PfK13-C580Y-dependent artemisinin resistance, the main liability of artemisinin derivatives nowadays.[32] Despite their potential medical and veterinary applications, fundamental studies on the structures of trioxolanes and tetraoxanes are scarce.

In the present section, we disclose results of our investigations on the structures of *p*-(dispiro-[cyclohexane-1,3'-[1,2,4]trioxolane-5',2''-tricyclo [3.3.1.1$^{3,7}$]decan]-4-yl)-phenyl acetate (**1**; **Figure 5.1**) and of *p*-(dispiro-[cyclohexane-1,3'-[1,2,4,5]tetraoxane-6',2''-tricyclo[3.3.1.1$^{3,7}$]decan]-4-yl)-phenyl acetate (**2**; **Figure 5.1**), the peroxide

building blocks used in the synthesis of the antimalarial candidates **OZ439** and **E209** (**Figure 5.1**). Since compounds **1** and **2** differ only in their peroxide pharmacophoric moiety, a detailed analysis of their structure, more precisely the relative effect of a trioxolane or a tetraoxane ring on the overall molecule, may contribute to a better understanding of the reactivity and activity of these classes of endoperoxides.

Over the last few years, tools based on Hirshfeld surfaces have become increasingly popular for molecular crystal structure investigation, proving to be an excellent tool to analyse intermolecular interactions by an unbiased identification of all close contacts.[33] Hence, the structures of compounds **1** and **2** were investigated in the condensed phase, using X-ray crystallography and infrared spectroscopy. A deep analysis of the intermolecular contacts existing in the crystal structure of both compounds was then undertaken by performing a Hirshfeld surface analysis, followed by a calculation of the pairwise interaction energies.

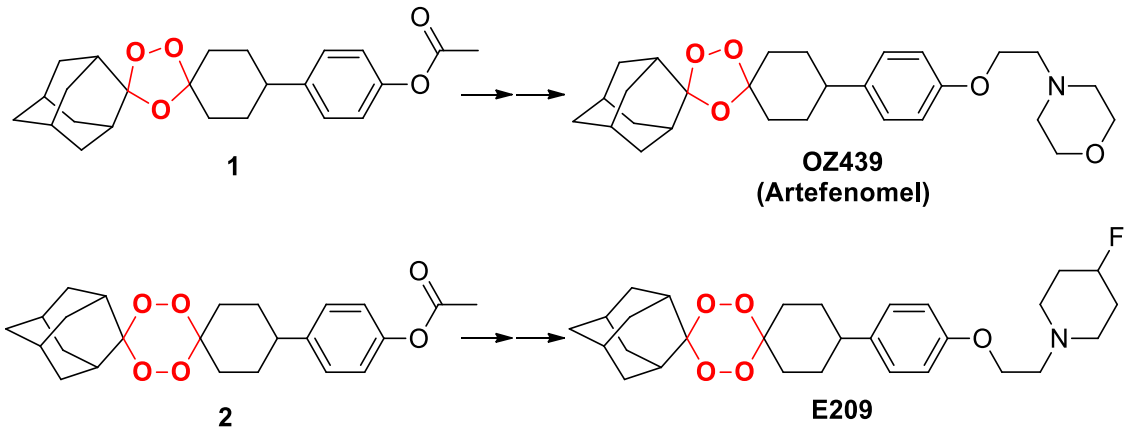


**Figure 5.1.** Structural representations of endoperoxides **1**, **2** and antimalarial candidates **OZ439** and **E209**.

## 5.3. Results and discussion

### 5.3.1. Synthesis

1,2,4-trioxolane **1**, 1,2,4,5-tetraoxane **2**, and the intermediate compounds for their preparation were synthesized using the synthetic strategies depicted in **Scheme 5.1**. Detailed procedures for compounds synthesis and characterization are described in the Experimental Section (Section 5.5.1). The synthesis starts with acetate protection of the commercially available 4-(4-hydroxyphenyl) cyclohexanone to achieve **5.1** and

preparation of the *O*-methyloxime derivative **5.2** from adamantan-2-one. A convergent strategy was followed, whereby the intermediate building blocks prepared were assembled through a Griesbaum coozonolysis reaction, as described in the literature,[2] affording 1,2,4-trioxolane **1** in 33% yield. Peroxidation of **5.1** allows the formation of the *gem*-dihydroperoxide **5.3** when using the heterogeneous catalyst SSA *(Please see more details about this procedure in Chapter 4*). After work-up, and without any further purification, this intermediate was subjected to a cyclisation reaction with adamantan-2-one in the presence of the heterogeneous catalyst silica sulfuric acid, according to the procedure developed and described in Chapter 4, providing the 1,2,4,5-tetraoxane **2** in 67% yield.

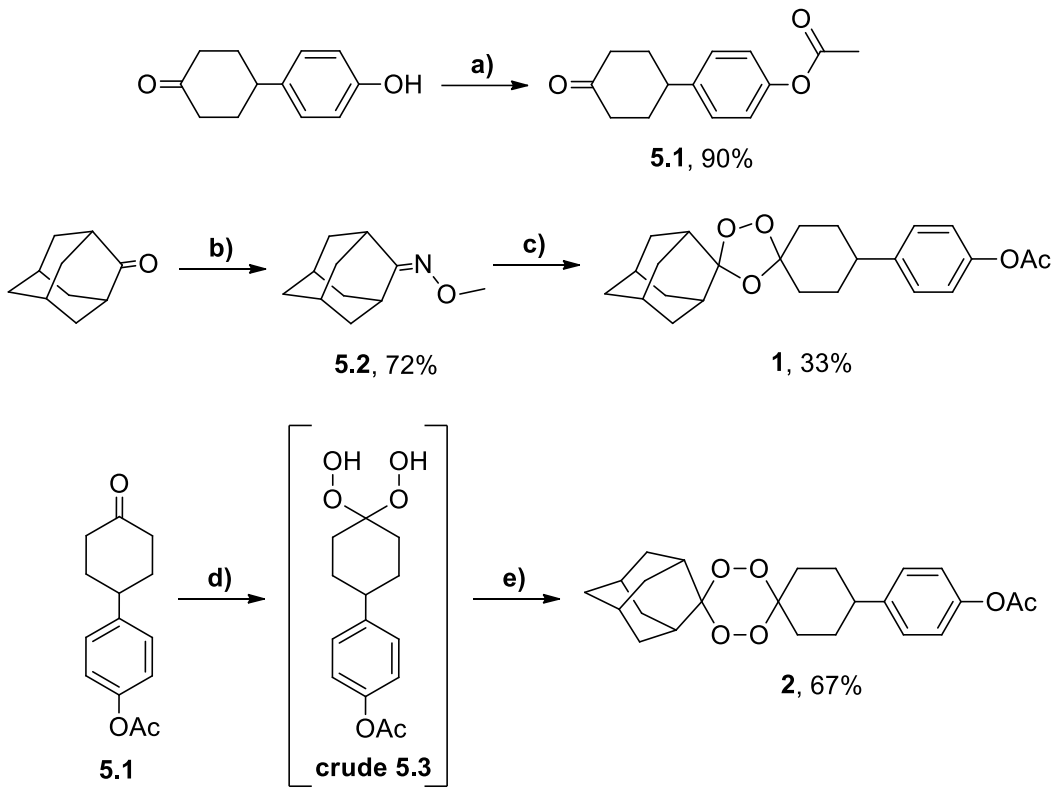


**Scheme 5.1.** Synthetic routes for the preparation of 1,2,4-trioxolane **1,** 1,2,4,5-tetraoxane **2**. Reagents and conditions: (a) Acetic anhydride, $Et_3N$, $CH_2Cl_2$, 0 ºC-r.t., 12 h; (b) $MeONH_2$, Pyridine, MeOH, r.t., 72 h; (c) **5.1**, $O_3$, $CH_2Cl_2$/pentane, 0 ºC, 30 min; (d) $H_2O_2$ (50% *w/w*), $H_2SO_4$-$SiO_2$, $CH_3CN$, 0 ºC-r.t., 2 h; (e) Adamantan-2-one, $H_2SO_4$-$SiO_2$, anhydrous $CH_2Cl_2$, 0 ºC-rt, 1 h.

## 5.3.2. Crystal structure of the title compounds

X-ray crystallographic analysis shows that compound **1** crystallizes in the monoclinic, non-centrosymmetric, *Cc* space group with $a$ = 6.7018(5), $b$ = 29.084(2), $c$ = 10.8383(8) Å, $\beta$ = 97.618(3)º, with four molecules per unit cell ($Z$ = 4). Crystals of compound **2** are also monoclinic, belonging to the centrosymmetric $P2_1/c$ space group, with $a$ = 19.4375(6), $b$ = 8.3355(2) and $c$ = 13.8160(4) Å, $\beta$ = 107.6820(10)º and $Z$ = 4. Details of the crystallographic results, data collection and structure refinement are given in **Table 5.1**.

Compounds **1** and **2** exhibit conformational disorder in the crystalline state. In **1** it affects one of the trioxolane ring atoms (O1), which may assume two positions, and the whole adamantane fragment (see **Figures 5.2** and **5.3**). The occupation of the two alternative conformations (**1A** and **1B**) are almost identical: 52% for **1A** and 48% for **1B**. In **2**, the disorder affects only the tetraoxane ring, with the four oxygen atoms assuming two positions, originating two different conformations (**2A** and **2B**), which can be interconverted by ring flipping (see **Figures 5.2** and **5.3**). Their relative occurrence in the crystal was determined to be 87 and 13%, respectively.

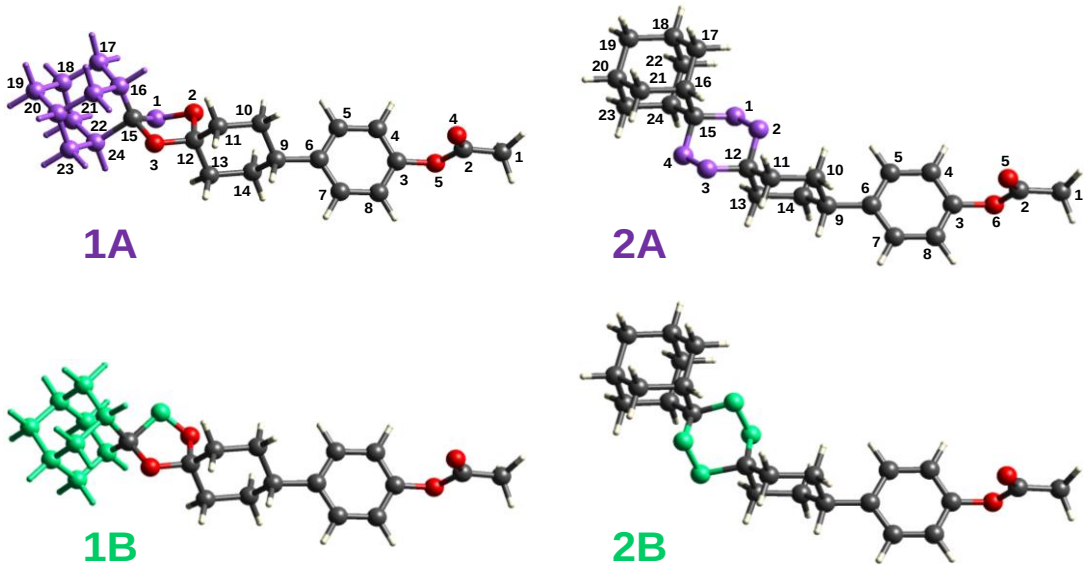


**Figure 5.2.** Conformations **A** and **B** adopted by compounds **1** and **2** in the crystal structure. Disordered fragments are highlighted as violet in conformation **A** and as green in conformation **B**. Atom numbering of the heavy atoms is included in conformation **A** of both compounds.

**Table 5.1.** Summary of the single-crystal X-ray data collections and crystal structure refinements.

| | **Compound 1** | **Compound 2** |
|---|---|---|
| **Chemical formula** | $C_{24}H_{30}O_5$ | $C_{24}H_{30}O_6$ |
| **Formula weight** | 398.48 | 414.48 |
| **Color, shape** | Colourless, block | Colourless, block |
| **Space group** | *Cc* | $P2_1/c$ |
| **Temperature (K)** | 293(2) | 294(2) |
| **Cell volume (Å $^3$)** | 2093.9(3) | 2132.73(10) |
| **Crystal system** | monoclinic | monoclinic |
| ***a* (Å)** | 6.7018(5) | 19.4375(6) |
| ***b* (Å)** | 29.084(2) | 8.3355(2) |
| ***c* (Å)** | 10.8383(8) | 13.8160(4) |
| ***α* (deg)** | 90 | 90 |
| ***β* (deg)** | 97.618(3) | 107.6820(10) |
| ***γ* (deg)** | 90 | 90 |
| ***Z,Z´*** | 4,1 | 4,1 |
| $D_c$ **(Mg m$^{-3}$)** | 1.264 | 1.291 |
| **Radiation (Å)** | 0.71073 | 0.71073 |
| **Max. crystal dimensions (mm)** | 0.26×0.21×0.18 | 0.32×0.25×0.22 |
| ***θ* range (deg)** | 3.383 – 27.490 | 2.199 – 27.499 |
| **Range of *h, k, l*** | –8,8; –37,37; –14,14 | –25,25; –10,10; –17,17 |
| **Reflections measured/independent** | 25764 / 4792 | 118816 / 4884 |
| **Reflections observed (*I* > 2 σ)** | 2925 | 3349 |
| **Data/restraints/parameters** | 4792/2/355 | 4884/0/309 |
| **GOF** | 1.006 | 1.019 |
| $R_1$ **(*I* >2 σ)** | 0.0437 | 0.0589 |
| $wR_2$ | 0.1073 | 0.1719 |
| **Function minimized** | $\Sigma\, w\,(\|F_o\|^2 - S\|F_c\|^2)$ | $\Sigma\, w\,(\|F_o\|^2 - S\|F_c\|^2)$ |
| **Diff. density final max/min (*e* Å$^{-3}$)** | 0.203, –0.158 | 0.366, –0.251 |

In addition to the conformational disorder of the trioxolane/tetraoxane rings, both molecules of compounds **1** and **2** feature conformational flexibility on rotation around the single C6−C9, C3−O5 (**1**) or C3−O6 (**2**), and C2−O5 (**1**) or C2−O6 (**2**) bonds (**Figure 5.3**).

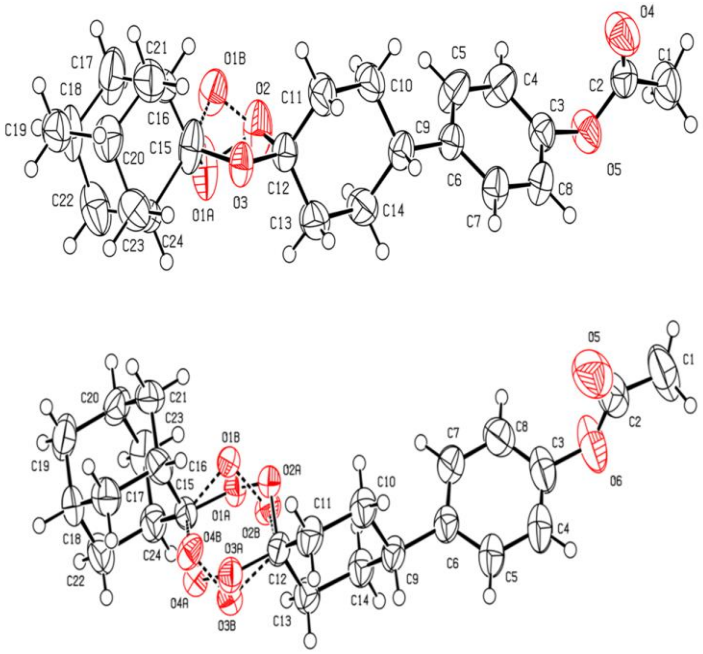


**Figure 5.3.** Oak Ridge Thermal Ellipsoid Plots (ORTEP) depicting the anisotropic displacement ellipsoids drawn at the 50 % probability level and the atom numbering schemes for compound **1** (*top*) and compound **2** (*bottom*). In compound **1** the adamantane group is disordered over two alternate positions; for the sake of clarity, only one of the two alternate conformations of the adamantane fragment is shown.

In compound **1**, the cyclohexane ring occurs in the usual chair conformation, with a weighted average torsion angle of 55.0(6)º and Cremer-Pople[34] puckering parameters $Q$ = 0.588(4) Å, $\theta$ = 177.2(4)º, $\varphi$ = 181(7)º and an average C−C bond length of 1.513(6) Å. The bond linking the phenylacetate substituent to the cyclohexane ring is in equatorial position. The cyclohexane ring is closely orthogonal to the approximate mirror plane passing through atoms C15−O3−C12 of the (disordered) adamantane-trioxolane part of the molecule, but the phenyl ring is neither coplanar nor orthogonal to this mirror plane. The angle between the least squares plane of the phenyl and cyclohexane rings is 52.7(1)º whereas that between the phenyl and acetate planes is 74.9(1)º, with a C4−C3−O5−C2 torsion angle of 75.7(4)º. Both components of the disordered 5-membered trioxolane ring have conformations close to O1A/O1B-envelope, as shown by the puckering parameters (for the main component) of $q_2$= 0.511(5) Å and $\varphi_2$ =178.7(4)º, corresponding to pseudo-rotation parameters[35] $P$ = 268.6(3)º and $\tau_m$ =53.0(3)º, taking C12−O3 as the reference bond.

In compound **2**, the cyclohexane is close to an ideal chair conformation ($Q$ = 0.555(2)

Å, $\theta$ = 179.8(2)º, $\varphi$ = 309(11)º), with average ring torsion angle of 54.6(5)º and C—C bond length of 1.520(3) Å. The same statement is true also for the two alternate conformations of the 6-membered tetraoxane ring (A: $Q$ = 0.665(2) Å, $\theta$ = 1.6(2)º, $\varphi$ = 269(7)º; B: $Q$ = 1.065(11) Å, $\theta$ = 178.1(6)º, $\varphi$ = 333(17)º.

Interestingly, and differently from compound **1**, the least-squares plane of tetraoxane and phenyl rings are almost coplanar [angle is 7.8(4)º], and close to orthogonal [angle is 86.46(8)º] to the least-squares plane of the cyclohexane ring. Also, the acetate moiety is closer to orthogonality with respect to the phenyl ring [85.12(12)º].

**Figure 5.4** shows the packing of the molecules in the crystals of compound **1** and **2**, depicting also the main intermolecular interactions. These are analysed in detail in the next section, thereby here only a brief description is presented. For both compounds, as they lack a strong donor for hydrogen bonding, cohesion of the crystals is achieved through van der Walls interactions and weak C−H···O and C-H···**π** interactions only. In compound **1**, the most relevant of the C−H···O interactions, based only on the analysis of the H···O distances and C−H···O angles in the crystal, is that between an H atom of the adamantane moiety (adopting configuration B) and the O2 atom of the trioxolane ring, acting as acceptor. This bond links the molecules in chains propagating along the *c*-axis as shown in **Figure 5.4A**. In compound **2** the most relevant of such interactions involves atom O5 of the acetate substituent, acting as double acceptor from the H-atoms of the phenyl ring connected to C5 and C7, in this case linking molecules in chains propagating along the crystallographic *b*-axis, as shown in **Figure 5.4B**.

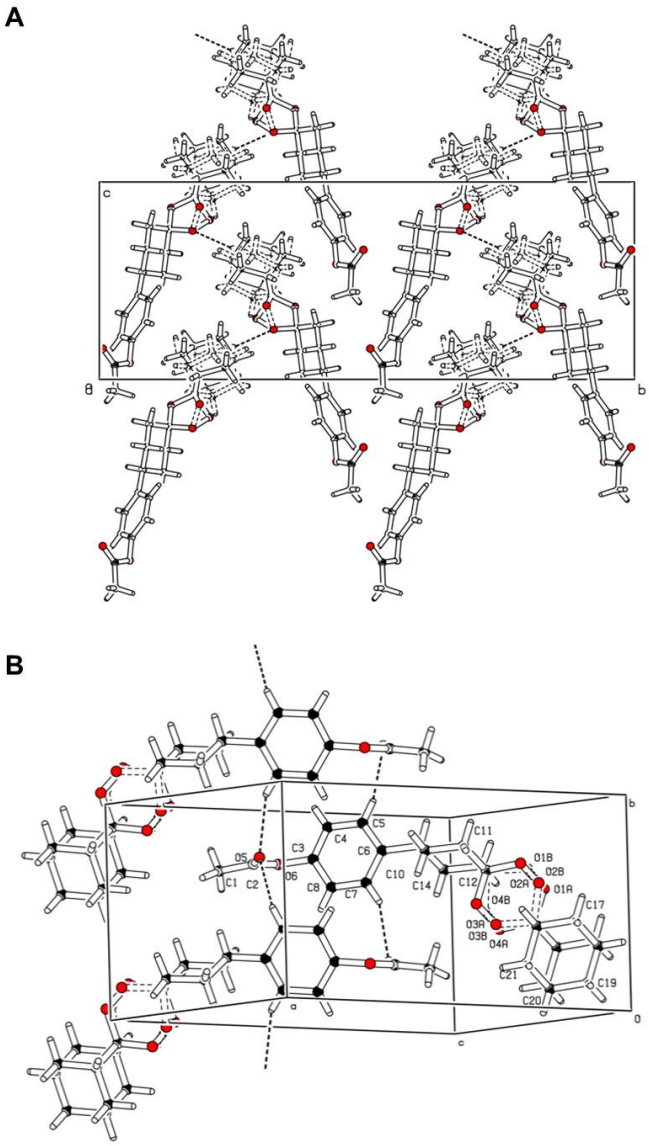


**Figure 5.4.** Crystal packing of the molecules of compound **1** (**A**) and **2** (**B**), depicting the main C−H···O interactions as dotted lines (**1**: C19−H···O2$^{i}$, i = −1/2+*x*,1/2−*y*,1/2+*z*; **2**: C5−H···O5$^{ii}$ ii= 1−*x*, 1/2+*y*,3/2−*z*) and C7−H···O5$^{iii}$ , iii= 1−*x*, −1/2+*y*,3/2−*z*).

## 5.3.3. Hirshfeld surface analysis

The $d_{norm}$ Hirshfeld surfaces (HSs) generated for compounds **1** and **2** are represented in **Figure 5.5.** For better visualization of the contacts, labelled as lower-case letters, the surfaces are presented as transparent and some of the molecules closer to the mapped molecule are also shown. The identified D−H···A hydrogen bonds (D and A are the donor and acceptor atoms, respectively) keep the label of the corresponding H···A contacts and are geometrically characterized in **Table 5.2**.

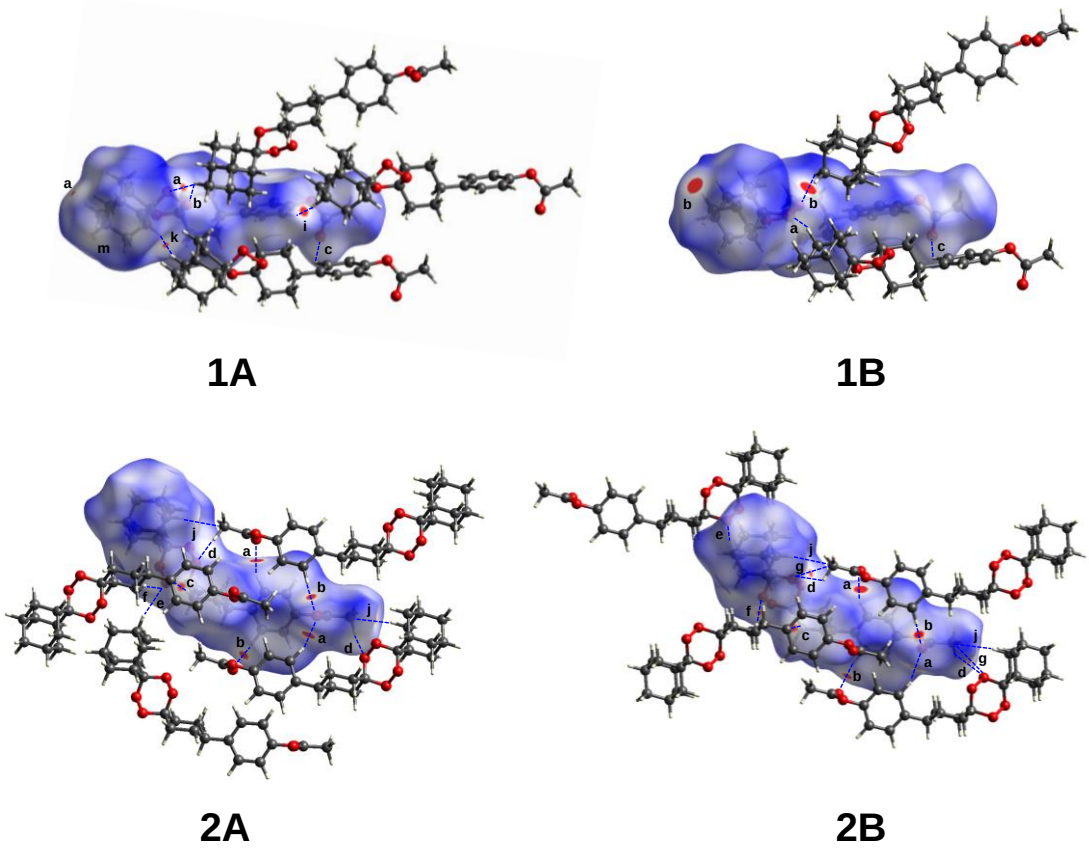


**Figure 5.5.** Three-dimensional Hirshfeld surface generated for conformations **A** and **B** of compounds **1** and **2**, mapped with the normalized contact distance ($d_{norm}$). Relevant intermolecular contacts are denoted by small letters and represented as dashed lines.

**Table 5.2.** Geometric characterization of the intermolecular hydrogen bonds (D−H···A) found in the crystal structure of compounds **1** and **2**.[a]

| Interaction | Label | Conf. | H···A / Å | D···A / Å | D−H···A / º |
|---|---|---|---|---|---|
| **Compound 1** | | | | | |
| **C19−H···O1** (i) | a | A | 2.54 | 3.57 | 160.1 |
| **C23−H···O1** (ii) | a | B | 2.66 | 3.31 | 117.8 |
| **C19−H···O2** (i) | b | A | 2.66 | 3.44 | 129.2 |
| **C19−H···O2** (i) | b | B | 2.34 | 3.21 | 136.7 |
| **C7−H···O4** (ii) | c | A/B | 2.72 | 3.47 | 126.4 |
| **C1−H···π** (iii) | d | A/B | 2.84 | 3.85 | 154.5 |
| **C21−H···π** (iv) | e | A | 3.00 | 3.58 | 114.1 |
| **C21−H···π** (iv) | e | B | 3.33 | 3.98 | 120.1 |
| **Compound 2** | | | | | |
| **C5−H···O5** (v) | a | A/B | 2.39 | 3.41 | 155.3 |
| **C7−H···O5** (vi) | b | A/B | 2.47 | 3.35 | 136.8 |
| **C11−H···π** (vii) | c | A/B | 2.63 | 3.59 | 147.3 |
| **C1−H···O2** (vi) | d | A | 2.63 | 3.27 | 117.5 |
| **C1−H···O1** (vi) | d | B | 2.64 | 3.16 | 108.9 |
| **C18−H···O3** (viii) | e | A | 2.70 | 3.65 | 146.3 |
| **C23−H···O3** (ix) | e | B | 2.52 | 3.51 | 150.8 |
| **C14−H···O3** (x) | f | A | 2.65 | 3.73 | 175.8 |
| **C14−H···O4** (x) | f | B | 2.54 | 3.57 | 158.7 |

[a] Values were extracted from the X-ray diffraction data with the C−H distances normalized to 1.083 Å. For the C−H···π interactions, the H-bond acceptor A was taken as the centroid of the phenyl ring ($C_g$). Symmetry codes: (i) -1/2+*x*, 1/2-*y*, 1/2+*z*; (ii) -1+*x*, *y*, *z*; (iii) *x*, -*y*, -1/2+*z*; (iv) *x*, *y*, 1+*z*; (v) 1-*x*, -1/2+*y*, 3/2-*z*; (vi) 1-*x*, 1/2+*y*, 3/2-*z*; (vii) *x*, 3/2-*y*, -1/2+*z*; (viii) *x*, -1+y, *z*; (ix) -*x*, -1/2+*y*, 1/2-*z*; (x) *x*, 3/2-*y*, 1/2+*z*;

One of the red spots observed in the HS generated for compound **1**, labelled as **a** in **1A** and as **b** in **1B**, is associated to the formation of a H···O contact between one of the oxygen atoms of the trioxolane ring: O1 in **1A** and O2 in **1B**, and one of the H-atoms connected to C19 of the adamantane ring of a neighbour molecule. In both cases, the geometric parameters characterizing this interaction [H···O distance = 2.3-2.5 Å; C···O distance = 3.2-3.6 Å; C−H···O angle = 137-160º, see **Table 5.2**] are well within the range of values commonly acceptable for the formation of a C−H···O H-bond.[36–39] Although in **1A** the bond angle is closer to the linearity, the C···O and H···O distances are shorter in **1B**, as reflected by the brighter/larger red spot found in the respective HS, meaning that the H-bond should be stronger in this conformation. Weaker C−H···O interactions, characterized by H···O distances 0.05-0.11 Å longer that the sum of the van der Waals radii of the O and H atoms (2.61 Å), are evidenced in the HSs by the existence of white regions in the proximity of O2 in **1A** (**b**), O1 in **1B** (**a**) and O4 both in **1A** and **1B** (**c**), and their geometrical parameters have been included in **Table 5.2**.

Additional bright red spots were only identified in the HS generated for **1A** and are ascribed to the presence of short intermolecular H···H contacts: one involves the H-atoms

connected to C4 and C20 (**i**, 2.07 Å), while the other one is established between H-atoms connected to C16 and C23 (**k**, 2.12 Å) (see **Table 5.3**). H···H contacts with distances slightly longer the van der Waals separation of 2.18 Å were also found to be present in the crystal packing of **1** (see **Table 5.2**). A very small and faint red spot has been further located in the HS of **1A**, revealing the presence of a H···C contact (**m**).

The existence of white areas near the phenyl ring led us to check for the possible formation of C−H···π H-bonds. The candidate atoms to act as hydrogen donors to the π-system of the phenyl ring were found to be C1 of the methyl group and C21 of the adamantyl fragment. In both cases, the H···$C_g$ (2.8-3.3 Å) and C···$C_g$ (3.6-4.0 Å) distances ($C_g$ = centroid of the phenyl ring), as well as the C-H···$C_g$ angle (114-155º) are consistent with the existence of two C−H···π H-bonds,[40–42] labelled as **d** and **e**, with the former (C1−H···π) being geometrically more favourable than the latter (C21−H···π), see **Table 5.2**.

**Table 5.3.** Additional contacts identified in the crystalline structure of compounds **1** and **2**.[a]

| Contact | Label | Conf. | Distance / Å |
|---|---|---|---|
| **Compound 1** | | | |
| **C1H···HC7** (i) | f | A/B | 2.20 |
| **C1H···HC23** (ii) | g | A | 2.39 |
| **C4H···HC14** (iii) | h | A/B | 2.32 |
| **C4H···HC20** (ii) | i | A | 2.07 |
| **C8H···HC9** (iv) | j | A/B | 2.26 |
| **C16H···HC23** (v) | k | A | 2.12 |
| **C18H···HC24** (vi) | l | B | 2.27 |
| **C19H···C22** (vi) | m | A | 2.76 |
| **C19H···HC22** (vi) | n | A | 2.36 |
| **Compound 2** | | | |
| **C1···O1** (vii) | g | B | 3.16 |
| **C1H···HC17** (vii) | h | A/B | 2.28 |
| **C13H···HC19** (viii) | i | A/B | 2.26 |
| **C17H···C1**(ix) | j | A/B | 2.73 |
| **C19H···HC19** (x) | k | A/B | 2.26 |
| **C20H···HC21** (xi) | l | A/B | 2.38 |
| **C22H···HC23** (xii) | m | A/B | 2.28 |

[a] Values were extracted from the X-ray diffraction data with the C−H distances normalized to 1.083 Å. Symmetry codes: (i) 1+*x*, -*y*, -1/2+*z*; (ii) 1+*x*, *y*, -1+*z*; (iii) 1+*x*, *y*, *z*; (iv) *x*, -*y*, -1/2+*z*; (v) 1+*x*, *y*, *z*; (vi) 1/2+*x*, 1/2-*y*, 1/2+*z*; (vii) 1-*x*, 1/2+*y*, 3/2-*z*; (viii) *x*, 1/2-*y*, 1/2+*z*; (ix) 1-*x*, -1/2+*y*, 3/2-*z*; (x) -*x*, -*y*, -*z*; (xi) -*x*, 1-*y*, -*z*; (xii) -*x*, -1/2+*y*, 1/2-*z*.

The 2D-fingerprint plots extracted from the Hirshfeld surface of **1**, decomposed into contributions from the H···H, O···H/H···O and C···H/H···C contacts, are displayed in **Figure 5.6**. Due to the large number of hydrogen atoms in the molecular composition of **1**, the H···H contacts make up 70-71% of the HS, with the shortest ones indicated by the feature with edge at $d_i + d_e \sim 2.1$ Å in **1A** and at $d_i + d_e \sim 2.2$ Å in **1B**. The O···H / O···H contacts comprise 19-20% of the surface area. The shortest ones in **1A** are found at $d_i + d_e \sim 2.5$ Å and are attributable to the C19−H···O1 hydrogen bond, while in **1B** they are represented as a pair of sharp features ending at $d_i + d_e \sim 2.3$ Å, in consonance with the stronger C19−H···O2 H-bond in this conformation. The C···H/H···C contacts account for 10% of the HS surface. The shortest ones are found at $d_i + d_e = 2.8$-$2.9$ Å and are mainly attributable to the C−H···π interactions.

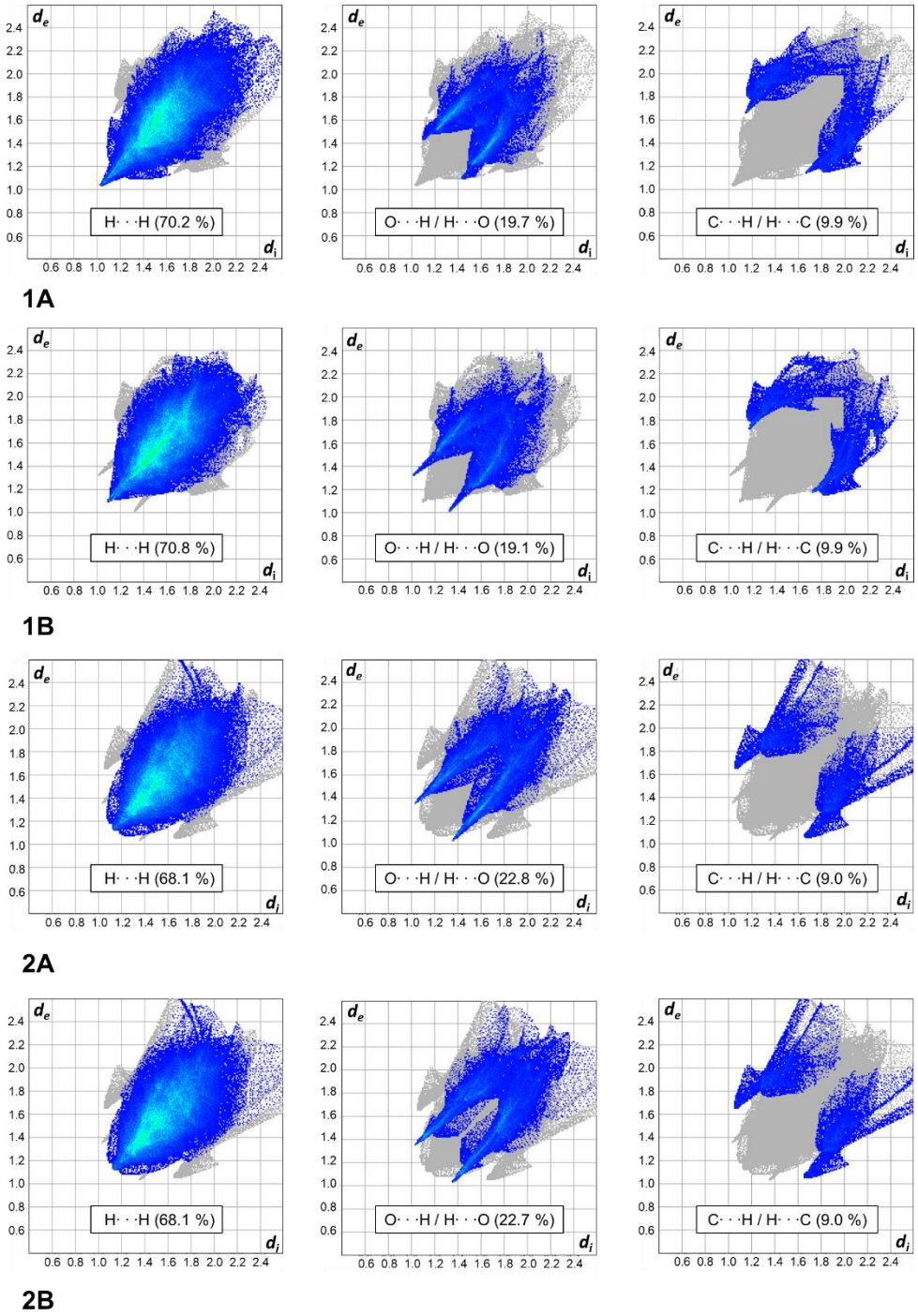


**Figure 5.6.** $d_e$ *vs.* $d_i$ fingerprint plots calculated for the conformations **A** and **B** of compounds **1** and **2**, showing the regions corresponding to the H···H, O···H / H···O and C···H / H···C contacts. The $d_i$ and $d_e$ values correspond, respectively, to the closest internal and external distances (Å) to the Hirshfeld surface. The contributions (in %) of the different contacts to the total Hirshfeld surface area of the molecule are included.

The larger and brighter red spots in the HS generated for **2** appear near the carbonyl oxygen O5 (labelled as **a** and **b**) and are common to both crystal conformations. These red spots highlight the formation of two C−H···O hydrogen bonds, with O5 acting as

double acceptor from the C5 and C7 phenyl carbon atoms of two nearby molecules. Although the H···O (2.4-2.5 Å) and C···O (3.3-3.4 Å) distances are not very different in the two interactions, the bond angle is more favorable in C5−H···O5 than in the C7−H···O5 H-bond (155º vs. 137º), making the former stronger. Weaker C−H···O interactions involving the tetraoxane oxygen atoms and C−H groups of the cyclohexane or adamantane fragments are highlighted in the HSs as faint/small red spots or white regions (labeled as **d**, **e** and **f**) and exhibit different geometric parameters depending on the conformation adopted by the tetraoxane ring (see **Table 5.2** for details). Two other faint and small red spots, also common to both conformations, have been identified. One of them, labeled as **c**, corresponds to a close contact between the H-atom connected to C11 of the cyclohexane ring and three carbon atoms of the phenyl ring of a neighbor molecule, clearly indicating the formation of a C−H···π H-bond. According to the geometric parameters given in **Table 5.2**, this H-bond is stronger than the equivalent ones established in compound **1**. The other light red spot denotes the presence of a H···C contact (**j**) between the H-atom connected to the C17 of the adamantyl ring and the terminal methyl carbon atom C1 of another molecule. It is also worth noting the presence of a red spot in the HS of **2B** resulting from a short contact between the C1 and O1 atoms of two neighbor molecules (**g**, 3.16 Å).

Analogously to **1**, the H···H contacts represent the largest contribution of the surface area of **2** (68%), appearing in the 2D-fingerprint plot at $d_i + d_e > 2.3$ Å (see **Figure 5.6**), thereby indicating their minor relevance in the crystal packing of **2** as compared to **1**. The O···H/H···O contacts comprise 23% of the surface area, which is slightly larger than that calculated for **1** due to the greater participation of the carbonyl oxygen in C-H···O H-bonds. The most relevant ones are evidenced by a pair of sharp spikes in the 2D-fingerprint plots ending at $d_i + d_e \sim 2.4$ Å, attributable to the stronger C-H···O5 hydrogen bond. The third most representative contacts are the C···H/H···C ones (9%), which are evidenced by the pair of wings with tips at $d_i + d_e \sim 2.6$ Å, reflecting the formation of C−H···π interactions.

### 5.3.3.1. Pairwise interaction energies

In order to have a more quantitative picture of the molecular packing in crystals **1** and **2**, the total CE-B3LYP/6-31G(d,p) interaction energies ($E_{tot}$) and respective dispersive ($E_{disp}$), electrostatic ($E_{ele}$), exchange-repulsion ($E_{ex\text{-}rep}$) and polarization ($E_{pol}$)

components were calculated for the molecular pairs involving a central molecule and all neighbouring molecules within a cluster of 3.8 Å. The values obtained for the molecular pairs with $|E_{tot}| > 10$ kJ mol$^{-1}$ are given in **Table 5.4**. These pairs are labelled as **I-VIII** from the one with a more negative to that with a less negative value of $E_{tot}$. The two most stabilizing pairs of each compound are presented in **Figures 5.7** and **5.8**, while the remaining ones are provided as supporting information (see **Figures S1** and **S2**, in the *Appendix*).

As expected from the type of interactions present in the crystal structure of both compounds, $E_{disp}$ is by far the main contribution of $E_{tot,}$ while the repulsion-exchange ($E_{ex-rep}$) and electrostatic ($E_{ele}$) components are only significant for some molecular pairs. In the opposite side is the polarization component, whose energy values are not relevant.

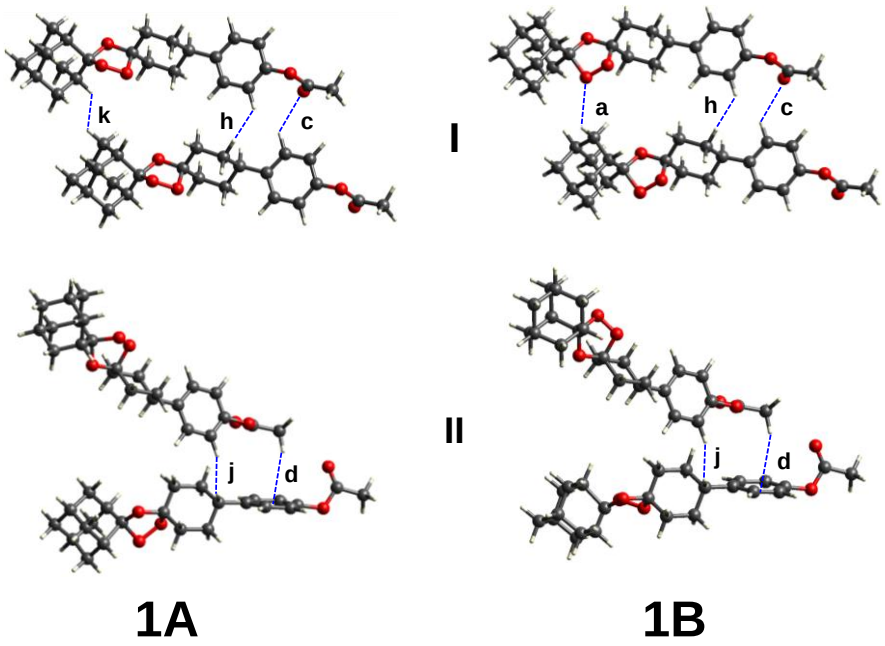


**Figure 5.7.** Most stabilizing molecular pairs of the crystal structure of **1**, including the identification of the intermolecular contacts.

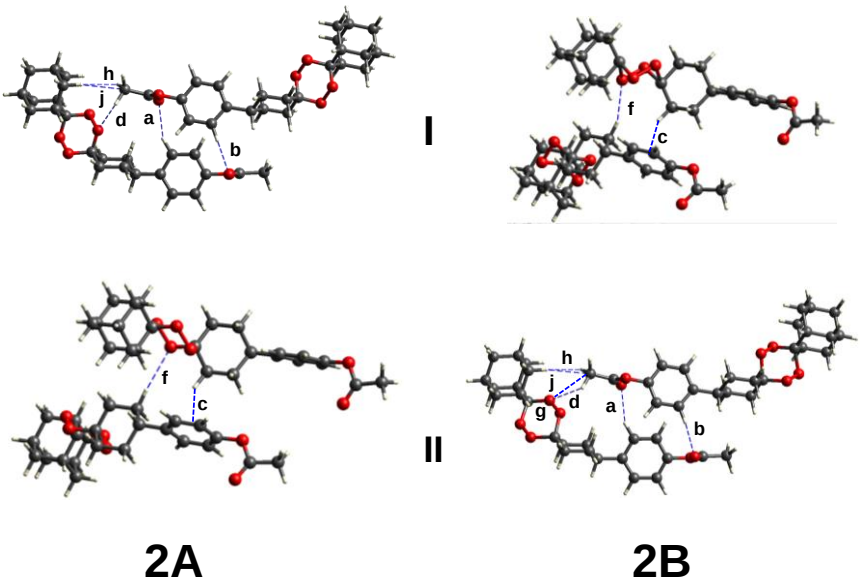


**Figure 5.8.** Most stabilizing molecular pairs of the crystal structure of **2**, including the identification of the intermolecular contacts.

In **1**, the most stabilized molecular pair **I** is characterized by the formation of a C−H···O interaction (**c**) and two H···H contacts (**h** and **k**) in **1A**, or by two C−H···O interactions (**a** and **c**) and one H···H contact (**h**) in **1B** (see **Figure 5.7**) The values of $E_{tot}$ calculated for **1A** and **1B** are –34.8 kJ mol$^{-1}$ and –36.8 kJ mol$^{-1}$, respectively, meaning that the replacement of a H···H short contact **k** in **1A** by a C19−H···O1 interaction **a** in **1B** causes only a small increase (2 kJ mol$^{-1}$) of the stabilization energy. The second most relevant molecular pair (**II**) exhibits an identical interaction energy for the two conformations: −30.2 (**1A**) and −29.3 (**1B**) kJ mol$^{-1}$ and its stabilization arise from the formation of a C1−H···π interaction (**d**) plus the contribution of a H···H contact (**j**). Pairs **III** and **IV** exhibit identical values of $E_{tot}$ but their stabilization results from different types of interactions (**Figure S1**, in the *Appendix*). In fact, while the stabilization of **III** is mostly originated by two H···H contacts (**i** and **g**), that of **IV** results from the formation of the C21−H···π interaction (**e**). Pair **V** is formed by two C−H···O H-bonds in **1A** (**a** and **b**) or only one (**b**) in **1B**. The resulting stabilization energy is −20.0 and −17.1 kJ mol$^{-1}$, respectively. Interestingly, it is less negative than that computed for molecular pair **III**, thus confirming the minor role of the C−H···O interactions in the molecular packing of **1**.

As shown in **Table 5.4**, the crystal packing of compound **2** is strongly determined by molecular pairs **I** and **II** (see **Figure 5.8**), whose interaction energies range from −43.1 to −39.2 kJ mol$^{-1}$. These energies are more negative than those calculated for the two most stabilizing pairs in compound **1** and have an appreciable contribution of the electrostatic

component. The stabilization of pair **I** in **2A**, which is structurally equivalent to pair **II** in **2B**, is essentially determined by the simultaneous formation of three C−H···O interactions (**a**, **b** and **d**). The value of $E_{tot}$ calculated for this pair amounts to –43.1 kJ mol$^{-1}$ in **2A** and to −40.4 kJ mol$^{-1}$ in **2B**. The stabilization of pair **II** in **2A**, or of pair **I** in **2B**, is governed by the C−H···π H-bond (**c**) plus the contribution of a C−H···O interaction (**f**) and the value of $E_{tot}$ is similar for the two conformations: −40.9 kJ mol$^{-1}$ for **2A** and −39.2 kJ mol$^{-1}$ for **2B**. For the remaining molecular pairs (**Figure S2**, in the *Appendix*), the values of $E_{tot}$ fall between −21.0 and −13 kJ mol$^{-1}$ (**Table 5.4**).

**Table 5.4.** CE-B3LYP interaction energies (in kJ mol$^{-1}$) calculated for the most relevant molecular pairs in the crystalline structure of compounds **1** and **2**.[a]

| Molecular pair | Conf. | $R$ | $E_{ele}$ | $E_{pol}$ | $E_{disp}$ | $E_{ex-rep}$ | $E_{tot}$ |
|---|---|---|---|---|---|---|---|
| **Compound 1** | | | | | | | |
| **I** | A | 6.7 | -8.4 | -1.9 | -44.1 | 22.5 | -34.8 |
| | B | 6.7 | -8.1 | -2.7 | -45.5 | 21.6 | -36.8 |
| **II** | A | 9.2 | -9.3 | -3.3 | -32.7 | 17.1 | -30.2 |
| | B | 9.1 | -8.5 | -3.2 | -32.8 | 17.2 | -29.3 |
| **III** | A | 13.5 | -3.8 | -0.8 | -23.3 | 0.0 | -24.9 |
| | B | 13.5 | -2.5 | -0.7 | -24.6 | 0.0 | -24.6 |
| **IV** | A | 10.8 | -4.0 | -0.7 | -34.1 | 16.5 | -24.3 |
| | B | 10.8 | -2.3 | -0.7 | -31.3 | 11.6 | -23.1 |
| **V** | A | 9.8 | -4.1 | -1.8 | -24.5 | 11.3 | -20.0 |
| | B | 9.8 | -4.5 | -1.8 | -23.0 | 14.6 | -17.1 |
| **VI** | A | 9.2 | -4.1 | -0.7 | -24.4 | 12.2 | -18.5 |
| | B | 9.3 | -1.4 | -0.3 | -22.8 | 9.9 | -15.5 |
| **VII** | A | 11.8 | -2.4 | -1.6 | -11.6 | 6.5 | -9.9 |
| | B | 11.7 | -2.5 | -1.7 | -11.7 | 6.4 | -10.1 |
| **Compound 2** | | | | | | | |
| **I** | A | 10.5 | -18.2 | -5.6 | -48.8 | 36.7 | -43.1 |
| | B | 7.5 | -11.9 | -2.0 | -51.6 | 29.2 | -40.9 |
| **II** | A | 7.5 | -10.2 | -1.6 | -51.1 | 27.9 | -39.2 |
| | B | 10.5 | -15.9 | -5.7 | -48.7 | 37.3 | -40.4 |
| **III** | A | 8.7 | -3.5 | -0.3 | -28.6 | 12.6 | -21.0 |
| | B | 8.7 | -3.4 | -0.2 | -28.9 | 12.9 | -21.0 |
| **IV** | A | 14.3 | -1.6 | -0.2 | -19.9 | 0.0 | -19.2 |
| | B | 16.1 | -1.9 | -0.7 | -17.4 | 0.0 | -17.7 |
| **V** | A | 16.1 | -2.0 | -0.6 | -17.4 | 0.0 | -17.7 |
| | B | 14.3 | 0.1 | -0.3 | -20.0 | 0.0 | -17.6 |
| **VI** | A | 11.5 | -3.0 | -0.7 | -20.9 | 9.5 | -16.0 |
| | B | 11.4 | -4.2 | -1.0 | -21.0 | 12.1 | -16.1 |
| **VII** | A | 8.3 | -1.7 | -0.9 | -17.0 | 4.9 | -14.2 |
| | B | 8.3 | -1.5 | -1.0 | -16.4 | 2.8 | -14.9 |
| **VIII** | A | 14.5 | -2.5 | -0.4 | -12.2 | 0.0 | -13.5 |
| | B | 14.5 | -2.2 | -0.4 | -12.2 | 0.0 | -13.2 |

[a] $R$ is the distance (Å) between the molecular centroids.

## 5.3.4. Infrared spectra of the title compounds

The compounds were investigated by infrared spectroscopy. Their room temperature IR (ATR) spectra are shown in **Figure 5.9** (**1**) and **Figure 5.10** (**2**), together with the B3LYP/6-311++G(d,p) theoretical spectra calculated for the two crystal conformations (**A** and **B**) of **1** and **2**, after their full geometry optimization at the same level of theory. Three main conclusions can be immediately extracted from the data shown in these figures: (i) the calculated spectra of the two forms (**A** and **B**) of each compound are practically coincident, (ii) the experimental spectra of the two molecules are also very similar to each other (see also **Figure S3** in the *Appendix*), and (iii) for both compounds, the calculated spectra for the isolated molecules provide a good description of the experimental spectra of the crystalline compounds.

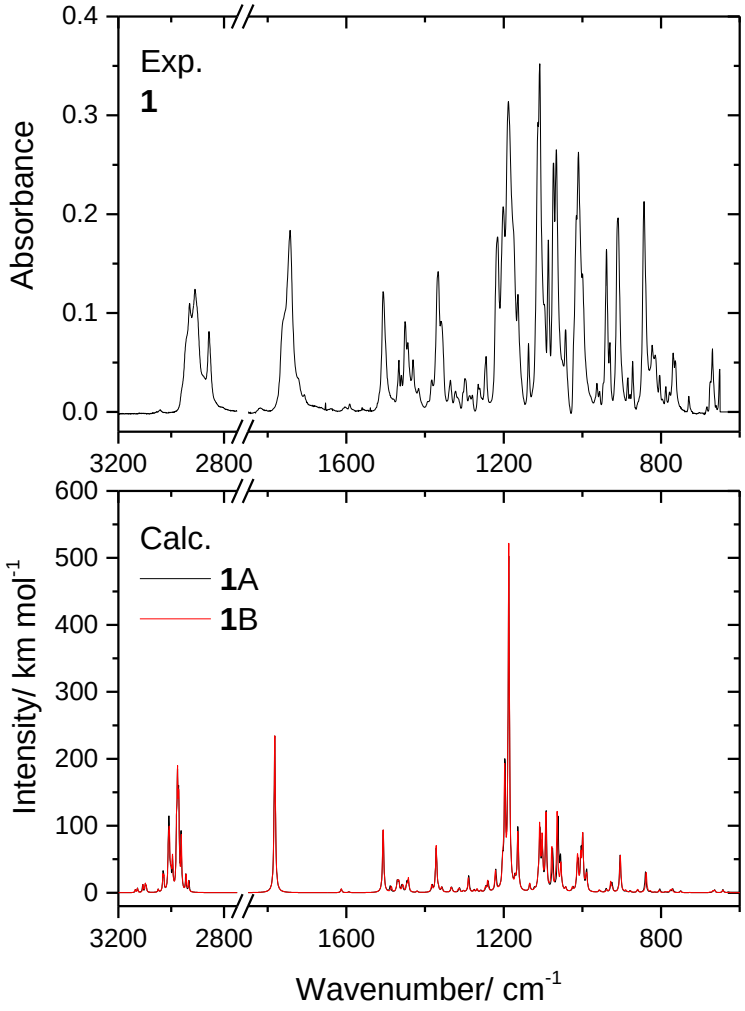


**Figure 5.9**. Experimental IR spectrum (ATR; room temperature) of compound **1** (*top*) and calculated IR spectra for the isolated molecule of the compound, forms **A** and **B** (*bottom*). Calculated wavenumbers were scaled by 0.980.

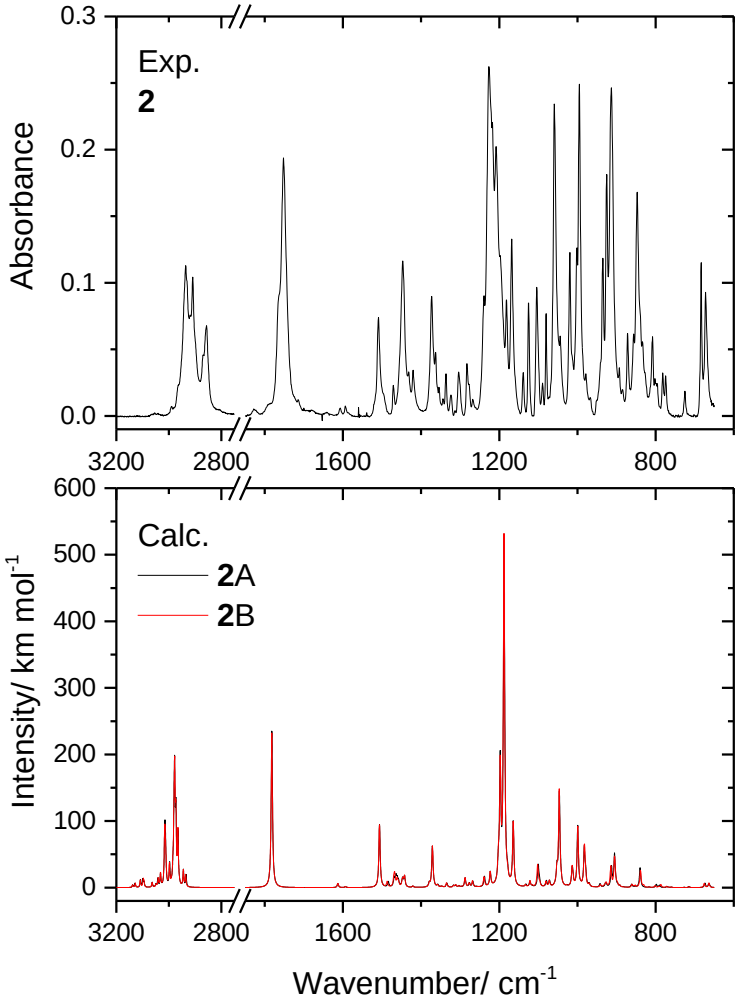


**Figure 5.10.** Experimental IR spectrum (ATR; room temperature) of compound **2** (*top*) and calculated IR spectra for the isolated molecule of the compound, forms **A** and **B** (*bottom*). Calculated wavenumbers were scaled by 0.980.

Conclusions (i) and (ii) were expected, considering the structural similarity of the two crystal conformations of each molecule and the close resemblance of the molecules of the two compounds. Most of the vibrations are in fact localized in the adamantane, cyclohexane and substituted-phenyl rings of the molecules, which have nearly identical structural arrangements. On the other hand, the fact that the calculated spectra for the isolated molecules provide a good description of the experimental spectra of the crystalline compounds indicates that the intermolecular interactions in the crystals do not disturb significantly the intramolecular vibrational potentials. This is in line with the prevalence of dispersive-type interactions, as described in detail in the previous sections of this article.

**Table 5.5.** Assignment of the infrared spectrum of **1**.[a]

| Calc. 1A | | Calc. 1B | | Exp. | Assignment |
|---|---|---|---|---|---|
| ν [cm$^{-1}$] | $I^{IR}$ [km mol$^{-1}$] | ν [cm$^{-1}$] | $I^{IR}$ [km mol$^{-1}$] | | |
| 1092.2 | 117.2 | 1092.6 | 114.5 | 1109 | νC12-O3 – νC12-O2 |
| 1075.6 | 60.6 | 1077.6 | 63.0 | 1086 | νC15-O3 + νC15-O1 |
| 1062.0 | 107.3 | 1064.1 | 117.2 | 1073 | νC12-O3 + νC12-O2 |
| 989.1 | 29.0 | 989.0 | 22.0 | 999 | νC15-O3 – νC15-O1 |
| 889.5 | 1.1 | 890.2 | 3.1 | 885 | νC15-O3 – νC15-O1 |
| 886.5 | 0.6 | 883.9 | 0.5 | 879 | νO1-O2 |
| 786.1 | 0.3 | 789.6 | 1.4 | 487 | δring |
| 775.8 | 3.0 | 776.4 | 3.5 | 769 | δring |
| 750.0 | 2.8 | 750.0 | 2.3 | 729 | δring |
| 3000.5 | 16.8 | 3001.9 | 11.6 | 2924 (sh) | νC16-H |
| 2994.8 | 43.8 | 2995.2 | 46.6 | 2917 (sh) | νC24-H |
| 1313.7 | 2.5 | 1316.1 | 2.9 | 1324 | δC16-H – δC24-H |
| 1312.1 | 5.1 | 1313.1 | 5.2 | 1322 | δC16-H + δC24-H |
| 1301.7 | 0.5 | 1302.2 | 1.1 | 1314 | γC16-H + γC24-H |
| 1250.8 | 0.03 | 1250.4 | 0.03 | n.obs. | γC16-H – γC24-H |
| 1245.1 | 7.7 | 1246.6 | 6.4 | 1264 | δC16-H – δC24-H |
| 1782.1 | 235.3 | 1782.0 | 234.2 | 1760,1753,1743 | νC2=O4 |
| 1202.9 | 34.8 | 1202.4 | 31.3 | 1201 | νC3-O5 |
| 1187.1 | 495.1 | 1187.1 | 514.7 | 1188,1177 | νC2-O5 |
| 663.8 | 4.1 | 663.7 | 3.6 | 669 | δO5-C2=O4 |
| 586.3 | 4.0 | 585.9 | 3.9 | n.i. | γC2=O4 |
| 339.6 | 5.1 | 339.2 | 4.7 | n.i. | δC1-C2=O4 |
| 1506.4 | 93.5 | 1506.5 | 93.7 | 1506 | νC=C ph; δCH ph |
| 1196.9 | 176.5 | 1197.4 | 169.7 | 1201 | νC-C ph; νC6-C9 |
| 3094.4 | 7.6 | 3094.4 | 7.6 | 3042 | $\nu CH_3$ s |
| 3049.3 | 4.3 | 3049.2 | 4.2 | 3001 | $\nu CH_3$ as |
| 2990.4 | 2.1 | 2990.3 | 2.1 | n.obs. | $\nu CH_3$ as |
| 1445.6 | 4.1 | 1442.7 | 4.9 | 1431 | $\delta CH_3$ as |
| 1420.0 | 2.0 | 1420.5 | 2.2 | 1416 | $\delta CH_3$ as |
| 1371.0 | 25.8 | 1371.6 | 67.9 | 1367 | $\delta CH_3$ s |
| 1042.3 | 5.7 | 1042.4 | 5.6 | 1042 | $\gamma CH_3$ |
| 999.2 | 78.1 | 999.1 | 80.4 | 1009 | $\gamma CH_3$ |
| 44.9 | 0.6 | 41.2 | 0.6 | n.i. | $\tau CH_3$ |

[a] Frequencies (ν) in cm$^{-1}$; calculated infrared intensities ($I^{IR}$) in km mol$^{-1}$; calculated frequencies were scaled by 0.980; ν, stretching, δ, bending; γ, rocking; τ, torsion; s, symmetric; as, anti-symmetric; ph, phenyl; + and – signals define mixing modes in-phase or in anti-phase; sh, shoulder; n.obs., not observed; n.i., not investigated; see **Figure 5.2** for atom numbering. For full calculated frequencies and intensities, see **Table S6** (*Appendix*).

The full calculated vibrational data for **1** and **2** are provided in **Tables S6** and **S7** in the **Appendix**, respectively. **Tables 5.5** and **5.6** present the assignments for the bands of the two compounds which originate in the trioxolane (for **1**) or tetraoxane (for **2**) moieties, in the acetate substituent, and in the C−H adamantane bonds closest to the trioxolane or tetraoxane rings (C16−H; C24−H), as well as two additional strong bands that are ascribable to modes belonging to the phenyl ring (one of them containing also a

significant contribution from the stretching of the $C_6$–$C_9$ bond that connects the phenyl and cyclohexyl groups). These set of bands include all the most intense bands observed experimentally, with the frequencies of the bands due to the acetate substituent appearing in the usual ranges,[43,44] and being good agreement with the calculated values.

**Table 5.6.** Assignment of the infrared spectrum of **2**.[a]

| Calc. 2A | | Calc. 2B | | Exp. | Assignment |
|---|---|---|---|---|---|
| ν [cm$^{-1}$] | $I^{IR}$ [km mol$^{-1}$] | ν [cm$^{-1}$] | $I^{IR}$ [km mol$^{-1}$] | | |
| 1052.4 | 25.6 | 1052.5 | 22.6 | 1067 (sh) | νC15-O1 + νC15-O4 |
| 1046.3 | 140.5 | 1046.6 | 145.0 | 1058 | νC12-O3 + νC12-O2 |
| 991.5 | 1.6 | 992.3 | 1.6 | 1001 | νC15-O4 |
| 982.5 | 56.5 | 982.3 | 55.9 | 994 | νC15-O1 |
| 933.4 | 0.2 | 933.0 | 1.5 | 935 | νC12-O3 + νC12-O2 |
| 891.5 | 2.1 | 891.7 | 2.1 | 885 | νO1-O2 + νO3-O4 |
| 856.4 | 0.6 | 856.9 | 1.0 | 872 | νO1-O2 – νO3-O4 |
| 852.1 | 1.2 | 852.1 | 2.8 | 856 | νO1-O2 – νO3-O4 |
| 798.4 | 4.7 | 801.5 | 2.7 | 808 | δring |
| 790.5 | 2.8 | 792.5 | 1.0 | 781 | δring |
| 714.8 | 1.3 | 714.6 | 1.4 | 725 | δring |
| 3010.6 | 4.6 | 3010.3 | 10.7 | 2932 (sh) | νC16-H |
| 2997.0 | 32.6 | 2997.8 | 31.7 | 2919 | νC24-H |
| 1317.0 | 3.1 | 1316.5 | 2.7 | 1323 | δC16-H – δC24-H |
| 1311.3 | 3.4 | 1311.3 | 3.6 | 1313 | δC16-H + δC24-H |
| 1302.3 | 0.3 | 1302.9 | 1.9 | 1303 | γC16-H + γC24-H |
| 1251.7 | 0.1 | 1252.5 | 0.1 | n.obs. | γC16-H – γC24-H |
| 1237.9 | 15.2 | 1239.1 | 14.5 | 1260 | δC16-H – δC24-H |
| 1782.0 | 232.4 | 1782.0 | 232.4 | 1763,1752 | νC2=O5 |
| 1202.4 | 28.3 | 1202.4 | 28.3 | 1239 | νC3-O6 |
| 1187.9 | 523.8 | 1187.9 | 523.8 | 1217,1207 | νC2-O6 |
| 663.6 | 4.6 | 663.6 | 4.6 | 670 | δO6-C2=O5 |
| 585.3 | 3.8 | 585.3 | 3.8 | n.i. | γC2=O5 |
| 336.4 | 6.4 | 336.4 | 6.4 | n.i. | δC1-C2=O5 |
| 1506.4 | 94.4 | 1506.5 | 94.0 | 1509 | νC=C ph; δCH ph |
| 1197.7 | 181.2 | 1197.6 | 173.1 | 1225 | νC-C ph; νC6-C9 |
| 3094.6 | 7.6 | 3094.5 | 7.6 | 3042 | $\nu CH_3$ s |
| 3049.2 | 4.2 | 3048.9 | 4.2 | 3002 | $\nu CH_3$ as |
| 2990.3 | 2.0 | 2990.0 | 2.0 | n.obs. | $\nu CH_3$ as |
| 1446.8 | 9.7 | 1446.5 | 9.8 | 1432 | $\delta CH_3$ as |
| 1421.1 | 1.9 | 1421.0 | 1.9 | 1420 | $\delta CH_3$ as |
| 1371.2 | 59.3 | 1371.0 | 61.2 | 1373 | $\delta CH_3$ s |
| 1042.4 | 5.8 | 1042.1 | 5.9 | 1044 | $\gamma CH_3$ |
| 999.3 | 91.3 | 999.1 | 90.3 | 994 | $\gamma CH_3$ |
| 44.5 | 1.2 | 44.3 | 1.1 | n.i. | $\tau CH_3$ |

[a] Frequencies (ν) in cm$^{-1}$; calculated infrared intensities ($I^{IR}$) in km mol$^{-1}$; calculated frequencies were scaled by 0.980; ν, stretching, δ, bending; γ, rocking; τ, torsion; s, symmetric; as, anti-symmetric; ph, phenyl; + and – signals define mixing modes in-phase or in anti-phase; sh, shoulder; n.obs., not observed; n.i., not investigated; see **Figure 5.2** for atom numbering. For full calculated frequencies and intensities, see **Table S7** (*Appendix*).

The bands due to the trioloxane and tetraoxane rings are also observed at frequencies closely matching the calculated frequencies for the isolated molecule (see **Tables 5.5** and **5.6**).

In the case of the trioxolane modes of **1**, all νC–O stretching vibrations give rise to intense bands (with calculated intensities over 22 km $mol^{-1}$), while both the ring deformational modes and the νO1–O2 stretching mode give rise to low intensity bands (calculated intensities below 4 km $mol^{-1}$), the latter vibration being observed at 879 $cm^{-1}$ (the calculated values for forms **A** and **B** are 886.5 and 883.9 $cm^{-1}$, respectively).

The bands due to the vibrations located in the tetraoxane moiety of compound **2** follow the same general trends as those originated in the trioxolane ring of compound **1**, with the νC–O stretching vibrations giving rise to intense bands (over 22 km $mol^{-1}$) and both the ring deformational modes and νO–O stretching vibrations giving rise to low intensity bands (below 5 km $mol^{-1}$). It is interesting to note that the calculations predicted that the vibrations of the two O–O bonds are combined, giving rise to a symmetric and an anti-symmetric mode, the first being ascribed to the experimental band at 885 $cm^{-1}$, and the second contributing significantly to the bands observed at 872 and 856 $cm^{-1}$.

## 5.4. Conclusion

In this work, the crystalline structures of the precursors of the antimalarial candidates **OZ439** and **E209**, endoperoxides **1** (*p*-(dispiro-[cyclohexane-1,3'-[1,2,4]trioxolane-5',2''-tricyclo [3.3.1.1$^{3,7}$]decan]-4-yl)-phenyl acetate) and **2** (*p*-(dispiro-[cyclohexane-1,3'-[1,2,4,5]tetraoxane-6',2''-tricyclo[3.3.1.1$^{3,7}$]decan]-4-yl)-phenyl acetate), were investigated by single crystal X-ray diffraction studies. Compounds **1** and **2** were found to crystallize in the monoclinic *Cc* and $P2_1/c$ space groups, respectively, with four molecules within the unit cell. Moreover, in the crystalline state the tetraoxane ring in **2** and the trioxolane-adamantane fragment in **1** were found to be disordered, with molecules of **1** and **2** existing as two distinct, stable conformations.

From the Hirshfeld surface analysis, it was shown that the crystal packing of both compounds is dominated by H···H (68-70%), H···O/O···H (19-23%) and H···C/C···H (9-10%) contacts, which are associated to the formation of C−H···H−C van der Waals interactions, as well as of C−H···O and C−H···**π** H-bond like interactions. In this regard, the following differences between the two endoperoxides must be underlined: (1) The

dominant C−H···O H−bonds in **1** connect a C−H group of the adamantane and the O1 or O2 oxygen atoms of the trioxolane ring, whereas in **2** they involve the carbonyl oxygen, which acts as double acceptor from C−H groups of the phenyl ring; (2) The C−H···O and C−H···π H-bonds play a more important role in the molecular packing of **2**, while the C−H···H−C van der Waals interactions are more relevant in the molecular packing of **1**.

In consonance with the large contribution of the H···H contacts to the Hirshfeld surfaces of the two compounds, the CE-B3LYP/6-31G(d,p) interaction energies calculated for the most representative molecular pairs are dominated by the dispersive component. Furthermore, in accordance with the more important role of the H-bonds in **2**, the largest pairwise interaction energies were estimated for this compound.

Because of the structural similarity between the molecules of **1** and **2**, the IR spectra recorded for the two compounds are also very similar. Moreover, due to the lack of strong intermolecular interactions in the crystals, the molecular conformation adopted by the molecules in the crystal structure is not much different from that of the fully optimized isolated molecules, the respective calculated spectra thus providing a good description of the experimental data.

As a final remark, this study provides valuable structural information that may be useful to better understand the reactivity and structure-activity relationship for these classes of antimalarial endoperoxides.

## 5.5. Experimental section

***Chemicals***. All reagents for synthesis were purchased from commercial sources and used without further purification. Analytical thin layer chromatography (TLC) was carried out using Merck (Germany) TLC Silica gel 60 F254 aluminium sheets and visualized under UV or by appropriate stain. p-Anisaldehyde and potassium permanganate were the most used. Column chromatography was carried out using Sigma Aldrich (Germany) technical grade silica gel (pore size 60 Å, 230–400 mesh particle size, 40–63 μm particle size).

***Equipment.*** $^{1}$H and $^{13}$C Nuclear Magnetic Resonance (NMR) spectra were recorded using a Bruker AMX400 spectrometer or a 500 MHz JEOL system equipped with a Royal HFX probe, in solution, using the deuterated solvents described in each experimental procedure. The chemical shifts (δ) are described in parts per million (ppm) downfield

from an internal standard of tetramethylsilane (TMS). Melting points (°C) were obtained on an SMP30 melting point apparatus and are uncorrected. High Resolution Mass Spectrometry (HRMS) was recorded using the analytical services within the Chemistry Department at the University of Liverpool (UoL), and within the Centre of Marine Sciences (CCMar). HRMS was conducted on a VG analytical 7070E machine, Frisons TRIO mass spectrometer, or Agilent QTOF 7200, using chemical ionisation (CI) or electrospray (ESI) (UoL), and on Thermo Scientific High Resolution Mass Spectrometer (HRMS), model Orbitrap Elite, capable of MSn, n up to 10 (CCMar). X-ray diffraction data were collected on a Bruker Kappa Apex II diffractometer (Massachusetts, USA), equipped with a 4K CCD detector, using graphite monochromated MoKα (λ = 0.71073 Å) radiation. Infrared spectra were recorded using a Perkin Elmer SPECTRUM 400 FT-IR Spectrometer equipped with a diamond crystal-based ATR device (more details are provided in the Infrared Spectroscopy and X-ray crystallography subsections).

## 5.5.1. Synthesis

### Preparation of 4-(4-oxocyclohexyl)phenyl) acetate (5.1)

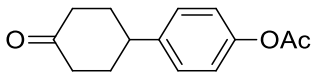


The synthesis for compound **5.1** is described in Chapter 4, section 4.7.2 (compound **4.11a**).

### Preparation of *O*-methyl-adamantan-2-one oxime (5.2)

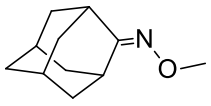


Procedure adapted from Cabral *et al.*[19] with slight modifications. To a solution of adamantan-2-one (7.00 g, 46.6 mmol) in methanol (50 mL) were added pyridine (6.00 mL, 74.18 mmol) and methoxylamine hydrochloride (5.06 g, 60.52 mmol). The reaction mixture was stirred at room temperature for 48 h. The final mixture was concentrated and then diluted with $CH_2Cl_2$ (50 mL) and water (50 mL). The organic layer was separated, and the aqueous layer was extracted with $CH_2Cl_2$ (30 mL). The combined organic extracts were washed with aqueous HCl (1 M; 30 mL × 2), then with brine (30 mL). The final

organic extract was dried over $MgSO_4$, filtered, and concentrated under reduced pressure to give *O*-methyl-adamantan-2-one oxime **5.2** (6.01 g, 72% yield) as a colourless solid. M.p. 342.15-343.15 K. Spectral data are in accordance with the reported in the literature.[19] $^1$H NMR (400 MHz, $CDCl_3$): δ 3.82 (s, 3H), 3.47 (s, 1H), 2.53 (s, 1H), 1.89 (m, 12H); $^{13}C\{^1H\}$ NMR (100 MHz, $CDCl_3$): δ 25.9, 26.31, 31.09, 32.59, 34.25, 35.70, 36.18, 37.35, 106.46, 111.95, 208.90 ppm. HRMS (ESI, *m/z*) calcd $C_{11}H_{18}NO$ $[M+H]^+$: 180.13829; found 180.13783. Diff: 2.55 ppm.

## Preparation of *p*-(dispiro[cyclohexane-1,3'-[1,2,4]trioxolane-5',2''-tricyclo [3.3.1.1$^{3,7}$]decan]-4-yl)-phenyl acetate (1)

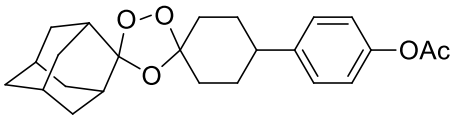


Procedure adapted from Cabral *et al.*[19] with slight modifications. Ozone, produced with an ozone generator Sander Labor-Ozonizator 301.7 (0.5 L/min $O_2$, 140 V), was passed through a solution of dichloromethane at 195.15 K and flushed into a solution of **5.1** (1.291 g, 5.56 mmol) and **5.2** (1.021 g, 5.70 mmol), in pentane/$CH_2Cl_2$ (6:4, 125 mL) at 273.15 K. After completion the reaction mixture was flushed with nitrogen for 5 min and concentrated under reduced pressure at room temperature to give a crude material. Separation by column chromatography (EtOAc: hexane, 1:99, *v/v*) and recrystallization from acetone gave 1,2,4-trioxolane **1** (0.753 g, 33%) as colourless crystals (m.p. 424.15-426.15 K). Spectral data are in accordance with literature reports.[45] $^1$H NMR (400 MHz, $CDCl_3$): δ 7.22 – 7.18 (d, *J* = 8.5 Hz, 2H), 7.02 – 6.97 (d, *J* = 8.5 Hz, 2H), 2.59 – 2.50 (t, *J* = 11.9 Hz, 1H), 2.28 (s, 3H), 2.07 – 1.67 (m, 22H), 1.55 (s, 2H) ppm. $^{13}C\{^1H\}$ NMR (100 MHz, $CDCl_3$): δ 169.68, 148.90, 143.69, 127.72, 121.36, 111.45, 108.33, 42.41, 36.82, 36.43, 34.83, 31.50, 26.91, 26.51, 21.14 ppm. HRMS (ESI, *m/z*) calcd $C_{24}H_{30}O_5Na$ $[M+Na]^+$ : 421.1985; found 421.1986. Diff: -0.10 ppm.

**Preparation of *p*-(dispiro[cyclohexane-1,3'-[1,2,4,5]tetraoxane-6',2''-tricyclo[3.3.1.1$^{3,7}$]decan]-4-yl)-phenyl acetate (2)**

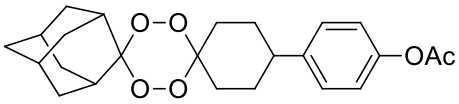


The synthesis for compound **2** is described in Chapter 4, section 4.7.2 (compound **4.13a**).

## 5.5.2. X-ray crystallography

Single crystal X-ray diffraction (XRD) measurements were performed at room temperature using graphite monochromated MoKα ($\lambda$ = 0.71073 Å) radiation. The structures were solved by the dual-space algorithm implemented in SHELXT-2018/2,[46] and refinement of the structural model was performed with full-matrix least-squares using SHELXL-2018/3.[47] All non-hydrogen atoms were refined anisotropically. Hydrogen atoms were placed at calculated idealized positions and refined as riding using SHELXL-2018/3 default values. Full details of the data collection and structure refinement procedures are provided in the Supporting Information (Crystallographic Data). A summary of the data collection and refinement is provided in **Table 5.1**. Deposition Numbers CCDC 2162410 (for **1**) and CCDC 2053084 (for **2**) contain the supplementary crystallographic data for this paper. These data are provided free of charge by the joint Cambridge Crystallographic Data Centre and Fachinformationszentrum Karlsruhe Access Structures service http://www.ccdc.cam.ac.uk/structures

## 5.5.3. Infrared spectroscopy

The infrared spectra of the compounds were obtained in the 4000-650 cm$^{-1}$ range with 4 cm$^{-1}$ resolution (64 accumulations), at room temperature, in the attenuated total reflexion mode (ATR), using a Perkin Elmer SPECTRUM 400 FT-IR Spectrometer equipped with a diamond crystal-based ATR device. The theoretical IR spectra were obtained after full geometry optimizations of the **1** and **2** crystal conformations, performed at the DFT(B3LYP)/6-311++G(d,p) level,[48–51] using the Gaussian 09 (revision A.2) suite of programs,[52] the calculated harmonic wavenumbers being scaled by 0.980. The spectra were simulated by using the Chemcraft software (version 1.8).[53]

### 5.5.4. Hirshfeld surface computations

A Hirshfeld surface (HS) analysis.[33,54–57] was carried out by using the *CrystalExplorer* software package (version 21.5).[58] The software used the CIF files as input and the C−H bonds length was set to the typical neutron diffraction value of 1.083 Å.[59] The Hirshfeld surfaces were generated with a very high resolution and were mapped with the normalized contact distance ($d_{norm}$), calculated from the following equation:[33,57]

$$d_{norm} = \frac{(d_i - r_i^{vdW})}{r_i^{vdW}} + \frac{(d_e - r_e^{vdW})}{r_e^{vdW}} \quad (1)$$

where $d_i$ and $d_e$ are, respectively, the distances from the point of the surface to the nearest atoms inside and outside the surface, and $r_i^{vdW}$ and $r_e^{vdW}$ are the van der Waals radii of the respective atoms: C (1.70 Å), O (1.52 Å), H (1.09 Å). Intermolecular contacts shorter than the sum of the van der Waals radii ($d_{norm} < 0$) appear as red spots on the surfaces, contacts around the van der Waals separation ($d_{norm} = 0$) are coloured white, and longer contacts ($d_{norm} > 0$) are represented by blue regions. Fingerprint plots, consisting of 2D-representations of $d_i$ versus $d_e$ at each point of the surface,[60] were also generated.

Pairwise intermolecular interaction energies in the crystal structure were computed using the CE-B3LYP/6–31G(d,p) energy model implemented in *CrystalExplorer*.[61,62] These energies were calculated between a central molecule and all neighbouring molecules within a cluster of 3.8 Å around the central molecule, generated by applying crystallographic symmetry operations. For each pair of molecules, the total inter-molecular energy ($E_{tot}$) is expressed as:

$$E_{tot} = E_{ele} + E_{pol} + E_{disp} + E_{ex-rep} \quad (2)$$

where $E_{ele}$, $E_{pol}$, $E_{disp}$ and $E_{ex\text{-}rep}$ are the electrostatic, polarization, dispersion and exchange-repulsion components, respectively.[36,63]

## 5.6. References

(1) Rosenthal, M. R.; Ng, C. L. *Plasmodium falciparum* Artemisinin Resistance: The Effect of Heme, Protein Damage, and Parasite Cell Stress Response. *ACS Infect. Dis.* **2020**, *6* (7), 1599–1614. https://doi.org/10.1021/acsinfecdis.9b00527.

(2) Lobo, L.; Cabral, L. I. L.; Sena, M. I.; Guerreiro, B.; Rodrigues, A. S.; de Andrade-Neto, V. F.; Cristiano, M. L. S.; Nogueira, F. New Endoperoxides Highly Active *in vivo* and *in vitro* against Artemisinin-Resistant *Plasmodium falciparum*. *Malar. J.* **2018**, *17* (1), 145. https://doi.org/10.1186/s12936-018-2281-x.

(3) Rawe, S. L. Artemisinin and Artemisinin-Related Agents. In *Antimalarial Agents*;

Elsevier Ltd, 2020; pp 99–132. https://doi.org/10.1016/B978-0-08-101210-9.00004-4.

(4) Vennerstrom, J. L.; Arbe-Barnes, S.; Brun, R.; Charman, S. A.; Chiu, F. C. K.; Chollet, J.; Dong, Y.; Dorn, A.; Hunziker, D.; Matile, H.; McIntosh, K.; Padmanilayam, M.; Santo Tomas, J.; Scheurer, C.; Scorneaux, B.; Tang, Y.; Urwyler, H.; Wittlin, S.; Charman, W. N. Identification of an Antimalarial Synthetic Trioxolane Drug Development Candidate. *Nature* **2004**, *430* (7002), 900–904. https://doi.org/10.1038/nature02779.

(5) Marti, F.; Chadwick, J.; Amewu, R. K.; Burrell-Saward, H.; Srivastava, A.; Ward, S. A.; Sharma, R.; Berry, N.; O'Neill, P. M. Second Generation Analogues of RKA182: Synthetic Tetraoxanes with Outstanding *in vitro* and *in vivo* antimalarial Activities. *Med. Chem. Commun* **2011**, *2* (7), 661–665. https://doi.org/10.1039/c1md00102g.

(6) O'Neill, P. M.; Stocks, P. A.; Sabbani, S.; Roberts, N. L.; Amewu, R. K.; Shore, E. R.; Aljayyoussi, G.; Angulo-Barturén, I.; Belén, M.; Jiménez-Díaz; Bazaga, S. F.; Martínez, M. S.; Campo, B.; Sharma, R.; Charman, S. A.; Ryan, E.; Chen, G.; Shackleford, D. M.; Davies, J.; Nixon, G. L.; Biagini, G. A.; Ward, S. A. Synthesis and Profiling of Benzylmorpholine 1,2,4,5-Tetraoxane Analogue N205: Towards Tetraoxane Scaffolds with Potential for Single Dose Cure of Malaria. *Bioorganic Med. Chem.* **2018**, *26* (11), 2996–3005. https://doi.org/10.1016/j.bmc.2018.05.006.

(7) O'Neill, P. M.; Sabbani, S.; Nixon, G. L.; Schnaderbeck, M.; Roberts, N. L.; Shore, E. R.; Riley, C.; Murphy, B.; McGillan, P.; Ward, S. A.; Davies, J.; Amewu, R. K. Optimisation of the Synthesis of Second Generation 1,2,4,5 Tetraoxane Antimalarials. *Tetrahedron* **2016**, *72* (40), 6118–6126. https://doi.org/10.1016/j.tet.2016.08.043.

(8) Woodley, C. M.; Amado, P. S. M.; Cristiano, M. L. S.; O'Neill, P. M. Artemisinin Inspired Synthetic Endoperoxide Drug Candidates: Design, Synthesis, and Mechanism of Action Studies. *Med. Res. Rev.* **2021**, *41* (6), 3062–3095. https://doi.org/10.1002/med.21849.

(9) O'Neill, P. M.; Amewu, R. K.; Nixon, G. L.; Bousejra ElGarah, F.; Mungthin, M.; Chadwick, J.; Shone, A. E.; Vivas, L.; Lander, H.; Barton, V.; Muangnoicharoen, S.; Bray, P. G.; Davies, J.; Park, B. K.; Wittlin, S.; Brun, R.; Preschel, M.; Zhang, K.; Ward, S. A. Identification of a 1,2,4,5-Tetraoxane Antimalarial Drug-Development Candidate (RKA 182) with Superior Properties to the Semisynthetic Artemisinins. *Angew. Chemie - Int. Ed.* **2010**, *49*, 5693–5697. https://doi.org/10.1002/anie.201001026.

(10) Crespo-Ortiz, M. P.; Wei, M. Q. Antitumor Activity of Artemisinin and Its Derivatives: From a Well-Known Antimalarial Agent to a Potential Anticancer Drug. *J. Biomed. Biotechnol.* **2012**, *2012*, 247597. https://doi.org/10.1155/2012/247597.

(11) Amewu, R. K.; Chadwick, J.; Hussain, A.; Panda, S.; Rinki, R.; Janneh, O.; Ward, S. A.; Miguel, C.; Burrell-Saward, H.; Vivas, L.; O'Neill, P. M. Synthesis and Evaluation of the Antimalarial, Anticancer, and Caspase 3 Activities of Tetraoxane Dimers. *Bioorg. Med. Chem.* **2013**, *21* (23), 7392–7397. https://doi.org/10.1016/j.bmc.2013.09.047.

(12) Yaremenko, I. A.; Syroeshkin, M. A.; Levitsky, D. O.; Fleury, F.; Terent'ev, A. O. Cyclic Peroxides as Promising Anticancer Agents: *in vitro* Cytotoxicity Study of Synthetic Ozonides and Tetraoxanes on Human Prostate Cancer Cell Lines. *Med. Chem. Res.* **2017**, *26* (1), 170–179. https://doi.org/10.1007/s00044-016-1736-2.

(13) Opsenica, D. M.; Radivojevic, J.; Matić, I. Z.; Štajner, T.; Kneževic-Ušaj, S.; Djurkovic-Djakovic, O.; Šolaja, B. A. Tetraoxanes as Inhibitors of Apicomplexan Parasites *Plasmodium falciparum* and *Toxoplasma gondii* Growth and Anti-Cancer Molecules. *J. Serbian Chem. Soc.* **2015**, *80* (11), 1339–1359. https://doi.org/10.2298/JSC150430063O.

(14) Vil', V. A.; Yaremenko, I. A.; Fomenkov, D. I.; Levitsky, D. O.; Fleury, F.; Terent'ev, A. O. Ion Exchange Resin-Catalyzed Synthesis of Bridged Tetraoxanes Possessing *in vitro* Cytotoxicity against HeLa Cancer Cells. *Chem. Heterocycl. Compd.* **2020**, *56* (6), 722–726. https://doi.org/10.1007/s10593-020-02722-4.

(15) Yaremenko, I. A.; Coghi, P.; Prommana, P.; Qiu, C.; Radulov, P. S.; Qu, Y.; Belyakova, Y. Y.; Zanforlin, E.; Kokorekin, V. A.; Wu, Y. Y. J.; Fleury, F.; Uthaipibull, C.; Wong, V. K. W.; Terent'ev, A. O. Synthetic Peroxides Promote Apoptosis of Cancer Cells by Inhibiting P-Glycoprotein ABCB5. *ChemMedChem* **2020**, *15* (13), 1118–1127. https://doi.org/10.1002/cmdc.202000042.

(16) Coghi, P.; Yaremenko, I. A.; Prommana, P.; Radulov, P. S.; Syroeshkin, M. A.; Wu, Y.

J.; Gao, J. Y.; Gordillo-Martinez, F. M.; Mok, S.; Wong, V. K. W.; Uthaipibull, C.; Terent'ev, A. O. Novel Peroxides as Promising Anticancer Agents with Unexpected Depressed Antimalarial Activity. *ChemMedChem* **2018**, *13* (9), 902–908. https://doi.org/10.1002/cmdc.201700804.

(17) Šolaja, B. A.; Terzić, N.; Pocsfalvi, G.; Gerena, L.; Tinant, B.; Opsenica, D.; Milhous, W. K. Mixed Steroidal 1,2,4,5-Tetraoxanes: Antimalarial and Antimycobacterial Activity. *J. Med. Chem.* **2002**, *45* (16), 3331–3336. https://doi.org/10.1021/jm020891g.

(18) Opsenica, I.; Opsenica, D.; Lanteri, C. A.; Anova, L.; Milhous, W. K.; Smith, K. S.; Šolaja, B. A. New Chimeric Antimalarials with 4-Aminoquinoline Moiety Linked to a Tetraoxane Skeleton. *J. Med. Chem.* **2008**, *51* (19), 6216–6219. https://doi.org/10.1021/jm8006905.

(19) Cabral, L. I. L.; Pomel, S.; Cojean, S.; Amado, P. S. M.; Loiseau, P. M.; Cristiano, M. L. S. Synthesis and Antileishmanial Activity of 1,2,4,5-Tetraoxanes against *Leishmania donovani*. *Molecules* **2020**, *25* (3), 465. https://doi.org/10.3390/molecules25030465.

(20) Antolínez, I. V.; Barbosa, L. C. A.; Borgati, T. F.; Baldaia, A.; Ferreira, S. R.; Almeida, R. M.; Fujiwara, R. T. Tetraoxanes as New Agents Agains *Leishmania amazonensis*. *Chem. Biodivers.* **2020**, *17* (6), e2000142. https://doi.org/10.1002/cbdv.202000142.

(21) Mendes, A.; Armada, A.; Cabral, L. I. L.; Amado, P. S. M.; Campino, L.; Cristiano, M. L. S.; Cortes, S. 1,2,4-Trioxolane and 1,2,4,5-Tetraoxane Endoperoxides against Old-World Leishmania Parasites: *In vitro* Activity and Mode of Action. *Pharmaceuticals* **2022**, *15* (4), 446. https://doi.org/10.3390/ph15040446.

(22) Wang, X.; Zhao, Q.; Vargas, M.; Dong, Y.; Sriraghavan, K.; Keiser, J.; Vennerstrom, J. L. The Activity of Dispiro Peroxides against *Fasciola hepatica*. *Bioorganic Med. Chem. Lett.* **2011**, *21* (18), 5320–5323. https://doi.org/10.1016/j.bmcl.2011.07.024.

(23) Kirchhofer, C.; Vargas, M.; Braissant, O.; Dong, Y.; Wang, X.; Vennerstrom, J. L.; Keiser, J. Activity of OZ78 Analogues against *Fasciola hepatica* and *Echinostoma caproni*. *Acta Trop.* **2011**, *118* (1), 56–62. https://doi.org/10.1016/j.actatropica.2011.02.003.

(24) Vil', V. A.; Yaremenko, I. A.; Ilovaisky, A. I.; Terent'ev, A. O. Peroxides with Anthelmintic, Antiprotozoal, Fungicidal and Antiviral Bioactivity: Properties, Synthesis and Reactions. *Molecules* **2017**, *22* (11), 1881. https://doi.org/10.3390/molecules22111881.

(25) Kirchhofer, C.; Vargas, M.; Huwyler, J.; Keiser, J. Pharmacokinetics of the Fasciocidal Drug Candidates MT04 and OZ78 in Uninfected Rats and *in vitro* Pharmacodynamic Studies. *Int. J. Parasitol. Drugs Drug Resist.* **2012**, *2*, 121–125. https://doi.org/10.1016/j.ijpddr.2012.03.003.

(26) Duan, W.-W.; Qiu, S.-J.; Zhao, Y.; Sun, H.; Qiao, C.; Xia, C.-M. Praziquantel Derivatives Exhibit Activity against Both Juvenile and Adult *Schistosoma japonicum*. *Bioorganic Med. Chem. Lett.* **2012**, *22* (4), 1587–1590. https://doi.org/10.1016/j.bmcl.2011.12.133.

(27) Cowan, N.; Yaremenko, I. A.; Krylov, I. B.; Terent'ev, A. O.; Keiser, J. Elucidation of the *in vitro* and *in vivo* Activities of Bridged 1,2,4-Trioxolanes, Bridged 1,2,4,5-Tetraoxanes, Tricyclic Monoperoxides, Silyl Peroxides, and Hydroxylamine Derivatives against *Schistosoma mansoni*. *Bioorg. Med. Chem.* **2015**, *23* (16), 5175–5181. https://doi.org/10.1016/j.bmc.2015.02.010.

(28) Ingram, K.; Yaremenko, I. A.; Krylov, I. B.; Hofer, L.; Terent'ev, A. O.; Keiser, J. Identification of Antischistosomal Leads by Evaluating Bridged 1,2,4,5-Tetraoxanes, Alphaperoxides, and Tricyclic Monoperoxides. *J. Med. Chem.* **2012**, *55* (20), 8700–8711. https://doi.org/10.1021/jm3009184.

(29) Charman, S. A.; Arbe-Barnes, S.; Bathurst, I. C.; Brun, R.; Campbell, M.; Charman, W. N.; Chiu, F. C. K.; Chollet, J.; Craft, J. C.; Creek, D. J.; Dong, Y.; Matile, H.; Maurer, M.; Morizzi, J.; Nguyen, T.; Papastogiannidis, P.; Scheurer, C.; Shackleford, D. M.; Sriraghavan, K.; Stingelin, L.; Tang, Y.; Urwyler, H.; Wang, X.; White, K. L.; Wittlin, S.; Zhou, L.; Vennerstrom, J. L. Synthetic Ozonide Drug Candidate OZ439 Offers New Hope for a Single-Dose Cure of Uncomplicated Malaria. *Proc. Natl. Acad. Sci. U. S. A.* **2011**, *108* (11), 4400–4405. https://doi.org/10.1073/pnas.1015762108.

(30) Phyo, A. P.; Jittamala, P.; Nosten, F. H.; Pukrittayakamee, S.; Imwong, M.; White, N. J.; Duparc, S.; Macintyre, F.; Baker, M.; Möhrle, J. J. Antimalarial Activity of Artefenomel

(OZ439), a Novel Synthetic Antimalarial Endoperoxide, in Patients with *Plasmodium falciparum* and *Plasmodium vivax* Malaria: An Open-Label Phase 2 Trial. *Lancet Infect. Dis.* **2016**, *16* (1), 61–69. https://doi.org/10.1016/S1473-3099(15)00320-5.

(31) Adoke, Y.; Rella Zoleko-Manego; Ouoba, S.; Tiono, A. B.; Kaguthi, G.; Bonzela, J. E.; Duong, T. T.; Nahum, A.; Marielle Bouyou-Akotet; Ogutu, B.; Ouedraogo, A.; Macintyre, F.; Jessel, A.; Laurijssens, B.; Cherkaoui-Rbati, M. H.; Cantalloube, C.; Marrast, A. C.; Bejuit, R.; White, D.; Wells, T. N. C.; Wartha, F.; Leroy, D.; Kibuuka, A.; Mombo-Ngoma, G.; Ouattara, D.; Mugenya, I.; Phuc, B. Q.; Bohissou, F.; Mawili-Mboumba, D. P.; Olewe, F.; Soulama, I.; Tinto, H.; FALCI Study Group. A Randomized, Double-Blind, Phase 2b Study to Investigate the Efficacy, Safety, Tolerability and Pharmacokinetics of a Single-Dose Regimen of Ferroquine with Artefenomel in Adults and Children with Uncomplicated *Plasmodium falciparum* Malaria. *Malar. J.* **2021**, *20* (1), 222. https://doi.org/10.1186/s12936-021-03749-4.

(32) O'Neill, P. M.; Amewu, R. K.; Charman, S. A.; Sabbani, S.; Gnädig, N. F.; Straimer, J.; Fidock, D. A.; Shore, E. R.; Roberts, N. L.; Wong, M. H.-L.; Hong, W. D.; Pidathala, C.; Riley, C.; Murphy, B.; Aljayyoussi, G.; Gamo, F. J.; Sanz, L.; Rodrigues, J.; Cortes, C. G.; Herreros, E.; Angulo-Barturén, I.; Jiménez-Díaz, M. B.; Bazaga, S. F.; Martínez-Martínez, M. S.; Campo, B.; Sharma, R.; Ryan, E.; Shackleford, D. M.; Campbell, S.; Smith, D. A.; Wirjanata, G.; Noviyanti, R.; Price, R. N.; Marfurt, J.; Palmer, M. J.; Copple, I. M.; Mercer, A. E.; Ruecker, A.; Delves, M. J.; Sinden, R. E.; Siegl, P.; Davies, J.; Rochford, R.; Kocken, C. H. M.; Zeeman, A.-M.; Nixon, G. L.; Biagini, G. A.; Ward, S. A. A Tetraoxane-Based Antimalarial Drug Candidate That Overcomes PfK13-C580Y Dependent Artemisinin Resistance. *Nat. Commun.* **2017**, *8*, 15159. https://doi.org/10.1038/ncomms15159.

(33) Spackman, M. A.; Jayatilaka, D. Hirshfeld Surface Analysis. *CrystEngComm* **2009**, *11* (1), 19–32. https://doi.org/10.1039/b818330a.

(34) Cremer, D.; Pople, J. A. A General Definition of Ring Puckering Coordinates. *J. Am. Chem. Soc.* **1975**, *97* (6), 1354–1358. https://doi.org/10.1021/ja00839a011.

(35) Rao, S. T.; Westhof, E.; Sundaralingam, M. Exact method for the calculation of pseudorotation parameters *P*, $\tau_m$ and their errors. A comparison of the Altona-Sundaralingam and Cremer-Pople treatment of puckering of five-membered rings. *Acta Crystallogr. Sect. A* **1981**, *A37*, 421–425. https://doi.org/10.1107/S0567739481000892.

(36) Spackman, M. A. Towards the Use of Experimental Electron Densities to Estimate Reliable Lattice Energies. *CrystEngComm* **2018**, *20* (36), 5340–5347. https://doi.org/10.1039/c8ce01108g.

(37) Gu, Y.; Kar, T.; Scheiner, S. Fundamental Properties of the CH···O Interaction: Is It a True Hydrogen Bond? *J. Am. Chem. Soc.* **1999**, *121* (31), 9411–9422. https://doi.org/10.1021/ja991795g.

(38) Desiraju, G. R. The C−H···O Hydrogen Bond in Crystals: What Is It? *Acc. Chem. Res.* **1991**, *24* (10), 290–296. https://doi.org/10.1021/ar00010a002.

(39) Steiner, T. C−H···O Hydrogen Bonding in Crystals. *Crystallogr. Rev.* **2003**, *9* (2–3), 177–228. https://doi.org/10.1080/0889311031000162177 2.

(40) Malone, J. F.; Murray, C. M.; Charlton, M. H.; Docherty, R.; Lavery, A. J. X−H···π (Phenyl) Interactions Theoretical and Crystallographic Observations. *J. Chem. Soc. Faraday Trans.* **1997**, *93* (19), 3429–3436. https://doi.org/10.1039/A700669A.

(41) Steiner, T.; Koellner, G. Hydrogen Bonds with π-Acceptors in Proteins: Frequencies and Role in Stabilizing Local 3D Structures. *J. Mol. Biol.* **2001**, *305* (3), 535–557. https://doi.org/10.1006/jmbi.2000.4301.

(42) G. R. Desiraju, T. Steiner. *The weak hydrogen bond: in structural chemistry and biology*, Vol. 9, Oxford University Press, **2001**, pp. 293–342.

(43) Teixeira-Dias, J. J. C.; Fausto, R. A Molecular Mechanics Force Field for Conformational Analysis of Simple Acyl Chlorides, Carboxylic Acids and Esters. *J. Mol. Struct.* **1986**, *144* (3–4), 199–213. https://doi.org/10.1016/0022-2860(86)85001-3.

(44) Fausto, R.; Teixeira-Dias, J. J. C. The High Energy *S-Trans* Conformers of $CH_3COOH$ and $CH_3COOCH_3$: A Molecular Mechanics and Vibrational Study of $CH_3COCl$,

$CH_3COOH$ and $CH_3COOCH_3$. *J. Mol. Struct.* **1986**, *144* (3–4), 215–223. https://doi.org/10.1016/0022-2860(86)85002-5.

(45) Tang, Y.; Dong, Y.; Karle, J. M.; DiTusa, C. A.; Vennerstrom, J. L. Synthesis of Tetrasubstituted Ozonides by the Griesbaum Coozonolysis Reaction: Diastereoselectivity and Functional Group Transformations by Post-Ozonolysis Reactions. *J. Org. Chem.* **2004**, *69* (19), 6470–6473. https://doi.org/10.1021/jo040171c.

(46) Sheldrick, G. M. SHELXT – Integrated Space-Group and Crystal-Structure Determination. *Acta Crystallogr. Sect. A* **2015**, *A71*, 3–8. https://doi.org/10.1107/S2053273314026370.

(47) Sheldrick, G. M. Crystal Structure Refinement with SHELXL. *Acta Crystallogr. Sect. C* **2015**, *C71*, 3–8. https://doi.org/10.1107/S2053229614024218.

(48) Becke, A. D. Density-Functional Exchange-Energy Approximation with Correct Asymptotic Behavior. *Phys. Rev. A* **1988**, *38* (6), 3098–3100. https://doi.org/10.1103/PhysRevA.38.3098.

(49) Lee, C.; Yang, W.; Parr, R. G. Development of the Colle-Salvetti Correlation-Energy Formula into a Functional of the Electron Density. *Phys. Rev. B* **1988**, *37* (2), 785–789. https://doi.org/10.1103/PhysRevB.37.785.

(50) Vosko, S. H.; Wilk, L.; Nusair, M. Accurate Spin-Dependent Electron Liquid Correlation Energies for Local Spin Density Calculations: A Critical Analysis. *Can. J. Phys.* **1980**, *58* (8), 1200–1211. https://doi.org/10.1139/p80-159.

(51) Mclean, A. D.; Chandler, G. S. Contracted Gaussian Basis Sets for Molecular Calculations. I. Second Row Atoms, *Z*=11–18. *J. Chem. Phys.* **1980**, *72* (10), 5639–5648. https://doi.org/10.1063/1.438980.

(52) M. J. Frisch, G. W. Trucks, H. B. Schlegel, G. E. Scuseria, M. A. Robb, J. R. Cheeseman, G. Scalmani, V. Barone, B. Mennucci, G. A. Petersson, H. Nakatsuji, M. Caricato, X. Li, H. P. Hratchian, A. F. Izmaylov, J. Bloino, G. Zheng, J. L. Sonnenberg, M. Hada, M. Ehara, K. Toyota, R. Fukuda, J. Hasegawa, M. Ishida, T. Nakajima, Y. Honda, O. Kitao, H. Nakai, T. Vreven, J. J. A. Montgomery, J. E. Peralta, F. Ogliaro, M. Bearpark, J. J. Heyd, E. Brothers, K. N. Kudin, V. N. Staroverov, R. Kobayashi, J. Normand, K. Raghavachari, A. Rendell, J. C. Burant, S. S. Iyengar, J. Tomasi, M. Cossi, N. Rega, J. M. Millam, M. Klene, J. E. Knox, J. B. Cross, V. Bakken, C. Adamo, J. Jaramillo, R. Gomperts, R. E. Stratmann, O. Yazyev, A. J. Austin, R. Cammi, C. Pomelli, J. W. Ochterski, R. L. Martin, K. Morokuma, V. G. Zakrzewski, G. A. Voth, P. Salvador, J. J. Dannenberg, S. Dapprich, A. D. Daniels, Ö. Farkas, J. B. Foresman, J. V. Ortiz, J. Cioslowski, D. J. Fox, *Gaussian 09 (Revision A.02)*, **2016**.

(53) "Chemcraft - Graphical Software for Visualization of Quantum Chemistry Computations," can be found under https://www.chemcraftprog.com, **2022**.

(54) Hirshfeld, F. L. Bonded-Atom Fragments for Describing Molecular Charge Densities. *Theor. Chim. Acta* **1977**, *44* (2), 129–138. https://doi.org/10.1007/BF00549096.

(55) Spackman, M. A.; Byrom, P. G. A Novel Definition of a Molecule in a Crystal. *Chem. Phys. Lett.* **1997**, *267* (3–4), 215–220. https://doi.org/10.1016/S0009-2614(97)00100-0.

(56) Mckinnon, J. J.; Mark, A.; Mitchell, A. S. Novel Tools for Visualizing and Exploring Intermolecular Interactions in Molecular Crystals. *Acta Crystallogr. Sect. B* **2004**, *B60* (6), 627–668. https://doi.org/10.1107/S0108768104020300.

(57) McKinnon, J. J.; Jayatilaka, D.; Spackman, M. A. Towards Quantitative Analysis of Intermolecular Interactions with Hirshfeld Surfaces. *Chem. Commun.* **2007**, No. 37, 3814–3816. https://doi.org/10.1039/b704980c.

(58) Spackman, P. R.; Turner, M. J.; McKinnon, J. J.; Wolff, S. K.; Grimwood, D. J.; Jayatilaka, D.; Spackman, M. A. CrystalExplorer: A Program for Hirshfeld Surface Analysis, Visualization and Quantitative Analysis of Molecular Crystals. *J. Appl. Crystallogr.* **2021**, *54* (3), 1006–1011. https://doi.org/10.1107/S1600576721002910.

(59) F. H. Allen, O. Kennard, D. G. Watson, L. Brammer, A. G. Orpen, R. Taylor. *International Tables for Crystallography*, Vol. C (Edited by AJC Wilson), **1995**, Dordrecht: Kluwer Academic Publishers.

(60) Spackman, M. A.; McKinnon, J. J. Fingerprinting Intermolecular Interactions in

Molecular Crystals. *CrystEngComm* **2002**, *4* (66), 378–392. https://doi.org/10.1039/b203191b.

(61) Turner, M. J.; Grabowsky, S.; Jayatilaka, D.; Spackman, M. A. Accurate and Efficient Model Energies for Exploring Intermolecular Interactions in Molecular Crystals. *J. Phys. Chem. Lett.* **2014**, *24* (4), 4249–4255. https://doi.org/10.1021/jz502271c.

(62) Mackenzie, C. F.; Spackman, P. R.; Jayatilaka, D.; Spackman, M. A. CrystalExplorer Model Energies and Energy Frame- Works: Extension to Metal Coordination Compounds, Organic Salts, Solvates and Open-Shell Systems. *IUCrJ* **2017**, *4* (5), 575–587. https://doi.org/10.1107/S205225251700848X.

(63) Thomas, S. P.; Spackman, P. R.; Jayatilaka, D.; Spackman, M. A. Accurate Lattice Energies for Molecular Crystals from Experimental Crystal Structures. *J. Chem. Theory Comput.* **2018**, *14* (3), 1614–1623. https://doi.org/10.1021/acs.jctc.7b01200.

# Chapter 6

## Conclusions

## 6.1. Conclusions and perspectives

The primary goal of this thesis was the development of new TB drugs by proposing an hybridization approach where two separate anti-TB classes were selected, the indole-2-carboxamide scaffold (MmpL3 inhibitors) and the benzothiazinone scaffold (DprE1 inhibitors), and independently combined with peroxide-containing moieties, choosing the 1,2,4-trioxane core for this research. The indole-2-carboxamide (IC) and the benzothiazinone (BTZ) scaffolds were selected due to their high potency against replicating *Mtb* but low activity against non-replicating persistent *Mtb*. We aimed to establish a dual mode of action, increasing *Mtb*'s sensitivity to the active anti-TB pharmacophore while targeting the DosRST signalling.

The screening of IC-based peroxide hybrids against replicating *Mtb* demonstrated poor activity for most of the compounds ($IC_{50}$ > 10 µM). However, the metabolite control compound **2.84** and the tetraoxane hybrid **2.86** exhibited moderate inhibitory activity of the *Mtb* growth ($IC_{50}$ = 5.680 and 2.634 µM, respectively). Docking studies explained the poor activity of IC compounds, as IC-peroxide hybrids displayed showed poor docking results, except for IC-analogue **TIC01**. However, this peroxide hybrid proved inactive against *Mtb.*

On the contrary, our research on BTZ analogues resulted in 16 novel BTZ-peroxide compounds and led to the identification of potent representatives in replicating *Mtb* assays, with $IC_{50}$ values in the nanomolar (1.32-870 nM) and picomolar range (< 0.457 nM). Docking studies demonstrated good overlap between the BTZ ring system of the hybrids and the reference ligand, supporting the potent sub-micromolar activity achieved by these series.

Moreover, *in silico* data were calculated for endoperoxide hybrids and compared to the *in vitro* DMPK results. Experimentally, the IC-trioxane hybrids **TIC01-03** were similarly lipophilic and poorly soluble at pH 7.4, as expected for indole-2-carboxamide compounds. The metabolic profiles of IC-based and BTZ043-based peroxide hybrids were moderate to good, whereas those derived from PBTZ169 were poor to moderate. The high cLogP values for all synthesized compounds are mirrored in the low anticipated aqueous solubility at pH 7.4.

*In vivo* pharmacokinetic profiles of **B3**, **P1**, and controls **BTZ043** and **PBTZ169**, indicate that peroxide-BTZs are less stable than standard BTZs, which could be due to the labile peroxide link in their structure, making them susceptible to extensive

metabolism. In contrast to the lead compounds, however, peroxide-BTZ **B3** exhibited sufficient PK data. Selected compounds were sent for screening against whole cell *Mtb* modified to express DosRST-dependent GFP and the testing is still ongoing. Further development in the BTZ series is required to improve the pharmacokinetics properties.

The flavoenzyme DprE1's non-specific vulnerability could explain our promising results during the development of BTZ-peroxide hybrids. Although the design of DprE1 inhibitors can be challenging, the prediction of PC descriptors and ADMET properties for these molecules may aid in designing new lead compounds. To deepen our understanding, a comprehensive PC descriptors analysis was conducted. Our results indicated that for inactive covalent DprE1 inhibitors to match the active set's corresponding properties more closely it may be necessary to optimize the compounds by increasing MW, ClogP, ClogD, HBA and TPSA, while reducing logS and HBD. On the other hand, for inactive non-covalent DprE1 inhibitors it may be required to optimize the compounds by increasing MW, HBA, HBD, TPSA, FInd, and ROTBS. All these changes are likely to increase the enthalpic component of drug binding through enhanced hydrogen bonding contacts with the enzyme. Covalent DprE1 inhibitors tend to violate the Ro5 more frequently than their non-covalent counterparts. However, only a small proportion fails the criteria by two or more violations, indicating that the DprE1 inhibitors are more likely to benefit from membrane permeability and, hence, will be more readily absorbed in the human digestive system via passive diffusion.

To predict and identify potent DprE1 inhibitors we built classification models of DprE1, a standard method for predicting the activity of a compound through its structural descriptors. We used the original dataset, with 1519 molecules, and another two modified datasets, with down or up-sampling pre-processing, to balance the active and inactive molecules in the sample.

A total of 105 models using five different algorithms (KNN, SVM, GBM, RF, and XGB) were built, in which the best models for each algorithm produced MCC values of 0.791, 0.775, 0.801, 0.842 and 0.882 on the test set, respectively, when using the up-sampling balanced subset. It was determined that the 35 generated models for the DS subset had a good performance, with accuracy >0.78, precision >0.78, sensitivity >0.78, specificity >0.78, MCC >0.57, ROC >0.78, and f1 score >0.78. Regarding the 35 constructed models for the US subset, these models had the best performance among the subsets, with accuracy >0.85, precision >0.85, sensitivity >0.85, specificity >0.85, MCC

>0.71, ROC >0.85, and f1 score >0.85. In comparison to the balanced subsets, the performance of the 35 generated models for the original subset was inferior, with an accuracy >0.80, precision >0.77, sensitivity >0.80, specificity >0.63, MCC >0.51, ROC >0.72, and f1 score >0.75. When examining the different metrics, it can be shown that the OS subset has the lowest metric specificity (>0.63), compared to the DS (>0.78) and US (>0.85) subsets, this result being ascribed to the imbalanced dataset between inactive and active compounds. The XGB models showed the best performance across most data sets during the 5 and 10-fold cross-validation training, in which the best model was model XGB21, using the US subset built with MACCS, ECFP4 and FCFP4 fingerprints.

MACCS and FCFP4 fingerprints were the most important features in GBM, RF, and XGB models. For each algorithm, such important properties feature the presence or absence of a nitro group that appears in determining whether a molecule inhibits or does not inhibit the DprE1enzyme. Therefore, models are better trained to identify covalent binders. Evaluation of peroxide hybrids in the best models for each algorithm was also performed and only model KNN16 could not appropriately classify IC-trioxane hybrids as non-inhibitors or inactive molecules. The remaining algorithms correctly identified the corresponding compounds as active, for the BTZ peroxide hybrids, and inactive, for IC peroxide hybrids. This result of high predictive performance was expected, since the models are better trained for identifying covalent binders. Further external validation data should be used to better evaluate these produced models.

In future work, refinement of these models is necessary for a more efficient selection of non-covalent binders. Splitting the collected dataset into subsets for covalent and non-covalent binders is a potential solution for this issue. Ensuring that overfitting does not occur is another crucial aspect of validation in future models to improve performance. In addition, developing regression (quantitative) models should be investigated since they will allow us to predict a molecule's MIC value instead of merely classifying it as active or inactive. Improvement of the applicability domain should also be addressed to optimize the reliability and decidability of these models.

Since there is a strong correlation between DprE1 inhibition and anti-TB activity, we were able to develop classification models that could identify either DprE1 inhibitors or new anti-TB drugs in this study.

Among organic peroxides, six-membered cyclic 1,2,4-trioxanes and 1,2,4,5-tetraoxanes have gained a great interest in medicinal chemistry due to their potential for

treating various parasite-borne diseases, including malaria. The work within this thesis also focused on improving methods for generating six-membered peroxides to expand their libraries, allowing the discovery of novel drug candidates.

The cyclocondensation of a representative library of ketones with *gem*-dihydroperoxides or peroxysilyl alcohols/β-hydroperoxy alcohols to afford the corresponding unsymmetrical 1,2,4,5-tetraoxanes or 1,2,4-trioxanes, mediated by the SSA catalyst, was systematically investigated. Silica-supported catalysts have attracted attention in recent years due to their promising reactivity and recoverable and reusable properties, leading to economic and environmental benefits. The elementary steps governing the cyclocondensation pathway were investigated through molecular orbital calculations, using the DFT method, at the ωB97XD/def2-TZVPP/PCM(DCM)//B3LYP/6-31G(d) level of approximation. The results support a mechanistic proposal that highlights the catalytic role of SSA, where SSA's initial protonation of the ketone carbonyl group emerges as a key step in the mechanism.

Among the advantages offered by this novel approach involving the silica-supported catalyst, the tolerance to a wide range of substrates should be highlighted. In addition, easy preparation, recyclability and eco-friendly properties of the SSA catalyst make this method appealing in broadening the design of new biologically active endoperoxides, therefore establishing a valid alternative approach for the synthesis of new biologically active endoperoxides.

Despite the endoperoxides' potential medical and veterinary applications, fundamental studies on the structures of trioxolanes and tetraoxanes are scarce. Within the work performed along the doctoral studies, described in this thesis, the crystalline structures of the precursors of the antimalarial candidates **OZ439** and **E209**, endoperoxides **1** (*p*-(dispiro-[cyclohexane-1,3'--[1,2,4]trioxolane-5',2''-tricyclo [3.3.1.1$^{3,7}$]decan]-4-yl)-phenyl acetate) and **2** (*p*-(dispiro-[cyclohexane-1,3'-[1,2,4,5]tetraoxane-6',2''-tricyclo[3.3.1.1$^{3,7}$]decan]-4-yl)-phenyl acetate), were also investigated by single crystal X-ray diffraction studies. Compounds **1** and **2** were found to crystallize in the monoclinic *Cc* and $P2_1/c$ space groups, respectively, with four molecules within the unit cell. Moreover, in the crystalline state, the tetraoxane ring in **2** and the trioxolane-adamantane fragment in **1** were disordered, with molecules of **1** and **2** existing as two distinct, stable conformations.

From the Hirshfeld surface analysis, it was shown that the crystal packing of both

compounds is dominated by H···H (68-70%), H···O/O···H (19-23%), and H···C/C···H (9-10%) contacts, which are associated to the formation of C−H···H−C van der Waals interactions, as well as of C−H···O and C−H···**π** H-bond like interactions. In this regard, the following differences between the two endoperoxides must be underlined: (1) The dominant C−H···O H−bonds in **1** connect a C−H group of the adamantane and the O1 or O2 oxygen atoms of the trioxolane ring, whereas in **2** they involve the carbonyl oxygen, which acts as double acceptor from C−H groups of the phenyl ring; (2) The C−H···O and C−H···π H-bonds play a more important role in the molecular packing of **2**, while the C−H···H−C van der Waals interactions are more relevant in the molecular packing of **1**.

In consonance with the large contribution of the H···H contacts to the Hirshfeld surfaces of the two compounds, the CE-B3LYP/6-31G(d,p) interaction energies calculated for the most representative molecular pairs are dominated by the dispersive component. Furthermore, in accordance with the more important role of the H-bonds in **2**, the largest pairwise interaction energies were estimated for this compound.

Because of the structural similarity between the molecules of **1** and **2**, the IR spectra recorded for the two compounds are also very similar. Moreover, due to the lack of strong intermolecular interactions in the crystals, the molecular conformation adopted by the molecules in the crystal structure is not much different from that of the fully optimized isolated molecules, the respectively calculated spectra thus providing a good description of the experimental data. As a final remark, this study provides valuable structural information that may be useful to a better understanding of the reactivity and structure-activity relationship for these classes of antimalarial endoperoxides.

# Appendix

# *List of Tables and Figures*

**Table S1:** Performances for all KNN models (the best model is highlighted in *green*).

| Model (KNN#) | Subset | FPS | Training set | | | | Test set | | | | | | |
|---|---|---|---|---|---|---|---|---|---|---|---|---|---|
| | | | Q | MCC | 5-CV | 10-CV | Q | P | SE | SP | MCC | AUC | f1 |
| **1** | **DS** | **M** | 0.907 | 0.815 | 0.803 ± 0.035 | 0.814 ± 0.036 | 0.784 | 0.786 | 0.784 | 0.789 | 0.573 | 0.787 | 0.784 |
| **2** | **DS** | **E** | 0.910 | 0.820 | 0.821 ± 0.020 | 0.826 ± 0.023 | 0.826 | 0.825 | 0.826 | 0.823 | 0.650 | 0.824 | 0.825 |
| **3** | **DS** | **F** | 0.899 | 0.799 | 0.811 ± 0.039 | 0.827 ± 0.039 | 0.826 | 0.826 | 0.826 | 0.822 | 0.650 | 0.824 | 0.824 |
| **4** | **DS** | **M + E** | 0.902 | 0.804 | 0.818 ± 0.013 | 0.821 ± 0.021 | 0.821 | 0.820 | 0.821 | 0.821 | 0.642 | 0.821 | 0.821 |
| **5** | **DS** | **M + F** | 0.904 | 0.807 | 0.808 ± 0.021 | 0.814 ± 0.031 | 0.826 | 0.825 | 0.826 | 0.824 | 0.650 | 0.825 | 0.825 |
| **6** | **DS** | **E + F** | 0.919 | 0.838 | 0.841 ± 0.019 | 0.844 ± 0.032 | 0.789 | 0.792 | 0.789 | 0.796 | 0.585 | 0.792 | 0.789 |
| **7** | **DS** | **M + E + F** | 0.904 | 0.807 | 0.827 ± 0.016 | 0.829 ± 0.022 | 0.812 | 0.811 | 0.812 | 0.811 | 0.623 | 0.811 | 0.811 |
| **Overall** | **DS** | **$\bar{x} \pm \sigma$** | **0.906 ± 0.005** | **0.813 ± 0.010** | - | - | **0.812 ± 0.015** | **0.812 ± 0.014** | **0.812 ± 0.015** | **0.812 ± 0.012** | **0.625 ± 0.027** | **0.812 ± 0.013** | **0.811 ± 0.014** |
| **8** | **OS** | **M** | 0.915 | 0.787 | 0.852 ± 0.017 | 0.843 ± 0.036 | 0.821 | 0.787 | 0.821 | 0.714 | 0.555 | 0.768 | 0.776 |
| **9** | **OS** | **E** | 0.925 | 0.814 | 0.863 ± 0.017 | 0.855 ± 0.029 | 0.832 | 0.801 | 0.832 | 0.729 | 0.581 | 0.781 | 0.789 |
| **10** | **OS** | **F** | 0.917 | 0.792 | 0.859 ± 0.011 | 0.850 ± 0.023 | 0.824 | 0.798 | 0.824 | 0.689 | 0.553 | 0.756 | 0.772 |
| **11** | **OS** | **M + E** | 0.922 | 0.805 | 0.861 ± 0.017 | 0.855 ± 0.029 | 0.829 | 0.797 | 0.829 | 0.728 | 0.575 | 0.779 | 0.787 |
| **12** | **OS** | **M + F** | 0.921 | 0.803 | 0.859 ± 0.016 | 0.850 ± 0.029 | 0.813 | 0.779 | 0.813 | 0.690 | 0.530 | 0.752 | 0.763 |
| **13** | **OS** | **E + F** | 0.928 | 0..821 | 0.865 ± 0.018 | 0.856 ± 0.029 | 0.832 | 0.804 | 0.832 | 0.719 | 0.578 | 0.775 | 0.787 |
| **14** | **OS** | **M + E + F** | 0.925 | 0.812 | 0.866 ± 0.017 | 0.856 ± 0.029 | 0.818 | 0.788 | 0.818 | 0.692 | 0.542 | 0.755 | 0.768 |
| **Overall** | **OS** | **$\bar{x} \pm \sigma$** | **0.922 ± 0.004** | **0.802 ± 0.008** | - | - | **0.824 ± 0.006** | **0.793 ± 0.008** | **0.824 ± 0.006** | **0.709 ± 0.016** | **0.559 ± 0.016** | **0.767 ± 0.010** | **0.777 ± 0.009** |
| **15** | **US** | **M** | 0.937 | 0.875 | 0.859 ± 0.012 | 0.865 ± 0.000 | 0.880 | 0.881 | 0.880 | 0.880 | 0.761 | 0.880 | 0.880 |
| **16** | **US** | **E** | **0.947** | **0.895** | **0.883 ± 0.010** | **0.886 ± 0.017** | **0.895** | **0.896** | **0.895** | **0.895** | **0.791** | **0.895** | **0.895** |
| **17** | **US** | **F** | 0.946 | 0.894 | 0.873 ± 0.011 | 0.873 ± 0.017 | 0.867 | 0.868 | 0.867 | 0.867 | 0.736 | 0.867 | 0.867 |
| **18** | **US** | **M + E** | 0.946 | 0.893 | 0.890 ± 0.016 | 0.893 ± 0.018 | 0.886 | 0.887 | 0.886 | 0.886 | 0.772 | 0.886 | 0.886 |
| **19** | **US** | **M + F** | 0.949 | 0.898 | 0.884 ± 0.015 | 0.886 ± 0.017 | 0.869 | 0.870 | 0.869 | 0.869 | 0.739 | 0.869 | 0.869 |
| **20** | **US** | **E + F** | 0.951 | 0.903 | 0.889 ± 0.012 | 0.893 ± 0.018 | 0.878 | 0.879 | 0.878 | 0.878 | 0.757 | 0.878 | 0.878 |
| **21** | **US** | **M + E + F** | 0.949 | 0.899 | 0.892 ± 0.016 | 0.895 ± 0.018 | 0.876 | 0.877 | 0.876 | 0.877 | 0.754 | 0.876 | 0.876 |
| **Overall** | **US** | **$\bar{x} \pm \sigma$** | **0.946 ± 0.003** | **0.894 ± 0.006** | - | - | **0.879 ± 0.007** | **0.880 ± 0.007** | **0.879 ± 0.007** | **0.879 ± 0.007** | **0.759 ± 0.014** | **0.879 ± 0.007** | **0.879 ± 0.007** |

| **KNN hyperparameters** |
|---|
| `KNeighborsClassifier(n_neighbors=3)` |

**Table S2:** Performances for all SVM models (the best model is highlighted in *green*).

| Model (SVM#) | Subset | FPS | Training set | | | | Test set | | | | | | |
|---|---|---|---|---|---|---|---|---|---|---|---|---|---|
| | | | Q | MCC | 5-CV | 10-CV | Q | P | SE | SP | MCC | AUC | f1 |
| **1** | **DS** | **M** | 0.872 | 0.743 | 0.819 ± 0.031 | 0.827 ± 0.028 | 0.830 | 0.830 | 0.830 | 0.831 | 0.660 | 0.830 | 0.830 |
| **2** | **DS** | **E** | 0.902 | 0.804 | 0.843 ± 0.021 | 0.838 ± 0.030 | 0.858 | 0.859 | 0.858 | 0.854 | 0.714 | 0.856 | 0.857 |
| **3** | **DS** | **F** | 0.888 | 0.778 | 0.837 ± 0.031 | 0.849 ± 0.034 | 0.849 | 0.853 | 0.849 | 0.841 | 0.698 | 0.845 | 0.847 |
| **4** | **DS** | **M + E** | 0.893 | 0.786 | 0.83.5 ± 0.023 | 0.836 ± 0.028 | 0.853 | 0.852 | 0.853 | 0.853 | 0.706 | 0.853 | 0.853 |
| **5** | **DS** | **M + F** | 0.893 | 0.786 | 0.828 ± 0.024 | 0.836 ± 0.034 | 0.853 | 0.853 | 0.853 | 0.851 | 0.705 | 0.852 | 0.852 |
| **6** | **DS** | **E + F** | 0.898 | 0.795 | 0.837 ± 0.010 | 0.842 ± 0.034 | 0.812 | 0.816 | 0.812 | 0.819 | 0.632 | 0.816 | 0.812 |
| **7** | **DS** | **M + E + F** | 0.893 | 0.786 | 0.839 ± 0.026 | 0.843 ± 0.029 | 0.853 | 0.853 | 0.853 | 0.851 | 0.705 | 0.852 | 0.852 |
| **Overall** | **DS** | **$\bar{x} \pm \sigma$** | **0.891 ± 0.006** | **0.783 ± 0.013** | - | - | **0.844 ± 0.013** | **0.845 ± 0.013** | **0.844 ± 0.013** | **0.843 ± 0.011** | **0.689 ± 0.024** | **0.843 ± 0.012** | **0.843 ± 0.013** |
| **8** | **OS** | **M** | 0.871 | 0.670 | 0.839 ± 0.017 | 0.845 ± 0.026 | 0.818 | 0.811 | 0.818 | 0.634 | 0.531 | 0.726 | 0.750 |
| **9** | **OS** | **E** | 0.896 | 0.739 | 0.865 ± 0.016 | 0.864 ± 0.024 | 0.847 | 0.837 | 0.847 | 0.709 | 0.613 | 0.778 | 0.799 |
| **10** | **OS** | **F** | 0.888 | 0.717 | 0.855 ± 0.011 | 0.859 ± 0.023 | 0.839 | 0.818 | 0.839 | 0.717 | 0.595 | 0.778 | 0.794 |
| **11** | **OS** | **M + E** | 0.891 | 0.725 | 0.860 ± 0.012 | 0.860 ± 0.025 | 0.837 | 0.827 | 0.837 | 0.684 | 0.584 | 0.760 | 0.782 |
| **12** | **OS** | **M + F** | 0.882 | 0.699 | 0.851 ± 0.015 | 0.858 ± 0.026 | 0.824 | 0.808 | 0.824 | 0.663 | 0.548 | 0.743 | 0.764 |
| **13** | **OS** | **E + F** | 0.898 | 0.743 | 0.861 ± 0.016 | 0.861 ± 0.023 | 0.853 | 0.842 | 0.853 | 0.722 | 0.627 | 0.787 | 0.807 |
| **14** | **OS** | **M + E + F** | 0.891 | 0.725 | 0.855 ± 0.017 | 0.861 ± 0.027 | 0.839 | 0.827 | 0.839 | 0.696 | 0.592 | 0.768 | 0.788 |
| **Overall** | **OS** | **$\bar{x} \pm \sigma$** | **0.888 ± 0.007** | **0.717 ± 0.018** | - | - | **0.837 ± 0.009** | **0.824 ± 0.010** | **0.837 ± 0.009** | **0.689 ± 0.025** | **0.584 ± 0.026** | **0.763 ± 0.017** | **0.783 ± 0.016** |
| **15** | **US** | **M** | 0.883 | 0.768 | 0.857 ± 0.011 | 0.862 ± 0.021 | 0.858 | 0.859 | 0.858 | 0.858 | 0.717 | 0.858 | 0.858 |
| **16** | **US** | **E** | 0.912 | 0.824 | 0.889 ± 0.010 | 0.895 ± 0.018 | 0.880 | 0.880 | 0.880 | 0.880 | 0.760 | 0.880 | 0.880 |
| **17** | **US** | **F** | 0.898 | 0.797 | 0.873 ± 0.017 | 0.881 ± 0.021 | 0.875 | 0.875 | 0.875 | 0.875 | 0.749 | 0.875 | 0.875 |
| **18** | **US** | **M + E** | 0.907 | 0.814 | 0.881 ± 0.016 | 0.884 ± 0.024 | 0.873 | 0.873 | 0.873 | 0.873 | 0.745 | 0.873 | 0.873 |
| **19** | **US** | **M + F** | **0.903** | **0.807** | **0.873 ± 0.016** | **0.878 ± 0.019** | **0.887** | **0.888** | **0.887** | **0.888** | **0.775** | **0.887** | **0.887** |
| **20** | **US** | **E + F** | 0.914 | 0.829 | 0.889 ± 0.014 | 0.896 ± 0.018 | 0.875 | 0.875 | 0.875 | 0.875 | 0.749 | 0.875 | 0.875 |
| **21** | **US** | **M + E + F** | 0.908 | 0.815 | 0.884 ± 0.015 | 0.888 ± 0.022 | 0.878 | 0.878 | 0.878 | 0.878 | 0.756 | 0.878 | 0.878 |
| **Overall** | **US** | **$\bar{x} \pm \sigma$** | **0.904 ± 0.008** | **0.808 ± 0.015** | - | - | **0.875 ± 0.006** | **0.875 ± 0.006** | **0.875 ± 0.006** | **0.875 ± 0.006** | **0.750 ± 0.012** | **0.875 ± 0.006** | **0.875 ± 0.006** |

| **SVM hyperparameters** |
|---|
| `svm.SVC(probability=True)` |

**Table S3:** Performances for all GBM models (the best model is highlighted in *green*).

| Model (GBM#) | Subset | FPS | Training set | | | | Test set | | | | | | |
|---|---|---|---|---|---|---|---|---|---|---|---|---|---|
| | | | Q | MCC | 5-CV | 10-CV | Q | P | SE | SP | MCC | AUC | f1 |
| **1** | **DS** | **M** | 0.914 | 0.829 | 0.813 ± 0.031 | 0.823 ± 0.041 | 0.830 | 0.830 | 0.830 | 0.828 | 0.659 | 0.829 | 0.829 |
| **2** | **DS** | **E** | 0.954 | 0.908 | 0.831 ± 0.031 | 0.821 ± 0.036 | 0.817 | 0.816 | 0.817 | 0.819 | 0.634 | 0.818 | 0.816 |
| **3** | **DS** | **F** | 0.950 | 0.899 | 0.825 ± 0.028 | 0.843 ± 0.031 | 0.830 | 0.830 | 0.830 | 0.827 | 0.659 | 0.829 | 0.829 |
| **4** | **DS** | **M + E** | 0.962 | 0.924 | 0.823 ± 0.022 | 0.837 ± 0.029 | 0.849 | 0.848 | 0.849 | 0.848 | 0.696 | 0.848 | 0.848 |
| **5** | **DS** | **M + F** | 0.956 | 0.911 | 0.833 ± 0.030 | 0.854 ± 0.030 | 0.844 | 0.844 | 0.844 | 0.840 | 0.687 | 0.842 | 0.843 |
| **6** | **DS** | **E + F** | 0.971 | 0.942 | 0.849 ± 0.015 | 0.850 ± 0.040 | 0.803 | 0.810 | 0.803 | 0.812 | 0.618 | 0.808 | 0.803 |
| **7** | **DS** | **M + E + F** | 0.972 | 0.945 | 0.835 ± 0.037 | 0.843 ± 0.033 | 0.849 | 0.849 | 0.849 | 0.846 | 0.696 | 0.847 | 0.848 |
| **Overall** | **DS** | **$\bar{x} \pm \sigma$** | **0.954 ± 0.013** | **0.908 ± 0.025** | - | - | **0.832 ± 0.013** | **0.832 ± 0.012** | **0.832 ± 0.013** | **0.831 ± 0.011** | **0.664 ± 0.025** | **0.832 ± 0.012** | **0.831 ± 0.013** |
| **8** | **OS** | **M** | 0.904 | 0.760 | 0.840 ± 0.012 | 0.844 ± 0.024 | 0.832 | 0.819 | 0.832 | 0.677 | 0.569 | 0.754 | 0.775 |
| **9** | **OS** | **E** | 0.932 | 0.831 | 0.859 ± 0.011 | 0.860 ± 0.029 | 0.863 | 0.844 | 0.863 | 0.769 | 0.659 | 0.816 | 0.828 |
| **10** | **OS** | **F** | 0.930 | 0.825 | 0.863 ± 0.009 | 0.867 ± 0.020 | 0.839 | 0.815 | 0.839 | 0.727 | 0.597 | 0.783 | 0.796 |
| **11** | **OS** | **M + E** | 0.933 | 0.835 | 0.859 ± 0.005 | 0.861 ± 0.028 | 0.858 | 0.837 | 0.858 | 0.761 | 0.646 | 0.810 | 0.821 |
| **12** | **OS** | **M + F** | 0.940 | 0.852 | 0.849 ± 0.014 | 0.857 ± 0.019 | 0.853 | 0.828 | 0.853 | 0.759 | 0.634 | 0.806 | 0.816 |
| **13** | **OS** | **E + F** | 0.939 | 0.850 | 0.867 ± 0.014 | 0.863 ± 0.018 | 0.863 | 0.846 | 0.863 | 0.764 | 0.658 | 0.813 | 0.827 |
| **14** | **OS** | **M + E + F** | 0.948 | 0.872 | 0.863 ± 0.005 | 0.865 ± 0.025 | 0.861 | 0.843 | 0.861 | 0.757 | 0.651 | 0.809 | 0.823 |
| **Overall** | **OS** | **$\bar{x} \pm \sigma$** | **0.932 ± 0.009** | **0.832 ± 0.023** | - | - | **0.853 ± 0.010** | **0.833 ± 0.011** | **0.853 ± 0.010** | **0.745 ± 0.024** | **0.631 ± 0.027** | **0.799 ± 0.017** | **0.812 ± 0.015** |
| **15** | **US** | **M** | 0.905 | 0.810 | 0.862 ± 0.006 | 0.863 ± 0.028 | 0.869 | 0.869 | 0.869 | 0.869 | 0.738 | 0.869 | 0.869 |
| **16** | **US** | **E** | 0.930 | 0.860 | 0.891 ± 0.012 | 0.892 ± 0.020 | 0.891 | 0.892 | 0.891 | 0.891 | 0.783 | 0.891 | 0.891 |
| **17** | **US** | **F** | 0.904 | 0.808 | 0.887 ± 0.010 | 0.884 ± 0.017 | 0.886 | 0.886 | 0.886 | 0.886 | 0.771 | 0.886 | 0.886 |
| **18** | **US** | **M + E** | **0.936** | **0.873** | **0.892 ± 0.015** | **0.896 ± 0.020** | **0.900** | **0.900** | **0.900** | **0.900** | **0.801** | **0.900** | **0.900** |
| **19** | **US** | **M + F** | 0.919 | 0.839 | 0.895 ± 0.015 | 0.899 ± 0.023 | 0.899 | 0.899 | 0.899 | 0.899 | 0.797 | 0.899 | 0.899 |
| **20** | **US** | **E + F** | 0.938 | 0.877 | 0.893 ± 0.008 | 0.892 ± 0.014 | 0.900 | 0.901 | 0.900 | 0.900 | 0.801 | 0.900 | 0.900 |
| **21** | **US** | **M + E + F** | 0.941 | 0.882 | 0.900 ± 0.014 | 0.899 ± 0.017 | 0.889 | 0.889 | 0.889 | 0.889 | 0.779 | 0.889 | 0.889 |
| **Overall** | **US** | **$\bar{x} \pm \sigma$** | **0.925 ± 0.013** | **0.850 ± 0.026** | - | - | **0.891 ± 0.008** | **0.891 ± 0.008** | **0.891 ± 0.008** | **0.891 ± 0.008** | **0.781 ± 0.016** | **0.891 ± 0.008** | **0.891 ± 0.008** |

## GBM hyperparameters

```
GradientBoostingClassifier(random_state=123)
```

**Table S4:** Performances for all RF models (the best model is highlighted in *green*).

| Model (RF#) | Subset | FPS | Training set | | | | Test set | | | | | | |
|---|---|---|---|---|---|---|---|---|---|---|---|---|---|
| | | | Q | MCC | 5-CV | 10-CV | Q | P | SE | SP | MCC | AUC | f1 |
| **1** | **DS** | **M** | 0.979 | 0.957 | 0.814 ± 0.025 | 0.829 ± 0.021 | 0.798 | 0.798 | 0.798 | 0.800 | 0.597 | 0.799 | 0.798 |
| **2** | **DS** | **E** | 0.995 | 0.991 | 0.839 ± 0.021 | 0.851 ± 0.030 | 0.853 | 0.853 | 0.853 | 0.852 | 0.705 | 0.853 | 0.853 |
| **3** | **DS** | **F** | 0.994 | 0.988 | 0.825 ± 0.030 | 0.844 ± 0.032 | 0.835 | 0.834 | 0.835 | 0.835 | 0.669 | 0.835 | 0.834 |
| **4** | **DS** | **M + E** | 0.995 | 0.991 | 0.829 ± 0.020 | 0.849 ± 0.023 | 0.849 | 0.848 | 0.849 | 0.848 | 0.696 | 0.848 | 0.848 |
| **5** | **DS** | **M + F** | 0.995 | 0.991 | 0.815 ± 0.033 | 0.836 ± 0.034 | 0.817 | 0.816 | 0.817 | 0.819 | 0.634 | 0.818 | 0.816 |
| **6** | **DS** | **E + F** | 0.998 | 0.997 | 0.849 ± 0.013 | 0.858 ± 0.036 | 0.826 | 0.829 | 0.826 | 0.833 | 0.658 | 0.829 | 0.826 |
| **7** | **DS** | **M + E + F** | 0.995 | 0.991 | 0.838 ± 0.027 | 0.847 ± 0.025 | 0.830 | 0.830 | 0.830 | 0.832 | 0.661 | 0.831 | 0.830 |
| **Overall** | **DS** | **$\bar{x} \pm \sigma$** | **0.993 ± 0.004** | **0.987 ± 0.008** | - | - | **0.830 ± 0.014** | **0.830 ± 0.013** | **0.830 ± 0.014** | **0.831 ± 0.012** | **0.660 ± 0.026** | **0.830 ± 0.013** | **0.829 ± 0.014** |
| **8** | **OS** | **M** | 0.959 | 0.898 | 0.853 ± 0.016 | 0.855 ± 0.029 | 0.816 | 0.789 | 0.816 | 0.670 | 0.530 | 0.743 | 0.759 |
| **9** | **OS** | **E** | 0.978 | 0.946 | 0.876 ± 0.011 | 0.868 ± 0.026 | 0.882 | 0.874 | 0.882 | 0.782 | 0.704 | 0.832 | 0.849 |
| **10** | **OS** | **F** | 0.966 | 0.915 | 0.879 ± 0.012 | 0.881 ± 0.026 | 0.876 | 0.864 | 0.876 | 0.780 | 0.691 | 0.828 | 0.843 |
| **11** | **OS** | **M + E** | 0.984 | 0.961 | 0.874 ± 0.018 | 0.874 ± 0.027 | 0.863 | 0.855 | 0.863 | 0.742 | 0.655 | 0.803 | 0.822 |
| **12** | **OS** | **M + F** | 0.975 | 0.939 | 0.874 ± 0.012 | 0.870 ± 0.026 | 0.853 | 0.835 | 0.853 | 0.738 | 0.629 | 0.795 | 0.811 |
| **13** | **OS** | **E + F** | 0.985 | 0.963 | 0.877 ± 0.011 | 0.870 ± 0.021 | 0.882 | 0.862 | 0.882 | 0.814 | 0.709 | 0.848 | 0.854 |
| **14** | **OS** | **M + E + F** | 0.991 | 0.978 | 0.877 ± 0.018 | 0.875 ± 0.023 | 0.874 | 0.860 | 0.874 | 0.779 | 0.685 | 0.826 | 0.840 |
| **Overall** | **OS** | **$\bar{x} \pm \sigma$** | **0.977 ± 0.009** | **0.943 ± 0.022** | - | - | **0.864 ± 0.017** | **0.848 ± 0.021** | **0.864 ± 0.017** | **0.758 ± 0.035** | **0.658 ± 0.045** | **0.811 ± 0.026** | **0.825 ± 0.024** |
| **15** | **US** | **M** | 0.942 | 0.883 | 0.904 ± 0.015 | 0.902 ± 0.022 | 0.893 | 0.895 | 0.893 | 0.893 | 0.788 | 0.893 | 0.893 |
| **16** | **US** | **E** | 0.967 | 0.934 | 0.912 ± 0.011 | 0.922 ± 0.021 | 0.913 | 0.914 | 0.913 | 0.913 | 0.827 | 0.913 | 0.913 |
| **17** | **US** | **F** | 0.961 | 0.921 | 0.908 ± 0.005 | 0.908 ± 0.015 | 0.919 | 0.919 | 0.919 | 0.919 | 0.838 | 0.919 | 0.919 |
| **18** | **US** | **M + E** | 0.973 | 0.946 | 0.926 ± 0.009 | 0.922 ± 0.022 | 0.915 | 0.916 | 0.915 | 0.915 | 0.831 | 0.915 | 0.915 |
| **19** | **US** | **M + F** | 0.967 | 0.934 | 0.916 ± 0.011 | 0.917 ± 0.023 | 0.913 | 0.914 | 0.913 | 0.913 | 0.827 | 0.913 | 0.913 |
| **20** | **US** | **E + F** | 0.972 | 0.945 | 0.926 ± 0.009 | 0.924 ± 0.018 | 0.917 | 0.917 | 0.917 | 0.917 | 0.834 | 0.917 | 0.917 |
| **21** | **US** | **M + E + F** | **0.972** | **0.945** | **0.928 ± 0.008** | **0.929 ± 0.016** | **0.921** | **0.921** | **0.921** | **0.921** | **0.842** | **0.921** | **0.921** |
| **Overall** | **US** | **$\bar{x} \pm \sigma$** | **0.965 ± 0.008** | **0.930 ± 0.016** | - | - | **0.913 ± 0.006** | **0.914 ± 0.005** | **0.913 ± 0.006** | **0.913 ± 0.006** | **0.827 ± 0.011** | **0.913 ± 0.006** | **0.913 ± 0.006** |

### Random Forest hyperparameters

```
RandomForestClassifier(n_estimators=120, criterion = 'entropy', max_leaf_nodes = 150, random_state=0)
```

**Table S5:** Performances for all XGB models (the best model is highlighted in *green*).

| Model (XGB#) | Subset | FPS | Training set | | | | Test set | | | | | | |
|---|---|---|---|---|---|---|---|---|---|---|---|---|---|
| | | | Q | MCC | 5-CV | 10-CV | Q | P | SE | SP | MCC | AUC | f1 |
| **1** | **DS** | **M** | 0.979 | 0.957 | 0.807 ± 0.028 | 0.812 ± 0.023 | 0.789 | 0.789 | 0.789 | 0.791 | 0.579 | 0.790 | 0.789 |
| **2** | **DS** | **E** | 0.995 | 0.991 | 0.827 ± 0.026 | 0.834 ± 0.029 | 0.853 | 0.854 | 0.853 | 0.850 | 0.705 | 0.851 | 0.852 |
| **3** | **DS** | **F** | 0.994 | 0.988 | 0.822 ± 0.038 | 0.826 ± 0.041 | 0.826 | 0.825 | 0.826 | 0.825 | 0.650 | 0.826 | 0.825 |
| **4** | **DS** | **M + E** | 0.995 | 0.991 | 0.813 ± 0.026 | 0.835 ± 0.032 | 0.867 | 0.867 | 0.867 | 0.865 | 0.733 | 0.866 | 0.866 |
| **5** | **DS** | **M + F** | 0.995 | 0.991 | 0.822 ± 0.035 | 0.830 ± 0.032 | 0.844 | 0.844 | 0.844 | 0.846 | 0.689 | 0.845 | 0.844 |
| **6** | **DS** | **E + F** | 0.998 | 0.997 | 0.841 ± 0.015 | 0.846 ± 0.039 | 0.803 | 0.807 | 0.803 | 0.810 | 0.613 | 0.806 | 0.803 |
| **7** | **DS** | **M + E + F** | 0.995 | 0.991 | 0.823 ± 0.025 | 0.847 ± 0.032 | 0.858 | 0.857 | 0.858 | 0.857 | 0.715 | 0.858 | 0.857 |
| **Overall** | **DS** | **$\bar{x} \pm \sigma$** | **0.993 ± 0.004** | **0.987 ± 0.008** | - | - | **0.834 ± 0.024** | **0.835 ± 0.024** | **0.834 ± 0.024** | **0.835 ± 0.022** | **0.669 ± 0.047** | **0.835 ± 0.023** | **0.834 ± 0.024** |
| **8** | **OS** | **M** | 0.977 | 0.944 | 0.848 ± 0.024 | 0.845 ± 0.036 | 0.808 | 0.777 | 0.808 | 0.661 | 0.510 | 0.735 | 0.750 |
| **9** | **OS** | **E** | 0.994 | 0.985 | 0.865 ± 0.022 | 0.857 ± 0.028 | 0.876 | 0.852 | 0.876 | 0.817 | 0.699 | 0.846 | 0.849 |
| **10** | **OS** | **F** | 0.985 | 0.963 | 0.864 ± 0.019 | 0.857 ± 0.023 | 0.861 | 0.838 | 0.861 | 0.773 | 0.654 | 0.817 | 0.826 |
| **11** | **OS** | **M + E** | 0.995 | 0.987 | 0.859 ± 0.015 | 0.858 ± 0.022 | 0.866 | 0.838 | 0.866 | 0.807 | 0.675 | 0.836 | 0.837 |
| **12** | **OS** | **M + F** | 0.995 | 0.987 | 0.864 ± 0.026 | 0.856 ± 0.039 | 0.861 | 0.836 | 0.861 | 0.778 | 0.656 | 0.819 | 0.827 |
| **13** | **OS** | **E + F** | 0.995 | 0.987 | 0.864 ± 0.024 | 0.866 ± 0.022 | 0.887 | 0.863 | 0.887 | 0.842 | 0.727 | 0.865 | 0.864 |
| **14** | **OS** | **M + E + F** | 0.995 | 0.987 | 0.859 ± 0.023 | 0.856 ± 0.026 | 0.863 | 0.834 | 0.863 | 0.811 | 0.671 | 0.837 | 0.835 |
| **Overall** | **OS** | **$\bar{x} \pm \sigma$** | **0.991 ± 0.006** | **0.977 ± 0.014** | - | - | **0.860 ± 0.015** | **0.834 ± 0.016** | **0.860 ± 0.015** | **0.784 ± 0.040** | **0.656 ± 0.042** | **0.822 ± 0.027** | **0.827 ± 0.022** |
| **15** | **US** | **M** | 0.977 | 0.955 | 0.921 ± 0.011 | 0.918 ± 0.014 | 0.908 | 0.909 | 0.908 | 0.908 | 0.817 | 0.908 | 0.908 |
| **16** | **US** | **E** | 0.994 | 0.989 | 0.931 ± 0.014 | 0.933 ± 0.022 | 0.939 | 0.940 | 0.939 | 0.939 | 0.879 | 0.939 | 0.939 |
| **17** | **US** | **F** | 0.988 | 0.975 | 0.930 ± 0.009 | 0.935 ± 0.014 | 0.937 | 0.938 | 0.937 | 0.937 | 0.875 | 0.937 | 0.937 |
| **18** | **US** | **M + E** | 0.996 | 0.993 | 0.932 ± 0.018 | 0.933 ± 0.016 | 0.935 | 0.937 | 0.935 | 0.936 | 0.873 | 0.936 | 0.935 |
| **19** | **US** | **M + F** | 0.996 | 0.993 | 0.938 ± 0.015 | 0.941 ± 0.017 | 0.941 | 0.941 | 0.941 | 0.941 | 0.882 | 0.941 | 0.941 |
| **20** | **US** | **E + F** | 0.997 | 0.994 | 0.931 ± 0.014 | 0.940 ± 0.016 | 0.932 | 0.932 | 0.932 | 0.932 | 0.864 | 0.932 | 0.932 |
| **21** | **US** | **M + E + F** | **0.997** | **0.994** | **0.933 ± 0.014** | **0.939 ± 0.016** | **0.941** | **0.941** | **0.941** | **0.941** | **0.882** | **0.941** | **0.941** |
| **Overall** | **US** | **$\bar{x} \pm \sigma$** | **0.992 ± 0.006** | **0.985 ± 0.011** | - | - | **0.933 ± 0.008** | **0.934 ± 0.008** | **0.933 ± 0.008** | **0.933 ± 0.008** | **0.867 ± 0.015** | **0.933 ± 0.008** | **0.933 ± 0.008** |

## XGB hyperparameters

```
XGBClassifier(base_score=0.5, colsample_bylevel=1, colsample_bynode=1,
colsample_bytree=1, gamma=0, gpu_id=0,
importance_type='gain', learning_rate=0.300000012, max_delta_step=0,
max_depth=6, min_child_weight=1, n_estimators=120, n_jobs=0,
num_parallel_tree=1, objective='binary:logistic', random_state=123, reg_alpha=0,
reg_lambda=1, scale_pos_weight=1, subsample=1)
```

**Table S6.** Calculated IR spectrum of **1**.[a]

| **1A** | | | | **1B** | | | |
|---|---|---|---|---|---|---|---|
| $\nu$ | $I^{IR}$ | $\nu$ | $I^{IR}$ | $\nu$ | $I^{IR}$ | $\nu$ | $I^{IR}$ |
| 3135.1 | 4.2 | 1092.2 | 117.2 | 3136.5 | 4.2 | 1092.6 | 114.5 |
| 3127.5 | 6.5 | 1075.6 | 60.6 | 3127.9 | 6.4 | 1077.6 | 63.0 |
| 3108.1 | 11.2 | 1062.0 | 107.3 | 3106.3 | 11.2 | 1064.1 | 117.2 |
| 3098.0 | 11.7 | 1056.1 | 18.0 | 3097.9 | 11.7 | 1055.0 | 7.0 |
| 3094.4 | 7.6 | 1055.4 | 29.9 | 3094.4 | 7.6 | 1054.6 | 32.8 |
| 3049.3 | 4.3 | 1050.7 | 2.7 | 3049.2 | 4.2 | 1050.3 | 1.4 |
| 3031.1 | 24.6 | 1042.3 | 5.7 | 3031.3 | 22.2 | 1042.4 | 5.6 |
| 3028.4 | 16.9 | 1024.0 | 6.1 | 3027.5 | 19.6 | 1025.4 | 6.0 |
| 3011.4 | 27.8 | 1013.4 | 23.2 | 3011.8 | 25.4 | 1013.7 | 19.6 |
| 3009.6 | 40.8 | 1010.8 | 36.7 | 3009.7 | 49.8 | 1011.9 | 41.1 |
| 3008.3 | 40.8 | 1003.4 | 51.0 | 3007.3 | 27.0 | 1004.1 | 47.8 |
| 3007.6 | 29.0 | 999.2 | 78.1 | 3007.0 | 30.9 | 999.1 | 80.4 |
| 3006.1 | 9.8 | 991.1 | 3.9 | 3005.7 | 20.1 | 991.6 | 10.0 |
| 3003.2 | 16.4 | 989.1 | 29.0 | 3001.9 | 11.6 | 989.0 | 22.0 |
| 3000.5 | 16.8 | 958.1 | 2.2 | 2999.9 | 15.7 | 956.9 | 3.4 |
| 2994.8 | 43.8 | 954.6 | 1.3 | 2995.2 | 46.6 | 953.6 | 0.9 |
| 2990.4 | 2.1 | 951.5 | 0.3 | 2990.3 | 2.1 | 951.8 | 0.3 |
| 2980.1 | 52.8 | 939.6 | 5.5 | 2979.9 | 56.7 | 938.2 | 3.7 |
| 2979.3 | 22.4 | 934.6 | 0.1 | 2978.7 | 23.3 | 933.9 | 0.1 |
| 2976.3 | 133.2 | 927.8 | 9.0 | 2976.2 | 129.5 | 927.9 | 15.4 |
| 2973.9 | 31.9 | 924.6 | 12.1 | 2974.3 | 33.7 | 924.0 | 5.5 |
| 2973.2 | 5.3 | 903.9 | 55.5 | 2972.8 | 3.1 | 903.6 | 54.7 |
| 2971.7 | 94.9 | 902.3 | 0.9 | 2971.4 | 96.2 | 901.8 | 0.6 |
| 2970.4 | 23.5 | 889.5 | 1.1 | 2970.1 | 24.5 | 890.2 | 3.1 |
| 2962.5 | 80.8 | 886.5 | 0.6 | 2961.7 | 76.8 | 883.9 | 0.5 |
| 2959.3 | 0.3 | 878.7 | 2.4 | 2959.0 | 0.7 | 878.3 | 0.2 |
| 2958.2 | 1.5 | 876.7 | 0.1 | 2957.6 | 1.0 | 876.7 | 1.8 |
| 2956.1 | 0.5 | 860.9 | 1.0 | 2955.9 | 0.6 | 863.1 | 0.3 |
| 2944.8 | 25.2 | 858.8 | 3.2 | 2943.8 | 24.7 | 859.6 | 4.5 |
| 2932.9 | 16.5 | 839.4 | 30.9 | 2934.4 | 15.5 | 837.8 | 30.2 |
| 1782.1 | 235.3 | 827.5 | 1.1 | 1782.0 | 234.2 | 827.1 | 2.1 |
| 1612.9 | 5.5 | 816.4 | 0.7 | 1612.9 | 5.7 | 814.6 | 0.7 |
| 1593.6 | 1.4 | 803.2 | 5.6 | 1593.4 | 1.4 | 804.5 | 4.0 |
| 1506.4 | 93.5 | 789.5 | 0.9 | 1506.5 | 93.7 | 789.6 | 1.4 |
| 1488.5 | 8.8 | 786.1 | 0.3 | 1485.7 | 8.3 | 783.8 | 0.9 |
| 1471.6 | 3.3 | 775.8 | 3.0 | 1472.5 | 3.5 | 776.4 | 3.5 |
| 1470.5 | 12.6 | 770.2 | 5.7 | 1469.9 | 13.3 | 771.9 | 5.0 |
| 1466.9 | 14.4 | 765.7 | 0.4 | 1466.5 | 14.1 | 762.2 | 0.2 |
| 1460.1 | 1.1 | 750.0 | 2.8 | 1458.0 | 5.2 | 750.0 | 2.3 |
| 1459.3 | 5.4 | 727.1 | 0.4 | 1456.9 | 1.5 | 726.2 | 0.4 |
| 1457.3 | 6.9 | 677.4 | 0.2 | 1455.6 | 6.1 | 675.4 | 0.8 |
| 1453.6 | 0.1 | 668.3 | 1.8 | 1453.5 | 0.4 | 667.9 | 2.4 |
| 1446.4 | 10.1 | 663.8 | 4.1 | 1446.6 | 9.7 | 663.7 | 3.6 |
| 1445.6 | 4.1 | 642.6 | 4.6 | 1442.7 | 4.9 | 642.5 | 3.9 |
| 1442.4 | 16.1 | 638.2 | 0.2 | 1442.2 | 15.6 | 638.0 | 0.1 |
| 1420.0 | 2.0 | 629.6 | 0.9 | 1420.5 | 2.2 | 626.4 | 0.6 |

| | | | | | | | |
|---|---|---|---|---|---|---|---|
| 1381.9 | 9.9 | 586.3 | 4.0 | 1383.0 | 9.8 | 585.9 | 3.9 |
| 1372.0 | 43.7 | 580.2 | 12.5 | 1372.5 | 2.0 | 579.9 | 11.2 |
| 1371.0 | 25.8 | 542.3 | 11.0 | 1371.6 | 67.9 | 541.8 | 7.6 |
| 1366.2 | 3.8 | 538.1 | 8.9 | 1366.6 | 4.1 | 538.2 | 13.9 |
| 1357.3 | 4.4 | 520.2 | 0.4 | 1358.2 | 5.8 | 519.0 | 0.3 |
| 1357.1 | 1.9 | 493.0 | 3.9 | 1356.5 | 1.5 | 492.2 | 4.0 |
| 1355.6 | 1.5 | 476.1 | 11.6 | 1355.9 | 0.2 | 477.1 | 11.6 |
| 1347.6 | 0.2 | 472.2 | 1.5 | 1347.1 | 0.1 | 471.4 | 1.1 |
| 1343.3 | 0.2 | 457.8 | 0.7 | 1342.2 | 0.2 | 455.9 | 1.3 |
| 1333.2 | 5.9 | 440.4 | 0.1 | 1334.0 | 6.5 | 436.8 | 0.2 |
| 1331.2 | 3.7 | 437.8 | 0.3 | 1331.3 | 2.9 | 436.2 | 0.1 |
| 1324.9 | 0.2 | 429.2 | 0.2 | 1324.6 | 0.04 | 423.9 | 0.4 |
| 1322.0 | 0.2 | 417.3 | 0.9 | 1322.4 | 0.03 | 416.8 | 0.3 |
| 1313.7 | 2.5 | 414.9 | 0.1 | 1316.1 | 2.9 | 414.7 | 0.2 |
| 1312.1 | 5.1 | 403.1 | 0.7 | 1313.1 | 5.2 | 401.5 | 1.0 |
| 1302.7 | 1.8 | 390.7 | 3.0 | 1302.7 | 1.2 | 388.0 | 1.4 |
| 1301.7 | 0.5 | 381.5 | 2.1 | 1302.2 | 1.1 | 380.8 | 3.4 |
| 1301.4 | 0.0 | 361.5 | 1.2 | 1301.1 | 0.01 | 357.4 | 2.0 |
| 1295.1 | 0.6 | 339.6 | 5.1 | 1295.0 | 0.7 | 339.2 | 4.7 |
| 1288.9 | 24.7 | 331.5 | 0.5 | 1289.7 | 21.9 | 329.1 | 0.5 |
| 1274.8 | 3.5 | 301.5 | 1.7 | 1276.0 | 3.3 | 302.9 | 1.6 |
| 1268.0 | 4.1 | 298.6 | 1.0 | 1267.5 | 4.9 | 294.6 | 1.0 |
| 1257.9 | 2.6 | 267.6 | 0.7 | 1258.8 | 2.1 | 268.8 | 0.5 |
| 1250.8 | 0.03 | 259.6 | 1.7 | 1250.4 | 0.03 | 259.6 | 1.6 |
| 1245.1 | 7.7 | 237.3 | 1.9 | 1246.6 | 6.4 | 232.9 | 0.4 |
| 1239.4 | 14.8 | 216.0 | 0.8 | 1240.6 | 16.4 | 214.3 | 2.3 |
| 1220.2 | 31.4 | 188.4 | 0.3 | 1221.0 | 29.9 | 188.0 | 0.5 |
| 1202.9 | 34.8 | 158.0 | 0.7 | 1202.4 | 31.3 | 157.3 | 0.7 |
| 1196.9 | 176.5 | 131.5 | 0.7 | 1197.4 | 169.7 | 127.8 | 0.3 |
| 1187.1 | 495.1 | 113.8 | 1.2 | 1187.1 | 514.7 | 114.9 | 1.1 |
| 1171.4 | 13.8 | 96.8 | 1.9 | 1170.6 | 12.9 | 99.1 | 2.0 |
| 1163.9 | 93.1 | 85.9 | 1.7 | 1163.9 | 85.7 | 87.3 | 1.9 |
| 1157.7 | 0.3 | 70.9 | 0.3 | 1158.2 | 0.4 | 72.2 | 0.3 |
| 1133.9 | 10.5 | 52.6 | 0.3 | 1133.9 | 11.5 | 51.0 | 0.2 |
| 1121.9 | 4.1 | 44.9 | 0.6 | 1120.4 | 2.7 | 41.2 | 0.6 |
| 1113.7 | 5.0 | 39.4 | 0.5 | 1113.0 | 8.4 | 34.3 | 0.5 |
| 1111.1 | 15.9 | 23.9 | 0.3 | 1110.7 | 1.5 | 20.1 | 0.7 |
| 1107.9 | 83.7 | 18.4 | 1.5 | 1108.5 | 93.2 | 16.6 | 0.2 |
| 1102.0 | 64.1 | 10.8 | 0.3 | 1102.4 | 73.9 | 15.4 | 1.1 |
| 1098.4 | 1.3 | | | 1097.8 | 1.7 | | |

[a] frequencies ($\nu$) in $cm^{-1}$ were scaled by 0.980; infrared intensities ($I^{IR}$) in km $mol^{-1}$.

**Table S7.** Calculated IR spectrum of **2**.[a]

| **2A** | | | | **2B** | | | | |
|---|---|---|---|---|---|---|---|---|
| $\nu$ | $I^{IR}$ | $\nu$ | $I^{IR}$ | $\nu$ | $I^{IR}$ | | $\nu$ | $I^{IR}$ |
| 1071.5 | 9.2 | 3138.1 | 3.8 | 1072.0 | 9.3 | 1071.5 | 9.2 | |
| 1059.2 | 1.2 | 3128.0 | 6.3 | 1058.4 | 0.6 | 1059.2 | 1.2 | |
| 1054.6 | 1.6 | 3108.9 | 11.2 | 1055.5 | 1.9 | 1054.6 | 1.6 | |
| 1052.4 | 25.6 | 3097.7 | 11.4 | 1052.5 | 22.6 | 1052.4 | 25.6 | |
| 1046.3 | 140.5 | 3094.5 | 7.6 | 1046.6 | 145.0 | 1046.3 | 140.5 | |
| 1042.4 | 5.8 | 3063.7 | 7.2 | 1042.1 | 5.9 | 1042.4 | 5.8 | |
| 1026.6 | 1.4 | 3048.9 | 4.2 | 1028.2 | 1.4 | 1026.6 | 1.4 | |
| 1013.8 | 21.5 | 3040.7 | 12.6 | 1013.7 | 27.2 | 1013.8 | 21.5 | |
| 1011.9 | 13.9 | 3031.8 | 20.0 | 1011.2 | 8.4 | 1011.9 | 13.9 | |
| 999.3 | 91.3 | 3016.7 | 29.4 | 999.1 | 90.3 | 999.3 | 91.3 | |
| 991.5 | 1.6 | 3015.8 | 30.0 | 992.3 | 1.6 | 991.5 | 1.6 | |
| 982.5 | 56.5 | 3014.5 | 39.1 | 982.3 | 55.9 | 982.5 | 56.5 | |
| 979.1 | 19.3 | 3013.0 | 19.9 | 980.0 | 19.1 | 979.1 | 19.3 | |
| 970.0 | 4.5 | 3011.2 | 13.1 | 969.9 | 4.5 | 970.0 | 4.5 | |
| 956.1 | 0.1 | 3010.3 | 10.7 | 955.9 | 0.1 | 956.1 | 0.1 | |
| 942.2 | 5.3 | 2997.8 | 31.7 | 941.3 | 3.7 | 942.2 | 5.3 | |
| 933.4 | 0.2 | 2990.0 | 2.0 | 933.0 | 1.5 | 933.4 | 0.2 | |
| 928.9 | 3.0 | 2985.0 | 18.0 | 928.5 | 4.1 | 928.9 | 3.0 | |
| 926.7 | 5.3 | 2980.9 | 63.4 | 926.1 | 4.9 | 926.7 | 5.3 | |
| 912.9 | 29.7 | 2980.1 | 3.1 | 914.6 | 30.4 | 912.9 | 29.7 | |
| 905.2 | 48.0 | 2978.2 | 60.1 | 905.2 | 39.6 | 905.2 | 48.0 | |
| 902.3 | 5.0 | 2977.8 | 90.3 | 903.4 | 11.0 | 902.3 | 5.0 | |
| 897.1 | 2.6 | 2975.6 | 24.9 | 898.2 | 4.3 | 897.1 | 2.6 | |
| 891.5 | 2.1 | 2973.2 | 88.2 | 891.7 | 2.1 | 891.5 | 2.1 | |
| 882.1 | 0.5 | 2965.5 | 77.2 | 883.1 | 0.2 | 882.1 | 0.5 | |
| 875.1 | 0.1 | 2962.7 | 1.3 | 876.6 | 0.1 | 875.1 | 0.1 | |
| 861.4 | 4.6 | 2960.6 | 2.6 | 860.5 | 4.3 | 861.4 | 4.6 | |
| 856.4 | 0.6 | 2958.8 | 0.9 | 856.9 | 1.0 | 856.4 | 0.6 | |
| 852.1 | 1.2 | 2944.9 | 24.1 | 852.1 | 2.8 | 852.1 | 1.2 | |
| 839.8 | 29.8 | 2936.0 | 17.6 | 838.7 | 25.9 | 839.8 | 29.8 | |
| 831.0 | 0.1 | 1782.0 | 232.4 | 830.5 | 2.9 | 831.0 | 0.1 | |
| 817.0 | 0.7 | 1612.9 | 6.2 | 815.9 | 0.8 | 817.0 | 0.7 | |
| 798.4 | 4.7 | 1593.4 | 1.4 | 801.5 | 2.7 | 798.4 | 4.7 | |
| 790.5 | 2.8 | 1506.5 | 94.0 | 792.5 | 1.0 | 790.5 | 2.8 | |
| 788.7 | 1.0 | 1486.8 | 8.2 | 786.6 | 4.5 | 788.7 | 1.0 | |
| 771.0 | 1.3 | 1470.6 | 2.3 | 772.1 | 1.8 | 771.0 | 1.3 | |
| 766.5 | 0.5 | 1469.3 | 11.1 | 766.0 | 0.2 | 766.5 | 0.5 | |
| 759.6 | 0.7 | 1467.4 | 15.4 | 760.2 | 0.8 | 759.6 | 0.7 | |
| 726.9 | 0.4 | 1461.5 | 10.5 | 726.9 | 0.3 | 726.9 | 0.4 | |
| 714.8 | 1.3 | 1459.7 | 1.7 | 714.6 | 1.4 | 714.8 | 1.3 | |
| 673.9 | 6.5 | 1457.7 | 6.0 | 675.5 | 6.2 | 673.9 | 6.5 | |
| 663.6 | 5.8 | 1453.4 | 0.1 | 664.0 | 2.3 | 663.6 | 5.8 | |
| 661.1 | 0.9 | 1448.4 | 5.1 | 663.6 | 4.6 | 661.1 | 0.9 | |
| 637.7 | 0.2 | 1446.5 | 9.8 | 637.9 | 0.2 | 637.7 | 0.2 | |
| 632.4 | 1.8 | 1442.3 | 16.0 | 633.7 | 1.3 | 632.4 | 1.8 | |
| 618.9 | 1.8 | 1421.0 | 1.9 | 618.0 | 2.3 | 618.9 | 1.8 | |

| | | | | | | | |
|---|---|---|---|---|---|---|---|
| 585.8 | 3.7 | 1378.9 | 5.7 | 585.3 | 3.8 | 585.8 | 3.7 |
| 564.0 | 18.3 | 1372.6 | 1.0 | 564.3 | 16.3 | 564.0 | 18.3 |
| 543.2 | 16.4 | 1371.0 | 61.2 | 542.9 | 10.5 | 543.2 | 16.4 |
| 540.5 | 1.0 | 1366.8 | 1.5 | 540.2 | 10.0 | 540.5 | 1.0 |
| 527.2 | 0.2 | 1359.6 | 1.2 | 528.0 | 0.9 | 527.2 | 0.2 |
| 517.4 | 1.7 | 1358.2 | 0.2 | 519.9 | 1.0 | 517.4 | 1.7 |
| 501.6 | 3.9 | 1357.6 | 2.2 | 501.7 | 5.4 | 501.6 | 3.9 |
| 484.7 | 16.6 | 1348.4 | 1.4 | 485.0 | 13.0 | 484.7 | 16.6 |
| 473.8 | 0.4 | 1345.7 | 0.6 | 473.1 | 0.6 | 473.8 | 0.4 |
| 456.7 | 1.1 | 1335.1 | 5.2 | 457.1 | 0.9 | 456.7 | 1.1 |
| 441.5 | 0.04 | 1334.5 | 1.7 | 442.1 | 0.6 | 441.5 | 0.04 |
| 438.0 | 0.4 | 1325.9 | 0.01 | 440.4 | 0.4 | 438.0 | 0.4 |
| 425.4 | 0.2 | 1325.2 | 0.1 | 427.5 | 0.4 | 425.4 | 0.2 |
| 419.8 | 0.4 | 1316.5 | 2.7 | 422.1 | 0.4 | 419.8 | 0.4 |
| 415.4 | 0.05 | 1311.3 | 3.6 | 415.4 | 0.04 | 415.4 | 0.05 |
| 402.6 | 1.0 | 1304.5 | 0.2 | 401.1 | 0.6 | 402.6 | 1.0 |
| 397.1 | 0.7 | 1303.7 | 0.2 | 397.8 | 1.0 | 397.1 | 0.7 |
| 379.8 | 2.7 | 1302.9 | 1.9 | 380.6 | 2.7 | 379.8 | 2.7 |
| 373.3 | 0.4 | 1296.9 | 0.8 | 378.4 | 0.5 | 373.3 | 0.4 |
| 335.8 | 7.0 | 1287.6 | 14.3 | 336.4 | 6.4 | 335.8 | 7.0 |
| 330.2 | 0.1 | 1277.8 | 2.7 | 331.1 | 0.5 | 330.2 | 0.1 |
| 324.7 | 0.05 | 1276.8 | 3.5 | 328.6 | 0.1 | 324.7 | 0.05 |
| 296.7 | 7.9 | 1268.6 | 9.4 | 298.8 | 7.8 | 296.7 | 7.9 |
| 272.5 | 1.6 | 1258.6 | 0.7 | 272.9 | 1.3 | 272.5 | 1.6 |
| 254.9 | 0.3 | 1252.5 | 0.1 | 261.0 | 1.7 | 254.9 | 0.3 |
| 252.3 | 1.9 | 1239.1 | 14.5 | 252.9 | 1.9 | 252.3 | 1.9 |
| 239.3 | 2.6 | 1223.2 | 21.1 | 227.6 | 0.3 | 239.3 | 2.6 |
| 212.8 | 0.6 | 1202.4 | 28.3 | 217.2 | 2.2 | 212.8 | 0.6 |
| 179.0 | 0.1 | 1197.6 | 173.1 | 189.0 | 0.5 | 179.0 | 0.1 |
| 155.6 | 1.4 | 1187.9 | 523.8 | 154.7 | 0.8 | 155.6 | 1.4 |
| 123.4 | 1.4 | 1178.6 | 8.7 | 120.6 | 0.4 | 123.4 | 1.4 |
| 118.9 | 0.4 | 1164.3 | 94.8 | 119.8 | 0.5 | 118.9 | 0.4 |
| 98.5 | 2.1 | 1163.2 | 1.5 | 102.0 | 2.7 | 98.5 | 2.1 |
| 86.9 | 1.8 | 1133.1 | 2.9 | 90.6 | 1.9 | 86.9 | 1.8 |
| 73.6 | 0.1 | 1121.5 | 9.0 | 74.9 | 0.3 | 73.6 | 0.1 |
| 60.5 | 0.2 | 1115.0 | 1.7 | 56.6 | 0.3 | 60.5 | 0.2 |
| 53.5 | 0.3 | 1111.5 | 0.0 | 53.9 | 0.1 | 53.5 | 0.3 |
| 44.5 | 1.2 | 1102.1 | 26.7 | 44.3 | 1.1 | 44.5 | 1.2 |
| 29.4 | 0.2 | 1100.9 | 8.4 | 29.3 | 0.05 | 29.4 | 0.2 |
| 19.9 | 1.3 | 1096.7 | 5.7 | 18.6 | 0.3 | 19.9 | 1.3 |
| 13.2 | 0.5 | 1080.6 | 7.9 | 13.8 | 1.8 | 13.2 | 0.5 |

[a] frequencies ($\nu$) in $cm^{-1}$ were scaled by 0.980; infrared intensities ($I^{IR}$) in km $mol^{-1}$.

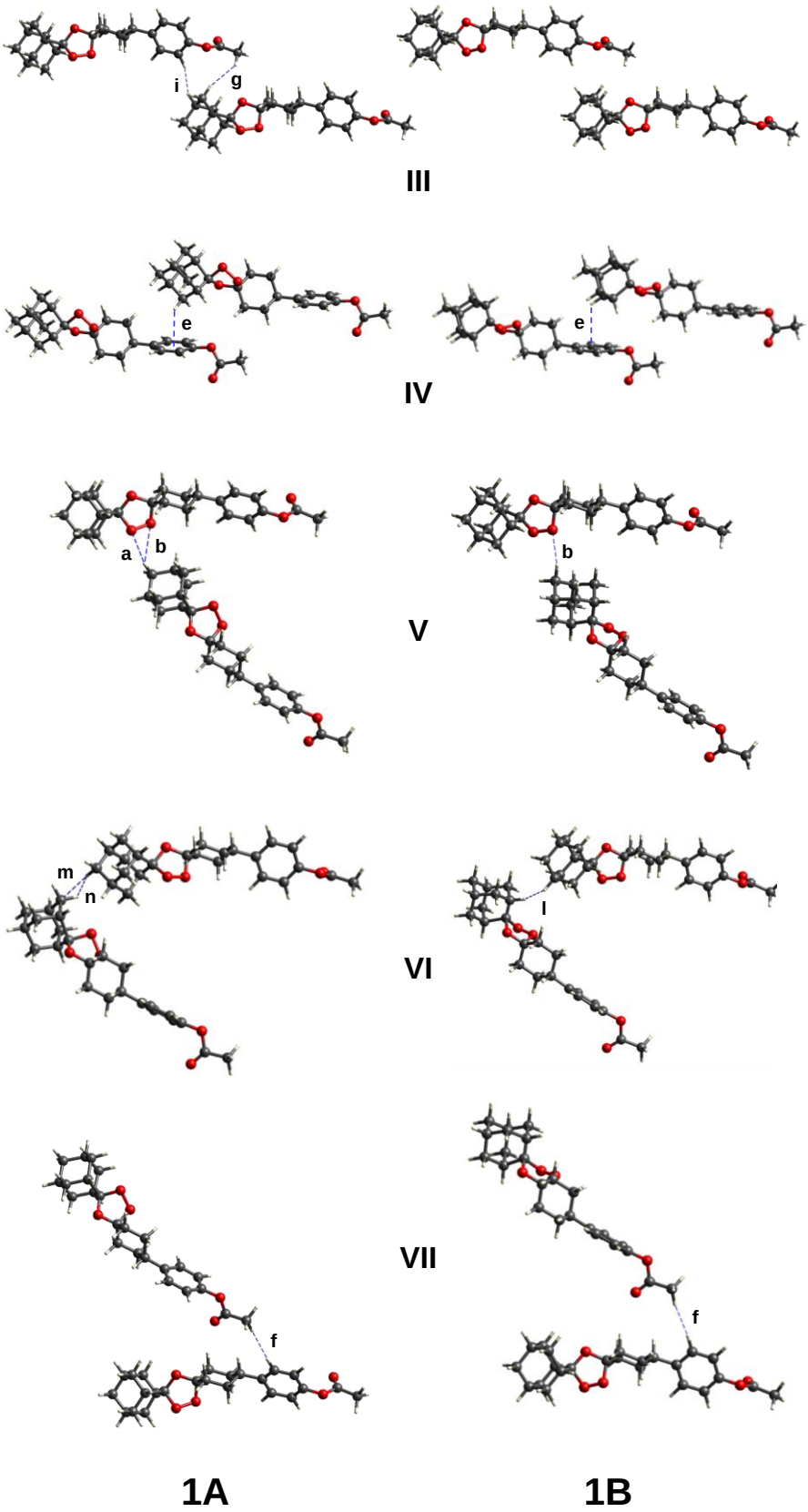


**Figure S1.** Molecular pairs of the crystal structure of **1**, including the identification of the intermolecular contacts.

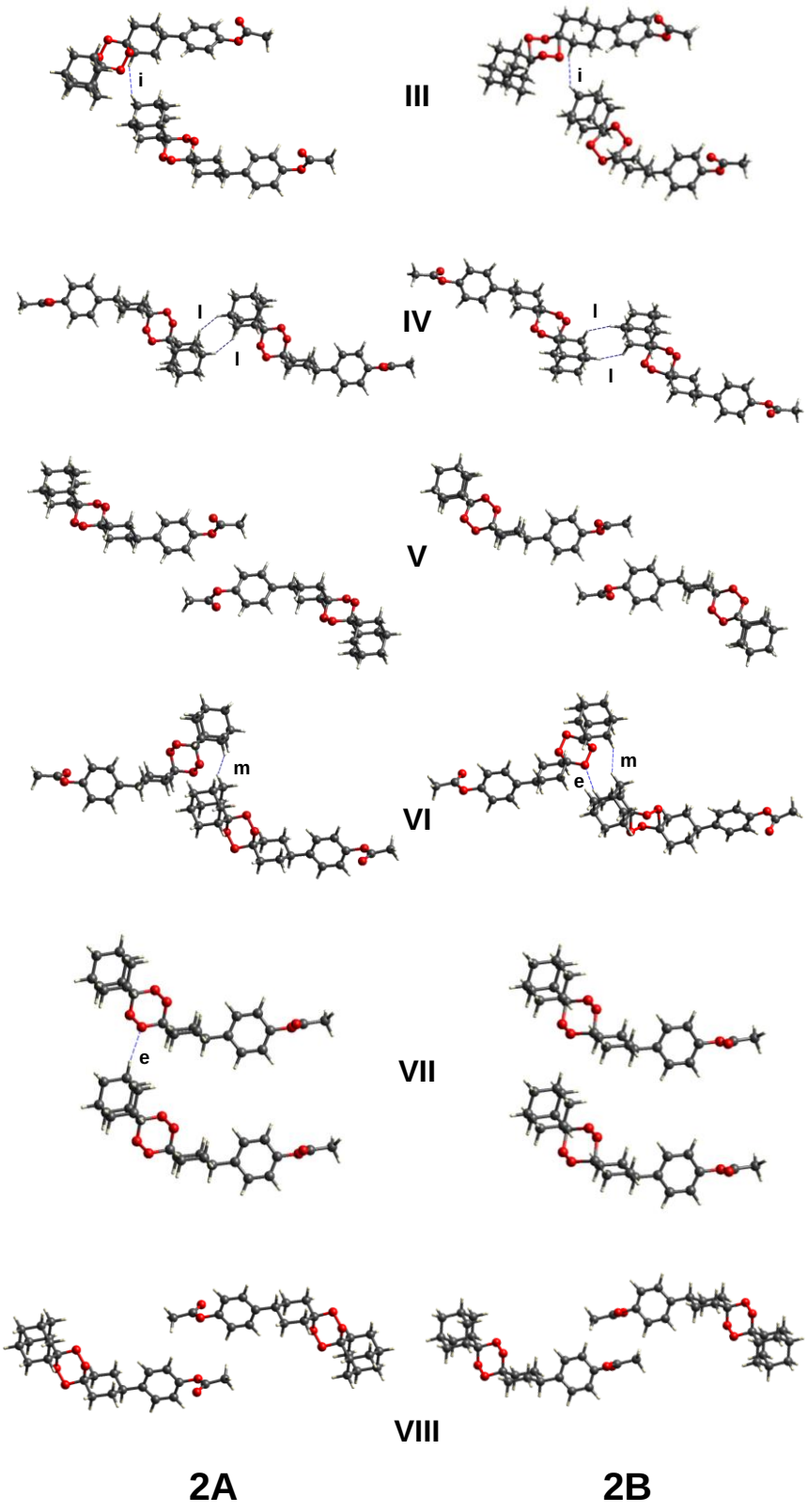


**Figure S2.** Molecular pairs of the crystal structure of **1**, including the identification of the intermolecular contacts.

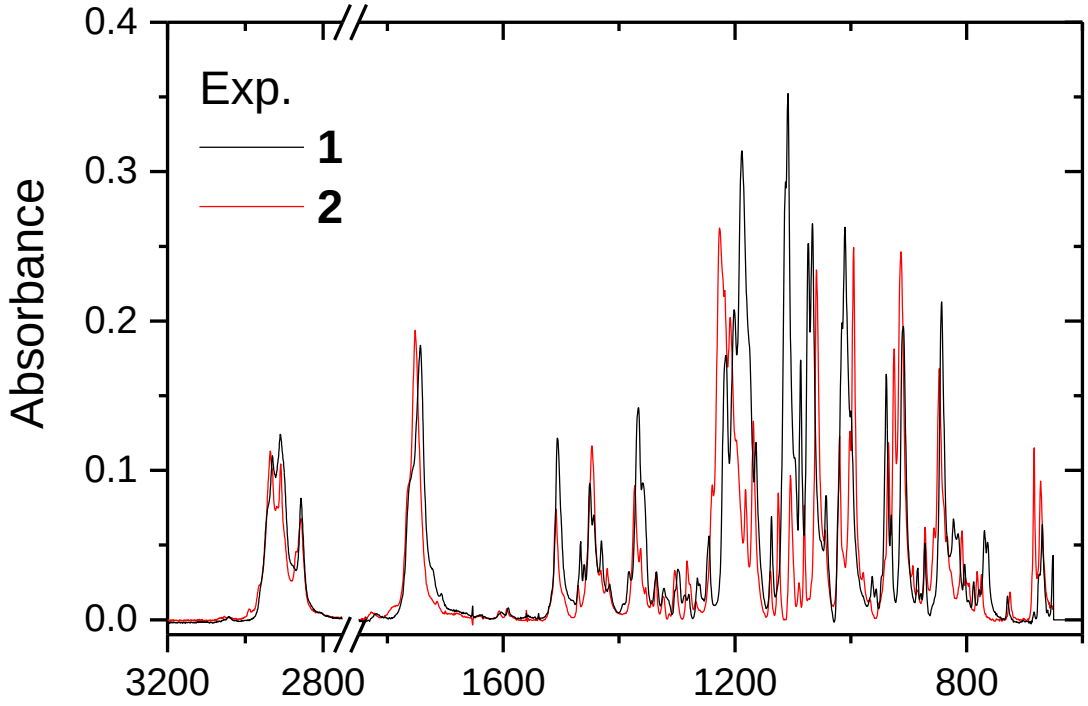


**Figure S3.** Infrared spectra (ATR; room temperature) of **1** and **2**.

# Appendix 1- DFT data: Energies and Cartesian Coordinates

**SSA**
**SCF energy:** -2433.96928181 Hartree
**Free energy correction:** 0.091992 Hartree

| | | | |
|---|---|---|---|
| 8 | -6.220583000 | 3.954129000 | -3.846679000 |
| 14 | -7.962409000 | 4.012027000 | -3.911384000 |
| 16 | -5.379858000 | 3.103235000 | -2.832415000 |
| 8 | -3.967861000 | 3.411075000 | -3.034574000 |
| 8 | -5.906551000 | 3.800398000 | -1.468127000 |
| 8 | -5.799357000 | 1.704450000 | -2.847496000 |
| 8 | -8.334712000 | 4.482351000 | -5.422616000 |
| 8 | -8.490153000 | 2.508088000 | -3.599277000 |
| 8 | -8.443839000 | 5.170945000 | -2.866124000 |
| 1 | -5.448394000 | 3.378592000 | -0.693753000 |
| 1 | -3.527184000 | 2.150853000 | -0.165712000 |
| 8 | -2.601153000 | 4.459194000 | 0.496332000 |
| 14 | -1.307491000 | 3.779864000 | -0.430857000 |
| 16 | -3.470834000 | 3.548778000 | 1.481821000 |
| 8 | -2.556637000 | 2.723521000 | 2.262006000 |
| 8 | -4.507025000 | 4.349938000 | 2.078900000 |
| 8 | -4.233690000 | 2.568464000 | 0.398262000 |
| 8 | -0.150877000 | 3.291992000 | 0.602431000 |
| 8 | -0.796971000 | 4.926537000 | -1.459875000 |
| 8 | -2.019356000 | 2.533931000 | -1.238253000 |
| 1 | -0.477232000 | 2.924200000 | 1.441865000 |
| 1 | -2.505350000 | 2.775234000 | -2.057401000 |
| 1 | -0.190229000 | 5.599071000 | -1.119804000 |
| 1 | -8.102504000 | 5.103025000 | -1.961701000 |
| 1 | -8.399709000 | 5.436301000 | -5.570776000 |
| 1 | -7.811778000 | 1.828918000 | -3.440007000 |

**2.38g**
**SCF energy:** -536.656531855 Hartree
**Free energy correction:** 0.151715 Hartree

| | | | |
|---|---|---|---|
| 6 | 1.676965000 | -0.653092000 | -0.347322000 |
| 6 | 1.086287000 | -0.777591000 | 2.125914000 |
| 6 | 0.717946000 | -0.194911000 | 0.756518000 |
| 8 | -0.578463000 | -0.571856000 | 0.291520000 |
| 8 | -1.563851000 | -0.332511000 | 1.337870000 |
| 8 | 0.536127000 | 1.904379000 | -0.315824000 |
| 8 | 0.702845000 | 1.223259000 | 0.959692000 |
| 1 | 1.405520000 | -0.170826000 | -1.288967000 |
| 1 | 1.531960000 | -1.732512000 | -0.473773000 |
| 1 | 0.415444000 | -0.373788000 | 2.887954000 |
| 1 | 0.891025000 | -1.855211000 | 2.066546000 |
| 1 | -0.318910000 | 1.533143000 | -0.615142000 |
| 1 | -1.467726000 | 0.632809000 | 1.468120000 |
| 6 | 3.136392000 | -0.350413000 | 0.024611000 |
| 1 | 3.276476000 | 0.736734000 | 0.065219000 |
| 1 | 3.792784000 | -0.727231000 | -0.768854000 |
| 6 | 3.512564000 | -0.973898000 | 1.376274000 |
| 1 | 3.473363000 | -2.070418000 | 1.294423000 |
| 1 | 4.546139000 | -0.716053000 | 1.637980000 |
| 6 | 2.557134000 | -0.510493000 | 2.485510000 |
| 1 | 2.694117000 | 0.563817000 | 2.659718000 |
| 1 | 2.791954000 | -1.017300000 | 3.429459000 |

**2.37b**
**SCF energy:** -464.792020119 Hartree
**Free energy correction:** 0.193117 Hartree

| | | | |
|---|---|---|---|
| 8 | -4.591163000 | -0.047254000 | 1.548610000 |
| 6 | -3.537681000 | -2.030777000 | -1.079866000 |
| 6 | -3.660603000 | -3.441031000 | -0.467432000 |
| 6 | -3.625384000 | -3.332494000 | 1.071171000 |
| 6 | -4.808786000 | -2.460515000 | 1.564321000 |
| 6 | -6.144676000 | -3.102852000 | 1.108690000 |
| 6 | -6.174124000 | -3.212384000 | -0.429836000 |
| 6 | -6.057331000 | -1.801996000 | -1.043208000 |
| 6 | -4.720858000 | -1.147346000 | -0.607143000 |
| 6 | -4.693319000 | -1.082616000 | 0.918111000 |
| 6 | -4.993015000 | -4.082167000 | -0.908724000 |
| 1 | -2.584710000 | -1.570312000 | -0.787986000 |
| 1 | -3.543250000 | -2.088153000 | -2.176928000 |
| 1 | -2.821020000 | -4.060822000 | -0.808057000 |
| 1 | -3.695236000 | -4.329505000 | 1.527295000 |
| 1 | -2.673483000 | -2.895758000 | 1.400889000 |
| 1 | -4.781534000 | -2.336677000 | 2.651715000 |
| 1 | -6.243668000 | -4.096936000 | 1.565766000 |
| 1 | -6.991617000 | -2.501549000 | 1.464674000 |
| 1 | -7.121398000 | -3.668991000 | -0.744718000 |
| 1 | -6.092723000 | -1.857451000 | -2.139846000 |
| 1 | -6.902868000 | -1.176996000 | -0.727080000 |
| 1 | -4.633919000 | -0.128738000 | -0.998763000 |
| 1 | -5.018658000 | -4.182343000 | -2.002509000 |
| 1 | -5.079087000 | -5.095833000 | -0.493693000 |

**I**
**SCF energy:** -3435.45999825 Hartree
**Free energy correction:** 0.478933 Hartree

| | | | |
|---|---|---|---|
| 8 | -5.894249000 | 3.439453000 | -3.769174000 |
| 14 | -7.387062000 | 4.320437000 | -3.939369000 |
| 16 | -5.555122000 | 2.461152000 | -2.585890000 |
| 8 | -4.169872000 | 2.025336000 | -2.719178000 |
| 8 | -5.692099000 | 3.511406000 | -1.372771000 |
| 8 | -6.590982000 | 1.435890000 | -2.466334000 |
| 8 | -7.504343000 | 4.721417000 | -5.512080000 |
| 8 | -8.575547000 | 3.300475000 | -3.503482000 |
| 8 | -7.234948000 | 5.687216000 | -3.058443000 |
| 1 | -5.334115000 | 3.099198000 | -0.531722000 |
| 6 | 1.675588000 | -0.663547000 | -0.345179000 |
| 6 | 1.092517000 | -0.754475000 | 2.132878000 |
| 6 | 0.722563000 | -0.183674000 | 0.757355000 |
| 8 | -0.572487000 | -0.564212000 | 0.298325000 |
| 8 | -1.550344000 | -0.464626000 | 1.371686000 |
| 8 | 0.638895000 | 1.921379000 | -0.319714000 |
| 8 | 0.746131000 | 1.231982000 | 0.957784000 |
| 8 | -4.740585000 | -0.063764000 | 1.575983000 |
| 1 | 1.401363000 | -0.195947000 | -1.293529000 |
| 1 | 1.524209000 | -1.744102000 | -0.453220000 |
| 1 | 0.430081000 | -0.329337000 | 2.889986000 |
| 1 | 0.884888000 | -1.830686000 | 2.090138000 |
| 1 | -0.294771000 | 1.752030000 | -0.589129000 |
| 1 | -4.602854000 | 1.294052000 | 1.024165000 |
| 8 | -3.072226000 | 4.252114000 | 0.586704000 |
| 14 | -1.835424000 | 4.225538000 | -0.599062000 |
| 16 | -3.437249000 | 3.102109000 | 1.620902000 |
| 8 | -2.275147000 | 2.248803000 | 1.865016000 |
| 8 | -4.140219000 | 3.705773000 | 2.729122000 |
| 8 | -4.472926000 | 2.282686000 | 0.681916000 |
| 8 | -0.361645000 | 4.511885000 | 0.013456000 |
| 8 | -2.351638000 | 5.448055000 | -1.555856000 |
| 8 | -1.825591000 | 2.732883000 | -1.291931000 |
| 1 | -1.721375000 | 0.502695000 | 1.421378000 |
| 1 | 0.213490000 | 3.716148000 | 0.075134000 |
| 1 | -2.601984000 | 2.460043000 | -1.821894000 |
| 1 | -1.641417000 | 5.963906000 | -1.963021000 |
| 1 | -6.864620000 | 5.583858000 | -2.168242000 |
| 1 | -7.110049000 | 5.569700000 | -5.759711000 |
| 1 | -8.293898000 | 2.425576000 | -3.183470000 |
| 6 | -3.525327000 | -2.042584000 | -1.084108000 |
| 6 | -3.659553000 | -3.449528000 | -0.471118000 |
| 6 | -3.612068000 | -3.334037000 | 1.065767000 |
| 6 | -4.793269000 | -2.458257000 | 1.562095000 |
| 6 | -6.138709000 | -3.098039000 | 1.110159000 |
| 6 | -6.170403000 | -3.204984000 | -0.427534000 |
| 6 | -6.048828000 | -1.793762000 | -1.036050000 |
| 6 | -4.698457000 | -1.147628000 | -0.602728000 |
| 6 | -4.711632000 | -1.102525000 | 0.905674000 |
| 6 | -4.996318000 | -4.083630000 | -0.908060000 |
| 1 | -2.567932000 | -1.591986000 | -0.806533000 |
| 1 | -3.561363000 | -2.093682000 | -2.180016000 |

| | | | |
|---|---|---|---|
| 1 | -2.823573000 | -4.073049000 | -0.812147000 |
| 1 | -3.693133000 | -4.324751000 | 1.532148000 |
| 1 | -2.663117000 | -2.892183000 | 1.387625000 |
| 1 | -4.765804000 | -2.326147000 | 2.647795000 |
| 1 | -6.227393000 | -4.089618000 | 1.572322000 |
| 1 | -6.982648000 | -2.497187000 | 1.473116000 |
| 1 | -7.122482000 | -3.652359000 | -0.740131000 |
| 1 | -6.074496000 | -1.833636000 | -2.131654000 |
| 1 | -6.887961000 | -1.160299000 | -0.722828000 |
| 1 | -4.608433000 | -0.137827000 | -1.011443000 |
| 1 | -5.026217000 | -4.184238000 | -2.001289000 |
| 1 | -5.090410000 | -5.095798000 | -0.491591000 |
| 6 | 3.138600000 | -0.366720000 | 0.015496000 |
| 1 | 3.287746000 | 0.719528000 | 0.044268000 |
| 1 | 3.789075000 | -0.756851000 | -0.776648000 |
| 6 | 3.515692000 | -0.979308000 | 1.372044000 |
| 1 | 3.468710000 | -2.076391000 | 1.300117000 |
| 1 | 4.552279000 | -0.726666000 | 1.627234000 |
| 6 | 2.568212000 | -0.499218000 | 2.481108000 |
| 1 | 2.715217000 | 0.574827000 | 2.647088000 |
| 1 | 2.803303000 | -1.000644000 | 3.427979000 |

**II**

**SCF energy:** -3435.46579315 Hartree

**Free energy correction:** 0.482087 Hartree

| | | | |
|---|---|---|---|
| 8 | -5.955530000 | 3.371929000 | -3.677491000 |
| 14 | -7.359555000 | 4.393994000 | -3.777255000 |
| 16 | -5.699338000 | 2.328996000 | -2.524819000 |
| 8 | -4.348858000 | 1.790285000 | -2.675352000 |
| 8 | -5.769886000 | 3.315807000 | -1.272966000 |
| 8 | -6.806006000 | 1.371814000 | -2.469606000 |
| 8 | -7.406672000 | 4.973370000 | -5.298376000 |
| 8 | -8.643139000 | 3.433385000 | -3.497287000 |
| 8 | -7.117680000 | 5.634267000 | -2.743130000 |
| 1 | -5.311367000 | 2.902398000 | -0.451857000 |
| 6 | 1.547097000 | -0.839986000 | -0.247127000 |
| 6 | 0.933465000 | -0.675840000 | 2.221132000 |
| 6 | 0.591684000 | -0.237121000 | 0.790916000 |
| 8 | -0.705922000 | -0.648252000 | 0.355824000 |
| 8 | -1.704778000 | -0.393714000 | 1.384305000 |
| 8 | 0.561040000 | 1.754909000 | -0.486248000 |
| 8 | 0.633637000 | 1.186310000 | 0.850995000 |
| 8 | -4.643739000 | -0.060799000 | 1.695385000 |
| 1 | 1.292304000 | -0.459598000 | -1.238858000 |
| 1 | 1.378539000 | -1.923587000 | -0.251868000 |
| 1 | 0.270050000 | -0.165670000 | 2.923127000 |
| 1 | 0.708620000 | -1.747895000 | 2.282993000 |
| 1 | -0.387711000 | 1.634954000 | -0.733187000 |
| 1 | -4.609525000 | 0.914764000 | 1.221977000 |
| 8 | -3.117774000 | 4.186414000 | 0.307780000 |
| 14 | -1.899733000 | 4.090901000 | -0.866828000 |
| 16 | -3.462072000 | 3.094487000 | 1.441476000 |
| 8 | -2.248077000 | 2.303313000 | 1.706615000 |
| 8 | -4.075219000 | 3.812227000 | 2.541026000 |
| 8 | -4.496349000 | 2.196123000 | 0.682370000 |
| 8 | -0.403238000 | 4.413844000 | -0.320414000 |
| 8 | -2.410108000 | 5.250540000 | -1.907356000 |
| 8 | -1.882910000 | 2.558277000 | -1.487051000 |
| 1 | -1.795262000 | 0.591968000 | 1.376075000 |
| 1 | 0.163309000 | 3.623147000 | -0.194261000 |
| 1 | -2.695611000 | 2.257127000 | -1.941253000 |
| 1 | -1.691532000 | 5.706381000 | -2.367790000 |
| 1 | -6.699061000 | 5.401477000 | -1.898966000 |
| 1 | -6.937115000 | 5.808467000 | -5.435190000 |
| 1 | -8.437425000 | 2.530679000 | -3.198216000 |
| 6 | -3.432029000 | -1.903660000 | -1.159119000 |
| 6 | -3.550873000 | -3.334982000 | -0.604959000 |
| 6 | -3.392105000 | -3.293303000 | 0.927507000 |
| 6 | -4.518875000 | -2.424817000 | 1.548031000 |
| 6 | -5.911331000 | -3.026965000 | 1.158614000 |
| 6 | -6.046238000 | -3.054032000 | -0.375797000 |
| 6 | -5.944108000 | -1.614995000 | -0.916696000 |
| 6 | -4.541906000 | -1.008609000 | -0.547754000 |
| 6 | -4.503655000 | -1.063470000 | 0.940953000 |
| 6 | -4.925268000 | -3.927130000 | -0.977742000 |
| 1 | -2.447965000 | -1.482709000 | -0.940343000 |
| 1 | -3.563063000 | -1.895425000 | -2.247987000 |
| 1 | -2.751473000 | -3.953093000 | -1.031405000 |
| 1 | -3.464284000 | -4.300758000 | 1.356020000 |
| 1 | -2.416787000 | -2.881187000 | 1.202260000 |
| 1 | -4.421034000 | -2.339892000 | 2.633756000 |
| 1 | -5.971608000 | -4.037201000 | 1.581161000 |
| 1 | -6.716159000 | -2.435541000 | 1.612460000 |
| 1 | -7.026581000 | -3.467591000 | -0.643354000 |
| 1 | -6.033261000 | -1.584588000 | -2.007996000 |
| 1 | -6.747179000 | -0.984286000 | -0.517855000 |
| 1 | -4.461650000 | 0.018325000 | -0.907173000 |
| 1 | -5.032217000 | -3.974467000 | -2.069177000 |
| 1 | -5.011217000 | -4.955881000 | -0.602981000 |
| 6 | 3.011162000 | -0.534443000 | 0.103220000 |
| 1 | 3.180369000 | 0.546324000 | 0.024620000 |
| 1 | 3.663406000 | -1.013613000 | -0.636897000 |
| 6 | 3.360397000 | -1.014620000 | 1.519377000 |
| 1 | 3.294888000 | -2.112550000 | 1.556743000 |
| 1 | 4.398233000 | -0.755040000 | 1.761990000 |
| 6 | 2.408896000 | -0.410272000 | 2.562237000 |
| 1 | 2.570913000 | 0.672634000 | 2.620536000 |
| 1 | 2.624427000 | -0.817126000 | 3.557800000 |

**TS1**

**SCF energy:** -3435.44919172 Hartree

**Free energy correction:** 0.486319 Hartree

**Imaginary Frequency:** 448.8 *i*cm$^{-1}$

| | | | |
|---|---|---|---|
| 8 | -6.095728000 | 3.395105000 | -3.801038000 |
| 14 | -7.694780000 | 4.078034000 | -3.867310000 |
| 16 | -5.574275000 | 2.473013000 | -2.634882000 |
| 8 | -4.166102000 | 2.176005000 | -2.877358000 |
| 8 | -5.731652000 | 3.510750000 | -1.425557000 |
| 8 | -6.487724000 | 1.345440000 | -2.445804000 |
| 8 | -7.928930000 | 4.573372000 | -5.400187000 |
| 8 | -8.726784000 | 2.876429000 | -3.498462000 |
| 8 | -7.684573000 | 5.382908000 | -2.882874000 |
| 1 | -5.316822000 | 3.126615000 | -0.577159000 |
| 6 | 1.109405000 | -0.998212000 | -0.194738000 |
| 6 | 0.294420000 | -0.797707000 | 2.216683000 |
| 6 | 0.164304000 | -0.278061000 | 0.780233000 |
| 8 | -1.136651000 | -0.497638000 | 0.187732000 |
| 8 | -2.200170000 | -0.191735000 | 1.156648000 |
| 8 | 0.518508000 | 1.712543000 | -0.432482000 |
| 8 | 0.400050000 | 1.110590000 | 0.885559000 |
| 8 | -4.382138000 | -0.094157000 | 1.756822000 |
| 1 | 1.004822000 | -0.564510000 | -1.191424000 |
| 1 | 0.794998000 | -2.047025000 | -0.247937000 |
| 1 | -0.346781000 | -0.206826000 | 2.875602000 |
| 1 | -0.085367000 | -1.826513000 | 2.222905000 |
| 1 | -0.417070000 | 1.741577000 | -0.754587000 |
| 1 | -4.645151000 | 0.749869000 | 1.311546000 |
| 8 | -2.999601000 | 4.298458000 | 0.319011000 |
| 14 | -1.734739000 | 4.260542000 | -0.815178000 |
| 16 | -3.433985000 | 3.136514000 | 1.334456000 |
| 8 | -2.218865000 | 2.225350000 | 1.419906000 |
| 8 | -3.815662000 | 3.762931000 | 2.581162000 |
| 8 | -4.544088000 | 2.396313000 | 0.614750000 |
| 8 | -0.255807000 | 4.463457000 | -0.169828000 |
| 8 | -2.149284000 | 5.533716000 | -1.754706000 |
| 8 | -1.750229000 | 2.788703000 | -1.565322000 |
| 1 | -2.286382000 | 0.960884000 | 1.220228000 |
| 1 | 0.257885000 | 3.638960000 | -0.050909000 |
| 1 | -2.550491000 | 2.553621000 | -2.079192000 |
| 1 | -1.399714000 | 5.994116000 | -2.157427000 |
| 1 | -7.205925000 | 5.270321000 | -2.046334000 |
| 1 | -7.661136000 | 5.484364000 | -5.586556000 |
| 1 | -8.319787000 | 2.067099000 | -3.141992000 |
| 6 | -3.269912000 | -1.768599000 | -1.463258000 |
| 6 | -3.310073000 | -3.208022000 | -0.912239000 |
| 6 | -2.753967000 | -3.219720000 | 0.528288000 |
| 6 | -3.613636000 | -2.313294000 | 1.435693000 |
| 6 | -5.080074000 | -2.830241000 | 1.420844000 |
| 6 | -5.627414000 | -2.793766000 | -0.021755000 |
| 6 | -5.576133000 | -1.348524000 | -0.563042000 |

| | | | |
|---|---|---|---|
| 6 | -4.104781000 | -0.834629000 | -0.558264000 |
| 6 | -3.678524000 | -0.883349000 | 0.910207000 |
| 6 | -4.767073000 | -3.713346000 | -0.912350000 |
| 1 | -2.241787000 | -1.414790000 | -1.550062000 |
| 1 | -3.706657000 | -1.737320000 | -2.469296000 |
| 1 | -2.691301000 | -3.857246000 | -1.544520000 |
| 1 | -2.778712000 | -4.238816000 | 0.935563000 |
| 1 | -1.708767000 | -2.896984000 | 0.533532000 |
| 1 | -3.230309000 | -2.289917000 | 2.461350000 |
| 1 | -5.090760000 | -3.857418000 | 1.807144000 |
| 1 | -5.697002000 | -2.221450000 | 2.088856000 |
| 1 | -6.667949000 | -3.141864000 | -0.022857000 |
| 1 | -5.948125000 | -1.302881000 | -1.592170000 |
| 1 | -6.217427000 | -0.690733000 | 0.032947000 |
| 1 | -4.063229000 | 0.195965000 | -0.923001000 |
| 1 | -5.160192000 | -3.723422000 | -1.937745000 |
| 1 | -4.812451000 | -4.746395000 | -0.541265000 |
| 6 | 2.562151000 | -0.907804000 | 0.300080000 |
| 1 | 2.884748000 | 0.139848000 | 0.276107000 |
| 1 | 3.206606000 | -1.456514000 | -0.396781000 |
| 6 | 2.704572000 | -1.468437000 | 1.721939000 |
| 1 | 2.483025000 | -2.546166000 | 1.711417000 |
| 1 | 3.740660000 | -1.365589000 | 2.066063000 |
| 6 | 1.755447000 | -0.759342000 | 2.698675000 |
| 1 | 2.063774000 | 0.286126000 | 2.816280000 |
| 1 | 1.811932000 | -1.220433000 | 3.691774000 |

**III**

**SCF energy:** -3435.45404335 Hartree

**Free energy correction:** 0.487995 Hartree

| | | | |
|---|---|---|---|
| 8 | -6.284596000 | 3.505554000 | -3.719682000 |
| 14 | -7.908038000 | 4.137427000 | -3.699890000 |
| 16 | -5.650999000 | 2.625618000 | -2.580960000 |
| 8 | -4.255577000 | 2.369516000 | -2.921437000 |
| 8 | -5.742502000 | 3.699998000 | -1.383632000 |
| 8 | -6.514468000 | 1.484994000 | -2.282867000 |
| 8 | -8.263394000 | 4.537178000 | -5.236247000 |
| 8 | -8.868153000 | 2.934966000 | -3.177754000 |
| 8 | -7.870613000 | 5.498064000 | -2.795395000 |
| 1 | -5.288113000 | 3.331313000 | -0.566671000 |
| 6 | 1.167039000 | -1.148335000 | -0.065707000 |
| 6 | 0.172262000 | -0.744081000 | 2.248917000 |
| 6 | 0.121965000 | -0.380376000 | 0.757737000 |
| 8 | -1.111913000 | -0.688200000 | 0.115405000 |
| 8 | -2.221027000 | -0.182450000 | 0.946088000 |
| 8 | 0.487883000 | 1.506214000 | -0.621298000 |
| 8 | 0.322972000 | 1.032286000 | 0.745377000 |
| 8 | -4.298820000 | -0.115346000 | 1.598944000 |
| 1 | 1.121775000 | -0.816612000 | -1.105367000 |
| 1 | 0.889976000 | -2.208911000 | -0.041578000 |
| 1 | -0.534752000 | -0.121282000 | 2.801752000 |
| 1 | -0.174855000 | -1.781320000 | 2.331326000 |
| 1 | -0.442259000 | 1.511289000 | -0.953147000 |
| 1 | -4.544661000 | 0.711210000 | 1.138363000 |
| 8 | -2.673288000 | 4.413721000 | 0.441368000 |
| 14 | -1.604636000 | 4.162167000 | -0.875771000 |
| 16 | -3.352951000 | 3.360038000 | 1.408069000 |
| 8 | -2.171001000 | 2.378375000 | 1.786955000 |
| 8 | -3.809241000 | 4.065527000 | 2.577543000 |
| 8 | -4.343942000 | 2.588976000 | 0.604198000 |
| 8 | -0.048238000 | 4.255864000 | -0.430892000 |
| 8 | -2.047884000 | 5.399021000 | -1.844411000 |
| 8 | -1.887835000 | 2.647956000 | -1.458865000 |
| 1 | -2.247566000 | 1.468849000 | 1.357036000 |
| 1 | 0.407335000 | 3.387814000 | -0.361121000 |
| 1 | -2.696274000 | 2.501106000 | -1.995157000 |
| 1 | -1.335679000 | 5.778890000 | -2.377972000 |
| 1 | -7.384572000 | 5.436977000 | -1.958585000 |
| 1 | -8.040074000 | 5.441706000 | -5.497412000 |
| 1 | -8.417051000 | 2.135115000 | -2.855239000 |
| 6 | -3.214041000 | -1.864146000 | -1.607436000 |
| 6 | -3.275104000 | -3.292926000 | -1.028454000 |
| 6 | -2.696089000 | -3.295035000 | 0.402992000 |
| 6 | -3.509177000 | -2.337723000 | 1.303816000 |
| 6 | -4.982032000 | -2.824465000 | 1.330558000 |
| 6 | -5.562531000 | -2.810471000 | -0.100497000 |
| 6 | -5.492760000 | -1.380480000 | -0.678316000 |
| 6 | -4.018101000 | -0.898527000 | -0.705647000 |
| 6 | -3.518822000 | -0.901218000 | 0.753035000 |
| 6 | -4.742567000 | -3.765433000 | -0.991418000 |
| 1 | -2.178845000 | -1.533905000 | -1.711889000 |
| 1 | -3.661060000 | -1.847660000 | -2.610196000 |
| 1 | -2.683372000 | -3.967657000 | -1.660732000 |
| 1 | -2.755978000 | -4.305733000 | 0.829037000 |
| 1 | -1.639700000 | -3.015738000 | 0.384055000 |
| 1 | -3.099963000 | -2.309410000 | 2.320461000 |
| 1 | -5.009488000 | -3.843976000 | 1.737707000 |
| 1 | -5.575163000 | -2.189558000 | 1.995101000 |
| 1 | -6.609738000 | -3.138117000 | -0.070276000 |
| 1 | -5.887805000 | -1.358513000 | -1.700832000 |
| 1 | -6.112745000 | -0.699098000 | -0.086682000 |
| 1 | -3.958933000 | 0.124014000 | -1.098267000 |
| 1 | -5.157689000 | -3.785104000 | -2.008498000 |
| 1 | -4.801844000 | -4.790771000 | -0.600748000 |
| 6 | 2.576188000 | -0.959204000 | 0.517263000 |
| 1 | 2.871027000 | 0.092015000 | 0.412536000 |
| 1 | 3.286575000 | -1.549538000 | -0.073659000 |
| 6 | 2.630712000 | -1.371396000 | 1.994967000 |
| 1 | 2.440641000 | -2.451997000 | 2.077413000 |
| 1 | 3.635673000 | -1.198803000 | 2.398851000 |
| 6 | 1.591804000 | -0.604085000 | 2.825164000 |
| 1 | 1.861526000 | 0.458334000 | 2.857775000 |
| 1 | 1.590183000 | -0.961726000 | 3.861768000 |

**IV**

**SCF energy:** -3435.46774741 Hartree

**Free energy correction:** 0.494983 Hartree

| | | | |
|---|---|---|---|
| 8 | -5.080782000 | 3.770819000 | -0.346521000 |
| 14 | -4.835257000 | 4.177816000 | 1.310112000 |
| 16 | -5.948879000 | 2.428541000 | -0.725413000 |
| 8 | -6.029250000 | 2.429224000 | -2.200376000 |
| 8 | -5.080714000 | 1.296239000 | -0.203814000 |
| 8 | -7.210783000 | 2.540446000 | 0.005603000 |
| 8 | -3.757964000 | 5.385253000 | 1.350917000 |
| 8 | -6.251955000 | 4.675786000 | 1.941686000 |
| 8 | -4.214186000 | 2.792773000 | 2.002467000 |
| 6 | 0.299898000 | -0.670741000 | 2.201887000 |
| 6 | -2.144343000 | -0.308673000 | 2.833449000 |
| 6 | -1.088569000 | -0.189835000 | 1.729846000 |
| 8 | -1.351211000 | -1.003440000 | 0.586981000 |
| 8 | -2.807903000 | -1.184399000 | 0.385875000 |
| 8 | -2.021965000 | 1.789780000 | 0.814982000 |
| 8 | -0.830541000 | 1.165355000 | 1.353011000 |
| 8 | -3.101420000 | 0.200506000 | -1.411896000 |
| 8 | -2.689880000 | 3.020704000 | -2.415119000 |
| 14 | -2.120485000 | 4.563238000 | -1.866641000 |
| 16 | -3.071885000 | 2.642408000 | -3.914916000 |
| 8 | -4.481594000 | 3.319648000 | -4.118494000 |
| 8 | -3.214564000 | 1.174647000 | -3.888810000 |
| 8 | -2.149524000 | 3.251226000 | -4.853393000 |
| 8 | -0.818002000 | 4.965309000 | -2.752609000 |
| 8 | -1.752419000 | 4.283105000 | -0.295526000 |
| 8 | -3.314911000 | 5.656305000 | -2.025064000 |
| 6 | -2.078365000 | -3.498051000 | -1.300164000 |
| 6 | -3.483581000 | -4.127407000 | -1.413777000 |
| 6 | -4.475548000 | -3.309384000 | -0.563169000 |
| 6 | -4.516523000 | -1.849043000 | -1.072490000 |
| 6 | -4.960288000 | -1.833770000 | -2.554574000 |
| 6 | -3.981401000 | -2.667908000 | -3.408308000 |
| 6 | -2.567628000 | -2.060819000 | -3.308120000 |
| 6 | -2.102297000 | -2.042172000 | -1.833240000 |
| 6 | -3.094765000 | -1.259784000 | -0.961268000 |
| 6 | -3.945875000 | -4.118986000 | -2.886300000 |
| 6 | 0.743945000 | 0.023368000 | 3.499530000 |
| 6 | -0.317755000 | -0.118521000 | 4.599156000 |
| 6 | -1.685466000 | 0.391783000 | 4.124236000 |
| 1 | -3.864470000 | 0.727655000 | -0.939147000 |
| 1 | -2.893474000 | 5.168335000 | 0.942888000 |
| 1 | -7.018382000 | 4.202159000 | 1.574237000 |
| 1 | -4.584039000 | 1.996555000 | 1.565292000 |

| | | | |
|---|---|---|---|
| 1 | 1.019030000 | -0.504210000 | 1.393217000 |
| 1 | 0.220621000 | -1.752487000 | 2.357197000 |
| 1 | -3.097207000 | 0.097550000 | 2.487327000 |
| 1 | -2.309184000 | -1.376337000 | 3.020139000 |
| 1 | -2.486458000 | 2.179711000 | 1.594316000 |
| 1 | -3.122858000 | 0.405471000 | -2.395074000 |
| 1 | -5.122354000 | 3.001955000 | -3.400896000 |
| 1 | -0.911237000 | 4.827699000 | -3.709790000 |
| 1 | -1.611502000 | 3.346260000 | -0.016644000 |
| 1 | -4.131147000 | 5.443686000 | -1.541543000 |
| 1 | -1.728664000 | -3.514964000 | -0.262604000 |
| 1 | -1.354876000 | -4.069339000 | -1.894968000 |
| 1 | -3.448381000 | -5.158754000 | -1.041191000 |
| 1 | -5.484888000 | -3.732691000 | -0.640287000 |
| 1 | -4.193190000 | -3.335516000 | 0.494394000 |
| 1 | -5.194006000 | -1.245243000 | -0.460854000 |
| 1 | -5.971113000 | -2.255378000 | -2.611337000 |
| 1 | -5.034912000 | -0.808502000 | -2.935827000 |
| 1 | -4.310115000 | -2.654228000 | -4.454273000 |
| 1 | -1.854483000 | -2.669796000 | -3.877722000 |
| 1 | -2.539233000 | -1.065071000 | -3.761404000 |
| 1 | -1.114518000 | -1.584035000 | -1.743543000 |
| 1 | -3.263715000 | -4.721812000 | -3.500775000 |
| 1 | -4.940385000 | -4.577471000 | -2.969723000 |
| 1 | 0.931465000 | 1.084662000 | 3.298789000 |
| 1 | 1.695938000 | -0.412310000 | 3.825416000 |
| 1 | -0.405361000 | -1.176620000 | 4.887122000 |
| 1 | -0.004640000 | 0.425863000 | 5.497884000 |
| 1 | -1.633989000 | 1.475289000 | 3.956033000 |
| 1 | -2.443996000 | 0.234896000 | 4.899622000 |

**TS2**

**SCF energy:** -3435.45314152 Hartree

**Free energy correction:** 0.491813 Hartree

**Imaginary Frequency:** 23.4 *i*cm$^{-1}$

| | | | |
|---|---|---|---|
| 8 | -4.562717000 | 4.437042000 | -0.141072000 |
| 14 | -3.693419000 | 4.411615000 | 1.325376000 |
| 16 | -6.148372000 | 3.882199000 | -0.131904000 |
| 8 | -6.515054000 | 3.875308000 | -1.565375000 |
| 8 | -6.036899000 | 2.512603000 | 0.462600000 |
| 8 | -6.872863000 | 4.842998000 | 0.705971000 |
| 8 | -2.197562000 | 4.981281000 | 1.086042000 |
| 8 | -4.497762000 | 5.305307000 | 2.426019000 |
| 8 | -3.631619000 | 2.779919000 | 1.724202000 |
| 6 | -0.084610000 | -0.814707000 | 2.792317000 |
| 6 | -2.589458000 | -0.320054000 | 2.879204000 |
| 6 | -1.350655000 | -0.449782000 | 1.991726000 |
| 8 | -1.447280000 | -1.556039000 | 1.045583000 |
| 8 | -2.849192000 | -1.817963000 | 0.640639000 |
| 8 | -2.052812000 | 1.069979000 | 0.361665000 |
| 8 | -0.995431000 | 0.719973000 | 1.293444000 |
| 8 | -4.734742000 | 0.280305000 | -0.733864000 |
| 8 | -3.305020000 | 2.574371000 | -2.581244000 |
| 14 | -2.097599000 | 3.792721000 | -2.433916000 |
| 16 | -4.239647000 | 2.333192000 | -3.865150000 |
| 8 | -5.252851000 | 3.536885000 | -3.805683000 |
| 8 | -4.901701000 | 1.057350000 | -3.591745000 |
| 8 | -3.450605000 | 2.495016000 | -5.078581000 |
| 8 | -1.100661000 | 3.683174000 | -3.717951000 |
| 8 | -1.334224000 | 3.387842000 | -1.033100000 |
| 8 | -2.801549000 | 5.252380000 | -2.322466000 |
| 6 | -1.342398000 | -3.288967000 | -1.802366000 |
| 6 | -2.478421000 | -4.226588000 | -2.250762000 |
| 6 | -3.580716000 | -4.233933000 | -1.173828000 |
| 6 | -4.189219000 | -2.781766000 | -1.017392000 |
| 6 | -4.755475000 | -2.333334000 | -2.383154000 |
| 6 | -3.629264000 | -2.317094000 | -3.431697000 |
| 6 | -2.520940000 | -1.353184000 | -2.969327000 |
| 6 | -1.913745000 | -1.830183000 | -1.625140000 |
| 6 | -2.983875000 | -2.003440000 | -0.619342000 |
| 6 | -3.054435000 | -3.738868000 | -3.597935000 |
| 6 | 0.149979000 | 0.180087000 | 3.943257000 |
| 6 | -1.086448000 | 0.285998000 | 4.845824000 |
| 6 | -2.335515000 | 0.661833000 | 4.037255000 |
| 1 | -5.324929000 | 0.910300000 | -0.271964000 |
| 1 | -1.675702000 | 4.502878000 | 0.406343000 |
| 1 | -5.422394000 | 5.475247000 | 2.162667000 |
| 1 | -4.526224000 | 2.412436000 | 1.526155000 |
| 1 | 0.769677000 | -0.843152000 | 2.108405000 |
| 1 | -0.233820000 | -1.824497000 | 3.190448000 |
| 1 | -3.443829000 | -0.000651000 | 2.277753000 |
| 1 | -2.823256000 | -1.317069000 | 3.272353000 |
| 1 | -2.623805000 | 1.698349000 | 0.897572000 |
| 1 | -4.718550000 | 0.637036000 | -1.639586000 |
| 1 | -5.733341000 | 3.598695000 | -2.907350000 |
| 1 | -1.565526000 | 3.533096000 | -4.559538000 |
| 1 | -1.398929000 | 2.456484000 | -0.725076000 |
| 1 | -3.508206000 | 5.305147000 | -1.650519000 |
| 1 | -0.886537000 | -3.630927000 | -0.866045000 |
| 1 | -0.547416000 | -3.232254000 | -2.554675000 |
| 1 | -2.080241000 | -5.243392000 | -2.357829000 |
| 1 | -4.411896000 | -4.890256000 | -1.456300000 |
| 1 | -3.192375000 | -4.591422000 | -0.212370000 |
| 1 | -4.938955000 | -2.760381000 | -0.223337000 |
| 1 | -5.537250000 | -3.048278000 | -2.667805000 |
| 1 | -5.222163000 | -1.354796000 | -2.274586000 |
| 1 | -4.033912000 | -1.957670000 | -4.383750000 |
| 1 | -1.706298000 | -1.314959000 | -3.702436000 |
| 1 | -2.910606000 | -0.339278000 | -2.861854000 |
| 1 | -1.142102000 | -1.158157000 | -1.251229000 |
| 1 | -2.266329000 | -3.746450000 | -4.361956000 |
| 1 | -3.837898000 | -4.426483000 | -3.941344000 |
| 1 | 0.395054000 | 1.164198000 | 3.527675000 |
| 1 | 1.022965000 | -0.152721000 | 4.516865000 |
| 1 | -1.250359000 | -0.675787000 | 5.354548000 |
| 1 | -0.912998000 | 1.030356000 | 5.631442000 |
| 1 | -2.234624000 | 1.673902000 | 3.632396000 |
| 1 | -3.221212000 | 0.673197000 | 4.682308000 |

**V**

**SCF energy:** -3435.45703245 Hartree

**Free energy correction:** 0.490181 Hartree

| | | | |
|---|---|---|---|
| 8 | -4.321022000 | 4.470470000 | -0.199897000 |
| 14 | -3.589399000 | 4.184247000 | 1.308071000 |
| 16 | -5.995705000 | 4.328956000 | -0.311294000 |
| 8 | -6.240126000 | 4.416482000 | -1.767964000 |
| 8 | -6.270569000 | 2.979728000 | 0.268953000 |
| 8 | -6.510228000 | 5.446589000 | 0.486990000 |
| 8 | -1.990699000 | 4.422139000 | 1.195414000 |
| 8 | -4.264192000 | 5.172645000 | 2.415501000 |
| 8 | -3.896223000 | 2.561545000 | 1.624260000 |
| 6 | -0.011246000 | -0.460781000 | 2.846179000 |
| 6 | -2.564752000 | -0.589113000 | 2.972524000 |
| 6 | -1.338845000 | -0.487948000 | 2.064008000 |
| 8 | -1.170943000 | -1.673252000 | 1.214945000 |
| 8 | -2.487651000 | -2.232663000 | 0.829587000 |
| 8 | -2.448103000 | 0.680962000 | 0.366004000 |
| 8 | -1.292231000 | 0.656494000 | 1.254221000 |
| 8 | -5.198652000 | 0.574913000 | -0.780399000 |
| 8 | -3.398845000 | 2.444425000 | -2.641491000 |
| 14 | -2.012222000 | 3.441631000 | -2.447920000 |
| 16 | -4.298085000 | 2.296292000 | -3.961831000 |
| 8 | -5.122771000 | 3.638233000 | -3.980624000 |
| 8 | -5.149264000 | 1.136742000 | -3.697053000 |
| 8 | -3.440355000 | 2.302986000 | -5.139943000 |
| 8 | -1.016497000 | 3.180355000 | -3.712313000 |
| 8 | -1.371421000 | 2.871439000 | -1.040518000 |
| 8 | -2.447711000 | 5.000390000 | -2.320852000 |
| 6 | -1.229929000 | -3.246132000 | -2.192376000 |
| 6 | -2.413889000 | -4.102306000 | -2.676499000 |
| 6 | -3.281025000 | -4.482908000 | -1.463024000 |
| 6 | -3.858805000 | -3.183231000 | -0.797190000 |
| 6 | -4.699311000 | -2.396195000 | -1.845847000 |
| 6 | -3.802605000 | -2.028642000 | -3.041647000 |
| 6 | -2.642557000 | -1.149032000 | -2.544501000 |
| 6 | -1.767074000 | -1.937311000 | -1.513151000 |
| 6 | -2.663005000 | -2.379556000 | -0.427820000 |
| 6 | -3.252170000 | -3.308618000 | -3.701296000 |
| 6 | -0.022530000 | 0.652470000 | 3.910524000 |
| 6 | -1.230534000 | 0.513448000 | 4.845631000 |

| | | | |
|---|---|---|---|
| 6 | -2.545794000 | 0.505824000 | 4.055410000 |
| 1 | -5.755276000 | 1.298635000 | -0.428693000 |
| 1 | -1.547961000 | 3.922116000 | 0.476124000 |
| 1 | -5.086142000 | 5.588119000 | 2.090323000 |
| 1 | -4.837855000 | 2.397901000 | 1.388020000 |
| 1 | 0.813308000 | -0.328636000 | 2.138473000 |
| 1 | 0.104930000 | -1.440060000 | 3.323641000 |
| 1 | -3.475077000 | -0.515269000 | 2.372271000 |
| 1 | -2.553603000 | -1.582670000 | 3.437055000 |
| 1 | -3.050050000 | 1.347042000 | 0.821882000 |
| 1 | -5.198073000 | 0.756361000 | -1.737593000 |
| 1 | -5.563534000 | 3.845479000 | -3.084646000 |
| 1 | -1.484926000 | 3.089503000 | -4.560848000 |
| 1 | -1.662865000 | 1.977689000 | -0.756732000 |
| 1 | -3.138163000 | 5.162521000 | -1.647814000 |
| 1 | -0.597822000 | -3.803685000 | -1.490464000 |
| 1 | -0.592952000 | -2.935100000 | -3.027986000 |
| 1 | -2.024813000 | -5.018924000 | -3.137011000 |
| 1 | -4.139193000 | -5.096817000 | -1.759517000 |
| 1 | -2.703345000 | -5.062049000 | -0.731625000 |
| 1 | -4.441157000 | -3.426348000 | 0.096000000 |
| 1 | -5.523025000 | -3.050391000 | -2.156855000 |
| 1 | -5.130828000 | -1.503311000 | -1.381547000 |
| 1 | -4.390152000 | -1.448817000 | -3.761139000 |
| 1 | -1.980341000 | -0.859740000 | -3.369215000 |
| 1 | -3.017282000 | -0.234291000 | -2.081285000 |
| 1 | -0.954248000 | -1.328212000 | -1.120334000 |
| 1 | -2.633345000 | -3.053927000 | -4.570993000 |
| 1 | -4.078435000 | -3.930046000 | -4.069657000 |
| 1 | -0.044731000 | 1.629082000 | 3.413710000 |
| 1 | 0.915533000 | 0.599360000 | 4.475071000 |
| 1 | -1.139503000 | -0.417773000 | 5.424634000 |
| 1 | -1.237178000 | 1.335223000 | 5.570586000 |
| 1 | -2.708090000 | 1.479339000 | 3.581813000 |
| 1 | -3.395696000 | 0.340064000 | 4.727185000 |

**VI**

**SCF energy:** -3435.46606195 Hartree

**Free energy correction:** 0.491405 Hartree

| | | | |
|---|---|---|---|
| 8 | -4.613094000 | 3.931095000 | -0.328466000 |
| 14 | -5.050695000 | 3.091033000 | 1.057912000 |
| 16 | -5.590330000 | 4.803167000 | -1.332580000 |
| 8 | -4.540666000 | 5.368670000 | -2.263320000 |
| 8 | -6.468734000 | 3.830400000 | -2.009973000 |
| 8 | -6.248865000 | 5.796849000 | -0.480339000 |
| 8 | -3.830718000 | 3.276761000 | 2.136547000 |
| 8 | -6.493388000 | 3.622000000 | 1.606983000 |
| 8 | -5.118406000 | 1.482110000 | 0.649760000 |
| 6 | 0.201188000 | 0.222979000 | 1.838645000 |
| 6 | -1.593595000 | -0.958663000 | 3.225874000 |
| 6 | -1.130260000 | -0.553406000 | 1.827865000 |
| 8 | -0.766761000 | -1.712142000 | 1.001248000 |
| 8 | -1.941289000 | -2.615571000 | 0.911734000 |
| 8 | -3.380068000 | -0.353418000 | 1.218514000 |
| 8 | -2.044494000 | 0.240644000 | 1.117841000 |
| 8 | -5.940351000 | 1.116114000 | -1.857778000 |
| 8 | -2.747206000 | 2.629626000 | -2.130840000 |
| 14 | -1.572367000 | 3.541167000 | -1.267510000 |
| 16 | -2.907532000 | 2.548752000 | -3.725465000 |
| 8 | -3.436910000 | 3.976082000 | -4.113729000 |
| 8 | -3.920562000 | 1.513786000 | -3.942292000 |
| 8 | -1.594122000 | 2.374891000 | -4.336958000 |
| 8 | -0.107597000 | 3.093147000 | -1.846434000 |
| 8 | -1.706255000 | 2.993611000 | 0.286395000 |
| 8 | -1.867756000 | 5.124155000 | -1.394237000 |
| 6 | -1.738563000 | -3.046969000 | -2.495198000 |
| 6 | -2.959656000 | -3.957427000 | -2.717588000 |
| 6 | -3.328678000 | -4.627104000 | -1.382461000 |
| 6 | -3.693709000 | -3.527459000 | -0.331843000 |
| 6 | -4.891403000 | -2.674989000 | -0.865398000 |
| 6 | -4.512895000 | -2.035195000 | -2.212205000 |
| 6 | -3.306643000 | -1.105816000 | -2.006145000 |
| 6 | -2.090392000 | -1.919868000 | -1.457979000 |
| 6 | -2.516657000 | -2.623242000 | -0.232338000 |
| 6 | -4.155436000 | -3.130701000 | -3.236816000 |
| 6 | 0.151010000 | 1.416857000 | 2.814433000 |
| 6 | -0.326952000 | 1.004221000 | 4.212279000 |
| 6 | -1.674869000 | 0.273558000 | 4.144068000 |
| 1 | -6.409325000 | 1.973745000 | -1.965595000 |
| 1 | -2.980342000 | 3.419079000 | 1.673957000 |
| 1 | -6.709129000 | 4.519246000 | 1.290693000 |
| 1 | -5.452109000 | 1.301949000 | -0.285279000 |
| 1 | 0.434285000 | 0.555952000 | 0.821599000 |
| 1 | 0.982282000 | -0.482497000 | 2.143896000 |
| 1 | -2.557622000 | -1.464821000 | 3.167917000 |
| 1 | -0.856916000 | -1.672525000 | 3.613889000 |
| 1 | -3.977562000 | 0.457116000 | 1.083921000 |
| 1 | -5.212561000 | 1.205086000 | -2.505595000 |
| 1 | -4.007659000 | 4.447246000 | -3.386273000 |
| 1 | -0.089113000 | 3.020608000 | -2.817198000 |
| 1 | -1.736875000 | 2.024958000 | 0.384410000 |
| 1 | -2.805611000 | 5.393093000 | -1.524515000 |
| 1 | -0.872324000 | -3.624814000 | -2.150354000 |
| 1 | -1.443786000 | -2.539181000 | -3.420218000 |
| 1 | -2.695372000 | -4.733762000 | -3.445998000 |
| 1 | -4.203434000 | -5.278717000 | -1.490211000 |
| 1 | -2.504849000 | -5.247334000 | -1.008132000 |
| 1 | -3.914372000 | -3.967951000 | 0.644525000 |
| 1 | -5.747997000 | -3.351847000 | -0.967975000 |
| 1 | -5.160473000 | -1.909454000 | -0.131712000 |
| 1 | -5.357204000 | -1.434260000 | -2.566889000 |
| 1 | -2.997879000 | -0.647155000 | -2.949977000 |
| 1 | -3.543825000 | -0.298307000 | -1.312471000 |
| 1 | -1.233187000 | -1.278353000 | -1.263653000 |
| 1 | -3.905593000 | -2.673869000 | -4.201963000 |
| 1 | -5.016559000 | -3.789266000 | -3.408285000 |
| 1 | -0.508173000 | 2.189712000 | 2.406914000 |
| 1 | 1.154295000 | 1.855433000 | 2.858980000 |
| 1 | 0.422024000 | 0.349209000 | 4.681627000 |
| 1 | -0.411537000 | 1.892510000 | 4.848284000 |
| 1 | -2.450710000 | 0.954985000 | 3.773574000 |
| 1 | -1.987394000 | -0.051720000 | 5.142641000 |

**TS3**

**SCF energy** -3435.45775226 Hartree

**Free energy correction:** 0.493449 Hartree

**Imaginary Frequency:** 95.9 *i*cm$^{-1}$

| | | | |
|---|---|---|---|
| 8 | -4.645264000 | 3.746586000 | -0.290348000 |
| 14 | -4.956690000 | 2.716359000 | 0.984495000 |
| 16 | -5.710774000 | 4.690137000 | -1.141156000 |
| 8 | -4.731508000 | 5.402217000 | -2.040786000 |
| 8 | -6.580582000 | 3.757986000 | -1.884818000 |
| 8 | -6.366306000 | 5.534325000 | -0.140168000 |
| 8 | -3.719328000 | 2.843078000 | 2.047360000 |
| 8 | -6.417959000 | 3.017993000 | 1.642122000 |
| 8 | -4.913257000 | 1.167657000 | 0.346876000 |
| 6 | 0.292907000 | 0.059794000 | 1.871332000 |
| 6 | -1.624288000 | -0.970177000 | 3.212234000 |
| 6 | -1.047660000 | -0.689819000 | 1.824367000 |
| 8 | -0.715316000 | -1.889027000 | 1.090953000 |
| 8 | -1.960748000 | -2.680138000 | 0.956873000 |
| 8 | -3.200857000 | -0.557293000 | 0.918912000 |
| 8 | -1.908661000 | 0.112229000 | 1.007308000 |
| 8 | -5.918714000 | 1.098355000 | -2.053673000 |
| 8 | -2.769743000 | 2.736332000 | -2.238499000 |
| 14 | -1.607941000 | 3.633229000 | -1.344601000 |
| 16 | -2.998468000 | 2.791291000 | -3.826815000 |
| 8 | -3.583148000 | 4.236802000 | -4.057929000 |
| 8 | -3.991361000 | 1.750956000 | -4.094724000 |
| 8 | -1.710847000 | 2.726396000 | -4.506435000 |
| 8 | -0.150537000 | 3.343256000 | -2.026662000 |
| 8 | -1.632514000 | 2.924722000 | 0.153131000 |
| 8 | -2.011069000 | 5.195285000 | -1.280969000 |
| 6 | -1.702988000 | -3.103721000 | -2.113533000 |
| 6 | -2.956012000 | -3.969276000 | -2.349116000 |
| 6 | -3.551386000 | -4.371842000 | -0.986814000 |
| 6 | -3.954902000 | -3.079291000 | -0.195695000 |
| 6 | -4.995901000 | -2.282111000 | -1.019646000 |
| 6 | -4.402225000 | -1.900459000 | -2.389521000 |
| 6 | -3.153704000 | -1.022641000 | -2.179334000 |

| | | | |
|---|---|---|---|
| 6 | -2.098792000 | -1.785876000 | -1.351508000 |
| 6 | -2.680268000 | -2.299151000 | -0.074107000 |
| 6 | -4.003450000 | -3.175758000 | -3.160067000 |
| 6 | 0.224004000 | 1.320410000 | 2.755492000 |
| 6 | -0.346340000 | 1.015283000 | 4.147045000 |
| 6 | -1.710762000 | 0.319178000 | 4.047193000 |
| 1 | -6.415161000 | 1.949202000 | -2.045698000 |
| 1 | -2.888133000 | 3.074017000 | 1.582797000 |
| 1 | -6.728552000 | 3.927681000 | 1.478617000 |
| 1 | -5.302252000 | 1.102759000 | -0.598527000 |
| 1 | 0.605352000 | 0.303990000 | 0.850193000 |
| 1 | 1.028015000 | -0.645337000 | 2.276647000 |
| 1 | -2.603925000 | -1.441554000 | 3.121148000 |
| 1 | -0.952083000 | -1.691823000 | 3.692502000 |
| 1 | -3.868149000 | 0.225917000 | 0.655020000 |
| 1 | -5.242384000 | 1.258413000 | -2.744702000 |
| 1 | -4.165467000 | 4.598646000 | -3.291166000 |
| 1 | -0.175015000 | 3.332845000 | -3.000006000 |
| 1 | -1.518725000 | 1.959270000 | 0.157736000 |
| 1 | -2.965238000 | 5.420987000 | -1.362071000 |
| 1 | -0.941156000 | -3.654960000 | -1.549588000 |
| 1 | -1.249031000 | -2.796622000 | -3.062713000 |
| 1 | -2.666684000 | -4.875364000 | -2.895629000 |
| 1 | -4.456457000 | -4.977101000 | -1.113111000 |
| 1 | -2.838271000 | -4.963553000 | -0.401046000 |
| 1 | -4.326559000 | -3.340108000 | 0.799370000 |
| 1 | -5.879156000 | -2.919658000 | -1.145372000 |
| 1 | -5.324406000 | -1.392896000 | -0.474318000 |
| 1 | -5.149501000 | -1.332149000 | -2.951545000 |
| 1 | -2.708639000 | -0.755166000 | -3.143594000 |
| 1 | -3.408671000 | -0.082211000 | -1.686083000 |
| 1 | -1.211608000 | -1.184209000 | -1.162079000 |
| 1 | -3.594241000 | -2.908669000 | -4.142562000 |
| 1 | -4.886118000 | -3.802415000 | -3.341696000 |
| 1 | -0.386403000 | 2.083159000 | 2.260793000 |
| 1 | 1.235595000 | 1.734874000 | 2.831479000 |
| 1 | 0.355394000 | 0.373128000 | 4.699665000 |
| 1 | -0.439172000 | 1.945378000 | 4.718840000 |
| 1 | -2.444321000 | 0.999698000 | 3.598116000 |
| 1 | -2.084398000 | 0.064644000 | 5.045419000 |
| 6 | -4.168714000 | -1.906139000 | -2.575845000 |
| 6 | -2.857750000 | -1.114510000 | -2.389424000 |
| 6 | -1.925114000 | -1.855848000 | -1.406652000 |
| 6 | -2.635811000 | -1.998338000 | -0.048296000 |
| 6 | -3.849719000 | -3.315159000 | -3.117579000 |
| 6 | 0.328662000 | 1.229133000 | 2.725708000 |
| 6 | -0.344323000 | 0.999761000 | 4.086338000 |
| 6 | -1.726862000 | 0.353238000 | 3.919147000 |
| 1 | -6.433564000 | 2.484551000 | -1.946949000 |
| 1 | -2.932491000 | 2.959310000 | 1.579677000 |
| 1 | -6.752988000 | 3.995526000 | 1.707115000 |
| 1 | -5.676328000 | 1.243646000 | -1.153633000 |
| 1 | 0.804425000 | 0.113631000 | 0.897345000 |
| 1 | 1.089325000 | -0.779463000 | 2.390023000 |
| 1 | -2.636192000 | -1.392231000 | 2.973737000 |
| 1 | -1.060942000 | -1.704176000 | 3.691552000 |
| 1 | -4.470306000 | 0.539917000 | 0.633896000 |
| 1 | -5.377473000 | 1.516978000 | -2.761967000 |
| 1 | -4.241279000 | 4.667921000 | -3.235297000 |
| 1 | -0.269567000 | 3.200539000 | -2.996867000 |
| 1 | -1.568156000 | 1.796220000 | 0.188381000 |
| 1 | -2.968448000 | 5.357865000 | -1.245993000 |
| 1 | -0.944624000 | -3.798505000 | -1.262974000 |
| 1 | -1.103006000 | -3.180201000 | -2.908417000 |
| 1 | -2.713744000 | -5.064318000 | -2.500947000 |
| 1 | -4.588205000 | -4.728353000 | -0.859609000 |
| 1 | -3.022487000 | -4.731720000 | -0.044506000 |
| 1 | -4.442370000 | -2.833229000 | 0.775958000 |
| 1 | -5.806364000 | -2.618003000 | -1.321917000 |
| 1 | -5.180933000 | -1.054448000 | -0.834096000 |
| 1 | -4.819270000 | -1.375021000 | -3.281917000 |
| 1 | -2.344445000 | -1.000538000 | -3.352211000 |
| 1 | -3.067904000 | -0.102562000 | -2.024764000 |
| 1 | -0.995147000 | -1.299874000 | -1.270776000 |
| 1 | -3.356614000 | -3.239229000 | -4.095811000 |
| 1 | -4.780197000 | -3.878186000 | -3.272208000 |
| 1 | -0.223150000 | 1.991930000 | 2.163894000 |
| 1 | 1.344295000 | 1.619946000 | 2.857000000 |
| 1 | 0.292781000 | 0.348851000 | 4.703258000 |
| 1 | -0.433989000 | 1.951634000 | 4.622567000 |
| 1 | -2.403149000 | 1.049749000 | 3.408852000 |
| 1 | -2.172976000 | 0.150011000 | 4.899716000 |

**VII**

**SCF energy:** -3435.48649341 Hartree

**Free energy correction:** 0.495030 Hartree

| | | | |
|---|---|---|---|
| 8 | -4.788620000 | 3.688772000 | -0.226745000 |
| 14 | -5.062697000 | 2.698245000 | 1.107452000 |
| 16 | -5.783097000 | 4.744335000 | -0.986106000 |
| 8 | -4.811444000 | 5.428142000 | -1.897050000 |
| 8 | -6.740139000 | 3.874075000 | -1.748527000 |
| 8 | -6.401681000 | 5.574746000 | 0.040704000 |
| 8 | -3.763933000 | 2.810378000 | 2.081199000 |
| 8 | -6.482918000 | 3.065349000 | 1.807361000 |
| 8 | -5.189428000 | 1.171764000 | 0.431419000 |
| 6 | 0.410296000 | -0.068725000 | 1.902829000 |
| 6 | -1.645018000 | -0.963705000 | 3.130903000 |
| 6 | -0.935398000 | -0.791449000 | 1.785927000 |
| 8 | -0.632091000 | -2.023192000 | 1.148053000 |
| 8 | -1.896855000 | -2.724954000 | 0.920359000 |
| 8 | -2.964712000 | -0.716801000 | 0.557979000 |
| 8 | -1.714566000 | -0.007527000 | 0.841885000 |
| 8 | -6.086524000 | 1.484229000 | -2.048478000 |
| 8 | -2.930008000 | 2.714307000 | -2.216076000 |
| 14 | -1.690258000 | 3.503344000 | -1.307636000 |
| 16 | -3.204180000 | 2.807388000 | -3.784517000 |
| 8 | -3.662407000 | 4.306428000 | -3.989520000 |
| 8 | -4.324013000 | 1.877211000 | -4.002675000 |
| 8 | -1.979655000 | 2.620719000 | -4.538974000 |
| 8 | -0.265720000 | 3.169164000 | -2.025691000 |
| 8 | -1.749384000 | 2.756829000 | 0.159817000 |
| 8 | -2.030163000 | 5.079826000 | -1.199695000 |
| 6 | -1.621132000 | -3.272855000 | -1.945388000 |
| 6 | -2.936089000 | -4.059356000 | -2.120851000 |
| 6 | -3.644298000 | -4.178023000 | -0.755099000 |
| 6 | -3.964812000 | -2.764597000 | -0.207853000 |
| 6 | -4.882444000 | -2.035807000 | -1.215037000 |

**SSA-water**

**SCF energy:** -2510.45390319 Hartree

**Free energy correction:** 0.471917 Hartree

| | | | |
|---|---|---|---|
| 8 | -4.791906000 | 3.566738000 | -0.274753000 |
| 14 | -5.058337000 | 2.648622000 | 1.102798000 |
| 16 | -5.790089000 | 4.669049000 | -0.981066000 |
| 8 | -4.834317000 | 5.356527000 | -1.903449000 |
| 8 | -6.787285000 | 3.836128000 | -1.727367000 |
| 8 | -6.348476000 | 5.487600000 | 0.089591000 |
| 8 | -3.681363000 | 2.596759000 | 1.954911000 |
| 8 | -6.343244000 | 3.160340000 | 1.959059000 |
| 8 | -5.438230000 | 1.156920000 | 0.413392000 |
| 8 | -6.133786000 | 1.447330000 | -2.118866000 |
| 8 | -2.819221000 | 2.732411000 | -2.201573000 |
| 14 | -1.622131000 | 3.621982000 | -1.337871000 |
| 16 | -3.134151000 | 2.787996000 | -3.763513000 |
| 8 | -3.614139000 | 4.280099000 | -3.991568000 |
| 8 | -4.249500000 | 1.846323000 | -3.941084000 |
| 8 | -1.924296000 | 2.605754000 | -4.539958000 |
| 8 | -0.188286000 | 3.393285000 | -2.078275000 |
| 8 | -1.539841000 | 2.857697000 | 0.129447000 |
| 8 | -2.095631000 | 5.157728000 | -1.199297000 |
| 1 | -6.473052000 | 2.442019000 | -2.008670000 |
| 1 | -2.857907000 | 2.694815000 | 1.428516000 |
| 1 | -6.583060000 | 4.092614000 | 1.807739000 |
| 1 | -5.803551000 | 1.183130000 | -1.201005000 |
| 1 | -5.833879000 | 0.495349000 | 1.001037000 |
| 1 | -5.368981000 | 1.483255000 | -2.774467000 |
| 1 | -4.225782000 | 4.622049000 | -3.260240000 |
| 1 | -0.209478000 | 3.346899000 | -3.048479000 |
| 1 | -0.841125000 | 2.187330000 | 0.180228000 |
| 1 | -3.045825000 | 5.380976000 | -1.290591000 |

**2.39g**
**SCF energy:** -925.014696065 Hartree
**Free energy correction:** 0.122233 Hartree

| | | | |
|---|---|---|---|
| 6 | 0.425541000 | -0.106619000 | 1.920585000 |
| 6 | -1.619744000 | -1.007310000 | 3.143158000 |
| 6 | -0.908475000 | -0.849040000 | 1.794943000 |
| 8 | -0.581070000 | -2.099381000 | 1.188407000 |
| 8 | -1.835666000 | -2.811652000 | 0.928395000 |
| 8 | -2.918566000 | -0.801321000 | 0.598859000 |
| 8 | -1.669437000 | -0.083299000 | 0.854569000 |
| 6 | -1.628299000 | -3.297565000 | -1.971650000 |
| 6 | -2.965821000 | -4.043675000 | -2.156673000 |
| 6 | -3.654445000 | -4.193830000 | -0.784484000 |
| 6 | -3.927658000 | -2.796228000 | -0.183270000 |
| 6 | -4.837216000 | -1.990804000 | -1.139132000 |
| 6 | -4.146783000 | -1.840670000 | -2.510485000 |
| 6 | -2.809824000 | -1.093104000 | -2.325547000 |
| 6 | -1.886608000 | -1.893764000 | -1.381306000 |
| 6 | -2.588483000 | -2.049561000 | -0.016665000 |
| 6 | -3.878179000 | -3.238772000 | -3.106560000 |
| 6 | 0.263575000 | 1.238791000 | 2.648522000 |
| 6 | -0.432845000 | 1.068253000 | 4.006621000 |
| 6 | -1.779515000 | 0.345748000 | 3.853870000 |
| 1 | 0.847642000 | 0.029461000 | 0.919715000 |
| 1 | 1.104594000 | -0.763216000 | 2.478505000 |
| 1 | -2.587222000 | -1.488315000 | 2.992834000 |
| 1 | -1.007852000 | -1.686240000 | 3.750517000 |
| 1 | -0.960307000 | -3.865240000 | -1.314456000 |
| 1 | -1.118195000 | -3.190002000 | -2.938286000 |
| 1 | -2.776244000 | -5.038854000 | -2.579623000 |
| 1 | -4.611540000 | -4.721392000 | -0.893107000 |
| 1 | -3.032255000 | -4.786412000 | -0.105333000 |
| 1 | -4.391389000 | -2.886555000 | 0.805388000 |
| 1 | -5.790472000 | -2.525171000 | -1.247977000 |
| 1 | -5.063332000 | -1.007441000 | -0.713137000 |
| 1 | -4.797792000 | -1.269008000 | -3.184743000 |
| 1 | -2.309211000 | -0.969239000 | -3.295217000 |
| 1 | -2.984267000 | -0.090225000 | -1.920579000 |
| 1 | -0.942244000 | -1.365142000 | -1.237498000 |
| 1 | -3.402966000 | -3.142680000 | -4.092670000 |
| 1 | -4.826751000 | -3.772140000 | -3.260699000 |
| 1 | -0.322518000 | 1.919317000 | 2.018706000 |
| 1 | 1.251871000 | 1.696601000 | 2.776731000 |
| 1 | 0.217060000 | 0.487855000 | 4.678496000 |
| 1 | -0.577834000 | 2.047589000 | 4.479302000 |
| 1 | -2.469421000 | 0.973647000 | 3.275830000 |
| 1 | -2.241467000 | 0.187447000 | 4.835993000 |

# Appendix 2 – NMR spectra of the peroxide hybrids

**Compound TIC01-1:** $^{1}$H NMR (400 MHz, DMSO-$d_6$)

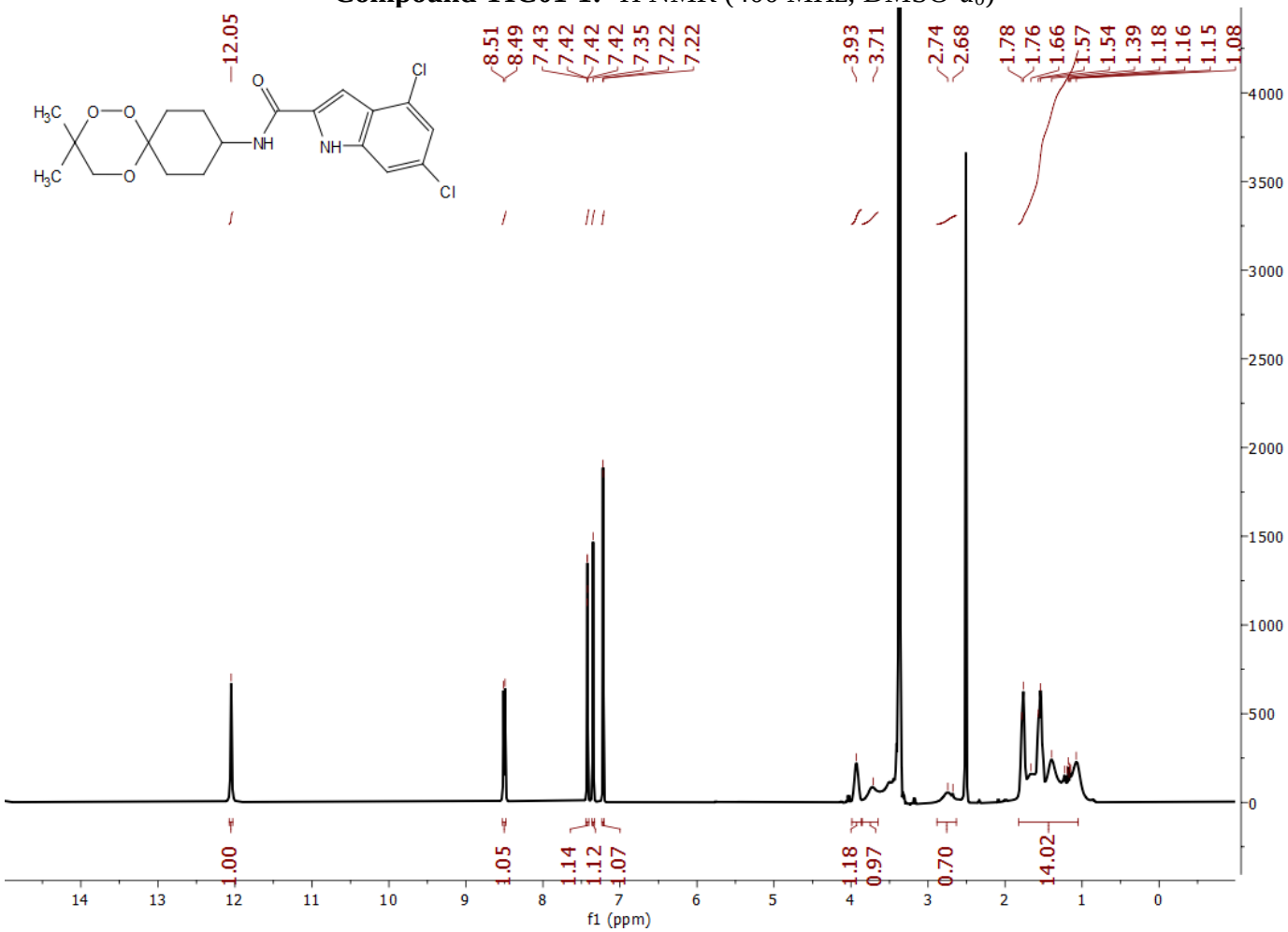

**Compound TIC01-1:** $^{13}C$ {$^{1}H$} NMR (101 MHz, DMSO-$d_6$)

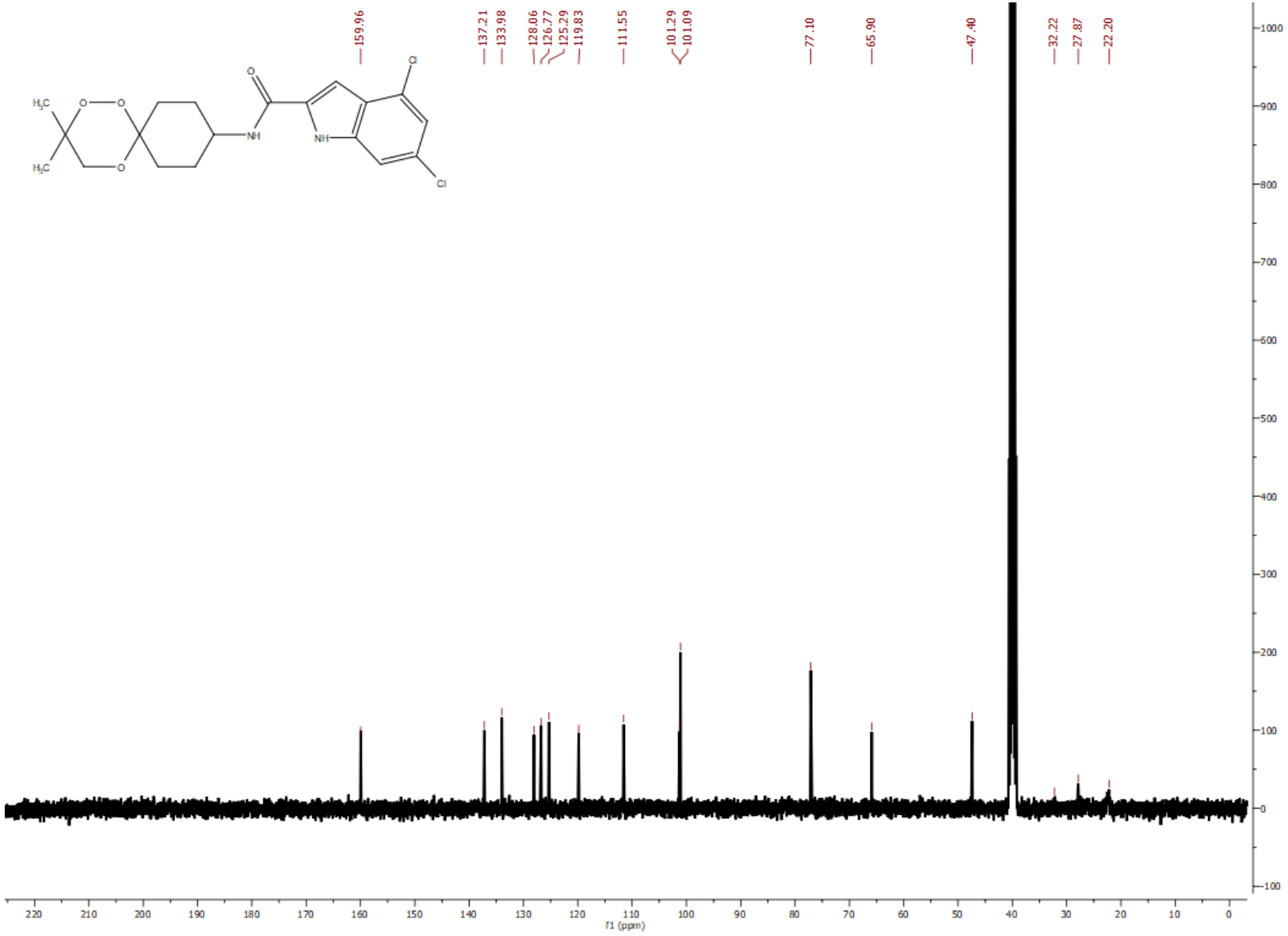

**Compound TIC01-2:** $^{1}$H NMR (400 MHz, DMSO-$d_6$)

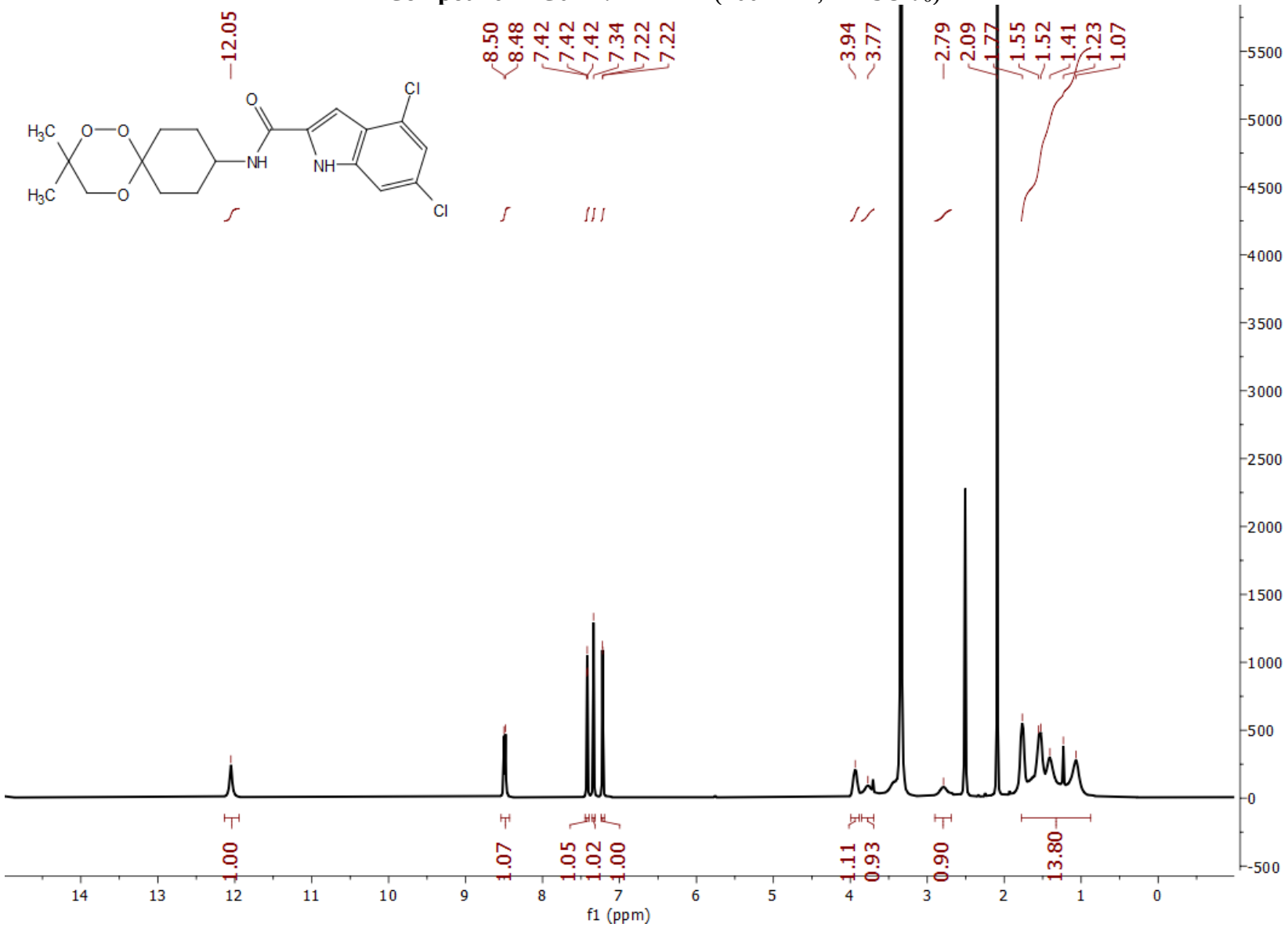

**Compound TIC01-2:** $^{13}C$ {$^{1}H$} NMR (101 MHz, DMSO-$d_6$)

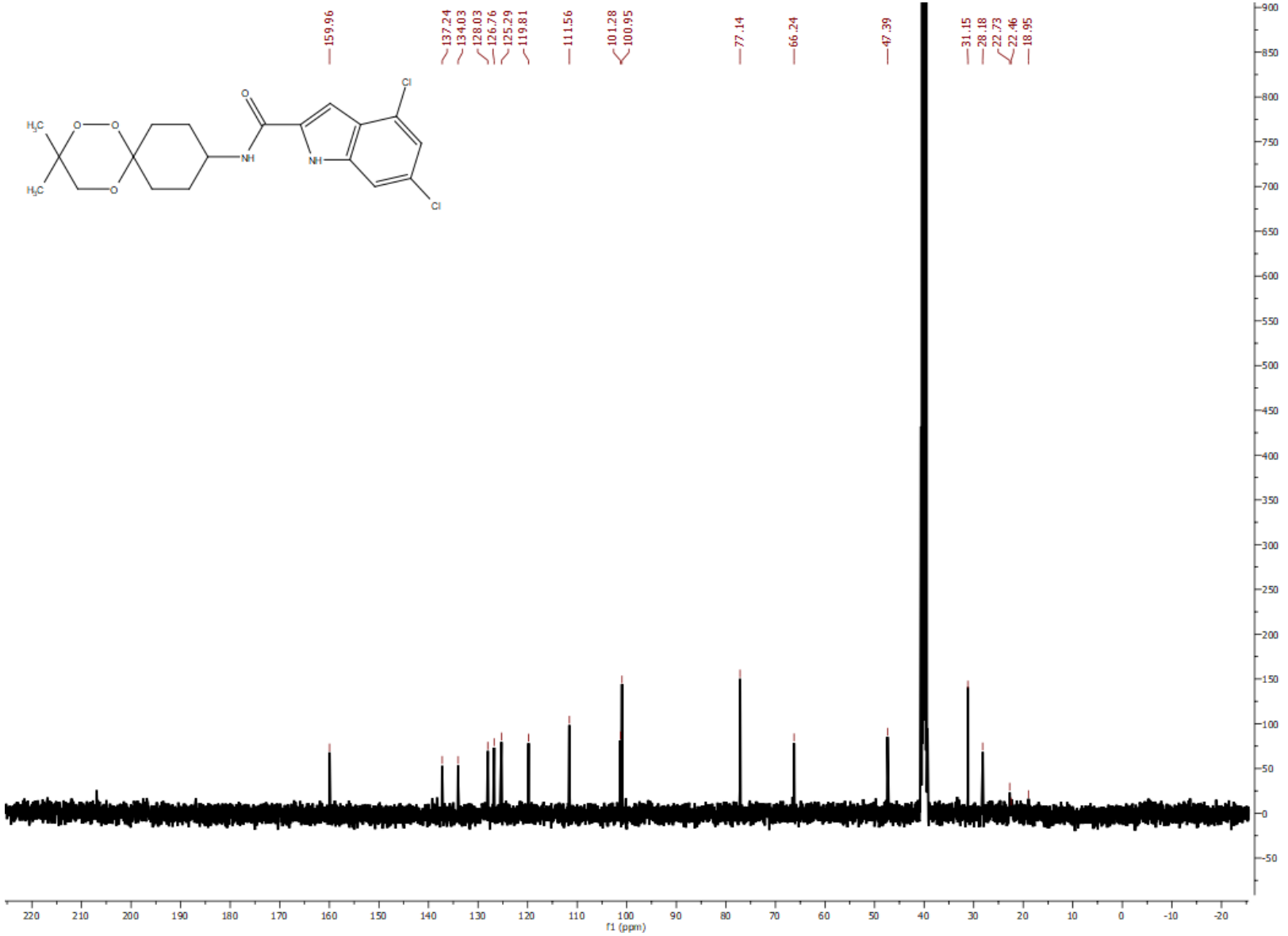

**Compound TIC02-1:** $^{1}$H NMR (400 MHz, DMSO-$d_6$)

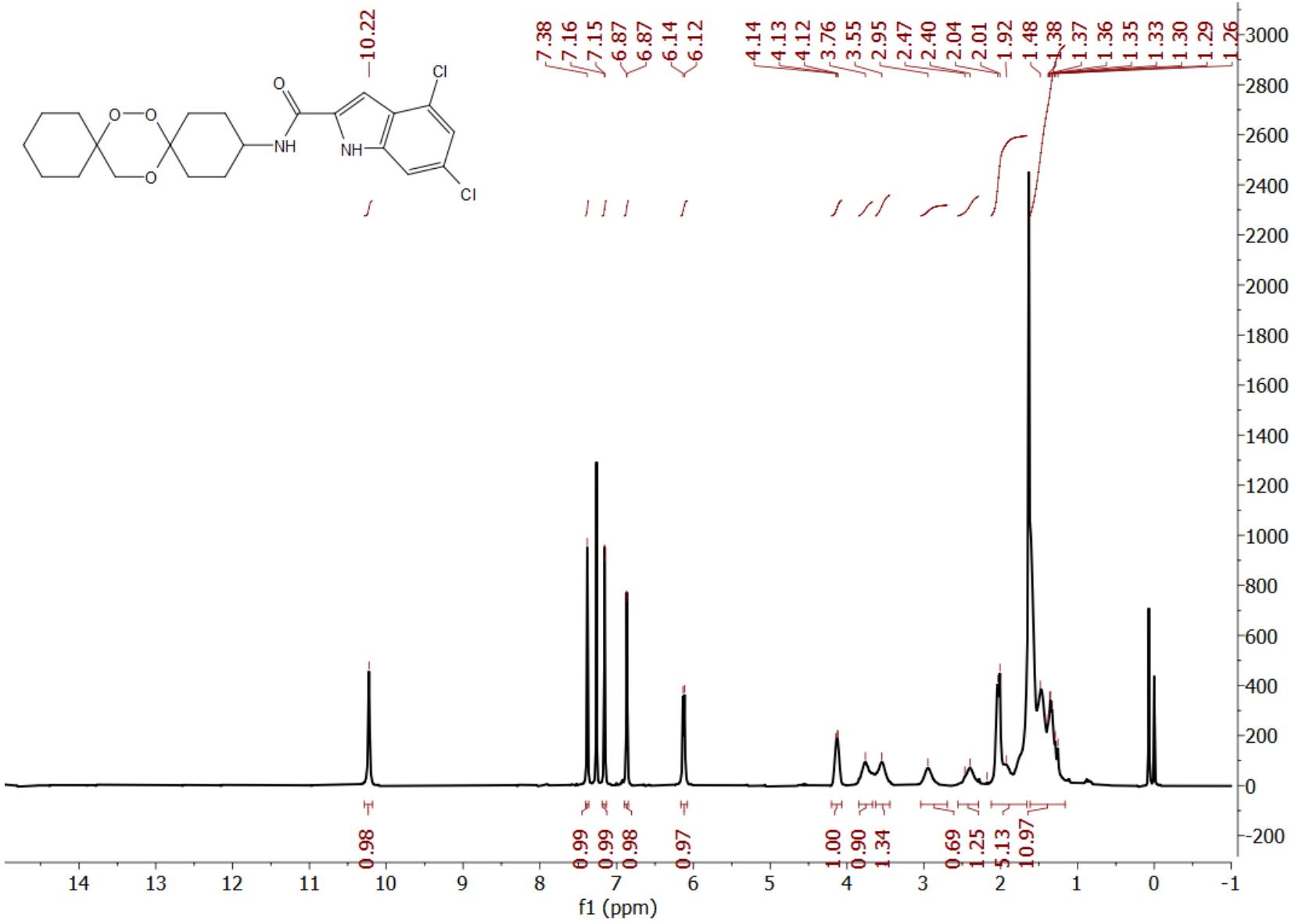

**Compound TIC02-1:** $^{13}C$ {$^{1}H$} NMR (101 MHz, DMSO-$d_6$)

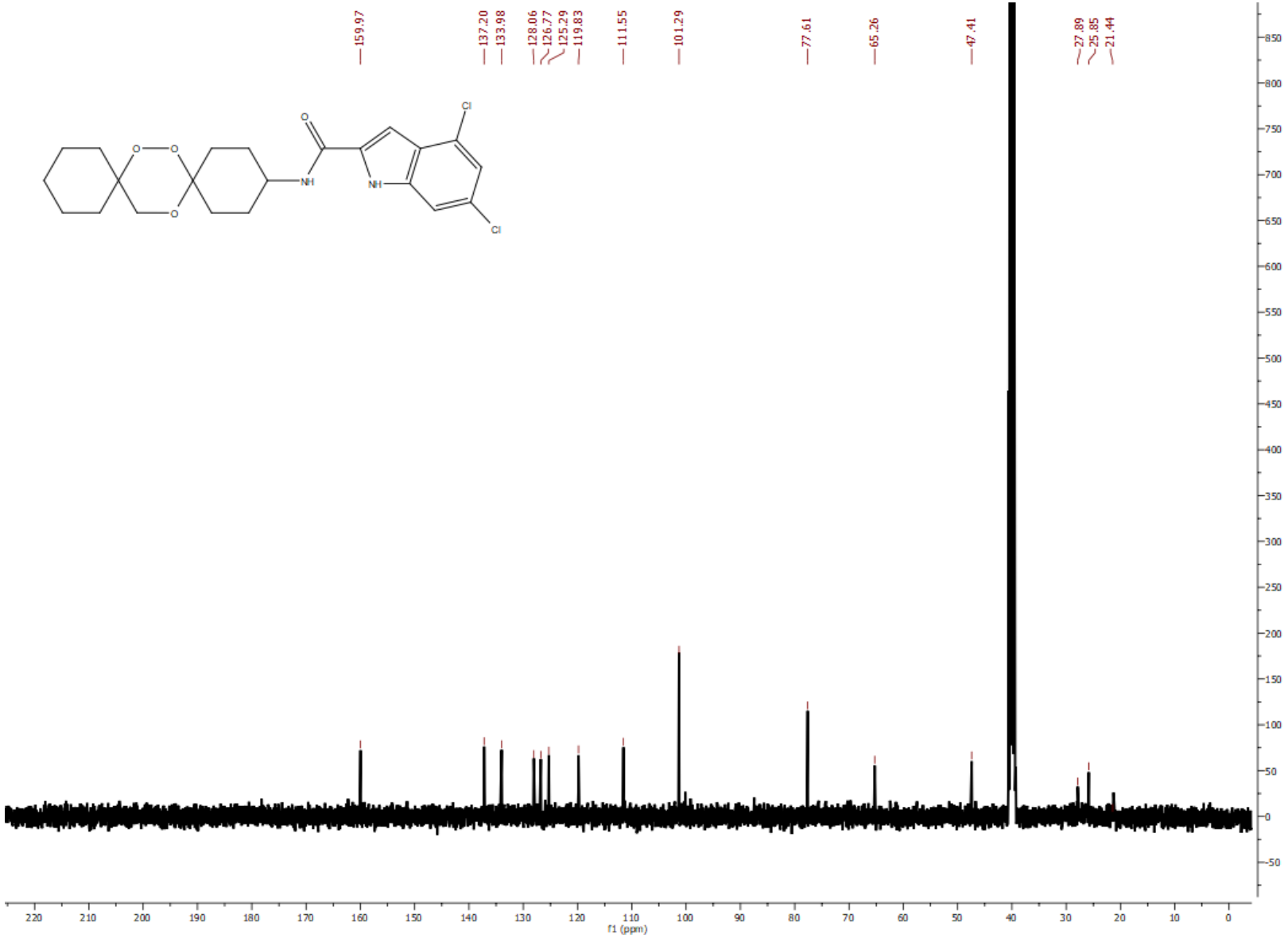

**Compound TIC02-2:** $^{1}$H NMR (400 MHz, $CDCl_3$-*d*)

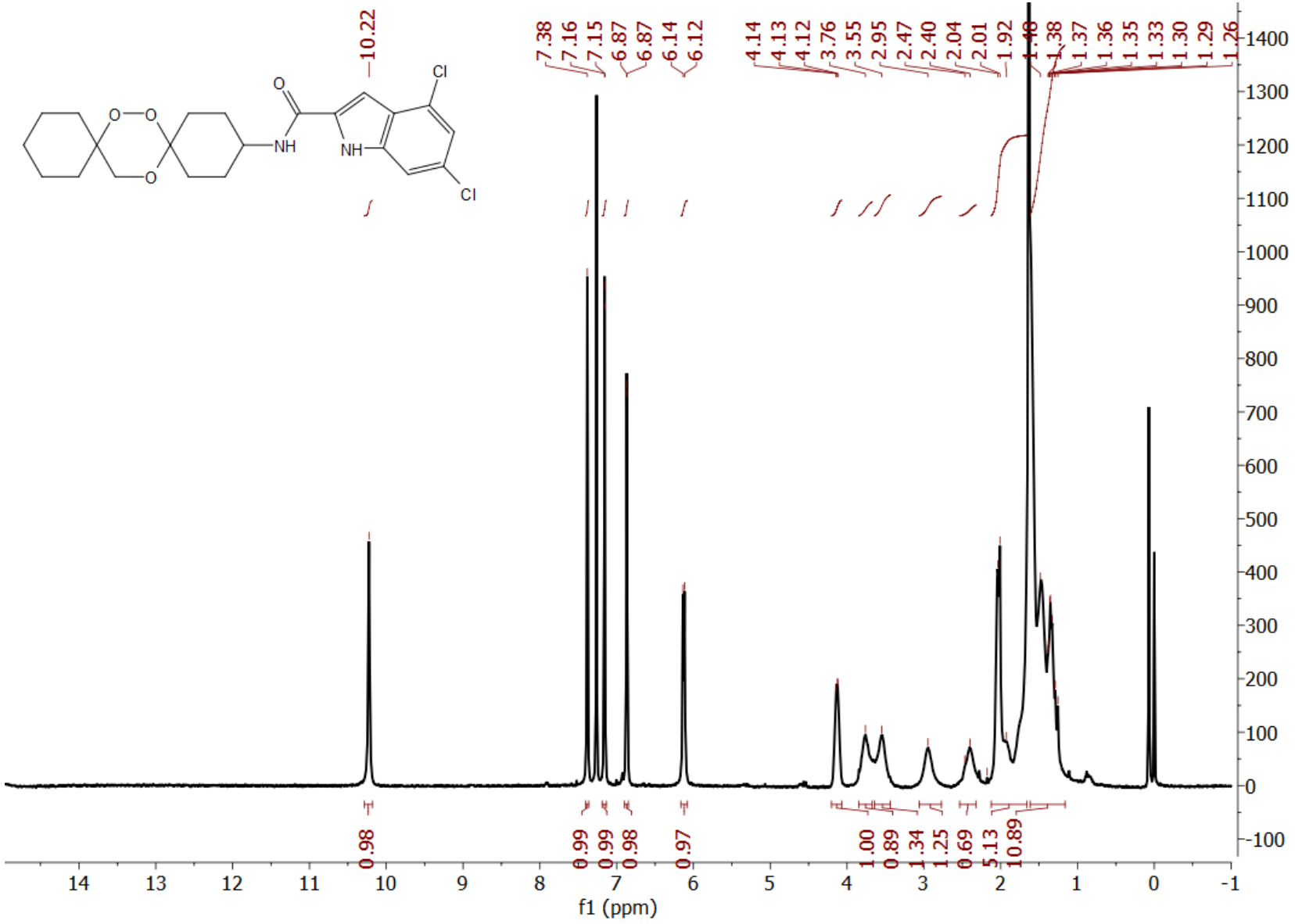

**Compound TIC02-2:** $^{13}C$ {$^{1}H$} NMR (101 MHz, $CDCl_3$-*d*)

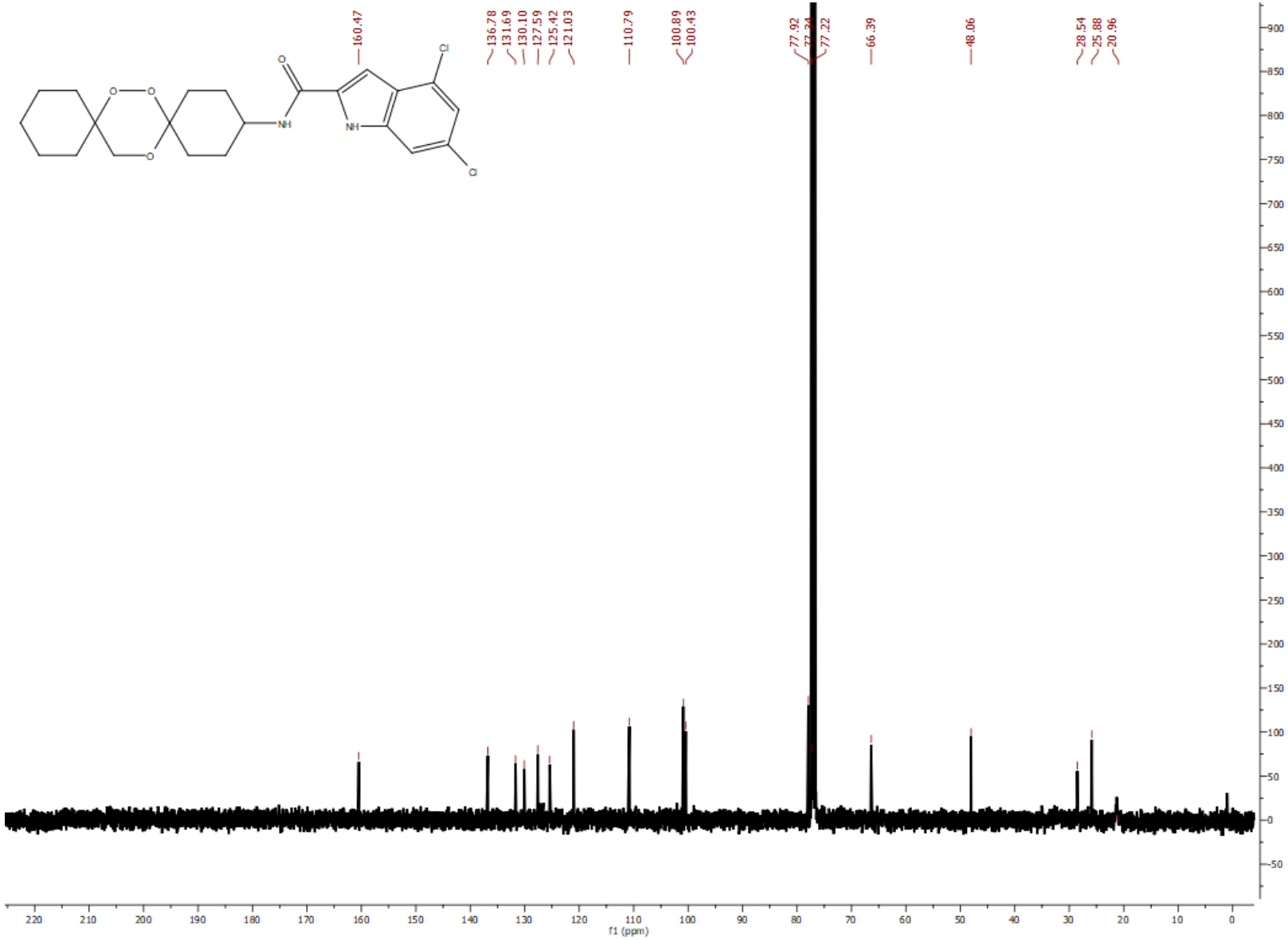

**Compound TIC03-1:** $^{1}$H NMR (400 MHz, $CDCl_3$-*d*)

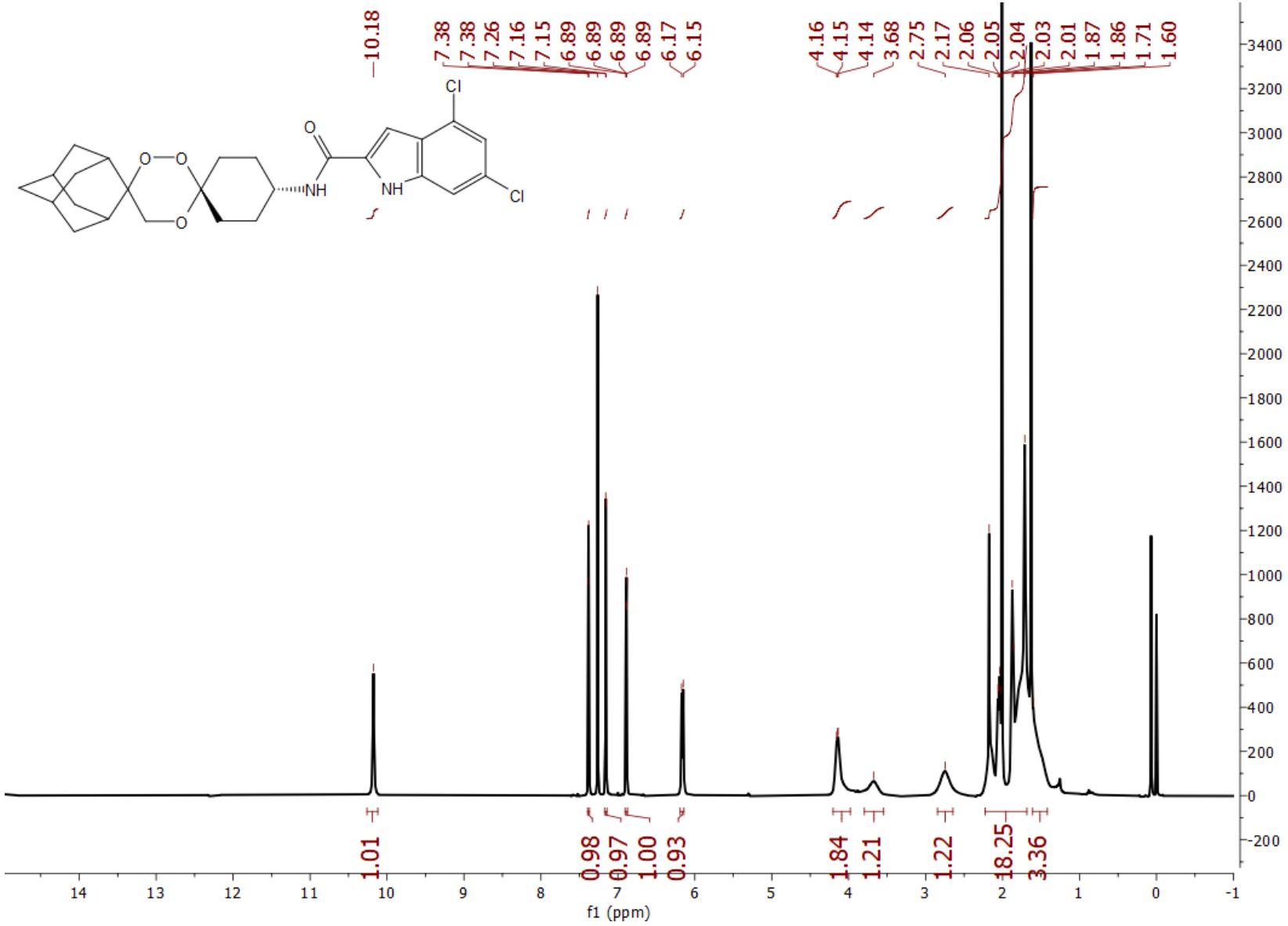

**Compound TIC03-1:** $^{13}C$ {$^{1}H$} NMR (101 MHz, $CDCl_3$-*d*)

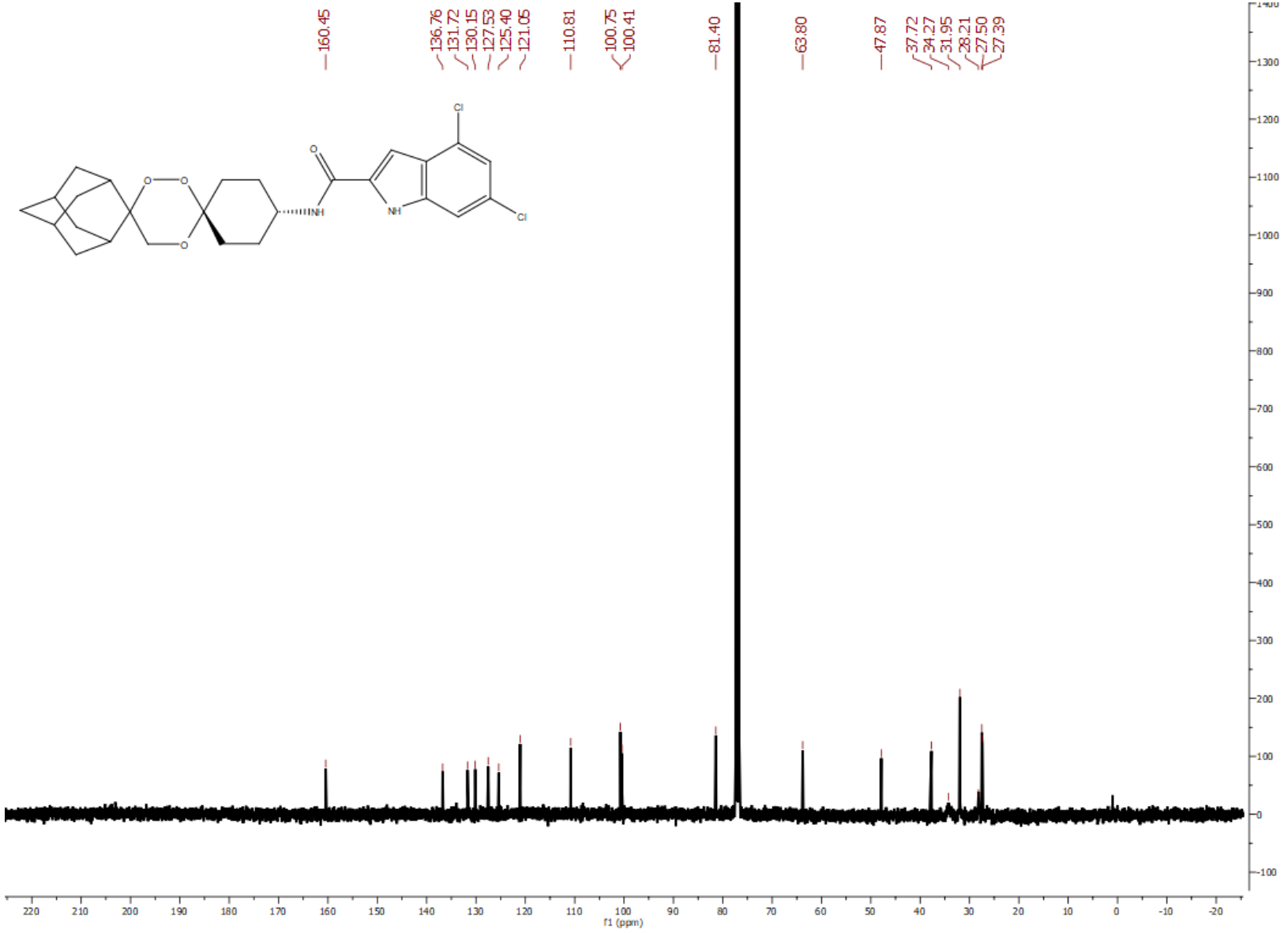

**Compound TIC03-2:** $^{1}$H NMR (400 MHz, DMSO-$d_6$)

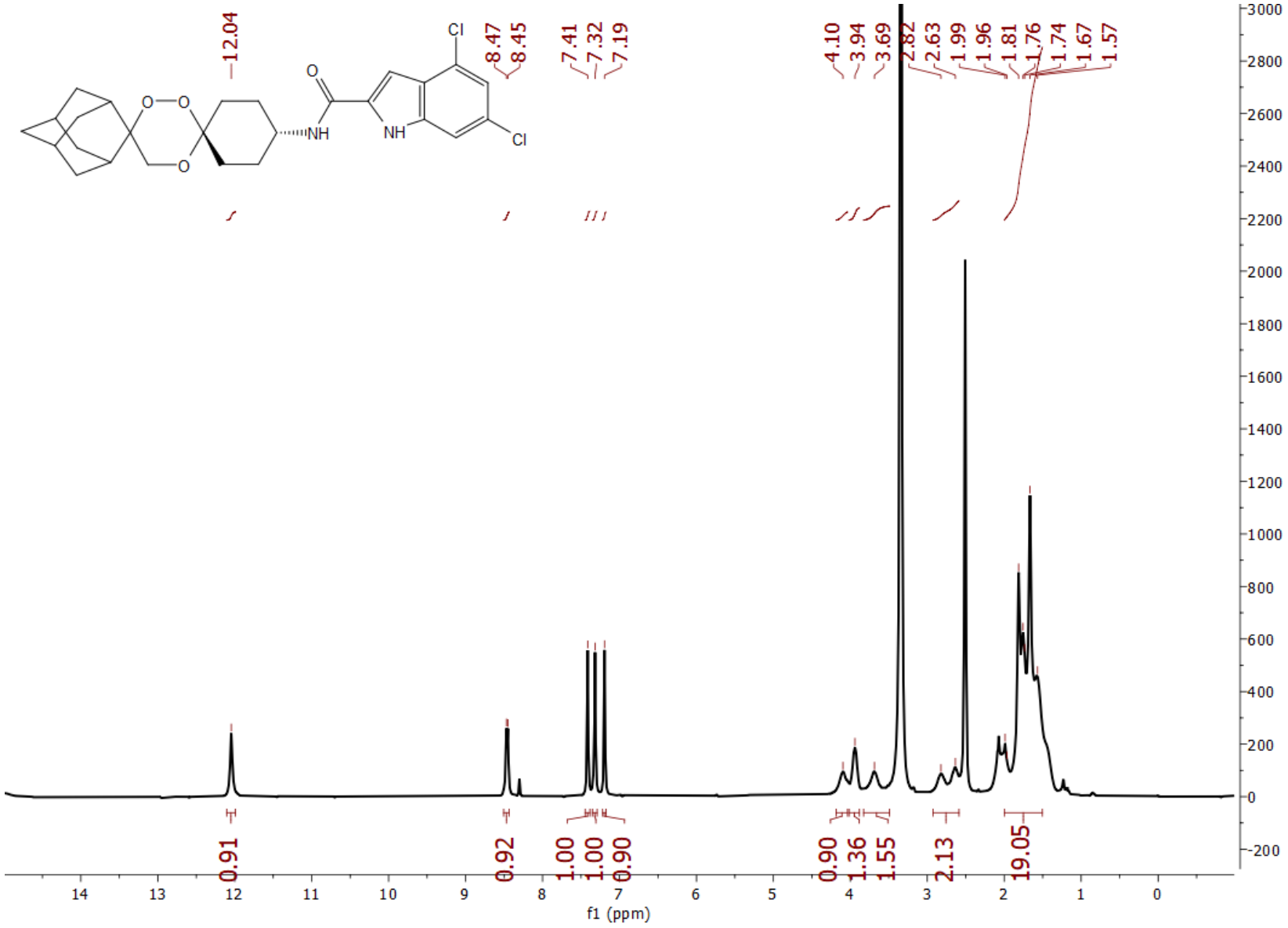

**Compound TC03-2:** $^{13}C$ {$^{1}H$} NMR (101 MHz, DMSO-$d_6$)

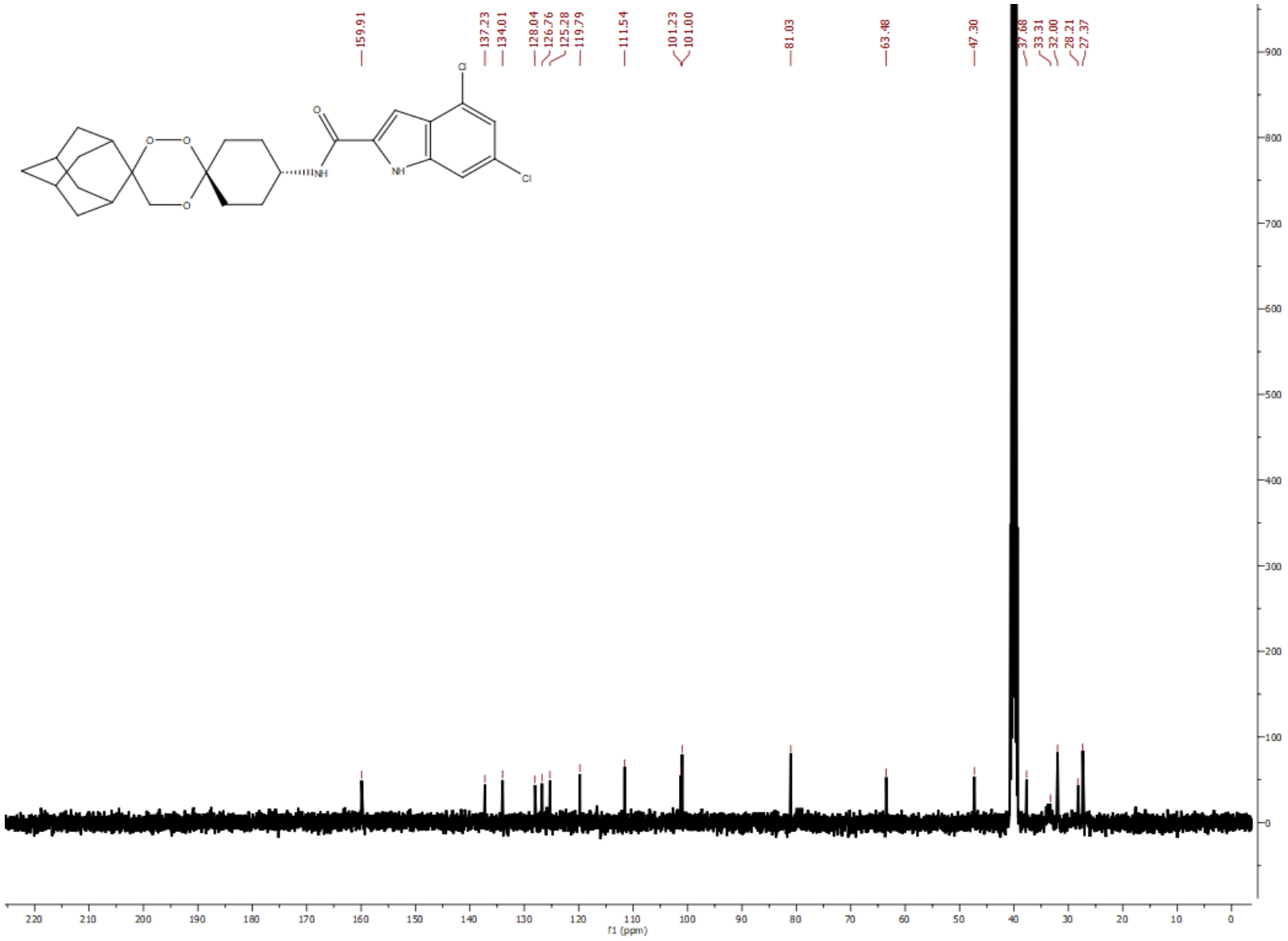

**Compound B3:** $^{1}H$ NMR (400 MHz, $CDCl_3$)

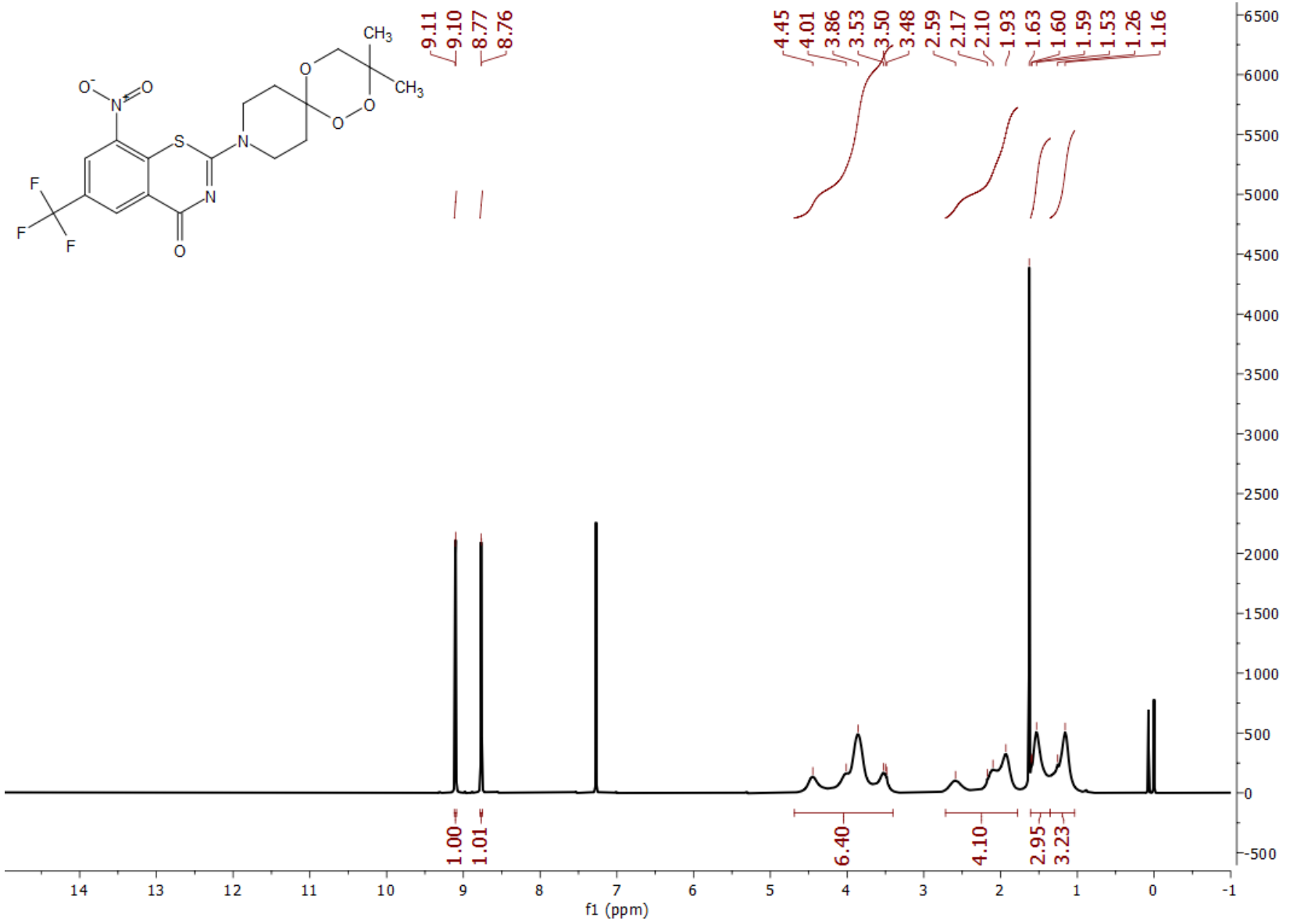

**Compound B3:** $^{13}C$ {$^{1}H$} NMR (101 MHz, $CDCl_3$)

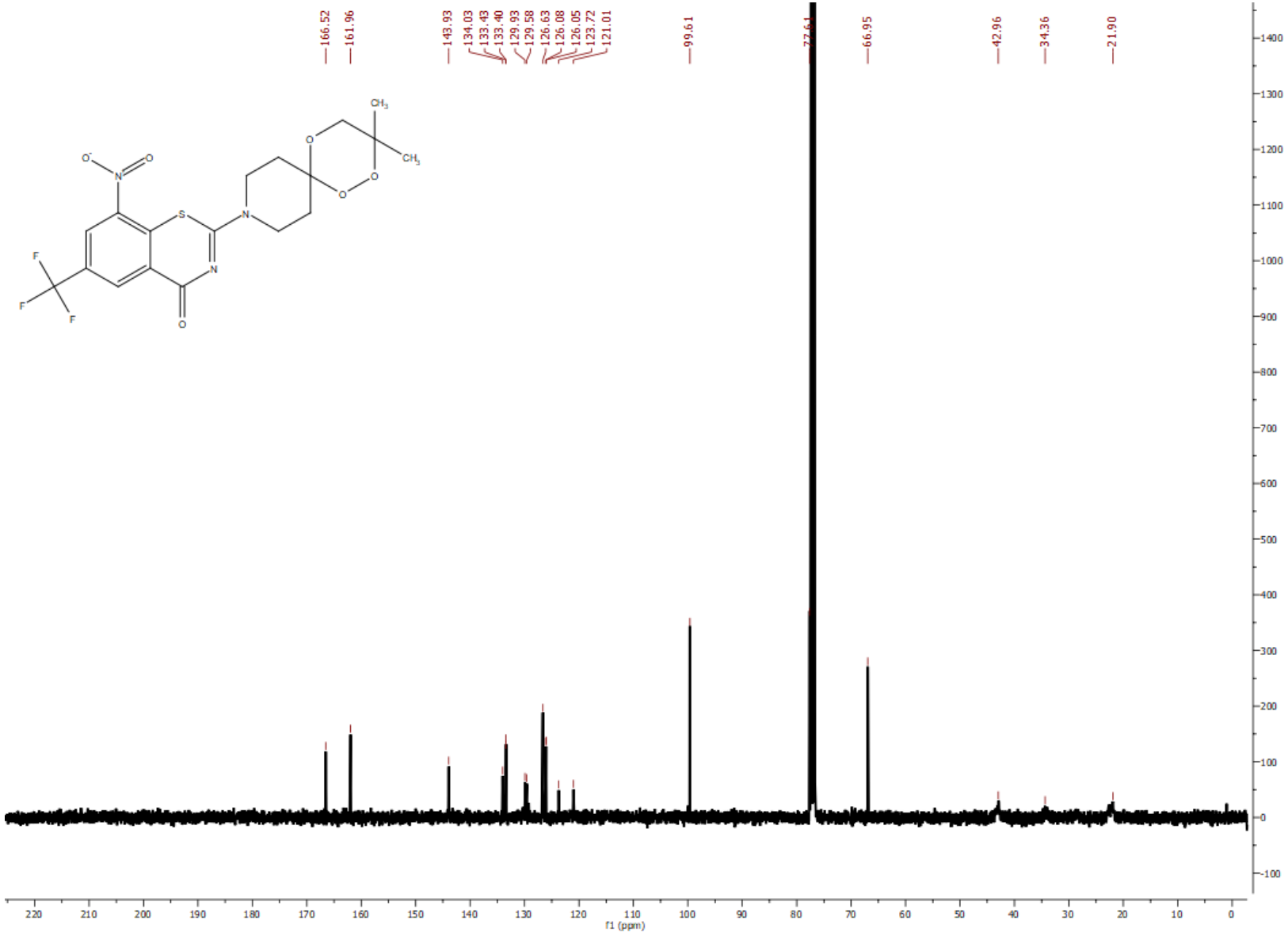

**Compound B4:** $^{1}H$ NMR (400 MHz, $CDCl_3$)

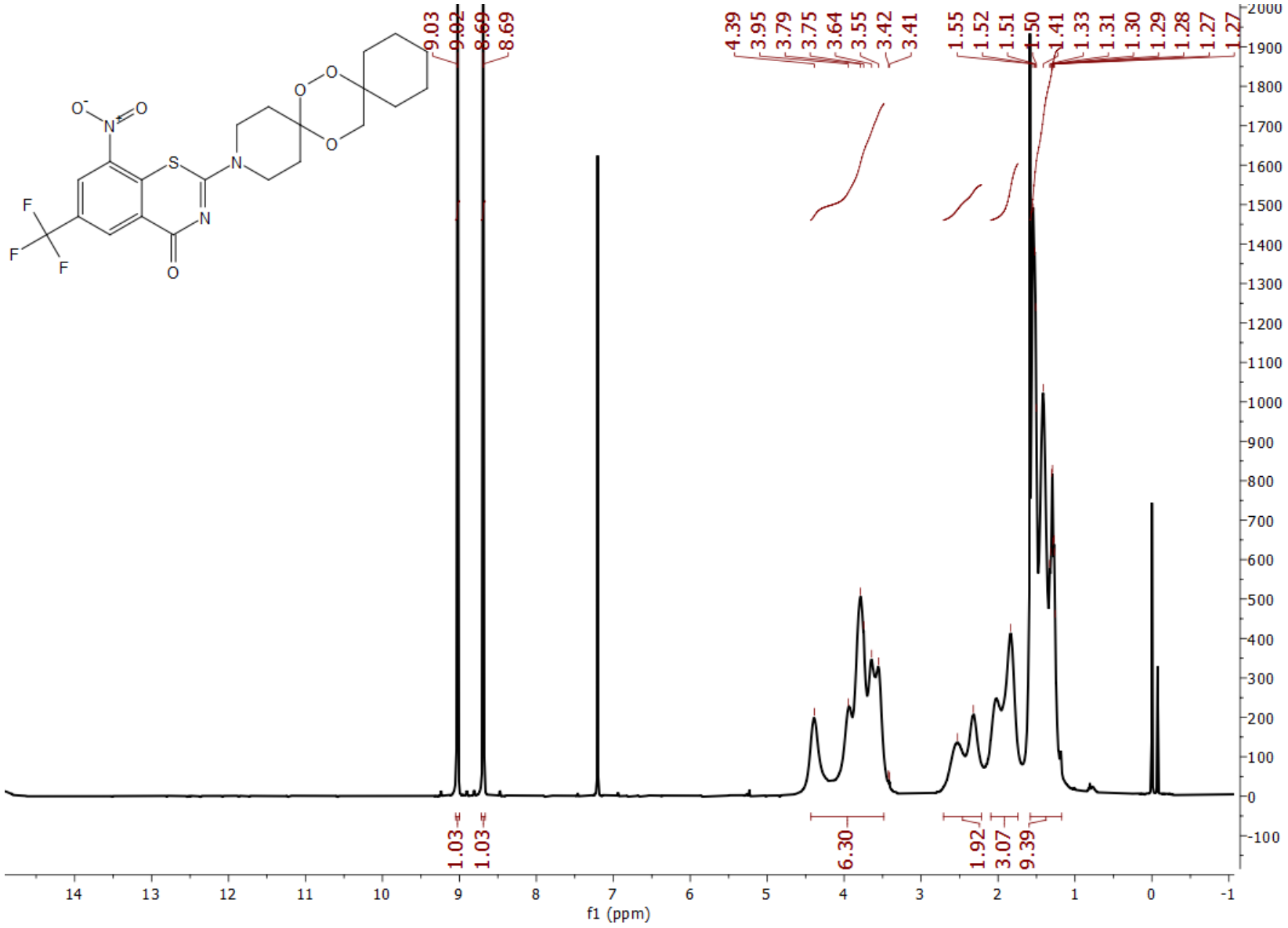

**Compound B4:** $^{13}C$ {$^{1}H$} NMR (101 MHz, $CDCl_3$)

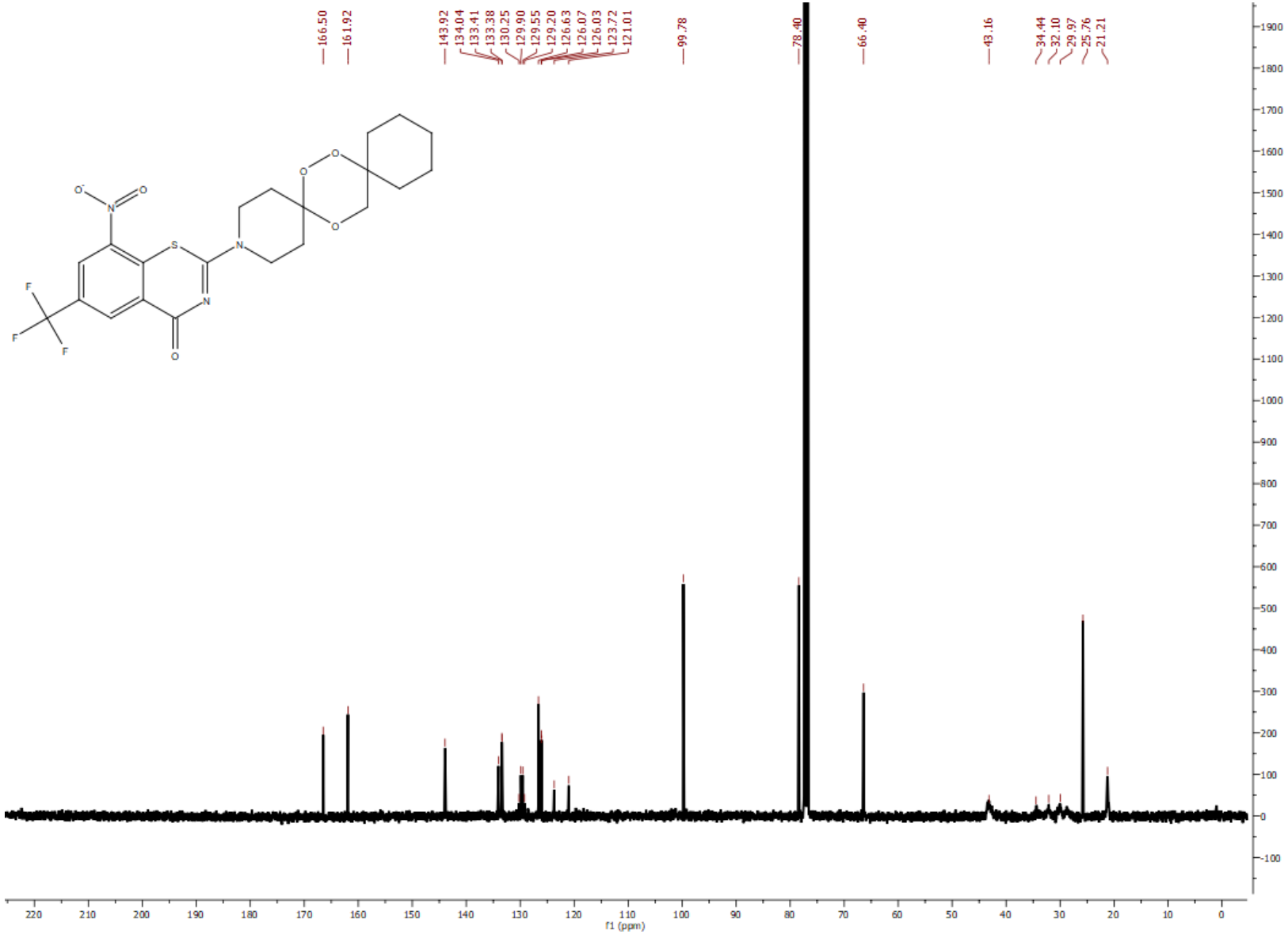

**Compound B5:** $^{1}H$ NMR (400 MHz, $CDCl_3$)

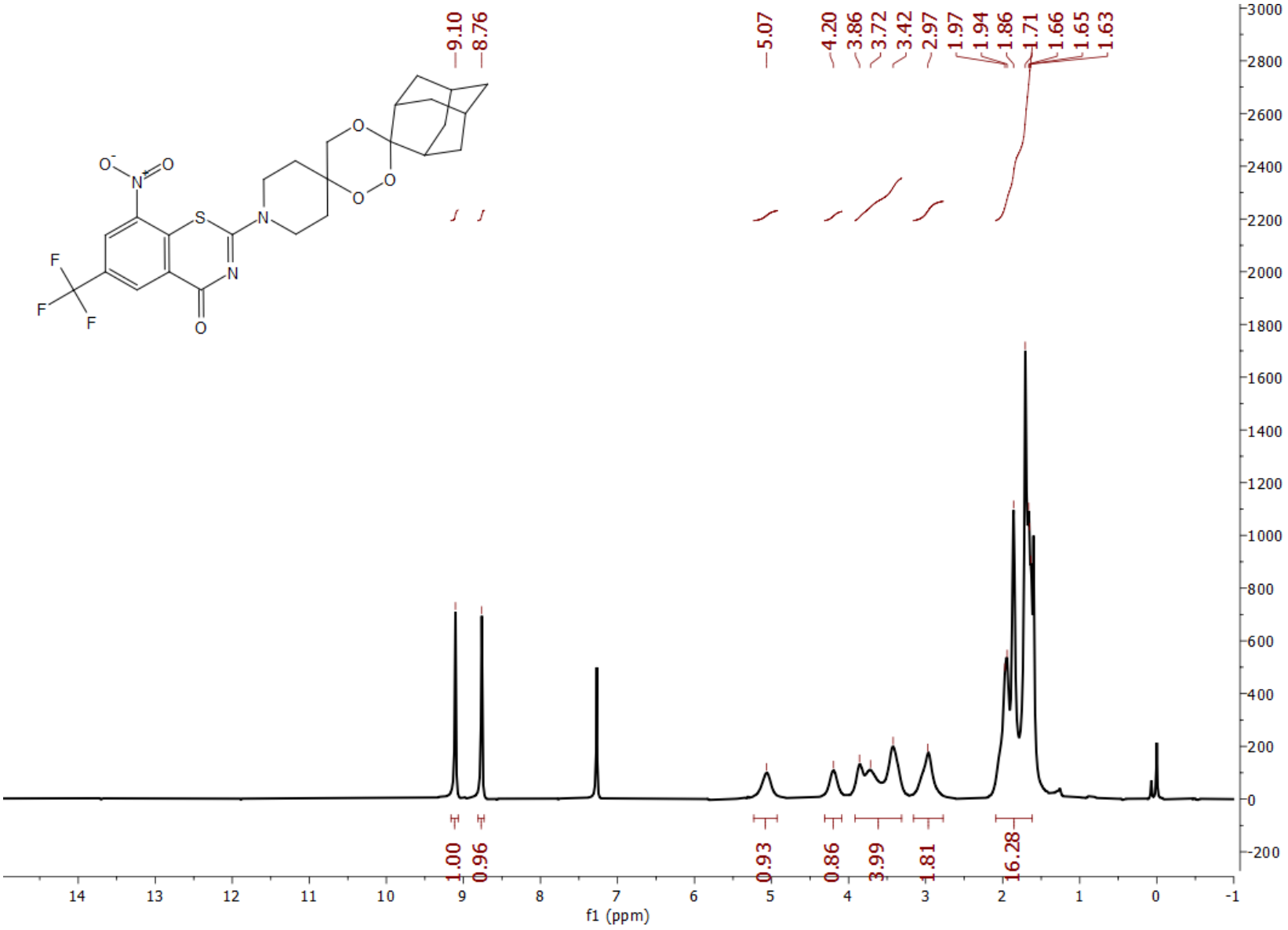

**Compound B5:** $^{13}C$ {$^{1}H$} NMR (101 MHz, $CDCl_3$)

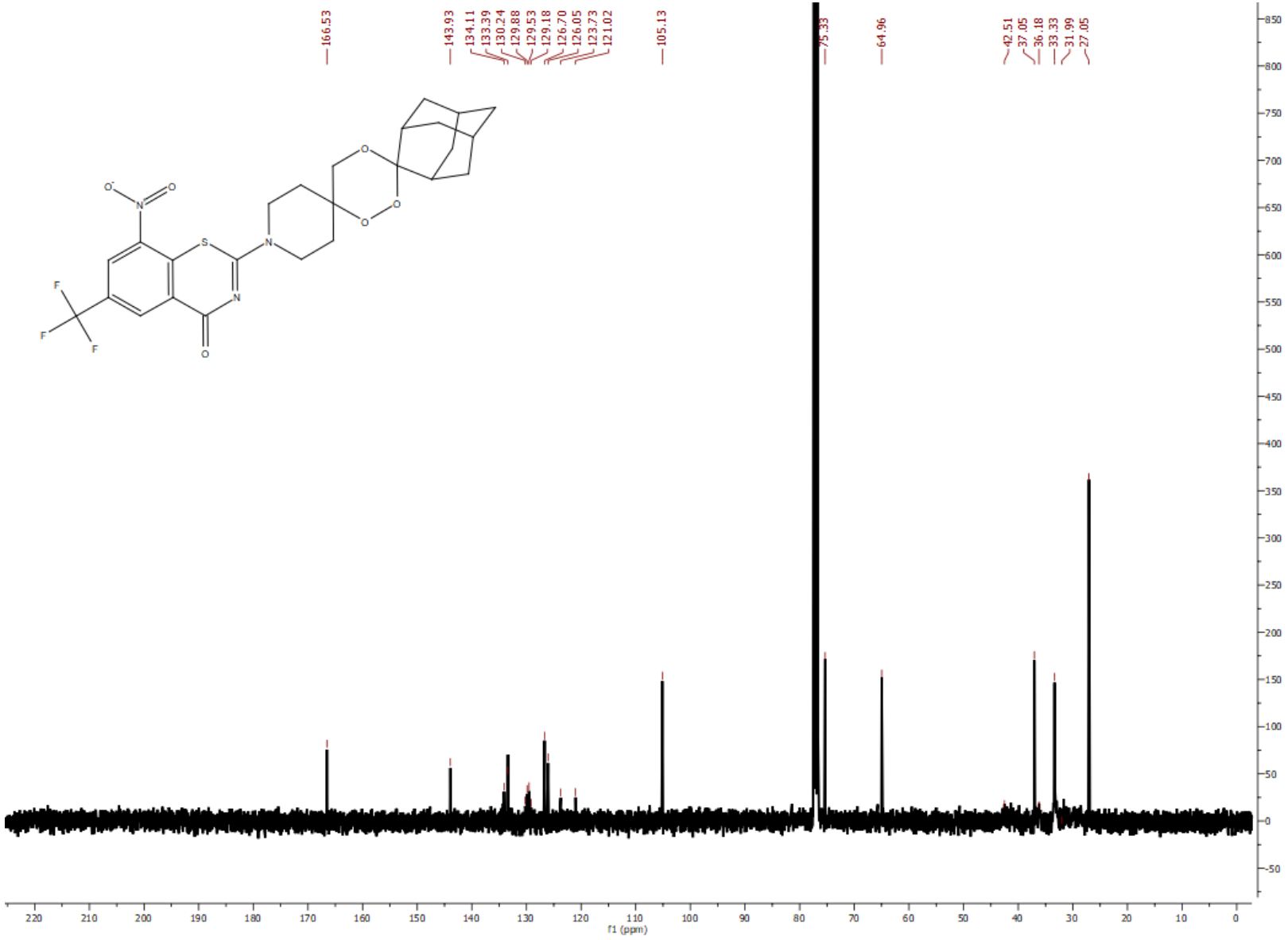

**Compound C1:** $^{1}H$ NMR (400 MHz, $CDCl_3$)

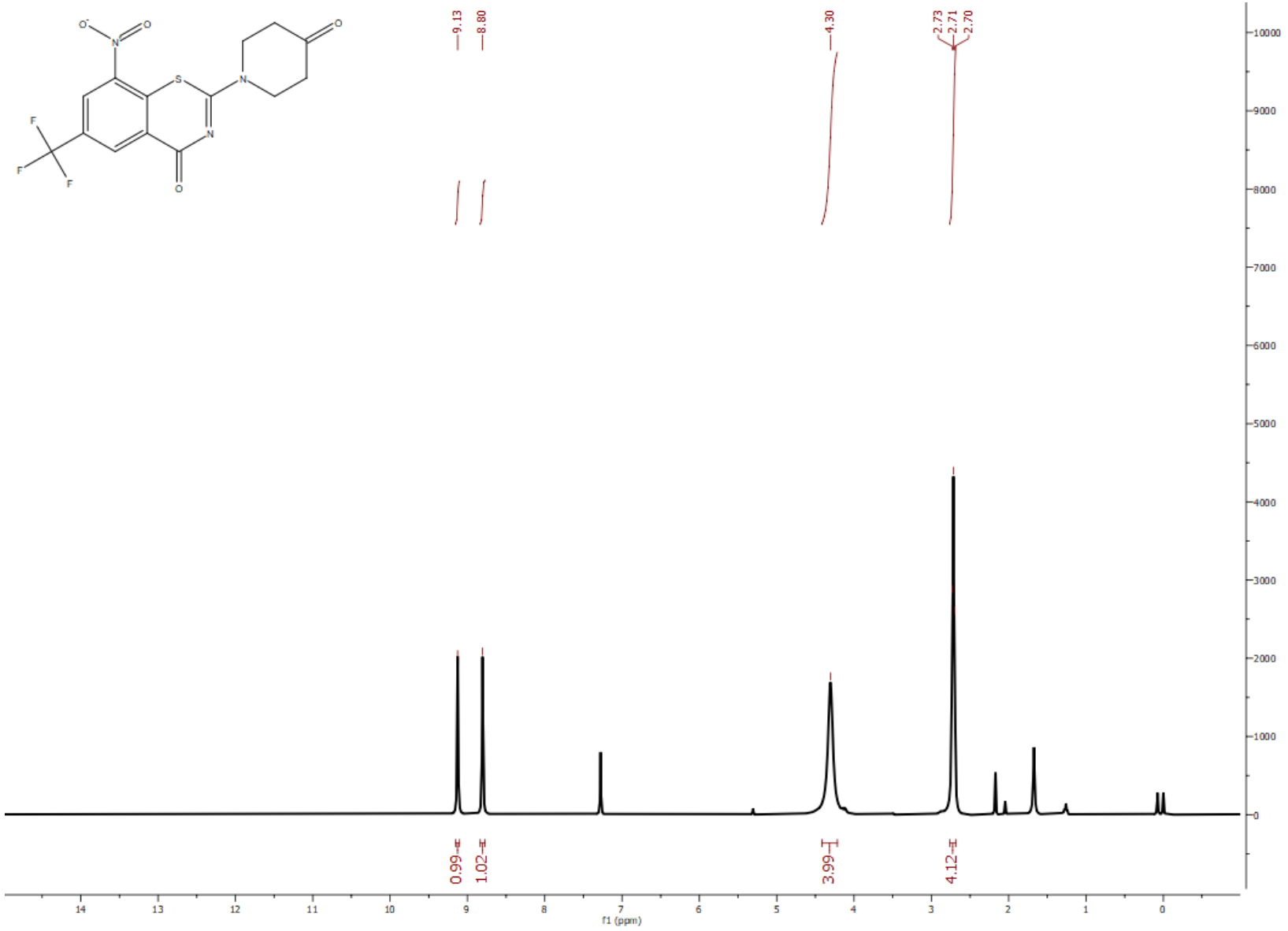

**Compound C1:** $^{13}C$ {$^{1}H$} NMR (101 MHz, $CDCl_3$)

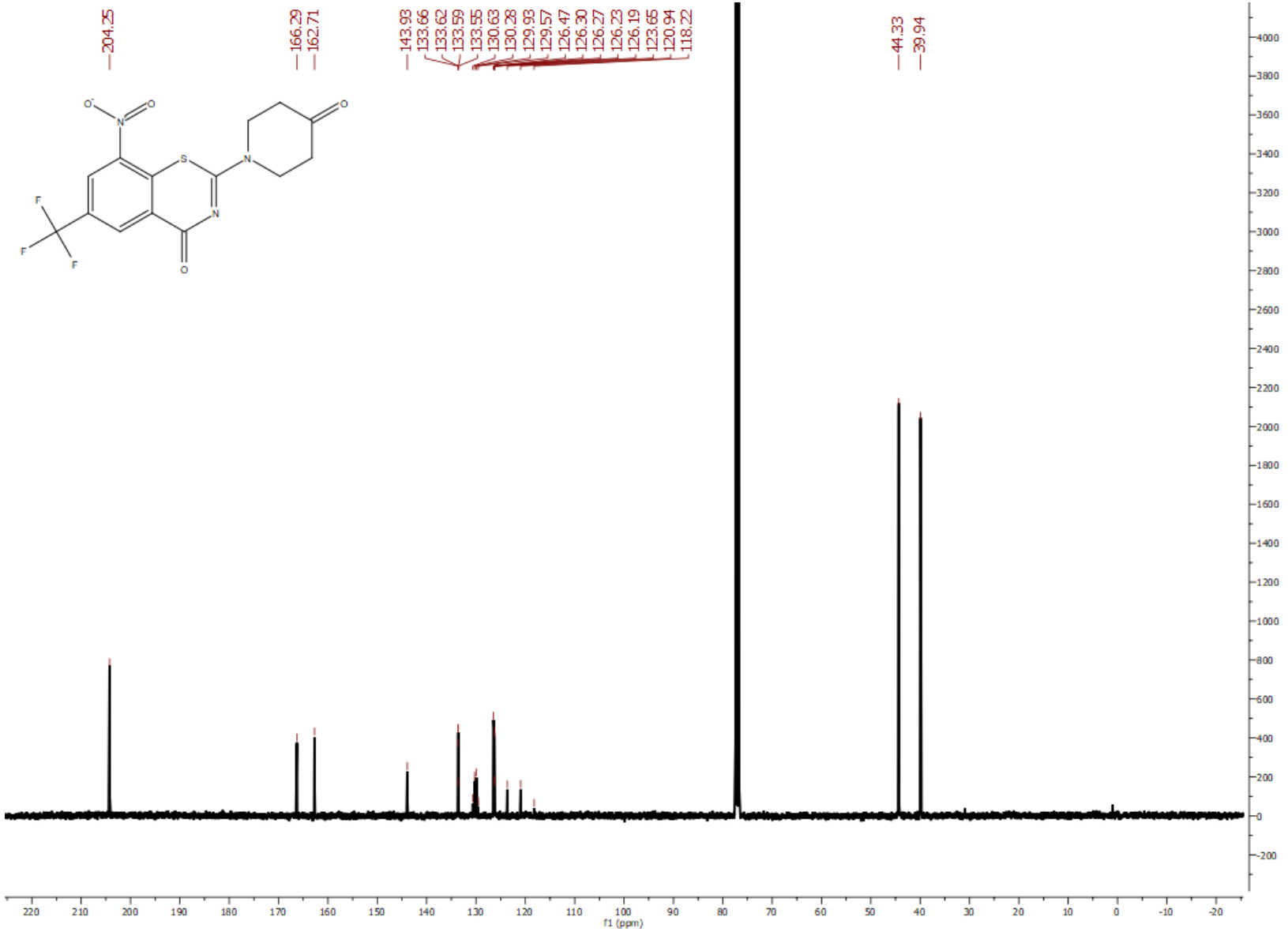

**Compound C2:** $^{1}H$ NMR (400 MHz, $CDCl_3$)

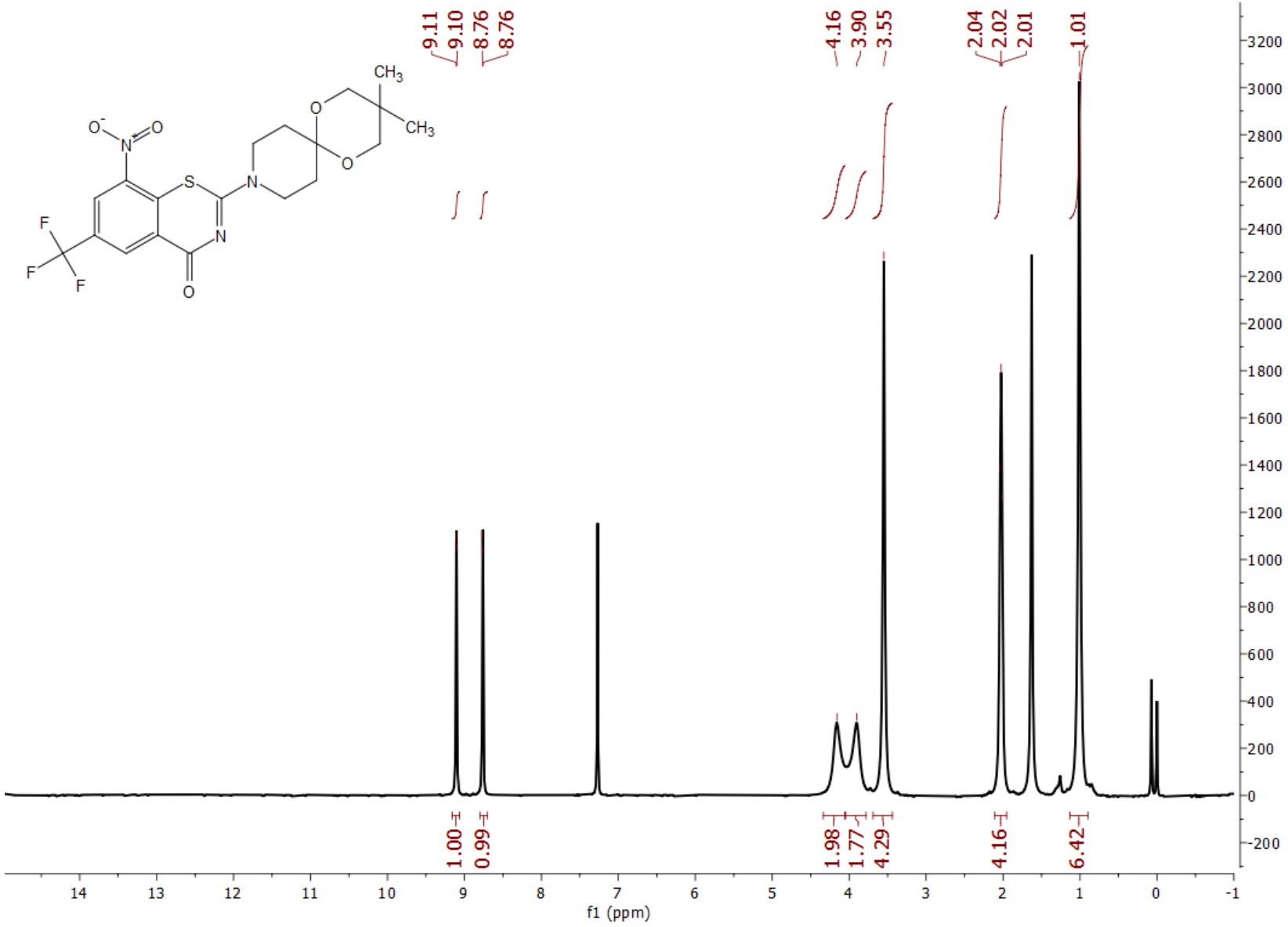

**Compound C2:** $^{13}C$ {$^{1}H$} NMR (101 MHz, $CDCl_3$)

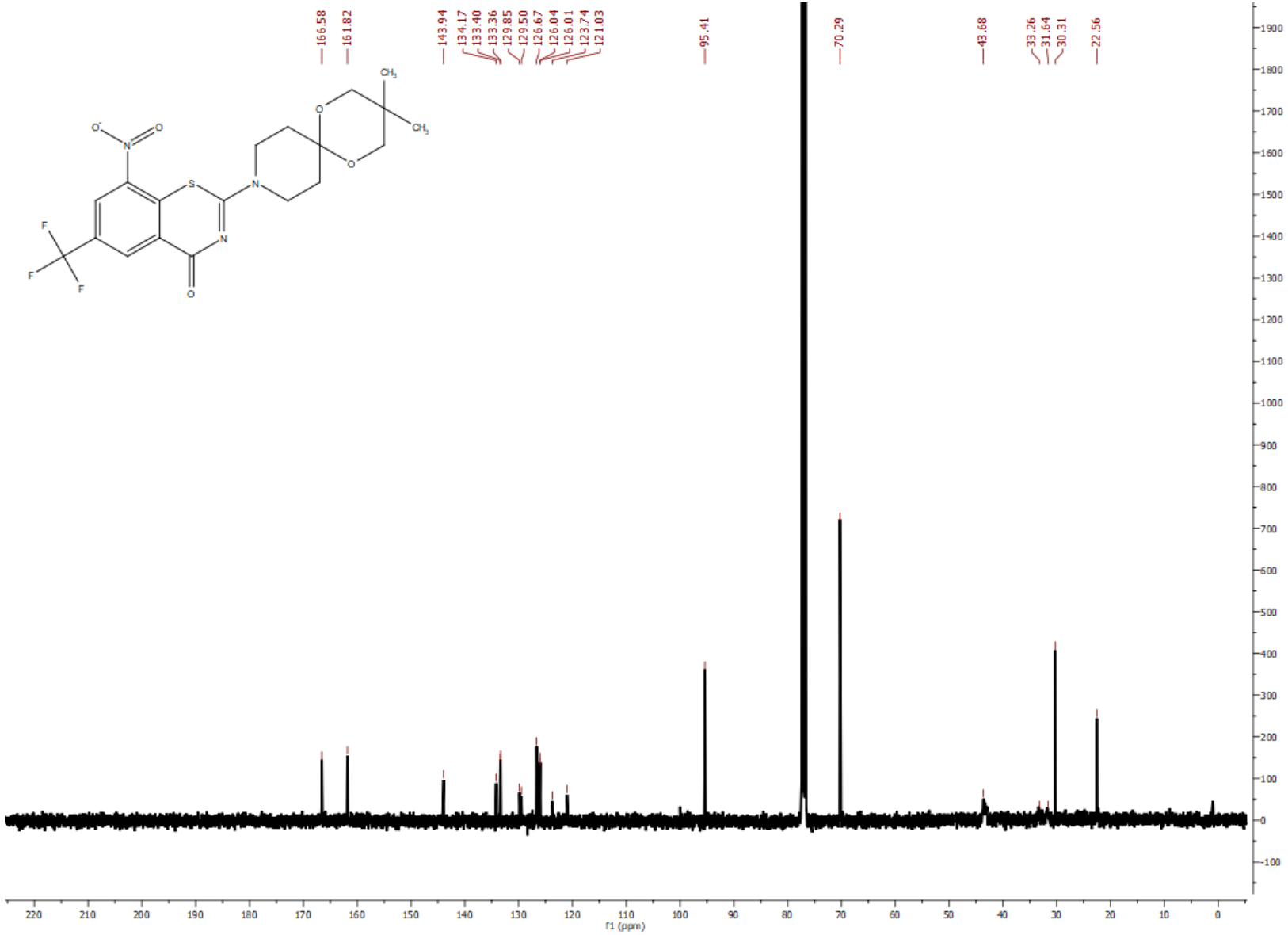

**Compound C3:** $^{1}H$ NMR (400 MHz, $CDCl_3$)

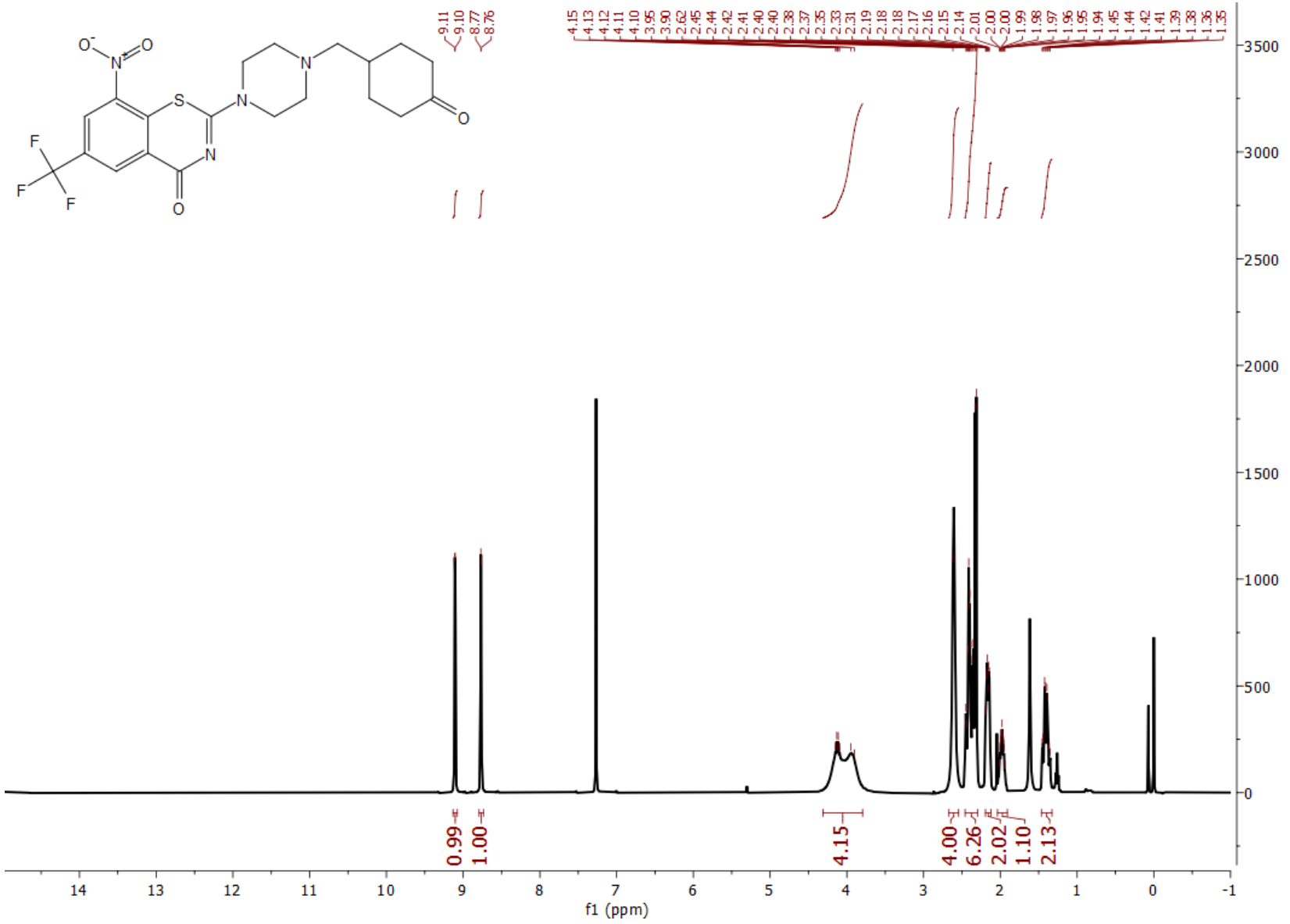

**Compound C3:** $^{13}C$ {$^{1}H$} NMR (101 MHz, $CDCl_3$)

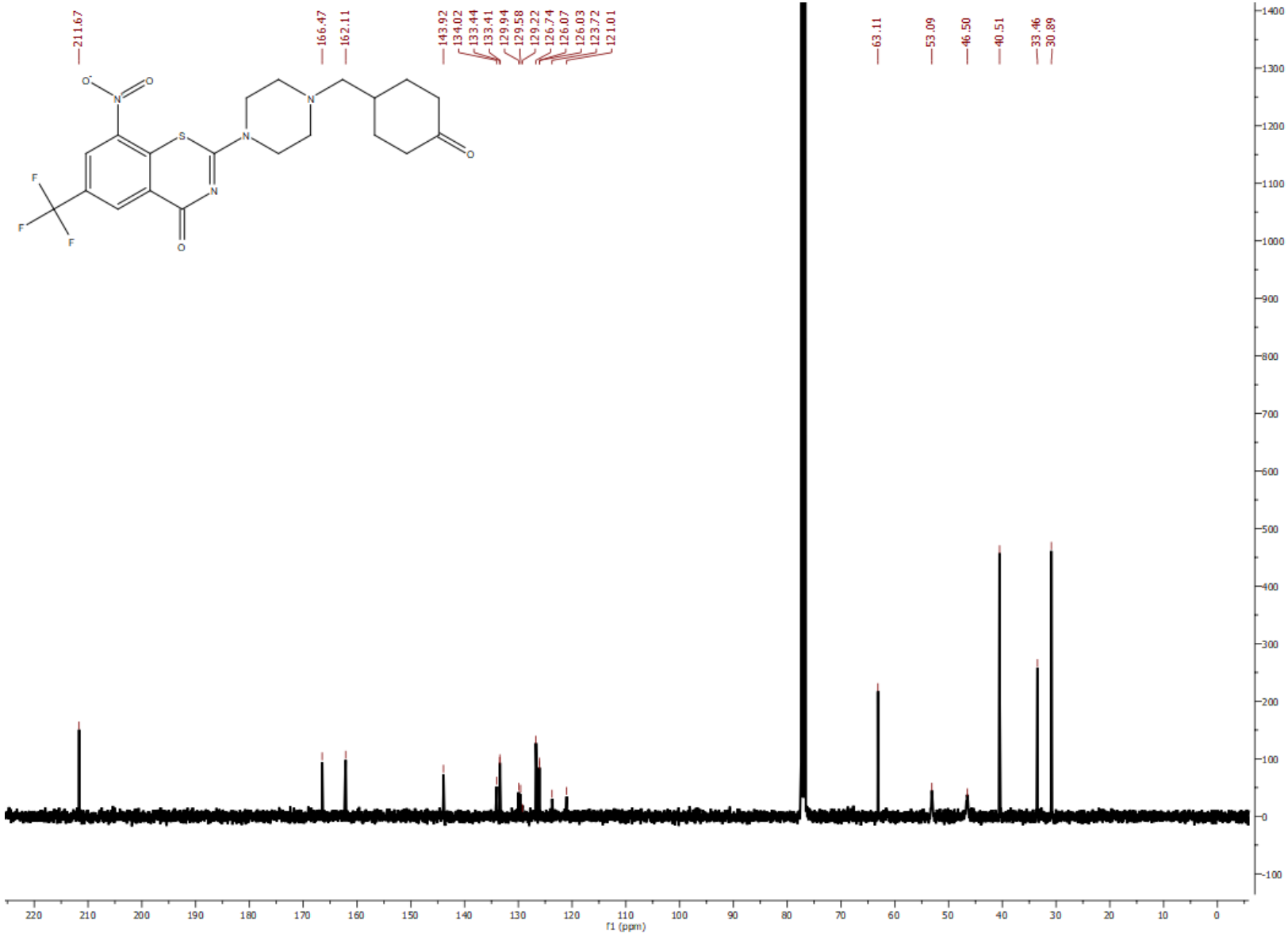

**Compound C4:** $^{1}H$ NMR (400 MHz, $CDCl_3$)

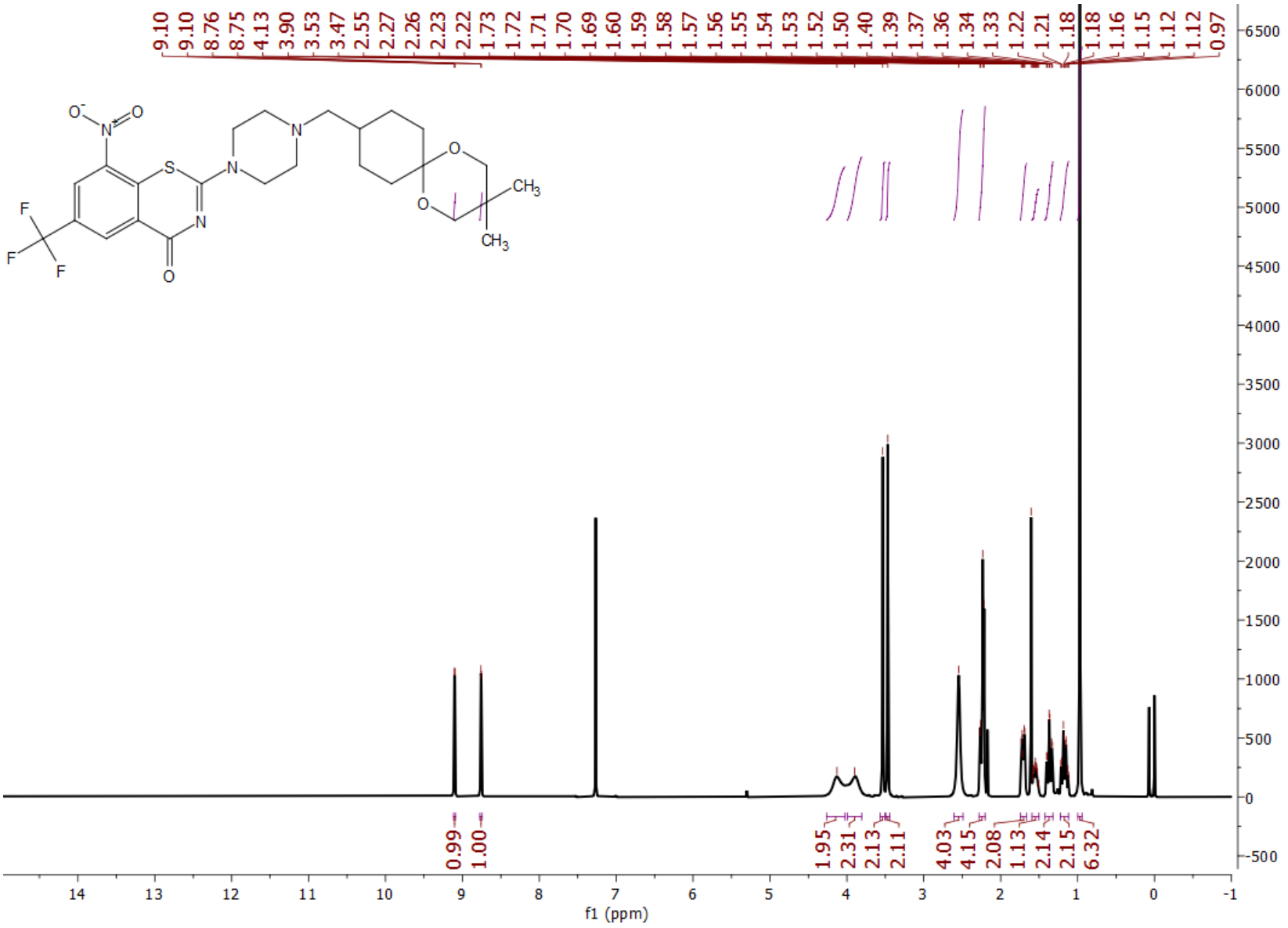

**Compound C4:** $^{13}C$ {$^{1}H$} NMR (101 MHz, $CDCl_3$)

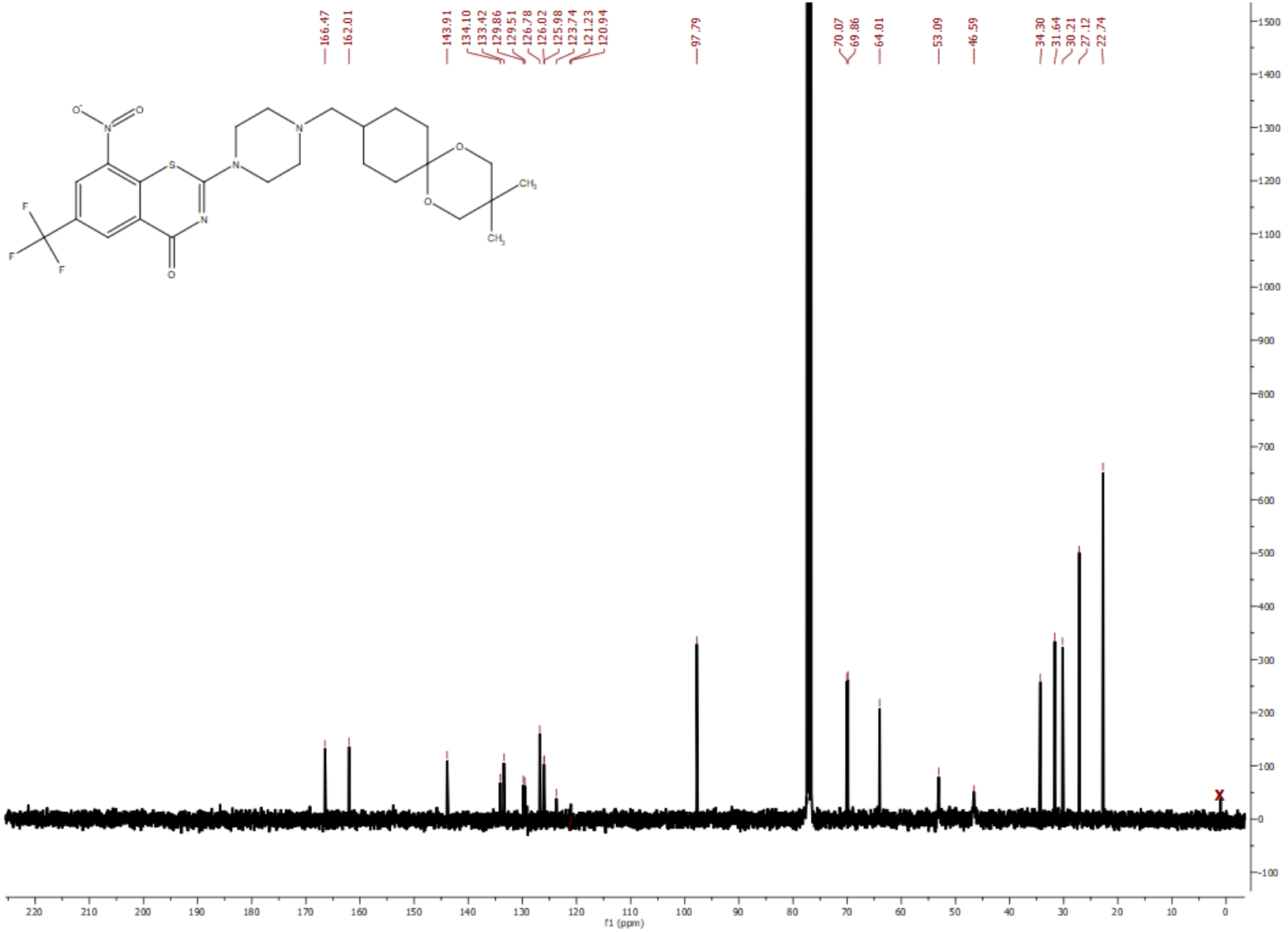

**Compound P4:** $^{1}H$ NMR (400 MHz, $CDCl_3$)

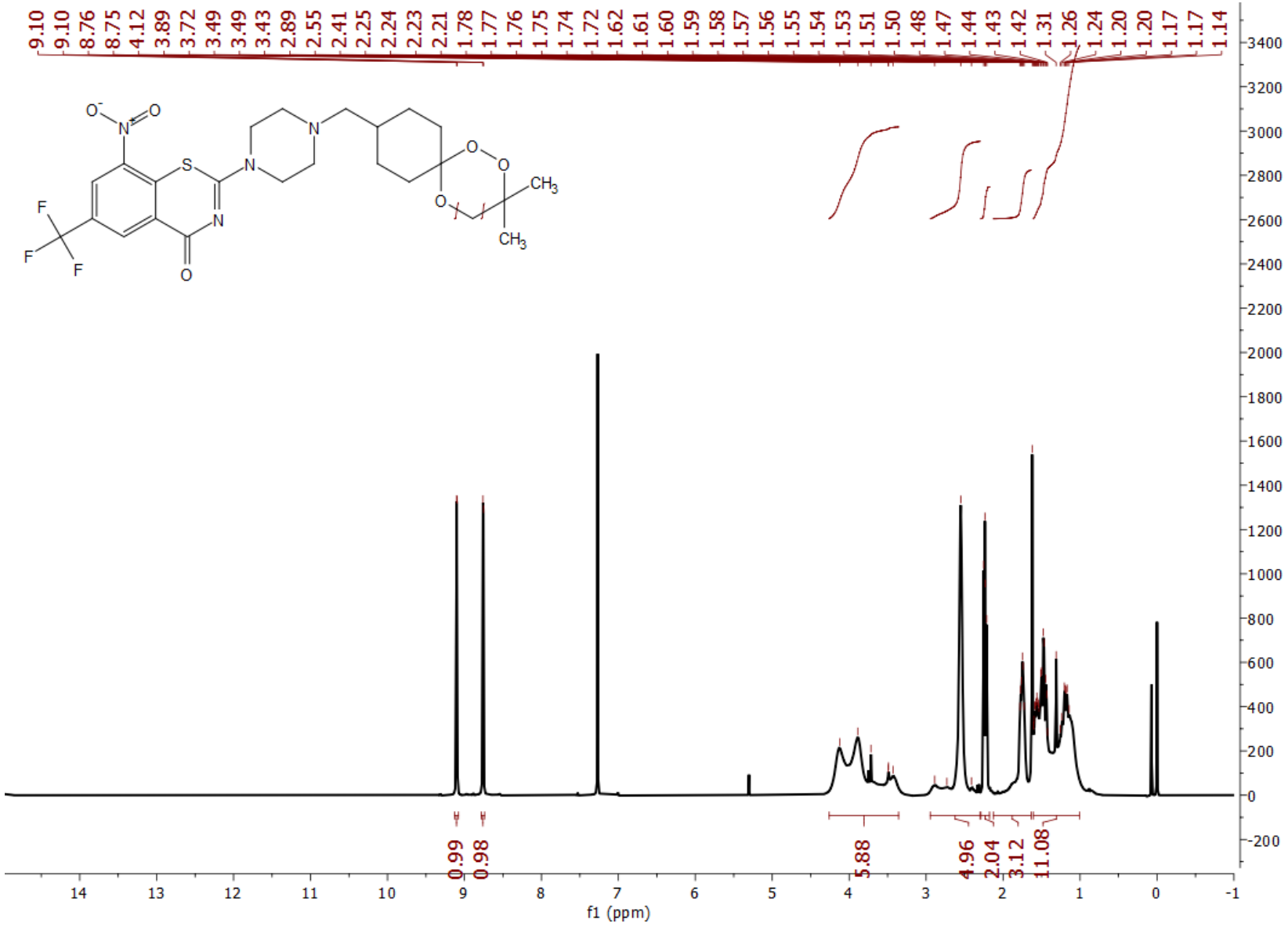

**Compound P4:** $^{13}C$ {$^{1}H$} NMR (101 MHz, $CDCl_3$)

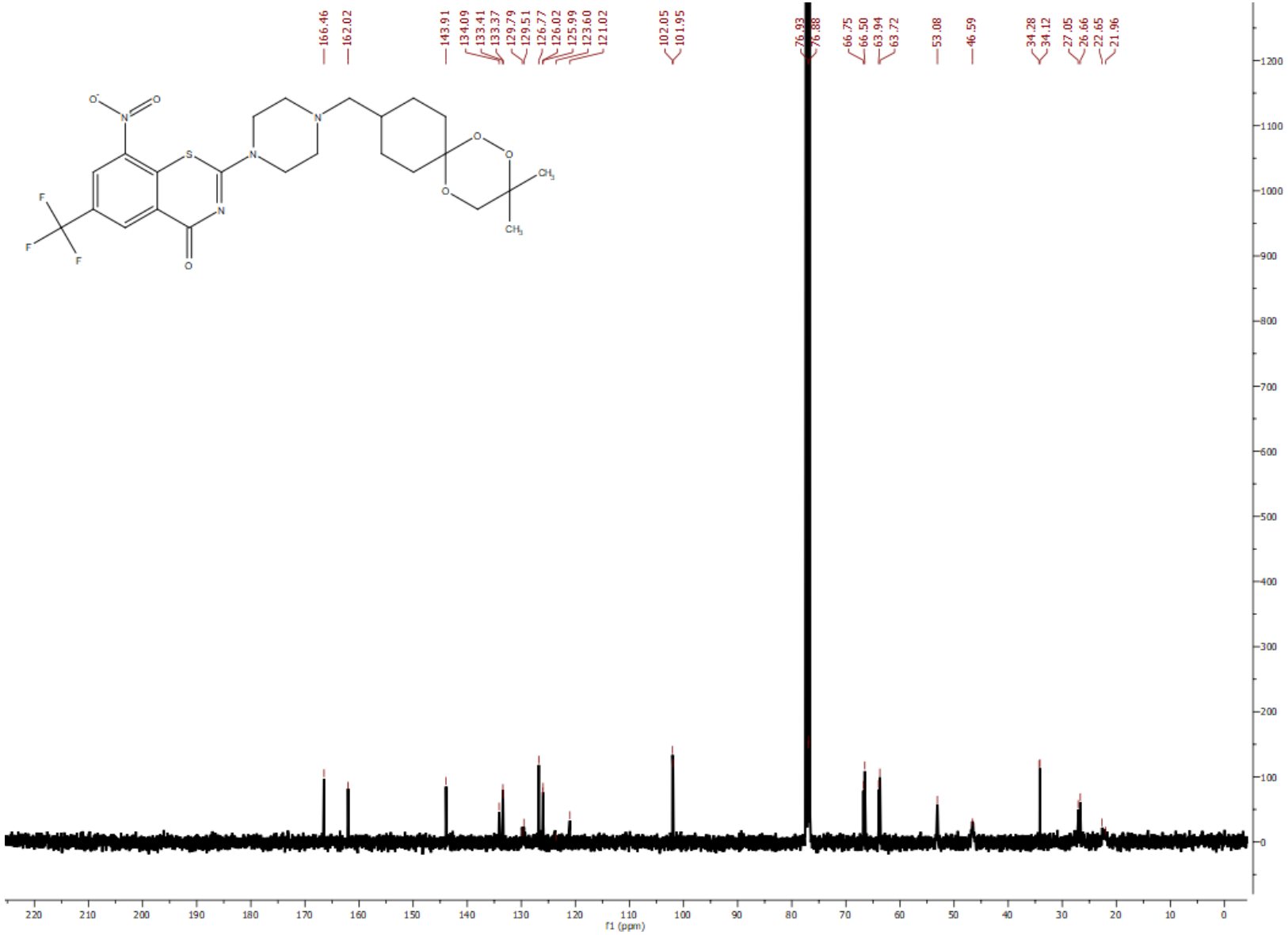

**Compound P5:** $^{1}$H NMR (400 MHz, $CDCl_3$)

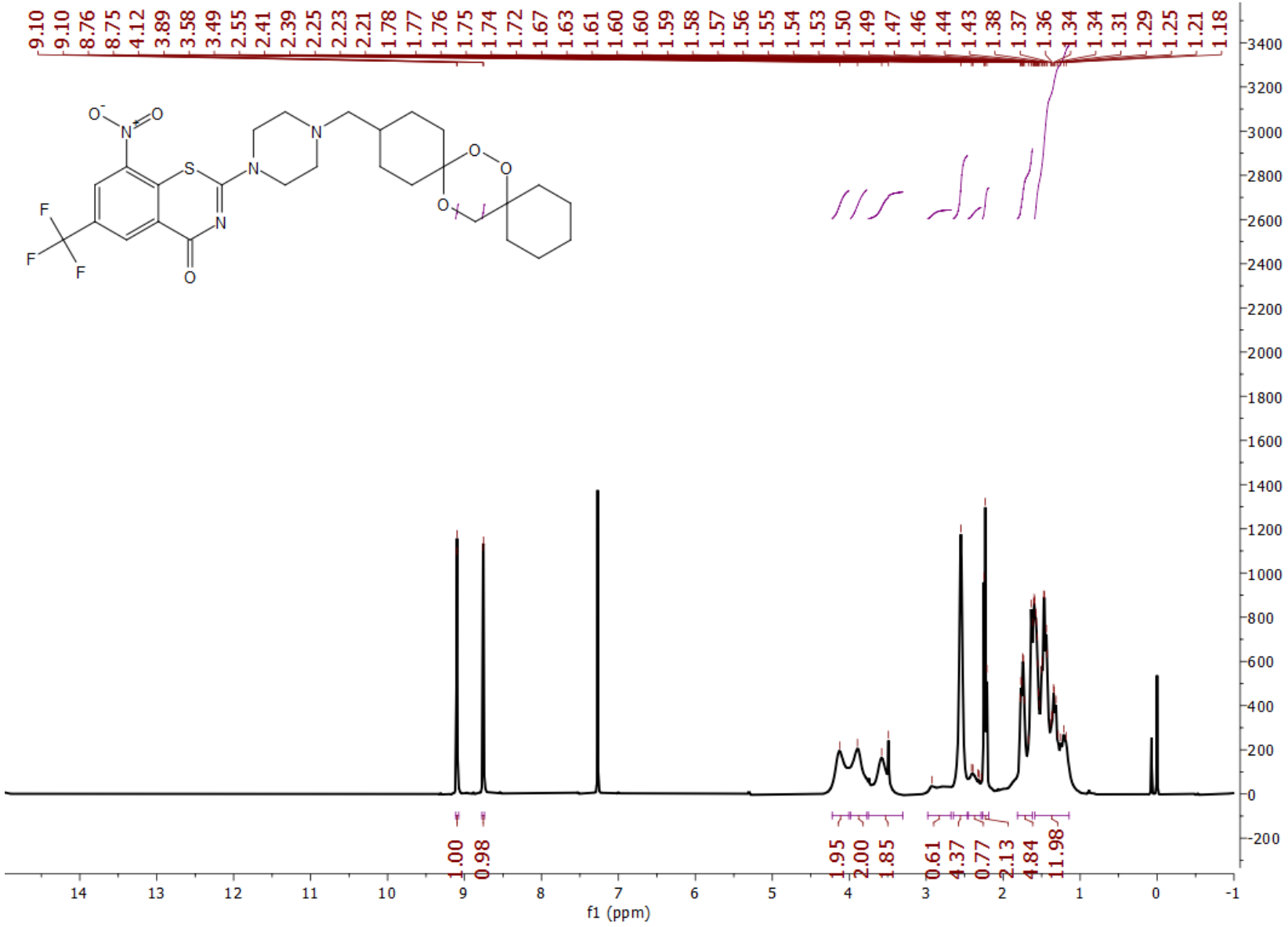

**Compound P5:** $^{13}C$ {$^{1}H$} NMR (101 MHz, $CDCl_3$)

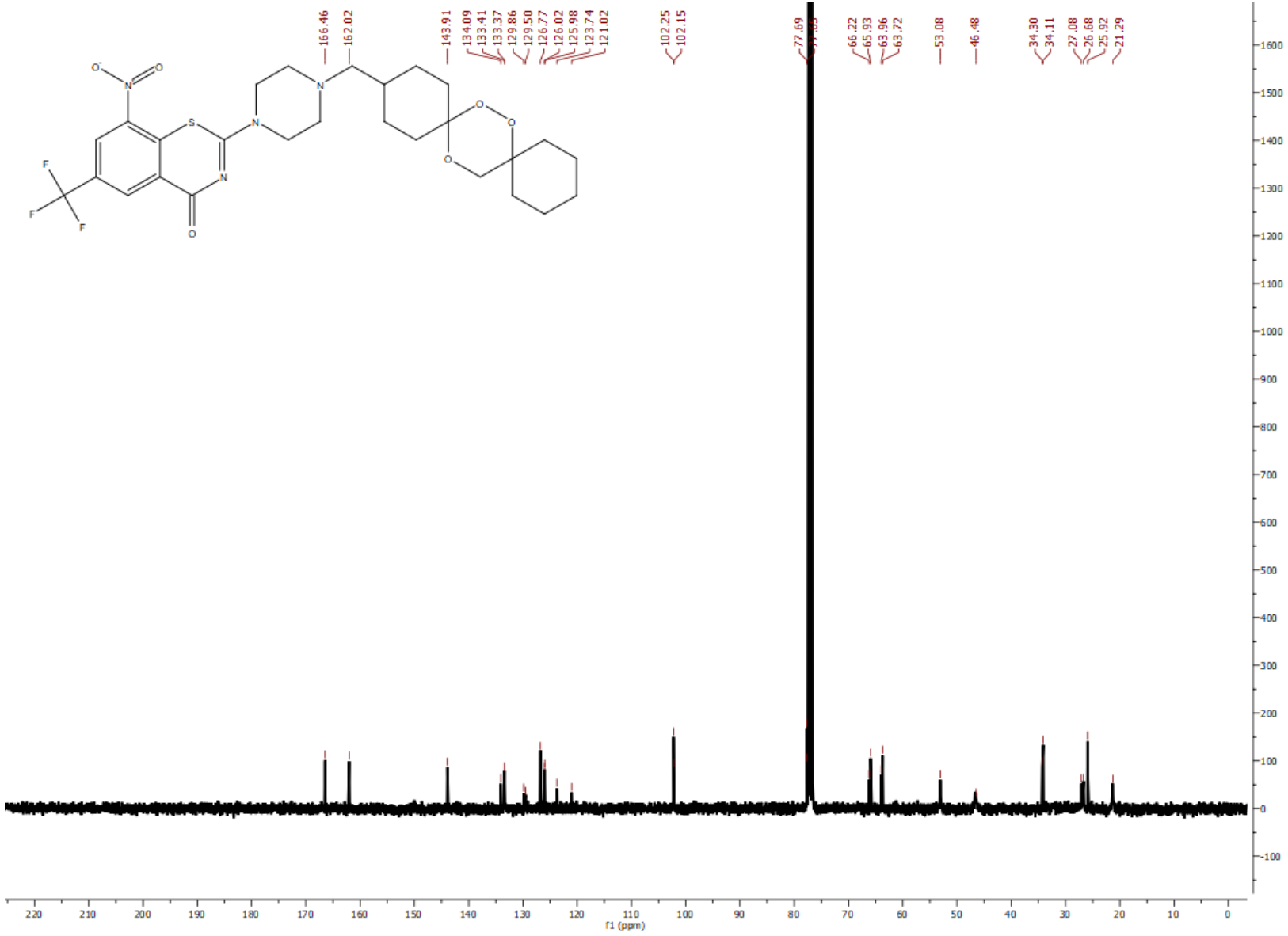

**Compound P6:** $^{1}H$ NMR (400 MHz, $CDCl_3$)

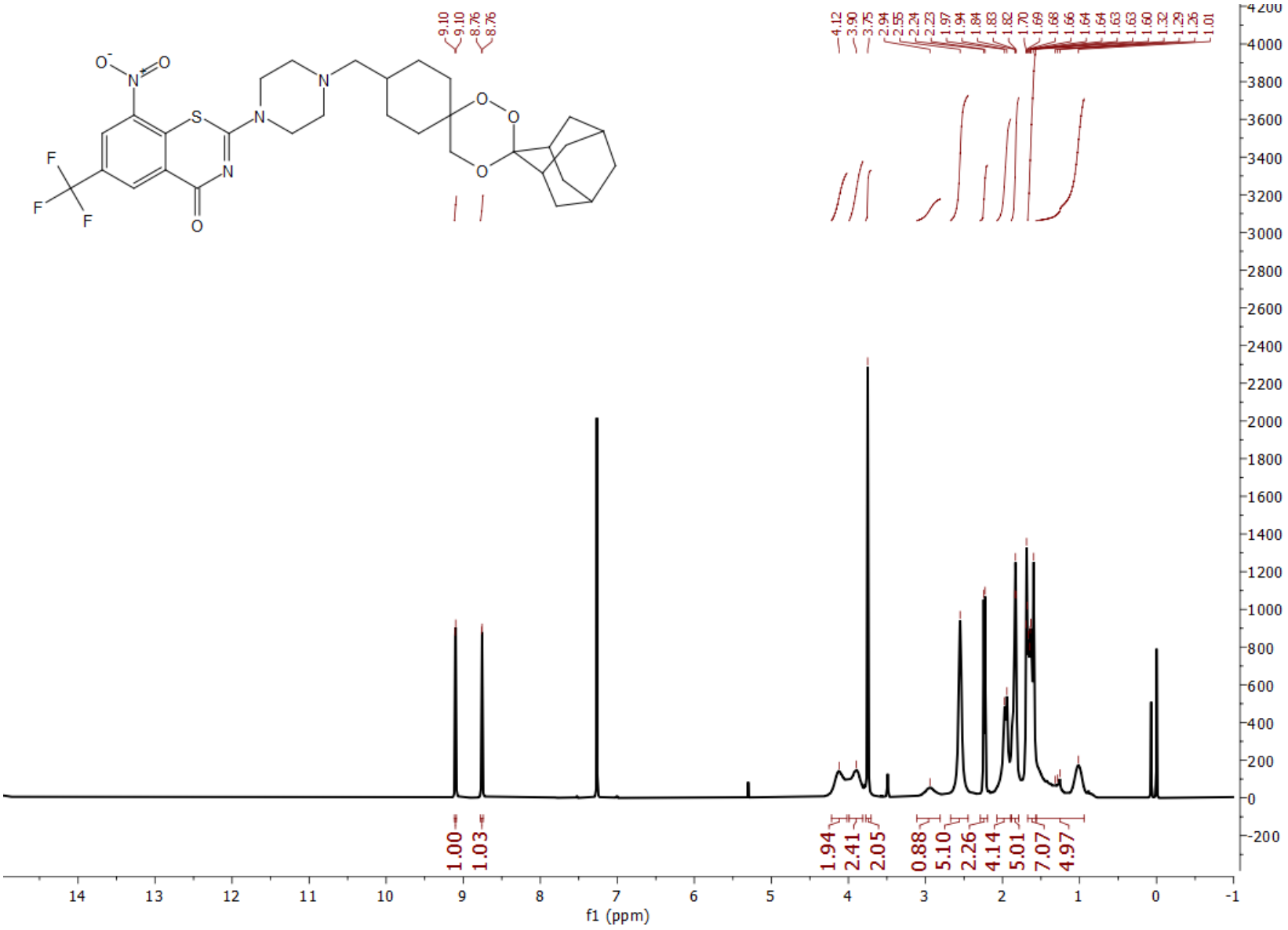

**Compound P6:** $^{13}C$ {$^{1}H$} NMR (101 MHz, $CDCl_3$)

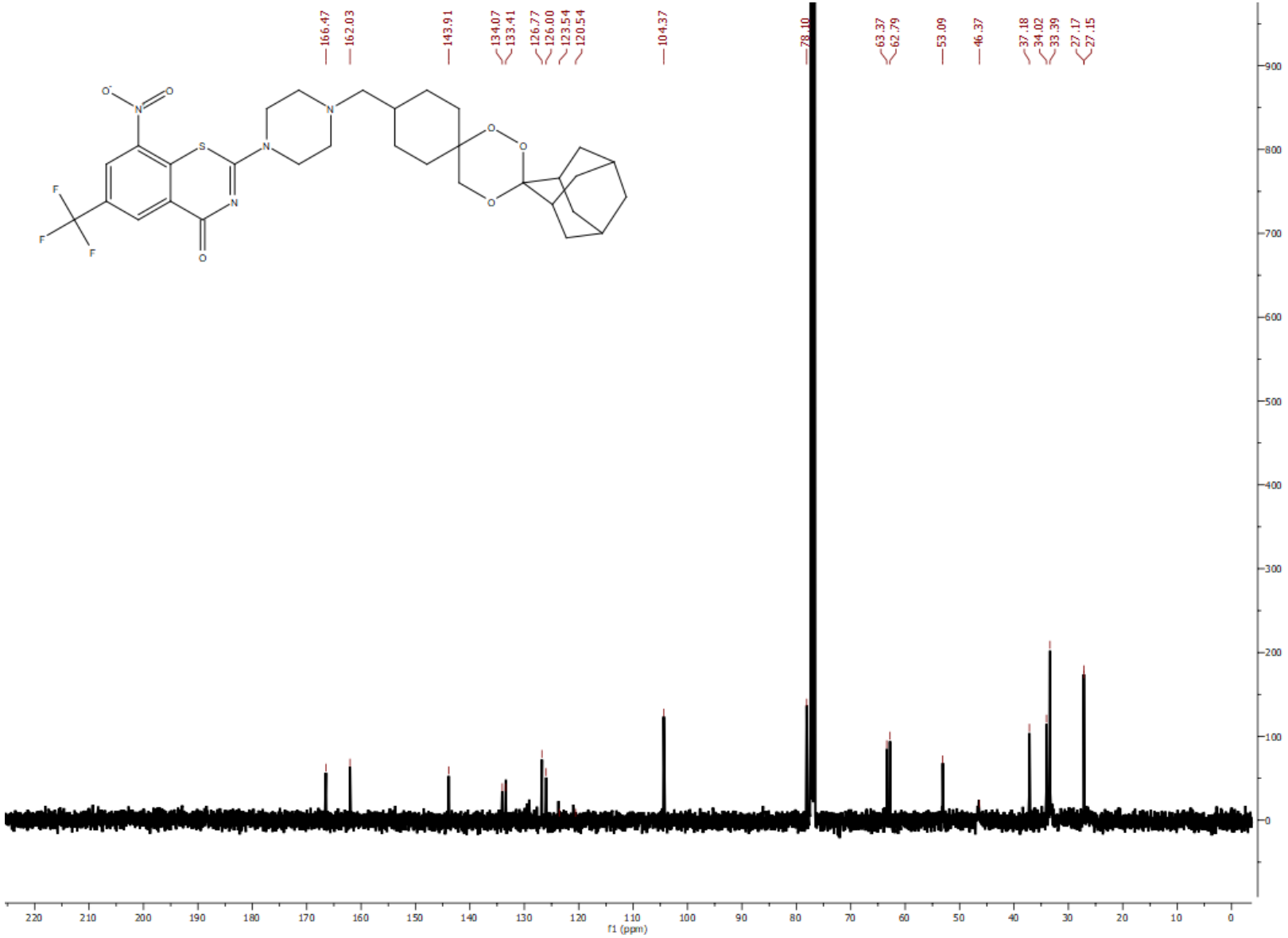

**Compound P7:** $^{1}$H NMR (400 MHz, DMSO-$d_6$)

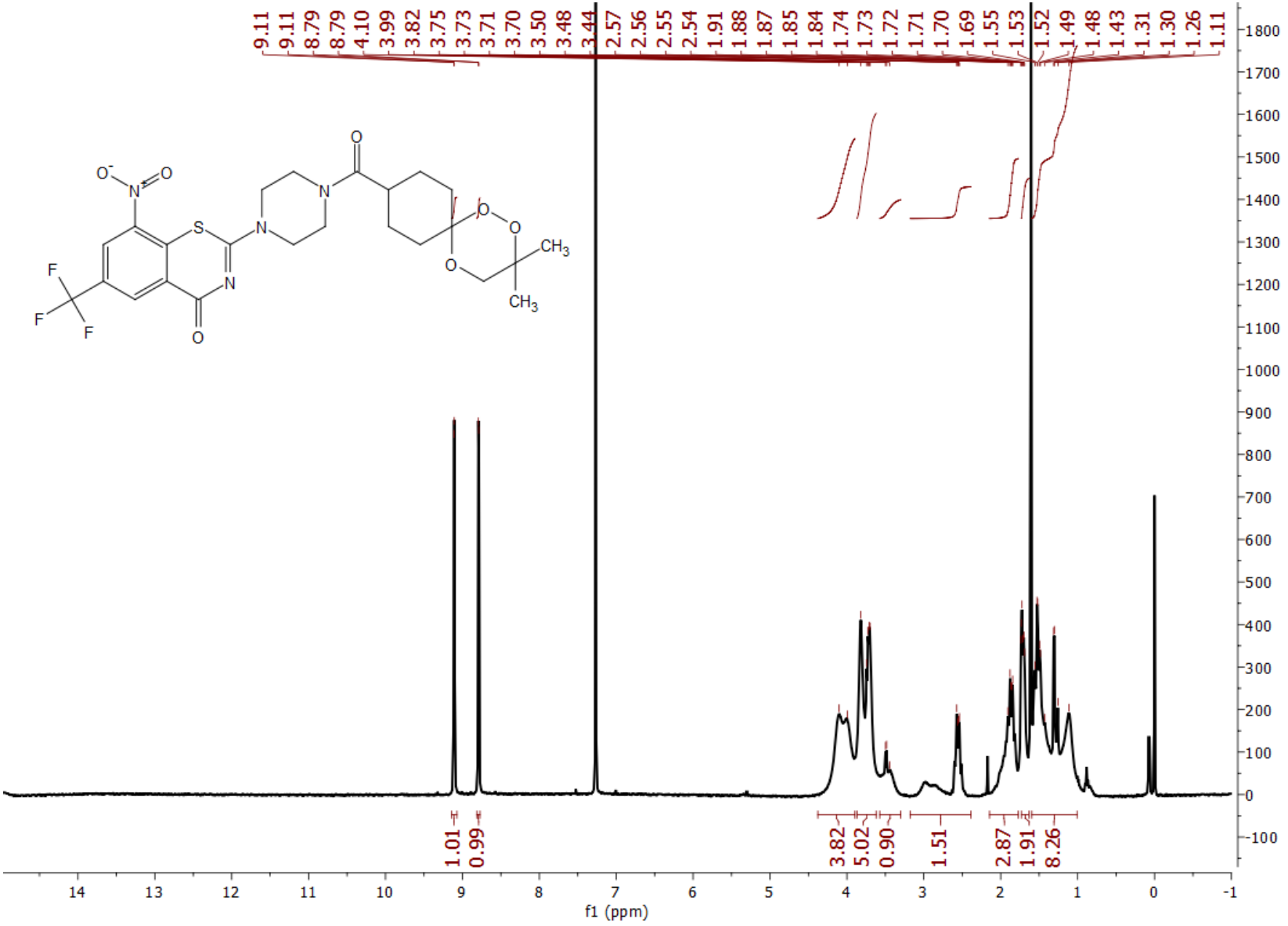

**Compound P7:** $^{13}C$ {$^{1}H$} NMR (101 MHz, DMSO-$d_6$)